DEVELOPMENT OF A VALIDATED MODEL FOR USE IN MINIMIZING NO_X EMISSIONS AND MAXIMIZING CARBON UTILIZATION WHEN CO-FIRING BIOMASS WITH COAL

Final Report

Project Start Date: 9/20/2001
Project End Date: 3/31/2003

Larry G. Felix, SoRI
P. Vann Bush, SoRI
Stephen Niksa, NEA, Inc.

April 30, 2003

DOE Cooperative Agreement No. DE-FC26-00NT40895

Southern Research Institute
2000 Ninth Avenue South
P. O. Box 55305
Birmingham, AL 35255-5305

DISCLAIMER

This report was prepared as an account of work sponsored by an agency of the United States Government. Neither the United States Government nor any agency thereof, nor any of their employees, makes any warranty, express or implied, or assumes any legal liability or responsibility for the accuracy, completeness, or usefulness of any information, apparatus, product, or process disclosed, or represents that its use would not infringe privately owned rights. Reference herein to any specific commercial product, process, or service by trade name, trademark, manufacturer, or otherwise does not necessarily constitute or imply its endorsement, recommendation, or favoring by the United States Government or any agency thereof. The views and opinions of authors expressed herein do not necessarily state or reflect those of the United States Government or any agency thereof.

Abstract

In full-scale boilers, the effect of biomass cofiring on NO_X and unburned carbon (UBC) emissions has been found to be site-specific. Few sets of field data are comparable and no consistent database of information exists upon which cofiring fuel choice or injection system design can be based to assure that NO_X emissions will be minimized and UBC be reduced. This report presents the results of a comprehensive project that generated an extensive set of pilot-scale test data that were used to validate a new predictive model for the cofiring of biomass and coal. All testing was performed at the 3.6 MMBtu/hr (1.75 MW_t) Southern Company Services/Southern Research Institute Combustion Research Facility where a variety of burner configurations, coals, biomasses, and biomass injection schemes were utilized to generate a database of consistent, scalable, experimental results (422 separate test conditions). This database was then used to validate a new model for predicting NO_X and UBC emissions from the cofiring of biomass and coal. This model is based on an Advanced Post-Processing (APP) technique that generates an equivalent network of idealized reactor elements from a conventional CFD simulation. The APP reactor network is a computational environment that allows for the incorporation of all relevant chemical reaction mechanisms and provides a new tool to quantify NO_X and UBC emissions for any cofired combination of coal and biomass.

Table of Contents

DISCLAIMER i

ABSTRACT ii

TABLE OF CONTENTS iii

LIST OF TABLES iv

LIST OF FIGURES v

1.0 INTRODUCTION 1
- 1.1 Task 1 – Project and Program Management 1
  - 1.1.1 Project Objectives 1
- 1.2 Task 2.0 – CFD Modeling 2
- 1.3 Task 3.0 – Simulation Tools Development 2
- 1.4 Task 4.0 – Fuels Selection 3
- 1.5 Task 5 – Cofiring Tests in the Combustion Research Facility 3
- 1.6 Task 6 – Model Simulations of Biomass Cofiring Cases 3
  - 1.6.1 Task 6.1 – Combustion Research Facility Results Verification 3
  - 1.6.2 Task 6.2 – Recommendations for Full-Scale Application of the Model 3
- 1.7 Task 7 – Reporting 3

2.0 EXECUTIVE SUMMARY 4
- 2.1 Introduction 4
- 2.2 Testing 4
- 2.3 Model Development 4
- 2.3 Results 6

3.0 EXPERIMENTAL 7
- 3.1 Background 7
- 3.2 Pilot-Scale Combustor Testing 7
  - 3.2.1 Combustion Research Facility 7
    - 3.2.1.1 Fuel Preparation 9
    - 3.2.1.2 Coal Feeding 10
    - 3.2.1.3 Burner Configurations 10
      - 3.2.1.3.1 Single-Register Burner 10
      - 3.2.1.3.2 Dual-Register Burner 11
    - 3.2.1.4 Radiant Furnace 11
    - 3.2.1.5 Convective Section 12
    - 3.2.1.6 Computer Data Acquisition and Control System 12
    - 3.2.1.7 CEM System 12
    - 3.2.1.8 Pollution Control Equipment 12

3.2.2 Comparison to Full-Scale Performance 13
3.2.3 Protocols for Testing 15
3.2.3.1 Modifications to Accommodate Biomass Cofiring 15
3.2.3.2 Testing Matrix 21
3.2.3.2.1 Coals Tested 21
3.2.3.2.2 Biomasses Tested 23
3.2.3.2.3 Tests Performed 26
3.2.4 Test Results 26
3.2.4.1 Single-Register Burner – Results from Cofiring Tests with Comilled Biomass 28
3.2.4.1.1 CRF Stability 28
3.2.4.1.2 Effect of Coal PSD on NO_X and UBC Emissions 30
3.2.4.1.3 Results of Cofiring Tests with Comilled Coal and Biomass 33
3.2.4.1.3.1 NO_X Reductions from Cofiring by Comilling SD with Coal 35
3.2.4.1.3.2 NO_X Reductions from Cofiring by Comilling SG with Coal 45
3.2.4.1.3.3 UBC Emissions from Cofiring by Comilling SD and SG with Coal 52
3.2.4.1.3.4 NO_X Reductions from Cofiring GL Coal with Simulated Poultry Litter 58
3.2.4.1.4 Results of Cofiring Tests by Comilling, Core Injection, and Side Injection 60
3.2.4.1.4.1 Biomass Particle Size Distribution 60
3.2.4.1.4.2 NO_X Reductions from Cofiring SD with JR and PR Coal 65
3.2.4.1.4.3 NO_X Reductions from Cofiring SG with JR and PR Coal 70
3.2.4.1.4.4 UBC Emissions from Cofiring SD and SG with Coal 75
3.2.4.2 Dual-Register Burner – Results from Cofiring Tests with Comilled Biomass 75
3.2.4.2.1 NO_X Reductions from Cofiring SD and SG with GL Coal 79
3.2.4.2.2 UBC Emissions from Cofiring SD and SG with GL Coal 79

4.0 MODEL DEVELOPMENT 86
4.1 Background 86
4.2 Advanced Post-Processing – Predicting Emissions with Detailed Chemical Reaction Mechanisms 87
4.2.1 Overview of APP 87
4.2.2 Bulk Flow and Temperature Patterns 88
4.2.2.1 CFD Simulations 88
4.2.2.2.1 Bulk Flow Patterns 88
4.2.2.1.2 Required CFD Variables for APP 89
4.2.3 Equivalent Reactor Network 90
4.2.3.1 Basis for an Equivalent Reactor Network 90

4.2.3.2 Steps in Developing an Equivalent Reactor Network....93
4.2.3.3 Delineating Regions....94
4.2.3.3.1 Combustibles Mass Fraction....94
4.2.3.3.2 Regions in the CRF....95
4.2.4 RTDs and Equivalent Reactor Assemblies....96
4.2.4.1 Basis for an Equivalent Reactor Assembly....96
4.2.4.2 An Equivalent Reactor Network for the CRF....96
4.2.5 Operating Conditions....97
4.2.5.1 Mean Gas Temperature Histories....97
4.2.5.2 Mean Particle Temperature Histories....98
4.2.5.3 Effective Radiation (Wall) Temperature....98
4.2.6 Entrainment Rates in Regions....98
4.2.6.1 Entrainment Rate by Fluid Tracking....99
4.2.6.2 Entrainment Histories....99
4.2.7 Detailed Chemical Reaction Mechanisms....99
4.2.8 Implementation....101
4.3 The Emissions Database – Nominal Fuel Properties....103
4.3.1 Overview....103
4.4 Reactor Network Specifications....104
4.4.1 Network Specifications for the PR Baseline Flame....104
4.4.1.1 Operating Conditions....105
4.4.1.2 Calibration Procedures....109
4.4.2 Extrapolation Procedures....110
4.4.2.1 Extrapolations for Furnace Stoichiometry....112
4.4.2.2 Extrapolations for Staging Level....112
4.4.2.3 Extrapolations for Cofiring Level and Biomass Form....113
4.4.2.4 Extrapolations for Injection Configuration....114
4.4.2.5 Extrapolations for the Dual-Register Burner....114
4.4.3 Ranges of Network Specifications....115
4.4.4 Complete Input Specifications....116
4.5 Results....116
4.5.1 Predicted Devolatilization Behavior....117
4.5.2 Flame Structures....119
4.5.2.1 Baseline PR-Only Flame Structure....119
4.5.2.1.1 Flame Core....119
4.5.2.1.2 Mixing Layer....121
4.5.2.1.3 OFA and Burnout Regions....122
4.5.2.2 Co-Milled PR/20%SG Flame Structure....122
4.5.2.3 Co-Milled PR/20%SD Flame Structure....126
4.5.3 NO_X Predictions....129

4.5.3.1 Fuel Quality Impacts 129
4.5.3.1.1 Calibration Factors 129
4.5.3.1.2 Fuel Quality Impacts On NO_X Emissions 130
4.5.3.2 Impacts of Furnace Stoichiometry and PSD 135
4.5.3.3 Effect of Biomass Injection Configuration 140
4.5.4 LOI Predictions 141
4.5.4.1 Fuel Quality Effects 143
4.5.4.2 Effects of Furnace Stoichiometry and PSD 144
4.5.4.3 Effect of Biomass Injection Configuration 147
4.5.5 Interpretations 147
4.5.5.1 Flame Structure Parameters 149
4.5.5.2 Fuel Quality Effects on NO_X Cofiring 151
4.5.5.3 Effect of Operating Conditions on NO_X 154
4.5.5.3.1 Effect of Staging 154
4.5.5.3.2 Effect of Furnace Stoichiometry 155
4.5.5.3.3 Effect of Cofiring Configuration 155
4.5.5.4 LOI Predictions 155
4.6 Recommendations for Full-Scale Applications 157
4.6.1 T-Fired Furnace Applications 157
4.6.2 Applications Involving Other Firing Configurations 158
4.7 Recommendations for Further Development 158

5.0 RESULTS AND DISCUSSION 160
5.1 Introduction 160
5.2 Testing 160
5.3 Model Development 161
5.4 Results of the Model Development 162

6.0 CONCLUSION 165

7.0 REFERENCES 166

APPENDIX A 167

APPENDIX B 217

LIST OF TABLES

3-1. Internal surface parameters compared for the CRF and full-scale units.....15

3-2. Typical as received (AR) fuel and ash analyses for the coals tested 22

3-3. Typical as received (AR) fuel and ash analyses for the sawdust (SD) tested.....24

3-4. Typical as received (AR) fuel and ash analyses for the switchgrass (SG) tested ..25

3-5. Pilot-Scale Furnace Tests.....27

3-6. Summary of test conditions in the database.....28

3-7. Fit parameters for the NO_X emissions curves in Figures 3-14 and 3-15.....35

3-8. NO_X reductions from cofiring with comilled sawdust.....37

3-9. Fuel stoichiometric ratio and volatile to fixed carbon ratio as a function of weight % biomass 44

3-10. Fuel Nitrogen as a function of weight % biomass 44

3-11. NO_X reductions from cofiring with comilled SG.....46

3-12. Results of increasing fuel nitrogen by ammonia addition in Test GL-11 59

3-13. Fit parameters for the NO_X emissions curves in Figures 3-33 through 3-36 63

3-14. NO_X reductions from cofiring PR and JR coals for comilled, center, and side injection of SD 66

3-15. NO_X reductions from cofiring PR and JR coals for comilled, center, and side injection of SG 71

3-16. Fit parameters for the NO_X emissions curves in Figure 3-50 80

3-17. NO_X reductions from cofiring GL coal with comilled SD and SG, dual-register burner and single-register burner 81

4-1. Nominal Fuel Properties used for model calculations 103

4-2. Cases With CFD Simulations 111

4-3. Matrix of Extrapolation Factors.....113

4-4. Ranges of Network Specifications 115

4-5. Distributions of Secondary Pyrolysis Products and Char Properties 118

4-6. Fuel-Specific Calibration Factors 130

4-7. Evaluation of Predicted NO_X for Co-Milled, Cofired Flames with 3.5 % O_2 133

4-8. Evaluation of Predicted NO_X for Core-Injected Co-Fired Flames with 3.5 % O_2 140

4-9. Evaluation of Predicted LOI for Co-Milled, Co-Fired Flames with 3.5 % O_2 145

4-10. Evaluation of Predicted LOI for Core-Injected Co-Fired Flames with 3.5 % O_2 148

4-11. Predicted N-Conversion Parameters for Coal-Only Flames with 15 % OFA and 3.5 % O_2 150

4-12. Predicted N-Conversion Parameters for Cofired Flames with 15 % OFA and 3.5 % O_2 153

4-13. Predicted N-Conversion Parameters for Coal-Only Flames with 0 % OFA and 3.5 % O_2 154

4-14. Predicted N-Conversion Parameters for Cofired Flames with 0 % OFA and 3.5 % O_2 155

4-15. Predicted N-Conversion Parameters for JR and JR/20%SD Flames with 15 % OFA 156

5-1. Summary of test conditions in the database 161

A-1A. Gas Flow Data from Tests PR-1, PR-1R, PR-2, and PR-10, Part 1 168

A-1B. Gas Flow Data from Tests PR-1, PR-1R, PR-2, and PR-10, Part 2 169

A-1C. Gas Flow Data for UBC Measurements from Tests PR-1, PR-1R, PR-2, and PR-10 170

A-1D. Gas Sampling Data from Tests PR-1, PR-1R, PR-2, and PR-10, Part 1 171

A-1E. Gas Sampling Data from Tests PR-1, PR-1R, PR-2, and PR-10, Part 2 172

A-1F. Gas Sampling Data for UBC Measurements from Tests PR-1, PR-1R, PR-2, and PR-10 173

A-2A. Gas Flow Data from Test PR-3 174

A-2B. Gas Flow Data for UBC Measurements from Test PR-3 175

A-2C. Gas Sampling Data from Test PR-3 176

A-2D. Gas Sampling Data for UBC Measurements from Test PR-3 177

A-3A. Gas Flow Data from Test PR-4 178

A-3B. Gas Flow Data for UBC Measurements from Test PR-4 179

A-3C. Gas Sampling Data from Test PR-4 180

A-3D. Gas Sampling Data for UBC Measurements from Test PR-4 181

A-4A. Gas Flow Data from Test GL-5 and PR-5 182

A-4B. Gas Flow Data for UBC Measurements from Test GL-5 and PR-5 183

A-4C. Gas Sampling Data from Test GL-5 and PR-5 184

A-4D. Gas Sampling Data for UBC Measurements from Test GL-5 and PR-5 185

A-5A. Gas Flow Data from Test GL-6 186

A-5B. Gas Flow Data for UBC Measurements from Test GL-6 187

A-5C. Gas Sampling Data from Test GL-6 188

A-5D. Gas Sampling Data for UBC Measurements from Test GL-6 189

A-6A. Gas Flow Data from Test JR-7 190

A-6B. Gas Flow Data for UBC Measurements from Test JR-7 191

A-6C. Gas Sampling Data from Test JR-7 192

A-6D. Gas Sampling Data for UBC Measurements from Test JR-7 193

A-7A1. Gas Flow Data from Test JR-8, Part 1 194

A-7A2. Gas Flow Data from Test JR-8, Part 2 195

A-7B. Gas Flow Data for UBC Measurements from Test JR-8.....196

A-7C1. Gas Sampling Data from Test JR-8, Part 1 197

A-7C2. Gas Sampling Data from Test JR-8, Part 2 198

A-7D. Gas Sampling Data for UBC Measurements from Test JR-8.....199

A-8A. Gas Flow Data from Test GL-9.....200

A-8B. Gas Flow Data for UBC Measurements from Test GL-9.....201

A-8C. Gas Sampling Data from Test GL-9.....202

A-8D. Gas Sampling Data for UBC Measurements from Test GL-9 203

A-9A. Gas Flow Data from Test PR-10 204

A-9B. Gas Flow Data for UBC Measurements from Test PR-10.....204

A-9C. Gas Sampling Data from Test PR-10 205

A-9D. Gas Sampling Data for UBC Measurements from Test PR-10.....205

A-10A. Gas Flow Data from Test GL-11.....206

A-10B. Gas Sampling Data from GL-11.....207

A-10C. Gas Flow Data for UBC Measurements from GL-11 208

A-10D. Gas Sampling Data for UBC Measurements from GL-11 208

A-11A. Gas Flow Data from Test JW-12.....209

A-11B. Gas Flow Data for UBC Measurements from JW-12 210

A-11C. Gas Sampling Data from JW-12.....211

A-11D. Gas Sampling Data for UBC Measurements from JW-12 212

A-12A. Gas Flow Data from Test JW-13.....213

A-12B. Gas Sampling Data from JW-13 214

A-12C. Gas Flow Data for UBC Measurements from JW-13 215

A-12D. Gas Sampling Data for UBC Measurements from JW-13 216

B-1A. Curvefits to NO_X emissions data for Tests PR-1, P-3, and PR-4 218

B-1B. Curvefits to NO_X emissions data for Tests GL-5&6, PR-6, JR-7, and JR-8 219

B-1C. Curvefits to NO_X emissions data for Tests GL-9, GL-11&12, and JW-12&13 220

B-2. Fuel stoichiometric ratio and volatile to fixed carbon ratio as a function of weight % biomass 221

B-3. Fuel Nitrogen as a function of weight % biomass 221

B-4A. Size distributions for coal and comilled biomass with component coal and biomass, Rosin-Rammler distribution fit parameters 222

B-4B. Size distributions for coal and comilled biomass with component coal and biomass, Rosin-Rammler distribution fit parameters 223

LIST OF FIGURES

3-1. NO_X concentrations measured when firing Pratt seam coal alone and with a comilled blend of 90% coal and 10% switchgrass....8

3-2. A summary of NO_X reduction from a number of biomass/coal cofiring full-scale and pilot-scale demonstration tests, based on the mass input of biomass. Dashed lines are 95% prediction limits that encompass the range of variability in the measured data....8

3-3. The combustion research facility....9

3-4. Comparison of the temperature-time history of the CRF with several Southern Company full-scale power plants....14

3-5. Cross section of the first section of the pilot-scale furnace with the single-register burner installed. The three locations employed for biomass injection are shown....16

3-6. Top view of modifications to primary air line and blast pilot to accommodate center-burner injection of biomass....17

3-7. Side view of modifications to primary air line and blast pilot to accommodate center-burner injection of biomass....18

3-8. Layout of apparatus used for the injection of biomass into the side of a pulverized coal flame....20

3-9. NO_X emissions for 100% PR coal firing in the CRF at 0%, 15%, and 30% OFA. These data span one year and cover five separate test series....29

3-10. Unburned carbon in fly ash from the combustion of 100% PR coal, 0% and 15% OFA, averages ± 1 standard deviation....31

3-11. Cumulative size distribution for a comilled mixture of 80% PR coal and 20% sawdust....32

3-12. NO_X emissions for normally and finely ground PR coal, test condition averages ± 1 standard deviation....32

3-13. UBC emissions for normally and finely ground PR coal, averages ± 1 standard deviation....33

3-14. Baseline NO_X emissions for 0% OFA....34

3-15. Baseline NO_X emissions for 15% OFA....34

3-16. Baseline UBC emissions for GL coal 36

3-17. NO_X reductions from comilling SD with JR coal, 0% and 15% OFA 38

3-18. NO_X reductions from comilling SD with GL coal, 0% and 15% OFA 39

3-19. NO_X reductions from comilling SD with PR coal, 0% and 15% OFA.....40

3-20. NO_X reductions from comilling SD with PR coal, 30% OFA 41

3-21. NO_X reductions from comilling SD with JW coal, 0% and 15% OFA.
Results for 5% biomass are not included.....42

3-22. NO_X reductions from comilling SD with JW coal, 0% and 15% OFA.
Results for 5% biomass are included.....43

3-23. NO_X reductions from comilling SG with JR coal, 0% and 15% OFA 47

3-24. NO_X reductions from comilling SG with GL coal, 0% and 15% OFA 48

3-25. NO_X reductions from comilling SG with PR coal, 0% and 15% OFA.....49

3-26. NO_X reductions from comilling SG with JW coal, 0% and 15% OFA 50

3-27. NO_X reductions from comilling SG with JW coal, 0% and 15% OFA.
Results for 5% biomass are included.....51

3-28. UBC emissions from comilling SD and SG with JR coal, for 0% OFA (top)
and for 15% OFA (bottom).....53

3-29. UBC emissions from comilling SD and SG with GL coal, for 0% OFA (top)
and for 15% OFA (bottom).....54

3-30. UBC emissions from comilling SD and SG with PR coal, (a) for 15% OFA,
varying FEO and (b) for ~3.5% FEO, varying OFA 55

3-31. UBC emissions from comilling SD with JW coal, 0 and 15% OFA 56

3-32. UBC emissions from comilling SG with JW coal, 0 and 15% OFA 57

3-33. Baseline NO_X emissions for 0% OFA, PR coal.....61

3-34. Baseline NO_X emissions for 15% OFA, PR coal.....61

3-35. Baseline NO_X emissions for 0% OFA, JR coal 62

3-36. Baseline NO_X emissions for 15% OFA, JR coal 62

3-37. Cumulative particle size distribution for the sawdust injected into the single-register burner in Tests PR-3 and PR-4 63

3-38. Cumulative particle size distribution for the switchgrass injected into the single-register burner in Tests PR-3 and PR-4 64

3-39. Cumulative particle size distribution for the sawdust injected into the single-register burner in Test JR-8.....64

3-40. Cumulative particle size distribution for the switchgrass injected into the single-register burner in Test JR-8.....65

3-41. NO_X reductions from cofiring SD with JR coal by injecting SD through the center of the single-register burner, 0% and 15% OFA.....67

3-42. NO_X reductions from cofiring SD with PR coal by injecting SD through the center of the single-register burner, 0% and 15% OFA.....68

3-43. NO_X reductions from cofiring SD with PR coal by injecting SD from the side into the exit of the single-register burner, 0% and 15% OFA 69

3-44. NO_X reductions from cofiring SG with JR coal by injecting SG through the center of the single-register burner, 0% and 15% OFA 72

3-45. NO_X reductions from cofiring SG with PR coal by injecting SG through the center of the single-register burner, 0% and 15% OFA 73

3-46. NO_X reductions from cofiring SG with PR coal by injecting SG from the side into the exit of the single-register burner, 0% and 15% OFA 74

3-47. UBC emissions from cofiring SD and SG with JR coal by injection through the burner center, 0% OFA (top) and 15% OFA (bottom) 76

3-48. UBC emissions from cofiring SD and SG with PR coal by injection through the burner center, 0% OFA (top) and 15% OFA (bottom) 77

3-49. UBC emissions from cofiring SD and SG with PR coal by injection from the side into the exit of the single-register burner, 0% OFA (top) and 15% OFA (bottom) 78

3-50. Baseline NO_X emissions for 16% TA and 30% TA for the dual-register burner and GL coal. Test GL-9.....80

3-51. NO_X reductions from comilling SD (top) and SG (bottom) with GL coal, 16% TA, dual-register burner 82

3-52. NO_X reductions from comilling SD (top) and SG (bottom) with GL coal, 30% TA, dual-register burner 83

3-53. UBC emissions from comilling SD and SG with GL coal in the dual-register burner, for 16% TA (top) and for 30% TA (bottom).....84

4-1. Schematic of the information flow in conventional and advanced post-processing 88

4-2. APP regions for the baseline Pratt hv bituminous flame delineated from the CFD simulation 95

4-3. Equivalent reactor network for the baseline Pratt hv bituminous flame.....97

4-4. Information flow in the computerized APP analysis for CRF flames 102

4-5. RTDs from the CFD simulation (columns) and assigned analytically (curves) for the core, mixing layer, and burnout zone of the PR-only flame with 15% OFA and 3.5 % O_2.....106

4-6. Gas temperature history assigned to the CSTR series for the core (histogram) compared to the history assigned from the CFD simulation (solid curve) for the PR-only flame with 15% OFA and 3.5 % O_2 106

4-7. Mean particle temperature history assigned for devolatilization simulations in the core (solid curve) compared to the history assigned from the CFD simulation (dashed curve) for the PR-only flame with 15% OFA and 3.5 % O_2.....107

4-8. Fraction of entrained secondary air into the mixing layer from the CFD simulation for the PR-only flame with 15% OFA and 3.5 % O_2.....108

4-9. Entrainment volumes for two limiting mixing models versus distance from the point of injection 108

4-10. Fit of predicted NO_X emissions to the data for the PR-only flames with 0 and 15% OFA and various O_2 levels 110

4-11. CFD-based temperature histories for PR only (dotted curves) and PR/20%SD (dashed curves), and the interpolated histories for PR/10%SD (solid curves) 114

4-12. Structure of the core of the baseline PR-only flame showing, in counterclockwise order from the upper left, the operating conditions, major species, char and soot burnout, and N-species 120

4-13. Structure of the mixing layer of the baseline PR-only flame showing, in counterclockwise order from the upper left, the operating conditions, major species plus entrainment fraction of secondary air, char and soot burnout, and N-species 121

4-14. Structure of the OFA and BO regions of the baseline PR-only flame showing (top) the operating conditions and (bottom) O_2 concentration and char burnout.....123

4-15. Extent of char burnout versus char size at the ends of the core, mixing layer, OFA region, and burnout region.....124

4-16. Structure of the core of the PR/20%SG flame showing, in counterclockwise order from the upper left, the operating conditions, major species, char and soot burnout, and N-species 124

4-17. Extent of char burnout of PR-char (solid curves) and SG-char (dashed curves) versus initial char size at the ends of the core, mixing layer, OFA region, and burnout region in the PR/20%SG flame 127

4-18. Structure of the core of the PR/20%SD flame showing, in counterclockwise order from the upper left, the operating conditions, major species, char and soot burnout, and N-species 127

4-19. Extent of char burnout of PR-char (solid curves) and SD-char (dashed curves) versus initial char size at the ends of the core, mixing layer, OFA region, and burnout region in the PR/20%SD flame 129

4-20. Parity plot for the data subset with co-milled injection, 3.5 % O_2, and 15 % OFA where the cases with NH_3 injection (□) are distinguished from all other test results (●) 131

4-21. Parity plot for the data subset with co-milled injection, 3.5 % O_2, and 0 % OFA where the cases with NH_3 injection (□) are distinguished from all other test results (●) 131

4-22. Evaluation of the predicted impact of biomass loading on NO_X emissions for PR/SD cases from test series 1 132

4-23. Evaluation of the predicted effect of biomass loading on NO_X emissions for test series with co-milled injection, 3.5 % O_2, and 0 % OFA 135

4-24. Evaluation for the full range of exhaust O_2 with 15 % OFA and co-milled injection. Each case contains a coal-only baseline (Δ, dashed curve) and, if available, cofired cases with 20 % SD (●, solid curve) and 20 % SG (○, dotted curve) 136

4-25. Evaluation for the full range of exhaust O_2 with 0 % OFA and co-milled injection. Each case contains a coal-only baseline (Δ, dashed curves) and, if available, cofired cases with 20 % SD (●, solid curves) and 20 % SG (○, dotted curves).....138

4-26. Evaluation of predicted NO_X emissions for finer grinds (filled symbols and solid curves) compared to baseline values (open symbols and dashed curves).....139

4-27. Evaluation for the full range of exhaust O_2 for core injection. Each case contains a coal-only baseline (Δ, dashed curves) and cofired cases with 15 % SD (●, solid curves) and 20 % SG (○, dotted curves).....142

4-28. Parity plot for the data subset with co-milled injection, 3.5 % O_2, and 15 % OFA where the cases with JR (Δ) and JW (○) are distinguished from all other test results (●) 143

4-29. Parity plot for the data subset with co-milled injection, 3.5 % O_2, and 0 % OFA where the cases with JR (Δ) and JW (○) are distinguished from all other test results (●) 146

4-30. Evaluation for the full range of exhaust O_2 with 15 % OFA and co-milled injection. Each case contains a coal-only baseline (Δ, dashed curves) and, if available, cofired cases with 20 % SD (●, solid curves) and 20 % SG (○, dotted curves).....147

4-31. Evaluation of predicted LOI for finer grinds (●and solid curve) compared to baseline values with 15 % OFA (○ and dashed curve).....148

4-32. Correlation of NO_C versus R_{DV} for coal-only flames 152

4-33. Submechanism for HCN oxidation in post-flame regions (Glarborg and Miller 1994) 152

1.0 INTRODUCTION

The work conducted in this project received funding from the Department of Energy under Cooperative Agreement No. DE-FC26-00NT40895. This project had a period of performance that commenced September 20, 2000 and, with approved time extensions, continued through March 31,2003. The project was divided into seven tasks.

1.1 Task 1 - Project and Program Management

Under Task 1.0, NEPA information (Task1.1) was submitted with the initial project proposal on March 30, 2000 and approval was obtained after project award before experimental work began. Task 1.2 involved overall project management, which was completed with the submission of this final project report. A project Work Plan (Task 1.3) was submitted to DOE on October 18, 2000 as the first deliverable under the cooperative agreement. The Work Plan is not included in this report, but below, the original objectives of the project are reproduced from the Work Plan.

1.1.1 Project Objectives

The project is designed to balance the development of a systematic and expansive database detailing the effects of co-firing parameters on nitrogen oxides (NO_X) formation with the complementary modeling effort that will yield a capability to predict, and therefore optimize, NO_X reductions by the selection of those parameters.

The database of biomass co-firing results will be developed through an extensive set of pilot-scale tests at the Southern Company/Southern Research Institute Combustion Research Facility. The testing in this program will monitor NO_X, unburned carbon (UBC), and other emissions over a broad domain of biomass composition, coal quality, and co-firing injection configurations to quantify the dependence of NO_X formation and LOI on these parameters. This database of co-firing cases will characterize an extensive suite of emissions and combustion properties for each of the combinations of fuel and injection configuration tested.

The complementary process modeling will expand the value of the raw test data by identifying the determining factors on NO_X emissions and UBC. Niksa Energy Associates (NEA) will develop and validate a detailed process model for predicting NO_X emissions and LOI from biomass co-firing that builds on a foundation of existing and proven fluid dynamics, reaction kinetics, and combustion products models. The fluid dynamics data will be produced from computer models developed by Reaction Engineering International (REI). The modeling process will resolve all major independent influences, including biomass composition, coal quality, chemical interactions among biomass-and coal-derived intermediate species, competitive O_2 consumption by biomass- and coal-derived intermediate species and chars, extent of biomass/coal mixing prior to combustion, and mixing intensity during biomass injection.

The overall goal of the project is to produce a validated tool or methodology to accurately and confidently design and optimize biomass co-firing systems for full-scale utility boilers to produce the lowest NO_X emissions and the least unburned carbon. Specific program objectives are:

- Develop an extensive data set under controlled test conditions that quantifies the relationships between NO_X emissions and biomass co-firing parameters.

- Provide a data set of the effects of biomass co-firing over a broad range of fuels and co-firing conditions on flame stability, carbon burnout, slagging and fouling, and particulate and gaseous emissions.

- Develop and validate a broadly applicable computer model that can be used to optimize NO_X reductions and minimize unburned carbon from biomass co-firing.

Once validated, the model provides a relatively inexpensive means to either (1) identify the most effective co-firing injection configuration for specified compositions of biomass and coal within a particular furnace environment, or (2) to forecast the emissions for a specified pair of fuels fired under an existing configuration. As such an important cost-saving tool, the modeling has the potential to accelerate widespread adoption of biomass co-firing as a NO_X control strategy in the electric utility industry.

Project partners included Southern Research Institute (project management and testing), Southern Company Services (SCS), Niksa Energy Associates (NEA, modeling), Reaction Engineering International (REI, CFD calculations), and MESA Reduction Engineering & Processing, Inc. (biomass processing).

1.2 Task 2.0 – CFD Modeling

Reaction Engineering International, Inc. completed Task 2. To complete the first part of this task, REI developed and coded a complete mesh for the Southern Research/Southern Company 3.6 MMBTU/hr Combustion Research Facility (CRF) and single-register burner and completed a variety of CFD simulations for this facility with their proprietary Glacier© code. Outputs from these CFD simulations are required as inputs for the computer modeling effort. As part of this task, REI also completed and delivered a fully functional version of their Configurable Fireside Simulator (CFS) that was used to complete the suite of CFD calculations for tests run at the CRF. The CFS is a completely functional version of their proprietary CFD simulation software that is tied to a specific mesh, in this case, a mesh representing the CRF. One goal was not completed. To remain within their budget, REI was not able to provide a simulation of the dual-register burner for the CRF, either for stand-alone CFD calculations or as part of the CFS. Thus, the set of tests carried out with this burner could not be modeled.

1.3 Task 3.0 – Simulation Tools Development

Niksa Energy Associates completed this task. Goals for this task included the configuration and integration of computer modules by NEA into a model to simulate the CRF cofiring cases to be investigated. In particular, the bio-FLASHCHAIN™, CHEMKIN III, and PC Coal Lab® modules have to be set up to accommodate the temperature and flow profiles that will be encountered in the pilot-scale cofiring test cases. NEA accomplished this task as part of their overall modeling responsibility.

1.4 Task 4.0 – Fuels Selection

This task involved fuels selection for testing at the CRF. Southern Company Services assisted Southern Research in identifying and locating coals to be burned. Four distinct types of coal were tested. The coals were: Pratt seam (an Alabama high volatility bituminous coal), Jim Walters #7 Mine (an Alabama low volatility bituminous coal), Galatia (an Illinois Basin high volatility bituminous coal), and Jacobs Ranch (a subbituminous Powder River Basin coal). Results from testing revealed that sawdust and switchgrass provided sufficient variety for the modeling effort and with this understanding, these two materials became the primary biomasses utilized for CRF testing. Poultry litter was simulated in one test by adding anhydrous ammonia to the primary air line in the CRF when comilled coal and sawdust were burned.

1.5 Task 5.0 – Cofiring Tests in the Combustion Research Facility

Task 5 was originally proposed to cover 18 weeks of testing over a period of 18 months. As the testing proceeded, results from the modeling effort were used to inform and guide the testing effort so that unnecessary testing could be eliminated. The lack of a CFD model for the dual-register burner also affected the testing program and eliminated several weeks of planned tests. Overall, 14 weeks of testing were performed with three biomass cofiring geometries: direct comilling, center-burner injection, and side injection of biomass into the flame. Two other schemes for biomass injection (biomass injection parallel to the side of the flame and biomass injection into the upper part of the flame) were not evaluated as they were found to be unneeded for the modeling effort. The testing effort is presented in detail in Sections 3 and 4 of this report.

1.6 Task 6.0 – Model Simulations of Biomass Cofiring Cases

Task 6 was divided into two subtasks, both which were performed by NEA and are documented in their final report, which has been incorporated into Sections 3 and 4 of this report.

1.6.1 Task 6.1 – Combustion Research Facility Results Verification

In this task, the computer model for NO_X and UBC predictions will be evaluated against experimental test results for each of the cofiring cases evaluated in Task 5. This task was expected to extend over the 18 months of pilot-scale testing.

1.6.2 Task 6.2 – Recommendations for Full-Scale Application of the Model

Results of the model validations in the pilot-scale tests are expected to provide a fairly rigorous model for the single-burner combustion configuration. In this task, key correlations that may be expected to be used for anticipating NO_X and UBC emissions in full-scale applications of cofiring, and prepare a detailed plan for developing the research version of the computer model into a software package for distribution and use for the benefit of full-scale applications.

1.7 Task 7 – Reporting

Under this task, the technical progress in the project is reported. This task included standard DOE reporting requirements. In addition, this task included the presentation of project results at an Annual Review Meeting and attendance at a project kick-off meeting at NETL. This project final report completes the reporting requirements of this Cooperative Agreement.

2.0 EXECUTIVE SUMMARY

2.1 Introduction

In carefully controlled pilot-scale testing, biomass cofiring has been found to reduce NO_X and unburned carbon (UBC) emissions. However, in field evaluations, the beneficial effect of biomass cofiring on NO_X and UBC emissions appears to be site-specific with few well-characterized sets of emissions data. Unfortunately, these data provide no suitable basis upon which fuel choice or injection system design can be based to insure that NO_X and UBC emissions will be minimized for biomass cofiring at an arbitrary combustion source. The premise for this research and development effort is that in field results, uncontrolled variables are responsible for ambiguities and that to realize the inherent benefits of biomass cofiring, a comprehensive understanding of the cofiring process must be developed.

The purpose of this project was to construct and validate a predictive computer model of biomass cofiring. To reach this goal, two advances were required in the state of the art. First, numerous well-characterized sets of emissions data were needed to define what efficiencies or penalties could be realized from biomass cofiring. Second, a comprehensive NO_X and UBC emissions model had to be developed and validated against the sets of experimental test results.

2.2 Testing

A rigorous testing campaign was designed to precisely define and assess those parameters most likely to affect NO_X and UBC emissions. These parameters include the type of biomass, type of coal, biomass injection configuration, burner geometry and staging, and furnace stoichiometry. All testing was carried out at a single combustion source whose emissions are representative of a full-scale boiler. In tandem with the testing effort, a comprehensive NO_X and UBC emissions model was developed and validated against the furnace test results.

For this investigation, the Southern Company Services/Southern Research Institute Combustion Research Facility (CRF) was fired at 1.75 MW_t (3.6 MMBtu/hr) to emulate the temperature-time profile of a typical pulverized coal-fired boiler in the Southern Company system. At the CRF, the testing campaign was designed to systematically vary those parameters most likely to affect NO_X and UBC emissions. This parameter set included two types of biomass, four types of coal, three locations for biomass injection, two nominal levels of burner staging, and three nominal stoichiometric ratios. A database of test results was generated from 14 weeks of testing that yielded 422 separate, stable test conditions. The database resulting from these tests also has an inherent value as a reference set of data for assessing the impact of biomass cofiring on NO_X emissions and carbon utilization. This characterization was considerably strengthened and guided by the connections between the pilot-scale tests and the detailed process model that was developed in tandem with the testing.

2.3 Model Development

It is not currently possible to incorporate detailed chemical reaction mechanisms into conventional CFD simulations of pulverized fuel (p. f.) flames. Therefore, to predict NO_X emissions at a combustion source, a common approach is to complete a CFD simulation of that source with a particular fuel and then use the results of that simulation for input to simplified

chemical submodels to predict NO_X emissions. This approach, called post-processing, has been applied to pulverized coal flames with varying degrees of success. The modeling protocol developed for this project also relies on post processing of a CFD simulation of the CRF for a particular fuel and biomass. However, in this model development, a new methodology was employed to perform the post processing and is able to incorporate all significant chemical mechanisms that are responsible for NO_X production and UBC emissions.

Because chemistry in the gas phase, especially volatile-N conversion chemistry, was suspected to play a dominant role in NO_X production during biomass cofiring, the modeling partner for this project, Niksa Energy Associates (NEA) developed a new computational approach for this application based on an "Advanced Post-Processing" or APP method. This approach proceeds through three stages: First, conventional computational fluid dynamics (CFD) simulations characterize the bulk flow patterns. Second, the bulk flow patterns are analyzed to specify an equivalent network of idealized reactors for the flow. Third, detailed chemical reaction mechanisms are used to determine the chemical composition across the entire reactor network, including the most important emissions.

Project partner Reaction Engineering International (REI) performed the CFD simulations of the CRF for many of the test cases in the experimental database. Other CFD simulations were performed at Southern Research, using REI's Configurable Fireside Simulator (CFS) for the CRF. The CFS is a stand-alone implementation of REI's proprietary *Glacier*© CFD code that imposes a fixed computational grid on the calculations, and is therefore suitable for parametric case studies with the same firing configurations.

In the APP method, the reactor network is a computational environment that accommodates realistic chemical reaction mechanisms. Under this formalism, mechanisms with a few thousand elementary chemical reactions can now be simulated on an ordinary personal computer, provided that the flow structures are restricted to the limiting cases of plug flow or perfectly stirred tanks. The network is equivalent to the CFD flowfield in so far as it represents the bulk flow patterns in the flow. Such equivalence is actually implemented in terms of the following set of operating conditions: The residence time distributions (RTDs) in the major flow structures are the same in the CFD flowfield and in the section of the reactor network that represents the flow region under consideration. Mean gas temperature histories and the effective ambient temperature for radiant heat transfer are also the same. The entrainment rates of surrounding fluid into a particular flow region are evaluated directly from the CFD simulation. To the extent that the RTD, thermal history, and entrainment rates are similar in the CFD flowfield and reactor network, the chemical kinetics evaluated in the network represent the chemistry in the CFD flowfield.

Model predictions have been validated across the database of test results to within useful quantitative tolerances. *This level of performance was achieved without any adjustments to the model parameters for any of the biomass cofiring cases*. Instead, calibration factors were specified to match the predicted and observed emissions for the coal-only tests for all excess O_2 levels, and extents of air staging.

2.3 Results

Overall, the predicted NO_X emissions agree with the experimental data within experimental uncertainties for all biomass fuel types, excess O_2 levels, and extents of air staging. The predicted unburned carbon (UBC) levels were less accurate, but were generally consistent with the qualitative tendencies in the data.

The database from the testing campaign was interpreted with simulations based on full chemistry for fuel decomposition, volatiles combustion including fuel-N conversion, soot conversion, and char burnout. Once the model predictions were demonstrated to be accurate, the simulation results were interrogated to determine how the biomass affected NO_X emissions. It was found that the answers to two questions determine whether biomass cofiring reduces NO_X emissions:

1. Does the abundance of gaseous volatiles, not soot, from biomass reduce away the NO formed near the burner?
2. Is significantly less char-N released into downstream flame zones by the addition of biomass?

The validated model now provides a relatively inexpensive means either (1) to identify the most effective cofiring injection configuration for specified compositions of biomass and coal within a particular furnace environment, or (2) to forecast the emissions for a specified pair of fuels fired under an existing configuration. As such, this model becomes an important cost-saving tool, and the modeling effort has the potential to help accelerate the widespread adoption of biomass cofiring as a NO_X control strategy in the electric utility industry.

3.0 EXPERIMENTAL

3.1 Background

In carefully controlled pilot-scale testing, biomass cofiring has been found to reduce NO_X and unburned carbon (UBC) emissions.[1-2] Figure 3-1 shows representative results for NO_X emissions from one of these pilot-scale evaluations.[3] In field evaluations, however, the beneficial effect of biomass cofiring on NO_X and UBC emissions is less clear and may be site-specific. Unfortunately, few well-characterized sets of field emissions data exist.[4-7] In 2002, Dayton reviewed the available results from full-scale and pilot-scale demonstration testing of biomass cofiring and in Figure 3-2 excerpted from his report, it is evident that there are significant scatter in these data.[8] Indeed, scatter within the results presented in Figure 3-2 is so large that the regression shown in this figure appears to fit the measurements from only one demonstration test (the Seward Station). Unfortunately, such data provide no suitable basis upon which fuel choice or injection system design can be based to insure that NO_X and UBC emissions will be minimized for biomass cofiring at an arbitrary combustion source.

Careful pilot-scale testing has shown that significant NO_X reductions can be achieved with biomass cofiring. Therefore, we are led to the premise that in tests such as those reviewed by Dayton, that unrecorded or uncontrolled variables are responsible for apparent scatter or ambiguities in the data and that to realize the inherent benefits of biomass cofiring, a comprehensive understanding of the cofiring process must be developed from a performance and a modeling perspective.

The purpose of this project was to construct and validate a predictive computer model of biomass cofiring. To reach this goal, two advances were required in the state of the art. First, a database of well-characterized sets of emissions data was required to define what efficiencies or penalties could be realized from biomass cofiring. Second, a comprehensive NO_X and UBC emissions model needed to be developed and validated against the sets of experimental test results.

3.2 Pilot-Scale Combustor Testing

3.2.1 Combustion Research Facility

All testing was performed at the Southern Company Services/Southern Research Institute Combustion Research Facility (CRF). The CRF is currently configured for firing on natural gas, coal, or mixtures of coals and biomass fuels, at up to 1.75 MW thermal which is equivalent to 3.8 GJ/hr (3.6 MMBtu/hr) or about 0.6 MW electric. The facility is designed to operate at up to 6.3 GJ/hr (6 MMBtu/hr). Because of its size and the time required to reach thermal equilibrium, the facility is operated around the clock during testing. Tests usually last 5-7 days.

The design of the facility was carefully chosen to provide a close simulation of the physical processes that occur in a full-scale utility boiler. The facility, shown in Figure 3-3, consists of a coal crushing and milling area, a coal feeding system, a vertical refractory lined furnace, a single up-fired burner, a horizontal convective section pass with air-cooled tube banks, a series of heat exchangers, an electrostatic precipitator, a pulse jet baghouse, and a packed column scrubber.

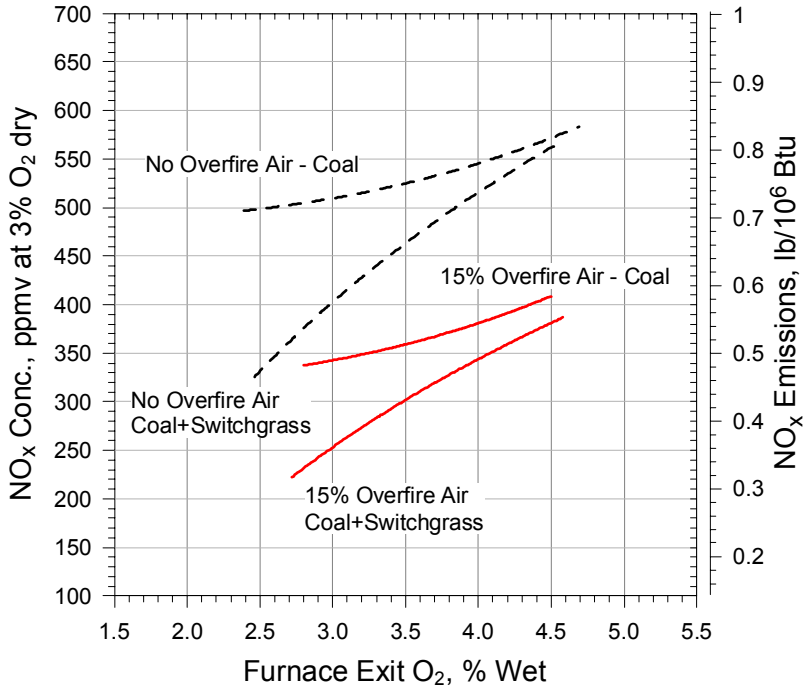

Figure 3-1. NO_X concentrations measured when firing Pratt Seam coal alone and with a comilled blend of 90% coal and 10% switchgrass.[3]

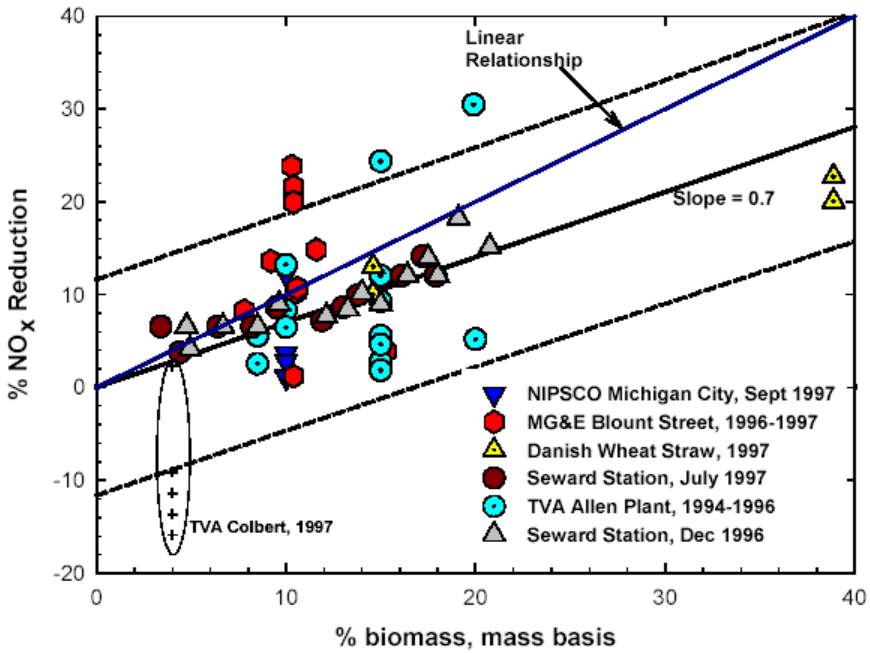

Figure 3-2. A summary of NO_X reduction from a number of biomass/coal cofiring full-scale and pilot-scale demonstration tests, based on the mass input of biomass. Dashed lines are 95% prediction limits that encompass the range of variability in the measured data.[8]

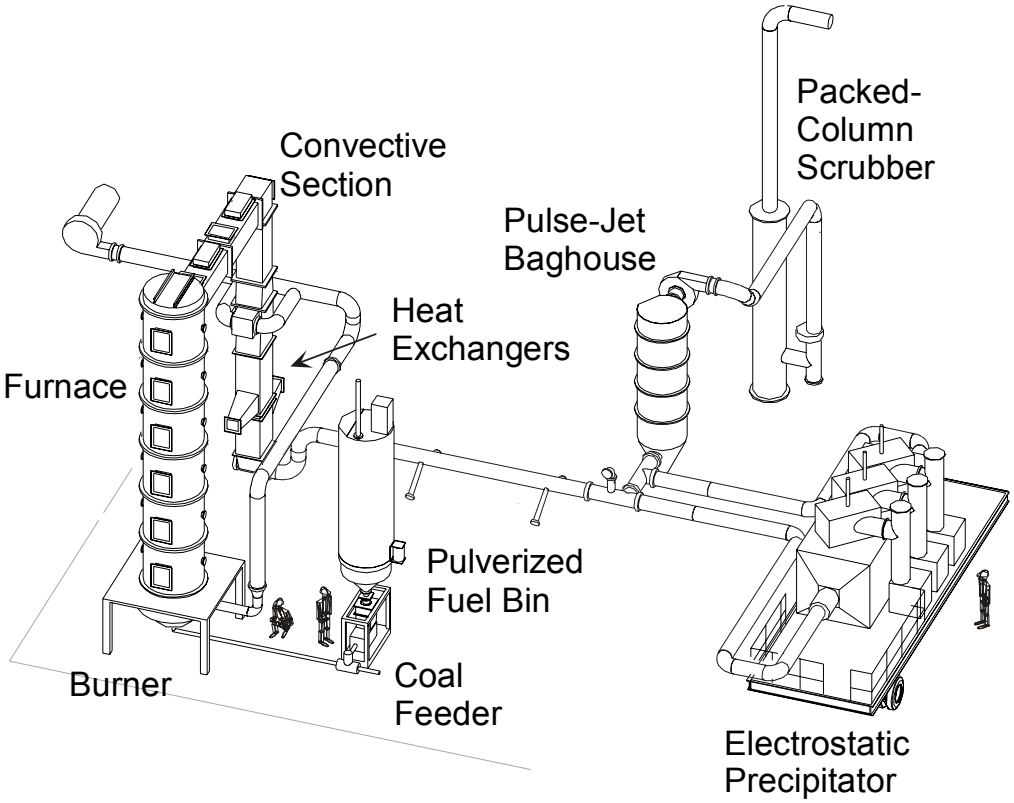

Figure 3-3. The combustion research facility.

3.2.1.1 Fuel Preparation The fuel preparation area includes an open area storage yard, covered on-site storage bins, a rotary drum coal crusher, a fully instrumented CE Raymond Model 352 bowl mill, and pulverized coal storage. Eighteen storage bins, each capable of holding up to 25 tons of coal or other fuel, are located adjacent to the coal preparation area. As-mined coal or coal premixed with biomass is loaded into the crusher with a small front-end loader and is crushed to a size of minus 3/8 inch. From the crusher, the coal is transported via a screw feeder and bucket elevator to one of two 3.54 m^3 (125 ft^3) storage bins located beside the mill. These bins are independently located on load cells and are equipped with integral vibrator/bridge-breakers and rotary lock feeders. The facility digital control system (DCS) is used to set the discharge rate for each bin so that combinations of different fuels can be fed to the mill while providing mass flow information for use with determining precise material balances for each fuel. The discharges of both hoppers is combined and fed to the mill. Fuel samples can be obtained from any part of the process.

The coal mill is a refurbished and instrumented Model 352 CE-Raymond bowl mill, which has a rated capacity of 1814 kg (2 tons) per hour. This type of mill should give representative milling simulations of the different air-swept table and roller mills normally used in power plant service. The mill air is preheated with a dedicated natural gas burner, which also helps inert the mill. For fuels that present an ignition hazard such as Powder River Basin coals and some biofuels, the facility is equipped to accept additional inerting from nitrogen tank trucks. The mill is

instrumented to report roller spring pressure, journal lift, motor amperage and voltage, gas flow, and mill rejects to the facility DCS. Coal is typically ground to a fineness of 70% < 75 micrometers (200 mesh), although finer and coarser grinds are easily accommodated.

Pulverized coal is captured in a pulse-jet baghouse and transported through a dedicated dense phase transport system to either an inerted pulverized fuel storage hopper (adjacent to the furnace) or to an inerted, separate waste hopper. Both hoppers are located on load cells. In such small-scale pulverized coal firing, it is normal practice to use indirect firing to help eliminate coal surges that can cause flame stability problems. The mill circuit can also be used to perform stand-alone milling experiments.

3.2.1.2 Coal Feeding The coal feeding system is designed to deliver a constant feed of pulverized fuel to the burner. The storage hopper is equipped with an orbital-motion live bottom to prevent bridging of the fuel within the hopper. An Acrison™ loss-in-weight auger-type feeder weighs a controlled amount of fuel that is discharged into the primary air line through a rotary airlock valve. This gravimetric feeder is suspended on a weighing mechanism, and the feed rate is controlled by varying the auger speed to maintain the desired fuel feed rate.

3.2.1.3 Burner Configurations Two burners are available for use. A single register conventional burner with variable swirl angle and variable fuel gun position is used in conventional wall-fired, as well as tangential firing mode with the addition of over-fire air. A dual register Low-NOx burner with variable swirl in both registers and variable fuel gun position is also available. Both burners attach to the water-cooled burner section, which is unlined and has a nominal cooling water flow of 284 liters/min. (75 gallons/min.). Two clean-out ports are provided in this section, to allow bottom ash to be periodically removed from the furnace. Both burners also use the same refractory quarl with a 25° half angle. The quarl exit is approximately 5 inches below the flange of the first water-cooled furnace section. This dimension is the same for either burner windbox. A closed-circuit television camera with a control-room monitor allows constant monitoring of the view of the flame from the top of the furnace.

Four basic configurations are available using the two burner windboxes. They are described as follows:

- T-Fired Conventional: Single register burner, swirl at 40° or less, no over-fire air.
- T-Fired Low NO_X: Single register burner, swirl at 40° or less, with over-fire air.
- Wall-Fired: Single register burner, swirl at 50 to 60°, no over-fire air.
- Wall-Fired Low NO_X: Dual register burner.

3.2.1.3.1 Single-Register Burner The single register burner windbox attaches to the water-cooled burner shell. Primary air at nominal 66°C (150°F) also carries natural gas or pulverized coal to the burner. The fuel gun is in the nominal "zero" position when the bottom of the fuel gun flange is 57.2 cm. (22.5 in.) from the bottom of the flange to the floor. Secondary air is at nominal 316°C (600°F) with varied swirl angle from 0 to 70° in 5° increments. Pilot air is not metered individually, but is included in the primary air rate measurement. When used, separated overfire air (OFA) is introduced through four injectors located in furnace section four, at a distance of 4.47 m (14.67 ft.) from the exit of the quarl. The injectors are constructed of 3.49 cm.

(1.38 in.) I.D. pipe with a 10 degree angled tip which barely protrudes through the furnace refractory lining, to introduce the over-fire with the same counter-clockwise rotation (as viewed from above) as the swirled secondary air. The over-fire air is at a nominal 316°C (600°F). Common operating air splits usually include 18 % primary air, with 0, 15 or 30 % OFA and the balance as secondary air. Other air splits between secondary and tertiary may be used.

3.2.1.3.2 Dual-Register Burner The dual register burner windbox attaches to the water-cooled burner shell. Quarl to furnace geometry is the same as with the single register burner, as well as the use of the same pilot air pipe size. The dual register burner features independently adjustable inner and outer swirl, as well as the ability to adjust the inner swirl windbox vertical position, as well as fuel gun position. The fuel gun is a nominal 8.26 cm. (3.25 in.) ID, 8.89 cm. (3.5 in.) OD. The fuel gun in the nominal "zero" position is 31.75 cm. (12.5 in.) from the bottom of the windbox flange to the floor which places the fuel gun tip at the same "zero" position as for the single register burner. This "zero" position is approximately 1.27 cm. (0.5 in.) into the tapered section of the quarl. As in the single register burner, the fuel gun carries the primary air as well as natural gas or pulverized coal. The inner swirl windbox swirl is adjustable from 0 to 80° in 10° increments with 60° being the most common operating position, with the inner windbox withdrawn 9.53 cm. (3.75 in.) from the outer windbox. The inner swirl air pipe is 14.12 cm. (5.56 in.) OD and 12.83 cm. (5.05 in.) ID, and in the nominal "zero" position (9.53 cm. or 3.75 in. withdrawn), extends to approximately the beginning of the quarl taper. Air enters the inner swirl pipe at a nominal 316°C (600°F). The outer swirl windbox swirl is adjustable from 0 to 60° in 5° increments, with 45° being the most common operating position. The outer swirl air annulus is 17.15 cm. (6.75 in.) ID and combustion air enters at a nominal 316 °C (600°F). Common operating conditions include 18 percent primary air, with 60 percent secondary and 22 percent tertiary air, but several combinations of secondary and tertiary air have been used.

<u>3.2.1.4 Radiant Furnace</u> The furnace is a vertical, up-fired 8.5 m (28 ft.) high cylinder, with an inner diameter of 1.07 m(3.5 ft.). Separated overfire air (OFA) is injected through 4 off-radius ports located 4.6 m (15 ft.) up the furnace. This allows gas velocities of 3.0 to 6.1 m/s (10 to 20 ft/sec.) and residence times of 1.3 to 2.5 seconds, depending upon the firing rate. The design furnace exit gas temperature is 1200°C (2200°F). The furnace diameter and height were chosen to best match the velocities and residence times found in full-scale units. Typical total furnace air flow is 21.2 sm^3/min. (750 scfm), with a primary air flow of 3.54 sm^3/min. (125 scfm).

The vertical furnace section is comprised of seven water-cooled refractory lined sections, stacked on top of a furnace base stand transfer plate. Each furnace section is nominally 1.22 m (48 in.) tall and has a nominal cooling water flow rate of 189 liters/min. (50 gallons/min.) to the outer furnace shell. The refractory lining is nominally 10 cm. (4 in.) thick, with the internal diameter of the furnace refractory lining a nominal 1.07 m. (3.5 ft.). The furnace sections are cast in two different refractory materials, one type being used on sections 2, 3 and 7, and a second refractory used in sections 4, 5, and 6. These refractory linings are used to limit the heat extraction and to ensure the proper simulation of the radiation environment found inside full-scale furnaces. Small furnaces have much higher ratios of inside surface area to total volume than full-scale furnaces, and the flame would be quenched if the entire interior were lined with a heat exchanging surface.

The cylindrical furnace section exits to a square convective section at furnace section 7 through a transition section. The transition section is a 46 by 46 cm. (18 by 18 in.) square duct centered vertically in furnace section 7 with a horizontal run of 32cm. (12.5 in.)

3.2.1.5 Convective Section Combustion gases exit the vertical furnace through a horizontal convection pass, which is designed to remove a substantial part of the heat from flue gas. The rate of heat extraction is designed to simulate the temperature-time profile found in a utility boiler. A series of three air-cooled tube banks are installed in the convective pass, the first two in series, with the third separated by a refractory lined elbow. Air cooling is used to control either the temperature profile of the flue gases or the tube metal surface temperatures for fouling/ash deposition studies. Air flow to each convective section tube bank is controlled by a temperature control loop with the flue gas temperature at the outlet of the section as the input, and the control signal to a control damper on the cooling air as the output. All three convective sections are identical; 2.13 m (84 in.) long and refractory lined, with an inside dimension of 46 by 46 cm. (18 by 18 in.). Each convective section contains a 5 wide X 10 deep array of tube-in-tube heat exchangers on 8.9 cm. (3.5 in.) centers, with each exchanger tube having an outside diameter of 4.8 cm. (1.9 in.), and a length of 43.2 cm. (17 in.) exposed to flue gas for cooling. Centers of the leading row of tubes are at a distance of 94 cm (37 in.) from the inlet to the section. The refractory elbow between convective sections 2 and 3 also has a flue gas path 46 by 46 cm., with a horizontal run of 46 cm. (18 in.) and a vertical run of 20.3 cm (8 in.).

A cross-flow tubular air preheater follows the convective tube banks and is used to preheat the primary and secondary air. Finally, four air-to-flue-gas recuperators are used to cool the flue gas down to a nominal 149°C (300°F) before the flue gas enters downstream pollution control devices.

3.2.1.6 Computer Data Acquisition and Control System The facility is controlled and monitored by networked combined digital control system (DCS) and data acquisition computers, managed by Yokogawa CS-1000 system software that runs under the Windows NT/2000/XP operating system. This DCS performs all process control for the facility and allows complex feed-forward and calculated variable control. This computer control also performs the safety monitoring needed for safe operation of combustion equipment, including flame scanning and interlocks, automatic startup and automatic shutdown of the entire facility. Process data acquisition and storage is accomplished within the Yokogawa software. Typically, about 200 channels of data are continuously logged during testing.

3.2.1.7 CEM System A complete extractive continuous emissions monitoring (CEM) system is installed in the facility, and it is also interfaced to the computer control system. A set of gas analyzers, which analyze the flue gas for concentrations of O_2, NOx, SO_2, CO_2, and CO, receives the dry flue gas sampled from a set of three extractive lines. Flue gas is sampled from the facility stack, the ESFF/baghouse inlet, and a multi-purpose spare line set up to sample from selective points through the system. The flue gas is dried before the analyzers by a sample conditioning system, which uses an ice bath to condense water from the sampled gases.

3.2.1.8 Pollution Control Equipment Particulate emissions are controlled by an Aeropulse pulse-jet baghouse, while sulfur dioxide emissions are controlled by an Indusco packed-column

caustic scrubber. Flue gas can be diverted by a set of valves through a pilot-scale electrically stimulated fabric filter (ESFF), which has been installed upstream of the baghouse.
The pulse-jet baghouse and the scrubber are required for the air quality permit of the facility issued by the Jefferson County Board of Health and are always on-line.

A four-field dry-wall electrostatic precipitator has been recently installed in the facility. With an interior that is nominally 1.37 m (4.5 ft) high by 0.61 m (2 ft.) wide by 4.88 m (16 ft.) long, the precipitator provides a maximum plate area of approximately 13.4 m^2 (144 ft^2) for an ESP sizing factor of 23.6 sec/m (120 ft^2 /kacfm). Plate width can be changed, allowing plate spacings up to a maximum of 0.61 m (2 ft.).

Particles are charged by a rigid electrode array. The discharge electrodes are suspended from high voltage structures located in the area above the gas passage. The high voltage structures are suspended from insulators, electrically isolating them from the precipitator casing. The discharge electrodes are attached to the upper high voltage frame and extend down through the gas passages. The lower high voltage frame is suspended from the rigid discharge electrodes and aligns the discharge electrodes. The discharge electrodes are centered in the gas passages, with anti-sway mechanisms attached to the lower high voltage frame to keep it from moving in the gas stream. As an aid to gas distribution, turning vanes, perforated plates, and baffles are used at the inlet and outlet of the precipitator chamber. The purpose is to provide uniform velocity distribution across the precipitator cross-section.

Impulse gravity impact rappers are used to remove dust deposits from collecting surfaces. The rappers are located on the precipitator roof. The plunger is allowed to fall, striking the rapper bar connected to a bank of collecting surfaces within the precipitator. The resulting shock dislodges the accumulated dust. Precipitator rapping is controlled through a microprocessor-based programmable controller

3.2.2 Comparison to Full-Scale Performance

The ability to predict the performance of full-scale equipment from pilot-scale experimental results is essential. Hence, the pilot-scale facility was designed to closely replicate the controlling mechanisms that occur in a large boiler. Fortunately, a great deal of previous work on scaling was available to guide the design of the facility. In particular, because of the focus of much NO_X reduction testing is on NO_X emissions and unburned carbon, the intensity of combustion in the radiant furnace of the full-scale equipment had to be matched in the pilot furnace. Therefore, the most common scaling parameter of combustion intensity, the volumetric heat release ratio (VHRR), from a variety of full-scale Southern Company plants was matched in the CRF. The VHRR is computed by dividing the fuel heat input, as GJ/hr, by the radiant furnace volume to yield GJ/hr•m^3. Testing has confirmed that NO_X and unburned carbon emissions are very close to that measured for full-scale boilers.[9]

Figure 3-4 shows that the CRF also meets another important criteria with respect to emulating the performance of a full-scale boiler. In this figure, the temperature-time history of the CRF is compared to that of a variety of full-scale boilers in the Southern Company system. As shown, the CRF in-furnace temperature-time history is very similar to that of the full-scale plants, with the exception of Branch, which is different from the other SCS plants. This similarity is a

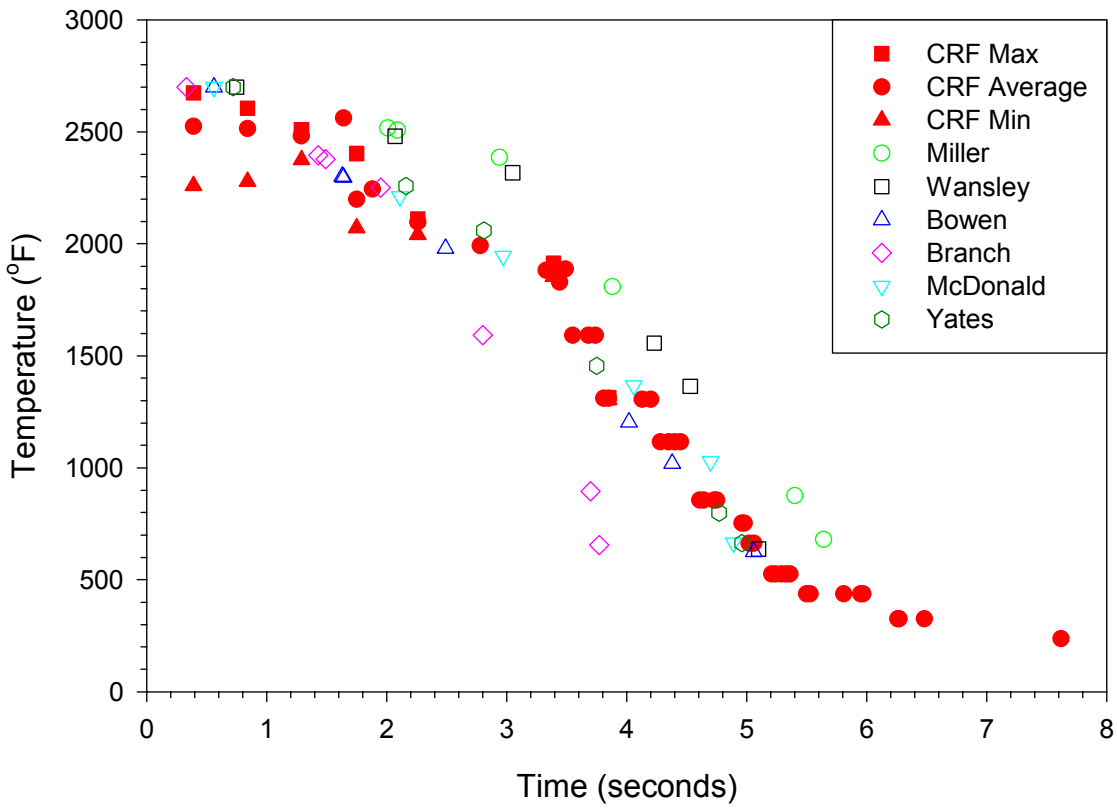

Figure 3-4. Comparison of the temperature-time history of the CRF with several Southern Company full-scale power plants.

reflection not only of the similar gas temperatures and residence times, but also of the similar cooling rates and overall heat transfer.

In addition to the similarity of the temperature/time histories, it is also of interest to compare the relative importance of in-furnace surface exposure to flue gas. A suitable dimensionless parameter allowing this comparison for the steam tube and economizer sections is:

$$\frac{A_S \cdot \upsilon}{Q} = \frac{A_S}{A_C}$$

Where A_S = External surface area of walls and steam tubes surfaces.
υ = Velocity of the flue gas in the duct.
Q = Volumetric flow rate of gas in the duct.
A_C = Cross sectional area of the duct.

As the external surface in the duct and the gas velocity in the duct increase, so does the gas contact with exposed surfaces, hence they are in the numerator. As the volumetric flow rate increases, the time for the contact to take place decreases, hence it is in the denominator. This dimensionless parameter reduces to an even simpler ratio of the surface area to cross sectional area, as shown. Since there are no surfaces extending across the flame and post flame zones of industrial boilers, a more appropriate dimensionless parameter for the furnace section is the height to diameter ratio. Table 3-1 compares these dimensionless parameters for the CRF with full-scale boiler types.

Table 3-1. Internal surface parameters compared for the CRF and full-scale units.

Combustion Source	In –Furnace Section 1400°C to 1150°C (~2550 ˚F to 2100 ˚F)	Superheater Section 1150°C to 600°C (~2100 ˚F to 1110 ˚F)	Economizer Section 600°C to 325°C (~1110 ˚F to 620 ˚F)
Parameter	H/D	A_S/A_C	A_S/A_C
125 MW CE	18	42	18
480 MW B&W	7.2	74	69
700 MW CE	14	3.6	3.8
245 MW CE	18	3.4	7.5
CRF at SRI	8	47	135

As shown in Table 3-1, the CRF has a similar H/D ratio in the furnace section as full-scale boilers. This comes at the price of having slower velocities in the CRF furnace section. The residence time in the CRF furnace is similar to that of a full-scale unit, as shown in Figure 3-4. Although the H/D ratio in the boiler is similar, the several seconds of in-furnace residence time is a limiting factor in full-scale boilers. Hence, transport limitations across a full-scale boiler prevent as much particulate from diffusing to the walls. However, for the convective sections of the boiler, the surface area contact with the flue gas in the CRF should be similar to that of a full-scale boiler, with perhaps a bit more surface contact in the economizer section.

3.2.3 Protocols for Testing

The test matrix employed for this project included four types of US coal and two biomasses. Two burner configurations were tested (single register tangentially-fired burner and generic low-NO_X dual-register burner). Three schemes for biomass cofiring were tested (biomass comilled with coal, separate biomass injection through the center of the burner, and off-axis direct injection into the flame). All three schemes for biomass injection were employed with the single-register burner. The dual-register burner was only used for one comilling test because the CFD model constructed by REI did not incorporate this burner and no modeling could be performed for results obtained with the pilot-scale furnace configured for operation with this burner.

<u>3.2.3.1 Modifications to Accommodate Biomass Cofiring</u> Figure 3-5 shows a cross-section drawing of the first section of the furnace with the single register burner in place. In this figure, the three locations where biomass was cofired are shown. Location 1 is the primary air line

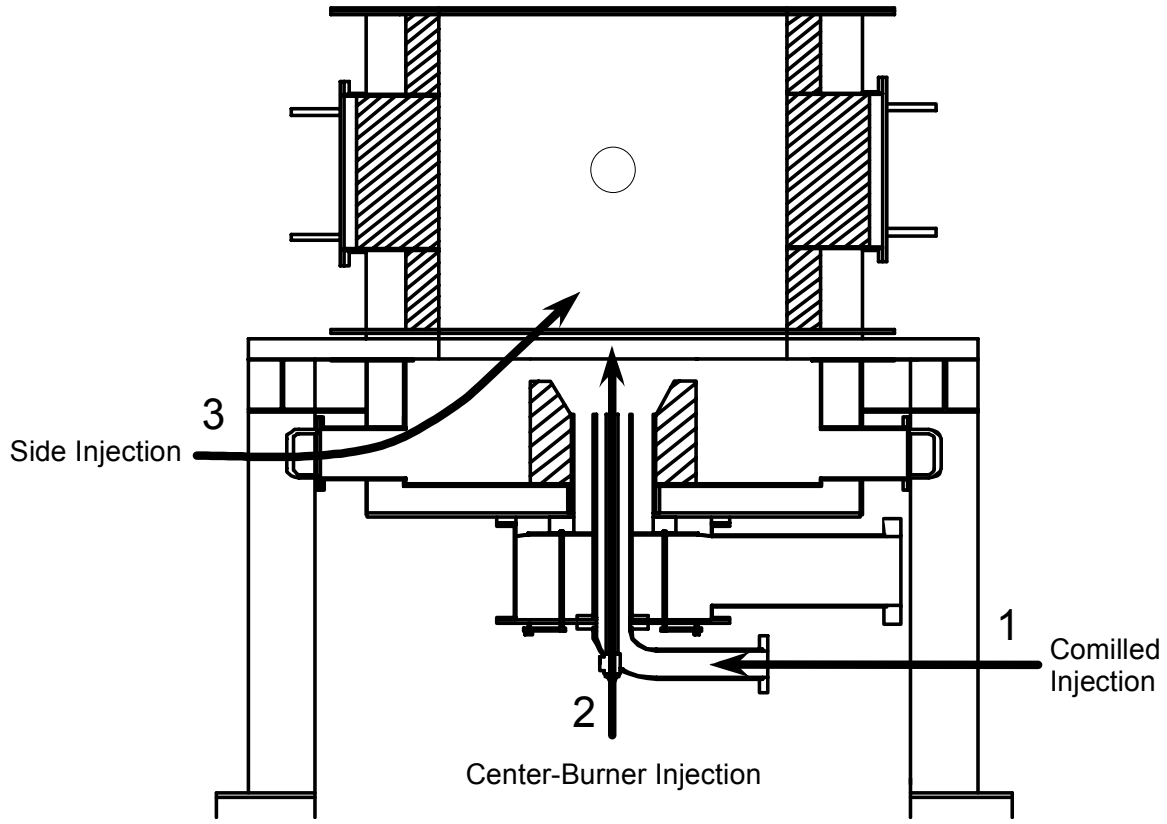

Figure 3-5. Cross section of the first section of the pilot-scale furnace with the single-register burner installed. The three locations employed for biomass injection are shown.

where comilled coal and biomass enter the burner. Location 2 is a center-burner biomass injection configuration, where finely divided biomass enters the burner through a tube centered in the furnace exit end of the primary air line. Location 3 is a side injection location, where finely divided biomass is injected into the furnace in a manner so that it intersects the pulverized coal flame as it exits the burner.

A gravimetric feeder was used to meter finely divided biomass into a compressed air-driven eductor that discharged into a nominal 1 in. diameter plastic transport line connected to the metal piping at location 2 or 3. Because large static electrical charges can be generated within the plastic transport line, the line is covered with a grounded metal mesh sheath. Biomass delivered to locations 2 or 3 was transported at a velocity high enough to avoid the possibility of flashback but low enough to minimize disruption of the flame.

Figures 3-6 and 3-7 show details of modifications that were made to the single-register burner to accommodate center-burner injection of biomass. The existing pilot assembly, a 2.639 cm. (1.039 in.) OD tube within a 8.26 cm. (3.25 in.) ID fuel gun, was replaced with a concentric pipe

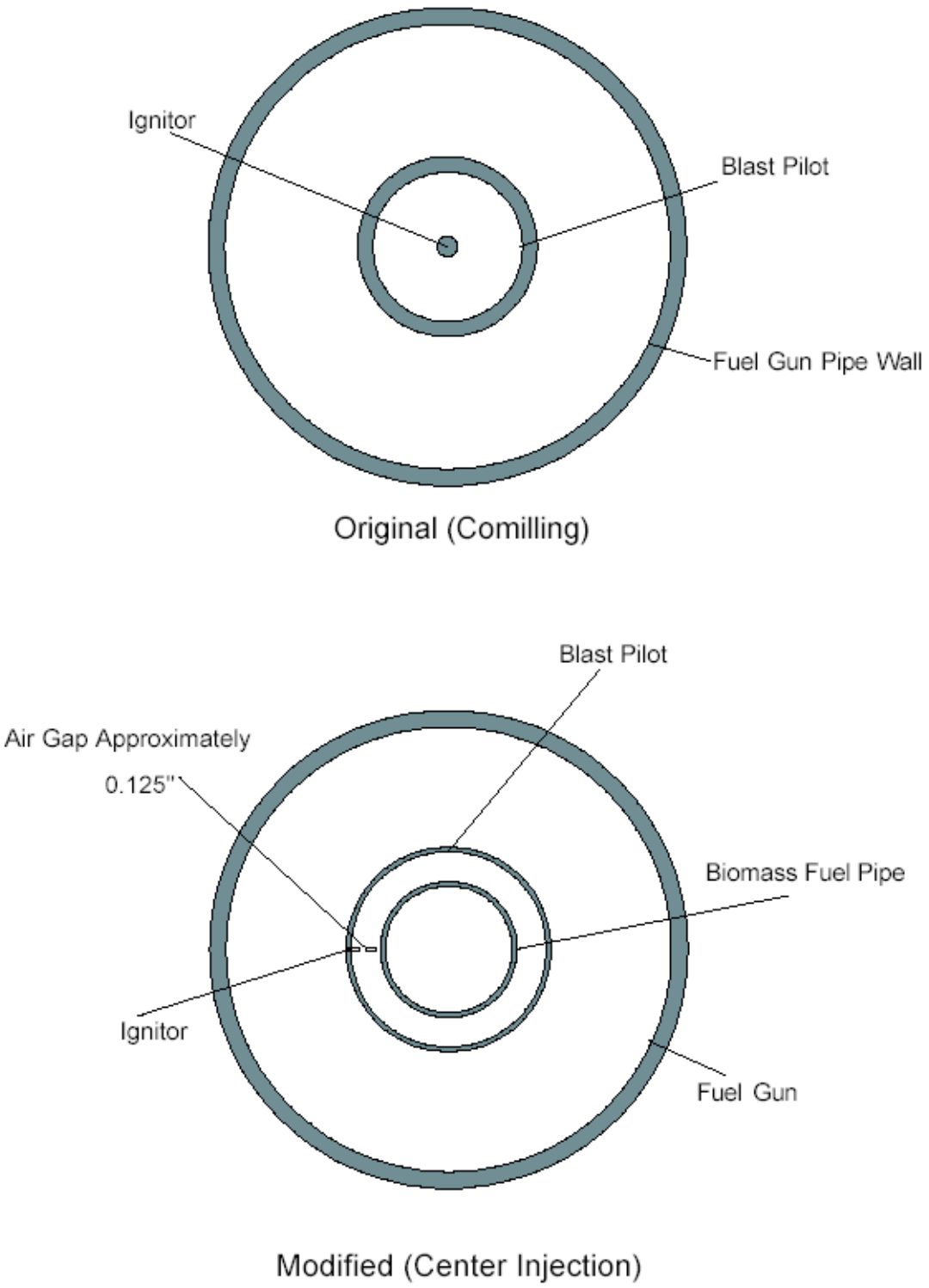

Figure 3-6. Top view of modifications to primary air line and blast pilot to accommodate center-burner injection of biomass.

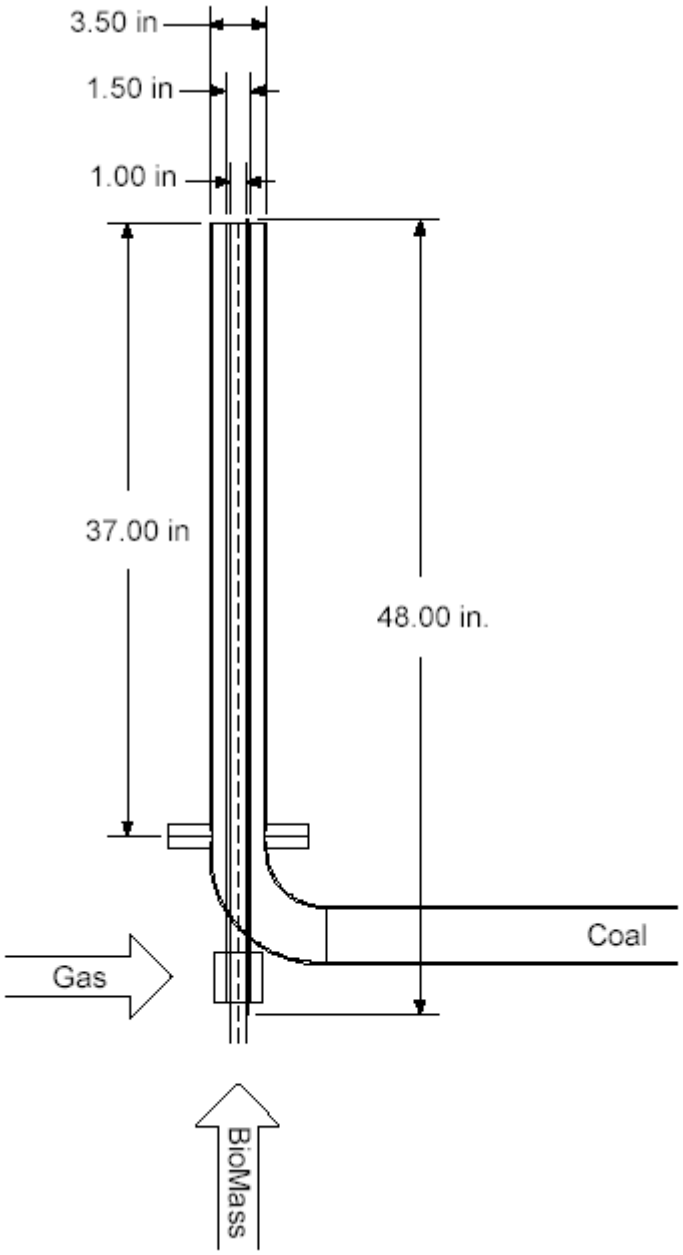

Figure 3-7. Side view of modifications to primary air line and blast pilot to accommodate center-burner injection of biomass.

assembly. The inner pipe is for the biomass with a nominal amount of conveying air, and the first annulus is a gas path for the blast (ignition) pilot. The biomass port has an ID of 2.36 cm. (0.93 in.), an OD of 2.54 cm. (1.00 in.), and a flow area of 5.063 cm^2 (0.00545 ft^2). The new blast pilot has an ID of 3.63 cm. (1.43 in.), an OD of 3.81 cm. (1.50 in.), and a resulting flow area of 5.30 cm^2 (0.00570 ft^2).

From comparing total air flow rates at equivalent levels of furnace exit oxygen (FEO), biomass is conveyed by an air flow of approximately 1.13 am^3/min (40 acfm). This air rate would have an exit velocity from the biomass gun of approximately 1829 m/min (6000 ft/min).

Under normal combustor operation, without injection of biomass or air directly into the flame, the Secondary air (SA) to primary air (PA) ratio (SA/PA) exit velocity ratios are as follows:

- for 0 % OFA, SA/PA exit velocity ratio = 2.0
- for 15 % OFA, SA/PA exit velocity ratio = 1.6
- for 30 % OFA, SA/PA exit velocity ratio = 1.2

This SA/PA exit velocity ratio is generally independent of FEO because the PA/SA/OFA split is controlled by the facility digital control system (DCS). The SA/PA ratio is affected somewhat at low values of FEO, as a minimum PA flow is required to convey fuel into the burner and also to prevent back-fire; this minimum level is set at 3.54 sm^3/min (125 scfm).

Because biomass is injected into the flame zone, approximately 0.85 to 1.13 sm^3/min (30-40 scfm) of combustion air is taken out of the DCS control loop for biomass conveying air. The remainder of the air is split by the DCS for PA/SA/TA. Using nominal splits, the SA/PA exit velocity ratio for biomass cofiring is:

- for 0 % OFA, SA/PA exit velocity ratio = 1.6
- for 15 % OFA, SA/PA exit velocity ratio = 1.2
- for 30 % OFA, SA/PA exit velocity ratio = 0.9

When the minimum PA flow is maintained at 3.54 sm^3/min (125 scfm), there is approximately 4.67 sm^3/min (165 scfm) of total PA flow with 1.13 sm^3/min (40 scfm) being the biomass conveying air.

Figure 3-8 shows details of the side biomass injection configuration (location 3 in Figure 3-5). The biomass injection tube was sized so that the injection velocities were equivalent to those used for center-burner biomass injection. Thus, the comments made above for center-burner injection of biomass also apply to this mode of delivery of biomass to the pilot-scale furnace.

To achieve comparable operation with coal-only firing (for baseline NO_X and UBC comparisons when biomass is injected at locations 2 or 3 in Figure 3-5), air-only injection through the biomass injection line at a rate of 40 scfm was maintained. This reduced the SA/PA exit velocity ratio to those typically observed during periods of biomass injection. As test results will reveal, in the absence of biomass, these directed air flows did affect NO_X and UBC emissions.

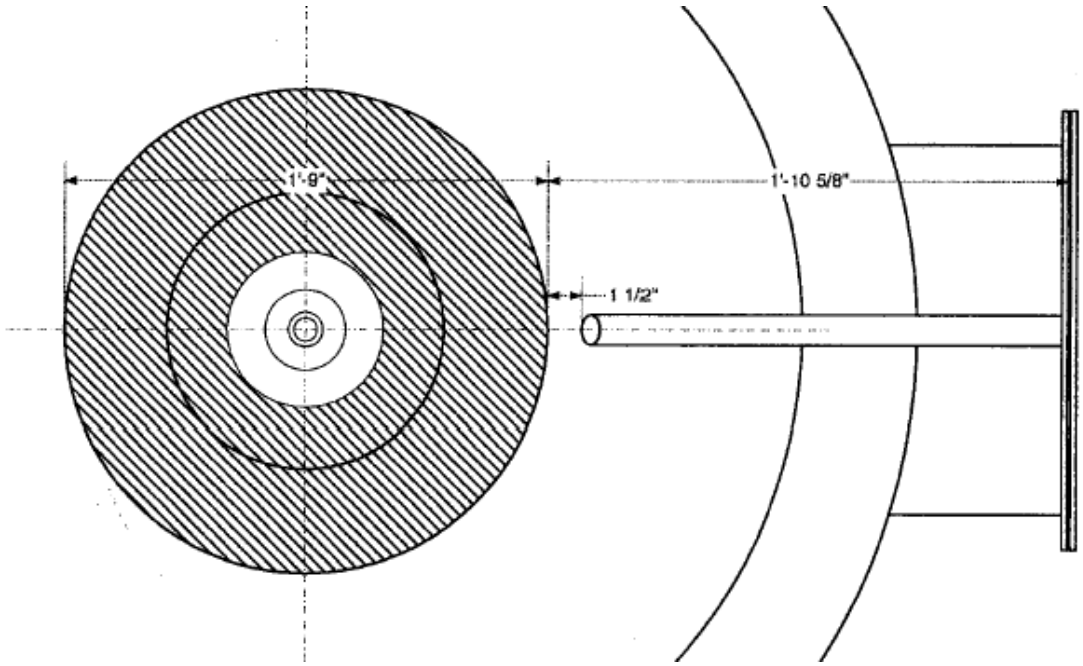

(a) Top View

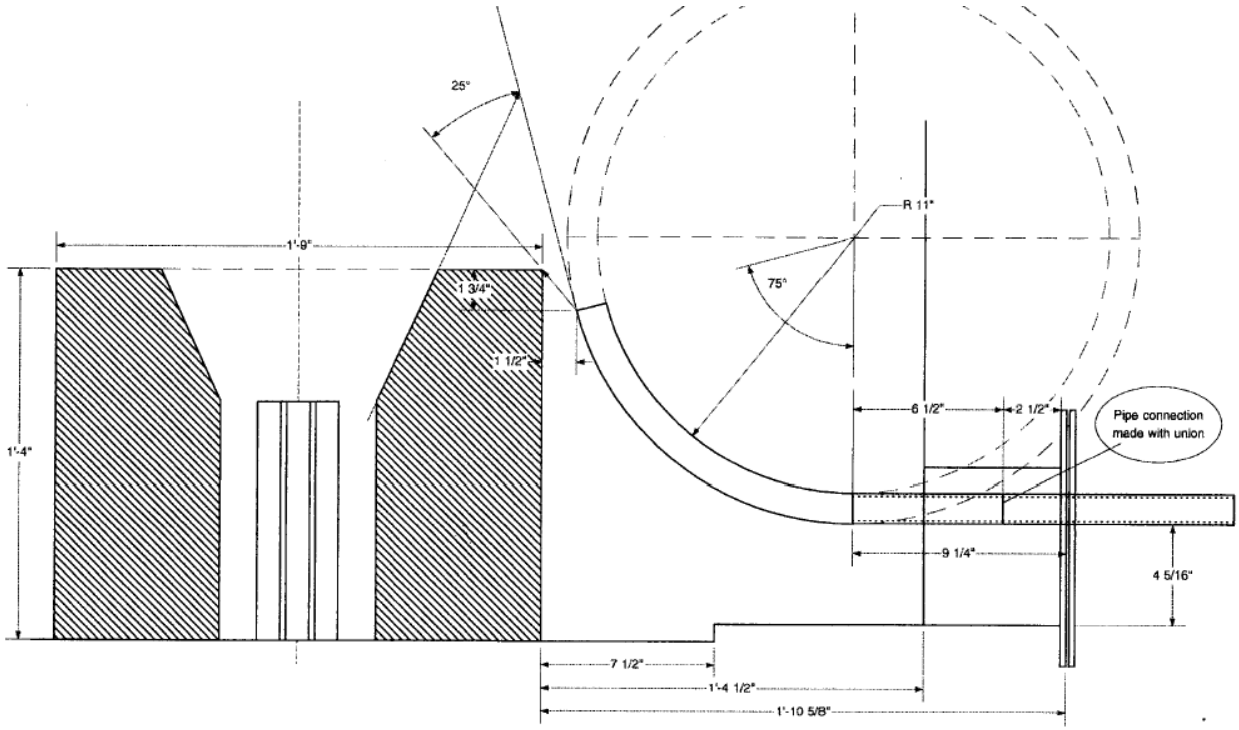

(b) Side View

Figure 3-8. Layout of apparatus used for the injection of biomass into the side of a pulverized coal flame.

3.2.3.2 Testing Matrix The testing matrix employed for this project included four types of US coal (Powder River Basin, Eastern bituminous high-volatility, Eastern bituminous low-volatility, and Illinois Basin coal) and two biomasses (sawdust and switchgrass). Poultry litter was simulated by adding anhydrous ammonia to the primary air line (to add fuel nitrogen) while a comilled mixture of coal and sawdust was combusted. Four discrete levels of biomass addition were tested, always as a percentage of the total mass fired (0%, 5%, 10% or 15%, and 20%). However, not every coal was tested at the four levels of biomass addition.

Testing with a particular fuel or blend of fuels usually requires a full 12-hour day of work; the other 12 hours are filled with fuel mixing and milling, preparation for the next day of work, and maintenance. During a day of testing with a selected fuel and burner combination, the furnace is nominally operated at three levels of FEO (usually 2.5%, 3.5%, and 4.5%) at up to two levels of separated OFA (usually 0% and 15% of the total furnace flow, although limited data were acquired at 30%OFA). At each level of FEO and OFA, gaseous and particulate emissions and furnace operating parameters were measured and recorded, usually for a minimum of one hour after the furnace had stabilized. Thus, within a typical week of testing, five major test conditions, each with 6 minor test conditions can be investigated (30 identifiable test conditions). Fourteen separate week-long tests were completed and 422 identifiable test conditions were logged. As testing proceeded, and the database of test results was compiled, the results of modeling were compared with the test results obtained to verify and tune the model and guide additional testing to exercise the model.

3.2.3.2.1 Coals Tested Table 3-2 presents typical proximate and ultimate analyses for the four coals tested along with mineral ash analyses. The analyses are arranged in columns in order of increasing rank, from left to right and are labeled with a two-letter code that will be used to identify these coals through the remainder of this report. Moisture levels are highest for the low-rank fuels, especially for Jacobs Ranch (JR). Ash levels are widely variable and especially high for Pratt Seam (PR) and Jim Walter #7 Mine (JW) coals.

Galatia coal (GL) is a high-volatility Illinois basin coal that is characterized by its relatively high chlorine content (~0.3% Cl) and moderate sulfur content (~1%). The American Coal Company mines Galatia coal from a deep mine located near the town of Galatia, in Saline County, Illinois.

JR coal is a Powder River Basin (PRB) coal surface mined by the Kennecott Energy Company from 3400 acres of land leased from the U.S. Government. The mine is located approximately 50 miles Southeast of Gillette, Wyoming where three seams are actively mined: the Upper, Middle, and Lower Wyodak seams. This is a typical PRB coal with a very high moisture content (~27%) and low sulfur content (~0.3%S).

PR and Jim JW coals are locally mined Alabama coals. PR coal was chosen for this test because it is a high volatility (~32%) Eastern bituminous coal that has been used in other biomass cofiring tests conducted at the CRF.[1,2] PR coal is mined by the Pittsburgh & Midway Coal Company at their North River No. 1 Mine in Walker County, Alabama. After testing had commenced, it was learned that PR coal is mined from at least two adjacent seams and the seam from which this type of coal was obtained for the previous biomass cofiring tests had been closed. Coals from the two test series differ mainly in ash content, with as received coal from

Table 3-2. Typical as received (AR) fuel and ash analyses for the coals tested.

Fuel Analysis	Jacobs Ranch Powder River Basin	Galatia Illinois Basin	Pratt Seam High Vol. Bit.	Jim Walters #7 Low Vol. Bit.
Proximate	**JR**	**GL**	**PR**	**JW**
Moisture, %	27.13	8.01	2.85	1.96
Ash, %	5.30	7.85	16.45	12.93
Volatile, %	34.53	32.76	31.90	20.45
Fixed C, %	33.04	51.38	48.80	64.66
Volatile/FC Ratio	1.045	0.638	0.654	0.316
Ultimate				
Carbon, %	50.75	69.47	66.96	75.43
Hydrogen, %	3.24	4.31	4.11	3.85
Nitrogen, %	0.65	1.52	1.68	1.45
Sulfur,%	0.29	1.01	1.53	0.73
Oxygen, %	12.64	7.83	6.42	3.65
Heat Value				
AR, kJ/kg	19890	28484	28621	30238
AR, Btu/lb	8551	12246	12035	13000
Dry, kJ/kg	27293	30964	28814	30843
Dry, Btu/lb	11734	13312	12388	13260
Chlorine, %	0.01	0.28	0.01	0.01
Mineral Ash Analysis				
As Oxide, wt %				
Li_2O	0.02	0.03	0.11	0.09
Na_2O	1.40	1.50	0.45	0.70
K_2O	0.47	2.80	1.60	2.30
MgO	4.20	1.00	0.91	0.30
CaO	22.30	2.00	1.60	4.10
Fe_2O_3	6.60	9.80	11.10	7.30
Al_2O_3	17.10	24.80	26.10	30.00
SiO_2	32.50	53.80	51.30	47.90
TiO_2	1.70	1.50	2.10	1.50
P_2O_5	1.60	0.65	1.40	0.58
SO_3	10.90	1.50	1.50	3.30
TOTAL	98.79	99.38	98.17	98.07
LOI, % (750°C, AR)	93.20	93.70	82.80	85.2
Silica Ratio	49.54	80.78	79.03	80.37
Base/Acid Ratio	0.68	0.21	0.20	0.19

the earlier testing averaging ~11% ash and coal obtained for this testing averaging ~15% ash (with a range of from 13% to 17%).

JW coal was obtained from Jim Walters Resource No. 7 mine located in Brookwood, Alabama. This coal is mined from the Blue Creek seam and is characterized by its low volatility (~20%), compared to that of other Blue Creek seam coals from the No. 4 mine. This is a low-sulfur coal (~0.7%S), compared to Pratt seam coal (~1.5%S).

3.2.3.2.2 Biomasses Tested Tables 3-3 and 3-4 present typical proximate and ultimate analyses for the two biomasses tested along with mineral ash analyses. Because biomass a crop material, there is typically much more variability in this material than is typical of coal. Therefore in these tables, analyses are presented that display the variability in constituency that was observed over the course of the project.

With respect to sawdust (hereafter SD), when testing commenced, a load of Red Oak SD was acquired from a local stair tread company. This material was tub ground to reduce long slivers of material to a size that could be easily fed through the fuel processing system when it was mixed with coal. Subsequent lots of SD were acquired and processed by MESA Reduction Engineering & Processing, Inc. located in Troy, NY. MESA uses a proprietary collision mill to process biomass to a uniformly small size that can be easily fed through an eductor (for center-burner or side injection of biomass) or can be mixed directly with coal for comilling. MESA acquired hardwood cut-offs from a toy manufacturer near their location in New York state. This material was usually Maple, but occasionally some Oak was present in the hardwood cut-offs supplied to MESA. Variability among the various lots of SD that were acquired for this project was evidenced by changes in the volatile/fixed carbon ratio and in certain metals measured in the ash mineral analysis (Na, K, Ca, Mg, Fe, and Si).

All of the switchgrass (hereafter SG) used for testing was grown and harvested by Wilson Farm, Inc. at two nearby locations (120 acres near Winterboro, AL and 80 acres near Lincoln, AL). In an earlier biomass-cofiring project, also sponsored by the U.S. DOE, these two stands of Alamo SG were planted and harvested to provide SG for biomass cofiring testing.[1] Table 3-4 shows that even though all of the SG used in our testing originated at these two sites, some variability in constituency remained. In particular, the greatest difference observed was due to the method of harvesting. SG that was field chopped (harvested and chopped in one operation), and then stacked in the field before being loaded and delivered for testing had a much higher ash content (~ 12% on a dry basis, probably from contamination by soil) than SG that was field chopped and immediately baled (from 3.8% to 7.8%, on a dry basis). The first batch of SG was taken from field chopped and stacked SG that had been acquired in an earlier biomass cofiring effort.[1] This material was tub ground to reduce long stalk segments to a size that could be easily fed through the fuel processing/milling system when mixed with coal. Subsequently, bales of SG were transported by truck to MESA Reduction Engineering & Processing, Inc. for processing. Table 3-4 shows less overall variability in constituency than was observed for SD. However, one sample (Baled, Lot 1) did have a much higher volatile content (and lower Si content) than the other three samples.

Table 3-3. Typical as received (AR) fuel and ash analyses for the sawdust (SD) tested.

Sawdust Analysis	Red Oak (Stair Tread Dust)	Maple (End Cuts) Lot 1	Maple & Oak (End Cuts) Lot 2	Maple & Oak (End Cuts) Lot 3
Proximate				
Moisture, %	3.11	5.44	7.06	7.21
Ash, %	0.52	0.37	0.64	0.64
Volatile, %	82.45	80.21	75.61	67.34
Fixed C, %	13.92	13.98	16.69	24.82
Volatile/FC Ratio	5.923	5.742	4.530	2.713
Ultimate				
Carbon, %	47.45	46.55	42.29	45.80
Hydrogen, %	5.90	5.64	5.99	5.59
Nitrogen, %	0.15	0.05	0.33	0.14
Sulfur,%	0.01	0.01	0.03	0.05
Oxygen, %	42.86	41.94	43.66	40.58
Heat Value				
AR, kJ/kg	18648	18245	18240	17503
AR, Btu/lb	8017	7844	7842	7525
Dry, kJ/kg	19246	19295	19626	18862
Dry, Btu/lb	8274	8295	8438	8109
Mineral Ash Analysis				
As Oxide, wt %				
Li_2O	0.13	0.11	0.11	0.10
Na_2O	1.70	2.97	4.00	2.23
K_2O	6.00	7.57	2.70	13.20
MgO	10.60	11.17	2.80	8.93
CaO	48.80	54.57	60.50	42.27
Fe_2O_3	11.50	3.60	4.50	2.00
Al_2O_3	1.70	1.47	2.80	2.80
SiO_2	7.40	4.67	13.20	18.13
TiO_2	0.20	0.32	1.90	0.57
P_2O_5	4.20	7.43	1.20	4.13
SO_3	3.60	4.83	3.60	4.17
TOTAL	95.83	98.70	97.31	98.54
LOI, % (750°C, AR)	99.60	97.73	99.60	99.55
Silica Ratio	9.45	6.31	16.30	25.42
Base/Acid Ratio	8.45	12.37	4.16	3.19

Table 3-4. Typical as received (AR) fuel and ash analyses for the switchgrass (SG) tested.[1]

Switchgrass[1] Analysis	Field Chopped, Field Stacked	Field Chopped, Baled, Lot 1	Field Chopped, Baled, Lot 2.	Field Chopped, Baled, Lot 3
Proximate				
Moisture, %	13.21	5.64	7.72	7.14
Ash, %	10.29	3.62	6.74	7.21
Volatile, %	60.03	72.85	62.76	62.98
Fixed C, %	16.47	17.90	22.78	22.67
Volatile/FC Ratio	3.645	4.071	2.755	2.778
Ultimate				
Carbon, %	39.06	44.24	42.90	42.72
Hydrogen, %	4.80	5.56	5.17	5.31
Nitrogen, %	0.50	0.70	1.07	1.18
Sulfur,%	0.22	0.07	0.05	0.08
Oxygen, %	31.92	40.17	36.35	36.36
Heat Value				
AR, kJ/kg	15626	17754	15249	16051
AR, Btu/lb	6718	7633	6556	6901
Dry, kJ/kg	18004	18816	16525	17285
Dry, Btu/lb	7741	8089	7104	7431
Chlorine, %				
Mineral Ash Analysis				
As Oxide, wt %				
Li_2O	0.07	0.12	0.04	0.14
Na_2O	1.40	2.90	1.00	4.70
K_2O	16.00	18.75	14.70	13.57
MgO	6.70	11.08	5.40	10.23
CaO	17.40	15.48	7.20	8.97
Fe_2O_3	3.60	3.15	4.70	2.83
Al_2O_3	5.10	1.43	5.50	3.37
SiO_2	40.10	34.88	49.70	45.07
TiO_2	0.41	0.31	0.50	0.32
P_2O_5	4.50	6.00	3.90	4.87
SO_3	5.70	5.33	5.10	4.07
TOTAL	100.98	99.40	97.74	98.13
LOI, % (750°C, AR)	93.50	98.20	93.40	95.07
Silica Ratio	59.14	54.01	74.18	67.16
Base/Acid Ratio	0.99	1.40	0.59	0.83

1. All switchgrass was grown by Wilson Farm, Inc. at their Winterboro, AL and Lincoln, AL farms, and was of the Alamo variety. See Reference 1.

As Tables 3-2 and 3-3 show, with SD, fuel nitrogen will always be reduced when coal is cofired with this biomass, even for JR coal. For a coal-bound fuel nitrogen level of 1.5% and an average SD fuel nitrogen level of 0.1%, at a 10% level of biomass addition, fuel N is reduced by ~ 9%. At a 20% level of SD addition, fuel N is reduced by ~ 19 %. For SG, as Tables 3-2 and 3-4 show, fuel nitrogen will also generally be reduced when coal is cofired with SG (with the possible exception of JR coal), but to a much lesser extent than with SD. For a coal-bound fuel nitrogen level of 1.5% and an average SG fuel nitrogen level of 1.0%, at a 10% level of biomass addition, fuel N is reduced by ~ 3%. At a 20% level of biomass addition, fuel N is reduced by ~ 7 %.

When coal is cofired with biomass, if the primary mechanism for reducing nitrogen emissions is the simple reduction of fuel nitrogen, the addition of SD or SG could usually be expected to result in a reduction of NO_X in proportion to the reduction in fuel N. When NO_X reductions are not proportional to the net fuel N reduction from biomass addition, other NO_X reduction or production mechanisms must be at work. The results of this work reveal that NO_X emissions can be increased, unaffected, or decreased by the addition of biomass.

3.2.3.2.3 Tests Performed Fourteen separate test series were required to generate the database of 422 results that was used to validate the model. Table 3-5 enumerates these tests by date with a brief description of the fuels that were burned and the furnace test conditions for each test. Table 3-6 lists these tests by coal, biomass, injection geometry, and burner. Inspection of this table shows that 76% of all test conditions were for pulverized coal (32%) or for coal comilled with biomass (44%). This relatively high proportion is indicative of the relative importance of testing with comilled biomass for validating the model as compared to the other injection geometries. Tests with core injection (16%) and side injection (8%) constitute the balance of the database of results.

The full database of test results is tabulated in Appendices A and B of this report. Appendix A (part 1) catalogs averages and standard deviations of FEO, NO_X, and UBC emissions for each test result along with averages and standard deviations of furnace air flows (total, primary, secondary, and OFA flows) and coal feed rates for each condition in the database. Appendix A (part 2) catalogs averages and standard deviations for CEM emissions data recorded for each test result and Appendix B tabulates curve fits to NO_X emissions data as a function of FEO and although included in the body of this report, Appendix B also includes relationships between FEO and fuel stoichiometry, volatile/fixed carbon ratio and weight % biomass, fuel-bound nitrogen and weight % biomass, and fits to sieve data for samples of comilled coal and biomass.

3.2.4 Test Results

Tables 3-5 and 3-6 show that a significant body of test results was acquired. We first present results related to cofiring biomass and coal by comilling, then results from cofiring by center-burner injection, and finally, results from cofiring by side injection. This order follows the relative number of test results for each cofiring case as shown in Table 3-6. After these results have been presented and compared with other results for the same mode of cofiring, we will discuss the results as a whole and draw general conclusions from the experimental effort.

Table 3-5. Pilot-Scale Furnace Tests.

Test 1: PR coal comilled with biomass, single register burner (Location 1), 15%, 20% SG, 10%, 20% SD. 0%, 15%, 30% OFA. 1/28-2/3/01

Test 2: PR coal – biomass through center of burner (Location 2), single register burner, 10% SD. 0%, 15%, 30% OFA. Problems with biomass injection scheme and flame stability. 2/25-3/2/01

Test 3: PR coal – biomass through center of burner (Location 2), single register burner, 10%, 20% SG, 10%, 20% SD. 0%, 15% OFA. Continued problems with flame stability. 4/8-14/01

Test 1R: Repeat of Test 1 for 100% PR coal – no biomass, single register burner (Location 1), extensive characterization of coal-only firing at 0% and 15% OFA. Corrected flame stability problem. 5/14-17/01

Test 4: PR coal – biomass injection toward quarl (Location 3), single register burner, 10%, 20% SG, 10%, 20% SD. 0%, 15% OFA. 6/10-15/01

Test 5: GL coal comilled with SD, single register burner (Location 1), 10%, 20% SD. 0%, 15%, OFA. 100% PR coal, 0%, 15%, OFA. 7/8-7/13/01 (SG supply exhausted)

Test 6: GL coal comilled with SG, single register burner (Location 1), 10%, 20% SG. 0%, 15%, OFA. PR Coal comilled with 20% SD. 8/5-10/01

Test 7: JR coal comilled with biomass, single register burner (Location 1), 10%, 20% SG, 10%, 20% SD. 0%, 15% OFA. 9/16-21/01

Test 8: JR coal – biomass through center of burner (Location 2), single register burner, 10%, 20% SG, 10%, 20% SD. 0%, 15% OFA. 10/21-26/01

Test 9: GL coal comilled with biomass, dual register burner (Location 1), 10%, 20% SG, 10%, 20% SD. 0%, 15%, overfire air. 1/6-11/02

Test 10: PR coal – no biomass, single register burner (Location 1), regular (~70%<200 mesh) and finely ground (~90%<200 mesh) coal at 0% and 15% OFA. 2/10-13/02

Test 11: GL coal comilled with SD, GL coal with liquid NH_3 injected into primary air line to increase fuel-bound nitrogen, single register burner (Location 1), 5%, 10%, 20% SD, 0%, 15%, OFA. 4/7-13/02

Test 12: GL coal (no biomass) and JW coal with comilled SD, single register burner (Location 1), 5%, 10%, 20% SD. 0%, 15%, OFA. Char sampling below OFA ports. 5/19-24/02

Test 13: JW #7 coal comilled with SG, single register burner (Location 1), 5%, 10%, 20% SG. 0%, 15%, OFA. Char sampling below OFA ports. 7/14-19/02

Table 3-6. Summary of test conditions in the database.

COAL	TYPE	BIOMASS	BURNER GEOMETRY				TOTAL
			Single Register			Dual-Register	
			Comilled	Core	Side	Comilled	
JR	PRB	None	6	7			**13**
		SD	13	15			**28**
		SG	13	17			**30**
GL	Ill. Basin	None	26			6	**32**
		None-NH_3	2				**2**
		SD	42			12	**54**
		SD-NH_3	14				**14**
		SG	17			14	**31**
PR	hv bit.	None	54	8	8		**70**
		SD	30	11	13		**54**
		SG	16	11	12		**39**
JW	lv bit.	None	13				**13**
		SD	21				**21**
		SG	21				**21**
TOTAL			**288**	**69**	**33**	**32**	**422**

3.2.4.1 Single-Register Burner - Results from Cofiring Tests with Comilled Biomass More testing was conducted with comilling than for any other method of biomass cofiring, regardless of burner geometry. This is because from a modeling perspective, predicting emissions for comilling is more challenging than for predicting emissions for center-burner or side injection of biomass. When biomass and coal are comilled and the resulting mixture is burned, the intimate association of coal and biomass during devolatilization and combustion produce more of a reducing environment (with more complex chemistry) than is possible when finely divided biomass entrained in air is injected to a pulverized coal flame.

In terms of the number of tests performed with the single-register burner, 100 comilling test conditions were recorded with PR coal comilled with SD and SG. As these results form the largest set of test conditions for a single coal, we use these data to illustrate the techniques that were developed to analyze and present the entirety of the data.

3.2.4.1.1 CRF Stability When biomass was cofired with coal, NO_X and UBC emissions were first determined for 100% coal firing so that the effect of adding biomass on NO_X and UBC emissions can be quantified within that test series. The establishment of such a reference point is important because in full-scale cofiring tests, baseline emissions information may be available only at the beginning or the end of testing and the variability of emissions data over time may not be known. For this investigation, tests with the same coal (PR) were conducted over five test series spanning one calendar year and baseline (100% coal) testing was conducted during each test. NO_X and UBC emissions from these baseline tests can be compared to assess the overall

stability of the pilot-scale furnace over time. Analyses of samples of PR coal taken throughout these five test series revealed no significant differences in fuel or ash chemistry.

Figure 3-9 shows NO_X emissions data as a function of FEO taken over the period from February 2001 to February 2002 for 100% PR coal at 0%, 15%, and 30% OFA. Note that 30% FEO results were only available from one test. In this figure, each ordered pair of results represents a measurement made during one minute of stable CRF operation at a particular test condition. All FEO measurements are in situ (wet measurements), taken with a zirconia O_2 cell located as close to the furnace exit as port availability and temperature limits of the O_2 sensor allow. All NO_X concentrations are reported as ppm, normalized to 3% O_2 (dry) in the flue gas at the point of extraction for the CEM system.

In this figure it is clear that while there are scatter within these data, NO_X emissions generally conform well to the same relationship for 0% and 15% OFA and exhibit no time-related trends. Thus, the CRF appears to be a stable platform for comparative emissions testing.

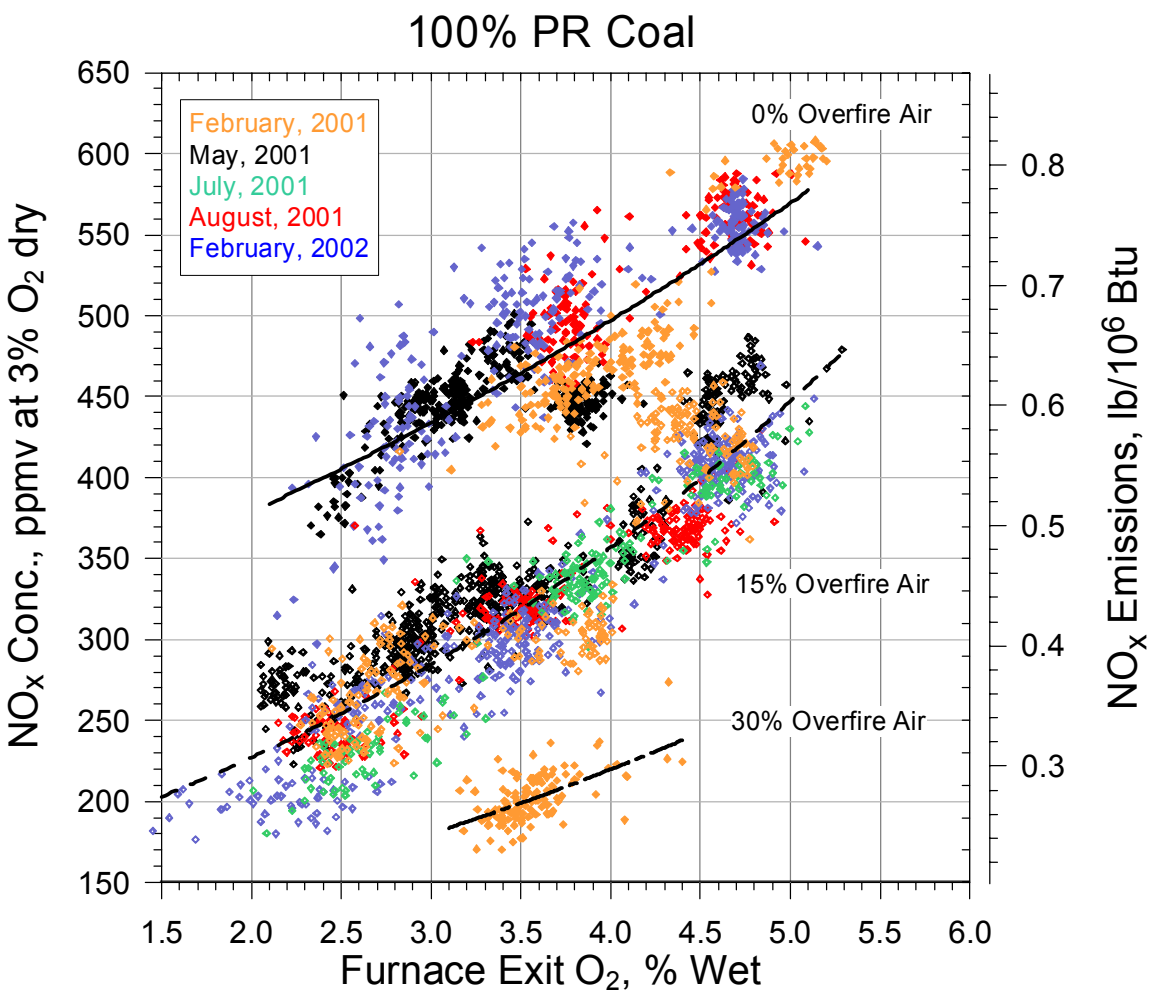

Figure 3-9. NO_X emissions for 100% PR coal firing in the CRF at 0%, 15%, and 30% OFA. These data span one year and cover five separate test series.

With respect to repeatability of UBC emissions, Figure 3-10 shows how UBC emissions compare when measured over roughly the same time period as shown in Figure 3-9. UBC is measured by determining the carbon content in fly ash that has been isokinetically sampled near the point where CEM measurements are made at the entrance of the CRF permit baghouse. Carbon is measured with a CHN analyzer that first pyrolyzes a 5 mg. sample of ash at 1000°C, then analyzes the off gases from pyrolysis for CO_2 (carbon) converts NO_X to N_2 and measures N_2 (for nitrogen), and water (for hydrogen). Figure 3-10 shows that UBC emissions for PR coal are quite low for 0% OFA, a fact that may contribute to the scatter in UBC measurements at lower values of FEO. At 15% OFA, UBC emissions increase and the overall agreement is better. These results also conform well to the same relationship for each level of OFA, exhibit no time-related trends, and reinforce the conclusion that the CRF appears to be a stable platform for comparative emissions testing.

3.2.4.1.2 Effect of Coal PSD on NO_X and UBC Emissions When a mixture of coal and biomass is pulverized, two distinct particle size distributions (PSDs) are present in the comilled product (see Appendix B for specific examples). Each PSD can be recovered by sieving a sample of the comilled fuel and determining the heat value of each sieve fraction compared to the heat value of each component of the comilled mixture. When making such determinations it is also important to determine the moisture content of each component and each sieve fraction.

Figure 3-11 shows measured and recovered cumulative size distributions for pulverized samples of a comilled 80% PR coal - 20% sawdust mixture. In this figure, the cumulative size distributions of the pulverized mixture (from 3 samples), coal portion, and sawdust portion are shown with fit parameters to a Rosin-Rammler size distribution. Size distributions result from grinding or comminution and are typically fit by a Rosin-Rammler distribution, defined as:

$$F(x; n,x_0) = 1-\exp[-(x/x_0)^n]; \quad 0< x < \infty$$

$$MMD = x_0 \bullet (0.693)^{1/n}$$

Where x_0 and n are known as the size parameter and the distribution parameter, respectively and MMD is the mass median diameter of the distribution.

The results shown in Figure 3-11 are typical for a pulverized mixture of coal and biomass. While the comilled mixture passes the nominal utility milling requirement of 70% < 75 micrometers (200 mesh), the recovered coal distribution is much finer (~90% < 75 μm) and the sawdust portion of the distribution is much coarser (~15% < 75 μm).

Because coal is so finely ground in a pulverized mixture of coal and biomass it is possible that some or all of the NO_X reduction attributed to cofiring is actually due to more finely ground coal. To address this issue, Test 10 (or PR-10) was performed with 100% PR coal ground to a nominal 70% < 75 μm (MMD ~ 48 μm) and PR coal ground to ~92% < 75 μm (MMD ~ 31 μm). NO_X and UBC emissions were compared for the two fuels and as Figures 3-12 and 3-13 show, differences were negligible for 15% OFA while NO_X and UBC emissions were slightly lower at 0% OFA but still within experimental uncertainty. Thus, we conclude that the influence of coal PSD on NO_X and UBC emissions is a factor that can be dismissed in our analyses.

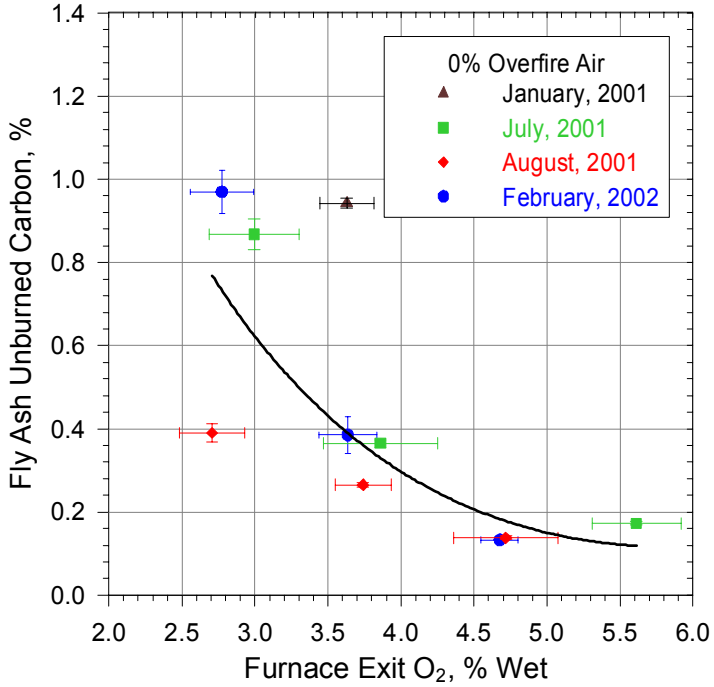

(a) 100% PR coal, 0% OFA

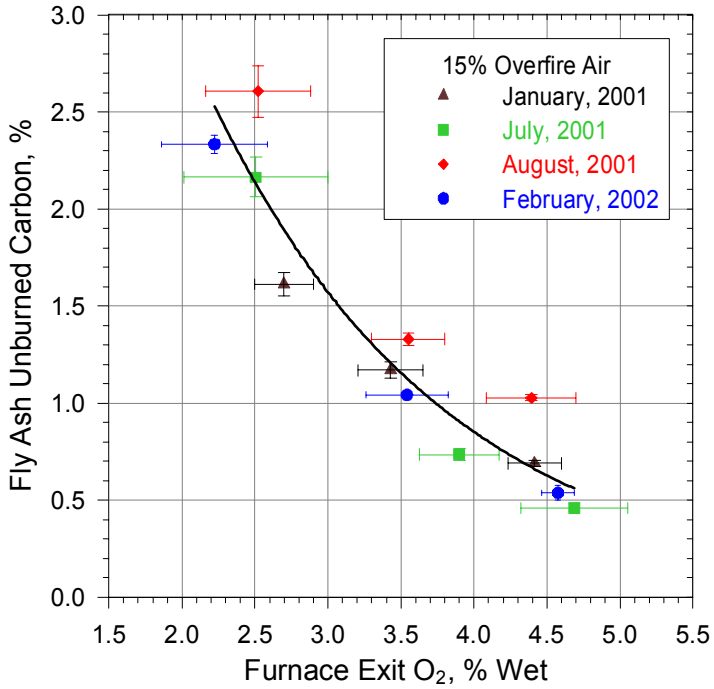

(b) 100% PR coal, 15% OFA

Figure 3-10. Unburned carbon in fly ash from the combustion of 100% PR coal, 0% and 15% OFA, averages ± 1 standard deviation.

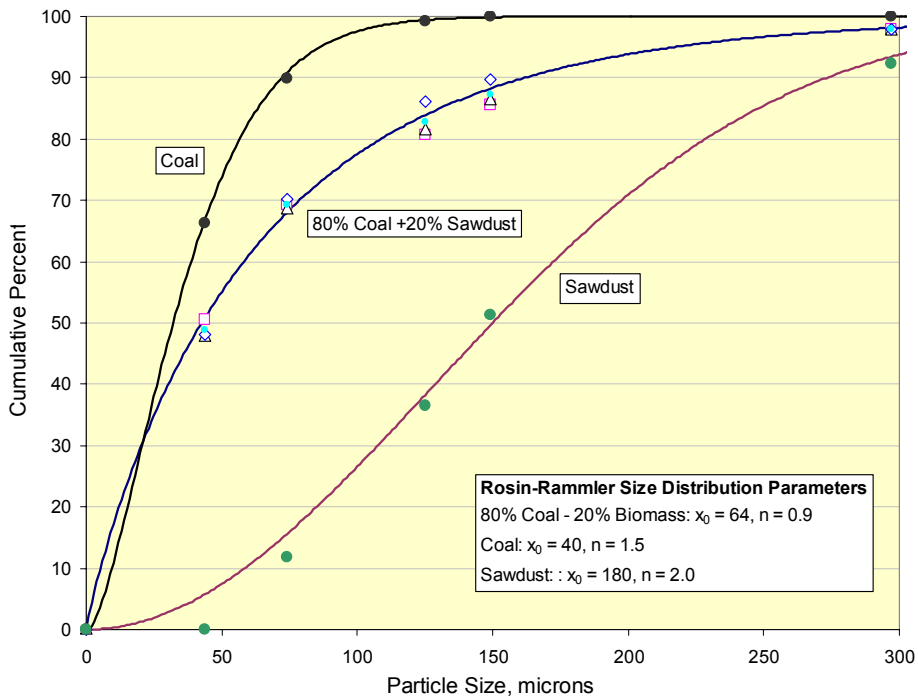

Figure 3-11. Cumulative size distribution for a comilled mixture of 80% PR coal and 20% sawdust.

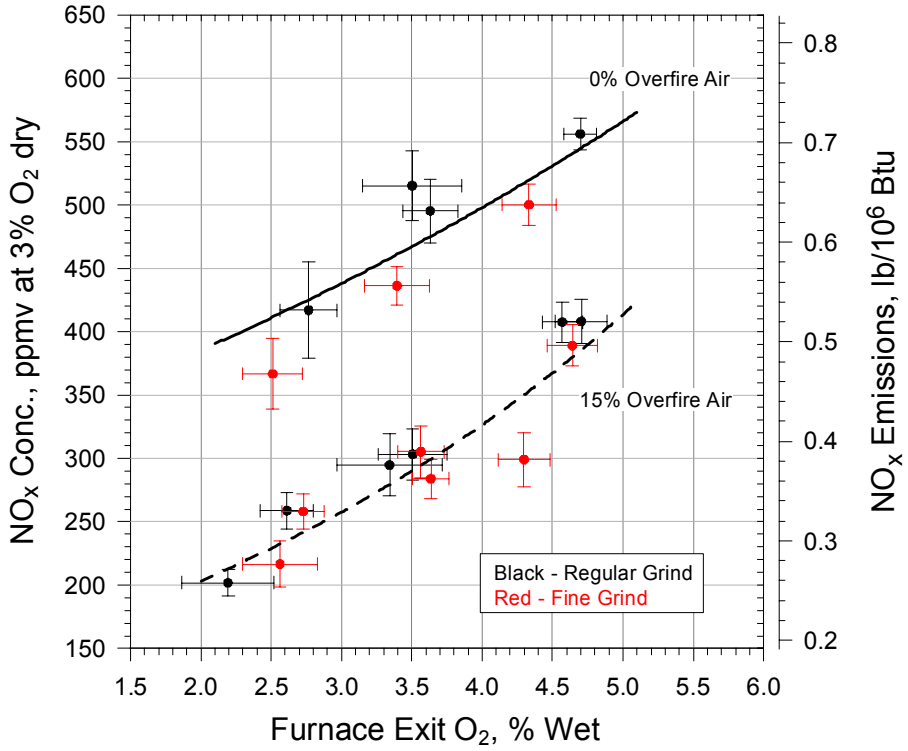

Figure 3-12. NO_X emissions for normally and finely ground PR coal, test condition averages ± 1 standard deviation.

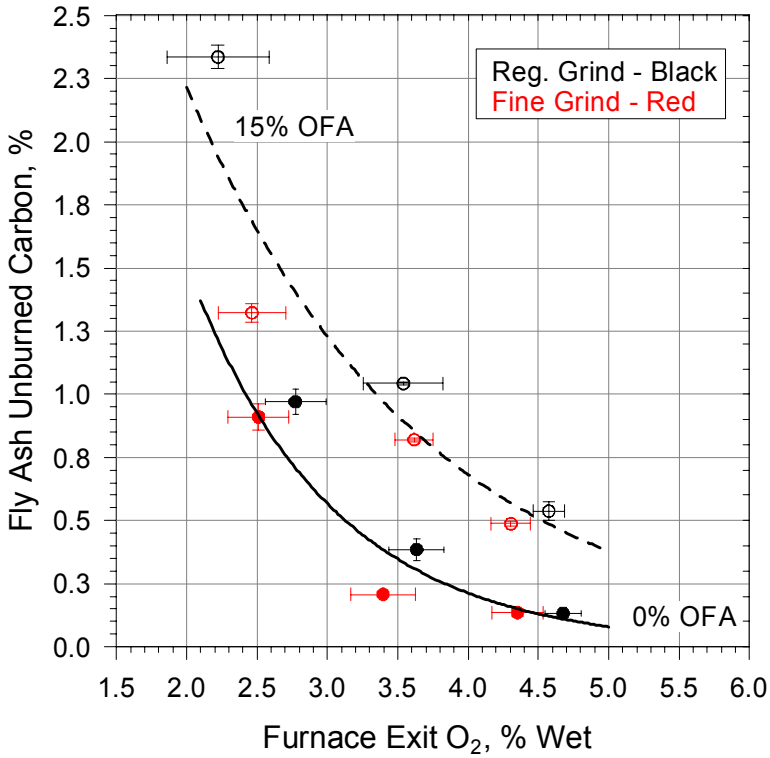

Figure 3-13. UBC emissions for normally and finely ground PR coal, averages ± 1 standard deviation.

3.2.4.1.3 Results of Cofiring Tests with Comilled Coal and Biomass For comilling, the choice of coal and biomass substantially affected NO_X and UBC emissions. To review these results in a systematic manner, we will first examine the effect of biomass cofiring with SD on NO_X reductions and UBC emissions for PR, GL, JR, and JW coals. Then, we present NO_X reductions and UBC emissions results for the same four coals comilled with SG. For each case, we will present results for 0%, 15% and 30% OFA (where available) in that order.

So that NO_X reductions can be referenced to NO_X concentrations, Figures 3-14 and 3-15 present graphs of curve fits to baseline NO_X emissions for 100% pulverized coal firing of PR, GL, JR, and JW coals as a function of FEO for 0%, 15% OFA. The curve fits shown in these figures are tabulated in Table 3-7 along with a curve fit to the single example with PR coal for 30% OFA.

These figures include two sets of curves for GL coal. The set of NO_X emissions curves labeled 2001 were determined in Tests 5 and 6 (or GL-5 and GL-6), in July and August of 2001. The set of NO_X emissions curves labeled 2002 were determined in Tests GL-11 and GL-12 in April and May of 2002. Between these two series of tests, in January 2001, the single-register burner was completely removed from the furnace so that the dual-register burner could be installed for Test GL-9. Subsequently, when the single-register burner was reinstalled, NO_X and UBC emissions for 100% PR coal firing were measured in Test PR-10 and though slightly different from those recorded in earlier tests no significant differences were noted (see February 2002 results in Figure 3-9 and UBC results in Figure 3-10). Subsequently, with Tests GL-11 and 12, NO_X

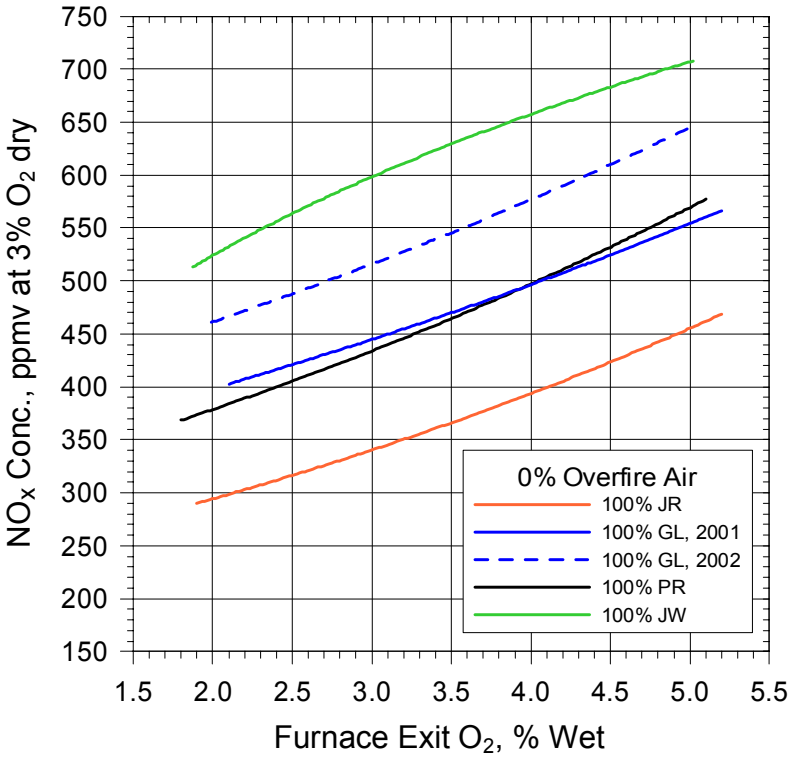

Figure 3-14. Baseline NO_X emissions for 0% OFA.

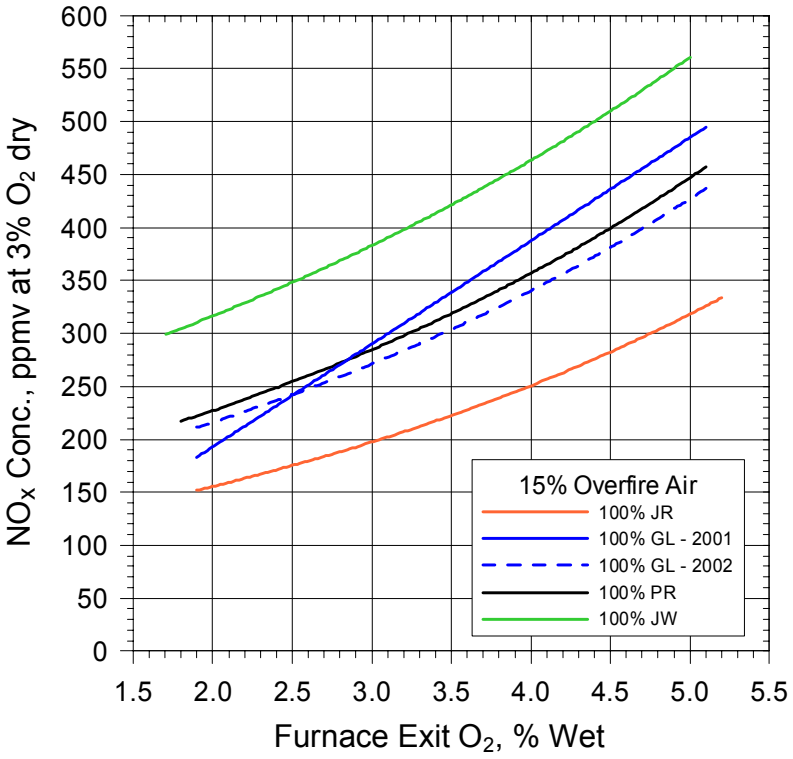

Figure 3-15. Baseline NO_X emissions for 15% OFA.

Table 3-7. Fit parameters for the NO_X emissions curves in Figures 3-14 and 3-15.

COAL	Fit*	Fitting Parameters	
0% OFA		A	B
PR	E	0.135906	288.624
GL-2001	E	0.109973	319.805
GL-2002	E	0.111567	369.156
JR	E	0.145559	219.918
JW	P	0.326872	417.801
15% OFA			
PR	E	0.225617	144.683
GL-2001	P	1.005719	96.0934
GL-2002	E	0.227053	137.263
JR	E	0.238524	96.5527
JW	E	0.190693	216.158
30% OFA			
PR	E	0.198759	99.2579

* E = Exponential fit: NO_X (ppm) = $B \bullet e^{(A \bullet \%FEO)}$
P = Power fit: NO_X (ppm) = $B \bullet (\%FEO)^A$

emissions for 100% coal firing were observed to be ~ 80 ppm higher than those measured during tests GL-5 and 6. NO_X emissions for 15% OFA were slightly, but measurably, different from those measured during tests GL-5 and 6. As Figure 3-16 shows, no differences in UBC emissions were measured in the four tests.

While these differences among NO_X emissions are small and not significant because baseline NO_X (and UBC) emissions are measured as part of every test, it is important to identify why NO_X emissions differed between the two tests performed before switching out the single-register burner with the dual-register burner and two tests performed after the single-register burner was reinstalled. With no difference in coal, UBC emissions, burner settings, or furnace operation, the differences in NO_X emissions were determined to be due to slight changes in burner geometry and windbox alignment resulting from removing and replacing the complete burner assembly. Specifically, while the single-register burner was uninstalled, the windbox and burner were cleaned and refurbished. Some of the bushings holding the vanes in the burner were replaced and a perforated screen at the exit of the windbox was found to have separated along a weld seam around a portion of its periphery. This screen was replaced with a similar but more robust screen with the same open area percentage as the original screen. The effect of such slight changes serves to illustrate the sensitivity of NO_X emissions to internal and external details of burner flow and alignment, particularly NO_X emissions for unstaged combustion. Such effects would not be noticed in a multi-burner system as the results of many slight misalignments are averaged over burner rows and elevations.

<u>3.2.4.1.3.1 NO_X Reductions from Cofiring by Comilling SD with Coal</u>. Table 3-8 and Figures 3-17 through 3-25 show NO_X reductions as a function of FEO and weight % of SD added for 0%, 15%, and 30% (where available) OFA. These figures also display stoichiometric ratio and

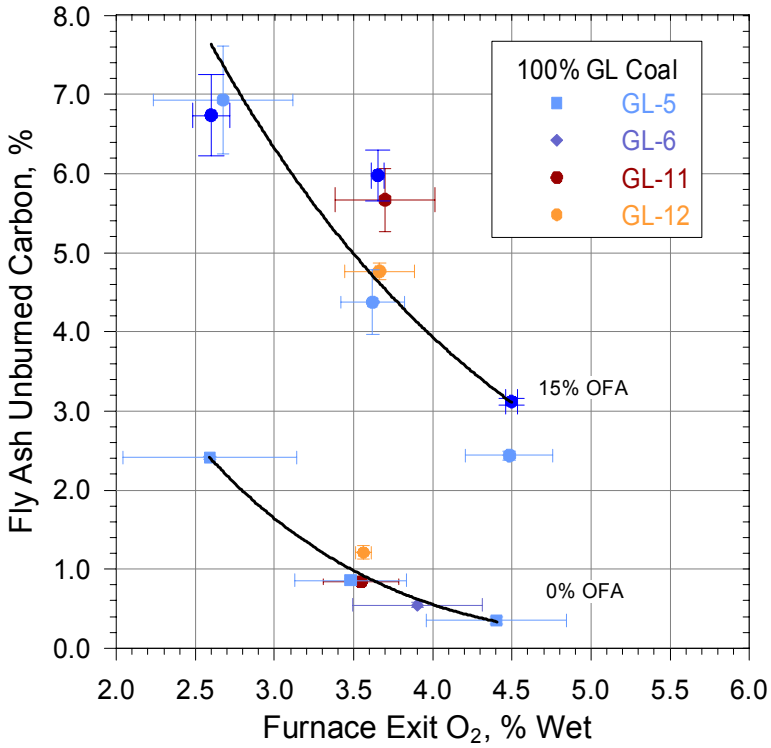

Figure 3-16. Baseline UBC emissions for GL coal.

volatile-to-fixed carbon ratio (V/FC) on alternate axes so that NO_X emissions and biomass content can be directly related to these quantities. These graphs were constructed by first fitting curves through experimental NO_X emissions data for weight percents of 0% (or 100% coal), 10%, and 20% biomass mixed with coal. Then, a three dimensional surface was constructed and imaged in the FEO-Biomass Weight % plane as the contour plots presented here. Fuel analyses and standard combustion calculations were used to relate fuel stoichiometry to FEO and weight % biomass to V/FC ratio for each coal and biomass. These relationships are tabulated in Table 3-9. Table 3-10 tabulates the relationship of fuel N to coal and biomass as a function of the weight % of biomass added. The 100% coal NO_X emissions curve fits presented in Table 3-7 and the fuel stoichiometry and V/FC ratio results presented in Tables 3-9 and 3-10 can be used with Figures 3-17 through 3-22 to recover NO_X emissions and fuel-bound nitrogen in each figure.

Note that while these graphs were constructed from tests results for 0, 10, and 20 weight percent biomass in the coal-biomass mixture, some tests were conducted with 5 weight percent biomass (in particular, JW-12, and JW-13). Because NO_X emissions at 5 weight percent biomass tend to add structure to these graphs that complicate comparisons with earlier results where 5 weight % biomass results were not available, these data are not included in Table 3-8 or in Figure 3-121 but are shown in Figure 3-22. NO_X emissions results for 5 weight percent addition of biomass will be discussed in detail after the presentation of results starting at a 10 weight percent addition of comilled biomass.

Table 3-8. NO_X reductions from cofiring with comilled sawdust.

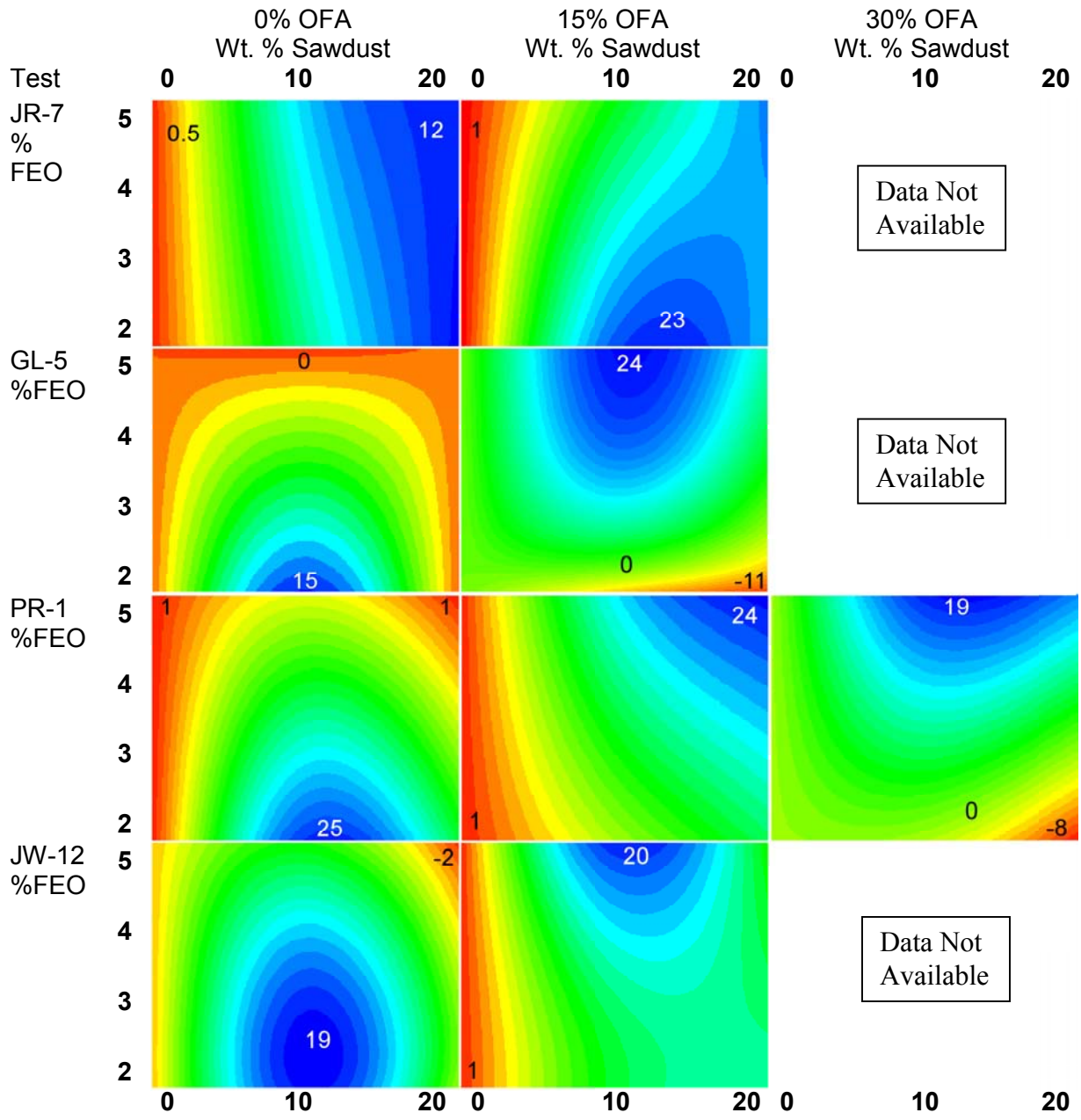

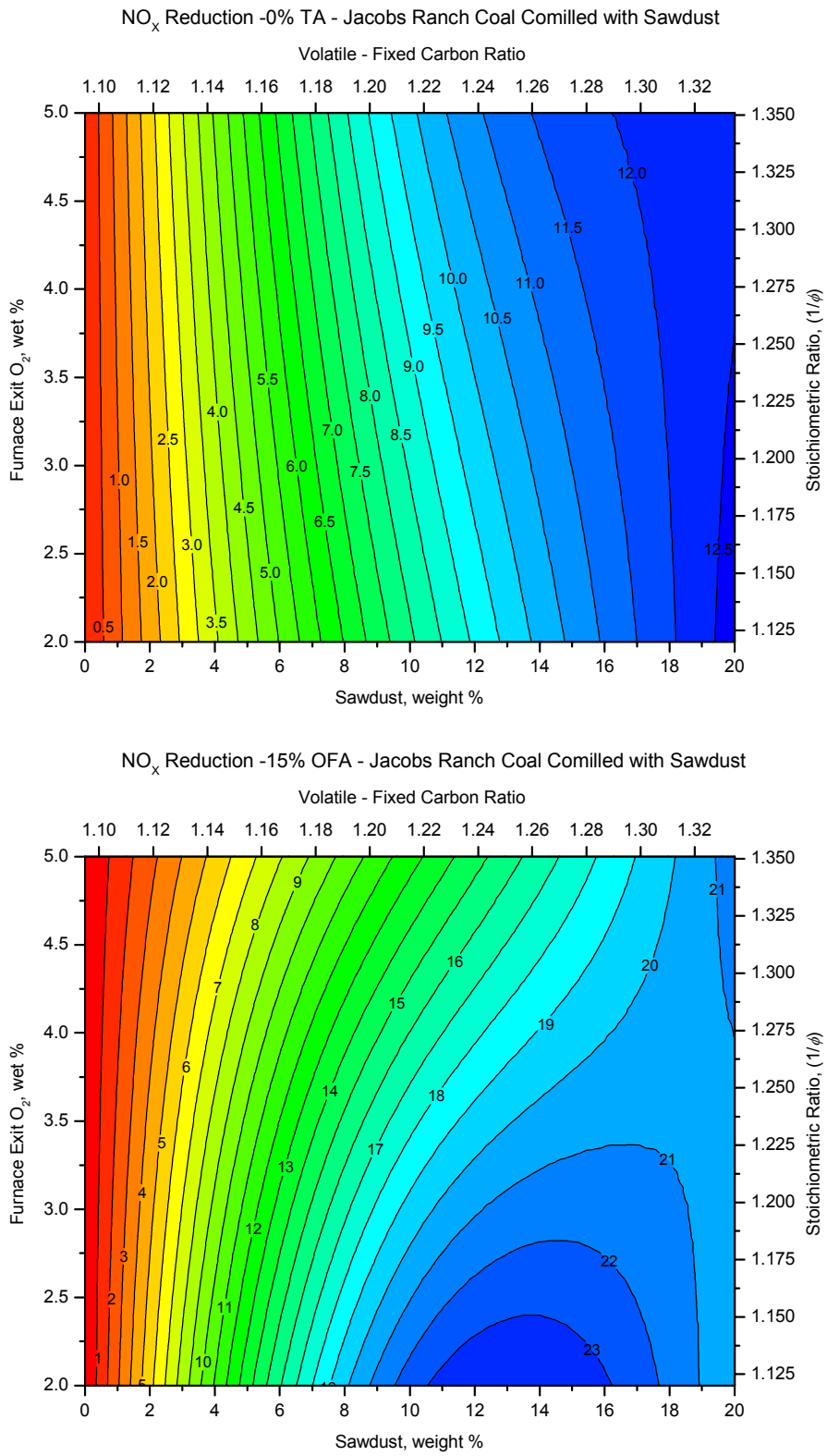

Figure 3-17. NO_X reductions from comilling SD with JR coal, 0% and 15% OFA.

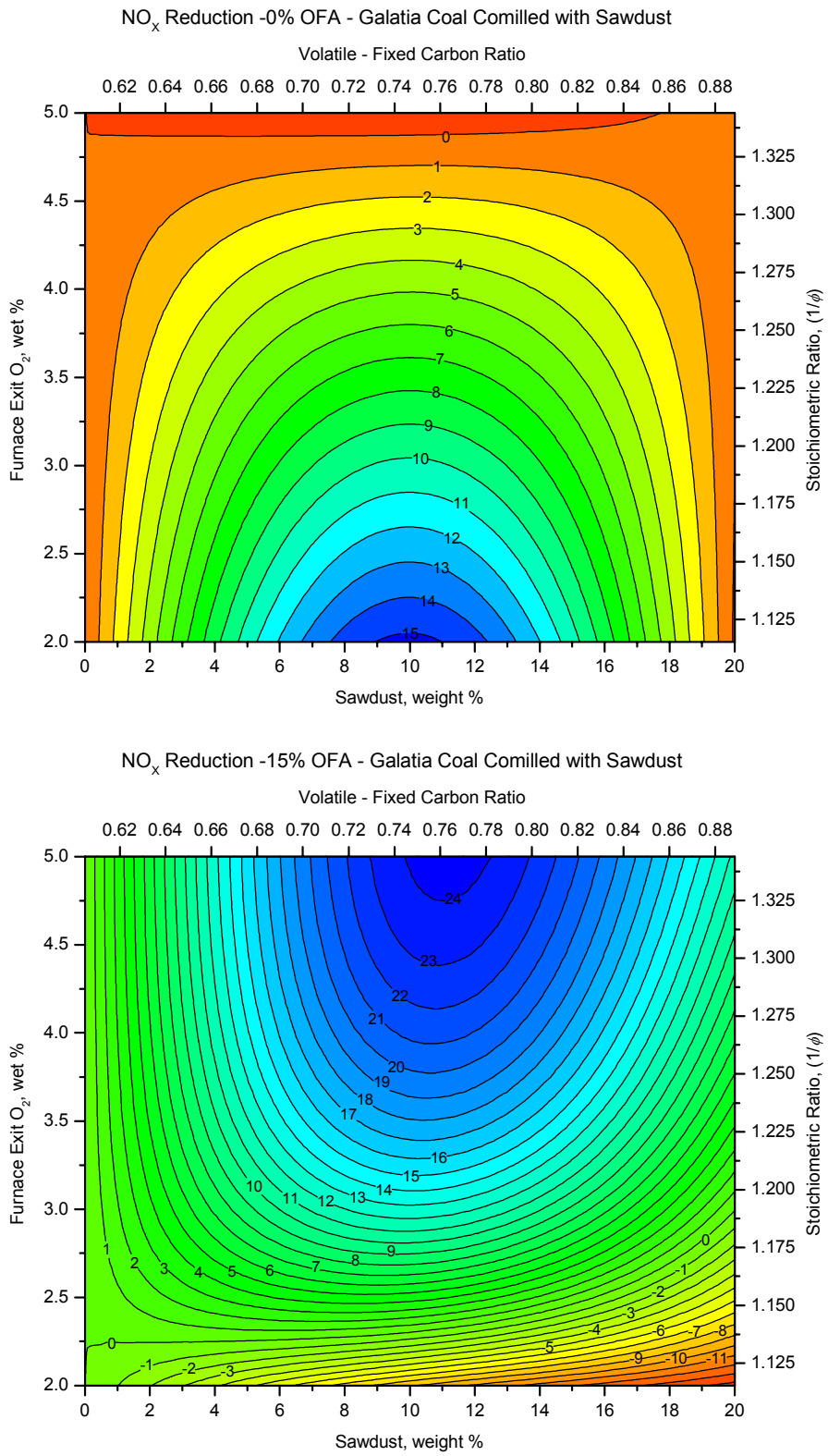

Figure 3-18. NO_X reductions from comilling SD with GL coal, 0% and 15% OFA.

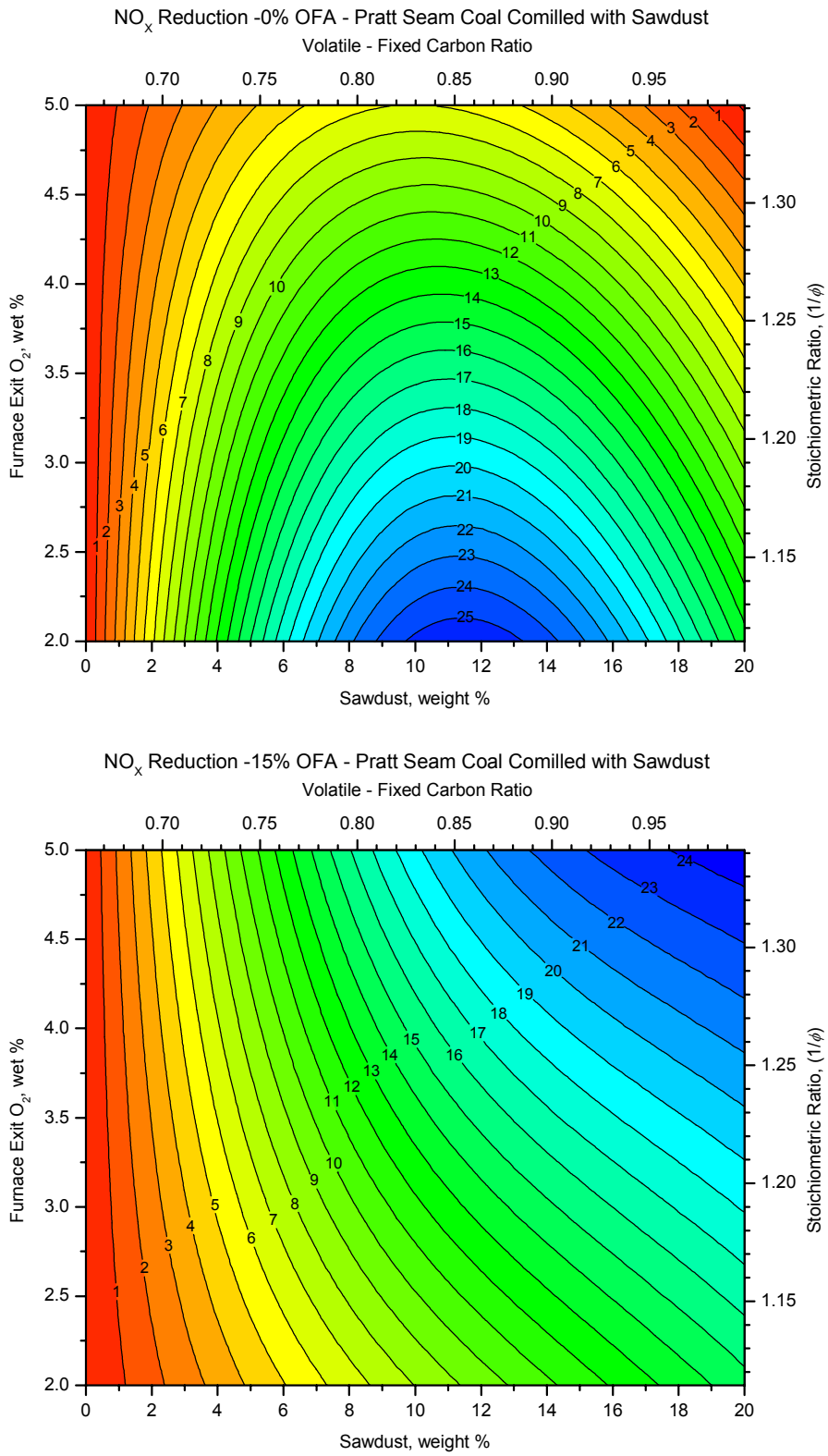

Figure 3-19. NO_X reductions from comilling SD with PR coal, 0% and 15% OFA.

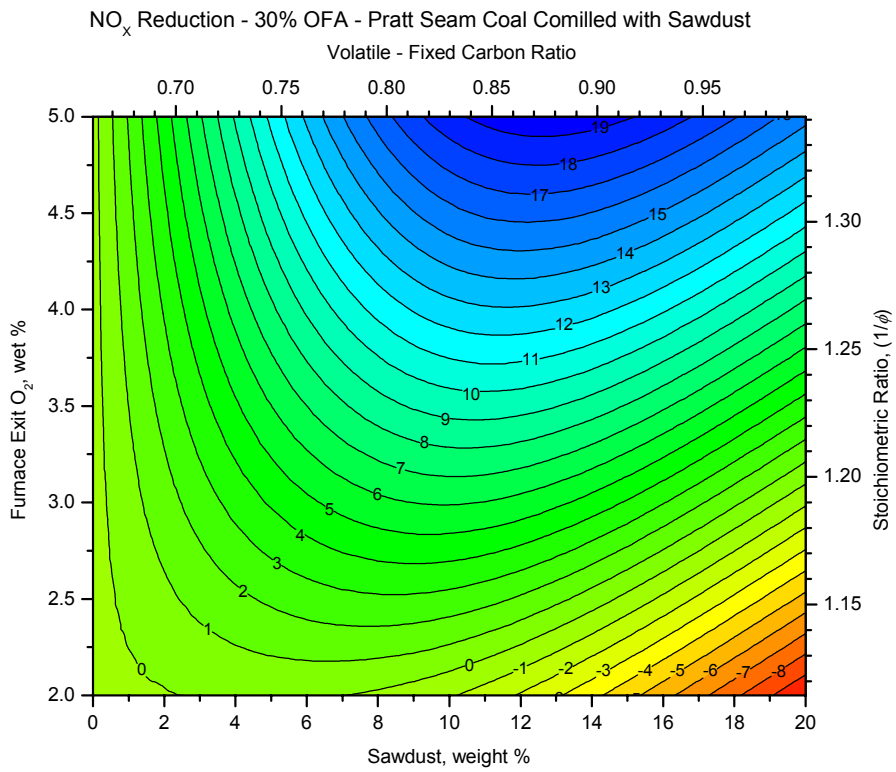

Figure 3-20. NO_X reductions from comilling SD with PR coal, 30% OFA.

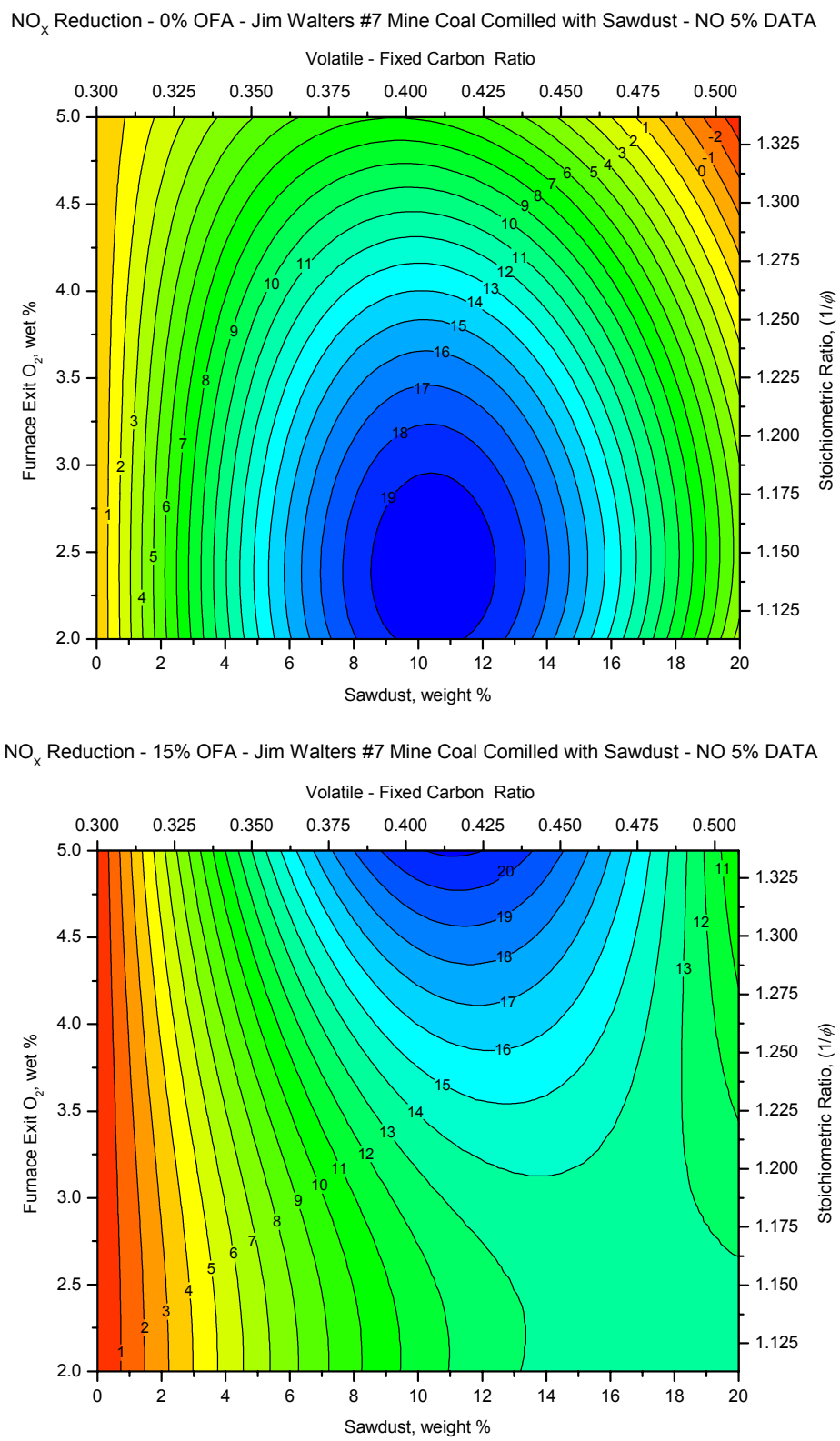

Figure 3-21. NO_X reductions from comilling SD with JW coal, 0% and 15% OFA. Results for 5% biomass are not included.

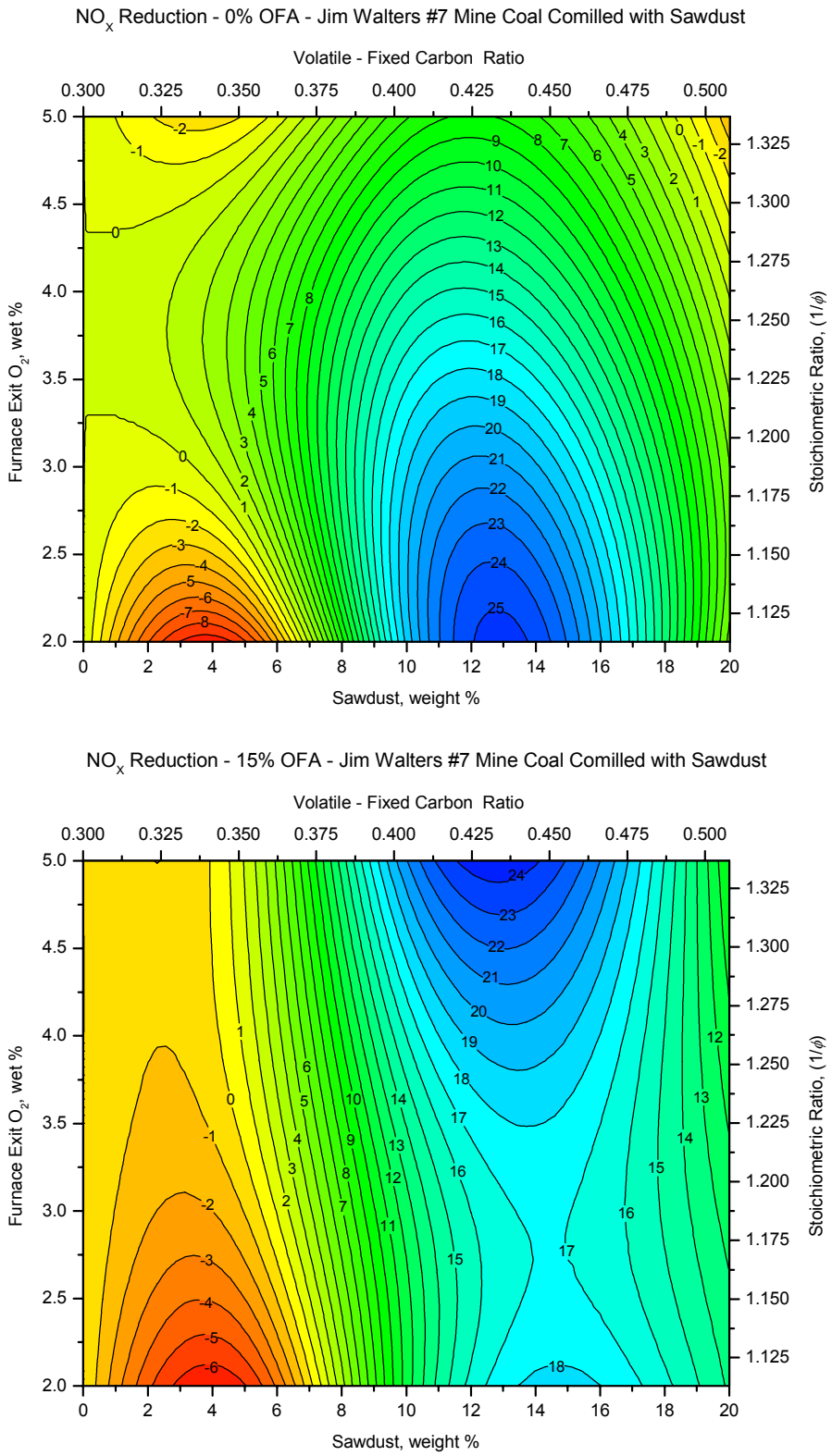

Figure 3-22. NO_X reductions from comilling SD with JW coal, 0% and 15% OFA. Results for 5% biomass are included.

Table 3-9. Fuel stoichiometric ratio and volatile to fixed carbon ratio as a function of weight % biomass.

Quantity/Biomass	Coal	Curvefit Coefficients		
		A	B	C
Stoichiometric Ratio*				
SD or SG	JR	1.0070	0.04746	0.004551
	GL	1.0076	0.04484	0.004451
	PR	1.0077	0.04451	0.004439
	JW	1.0079	0.04372	0.004408
Volatile/FC Ratio**				
SD	JR	1.0946	0.01101	5.012E-05
	GL	0.6174	0.01052	9.122E-05
	PR	0.6571	0.01437	1.332E-04
	JW	0.3180	0.00906	6.953E-05
SG	JR	1.0946	0.01043	5.620E-05
	GL	0.6174	0.00876	7.142E-05
	PR	0.6581	0.01126	9.515E-05
	JW	0.3180	0.00853	6.988E-05

*SR = A + B•FEO+C•$(FEO)^2$
**V/FC = A + B•W% + C•$(Wt\%)^2$

Table 3-10. Fuel Nitrogen as a function of weight % biomass.

Biomass	Coal	Curvefit Coefficients	
		Slope	B
SD	JR	-0.0080	0.8510
	GL	-0.0142	1.7074
	PR	-0.0088	1.5693
	JW	-0.0120	1.4485
SG	JR	0.0047	0.8521
	GL	-0.0054	1.7074
	PR	-0.0089	1.5731
	JW	-0.0027	1.4482

% Fuel N = Slope•Wt% + B

To facilitate comparisons among Figures 3-17 through 3-25, thumbnail images of these figures are shown in Table 3-8. Maximum and minimum NO_X reductions are indicated in each thumbnail image. In this table and in the figures that follow, when the addition of biomass results in an increase in NO_X emissions, negative NO_X reductions are shown. Emissions reductions are coded by color: highest NO_X reductions are in regions of blue and lowest NO_X reductions (or increases) are in regions of red. The gradations in color follow the normal spectra of white light that can be resolved into red, orange, yellow, green, and blue.

In Table 3-8, coal is ordered by volatility, so that NO_X reductions for JR coal are located at the top and NO_X reductions for JW coal are located at the bottom of the table. Also, staging by the addition of separated OFA is shown as increasing from left to right.

Inspection of Table 3-8 shows that when SD is comilled with coal across all levels of FEO, the most consistent NO_X reductions are measured with JR coal. That is, regardless of OFA, as the amount of SD is increased, NO_X emissions are reduced. Equivalent reductions were measured for other coals, but these reductions depend strongly on FEO for a given level of SD addition. For non-PRB coals, some consistent trends appear as coal volatility is decreased and OFA is increased. First, for 0% OFA and FEO < 3.5%, NO_X reduction appears to be the greatest at SD levels of ~ 10 weight %. As coal volatility decreases, the dependence on FEO appears to relax so that NO_X reductions at FEO levels of 4% are considerable. For 15% OFA, NO_X reductions are higher at FEO levels greater than 3.5% and these results suggest that higher levels of SD addition improve NO_X reductions. With respect to the effect of increasing OFA, with PR coal, increasing the amount of OFA to 30% appears to move the region for greatest NO_X removals to higher levels of FEO and higher levels of SD addition. Table 3-8 also reveals complex relationships among these results that range from the expected (more biomass is better for PRB) to the counter-intuitive (increasing OFA eliminates NO_X reductions at low levels of FEO).

When NO_X reductions from testing with 5 weight % SD are added to the results shown in Figure 3-21, much more structure is apparent, as shown in Figure 3-22. Indeed, at the 5% level of comilled SD, NO_X emissions are increased for low values of FEO. In Figure 3-21, this trend is not apparent which points out the need for additional data at low values of biomass cofiring. The fact that NO_X emissions increase is reasonable from the combination of a higher flame temperature (from adding volatile biomass) with insufficient depletion of oxygen in the flame to produce the strongly reducing region required to reduce NO to N_2, leading to increased NO_X emissions.

<u>3.2.4.1.3.2 NO_X Reductions from Cofiring by Comilling SG with Coal</u>. Table 3-11 and Figures 3-23 through 3-28 provide a presentation of NO_X reduction results in a format similar to that employed for comilled SD. Thus, Tables 3-7 through 3-10 also provide assistance in recovering NO_X emissions, stoichiometric ratio, V/FC ratio, and Fuel N from Figures 3-23 through 3-28.

A side-by-side comparison of Table 3-8 with Table 3-11 clearly illustrates the effect of biomass choice on NO_X reduction. With comilled SG, increasing the amount of comilled SG does not tend to uniformly reduce NO_X emissions for any coal. However, higher NO_X reductions were achieved with comilled SG (~29%, JR coal, 15% OFA) than with SD (~25%, PR coal, 0% OFA). With JR coal, adding more SD tended to reduce NO_X emissions for all values of FEO at both 0% and 15% OFA. For JR coal comilled with SG, at 0% OFA, NO_X emissions are significantly reduced only at high levels of comilled SG and FEO above 4%. For 15% OFA, and greater than 10% comilled SG, NO_X emissions are significantly reduced for FEO less than 4%.

With GL coal, cofiring with SG is not as effective in reducing NO_X emissions as was cofiring with SD. At 0% OFA, small reductions in NO_X emissions were observed at ~10% comilled SG, for all values of FEO. However, larger amounts of SG tended to uniformly increase NO_X emissions. At 15% OFA, NO_X reductions exhibited the same overall trends as were seen with

Table 3-11. NO_X reductions from cofiring with comilled SG.

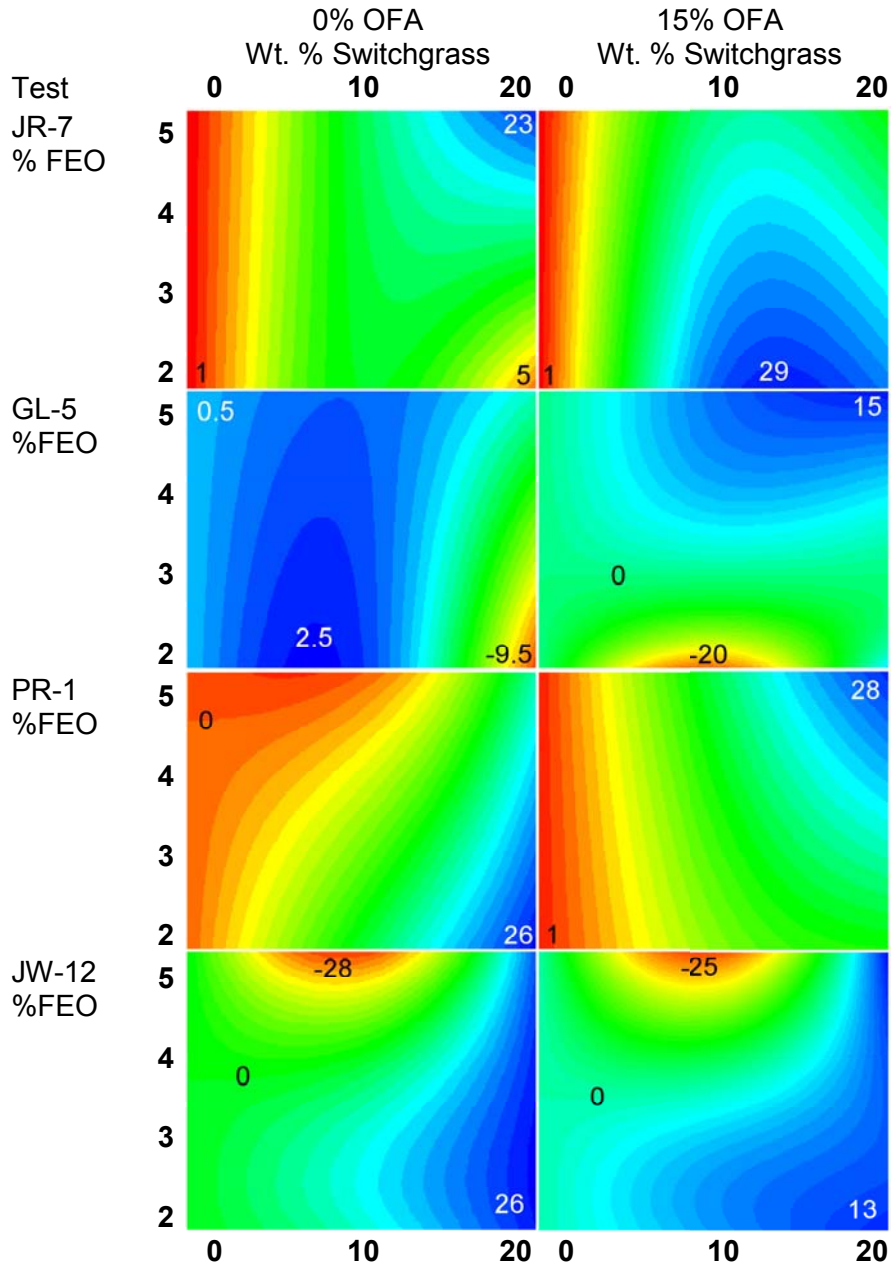

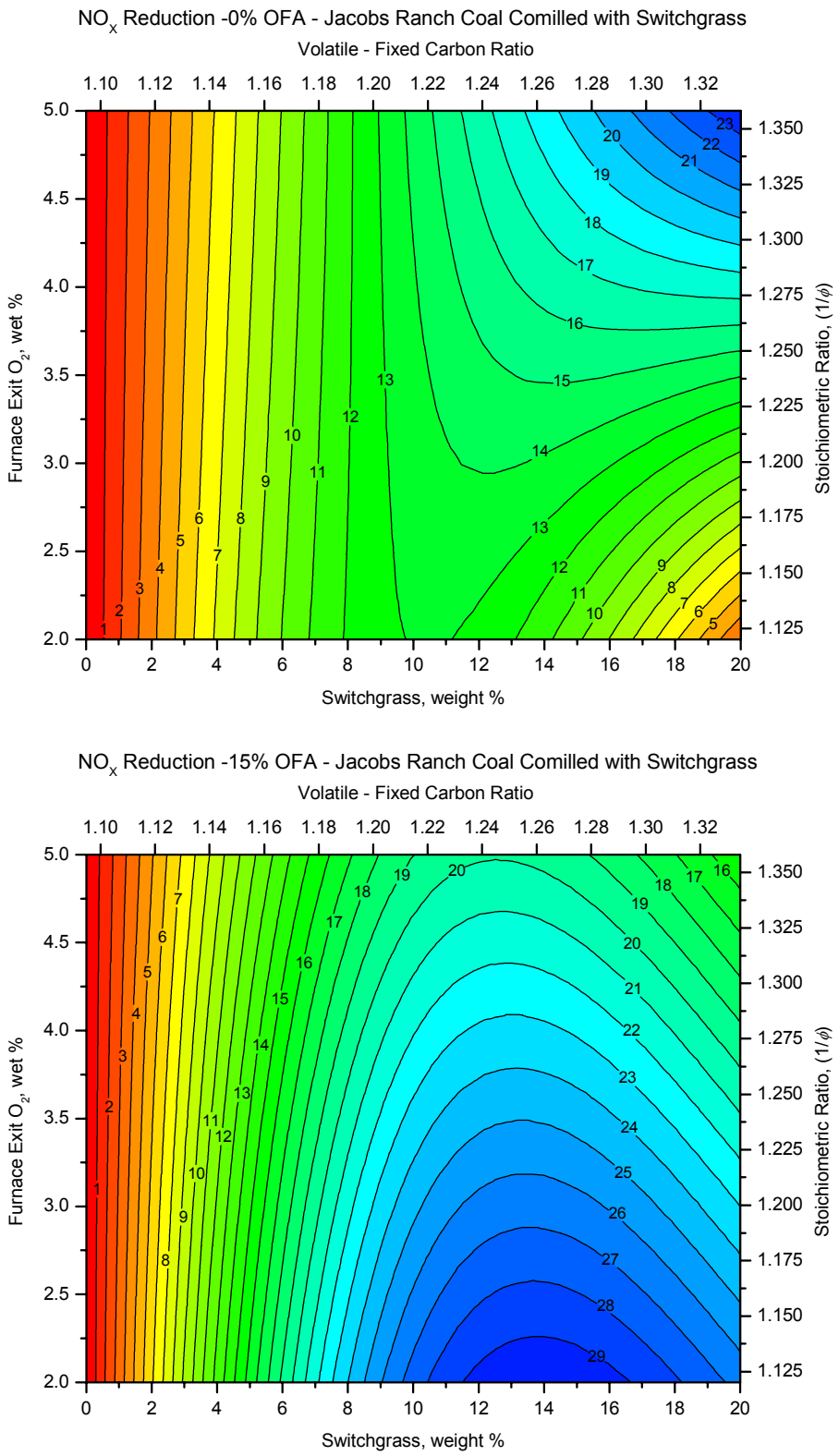

Figure 3-23. NO_X reductions from comilling SG with JR coal, 0% and 15% OFA.

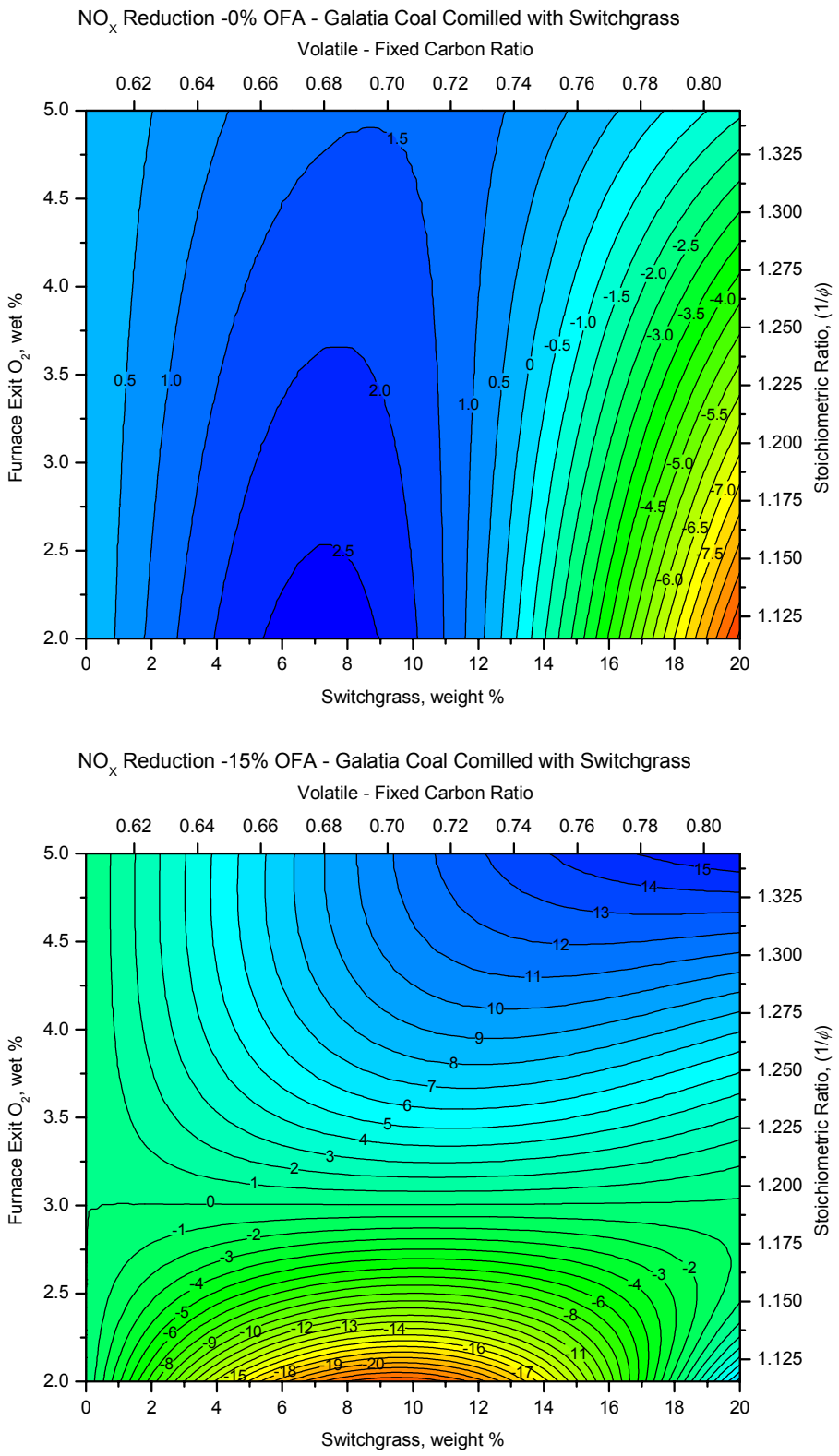

Figure 3-24. NO_X reductions from comilling SG with GL coal, 0% and 15% OFA.

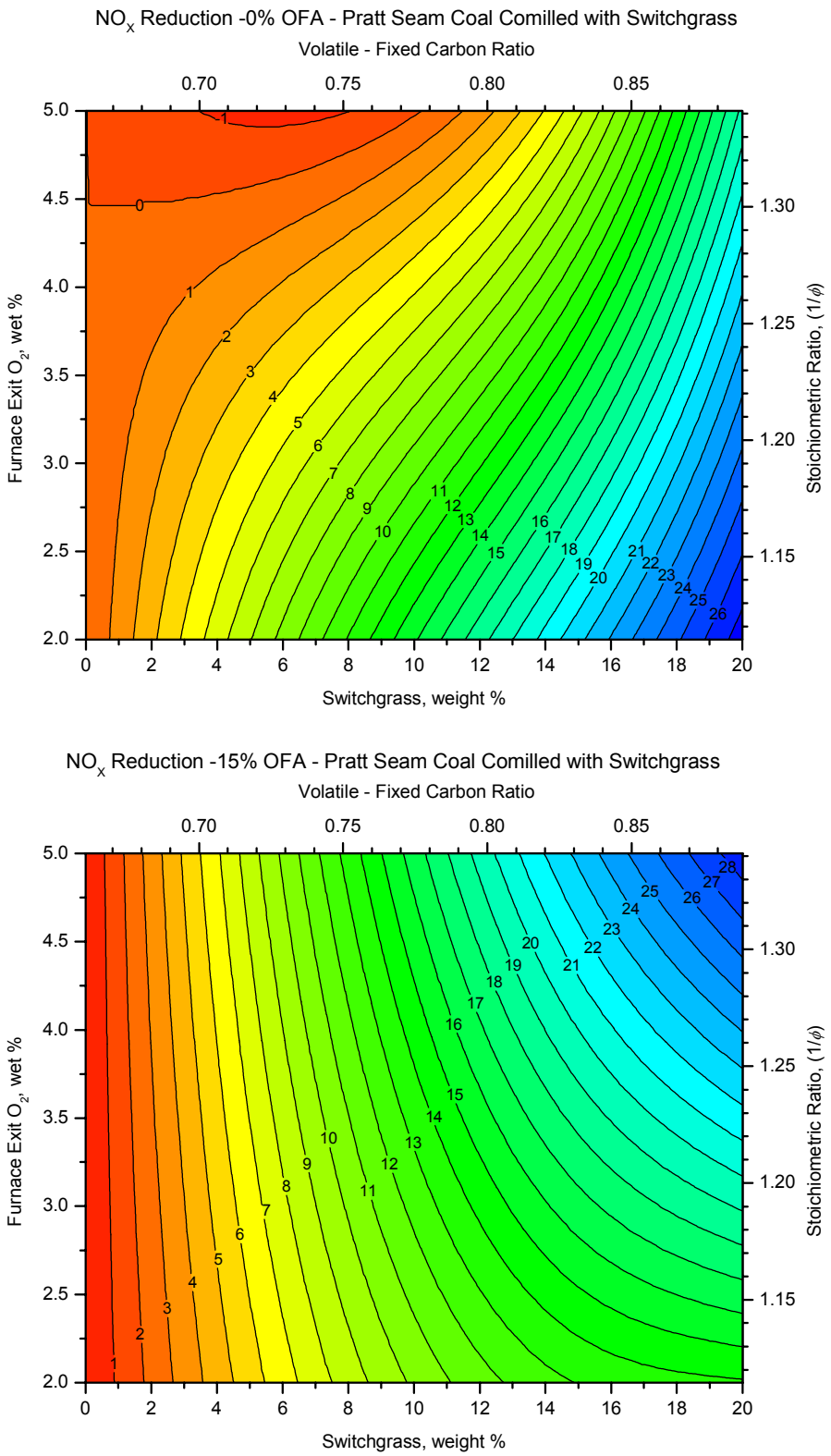

Figure 3-25. NO_X reductions from comilling SG with PR coal, 0% and 15% OFA.

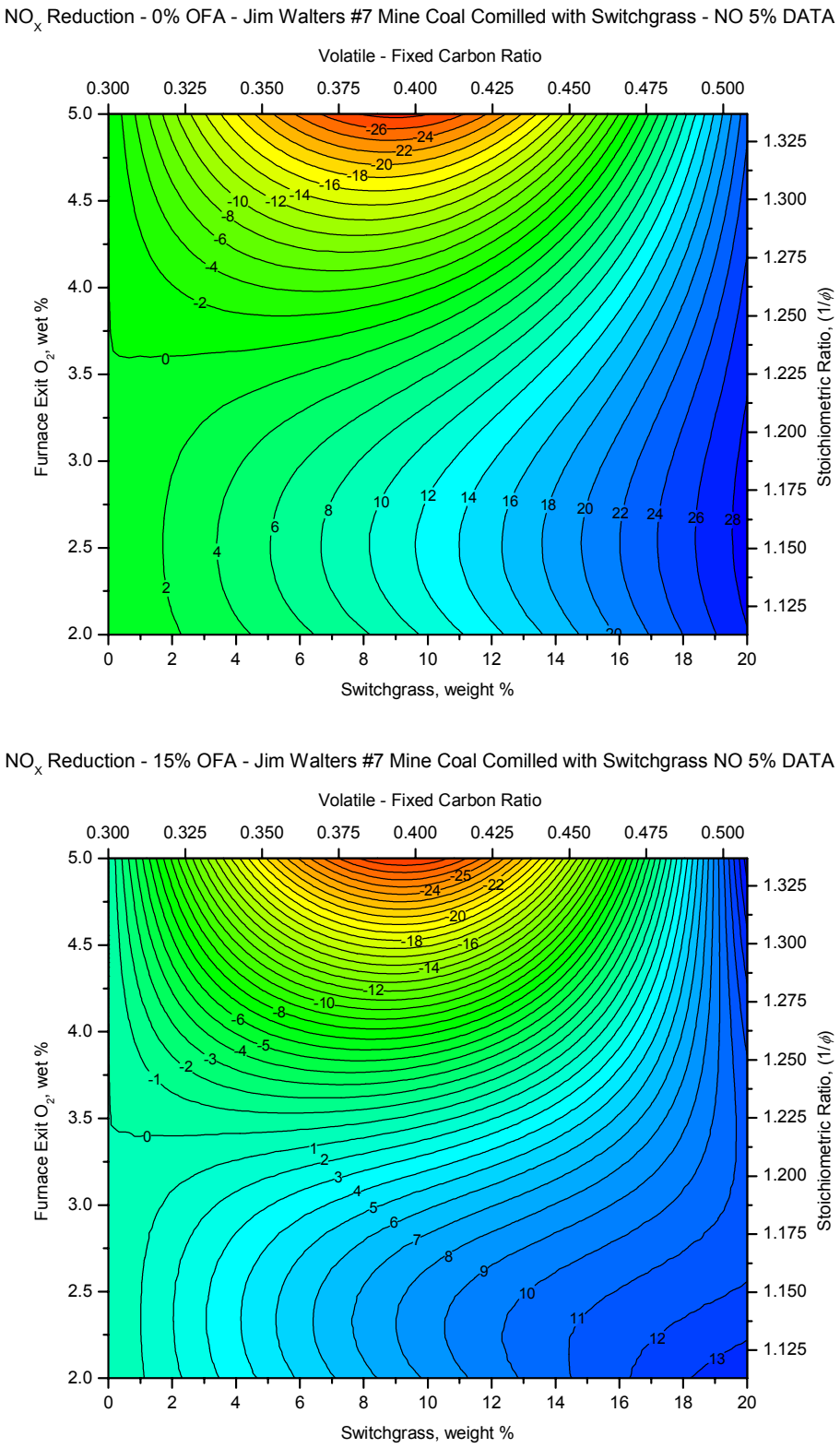

Figure 3-26. NO_X reductions from comilling SG with JW coal, 0% and 15% OFA.

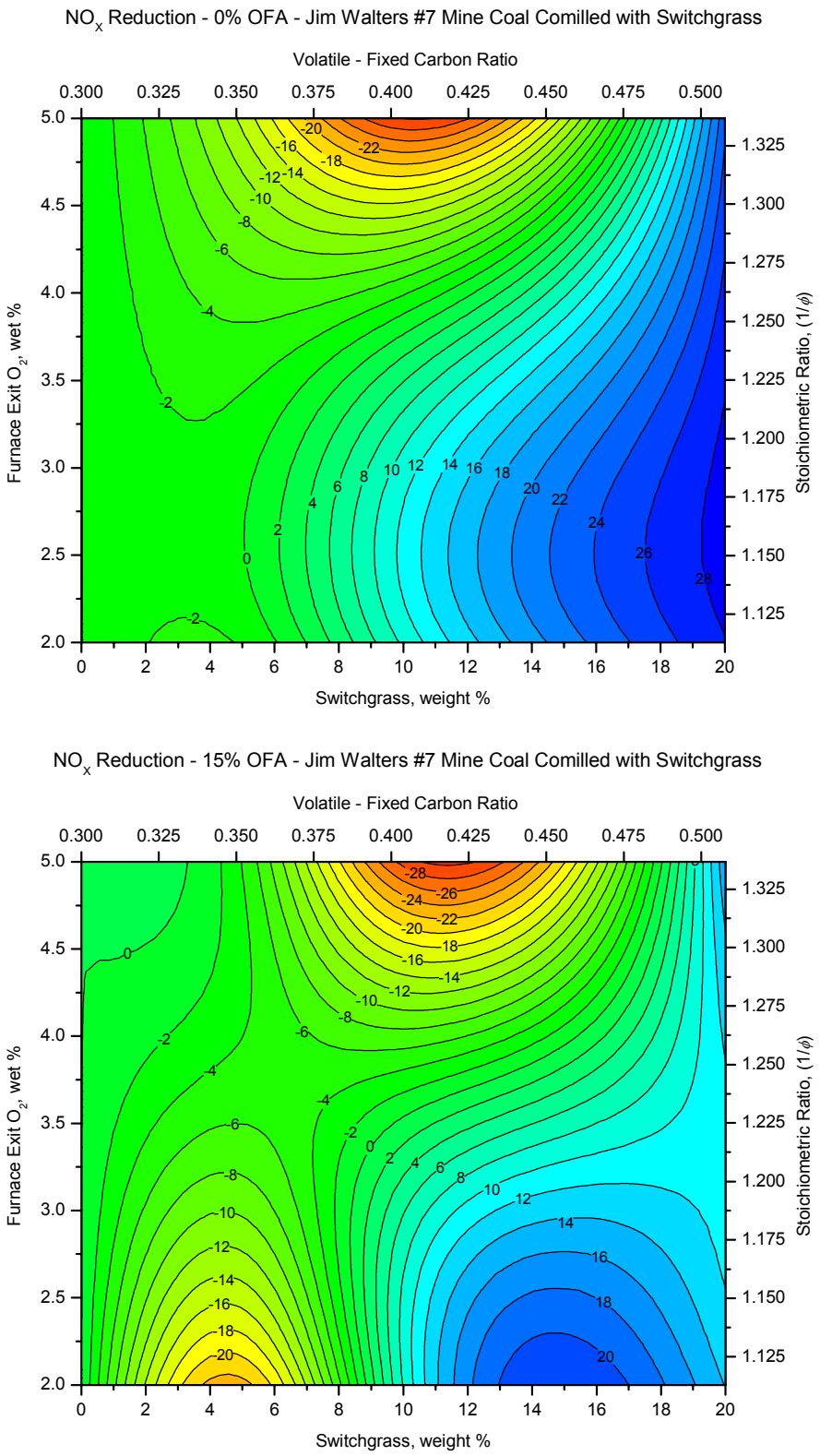

Figure 3-27. NO_X reductions from comilling SG with JW coal, 0% and 15% OFA. Results for 5% biomass are included.

Comilled SD, but with lower NO_X reductions at higher values of FEO and greater increases in NO_X emissions at lower values of FEO.

With PR coal, and 0% OFA, adding more SG tends to enhance NO_X reduction, particularly at lower values of FEO, different from the behavior measured doe comilled SD. However, at 15% OFA, NO_X reductions from the addition of SG or SD appear quite similar with slightly higher NO_X reductions measured for SG.

Adding comilled SG to JW coal provides the potential for much greater NO_X reductions than with SG, but only for 0% OFA and amounts of SD greater than 10 weight %. At 15% OFA, NO_X production is increased by 25% over that seen for 100% coal firing at the same relative amount of biomass addition that decreased NO_X emissions by 20% with comilled SD. As with comilled SD, when NO_X reductions from testing with 5 weight % SG are added, more structure is apparent, as shown in Figure 3-27. At 0% OFA, differences are insignificant. However, at 15% OFA, the effect of fitting a surface through four NO_X emissions curves (0%, 5%, 10%, and 20% SD) as opposed to three curves suggests that NO_X reductions up to 20% are possible at high levels of SG addition for FEO less than 3.5%.

<u>3.2.4.1.3.3 UBC Emissions from Cofiring by Comilling SD and SG with Coal</u>. Figures 3-28 through 3-32 present the results of UBC measurements made on isokinetically extracted samples of fly ash obtained during each major test condition. During the testing period of each fuel, fly ash was sampled using EPA Method 17. In this method, a fly ash sample is collected from the flue gas with a filter held in the duct at duct temperature while extracting an isokinetic stream through a nozzle. This is the best method to obtain a representative sample of fly ash and to calculate the flow rate of fly ash through the duct. These fly ash samples were collected, weighed for the method, ground in a mortar and pestle, and then analyzed for carbon. This is not the loss-on-ignition measurement of fly ash that is frequently used, but a more precise method that specifically and quantitatively identifies the carbon present. In this method, carbon is measured with a CHN analyzer that first pyrolyzes a 5 mg. sample of ash at 1000°C in 100% O_2, then analyzes the off-gases from pyrolysis for CO_2 (carbon), converts NO_X to N_2, and measures N_2 (for nitrogen), and water (for hydrogen).

As these results show, the complex behavior seen in NO_X emissions is not mirrored in UBC measurements. In general, adding comilled biomass serves to reduce UBC. However, with JR coal at 15% OFA, UBC emissions were uniformly increased by the addition of any comilled biomass. It should be noted that UBC emissions for PRB coals are generally very low, and UBC emissions for JR coal are uniformly very low (for 100% coal, < 0.25% for 0% OFA and <0.2% for 15% OFA).

Higher UBC emissions were measured for other coals, and the addition of comilled biomass did reduce UBC emissions for GL and JW coals. For GL coal at 15% OFA, the addition of comilled biomass reduced UBC by roughly a factor of two and greater reductions were also observed. At 3.5% FEO, UBC for 100% GL coal is ~ 5%. Adding 10% comilled switchgrass reduced UBC to 1%. This degree of reduction was the greatest measured. With JW coal, increasing the amount of comilled SD reduced UBC emissions better than increasing the amount of comilled SG. Adding 20% SG increased UBC emissions slightly beyond those measured for 100% coal.

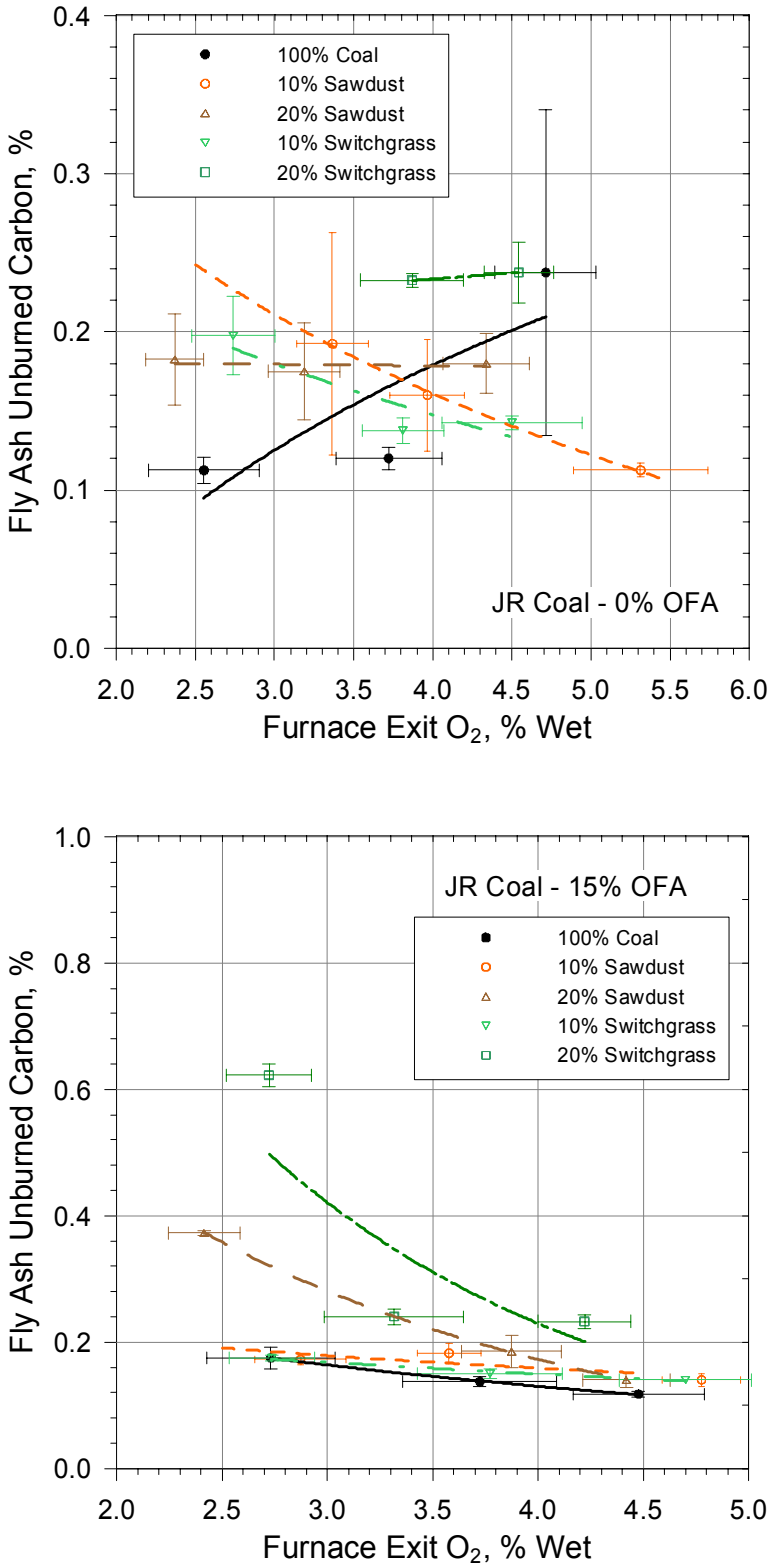

Figure 3-28. UBC emissions from comilling SD and SG with JR coal, for 0% OFA (top) and for 15% OFA (bottom).

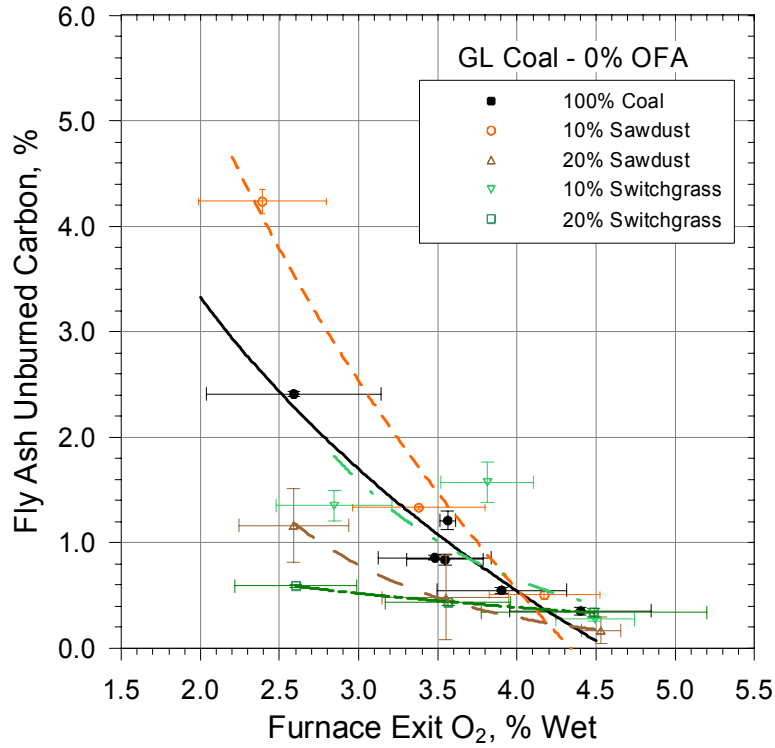

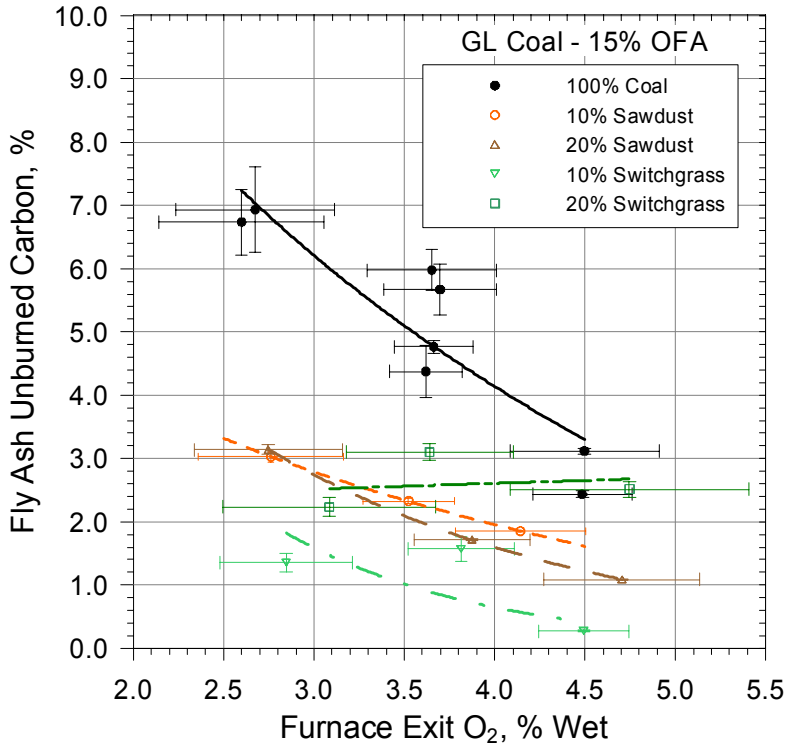

Figure 3-29. UBC emissions from comilling SD and SG with GL coal, for 0% OFA (top) and for 15% OFA (bottom).

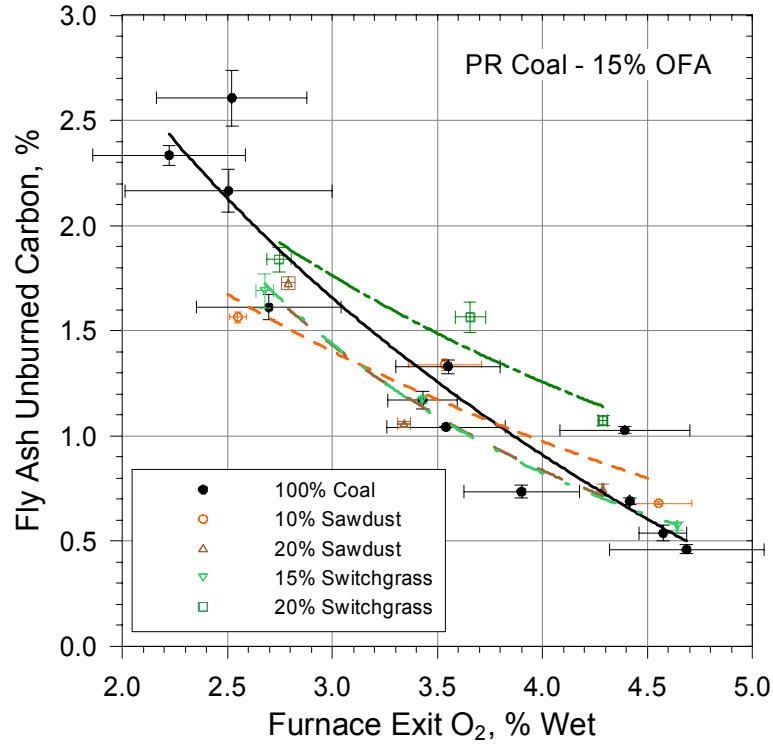

(a)

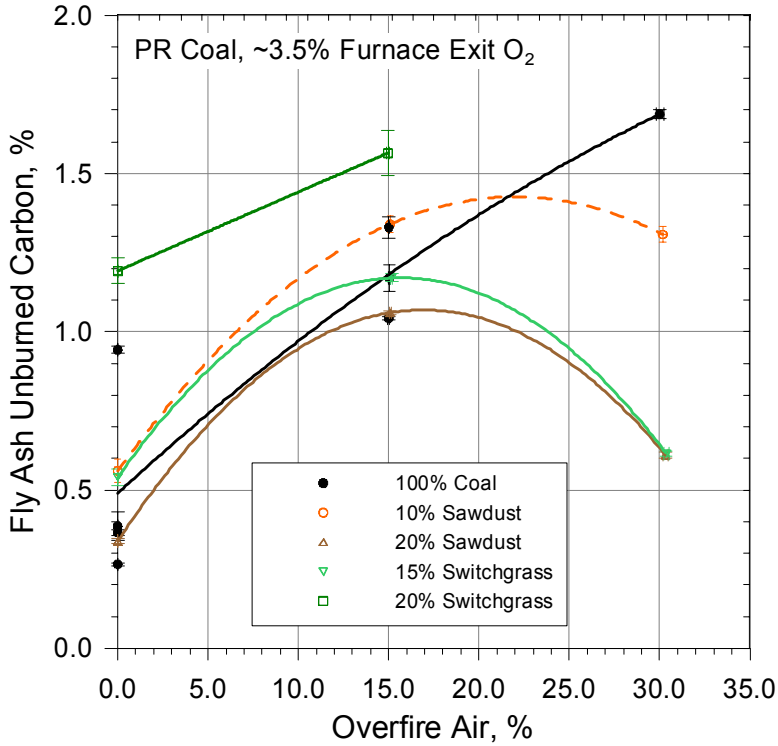

(b)

Figure 3-30. UBC emissions from comilling SD and SG with PR coal, (a) for 15% OFA, varying FEO and (b) for ~3.5% FEO, varying OFA.

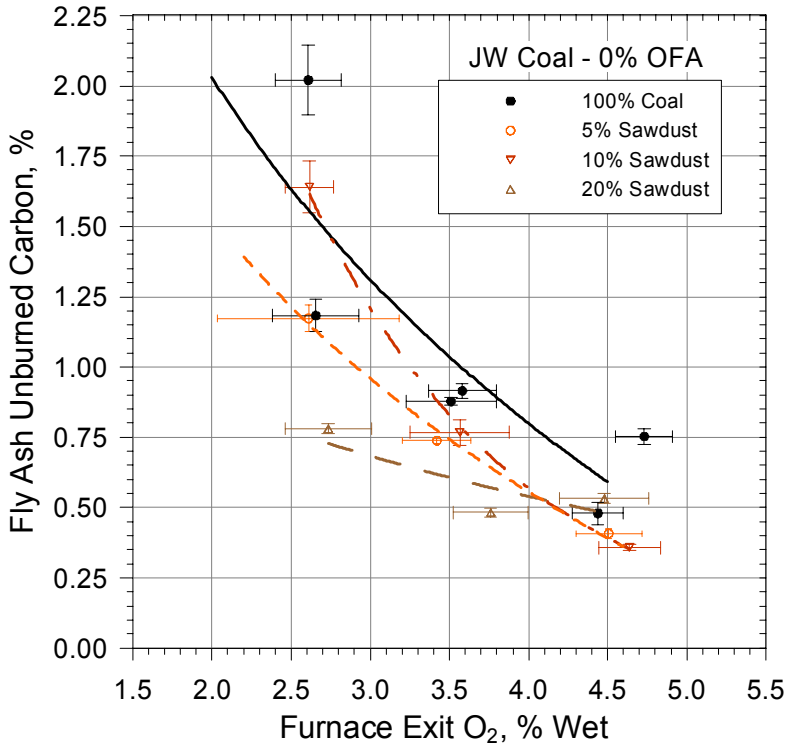

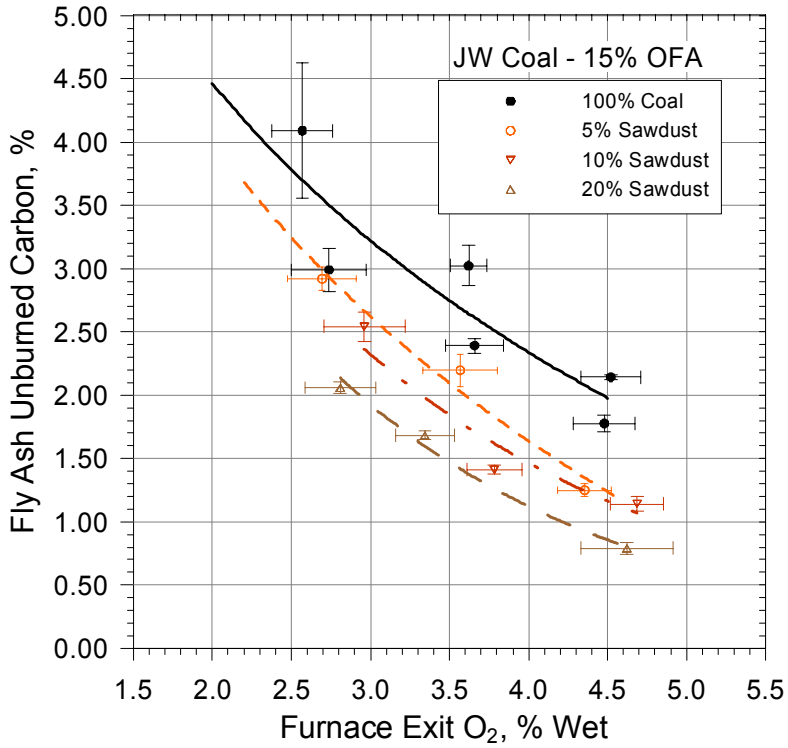

Figure 3-31. UBC emissions from comilling SD with JW coal, 0 and 15% OFA.

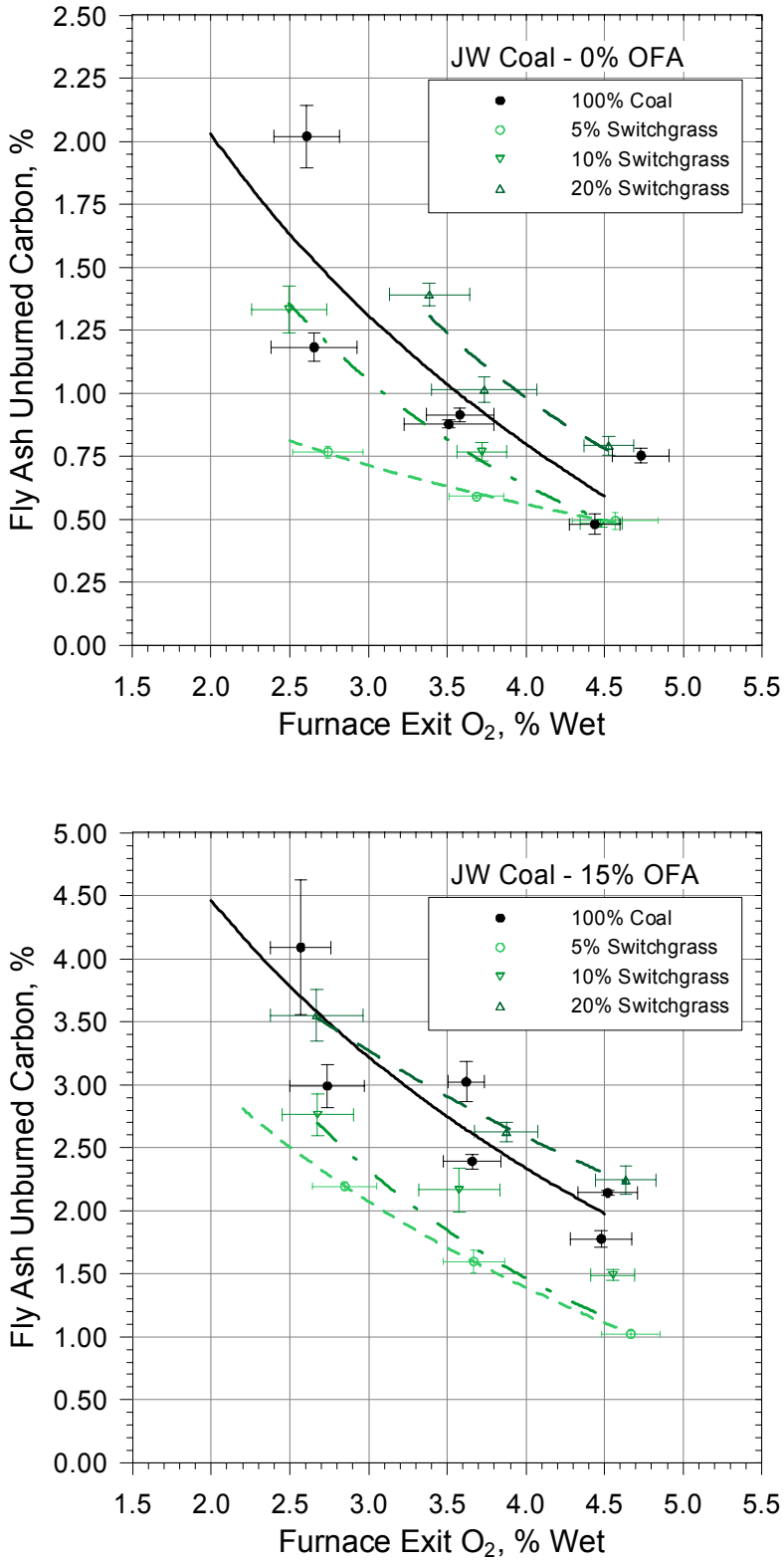

Figure 3-32. UBC emissions from comilling SG with JW coal, 0 and 15% OFA.

UBC emissions from PR coal were not significantly affected by the addition of comilled biomass. For PR coal, because UBC measurements were made at 30% OFA, it appears that increasing OFA beyond 30% tends to decrease UBC emissions for coal with comilled biomass than for 100% PR coal.

Recall that a compendium of UBC results for every test is included in Appendix A. Therefore, for details of individual measurements, the reader is referred to the appendices of this report.

3.2.4.1.3.4 NO_X Reductions from Cofiring GL Coal with Simulated Poultry Litter. Chicken litter is an interesting fuel because the amount of fuel nitrogen in this biomass can exceed 5%. Various attempts were made to secure several tons of dry chicken litter but none could be obtained locally or by MESA Reduction Engineering and Processing, Inc. Large quantities of relatively wet chicken litter are readily available. However, wet chicken litter has a strong odor and in a densely populated urban area such as the area that surrounds Southern Research, such odor is unacceptable. Further, wet chicken litter contains chicken urine and feces, which can be a biohazard to technicians who would spread the wet litter out to dry or mix the dried material with coal. When dry, dust from this material could constitute a breathing hazard for workers and nearby residents.

After determining that cofiring coal with chicken litter was not a viable approach, we decided to simulate the cofiring coal with chicken litter by comilling GL coal with sawdust (to simulate clean chicken litter) and approximate the fuel nitrogen in chicken litter with gaseous or liquid ammonia injected into the primary air line, just upstream of the single-register burner. Discussions with a local ammonia supplier revealed that liquid ammonia was the best choice, as the injection of gaseous ammonia would require large heated tanks to maintain the delivery rates necessary for testing. Accordingly, liquid ammonia was injected into the primary air line where it was allowed to flash into gaseous ammonia.

The configuration that was used for testing consisted of a ~350 lb tank of liquid ammonia mounted on a calibrated scale that reported the weight of the tank to the combustor data acquisition system. Instructions on each tank required horizontal mounting for proper delivery of liquid ammonia and a cradle was fabricated to hold each tank. Pressure within the tank was used to convey liquid ammonia through a liquid flow meter mounted at the tank discharge point that was connected to a coiled stainless steel transport line that discharged into the primary air line. Liquid ammonia was flashed to gaseous ammonia in the coiled section of the stainless steel line that was kept submerged in a warm water bath. Throughout the test, problems were continually encountered with uneven ammonia delivery to the liquid flow meter and some tests had to be curtailed. Extended conversations with the ammonia supplier revealed that the instructions printed on the side of each tank were in error and that the tanks should have been mounted in an upright position. Once the tanks were mounted upright, the delivery problems were corrected. Unfortunately, the test was nearly over when this discovery was made.

The results of ammonia testing were not as comprehensive as was planned, however, sixteen separate ammonia injection tests were completed for 100% GL coal, and GL coal with 5%, 10%, and 20% weight percent sawdust in Test GL-11. The results of these tests are presented in Table 3-12. In this table, FEO, NO_X emissions data, ammonia injection rate and equivalent fuel N

Table 3-12. Results of increasing fuel nitrogen by ammonia addition in Test GL-11.

Fuel	FEO Avg. S.D. %	NO_X @ 3% O_2 Avg. S.D. ppmv	NO_X @ 3% O_2 Calc., No NH_3[1] ppmv	Δ %	Ammonia Feed Rate lb/h	Equiv. Fuel N %
0% OFA						
100% Coal					0.0	1.70
	3.08 ± 0.14	632 ± 59	515	**19**	6.1	3.49
	2.88 ± 0.14	618 ± 80	503	**19**	13.1	5.46
5% SD					0.0	1.62
	3.27 ± 0.13	715 ± 67	523	**27**	9.6	4.35
10% SD					0.0	1.53
	3.33 ± 0.15	741 ± 59	553	**25**	7.0	3.51
	3.02 ± 0.09	550 ± 45	529	**4**	10.2	4.37
	3.11 ± 0.17	728 ± 70	536	**26**	13.4	5.20
20% SD					0.0	1.43
	3.13 ± 0.14	578 ± 47	469	**19**	7.2	3.38
	2.89 ± 0.15	586 ± 41	457	**22**	10.8	4.31
			Average[2]	**22**		
15% OFA						
5% SD					0.0	1.70
	3.64 ± 0.16	359 ± 21	319	**11**	2.2	2.25
	3.39 ± 0.20	328 ± 16	304	**7**	11.4	4.82
	3.63 ± 0.17	342 ± 27	319	**7**	17.2	6.36
10% SD					0.0	1.62
	3.44 ± 0.13	299 ± 17	292	**3**	0.8	1.77
	3.05 ± 0.22	286 ± 23	263	**8**	10.3	4.42
20% SD					0.0	1.43
	4.14 ± 0.17	355 ± 12	321	**9**	0.9	1.68
	3.29 ± 0.13	282 ± 19	267	**5**	2.5	2.13
	3.50 ± 0.18	332 ± 21	280	**16**	12.0	4.63
			Average	**8**		

[1] From curve fits to test data taken with no NH_3 injection
[2] Excluding low value of 4%

level (from coal, sawdust, and ammonia) are shown. Also presented for each of the 16 tests are expected NO_X emissions if ammonia was not injected. These estimations were derived from curve fits to NO_X emissions data taken during periods when ammonia was not injected. By comparing estimated NO_X emissions for no ammonia injection with NO_X emissions measured during periods of ammonia injection an estimate can be made of the effect of increasing fuel nitrogen through ammonia injection. As Table 3-12 shows, with 15% OFA, NO_X emissions were only slightly increased. That is, NO_X emissions were observed to increase with ammonia injection, but frequently by less that the uncertainty (1 standard deviation) in the measurement of the NO_X concentration. Indeed, with a mixture of 95% coal and 5% sawdust, when 17 lb/h of ammonia was added (equivalent to 6.4% fuel N), NO_X emissions were increased by only 7%, while the uncertainty in the NO_X measurement was 8% of the measurement.

With 0% OFA, NO_X emissions were noticeably increased by the addition of ammonia. As Table 3-12 shows, with the exception of one test period (a short test of less than 0.5 hours), NO_X emissions were increased by an average of 22% while the results in Table 3-12 show that the average uncertainty on the NO_X measurements was 9% of the measurement. The increase in NO_X emissions does not necessarily correlate with the rate of ammonia injection which may be due, in part, to variations in the amount of ammonia injected from moment to moment. However, there is no doubt that in the absence of overfire air, NO_X emissions are increased by the addition of ammonia.

3.2.4.1.4 Results of Cofiring Tests by Comilling, Core Injection, and Side Injection Three schemes for biomass cofiring with the single-register burner were tested with PR coal. Test PR-1 employed cofiring by comilling (location 1 in Figure 3-5), test PR-3 performed cofiring by injecting of biomass through the center of the single-register burner (location 2 in Figure 3-5), and test PR-4 performed cofiring by injecting of biomass through the side of the pilot-scale furnace into the single-register burner (location 3 in Figure 3-5). Two of these modes (comilling and center-burner injection) were tested with JR coal in Tests PR-7 and PR-8, respectively. The methodology for performing these tests and the burner modifications required were discussed earlier in section 3.2.3.1. Therefore we will present NO_X reduction results below for each test series and follow these results with a presentation and discussion of UBC measurements.

So that NO_X reductions can be referenced to NO_X concentrations, Figures 3-33 through 3-36 present graphs of curve fits to baseline NO_X emissions results for 100% pulverized coal firing of PR and JR coals taken as baseline NO_X emissions data during each of these tests. NO_X emissions are shown as a function of FEO for 0% and 15% OFA. The curve fits shown in these figures are tabulated in Table 3-13.

<u>3.2.4.1.4.1 Biomass Particle Size Distribution</u>. Figures 3-37 through 3-40 present particle size distributions of SD and SG that was injected through and into the single-register burner in tests PR-3 and PR-4, and tests JR-7 and JR-8. From a modeling standpoint, these distributions are required to help estimate biomass burnout times in the furnace. From a practical standpoint, fairly finely divided biomass is needed so that it will feed and transport easily through the eductor-pipe system used to convey biomass to the single-register burner in the base of pilot-scale furnace. In Test JR-8, SD from Lot 3 was used and from Figure 3-39, the MMD of this sawdust was 470 μm while the SD from Lot 2 had an MMD of 226 μm. In Test JR-8, the SD

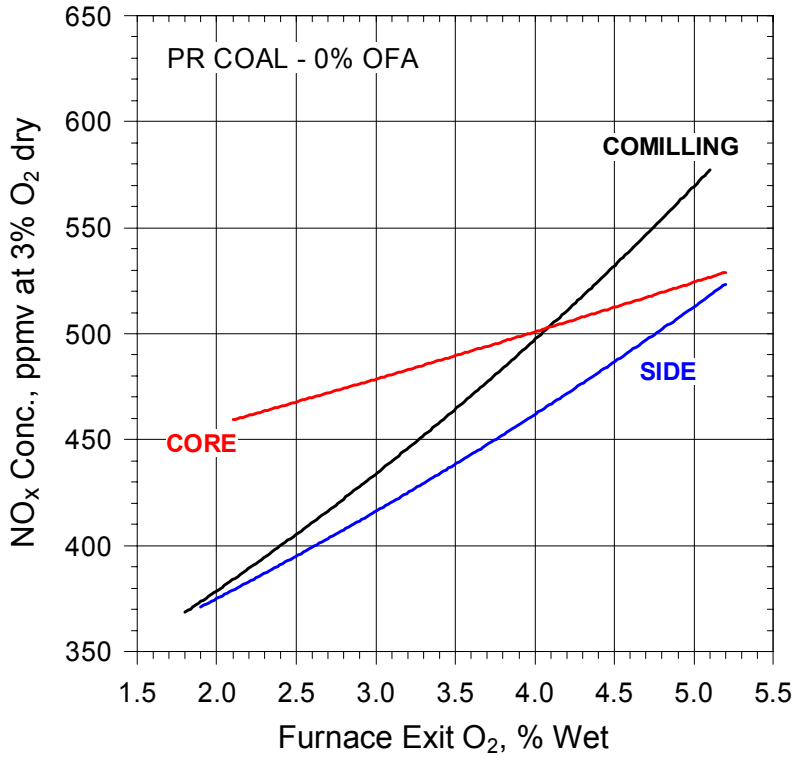

Figure 3-33. Baseline NO_X emissions for 0% OFA, PR coal.

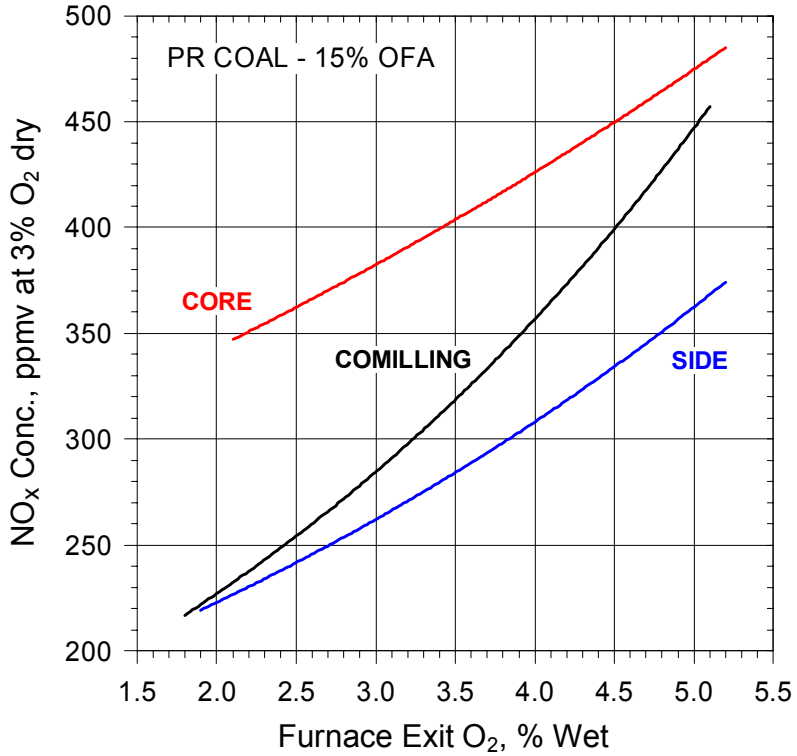

Figure 3-34. Baseline NO_X emissions for 15% OFA, PR coal.

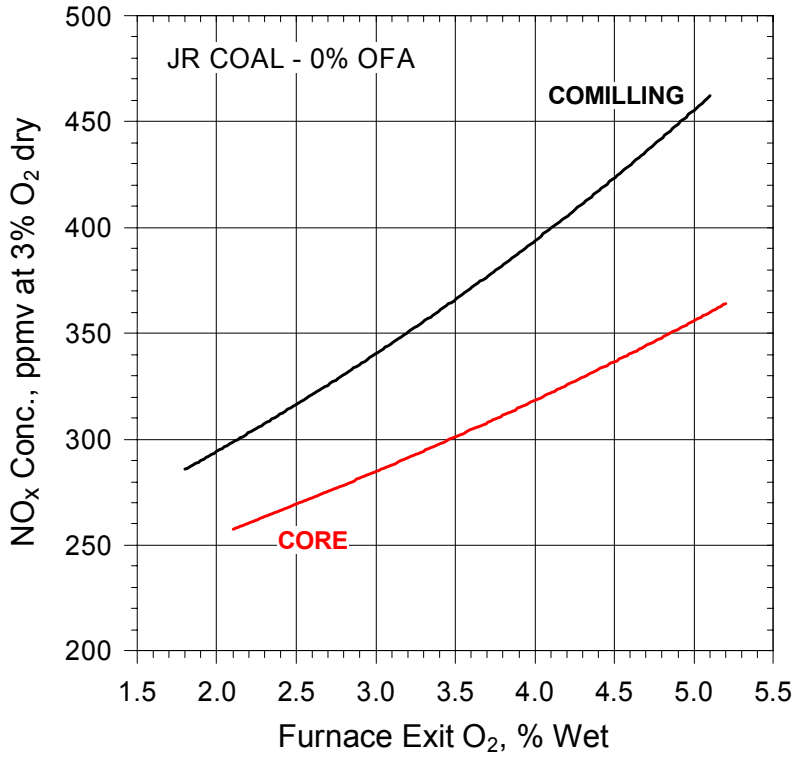

Figure 3-35. Baseline NO_X emissions for 0% OFA, JR coal.

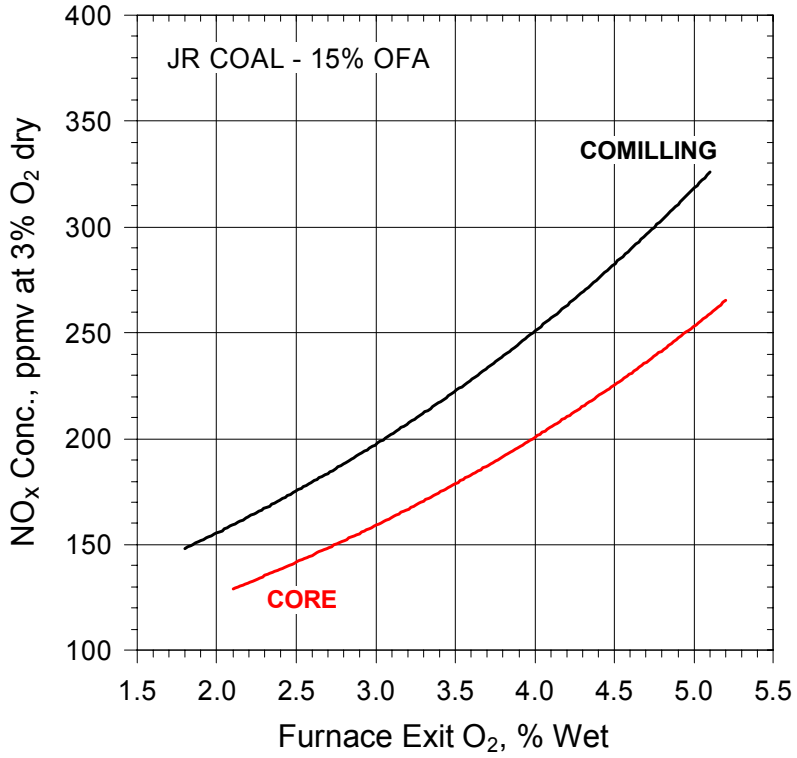

Figure 3-36. Baseline NO_X emissions for 15% OFA, JR coal.

Table 3-13. Fit parameters for the NO_X emissions curves in Figures 3-33 through 3-36.

TEST	Cofiring	Fit*	Fitting Parameters	
0% OFA			A	B
JR-7	Comill	E	0.145559	219.918
JR-8	Center	E	0.111516	203.781
PR-1	Comill	E	0.135906	288.624
PR-3	Center	E	0.045562	417.421
PR-4	Side	E	0.104231	304.456
15% OFA				
JR-7	Comill	E	0.238524	96.5527
JR-8	Center	E	0.232116	79.3175
PR-1	Comill	E	0.225617	144.683
PR-3	Center	E	0.107907	276.709
PR-4	Side	E	0.161885	161.341

*E = Exponential fit: NO_X (ppm) = $B \bullet e^{(A \bullet \%FEO)}$

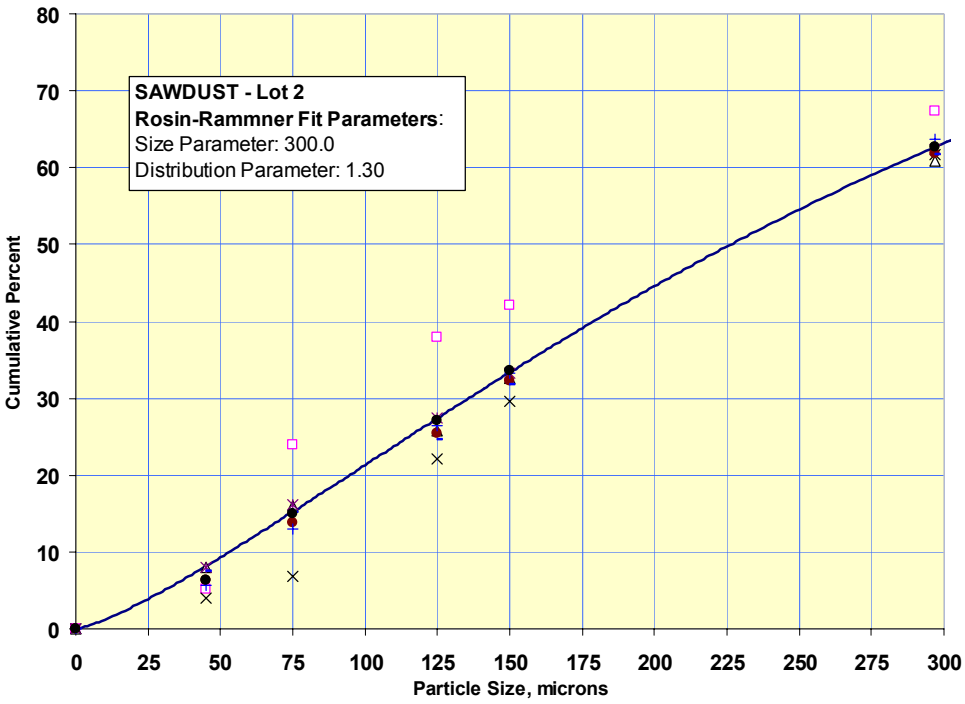

Figure 3-37. Cumulative particle size distribution for the sawdust injected into the single-register burner in Tests PR-3 and PR-4.

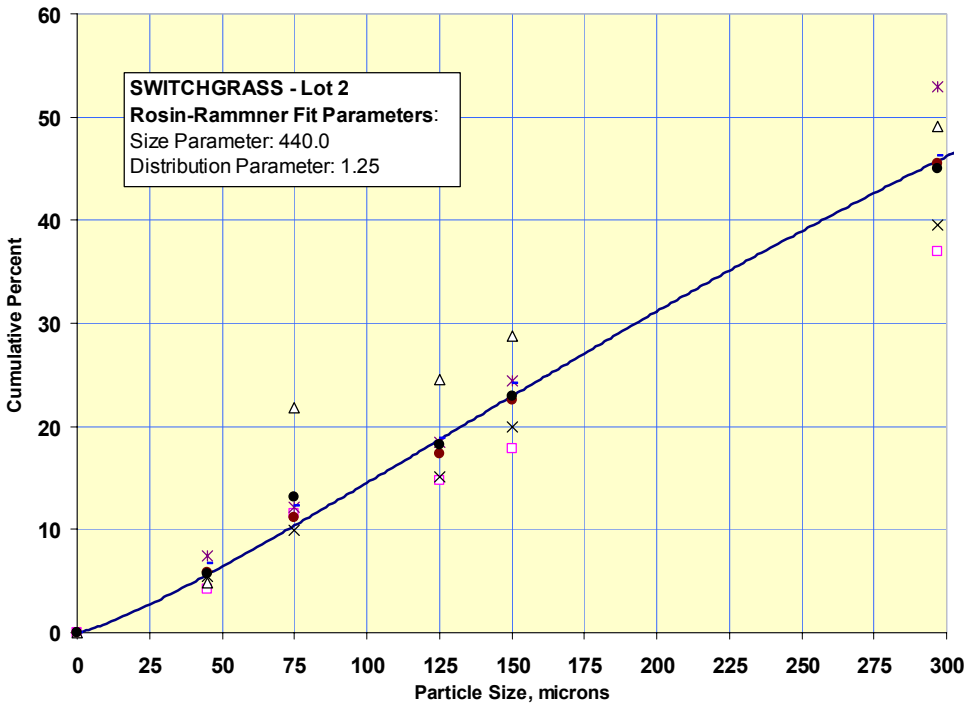

Figure 3-38. Cumulative particle size distribution for the switchgrass injected into the single-register burner in Tests PR-3 and PR-4.

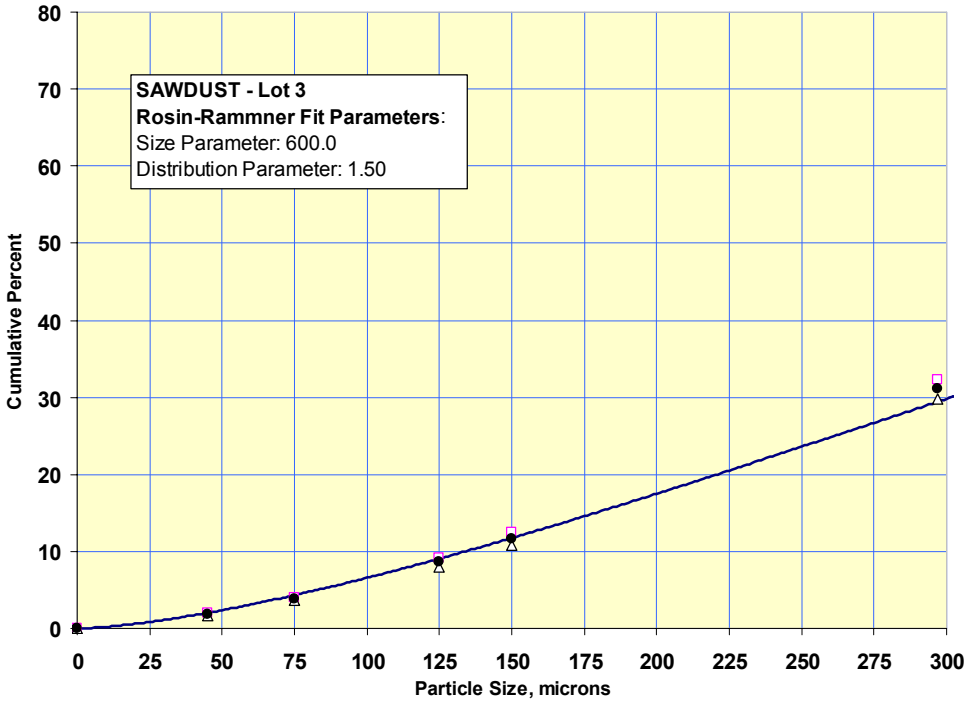

Figure 3-39. Cumulative particle size distribution for the sawdust injected into the single-register burner in Test JR-8.

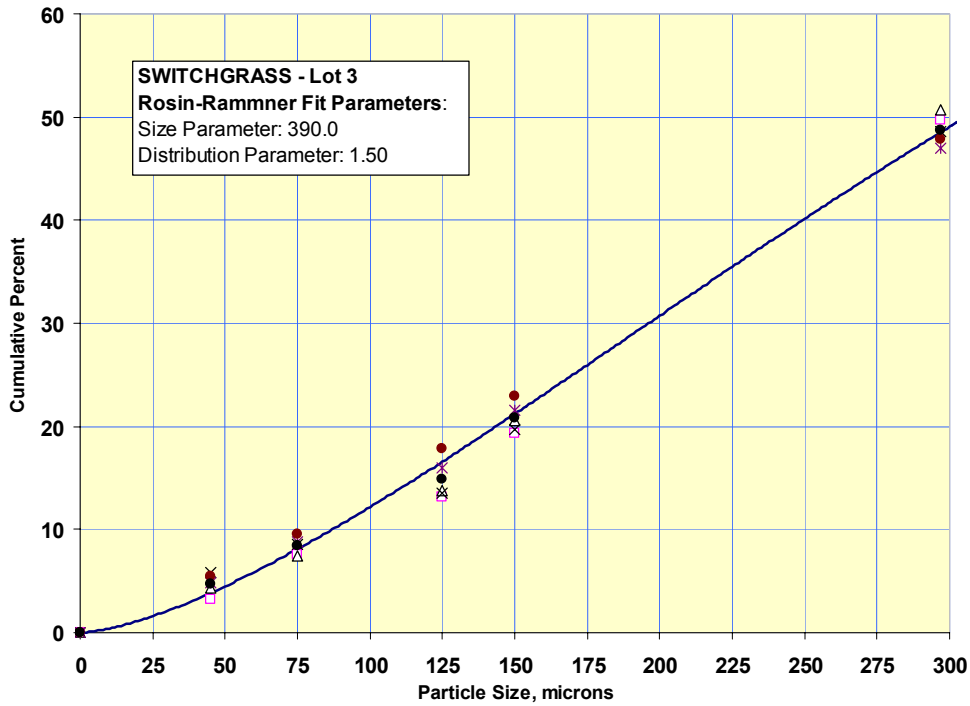

Figure 3-40. Cumulative particle size distribution for the switchgrass injected into the single-register burner in Test JR-8.

from Lot 3 could not be fed at a rate sufficient to maintain 20 weight % cofiring because of the larger average size of this biomass. For this test, the maximum feed rate that could be maintained corresponded to cofiring at a 15 weight % of SD. No problems were encountered in feeding SD from Lot 2 or SG from Lots 2 or 3 at a maximum cofiring level of 20 weight %.

<u>3.2.4.1.4.2 NO_X Reductions from Cofiring SD with JR and PR Coal</u>. Table 3-14 and Figures 3-41 through 3-43 provide a presentation of NO_X reduction results in a format similar to that employed earlier for comilled SD. For details of NO_X reductions from cofiring with comilled SD, refer to Figures 3-17 (Test JR-7) and 3-19 (Test PR-1), above. As for comilling, Tables 3-13, 3-9, and 3-10 also provide assistance in recovering NO_X emissions, stoichiometric ratio, V/FC ratio, and Fuel N from Figures 3-41 through 3-43.

For JR coal, Table 3-14, and Figures 3-17 and 3-41show that when SD is injected through the center of the single-register burner, NO_X reductions are lessened, compared to cofiring by comilling. For 0% OFA, both maximal and minimal NO_X emissions were observed at a cofiring level of ~10 weight % SD. For low values of FEO, (< 2.5%) NO_X emissions were significantly decreased. However, for FEO values greater than 4.5%, NO_X emissions were increased up to 25% over those measured for 100% coal. With center-burner cofiring, the addition of overfire air served to dramatically increase NO_X emissions. At a 10% level of biomass addition, for low values of FEO (~<3.5%), NO_X emissions increased up to 56% above those measured for 100% coal firing. It should be noted that during this test, SD cofiring had to be limited to a maximum of 15 weight % because of the coarseness of the SD. It is possible that NO_X emissions were

Table 3-14. NO_X reductions from cofiring PR and JR coals for comilled, center, and side injection of SD.

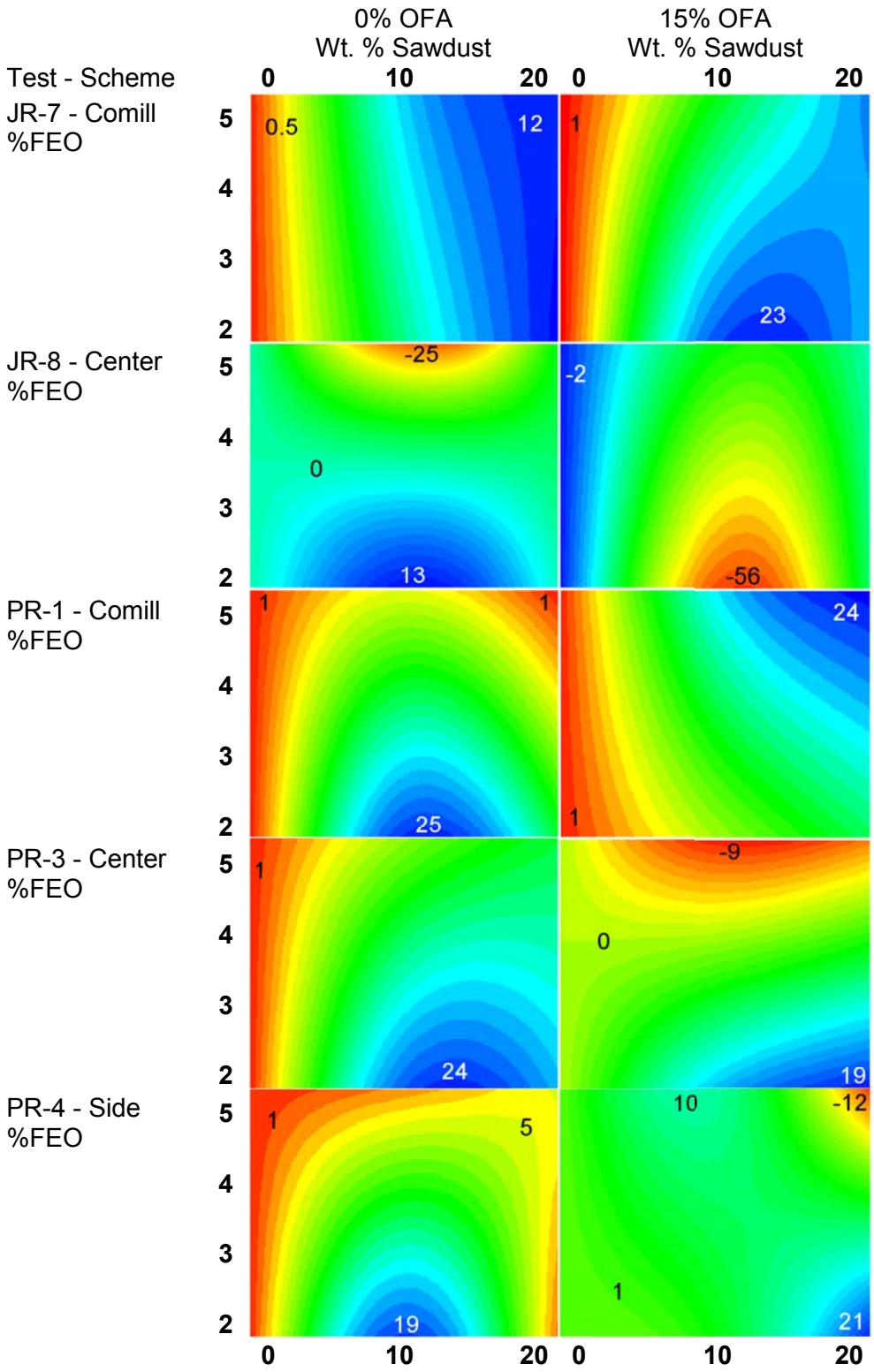

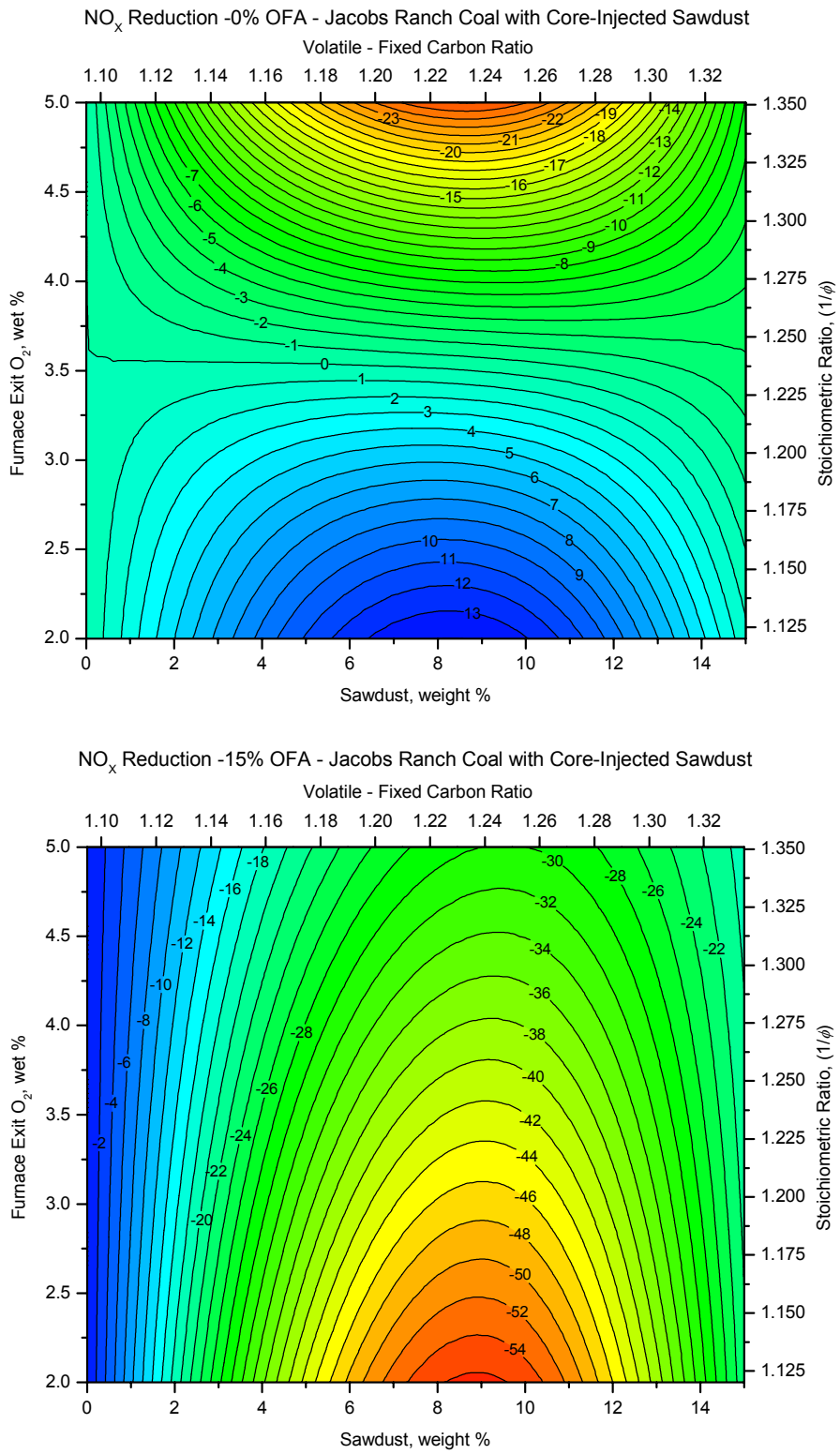

Figure 3-41. NO_X reductions from cofiring SD with JR coal by injecting SD through the center of the single-register burner, 0% and 15% OFA.

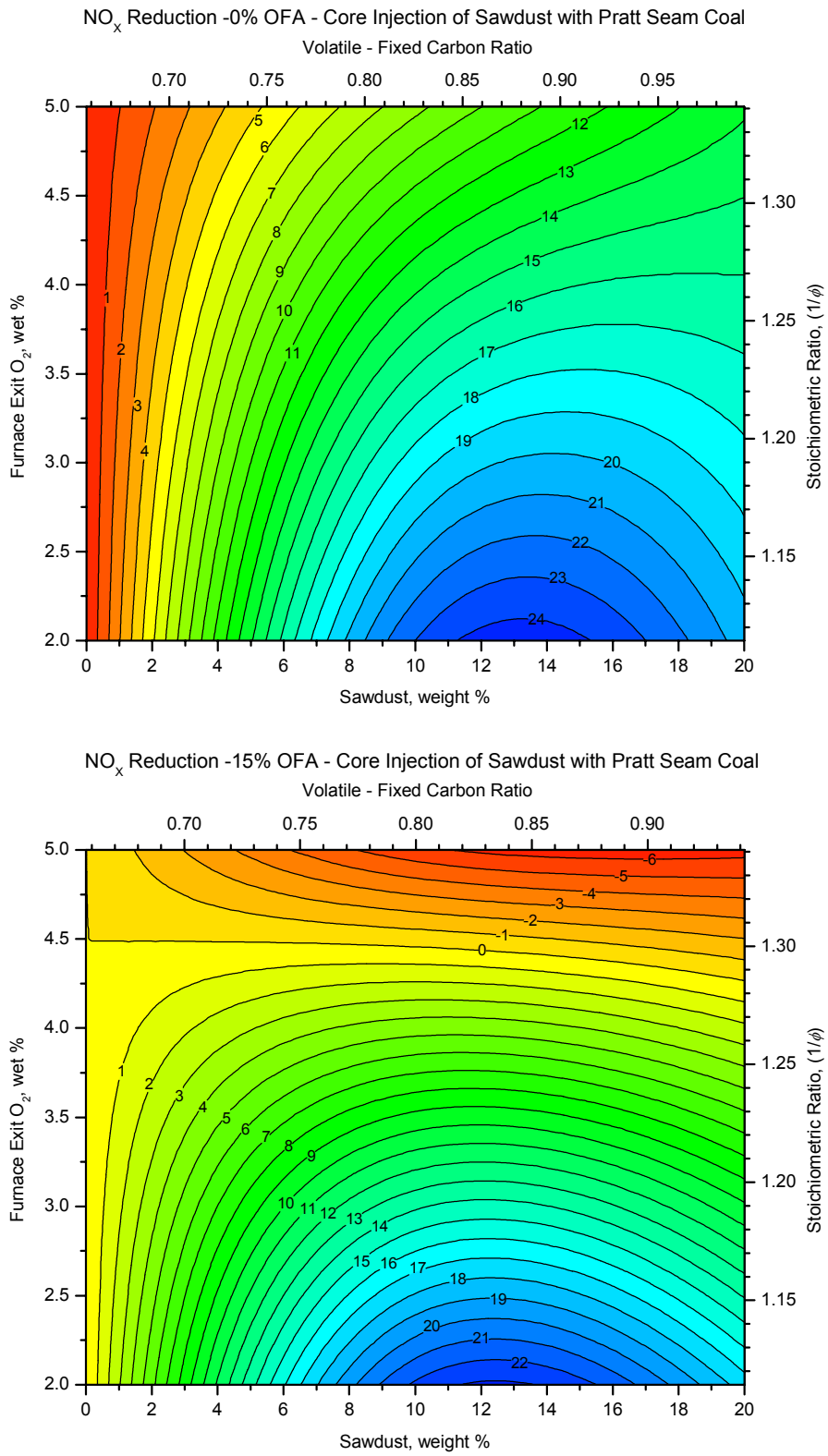

Figure 3-42. NO_X reductions from cofiring SD with PR coal by injecting SD through the center of the single-register burner, 0% and 15% OFA.

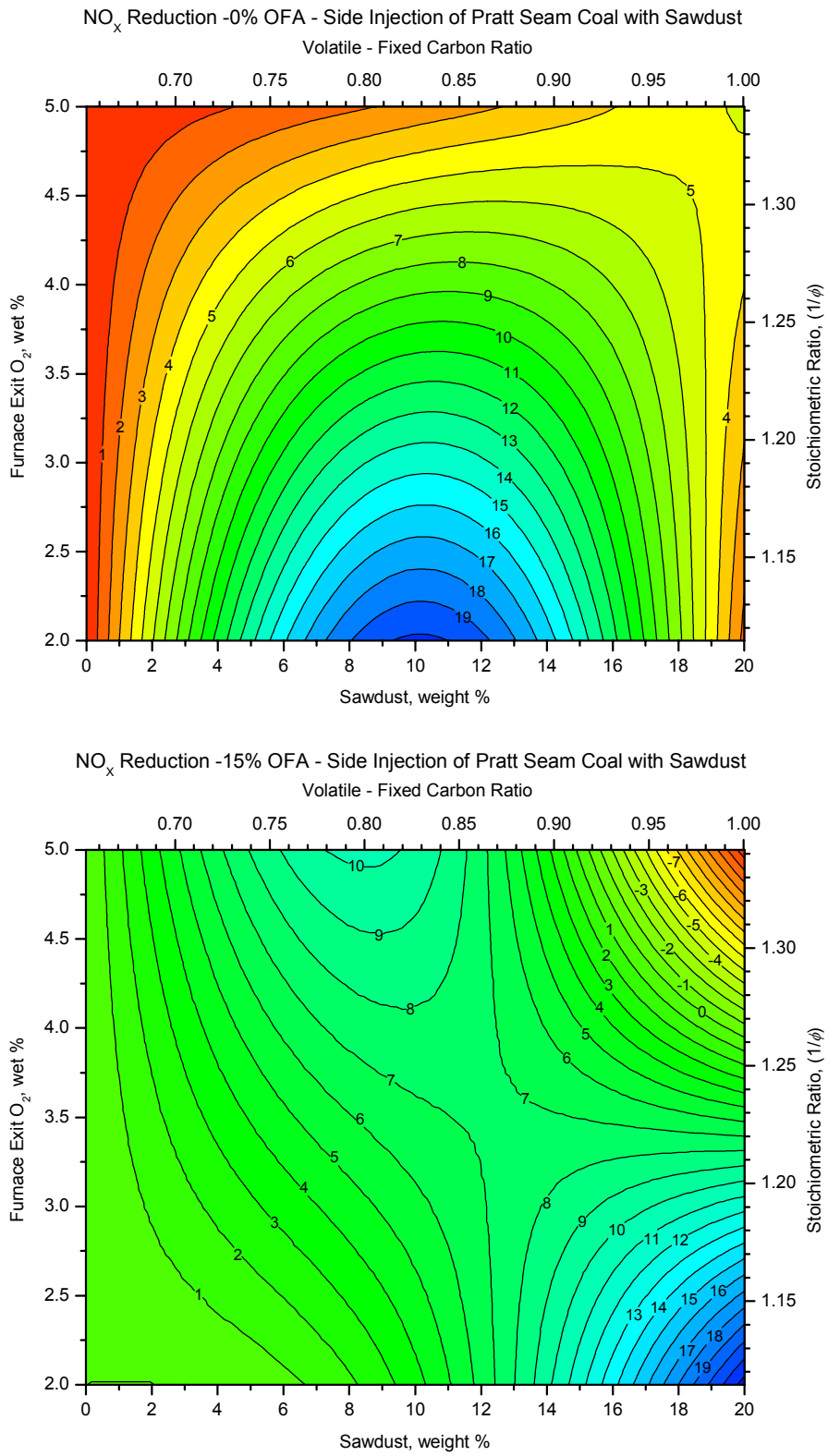

Figure 3-43. NO_X reductions from cofiring SD with PR coal by injecting SD from the side into the exit of the single-register burner, 0% and 15% OFA.

affected by larger than normal (i.e., ~ 6 mm) toothpick-like pieces of wood in the processed sawdust.

With PR coal, cofiring of SD by center-burner injection or by injection from the side into the PC flame at the exit of the single-register burner did not produce the very large increases in NO_X emissions that were measured for JR coal. In fact, as Table 3-14 shows, at 0% OFA, cofiring by comilling, center-burner injection, or side injection of processed SD produced similar NO_X reductions for the range of FEO tested and the amounts of SD added. As with JR coal, adding 15% OFA did significantly modify the locations of greatest NO_X reductions and increases. Highest NO_X reductions were still measured for SD addition at greater than 10 weight %. However, for center-burner or side injection of biomass, increases in NO_X emissions were observed at high values of FEO (the reverse of what was observed for comilling) and NO_X reductions were greatest at low values of FEO (again, the reverse of what was observed for comilling).

3.2.4.1.4.3 NO_X Reductions from Cofiring SG with JR and PR Coal. Table 3-15 and Figures 3-44 through 3-46 provide a presentation of NO_X reduction results in a format similar to that employed earlier for comilled SG. For details of NO_X reductions from cofiring with comilled SG, refer to Figures 3-23 (Test JR-7) and 3-25 (Test PR-1), above. As for comilling, Tables 3-13, 3-9, and 3-10 also provide assistance in recovering NO_X emissions, stoichiometric ratio, V/FC ratio, and Fuel N from Figures 3-44 through 3-46.

For JR coal, Table 3-15, and Figures 3-23 and 3-44 show that when SG is injected through the center of the single-register burner, NO_X reductions are generally lessened, compared to cofiring by comilling. For 0% OFA, increases in NO_X emissions of 30% were measured where the greatest reductions in NO_X emissions were measured with comilled SG. In contrast to the results observed for comilled SG, at very low values of FEO large NO_X reductions do appear possible for JR coal. With 15% OFA, slight decreases in NO_X emissions were seen for less that 10 weight % SG, but increasing the amount of injected SG only increased NO_X emissions, regardless of the value of FEO.

With PR coal and no OFA, for center-burner or side injection, NO_X reductions were improved with added SG. For center-burner injection, at high levels of biomass addition and high values of FEO, NO_X emissions increased by as much as 13% however, for low values of FEO, NO_X emissions were reduced by as much as 28%. With no OFA and side injection of SG, NO_X emissions were increased above those measured for baseline cofiring for levels of SG addition of less than 10 weight %. As for center-burner injection, at high levels of SG addition and at low FEO, NO_X emissions were substantially reduced.

With PR coal, 15% OFA, and center-burner injection of SG, the landscape of NO_X reductions appears similar to that determined for 0% OFA. However, at high levels of FEO, increases in NO_X emissions are less and NO_X reductions are less than those measured for 0% OFA. With side injection at 15% OFA, NO_X emissions were generally increased above those measured for baseline 100% PR coal. At 10 weight % SG addition, NO_X emissions increased to greater than 30% above those measured for baseline 100% PR coal for FEO greater than 3.5%.

Table 3-15. NO_X reductions from cofiring PR and JR coals for comilled, center, and side injection of SG.

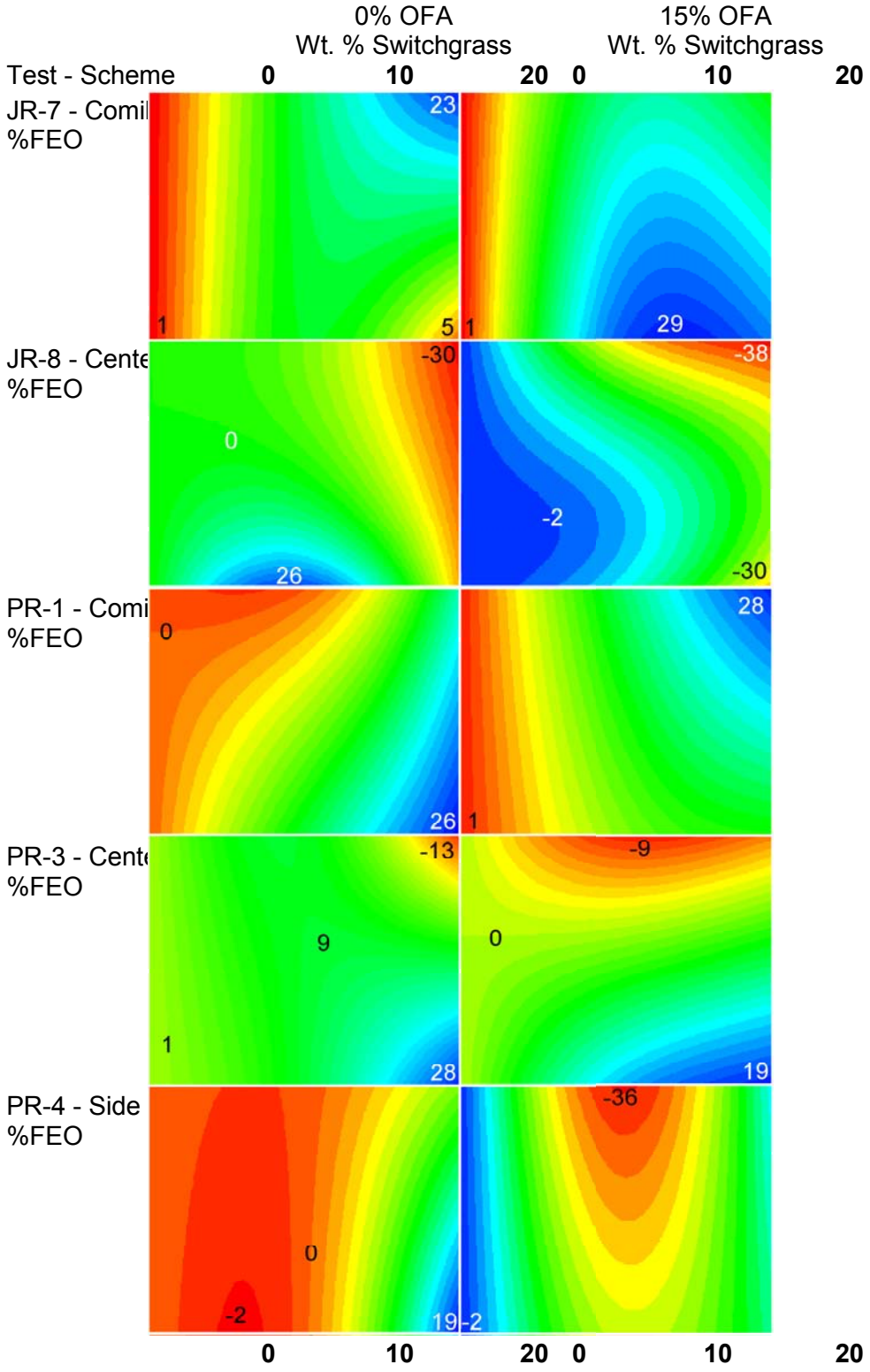

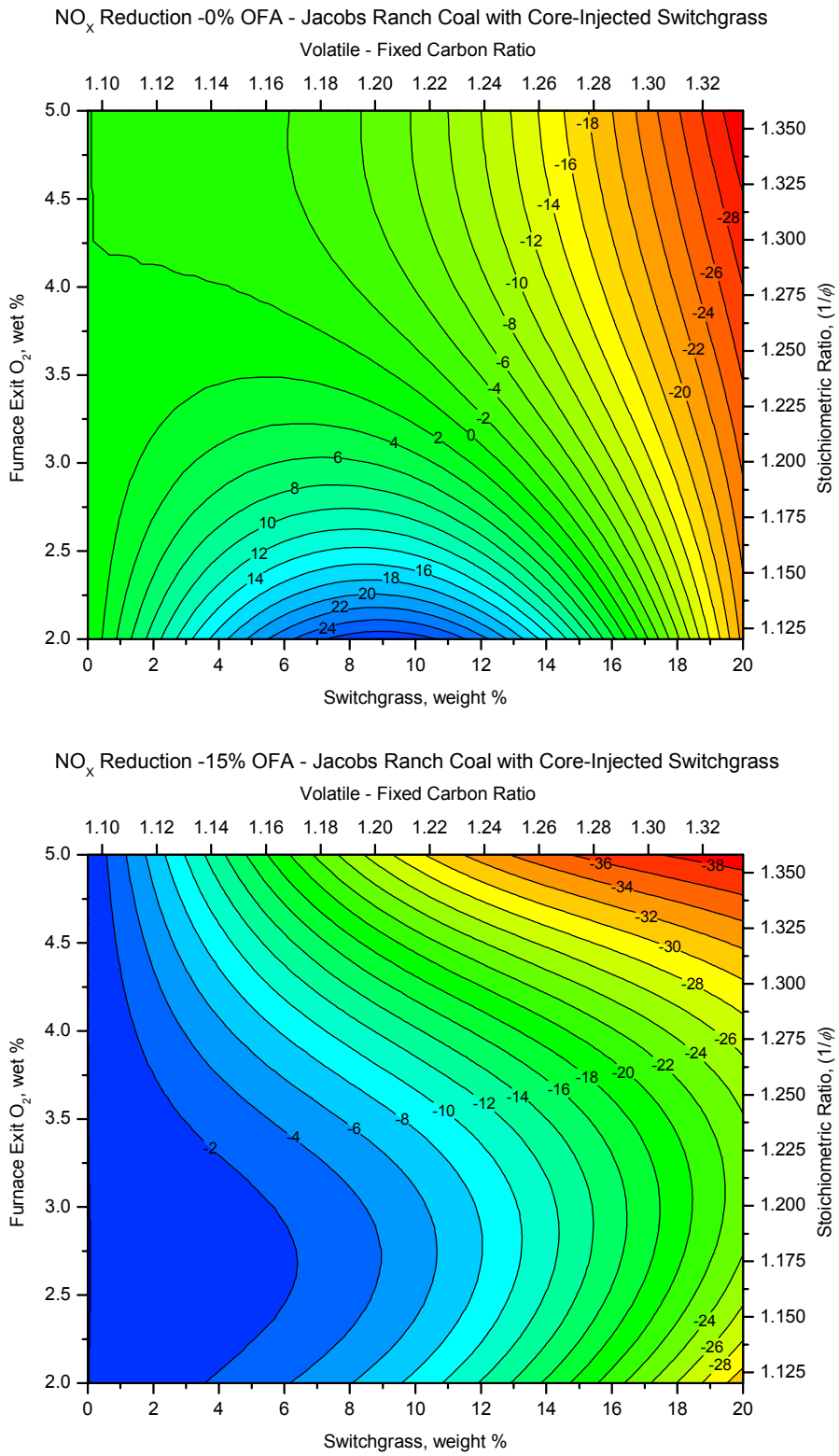

Figure 3-44. NO_X reductions from cofiring SG with JR coal by injecting SG through the center of the single-register burner, 0% and 15% OFA.

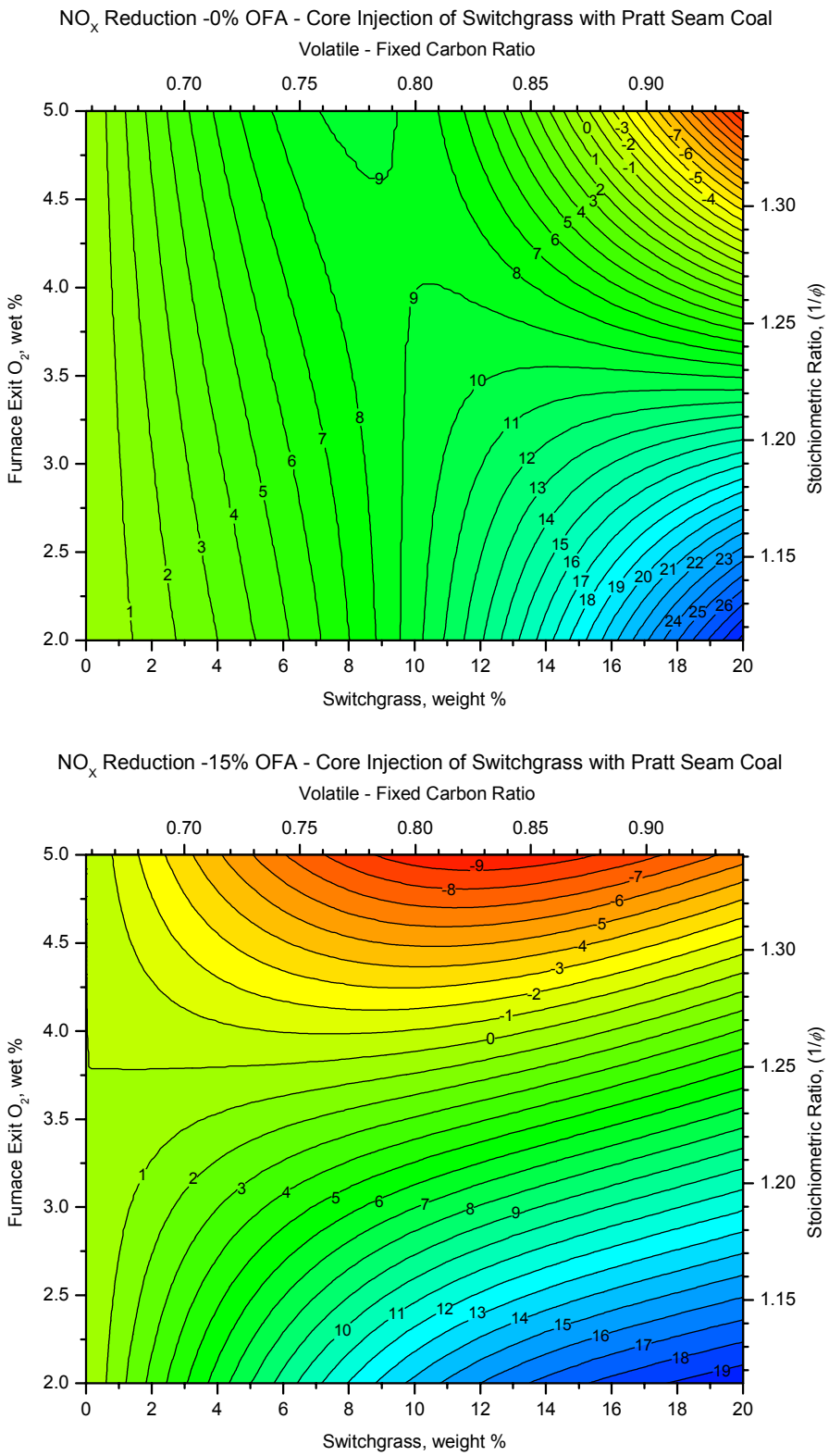

Figure 3-45. NO_X reductions from cofiring SG with PR coal by injecting SG through the center of the single-register burner, 0% and 15% OFA.

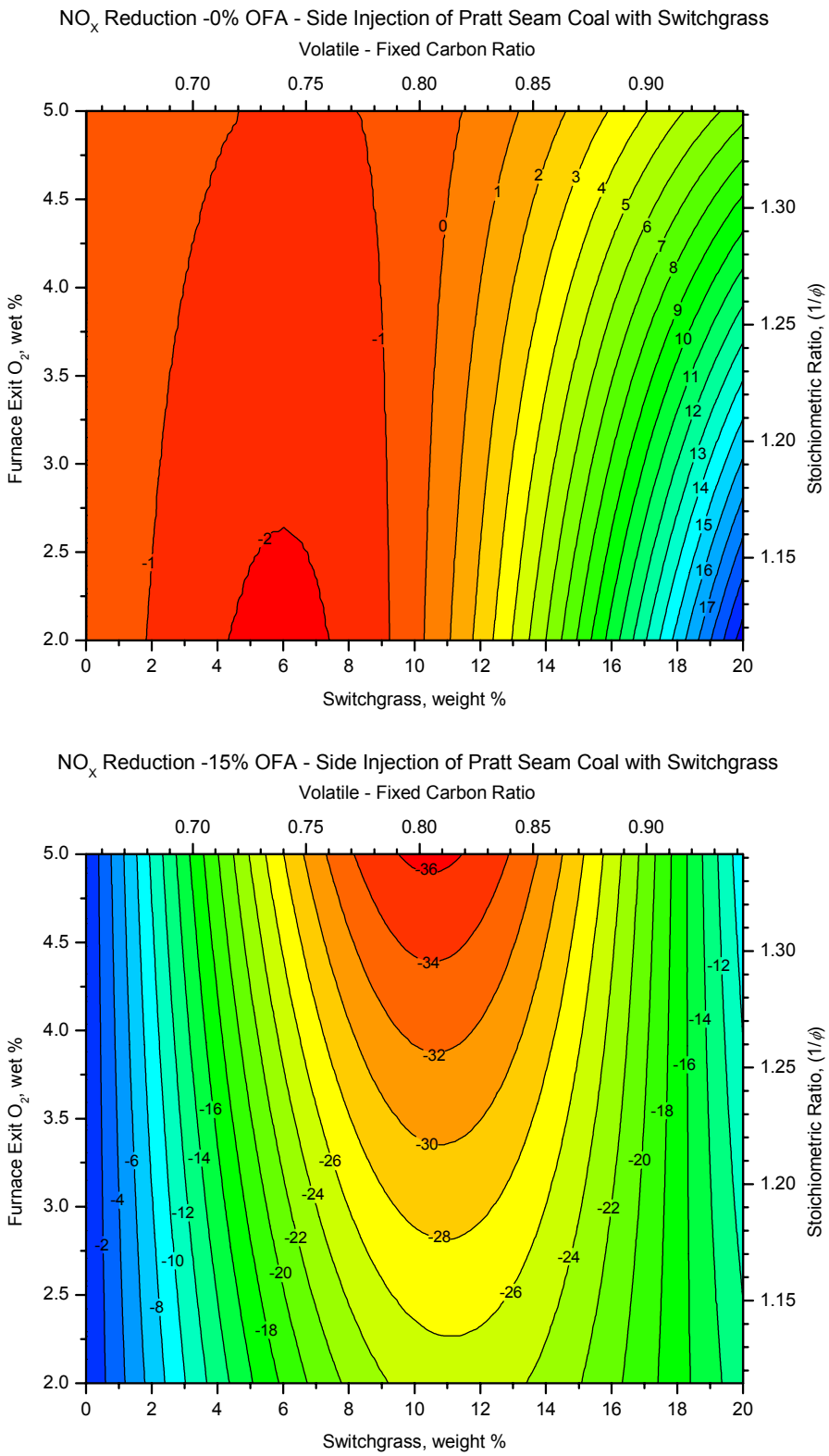

Figure 3-46. NO_X reductions from cofiring SG with PR coal by injecting SG from the side into the exit of the single-register burner, 0% and 15% OFA.

3.2.4.1.4.4 UBC Emissions from Cofiring SD and SG with Coal. Figures 3-47 through 3-49 present the results of UBC measurements made on isokinetically-extracted samples of fly ash obtained during each major test condition.

As with comilled biomass, the complex behavior seen in NO_X emissions is not mirrored in UBC measurements. In general, adding comilled biomass serves to reduce UBC. However, as for comilling, with center-burner injection of SD or SG and JR coal, UBC emissions were uniformly increased by the addition of any comilled biomass, but not above 1%. Again, as we noted for the comilled case, UBC emissions for PRB coals are generally very low, and UBC emissions for JR coal are uniformly extremely low (for 100% coal, ~ 0.1% for 0% or 15% OFA).

With PR coal, adding biomass generally reduced UBC emissions although for 100% coal firing UBC emissions never exceeded 3%. The greatest reduction in UBC emissions was measured for center-burner injection of SG at 15% OFA, where UBC was reduced by about a factor of two by the addition of biomass, regardless of FEO.

3.2.4.2 Dual-Register Burner - Results from Cofiring Tests with Comilled Biomass Because no CFD modeling could be carried out for the dual-register burner, only one test was completed, GL coal comilled with SD and SG (Test GL-9). Therefore, limited results (32 test conditions) are available for this burner-coal combination.

The dual-register burner is a complex device, with five degrees of freedom (three independent flows and two different swirl settings). Because this burner has two independent wind boxes, or registers (each register has a set of swirl vanes), overfire air is incorporated into the second register with secondary air fed to the first register. Two stable regimes were established. The first regime, characterized by low-NO_X emissions, exists at a flow split of 18% primary (fuel) air, 66% secondary air at 60° swirl (the first register), and 16% tertiary air (or TA) with 45° swirl (the second register). The second regime, characterized by higher NO_X emissions, exists at a flow split of 18% primary (fuel) air, 52% secondary air at a swirl of 60° (the first register), and 30% TA at a swirl of 45° (the second register).

Because two stable emissions regimes exist for the same burner, it can sometimes be difficult to force the burner to change from one regime to another. After the two emissions regimes were established and testing in the low-NO_X regime and high-NO_X regime had concluded for 100% GL coal, several hours of tedious flow, swirl, and burner adjustments were required to force the burner into the low-NO_X condition with a 10% switchgrass – 90% coal mixture. Subsequent adjustments were made easier by slightly increasing the coarseness of the coal-biomass grind (from ~70% < 200 mesh to ~66% < 200 mesh). Fine coal tends to cause a very stable high-NO_X flame. That is, fine coal particles tend to diffuse from the coal jet, breaking down the jet and causing some early mixing. Coarsening the fuel grind serves to reduce this mixing. This was a likely cause for this difficulty because a pulverized coal-biomass mixture tends to have a finer coal grind and a coarser biomass grind.

As with testing with the single-register burner, so that NO_X reductions can be referenced to NO_X concentrations, Figure 3-50 presents graphs of curve fits to baseline NO_X emissions as a function of FEO for 100% pulverized coal firing of GL coal for the dual-register burner (at 16% and 30%

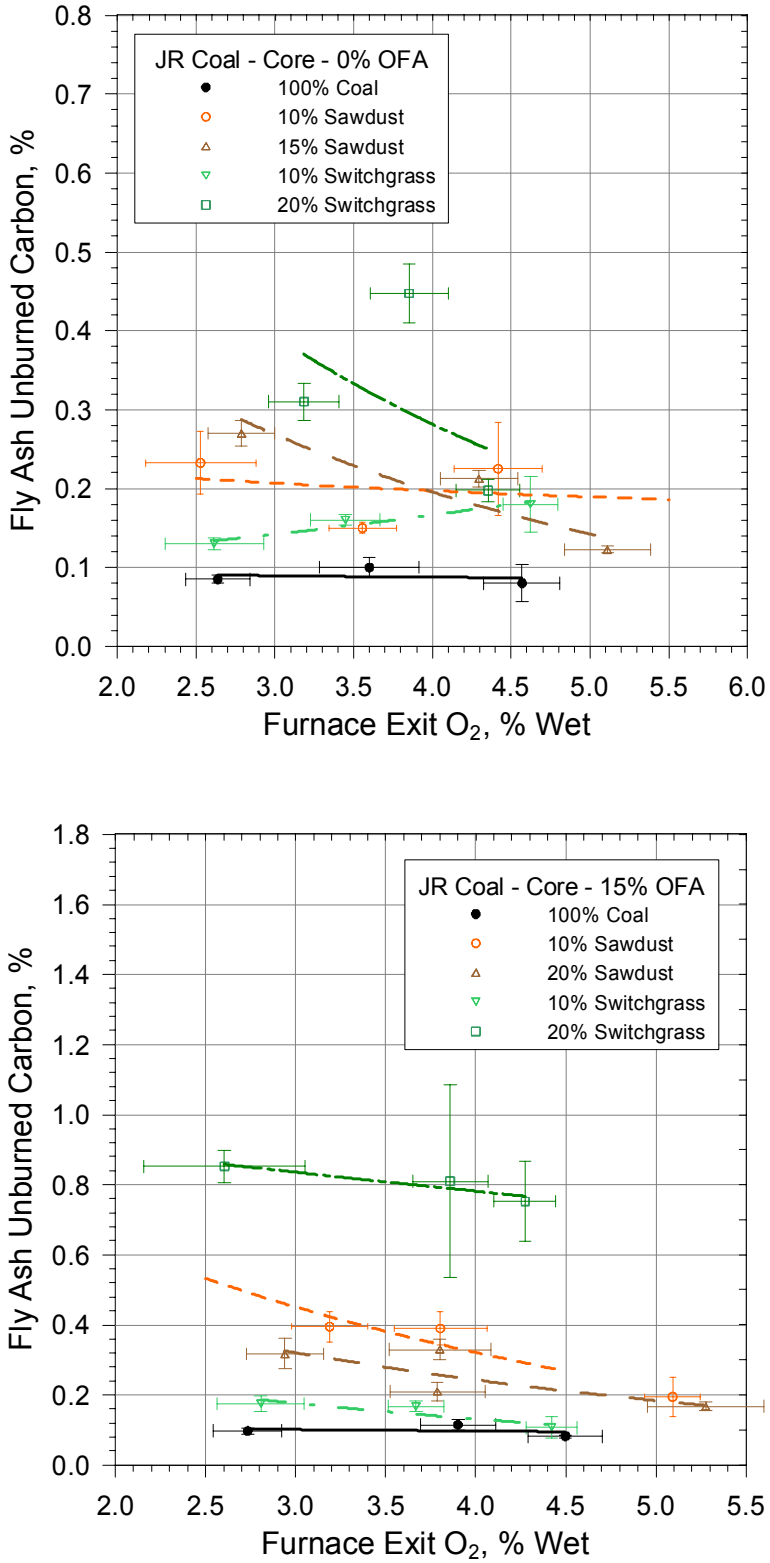

Figure 3-47. UBC emissions from cofiring SD and SG with JR coal by injection through the burner center, 0% OFA (top) and 15% OFA (bottom).

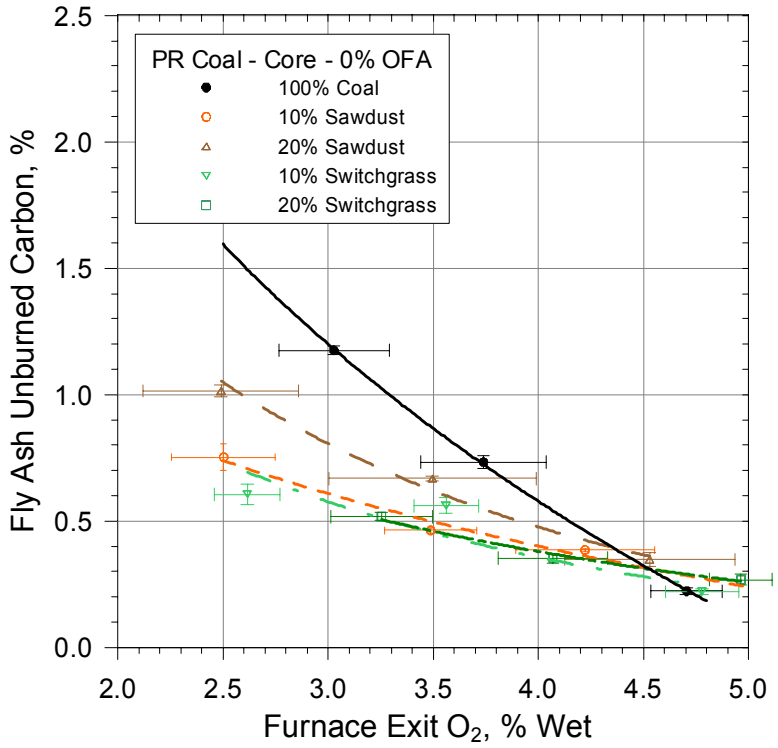

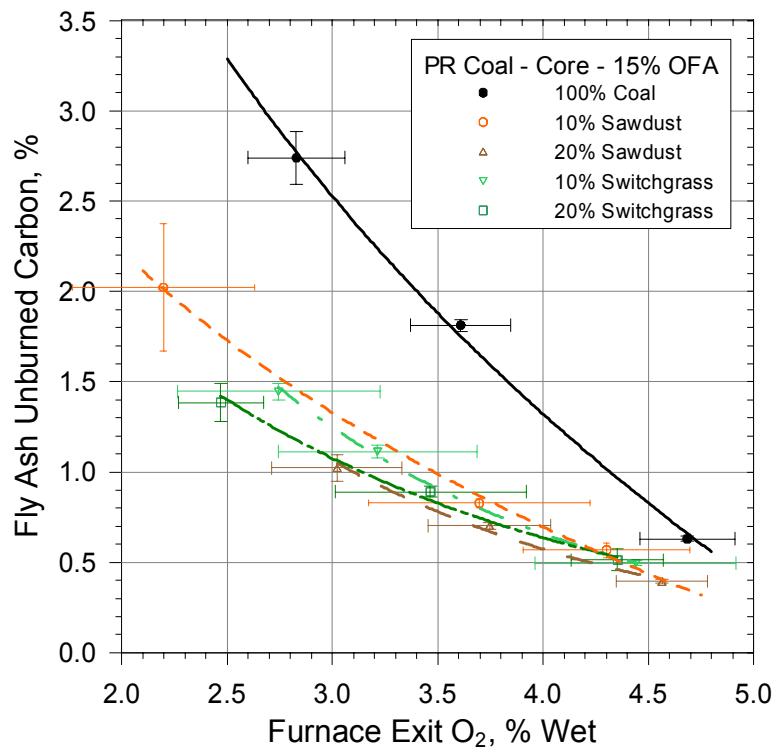

Figure 3-48. UBC emissions from cofiring SD and SG with PR coal by injection through the burner center, 0% OFA (top) and 15% OFA (bottom).

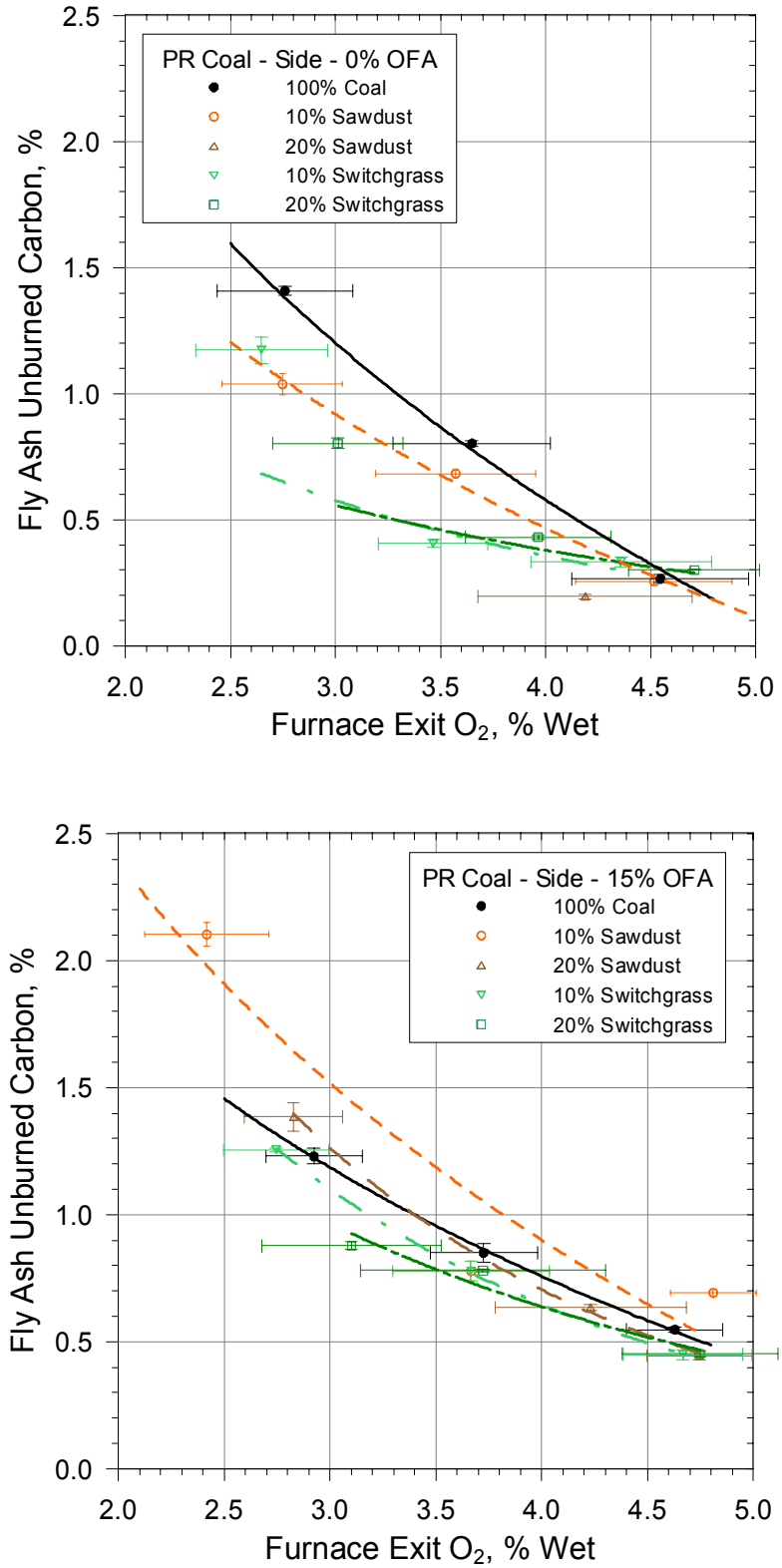

Figure 3-49. UBC emissions from cofiring SD and SG with PR coal by injection from the side into the exit of the single-register burner, 0% OFA (top) and 15% OFA (bottom).

TA) and the single-register burner (at 0% and 15% OFA). Notwithstanding slight differences in GL coal from Tests 5 and 6 to Test 9 (two different deliveries), in a high-NO_X mode of firing (0% OFA with the single-register burner and 30% TA with the dual-register burner) emissions were always greater for the single-register burner. In a low-NO_X firing mode (15% OFA with the single-register burner and 16% TA with the dual-register burner) at low levels of FEO, NO_X emissions are up to 50 ppm lower with the single-register burner. However, for ~3.5% FEO and above, NO_X emissions are generally lower with the dual-register burner so that at 4.5% FEO, NO_X emissions are up to 50 ppm higher with the single-register burner. The curve fits shown in Figure 3-50 are tabulated in Table 3-16.

3.2.4.2.1 NO_X Reductions from Cofiring SD and SG with GL Coal. Table 3-17 and Figures 3-51 and 3-52 provide a presentation of NO_X reduction results in a thumbnail format similar to that we have employed earlier. In Table 3-17, results of NO_X reductions measured with the dual-register burner are compared with NO_X reductions measured with the single-register burner. Recall that Figure 3-50 shows that the two burners exhibit different trends in NO_X emissions as a function of FEO. Thus, NO_X reductions with one burner cannot be equated to NO_X reductions with the other burner. Figure 3-50 and Table 3-16 will facilitate this comparison. Tables 3-9 and 3-10 also provide assistance in recovering stoichiometric ratio, V/FC ratio, and Fuel N from Figures 3-51 and 3-52.

In the high-NO_X mode of firing (30% TA), the addition of comilled SD or SG generally raises NO_X emissions, particularly for SD where at the 10 weight % level of addition, NO_X emissions increased by 90% at low levels of FEO (from 2% to 3%) and by as much as 45% at high levels of FEO (from 4% to 5%). At very high levels of added SD, NO_X reductions of up to 10% were obtained. With SG, moderate levels of addition (~10 weight %) led to low levels of NO_X reductions (a maximum of 9% for FEO < 3%). At higher levels of SG (~20 weight %), NO_X emissions increased by ~20%, regardless of FEO.

In the low-NO_X firing mode (16% TA), Table 3-17 shows that NO_X emissions were effectively reduced by the addition of comilled SD or SG. Higher NO_X reductions were measured with comilled SD. At 10 weight % SD, regardless of FEO, NO_X reductions of ~25% were measured. For 15 to 20 weight % SD, NO_X reductions depend on FEO with highest NO_X reductions occurring for FEO < 3.5%. With SG, below ~3.2% FEO, NO_X emissions are increasingly reduced as the amount of SG is increased (maximum of 33% for weight % SG > 10%). Above 3.2% FEO, NO_X reductions are small for SG levels lower than 10 weight %. Above 10 weight % SG, NO_X reductions diminish and for SG additions of greater than 15 weight %, NO_X emissions increase up to 12% above those measured for 100% coal.

Table 3-17 shows that comparisons of NO_X reductions for single and dual-register burners fueled with the same coal and biomass cannot be made on an intuitive basis. In general, where NO_X reductions are found with the single register burner is not where NO_X reductions occur for the single-register burner, with the same coal and biomass.

3.2.4.2.2 UBC Emissions from Cofiring SD and SG with GL Coal. Figure 3-53 shows the results of UBC measurements made on made on isokinetically-extracted samples of fly ash obtained during each major test condition. Overall, the addition of biomass does not affect

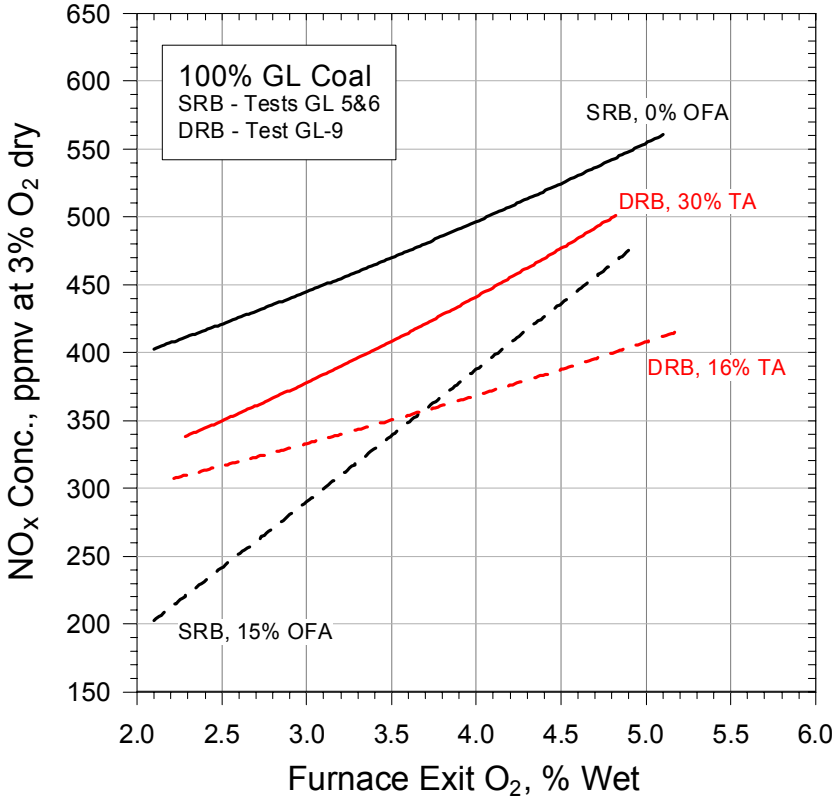

Figure 3-50. Baseline NO_X emissions for 16% TA and 30% TA for the dual-register burner and GL coal, Test GL-9, and for the single-register burner and GL coal, Tests GL 5&6.

Table 3-16. Fit parameters for the NO_X emissions curves in Figure 3-50.

TEST	Cofiring	Fit*	Fitting Parameters	
			A	B
GL-9				
16% TA	Comill	E	0.145559	219.918
30% TA	Comill	E	0.161885	161.341
GL-5&6				
0% OFA	Comill	E	0.109973	319.805
15% OFA	Comill	P	1.005719	96.0934

* E = Exponential fit: NO_X (ppm) = $B \cdot e^{(A \cdot \%FEO)}$
P = Power fit: NO_X (ppm) = $B \cdot (\%FEO)^A$

Table 3-17. NO_X reductions from cofiring GL coal with comilled SD and SG, dual-register burner (DRB) and single-register burner (SRB).

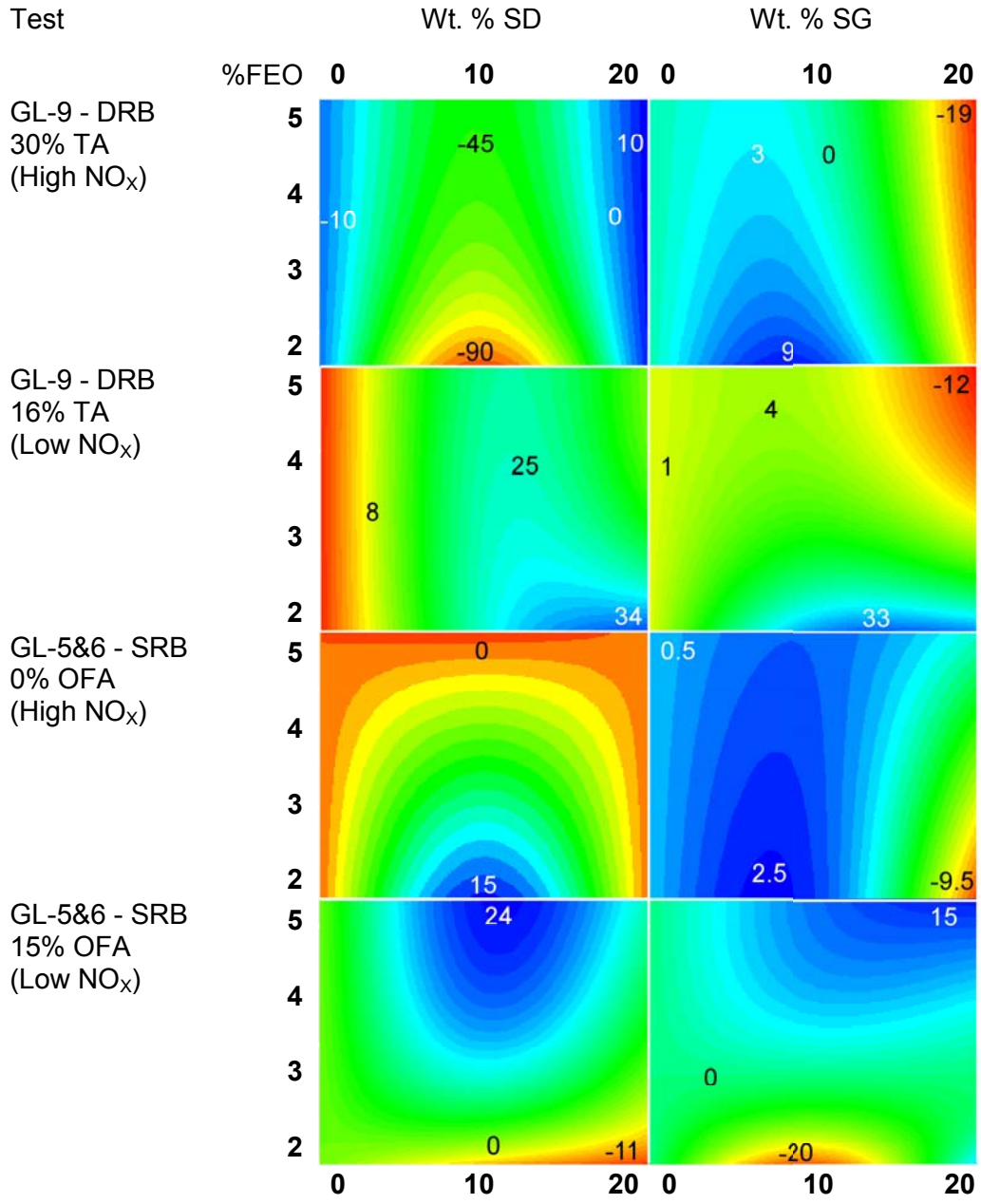

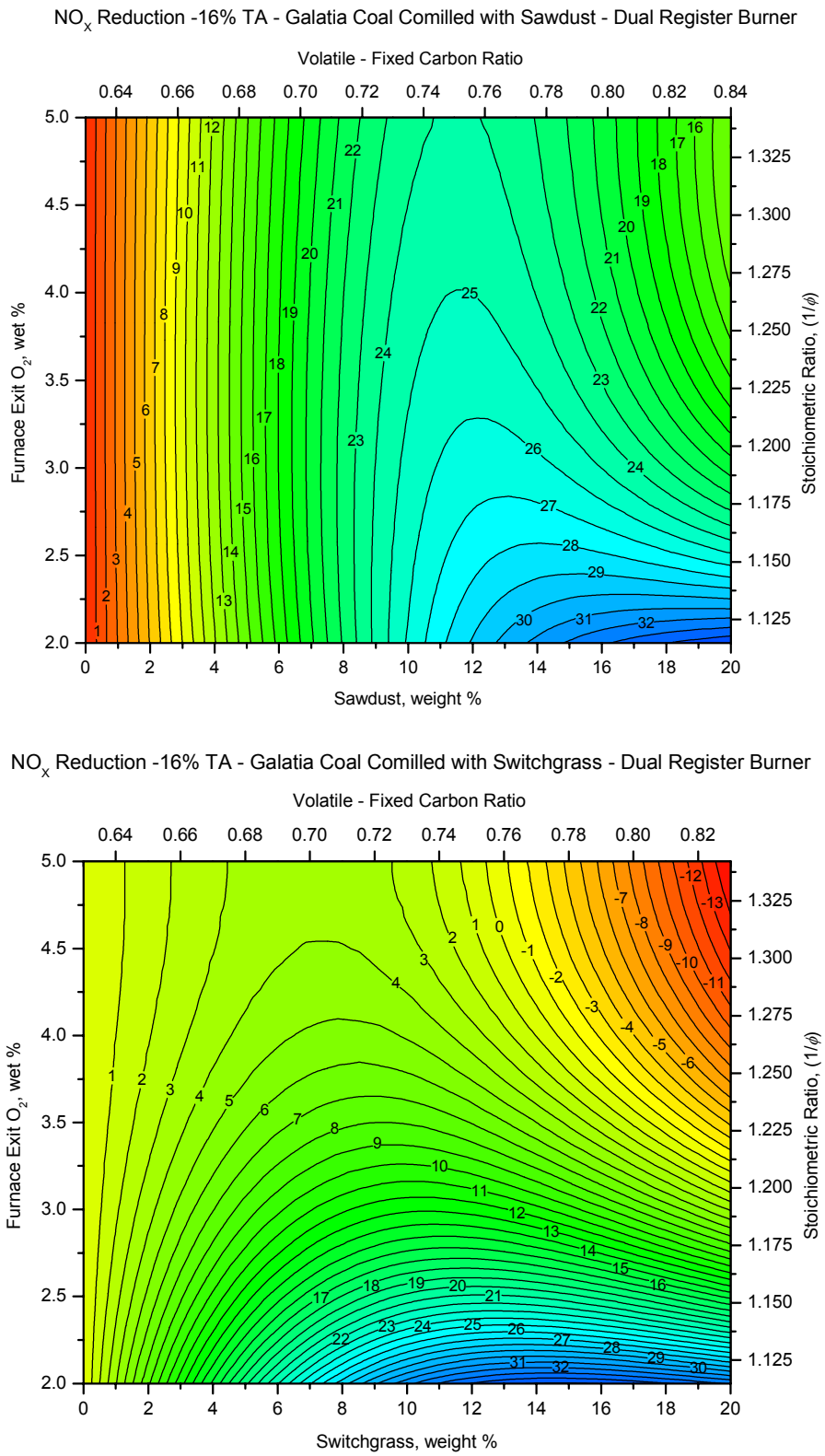

Figure 3-51. NO_X reductions from comilling SD (top) and SG (bottom) with GL coal, 16% TA, dual-register burner.

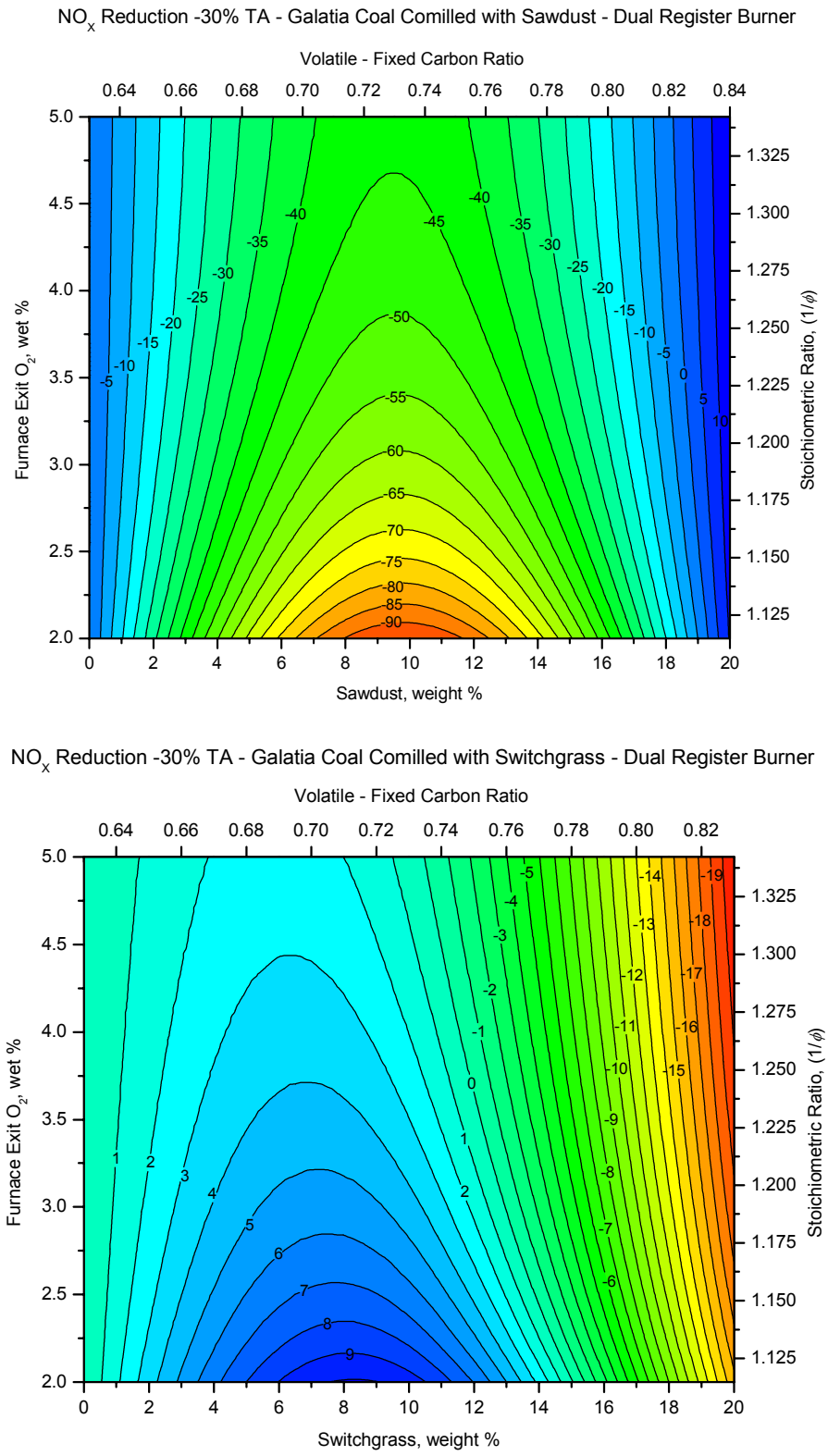

Figure 3-52. NO_X reductions from comilling SD (top) and SG (bottom) with GL coal, 30% TA, dual-register burner.

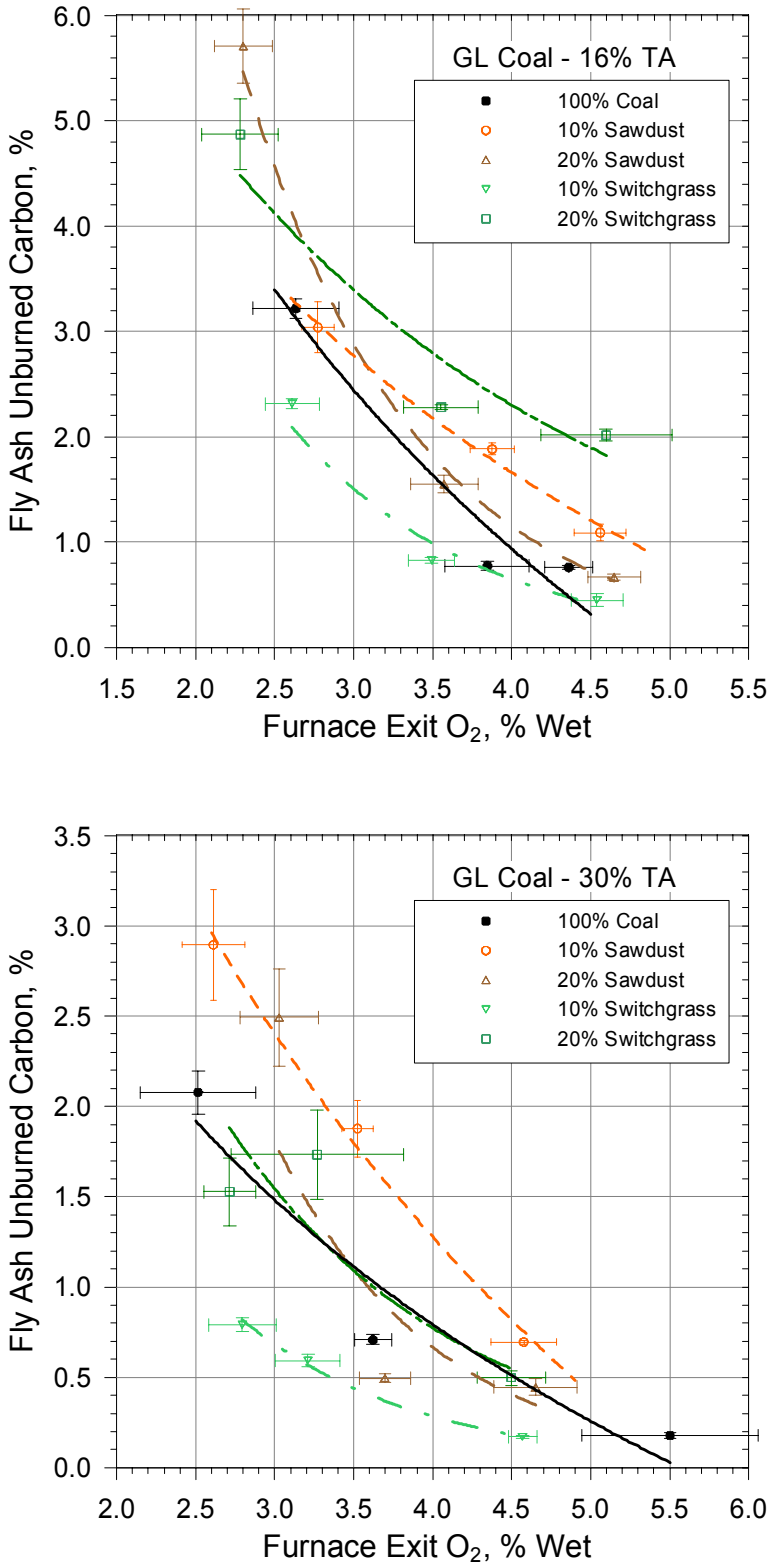

Figure 3-53. UBC emissions from comilling SD and SG with GL coal in the dual-register burner, for 16% TA (top) and for 30% TA (bottom).

UBC emissions in a significant manner. For low-NO_X firing with the dual-register burner (16% TA), UBC emissions for 100% coal are half of those measured for the single-register burner with GL coal at 15% OFA, as shown in Figure 3-29. For high-NO_X firing (30% TA), 100% coal UBC emissions for the dual-register burner are approximately a third lower than those measured for 0% OFA for the single-register burner with GL coal.

4.0 MODEL DEVELOPMENT

4.1 Background

Model development was the specific responsibility of project partner Niksa Energy Associates (NEA). Three technical tasks were defined for NEA that address this portion of our effort:

Task 3.0 Simulation Tools Development
Set up NEA's *bio*-FLASHCHAIN®, PC Coal Lab®, and CHEMKIN III for the fuels and operating conditions in Southern Research's testing program. Integrate all necessary submodels into a simulator for the Southern Research Institute/Southern Company CRF pilot-scale test facility.

Task 6.1 Validate the Simulation Results with All CRF Datasets
Develop calibration procedures for the simulations for the domain of operating conditions in the CRF tests. Predict emissions for all test cases, and compare to the reported values.

Task 6.2 Recommendations for Full-Scale Applications
Use the simulator to develop engineering guidance to obtain the benefits of biomass cofiring in full-scale, multiburner installations.

Our overall program objective is to develop and validate a broadly applicable computer model that can be used to optimize NO_X reductions and minimize unburned carbon (UBC) from biomass cofiring. The model was developed as a computer simulator for the Southern Research Institute/Southern Company Combustion Research Facility (CRF) test facility based on NEA's Advanced Post-Processing (APP) methodology. This approach proceeds through three stages: First, conventional computational fluid dynamics (CFD) simulations characterize the bulk flow patterns. Second, the bulk flow patterns are analyzed to specify an equivalent network of idealized reactors for the flow. Third, detailed chemical reaction mechanisms are used to determine the chemical composition across the entire reactor network, including the most important emissions.

Under this project, an APP simulator was developed for flames in the CRF, and used to predict the emissions for the broad ranges of coal quality, biomass quality, staging level, and furnace stoichiometry in Southern Research's testing program. Based on the satisfactory performance in this evaluation, we suggested a few strategies to achieve the benefits of biomass cofiring in full-scale utility furnaces, although additional simulations are needed to accurately extrapolate APP's performance in this project to full-scale applications. This work was completed from December 2000 through February 2003.

Section 4.2 surveys the modeling approach, emphasizing the application of APP to interpret the CRF test datasets because much of the detail on Task 3.0 was previously reported in NEA's first annual report under this project. Sections 3 and 4.3 characterize the datasets and describes how the operating conditions in the tests were imposed in the simulations. Section 4.4 explains how the bulk flow patterns were used to specify an equivalent reactor network for the CRF, and introduces the results of the analysis with detailed chemical reaction mechanisms. Section 4.5 compares the predictions to the CRF datasets all the most important test series. Extensions of the analysis for cofiring applications in full-scale furnaces are outlined in Section 4.6. A final

chapter summarizes the current status of the modeling capability. It also recommends several immediate extensions that support biomass cofiring in full-scale utility furnaces as well as a diverse assortment of near- and far-term applications.

4.2 Advanced Post-Processing – Predicting Emissions with Detailed Chemical Reaction Mechanisms

4.2.1 Overview of APP

NEA's Advanced Post-Processing (APP) Method generates an equivalent network of idealized reactor elements from a conventional CFD simulation. The reactor network is a computational environment that accommodates realistic chemical reaction mechanisms; indeed, mechanisms with a few thousand elementary chemical reactions can now be simulated on ordinary personal computers, provided that the flow structures are restricted to the limiting cases of plug flow or perfectly stirred tanks. The network is equivalent to the CFD flowfield in so far as it represents the bulk flow patterns in the flow. Such equivalence is actually implemented in terms of the following set of operating conditions: The residence time distributions (RTDs) in the major flow structures are the same in the CFD flowfield and in the section of the reactor network that represents the flow region under consideration. Mean gas temperature histories and the effective ambient temperature for radiant heat transfer are also the same. The entrainment rates of surrounding fluid into a particular flow region are evaluated directly from the CFD simulation. To the extent that the RTD, thermal history, and entrainment rates are similar in the CFD flowfield and reactor network, the chemical kinetics evaluated in the network represents the chemistry in the CFD flowfield.

The information flow is sketched and compared with conventional CFD post-processing in Figure 4-1. In conventional CFD post-processing, a first-pass calculation imposes a radically reduced set of chemical species with rudimentary reaction mechanisms to predict the heat release and its impact on the flowfield, but not the emissions. Then the converged solutions for the flowfield, temperature field, and major species concentration fields are re-analyzed with additional species and more global reaction processes to predict emissions. In contrast, APP utilizes the flow and temperature fields but not the species concentration fields from the first pass, because these were determined with the rudimentary reaction submodels. In addition, APP uses fields of the turbulent diffusivity and selected conserved scalar variables, which are always computed in CFD but not normally reported to the user. The APP method then specifies an equivalent reactor network directly from the CFD flow and temperature fields. Finally, realistic elementary reaction mechanisms are used to determine the concentrations of all major and various minor species across the reactor network, including any emissions of particular interest.

From a practical perspective, it is only possible to implement APP after the CFD flowfield has first been subdivided into regions. The regions are the rudimental elements of the chemical structure of the flowfield. As such, each region sustains a collection of chemical reaction mechanisms that are distinctive. Regions are usually much more extensive than any distinct flow structures. For example, the core formed by the primary jet within a dual register burner is a region, because the very high loadings of particles and soot in this region will significantly perturb the chemical reaction rates in the gas phase, especially the N-conversion mechanisms. Mixing layers formed by simultaneous entrainment of fuel-rich fluid into secondary or tertiary

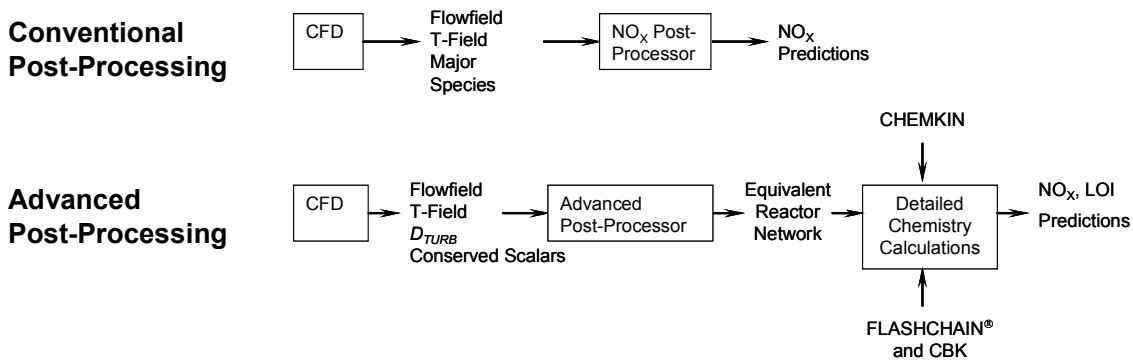

Figure 4-1. Schematic of the information flow in conventional and advanced post-processing.

air streams are also regions, because the temperature profiles along the direction of mixing exhibit similar maximum values across the entire layer. The portion of an OFA jet remaining to be mixed with a process stream is another region, because the absence of fuel essentially eliminates all chemistry.

This section describes how APP was applied to the CRF test facility; in particular, how the flow was subdivided and how the operating conditions were assigned for the various regions. Whereas the equivalent network for the furnace is actually presented in Section. 4.4, the analyses in this chapter comprise the technical foundations for APP. They also differentiate NEA's APP from other methods that assign equivalent reactor networks to pulverized fuel flames and furnaces.[10-12]

4.2.2 Bulk Flow and Temperature Patterns

4.2.2.1 CFD Simulations CFD simulations of the CRF were performed by Reaction Engineering International (REI) for all tests with Pratt seam high volatile (hv) bituminous coal and various biomass. Cases with Jacobs Ranch subbituminous and Jim Walters low volatile (lv) bituminous were performed at Southern Research, using REI's Configurable Fireside Simulator (CFS) for the CRF. The CFS imposes a fixed computational grid on the calculations, and is therefore suitable for parametric case studies with the same firing configurations. No CFD were available for cases with Galatia coal because these flame structures were expected to be very similar to the Pratt flames.

4.2.2.1.1 Bulk Flow Patterns Perhaps the most surprising feature in the CFD simulations is that in the co-milled and core injection configurations, all fuel particles remain on the furnace axis in the lower furnace and throughout most of the upper furnace as well. Neither mixing in the near-burner zone nor radial OFA injection disperses the particles off their original trajectories.

Near the burner, the primary air stream is significantly expanded by the release of volatiles from the fuel suspension and by thermal expansion. This expansion zone delineates a fuel-rich core from the outer, annular flow of secondary air. Nominal residence times in the core range from 120 to 170 ms. The expansion of the primary flow promotes entrainment of secondary air into the core, because some of the secondary flow penetrates the expansion boundary. In addition, a

portion of secondary air is entrained into the core as soon as it passes the edge of its delivery tube in the fuel injector. Together, these entrainment mechanisms almost instantaneously mix about 20 % of the secondary air into the primary flow.

The flow of the core and secondary air streams gradually expands until it contacts the furnace wall midway to the OFA ports. A weak external recirculation zone (ERZ) forms in the corner bounded by the outer boundary of the secondary air stream. Since the ERZ is too weak to entrain particles or appreciable amounts of air or fuel compounds, it appears to be inconsequential.

As the fuel compounds in the flame core contact the secondary air stream, they mix and burn in an expanding mixing layer. This layer completely surrounds the core near the burner inlet, and fills the entire furnace downstream of the core. The most distinctive feature of the mixing layer is that the temperature profile across the layer in the normal direction passes through a maximum value which is essentially the same around the entire circumference of the core. Note the similarity to the structure of a laminar diffusion flame, although flow in the CRF is definitely turbulent. Maximum gas temperatures approach 1700°C in cases where fuels of the highest heating values were fired without OFA, and 1600°C in cases with 15 % OFA. Residence times in the mixing layer to the OFA location vary from 500 to 600 ms.

The four air jets from the OFA ports do not penetrate onto the centerline. They also do not fill the entire flow cross section. Since OFA injection does not impart significant swirl to the flow either, sectors of the post-flame gases mix independently with only one of the OFA jets. Downstream of the OFA ports, the flow relaxes to a plug flow pattern that carries ash and exhaust into an exhaust system. The total residence times to the furnace exit are approximately 2.5 s.

4.2.2.1.2 Required CFD Variables for APP We use a commercial software package called FIELDVIEW to characterize the bulk flow patterns in the CFD simulations. This work was based on a custom output file for the CFD simulations prepared by REI or Southern Research staff according to NEA's specifications. The following field variables are used in APP:

(1) Gas density (kg/m^3)
(2) Gas temperature (K)
(3) Mass fractions of all gas species (-)
(4) Effective mass diffusivities of all gas species (m^2/s)
(5) U velocity component (m/s)
(6) V velocity component (m/s)
(7) W velocity component (m/s)
(8) Wall temperature (°C)
(9) Dry-ash free (daf) mass concentration of particles (kg/m^3)

Variables 1 – 8 are directly determined by the CFD simulation, but not the daf mass concentration of particles. The daf mass concentration of particles ρ_{daf} (kg/m^3) is evaluated from

$$\rho_{daf} = \frac{\sum_{i=1}^{n_p}(m_i - m_{i0} f_{ash})}{V_{cell}} \tag{4.2.1}$$

where n_p is the total number of particles in a computational cell; m_i is the remaining mass of particle i; m_{i0} is the initial mass of particle i; f_{ash} is the ash fraction in the original coal particles, and V_{cell} is the control volume.

Particle trajectories also need to be exported from the CFD simulation. The required particle trajectory file includes the following information:

(1) x location (m)
(2) y location (m)
(3) z location (m)
(4) Residence time (s)
(5) Particle temperature (K)
(6) Particle mass (kg)
(7) Particle size (μm)

4.2.3 Equivalent Reactor Network

4.2.3.1 Basis for an Equivalent Reactor Network A coal-fired furnace cannot be analyzed as a homogeneous reaction system like other chemical processes. One reason is that coal flames comprise several separate regions, each with its own distinctive chemical reaction and transport mechanisms. And these distinctive mechanisms determine the most important species concentrations, especially the species associated with NO_X emissions. Another reason is that the flowfield in the CRF governs the mixing rates between fuel and oxidizer streams which, in turn, govern the combustion intensity. Interactions and entrainment among these flows directly affect emissions.

Thus, the first step in developing an equivalent reactor network is to subdivide the CFD flowfield into its distinctive regions. These regions are distinctive in terms of their chemical reaction mechanisms, rather than their fluid dynamic structure. In addition to distinctive chemistry, regions must have operating conditions that can be expressed as functions of time only because, by definition, a network of idealized reactors reduces all spatial variations to a time dependence. This condition imposes several constraints on how regions are defined, as follows.

The flowfield determines the residence times of all fluid particles moving across a particular region. Since regions are generally fed by multiple streams of grossly different compositions, the flowfields within regions are rarely one-dimensional. Multi-dimensional flowfields determine RTDs, rather than a nominal residence time. For example, suppose that a region was defined as a round turbulent jet emanating from a cylindrical injector. Most of the fluid remains near the jet axis and travels far downstream from the injector within this region. This fluid has the longest residence times. But some of the fluid has a sufficiently fast radial velocity

component to quickly move off axis and cross the boundary into another region. Such fluid has much shorter residence times. By tracking many fluid particles over the injector cross section, we can formulate an RTD for the region that accounts for the multi-dimensional character of the flowfield, without reducing the flowfield to a single spatial coordinate. The RTDs for all regions in the CFD simulation must be matched in the equivalent reactor network to depict the impact of the multi-dimensional flow character on the chemical kinetics.

The most versatile way to match the RTDs is to represent the operating conditions in each region by an assembly of idealized reactor elements, either continuously stirred tank reactors (CSTRs) or plug flow reactors (PFRs). These two reactors represent the extreme extents of backmixing of products with reactants, in that CSTRs are completely backmixed whereas PFRs have no backmixing. This feature is responsible for their characteristic RTDs as well. A CSTR RTD is an exponential decay, and therefore as broad as possible. The PFR RTD is a Dirac delta function with no dispersion whatsoever. Most important, the RTDs of CSTRs-in-series can be varied continuously between these limiting forms simply by varying the number of CSTRs in the series. In APP practice, only series of CSTRs are used because the RTD of a PFR equals that of a CSTR-series in the limit of a large number of reactors. We have encountered regions whose RTDs did not fall within this range, but were nevertheless able to represent the RTD with a more complicated reactor assembly, such as a CSTR-series in parallel with a PFR.

The multi-dimensional flow through a particular region can be reduced to a single function of time by evaluating the RTD with particle tracking. Hence, we are committed to re-casting the CFD flowfield into a Lagrangian field of individual trajectories in time for both fluid elements and actual fuel particles. In other words, all the operating conditions that affect chemical kinetics must be re-cast into functions of a common time coordinate.

The gas temperature field within each region must be reducible to a thermal history; i.e., an average temperature as a function of time. In principle, the profile could be expressed in terms of one spatial coordinate or in terms of a time coordinate. We always use the time coordinate because a thermal history maps directly onto the average residence time profile along a series of CSTRs. This stipulation is potentially confusing to implement because it certainly does not imply that the gas temperature field within each region must be one-dimensional. Rather, it means that the gas temperature field must be amenable to meaningful averaging, whereby each fluid particle is subjected to a similar thermal history, regardless of its particular residence time in the RTD.

To illustrate this point further, consider a 2-D, axisymmetric, laminar diffusion (Burke-Schumann) flame. This flame consists of a relatively cool core of fuel, surrounded by air at ambient temperature. The interface between these two regions is a reacting surface fed by fuel from one side and by air from the other. The interface also determines the locus of maximum temperatures for the entire flame, so the gas temperature field is definitely not one-dimensional. Nevertheless, each fluid particle that moves from the fuel core into the flame surface is rapidly heated to the flame temperature, then cooled as it penetrates into the air stream. The crucial point is that the imposed thermal history is essentially independent of position on the flame surface. Whether the fluid leaves the fuel core immediately after leaving the burner or from the streamline on the flame axis into the flame tip, essentially the same thermal history is imposed: it

rapidly increases from the low value in the fuel core, passes through the maximum value at the flame surface, then diminishes to the low value in the air stream.

We use fluid particle tracking to compile a population of thermal histories for all trajectories represented by the RTD. We then average the temperatures of the population in time to assign an average gas temperature history for the region under consideration. Once the average temperature history has been specified, it is rendered in a discretized version to each of the reactors in the CSTR-series for this particular region. Note that each individual CSTR is isothermal. Provided that many CSTRs are used to represent the region, there is little uncertainty introduced by rendering the average thermal history into a discrete form.

In addition to the gas temperature history, two additional thermal histories must be specified. Both pertain to the particulate phase. First, an effective ambient (wall) temperature for radiation transfer must be specified. During char oxidation, the instantaneous particle temperature represents the interplay among numerous heat transfer mechanisms, including thermal inertia, convection, radiation, and the heat release due to char oxidation. So, in our char oxidation simulations, we simultaneously assign particle temperature histories and burnout histories from coupled balances on particle mass, size, and enthalpy. The radiation flux in the enthalpy balance contains the effective ambient temperature, which must be specified as a function of the mean residence time throughout the region under consideration. We certainly do not want to apply the particle histories from the CFD simulation in the calculations with detailed chemistry, because that would compromise the benefits of the advanced reaction mechanisms for char oxidation in the detailed calculations.

In principle, the radiation analysis in the CFD simulation was already used to evaluate the radiation flux to the particle along each particle trajectory in the CFD simulation. This flux could be used to directly evaluate an effective ambient temperature. In practice, this would entail a deep interrogation of the CFD simulation that is hard to justify, because the effective ambient temperature is usually much lower than the particle temperature (after ignition), which often renders it negligible. In practice, we specify effective ambient temperatures as average values over various sections of the surroundings. Effective ambient temperature histories are also implemented in discrete forms across CSTR-series.

The second required thermal history for the particulate phase is only needed at fuel injectors. To evaluate our devolatilization mechanism, a representative thermal history must be specified for the entire suspension. Usually, this is not ambiguous because, for the relatively high mass loadings in commercial burners, the suspension and primary air streams have very similar temperature histories prior to ignition, and these histories are insensitive to particle size. We assign a thermal history for devolatilization as an average of the histories for all the available particle trajectories from each injector. It usually extends from 80 to 100 ms, although devolatilization is usually complete in significantly shorter periods.

The thermal history for devolatilization is not implemented in discrete form. Rather, it is used in a separate devolatilization simulation with PC Coal Lab® to determine the time-resolved yields of all the important volatile species. The product yield histories are then subdivided into increments for the mean residence time of each CSTR in a series for the near-injector region

under consideration. In other words, the fuel fed into a near-injector CSTR-series is a mixture of char and volatiles, where the volatiles are added in increments assigned for the residence times of individual reactors from a separate devolatilization simulation.

The final operating conditions to be specified are the entrainment rates into all regions. When the region under consideration is an injector, the flowrates of fuel and air into the region are unambiguous. However, for mixing layers, relatively thin zones for char burnout, OFA injection elevations, and other regions in which two or more streams mix, all flowrates into the region must be specified. In particular, all inlet flowrates must be specified as an entrainment rate in terms of the mean residence time across the region, because we have already mapped the flow and thermal fields from the CFD simulation into an average Lagrangian history on this time coordinate. For regions of simpler, axisymmetric shapes, the entrainment rates may be evaluated from the analytical definition for the turbulent flux across the boundary of the region. More generally, we use fluid element tracking from the surrounding flows that cover the entire surface of the region under consideration. The tracking directly indicates the flowrate entering the region, which is interpreted as the entrainment rate. The total entrainment flowrate is then distributed in time, based on the flowrates through particular locations on the regional boundary compiled in the particle tracking. This procedure bases the entrainment rate on the multi-dimensional gradients and turbulent transport rates in the CFD simulation, yet remains compatible with the Lagrangian trajectory in the reactor network calculations. Note, however, that the entrained fluid is assumed to be instantaneously dispersed over the cross section of the region in the directions transverse to the nominal flow (time) coordinate, as implemented in the governing equations for CSTRs and PFRs.

4.2.3.2 Steps in Developing an Equivalent Reactor Network To summarize the discussion in Sec. 4.2.3.1, the definition of an equivalent reactor network will proceed through the following sequence of steps:

(1) The CFD flowfield is delineated into regions whose chemistry is distinctive. The actual basis for the delineation may be the local concentrations of combustibles, especially soot and fuel particles, or a temperature field that can specify a meaningful average thermal history, or by an abundance of oxidizer and no fuel, which essentially suppresses the chemistry.

(2) The RTDs of each region are determined from the CFD simulations by fluid element tracking. Each RTD is then assigned a sequence of reactors, usually by fitting the analytical RTD for a CSTR-series to specify the number of CSTRs for the RTD under consideration.

(3) An average gas temperature history for each region is evaluated from the CFD gas temperature field by fluid particle tracking. The average history in then implemented in discrete form across the CSTR-series under consideration.

(4) An effective ambient (wall) temperature for radiation transfer is evaluated as an average over the surrounding sections around the region under consideration. It is also implemented in discrete form across the CSTR-series.

(5) If the region is a fuel injector, an average particle temperature history is assigned as the average of the thermal histories over all particle trajectories from the injector, so that the fuel's devolatilization behavior can be evaluated. The

predicted volatiles yields are implemented as discrete injections into all CSTRs whose residence times includes a portion of the predicted devolatilization period.

(6) Entrainment rates into all regions are evaluated as functions of the nominal time coordinate through the region under consideration. These rates are specified from the definition of the total mass flux into the boundary of the region, for simple shapes, or from fluid particle tracking from the surroundings into the region, in the more general situation.

4.2.3.3 Delineating Regions Subdivision of the CFD flowfield into regions with distinctive chemistry is the first step in APP. This section first introduces a conserved scalar variable that delineates regions near the fuel injectors, then discusses other criteria to specify regions for the bulk of the furnace volume.

4.2.3.3.1 Combustibles Mass Fraction Regions near the fuel injectors should be identified on the basis of the extents of mixing between the fuel suspension and any secondary air streams (since the primary fuel jets are premixed with primary air). To quantitatively characterize the mixing near fuel injectors, we introduce the mass fraction of all combustible material (C, H, O, N, S) in both the particle and gas phases, normalized by the inlet value, which is defined as:

$$\psi(x,y,z) = \frac{m_{chons}(x,y,z)}{m_{chons,0}} \tag{4.2.2}$$

where ψ is the local combustibles mass fraction; m_{chons} is the mass fraction of combustibles at any position; and $m_{chons,0}$ is the combustible mass fraction at the inlet plane of the injector. The mass fraction of combustibles is calculated from the mass fractions of volatiles, CO_2, CO, H_2O, SO_2 and daf mass concentration of particles, as follows:

$$m_{chons} = \frac{\rho_{daf} + \rho\left(m_{vol} + \frac{12}{44} m_{CO_2} + \frac{12}{28} m_{CO} + \frac{2}{18}(F_O) m_{H_2O} + \frac{32.06}{64.06} m_{SO_2} \right)}{\rho_{daf} + \rho} \tag{4.2.3}$$

where ρ_{daf} is the daf concentration of char particles (kg/m^3) calculated in eq. 4.2.1; ρ is the local gas density (kg/m^3); m_{vol}, m_{CO_2}, m_{CO}, m_{H_2O}, m_{SO_2} are mass fractions of volatiles, CO_2, CO, H_2O and SO_2, respectively. The factor F_O in the H_2O-term is one plus the ratio of the percentages of oxygen to hydrogen in the fuel, and it accounts for the contribution of fuel-O to the combustibles mass fraction. Coal-N was omitted from the CFD simulations, so it could not be included in the evaluation of combustibles mass fraction. This omission is inconsequential because nitrogen is a minor contributor to the combustibles mass fraction. Note that the combustibles mass fraction includes the combustible elements, *regardless of phase and regardless of whether they appear in reactants, intermediates, or products*.

The field of the combustibles mass fraction was evaluated by incorporating eqs. 4.2.2 and 4.2.3 into FIELDVIEW to process the CFD output files. Since this variable is a conserved scalar, its local value is determined entirely by the convective and diffusive transport mechanisms in the

CFD simulation. Sources and sinks, such as chemical reactions, do not affect its value. As such, the value of the combustibles mass fraction diminishes in proportion to the entrainment of surrounding fluid into the primary fuel stream and the dispersion of combustibles away from the primary fuel stream.

4.2.3.3.2 Regions in the CRF The regions of the CRF flame that were delineated from the CFD simulation for a baseline condition with Pratt seam hv bituminous coal with 15 % OFA and 3.5 % O_2 in the exhaust appears in Figure 4-2. The structure of this flame comprises the following five regions:

(1) Core (CR) – Since the swirl is weak, the primary air and fuel stream remains intact for several meters, and this flame core retains virtually all the fuel particles.

(2) Mixing layer (ML) – Secondary air contacts the fluid from the core in a mixing layer that remains thin over most of the core length, but then fans out over the entire cross section beyond the tip of the core. Almost all the secondary air mixes with the core flow downstream of the core tip.

(3) ERZ - A relatively thin external recirculation zone (ERZ) fills the upstream furnace corners, pulling products from the mixing layer into the upstream secondary air stream.

(4) OFA Zone – Downstream of the mixing layer, tertiary air is injected through four off-radius jets. Some eddies alter the gas flow streamlines near the injection ports but particle trajectories are hardly affected by the OFA flows.

(5) Burnout (BO) Zone – 1.5 seconds of residence time are available for the later stages of char oxidation downstream of the OFA injectors, before the exhaust passes through a convective section and exhaust cleaning systems.

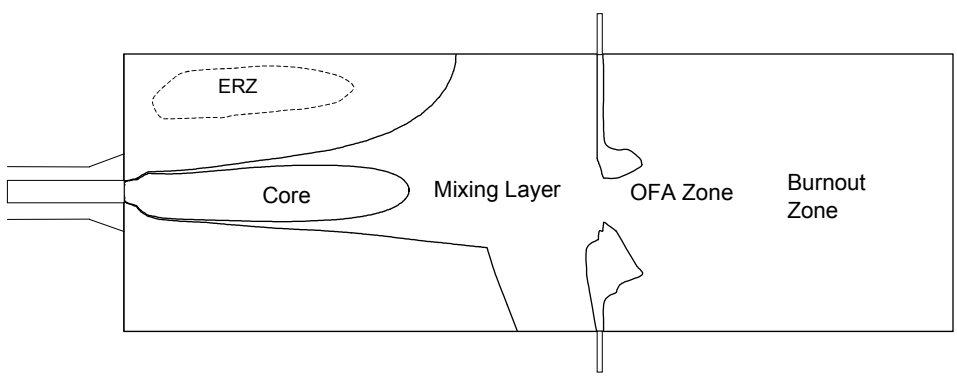

Figure 4-2. APP regions for the baseline Pratt seam hv bituminous flame delineated from the CFD simulation.

In this flame, the core was defined as the locus of points where the combustibles mass fraction equals a threshold value, and the extent of the mixing layer was based on a combustibles mass fraction equal to the well-mixed value for the primary and secondary streams in this burner. The OFA injection zones were delineated with O_2 mass fractions another threshold value. These criteria were applied uniformly to all flames of all fuel combinations, injector configurations, staging levels, and stoichiometric ratios (S. R.). Indeed, the structures of all flames were similar, in that they could be developed with the same regions. However, there are significant differences among the quantitative operating conditions specified for the same regions in different flames.

4.2.4 RTDs and Equivalent Reactor Assemblies

4.2.4.1 Basis for an Equivalent Reactor Assembly As explained in Sec. 4.2.3.1, once a boundary for a region has been assigned, the residence time of a single fluid particle is easily evaluated with fluid element tracking, based on the difference between the initial time that a fluid enters the region and the elapsed time to its departure. Then a statistical analysis compiles an RTD from the residence times for the population of individual trajectories.

Such CFD-based RTDs are then used to specify the number of CSTRs in a series that will represent the region under consideration in the equivalent reactor network. The section of the network for a specific region is called an "equivalent reactor assembly." We try to exclusively use CSTR-series for all reactor assemblies but, occasionally, more complicated configurations are necessary. CSTR-series are emphasized because the CSTR-number in the series is easily determined from a least-squares fit of the following analytical expression to the CFD-based RTD:

$$RTD(t) = \frac{1}{(N-1)!\,\bar{t}_i}\left(\frac{t}{\bar{t}_i}\right)^{N-1} \exp\left(-\frac{t}{\bar{t}_i}\right) \qquad (4.2.4)$$

where *RTD(t)* is the exit age distribution of fluid in the region as a function of time, t; N is the number of CSTRs in the series; and t_i-bar is the mean residence time of an individual CSTR. All reactors in the series have the same properties. The assignment of N in the least-squares fit to the CFD-based RTD is particularly efficient because only integer values are acceptable. Cases which have N greater than 125 during the analysis are aborted to avoid overflows and interpreted as plug flow systems.

4.2.4.2 An Equivalent Reactor Network for the CRF The CSTR network from the APP analysis of the baseline flame fired with Pratt seam hv bituminous coal appears in Figure 4-3. The networks for all other CRF flames have similar branches and feedstreams but appreciably different quantitative specifications. Only the four regions of the flame that contain fuel particles appears in Figure 4-3. The ERZ was omitted because it is not strong enough in this furnace to entrain fuel particles and, also, because its extent was fairly small.

In Figure 4-3, the flame core has been subdivided into two regions. The devolatilization zone covers the upstream portion of the core in which volatiles are being released from the fuel suspension and burned with primary air. Since the primary stream is reducing, very little

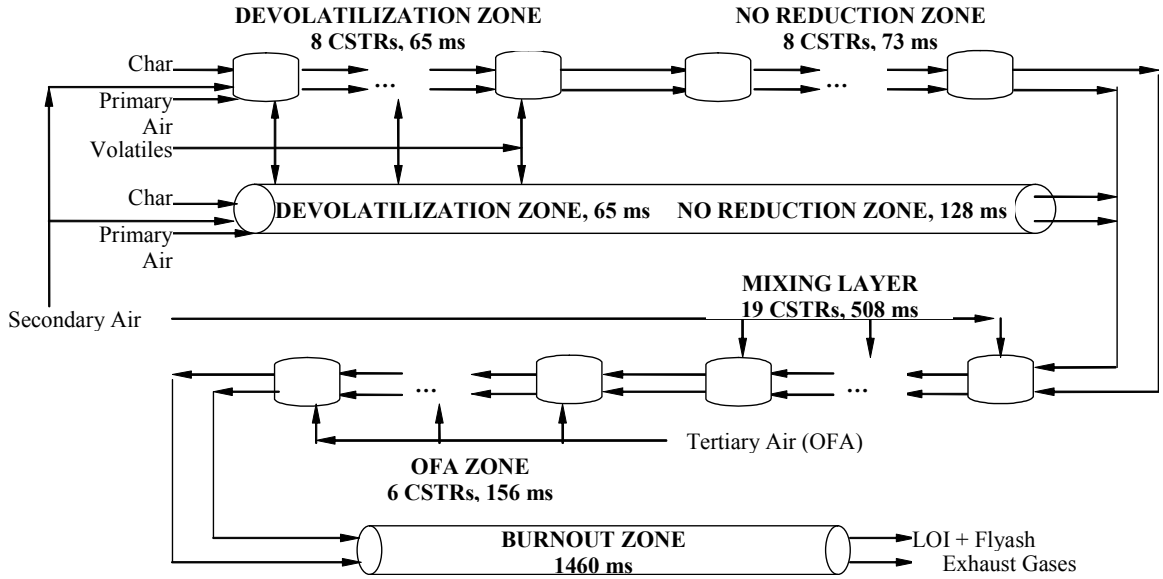

Figure 4-3. Equivalent reactor network for the baseline Pratt seam hv bituminous flame.

residual O_2 leaves the devolatilization zone. The NO_X reduction zone covers the downstream portion of the core in which only the N-species are converted under the influence of water gasshifting, due to the absence of O_2. The CSTR-series for the mixing layer and the SOFA zone represent the mixing of secondary and tertiary air streams, respectively. But there are no additional flows into the CSTR-series for the BO zone.

The RTD for this particular core was deconvoluted into one component for 16 CSTRs-in-series and another for plug flow with respective mean residence times of 138 and 193 ms. The plug flow component represents the near-axial fluid motion under the influence of particle drag, and the CSTR-component represents flow with significant radial velocities. The networks for other fuels usually have only one flow channel for the entire core, and the bulk flow pattern is plug flow. The RTD for the mixing layer was matched with a series of 19 CSTRs, and that for the OFA zone was represented by 6 CSTRs-in-series. The burnout zone is essentially in plug flow.

Note that entrainment into the various CSTR-series is represented as a series of discrete additions over several reactors in the series. Volatiles are entrained into the series for the first part of the flame core; secondary air is entrained into the series for the mixing layer; and tertiary air is entrained into the series for the OFA zone. The addition rates of volatiles were specified from the stand-alone devolatilization simulation with the average thermal history of particles from the CFD simulation. The specific addition rates of the air streams were specified from the continuous entrainment profiles evaluated from the CFD simulation.

4.2.5 Operating Conditions

4.2.5.1 Mean Gas Temperature Histories The mean gas temperature histories were simultaneously assigned with the RTDs. The time scale for the temperature history was specified with 50 equal increments of the longest populated residence time in the RTD. The

longest populated time was evaluated as the time in the RTD which was longer than the residence times of 95 % of the individual fluid particle residence times. Then the temperatures along the trajectories of individual fluid particles were recorded in the same time increments. This operation puts the individual temperature histories on a consistent time scale for averaging. The gas temperatures for all fluid particles in the region were averaged at each time increment, according to:

$$\overline{T}_{gi} = \frac{\sum_{j=1}^{N_f} \left(u_{0j} \cdot T_{gi,j} \right)}{\sum_{j=1}^{N_f} u_{0j}} \tag{4.2.5}$$

where subscript i represents the i th time increment in the time scale and j represents the j th fluid trajectory; N_f is the total number of fluid tracks in the region; and u_0 is the fluid velocity at the injector, which is used to mass-weight the average, since the gas density at the injection plane is uniform because the temperatures are uniform.

<u>4.2.5.2 Mean Particle Temperature Histories</u> Particle temperature histories are only used to assign a thermal history for the devolatilization simulation, so only particle temperature histories within the cores were analyzed. Particle temperature histories were evaluated from the particle trajectories assigned in the CFD simulation. These particle trajectory data files are structured like the fluid tracking files, so the same analytical procedure was implemented. One important difference is that the boundaries for regions cannot be identified with particle trajectories, because the combustibles mass fractions that define the extents of cores were not included in the particle trajectory data files. In the analysis, we imported the regional boundaries from the fluid trajectories into the analysis of particle tracks. Mass-weighting was also applied in the averaging of particle temperature histories, based on the initial masses of particles.

<u>4.2.5.3 Effective Radiation (Wall) Temperature</u> An effective ambient temperature is required by our char oxidation submodel to evaluate the incident radiation flux in an energy balance for a burning char particle. In the energy balance, wall temperature only appears in the definition of the radiation flux between a particle and its environment. In principle, it should be evaluated as an effective ambient temperature for radiant transfer; i.e., one that delivers the same flux as the actual collection of nonisothermal sources surrounding the particle. A legitimate implementation of this definition requires a comprehensive radiation analysis like the one in the CFD simulation. Such an effort cannot be justified by the impact of the assigned value on the char burnout predictions, which is fairly weak. Consequently, the effective wall temperature histories were assigned from mean wall temperatures.

4.2.6 Entrainment Rates in Regions

The entrainment of oxidizing streams into fuel-rich streams is obviously crucial to accurate predictions of furnace exhaust compositions. In furnaces where the regions have simple shapes and regular boundaries such as the CRF, entrainment rates can be directly specified from the entrainment flux across the boundary of a region. This flux, Q_{O_2} in kg/m^2-s of O_2, is defined as follows:

$$Q_{O_2}(s) = -\rho D_{eff,O_2}\left(\vec{n}\cdot\nabla m_{O_2}\right) + \rho m_{O_2}(\vec{v}\cdot\vec{n}) \qquad (4.2.6)$$

where m_{O_2} is O_2 mass fraction; D_{eff,O_2} is the effective (turbulent) diffusivity of O_2; $\vec{n}$ is the unit vector normal to the boundary; and $\vec{v}$ is the velocity vector. The two terms on the right hand side of eq. 4.2.6 represent diffusion and convection of O_2, respectively.

The entrainment rate $\dot{m}_{O_2}$ (kg/s) is evaluated by integrating the entrainment flux over the entire boundary, according to:

$$\dot{m}_{O_2} = \iint_s Q_{O_2}(s)ds \qquad (4.2.7)$$

where s is the boundary of the region.

These expressions can be evaluated in FIELDVIEW, then the assigned entrainment rates can be transformed onto the mean residence time coordinate used for the temperature histories.

4.2.6.1 Entrainment Rate by Fluid Tracking Fluid particle tracks from all air streams were generated with FIELDVIEW based on the velocity field in the CFD simulation. Entrainment of these air streams into furnace regions was analyzed in a separate FORTRAN program. The program records where the fluid track crosses the boundary into a certain region, if it does. An overall entrainment rate is evaluated as a mass-weighted sum of all tracks that crossed a boundary. The overall entrainment is distributed along the regional boundary according to the recorded locations of the penetrations from the fluid particle tracking. These locations are expressed along the one of the major coordinate axes that aligns best with the dominant flow direction of the region.

4.2.6.2 Entrainment Histories The spatial entrainment profiles must be converted into time-histories for compatibility with all the other operating conditions and the sequencing in the detailed chemistry calculations. Of course, the time coordinate in this history must be the same as in the temperature histories. In the evaluations of the gas temperature histories, position along the dominant flow direction was already assigned a nominal residence time. This same time line is applied to the entrainment positions.

4.2.7 Detailed Chemical Reaction Mechanisms

Once the equivalent reactor network has been specified, the chemistry in each reactor in the network is sequentially evaluated from the species balances based on elementary reactions for the gas phase and on soot. The chemical reaction mechanisms incorporated into our simulations, and how they were used in APP have been described in a previous report.[13] This section briefly reviews the reaction mechanisms. Detailed discussions on the structure of CRF flames are presented in Section 4.5.

A multitude of fuel species – CO, H_2, CH_4, C_2H_2, HCN, soot, and char – compete for the available O_2 in a p. f. flame. This competition determines local heat release rates, which govern flame stability, combustion efficiency and UBC, and the local oxidizing potential of the gas phase, which governs N-species conversion. The central premise behind our modeling approach

is that the crucial outcome of this competition cannot be forecast from the burning rates of the individual fuels determined in isolation. Instead, realistic chemical kinetics for each distinctive combustion process must be incorporated into a comprehensive analysis. Our analysis incorporates the most comprehensive chemical reaction submodels available, and imposes no *a priori* assumptions whatsoever regarding the apportioning of O_2.

The devolatilization submodel, called FLASHCHAIN®, distinguishes primary devolatilization, which relates fuel properties to the composition of volatiles, from secondary volatiles pyrolysis, which generates the volatiles that actually burn in p. f. flames. FLASHCHAIN® determines the complete distribution of primary products from almost any p. f., and also predicts the yield and elemental composition of char.[15] When combined with a swelling factor correlation and a correlation for the initial carbon density in char, it specifies all the necessary char properties for a char oxidation simulation. Hence, the complete distribution of volatiles, including gaseous fuels and soot, and all char properties are completely determined from the fuel's proximate and ultimate analyses.

The reaction mechanism for chemistry in the gas phase must describe the ignition and combustion of all secondary volatiles pyrolysis products, as well as the conversion of all N-species across the full range of S. R. values in p. f. flames. Our homogeneous reaction mechanism contains 444 elementary reactions among 66 species, including all relevant radicals and N-species.[16] It is implemented in the simulations without any approximations whatsoever. All rate parameters were assigned independently, so there are also no adjustable parameters in the submodel for gas phase chemistry.

Soot plays several important roles. As it burns, it directly competes for the available O_2 and also consumes O-atoms and OH that would otherwise sustain homogeneous chemistry. Soot also promotes recombinations of H-atoms and OH that could also sustain homogeneous chemistry.[17] And soot reduces NO directly into N_2. Our soot chemistry submodel depicts all these effects in the form of a collection of elementary reactions that can be coupled to the homogeneous reaction mechanism within the CHEMKIN/SURFACE CHEMKIN framework.

Char burning rates are determined by thermal annealing, ash encapsulation (of low-rank chars), and a transition to chemical kinetic control. The Char Burnout Kinetics (CBK) Model includes all these effects, and depicts the impact of variation in gas temperature, O_2 level, and char particle size within useful quantitative tolerances.[18] However, it is not yet possible to specify the initial char reactivity within useful tolerances from the standard coal properties. We must calibrate this value with LOI predictions or some other suitable index on combustion efficiency. The submodel for char-N conversion is subject to a similar calibration requirement (with NO emissions), compounded by its simplistic mechanistic premise; viz., that a fixed fraction of char-N is converted into NO at the overall burning rate throughout all stages of char oxidation.

To summarize the status of our reaction mechanisms, we believe that the submodels for devolatilization, homogeneous chemistry, and char burnout are complete, whereas those for soot/radical chemistry and for char-N conversion will probably be subject to revisions in the near term. Neither of these latter two situations introduces significant uncertainties into NEA's simulations of the CRF. Since these reaction mechanisms have already been independently

validated across an enormous domain of conditions, what matters most is the degree to which all model parameters can be specified from the available information on the furnace operating conditions. The initial char reactivity and the fraction of char-N converted to NO can only be specified from calibration procedures, whereby these parameters are adjusted to match the predicted LOI and NO_X emissions to reported values for a single set of operating conditions. Then the same values should be imposed for all other operating conditions. Except for these two parameters, all other model parameters can be assigned from the fuel's proximate and ultimate analyses within useful quantitative tolerances, or directly adopted from literature.

4.2.8 Implementation

A diagram of the information flow in the computerized version of the APP calculations appears in Figure 4-4. A custom FORTRAN program sequences through the reactor network region-by-region, and element-by-element within each region. All the chemical submodels were implemented in the conservation equations for each CSTR in the network, as follows: The jth CSTR is fed by an inlet char flow, F^C_j, an inlet flow of gaseous fuels and combustion products plus soot, F^P_j, and an entrainment flow, F^E_j, which consists of volatiles or secondary air or OFA in the CRF. In the analysis, the key organizational principle is the competition for O_2 among chemistry in the gas phase versus the oxidation of soot and char, which is apparent in the following oxygen balance for a CSTR in the network:

$$F_j^E y_{O_2,j}^E + F_j^P y_{O_2,j}^P - F_{j+1}^P y_{O_2,j+1}^P = \frac{\Delta X_j^C F_0^C (1 - x_0^A)\nu_C}{M_C^{'}} - M_{O_2} V_j \omega_{O_2} \qquad (4.2.8)$$

where subscript j denotes the index on the CSTR under consideration; superscripts E, P, and C denote entrainment, gaseous product, and char flows, respectively; and y^I denotes the oxygen mass fraction in stream I. The terms on the left of the balance represent the net efflux of O_2 from the jth CSTR. The two terms on the right represent the O_2 consumed by char oxidation and by oxidation of gaseous fuels and soot, respectively. The consumption term for char oxidation is written in terms of the burnout predicted by CBK for the residence time increment of the jth CSTR, ΔX^C_j, and the flowrate of ash-free combustibles into the furnace, $F^C_0(1-x_0^A)$. The stoichiometric O_2 requirement, ν_C, and the char molecular weight, M_C', account for the presence of heteroatoms in the char combustibles. The consumption term for oxidation of gaseous fuels and soot incorporates the molar rate of O_2 consumption per unit volume, ω_{O2}.

These rates were determined with CHEMKIN and SURFACE CHEMKIN software, then incorporated into the iteration routine that satisfied the oxygen balance. Rates were converted to a mass basis by multiplying by the molecular weight of O_2, M_{O2}, and the CSTR volume, V_j.

Note that the analysis does not determine the apportioning of O_2 among the various fuels in this reaction system in advance, or through any imposed constraints. The kinetics for oxidation of soot, char, and gaseous fuels govern O_2 apportioning, as in actual p. f. flames.

On a P4-based microprocessor operated at 1.5 GHz, each simulation of a CRF reactor network takes from 15 to 50 min, depending on the fuel combination and network specifications.

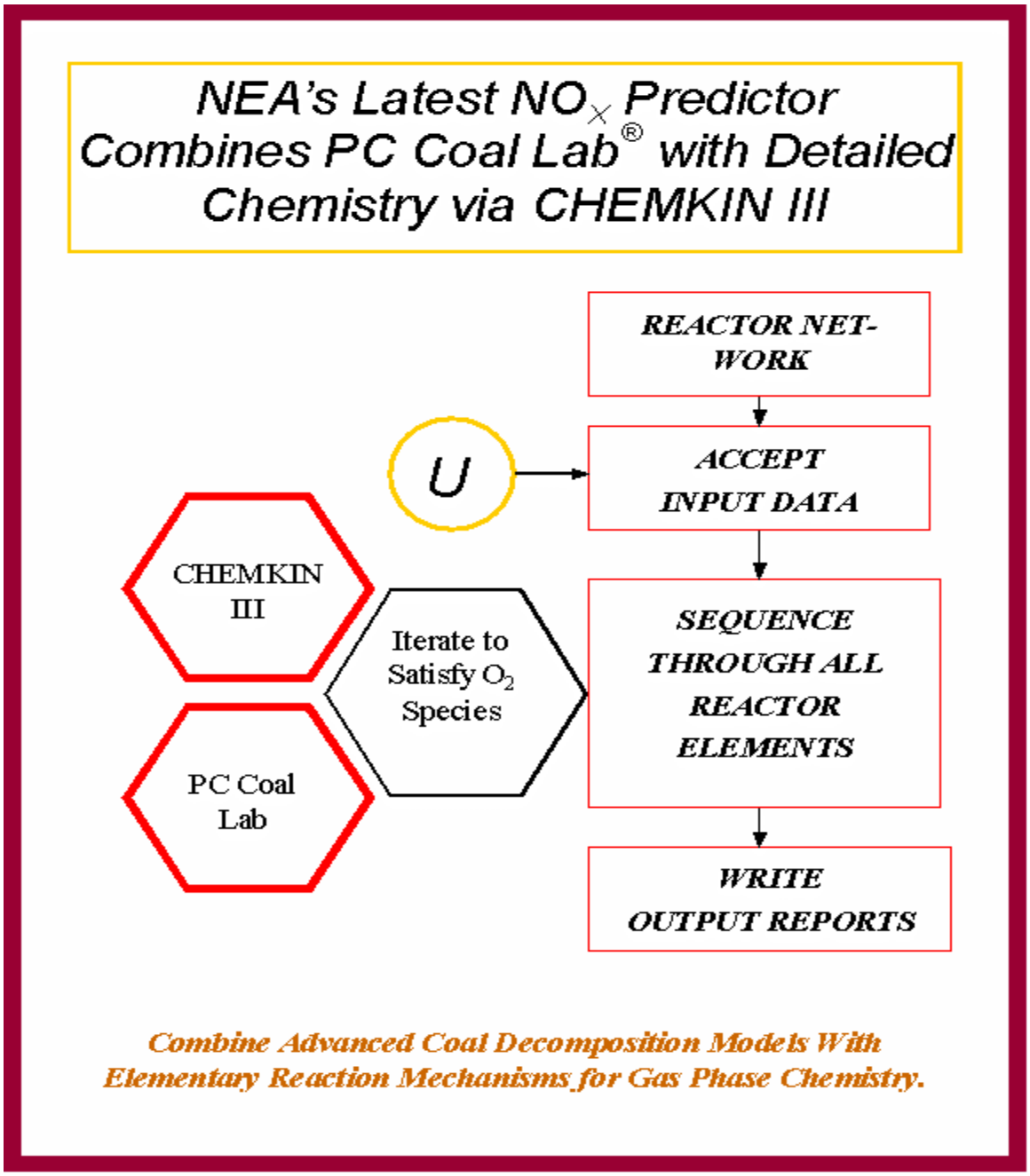

Figure 4-4. Information flow in the computerized APP analysis for CRF flames.

4.3 The Emissions Database – Nominal Fuel Properties

4.3.1 Overview

The testing program at Southern Research covered a broad domain of fuel quality, fuel injection configuration, burner type, staging level, and furnace stoichiometry. The nomenclature used to distinguish the various cases, and reports the fuel properties have been introduced in Section 3 and the database of information that was used to validate the modeling effort is presented in Appendices A and B.

The testing program characterized four major independent parameters: (1) Fuel quality, including fuel type, cofiring specifications, and grind size; (2) Injection configuration, including co-milling all blend components, core injection of biomass, and side (or off-axis) injection of biomass; (3) Staging level of 0, 15, or 30 % OFA; and (4) Furnace stoichiometry to impose exhaust O_2 levels (wet) from 2.5 to 4.5 (vol.) %. In addition to the major parameters, burner type was investigated in one test series by replacing the coaxial fuel injector with a dual-register burner. Variations in each of these parameters are discussed in Section 3.

Fuel quality was varied by firing four diverse coals with two forms of biomass. In addition, in one series one of the biomass forms was spiked with NH_3, to simulate the behavior of animal production wastes like poultry litter. Nominal properties of the six primary fuels appear in Table 4-1. The fuels are arranged in columns in order of increasing rank, from left to right, and labeled with a 2-letter code that has used throughout this report. More complete fuel information is included in Tables 3-2 through 3-4. These results are included because they represent the data

Table 4-1. Nominal Fuel Properties used for model calculations.

	Sawdust **SD**	Switch Grass **SG**	Jacobs Ranch **JR**	Galatia **GL**	Pratt **PR**	Jim Walters **JW**
Proximate, as rec'd						
Moisture	9.5	15.2	19.3	5.8	1.9	0.8
Ash	0.4	29.5	5.4	6.6	15.1	14.6
Volatile Matter	78.1	47.6	39.6	33.7	33.2	20.0
Fixed Carbon	11.9	7.7	35.7	54.0	49.9	64.6
Ultimate, daf wt. %						
C	49.8	56.1	74.9	81.8	83.4	89.5
H	6.1	5.4	4.9	5.0	5.5	4.6
O	43.9	35.7	18.8	10.0	7.5	3.3
N	0.2	2.4	0.9	2.0	1.8	1.7
S	0.0	0.4	0.4	1.1	1.8	0.9
PSD						
$\langle d_P \rangle$, μm	163	173	28.8	53	48	34
RR-n	2.1808	2.2617	0.9405	1.7353	1.3111	1.0082
RR-b, cm	5518.2	6728.2	169.71	6116.5	752.06	211.46

incorporated into the modeling effort. In particular, the results for SG in Table 4-1 were early results from Test PR-1. Later, reanalysis produced more correct results and these are included in Table 3-4.

Moisture levels are highest for the low-rank fuels, especially SG and JR. Ash levels are widely variable and especially high for biomass SG and for coals PR and JW. Whereas it appears that the volatility of SD is much higher than SG's, on a dry-ash-free (daf) basis, their volatilities are almost identical. However, the daf volatiles contents of the coals fall by more than a factor of two over this suite of samples, which will definitely affect the conversion of coal-N into NO_X. Carbon contents increase and oxygen contents decrease for fuels of progressively higher rank. The pair of biomass samples represents most of the range of elemental compositions seen for diverse forms of biomass. The represented range of coal rank, from subbituminous through lv bituminous, is similarly broad. The hydrogen, nitrogen, and sulfur levels are not rank-dependent. Whereas almost all biomass contains little nitrogen and sulfur, sample SG contained the most nitrogen of any of the fuels, due to its decomposition before firing.

The particle size distributions (PSDs) are typical utility grinds for the coals, except for the much finer grinds of JR and JW, whereas the biomass grinds are much coarser, as expected. The pairs of Rosin-Rammler parameters were assigned from pairs of size fractions provided by Southern Research.

All the fuel properties in Table 4-3. are nominal values. Some of them varied during the course of the testing program, especially the grind sizes of the coals that were co-milled to much finer PSDs with biomass. These properties and grind sizes were provided by Southern Research for each test series, and these values were used in the corresponding simulations and are included in Appendix B. Fuel properties evaluated with samples from the fuel discharge tube off the pulverizer were used whenever possible. It should be noted that at this point, pulverized fuel is typically found to be somewhat finer than is measured at the discharge point of the mill where particle size is controlled to be 70% ± 2% < 75mm. This additional milling is an artifact introduced by movement through a dense-phase transport system used to convey milled fuel to a day bin next to the furnace in the CRF and may mimic effects of coal transport in a full-scale facility.

4.4 Reactor Network Specifications

This section reports the specifications for the reactor networks used to simulate the various test series. First, the evaluation procedures are illustrated with the PR-only flame, and then the final specifications are surveyed for all other series. Since a small number of CFD simulations were provided for the APP analysis, various extrapolation and calibration procedures are also reported here.

4.4.1 Network Specifications for the PR Baseline Flame

As explained in Section 4.2, branches in the equivalent reactor network represent distinctive regions (or structural elements) in the flame. Temperature histories of gases and walls, mean residence times, the numbers of CSTRs in each CSTR-series, and the entrainment histories of all surrounding flows must be specified for each region. This section illustrates these specifications

from the analysis of the CFD simulation for the baseline PR-only flame with co-milled injection, 15 % OFA, and 3.5 % exhaust O_2.

4.4.1.1 Operating Conditions The operating conditions for four distinct regions must be specified: a flame core (CR), mixing layer (ML), OFA injection region (OF), and burnout region (BO). Fluid (massless) element tracking was used to assign thermal histories and residence time distributions (RTDs) for each region. Thermal histories of individual particles were averaged to assign nominal thermal histories throughout each region. A number of CSTRs in series was assigned to each region by fitting the analytical RTD expression for a series of CSTRs (in eq. 4.2.4) to the CFD-based RTDs. Whenever more than 25 CSTRs were assigned, the flow pattern was regarded as plug flow although, in practice, the CSTR-number for which the predictions become insensitive to the CSTR-number is determined by the governing chemical reaction mechanisms for the particular region under consideration.

RTDs for the core, mixing layer, and burnout zone determined with fluid element tracking throughout the CFD flow field appear in Figure 4-5, along with their analytical representations. The RTD for the core was deconvoluted into one component for 13 CSTRs-in-series and another for plug flow with respective mean residence times of 138 and 192 ms. The plug flow component represents the near-axial fluid motion under the influence of particle drag, and the CSTR-component represents flow with significant radial velocities. The RTD for the mixing layer was matched with a series of 19 CSTRs, and that for the OFA zone (not shown) was represented by 6 CSTRs-in-series. The burnout zone is essentially in plug flow.

Since the CFD-based RTDs determine the nominal residence time for each region, and the analytical fits to each RTD determine a CSTR-number, the incremental residence time for each CSTR can be evaluated as their ratio.

The CFD-based and discrete rendition of the gas temperature history for the core of the same flame appears in Figure 4-6. This particular determination was based on a series of 16 CSTRs, representing a total residence time of 163 ms. Each temperature in the CFD-based history was determined as the average temperature across the core, transverse to the flow direction. To specify the discrete version, this thermal history was subsequently averaged over each increment in residence time for the CSTR-series that represents the core. Since the incremental residence time is only 10 ms, the discrete rendition depicts the CFD-based thermal history without undue uncertainty. Thermal histories for wall temperature were assigned the same way, and both histories were assigned for all regions in the flame with the same method.

In addition to the ambient thermal history, an average thermal history of particles through the core is needed for the devolatilization simulation. The history used in the simulation is compared to the CFD-based history in Figure 4-7. There is a non-physical lag in the CFD-based history which was deliberately omitted in the assigned history. Even so, the heating rates for both cases are too similar to affect the predicted devolatilization behavior. The discrepancy for times longer than 60 ms is also inconsequential because devolatilization is complete by this time. A histogram of incremental residence times for the associated CSTR-series is superimposed on the thermal histories. This does not imply that the devolatilization simulation is based on a discrete rendition of the particle temperature history. Rather, the cumulative volatiles yields and

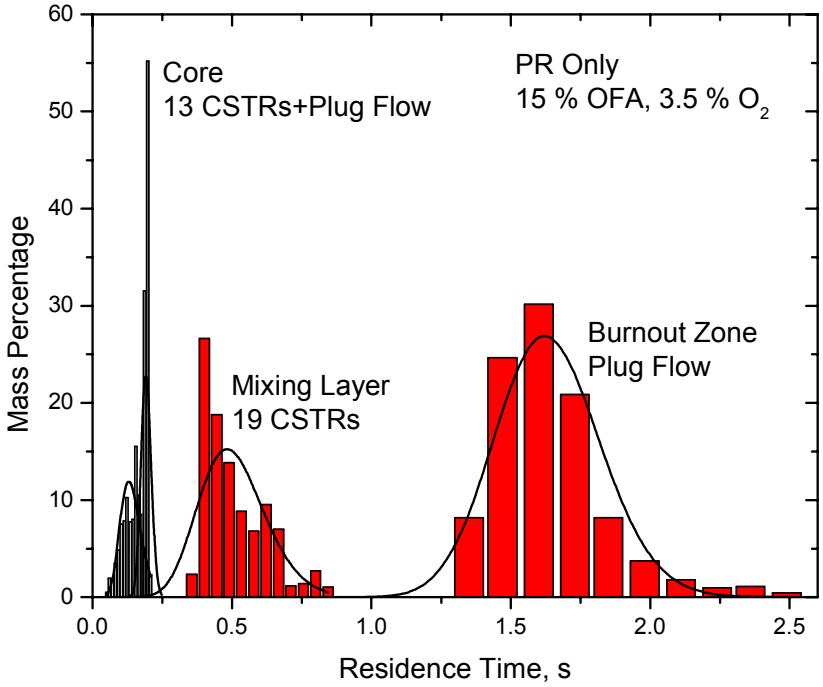

Figure 4-5. RTDs from the CFD simulation (columns) and assigned analytically (curves) for the core, mixing layer, and burnout zone of the PR-only flame with 15% OFA and 3.5 % O_2.

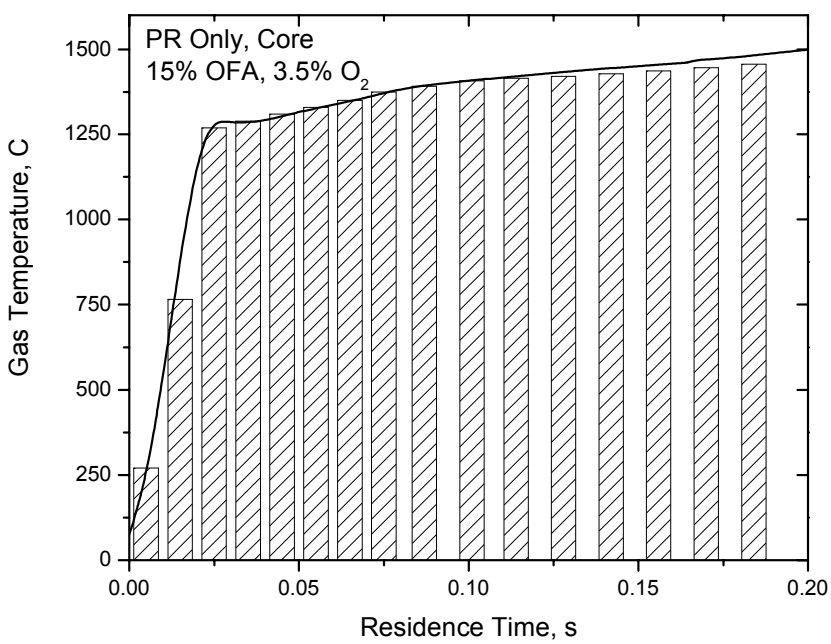

Figure 4-6. Gas temperature history assigned to the CSTR series for the core (histogram) compared to the history assigned from the CFD simulation (solid curve) for the PR-only flame with 15% OFA and 3.5 % O_2.

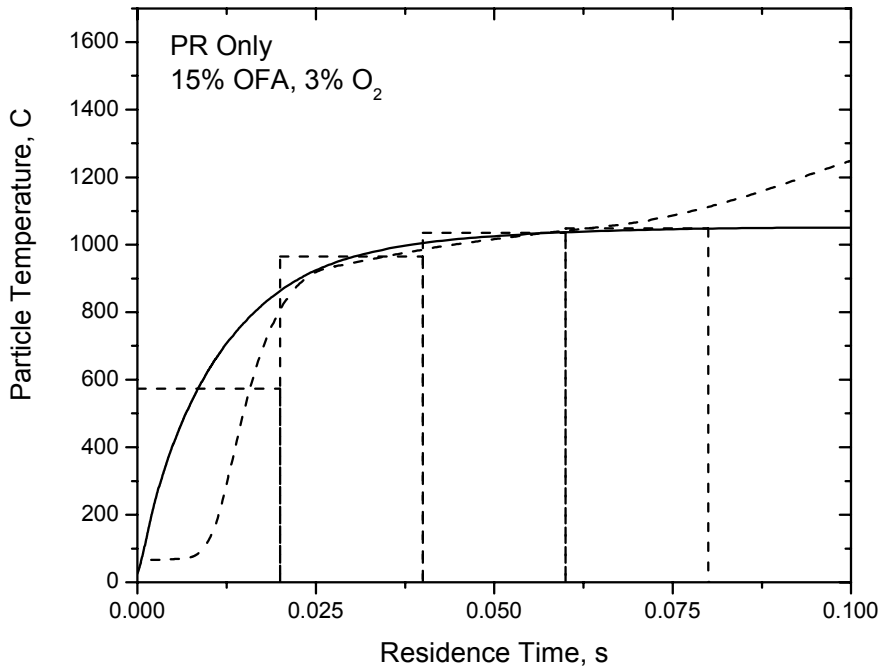

Figure 4-7. Mean particle temperature history assigned for devolatilization simulations in the core (solid curve) compared to the history assigned from the CFD simulation (dashed curve) for the PR-only flame with 15% OFA and 3.5 % O_2.

compositions are apportioned to each increment in residence time to specify the release of volatiles into individual reactors in the CSTR-series.

Entrainments of secondary air into the mixing layer and of OFA into the process flow were first evaluated directly from the CFD simulation with the method described in Sec. 4.2.6. The entrained fraction of secondary air into the ML in the baseline flame appears in Figure 4-8. The entrainment rate decays exponentially across the mixing layer, with substantial irregularities, and reaches an asymptotic value of 0.84, which is the portion of the secondary air not immediately entrained into the primary stream near the fuel injector outlet. Such air entrainment was incorporated into the simulations with detailed chemistry with either of two simple mixing models, whose behavior is illustrated in Figure 4-9. The curves in this figure depict the volumetric air entrainment rate at each point downstream of a common injection point. For jets in co-flow, the entrainment volume grows with distance from the injection point, according to the following functional form:

$$F_E = \exp(\beta_M (t - \tau_M)) - 1 \qquad for \quad t \geq \tau_M \tag{4.4.1}$$

where F_E is the fraction of the air stream that has been entrained into the process flow to time t; τ_M is a time lag equal to the nominal residence time to the injection point; and β_M is an empirical

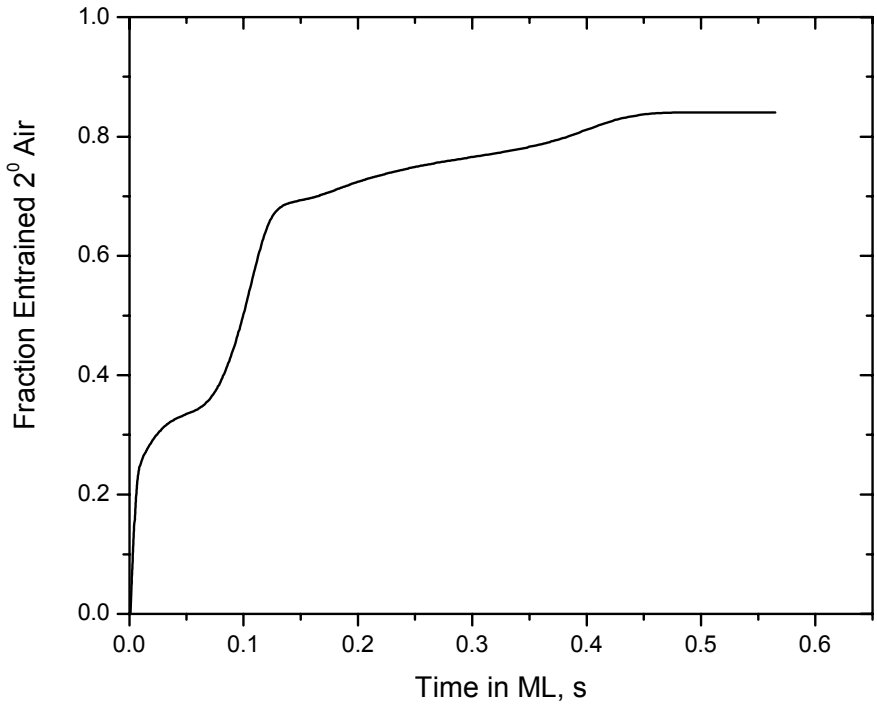

Figure 4-8. Fraction of entrained secondary air into the mixing layer from the CFD simulation for the PR-only flame with 15% OFA and 3.5 % O_2.

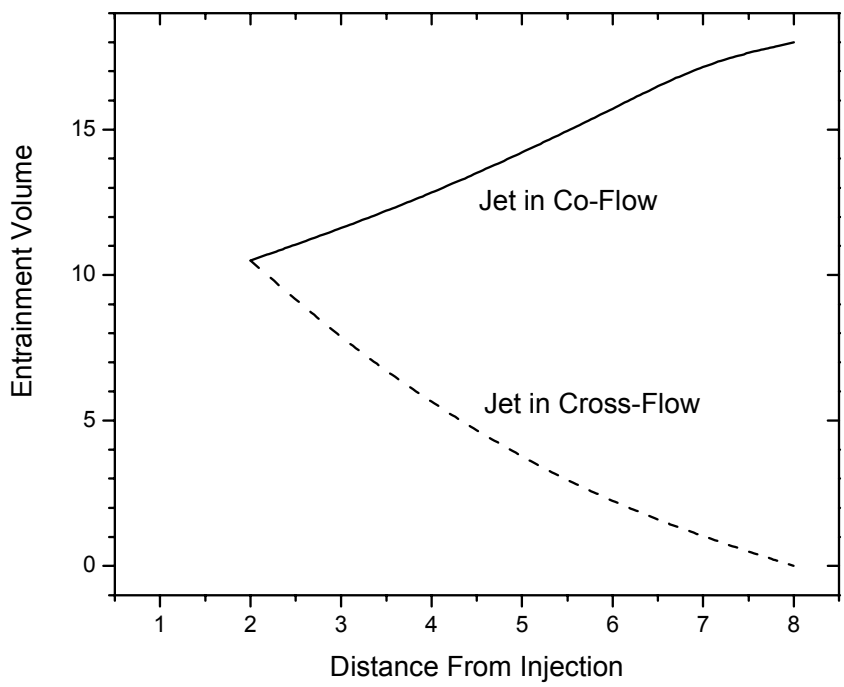

Figure 4-9. Entrainment volumes for two limiting mixing models versus distance from the point of injection.

mixing constant. According to equation 4.4.1, the entrainment rate grows with distance from the injection point until the entire secondary stream has been entrained.

For jets in cross-flow, the entrainment volume diminishes with distance from the injection point, according to

$$F_E = 1 - \exp(-\beta_M (t - \tau_M)) \qquad for \quad t \geq \tau_M \tag{4.4.2}$$

According to this relation, the entrainment rate diminishes with distance from the injection point until the entire secondary stream has been entrained.

Once the parameters in one of these mixing models were assigned by fitting an entrainment history, the continuous profile of entrainment fraction versus time from the injection point was resolved into discrete additions to each CSTR in a series. Since the entrainment of secondary air into the primary air stream is very rapid, no finite-rate mixing models were applied. That entrainment was simply added to the initial primary air stream.

To summarize, the mean residence times and the CSTR-number for each region were assigned from the CFD-based RTDs. Their ratio specified the nominal residence time for each CSTR. Temperatures were assigned to each isothermal CSTR from the CFD-based gas thermal histories. The effective radiation temperature in the energy balance for burning char was specified in the same way from the wall temperature history. But particle temperature histories did not need to be discretized, because a stand-alone devolatilization simulation could be based on essentially the same CFD-based particle temperature history. However, the release of volatiles and their compositions were rendered into discrete increments for each CSTR immediately downstream of the fuel injector. Rapid, near-burner entrainment of secondary air simply supplemented the primary air. But one of two finite-rate mixing models was fit to the CFD-based entrainment histories and implemented in the detailed chemistry simulations.

4.4.1.2 Calibration Procedures As explained in Sec. 4.2.7, two model parameters must be specified to fit the predicted emissions to the measured values for a baseline test condition. The fraction of char-N converted to NO during char oxidation was assigned to fit the NO_X emissions from the PR-only baseline flame, as shown in Figure 4-10. A fixed fraction of 0.38 was specified for this particular coal with data for the baseline flame, then the same value was used in all other test series with this coal, including all co-firing combinations and injector configurations. The fit of the baseline NO_X data is within experimental uncertainty at all operating conditions, except for the lowest O_2 levels with 15 % OFA and, perhaps, with the highest O_2 level in the unstaged flame. The discrepancy at low O_2 levels is not a symptom of flawed reaction mechanisms. Rather, it is a reflection of numerical instabilities that prevented converged solutions for the parameter assignments that would have better depicted this portion of the dataset. Note also that since the data in Figure 4-10 cover broad ranges of OFA and exhaust O_2, the fits of the predictions were also determined by the extrapolation procedures described below in Sec. 4.4.2, as well as the assigned value of the char-N conversion factor.

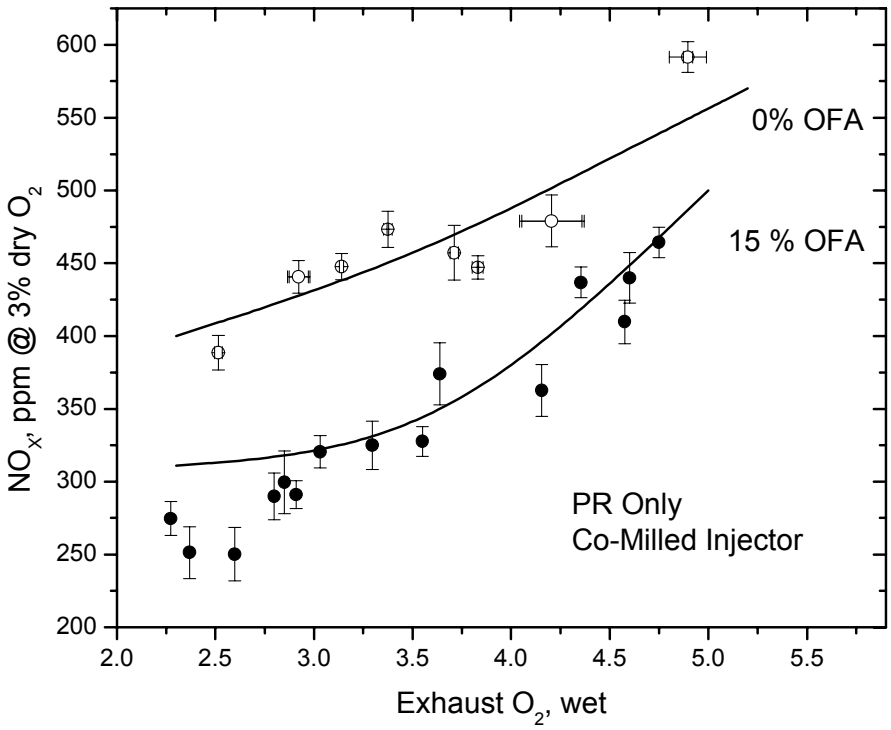

Figure 4-10. Fit of predicted NO_X emissions to the data for the PR-only flames with 0 and 15% OFA and various O_2 levels.

A second calibration was anticipated for the initial char oxidation reactivity, prior to annealing, because the default values assigned by CBK can depict the tendency for slower burning rates for chars of progressively higher rank, but not the sample-to-sample variability. We originally intended to specify the reactivity to match the LOI data for the baseline flames of each coal, and then apply the same value to all other test simulations with the same coal. Unfortunately, CBK was unable to predict LOI levels as low as reported in the vast majority of the Southern Research tests, so this calibration had to be omitted. The likely reasons for this problem are discussed in Section 4.5.4.2, after the NO_X predictions are presented. We did find, however, that the value for the initial char reactivity affected the predicted NO_X emissions, because O_2 consumed by char oxidation would otherwise be available for chemistry in the gas phase. So char reactivities were adjusted during the course of fitting the baseline NO_X emissions, but by no more than a factor of 3.

4.4.2 Extrapolation Procedures

Only several CFD simulations were developed for the CRF under this project, yet almost 300 tests had to be simulated with detailed reaction mechanisms. The extrapolation procedures reported in this section bridged the gaps in the conditions covered by CFD, and enabled complete network specifications for all test series. The conditions for which CFD simulations were provided are collected in Table 4-2. The high and low entries under both biomass forms denote cases with 15 or 20 wt. % biomass (high) and 5 or 10 % biomass (low). REI provided the simulations for series 1, 3, and 4 and Southern Research provided the simulations for series 7, 8,

Table 4-2. Cases With CFD Simulations.

Series	Injection	Coal-Only	Sawdust		Switchgrass	
			High	Low	High	Low
1	Co-Milled	15 % OFA	15 % OFA	-	-	-
3	Core	15 % OFA	-	-	-	-
4	Side	15 % OFA	-	-	-	-
7	Co-Milled	0, 15 % OFA	15 % OFA	-	15 % OFA	-
8	Core	15 % OFA	15 % OFA	-	15 % OFA	-
12	Co-Milled	15 % OFA	15 % OFA	-		-
13	Co-Milled	-	-	-	15 % OFA	-

12, and 13. Recall that series 1, 3, and 4 were run with PR coal; series 7 and 8 were run with JR; and series 12 and 13 were run with JW. No simulations were available for any tests with GL.

Four of the five series had co-milled injection, and core injection was only characterized for PR only, and for JR coal with and without both biomass forms. The PR-only case with core injection had the supplemental air flow through the core injection tube (which entrains biomass in the cofiring cases), but the JR-only case did not. So the differences between this JR-only case and the one in series 7 are difficult to pinpoint.

All CFD simulations were run for 15 % OFA, except for 1 run for series 7 with JR coal. None of the CFD simulations characterized furnace stoichiometries other than that for 3.5 % exhaust O_2. All the cofiring cases were for the high biomass levels. Given this CFD matrix, extrapolation procedures were needed for variations in exhaust O_2, coal type, and the low biomass cofiring level. Actually, the CFD simulations for series 1 were provided at the start of the second year of this 2-year project, those for series 7 and 8 were provided late in the second year, and those for series 12 and 13 were provided at the end of the second year. To maintain the project schedule, extrapolation procedures were also developed for variations in staging level and injection configuration as well, based on only the CFD simulations for series 1 and 3.

We were surprised to notice three significant differences among the CFD simulations from REI and from Southern Research, with REI's CFS package. First, in the REI simulations, the primary flow significantly expands at the point of devolatilization, but not by nearly as much in the Southern Research simulations for cases with the highest devolatilization yields of all. Second, the OFA jets mixed almost twice as fast in Southern's simulations as in REI's, for essentially the same flow conditions. Third, the entrainment rate of secondary air into the mixing layer of the JW baseline flame was much faster than for all other flames, even though the lower total flowrate should have had slightly slower entrainment. We did not try to compensate for the first two differences, but had to adjust parameters in the simulations to rectify the third. All the CFD simulations should all be examined further as an aspect of quality control.

4.4.2.1 Extrapolations for Furnace Stoichiometry To increase the exhaust O_2 level in the tests, and thereby impose a more oxidizing furnace stoichiometry, the flows of primary air,

secondary air, and OFA were increased while the fuel feedrate was fixed. Since the maximum gas and wall temperatures are always recorded in the mixing layer, where secondary air mixes with the primary flow, we extrapolated from the reference condition of 3.5 % O_2 by slightly elevating the temperature profiles for higher exhaust O_2. Gas and wall temperatures were increased by 5 % for each 1 % increase in O_2 level with 15 % OFA. With no OFA, the 5 % increase was imposed when the O_2 level was increased from 2.5 to 3.5 %, but not when it was increased from 3.5 to 4.5 %, to rectify systematic over predictions in trial simulations at the highest O_2 levels.

In addition, with 15 % OFA, the fraction of secondary air diverted into the primary air stream at the burnout outlet was increased from 0.18 to 0.20 to 0.22 as the exhaust O_2 level was increased from 2.5 to 3.5 to 4.5 %. With no OFA, only the first step change was imposed in the simulations for test series 1, 5, 6, and 7, similar to the extrapolation procedure for the temperature profiles. However, for series 11, 12, and 13, a uniform fraction of secondary air was diverted for all furnace stoichiometries. These incremental changes could not be compared to values from the CFD simulations, because all simulations were for 3.5 % O_2. But the absolute magnitudes are reasonably consistent with the CFD-values, which ranged from 0.14 to 0.21.

Finally, the reciprocal time constant in the mixing model for the mixing layer was reduced by a factor of 4 in cases with 15 % OFA at 2.5 % O_2, once it became apparent that the predicted NO_X emissions based on variations in temperature and diverted secondary air were consistently high. In some runs, the adjusted mixing constant prevented a converged solution and had to be increased to 2.5 s^{-1}, regardless of the mixing time for the baseline reference condition. So the adjustment to the mixing constant is either reduction by a factor of 4 or 2.5 s^{-1}, whichever is greater. Also, in the simulations for series 5 and 6 with no OFA, the baseline value of the mixing constant was applied, rather than the value enhanced by 50 %.

All three of these extrapolation procedures were adopted early in the simulation effort, and were imposed uniformly for all fuels, injection configurations, and test series, except where noted otherwise.

4.4.2.2 Extrapolations for Staging Level In all series except no. 1, staging levels with 0 and 15 % were evaluated. Without staging, the OFA was combined with secondary air, so staging is analogous to decreasing the furnace stoichiometry with respect to the near-burner flame structure: There is less secondary air at fixed conditions in the primary stream as the staging level is increased. Consequently, gas and wall temperature profiles for the staged case were increased by 5 % for the simulations of an unstaged case at the same O_2 level. The fraction of secondary air diverted into the primary stream was not increased, although the strength of the diverted flow increased in proportion to the increase in secondary air for unstaged cases.

The mixing constant was increased by 50 % for all unstaged cases, assuming that the much higher secondary air flows promoted faster mixing in the mixing layer. Since the geometry of the fuel injector was fixed, higher secondary air flowrates impose a greater velocity difference across the primary and secondary flows, which often enhances mixing. Even so, the magnitude of the enhancement was assigned by fitting baseline NO_X emissions, not from a legitimate mixing analysis.

The complete matrix of extrapolation factors appears in Table 4-3. The baseline reference conditions are 15 % OFA with 3.5 % O_2, and the baseline temperature profiles, $T_B(t)$, and mixing constant, R_B, are presumably available from a baseline CFD simulation. The baseline temperature profile is increased by 5 % for every 1 % change in the exhaust O_2 level, except for the highest O_2 without OFA. The secondary air entrainment fractions follow the same pattern, in increments of 0.02. The mixing constant is reduced for the lowest O_2 level with 15 % OFA, but increased by 50 % for all unstaged flames. This matrix of extrapolation factors was applied uniformly to all test series, unless explicitly noted otherwise.

Table 4-3. Matrix of Extrapolation Factors.

	Exhaust O_2, %		
OFA, %	2.5	3.5	4.5
15 % OFA			
T(t)	$0.95T_B(t)$	$T_B(t)$	$1.05T_B(t)$
2^0 Ent. Fr.	0.18	0.20	0.22
R_{MIX}, s^{-1}	$R_B/4$ or 2.50	R_B	R_B
0 % OFA			
T(t)	$T_B(t)$	$1.05T_B(t)$	$1.05T_B(t)$
2^0 Ent. Fr.	0.18	0.20	0.20
R_{MIX}, s^{-1}	$1.5R_B$	$1.5R_B$	$1.5R_B$

4.4.2.3 Extrapolations for Cofiring Level and Biomass Form None of the baseline CFD simulations represented a low cofiring level, which was either 5 or 10 wt. % in the tests. Many of the simulation parameters for such cases were specified by interpolating values for the coal-only and high cofiring cases. The interpolated parameters included residence times in the core, mixing layer, and burnout zones; mixing parameters; and temperature histories. CSTR-numbers were usually the same for all fuel combinations. Interpolated temperature histories for the sawdust cofiring cases from test series 1 appear in Figure 4-11. In general, biomass cofiring steepens the gas heating rate, and slightly increases the maximum temperatures of the gases and walls. Consequently, both the magnitudes of the temperatures and the heating time scales were adjusted to obtain the interpolated temperature histories.

CFD simulations were available for both sawdust and switchgrass for series 7, 8, 12, and 13. The temperature histories for the regions in the equivalent reactor network were very similar for both biomass forms, so the same temperature histories were applied for all biomass forms. The CFD-based regional residence times and mixing constants were used for each biomass form, although they were also very similar.

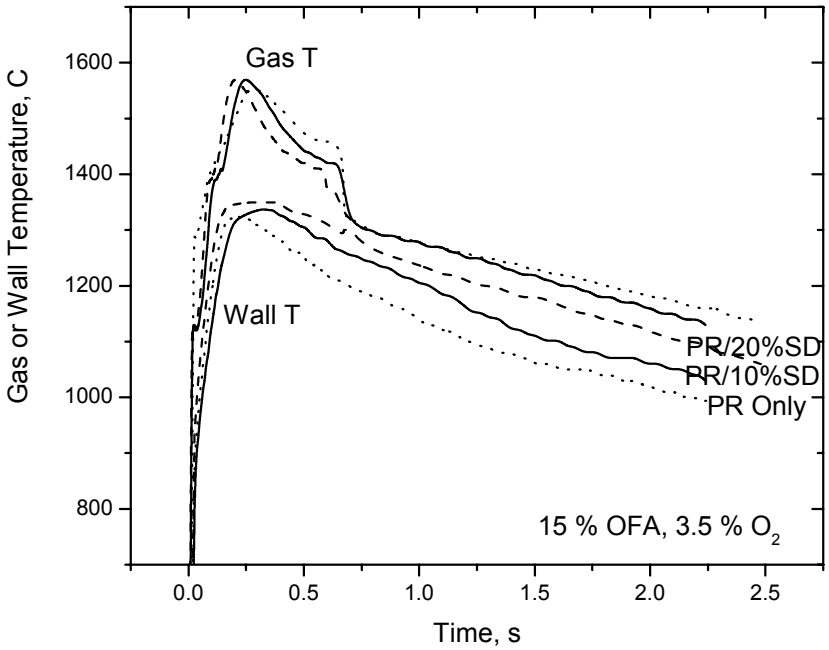

Figure 4-11. CFD-based temperature histories for PR only (dotted curves) and PR/20%SD (dashed curves), and the interpolated histories for PR/10%SD (solid curves).

4.4.2.4 Extrapolations for Injection Configuration In the core injection mode, biomass was entrained into the core of a coal flame through a separate flow tube on the fuel injector centerline. The entrainment medium was 30 SCFM air, in addition to the normal primary air flow. The supplemental flow represents an 11 to 15 % enhancement of the primary air stream. This perturbation is definitely significant for NO_X production, but it did not appear to appreciably perturb the flow field near the burner. The parameters assigned from the CFD simulations that included the supplemental air flow were not appreciably different from the comparable cases with co-milled injection. Consequently, no extrapolation procedure was devised for core injection, although the supplemental air flow was added to the reported primary air flowrates, and CFD-based parameters were used whenever possible for the core injection cases. The same extrapolation matrix (in Table 4-3) was applied to the series with core injection.

A CFD simulation was provided for series 4 with side injection, but this series was ignored because the NO_X reduction performance was poor in comparison to both other injection configurations.

4.4.2.5 Extrapolations for the Dual-Register Burner Series 9 used a dual-register burner (DRB) instead of the standard fuel injector. However, CFD simulation was not possible for this case. As it would not be feasible to extrapolate the performance of a DRB from the much simpler fuel injector, due to the formation of an internal recirculation zone in the near-burner region, series 9 was not simulated with detailed reaction mechanisms.

4.4.3 Ranges of Network Specifications

Complete sets of network specifications are too numerous to tabulate because even tests with very similar operating conditions often have slightly different network specifications. The reason is that many cases have CSTR-numbers for cores and mixing layers adjusted by one from the value based on the CFD-RTD. Such adjustments were necessary to obtain stable solutions that represent the ignition of volatiles within the core. Cores have gas temperature histories that rapidly increase from roughly 150°C to flame temperatures. Over this range, the volatiles burning rates increase from essentially zero, through ignition, to the quasi-steady values in flames. This transition is resolved in terms of discrete increments for each CSTR in the series that represents the flame core region. Occasionally, the solution for one of the CSTRs in the series becomes unstable, because the combustion kinetics vacillate between the slow-burn and fully ignited states. Whereas it is very difficult (if not impossible) to resolve the ignition event within a single CSTR, we were able to circumvent these problems by perturbing the number of CSTRs in the series. The CSTR-number had to be changed by only one or two units in all such cases in this project. Since the CSTR-numbers in all regions except the OFA region were usually greater than 10, the perturbation was probably inconsequential.

Ranges for the regional residence times and CSTR-numbers are collected in Table 4-4. The core values have been subdivided further into a devolatilization sub-region and a NO_X reduction sub-region, as illustrated in Figure 4-3 for the baseline PR flame. Residence times for the entire core range from 100 to 170 ms. But the more important specification is on the NO_X reduction region, because near-burner NO_X emissions are largely determined by the time available for NO reduction before the primary flow penetrates the mixing layer (as explained in Section 4.5.2). Cases with the lowest residence times in the NO_X reduction zone tend to have significantly higher NO_X emissions, all else being equal. The bulk flow pattern in the core is near-plug flow because the associated CSTR-series always contain more than 10 units, and often had about 20 units.

Table 4-4. Ranges of Network Specifications.

Region	Residence Time, s	CSTR-Number
Core – Devol.	0.060 – 0.080	5 – 12
NO_X Red.	0.040 – 0.110	7 – 20
Mixing Layer	0.530 – 0.575	12 – 25
OFA Jets	0.055 – 0.110	6
Burnout Zone	1.400 – 1.800	15 or 35

Residence times in the mixing layer were fairly similar at roughly 550 ms in all cases, and the flow pattern could be represented with CSTR-numbers similar to those in the core. The only region without a mostly plug flow pattern is the OFA zone. Six CSTRs were specified in all cases, although the CFD-based RTDs often indicated CSTR-numbers as few as three. Unfortunately, these cases caused convergence problems. Since gas phase chemistry in the OFA jets is negligible, the CSTR-numbers could be safely increased to circumvent the convergence issues. Assigned residence times for the OFA jets varied by a factor of two between the CFD-

providers (as noted in Sec. 4.4.2) even though the flow conditions and geometry were essentially the same in all cases. The nominal residence time for the burnout zone is 1.5 s or more. The flow pattern is definitely plug flow, so the simulations were initially conducted with 35 CSTRs. Succeeding cases demonstrated that the same results could be obtained with 15 CSTRs, because chemistry in the gas phase is negligible throughout this region.

Mixing constants varied from 6 to 9 s^{-1} for the mixing layer in the coal-only baseline cases, and roughly 9 s^{-1} for the OFA jets. Values tended to be lower for cofiring cases. These variations significantly affect the predicted NO_X emissions. Since the bulk flow patterns were very similar in all flames, variations in the network specifications on residence time and CSTR-number were not especially significant. But variations in the mixing intensities, especially in the mixing layer, were definitely important.

4.4.4 Complete Input Specifications

In addition to the network specifications discussed to this point, various additional properties and conditions were assigned for the APP simulations. Fuel properties consisted of the proximate analysis, on an as-received basis, and the ultimate analysis, on a daf basis, plus the two Rosin-Rammler parameters for the fuel PSD. The fuel analyses were updated for every test series, based on the analytical results provided by Southern Research. The Rosin-Rammler parameters were assigned from fits of two size fractions on standard sieves for each fuel provided by Southern Research. The proportions of biomass in cofiring tests were reported by Southern Research. Once the char-N conversion factor and initial char oxidation reactivity were specified in coal-only calibrations, the same values were used for all other simulation cases with that particular fuel.

The reported flowrates of all air streams were imposed in the APP simulations. Air stream compositions were taken from the initial series of CFD simulations from REI and used in all APP simulations. However, the reported fuel feedrates were found to be subject to calibration uncertainties late in the testing program. We adjusted the reported values to obtain the reported exhaust O_2 level in the simulation results. Generally, these adjustments were only about 5 %.

4.5 Results

Our main objective is to predict emissions that agree with the reported values within useful quantitative tolerances across the entire domain of operating conditions in the CRF database. Obviously, fuel quality impacts are the central focus, although variations in staging level and furnace stoichiometry are also important in applications. Injection configuration soon became unimportant after the testing program established that co-milling achieved the greatest extents of NO_X reduction with cofiring; in fact, the side injection scheme was omitted from the simulation cases due to poor performance.

This chapter presents NEA's APP predictions that demonstrate the accuracy of the NO_X predictions for biomass cofiring across the entire range of fuel quality of practical interest. We have also predicted essentially complete char burnout for most cases, although the predicted LOI values are often many times higher than the measured values (because the basis for LOI is the coal ash, not the portion of combustibles in the fuel). We remain confident that the accuracy of

the LOI prediction could be restored by additional analysis, but relegated that work to a continuation project, due to the current limitations on schedule and budget.

The discussion is this section moves through the mechanistic basis for NO_X reduction via biomass cofiring, beginning with the distinctive devolatilization behavior of the various fuels in the testing program. The detailed flame structure of CRF flames is then illustrated in detail, to provide a mechanistic basis to interpret the NO_X predictions for the various test series. Then the NO_X and LOI predictions are presented in turn, followed by our interpretations for the major trends.

4.5.1 Predicted Devolatilization Behavior

We will soon see significant NO_X reduction via biomass cofiring, even in cases in which the N-content of the biomass exceeded the coal-N level. These results are a clear indication of favorable perturbations to the N-conversion chemistry in the near-burner flame zone by the devolatilization products from the biomass. We therefore review the predicted distributions of the gaseous products and soot that burn and convert fuel-N during the initial stages of combustion. Since the heating rate of primary air in the CRF is very fast, the primary devolatilization products are instantaneously converted into secondary volatiles pyrolysis products. The predominant transformation during secondary pyrolysis is the conversion of tar into soot, with simultaneous release of tar-O as CO, tar-H as H_2, and most of the tar-N as HCN. In addition, all aliphatic hydrocarbons are converted into CH_4 and C_2H_2, which can add to the soot phase during the latest stages.

The predicted distributions of secondary pyrolysis products are collected in Table 4-5. Total volatiles yields are the same for both forms of biomass and, at 86 daf wt. %, much higher than the yields from any of the coals. The biomass product distributions are dominated by CO, with substantial amounts of hydrocarbons, especially CH_4, and CO_2 and H_2O. H_2 is another major fuel compound from biomass. But there is surprisingly little soot, considering that tar, the soot precursor, is 25 to 45 % of the daf fuel mass released during primary devolatilization. The reason is the abundance of tar-O, which approaches 40 % of the tar mass. This oxygen converts most of the tar into CO rather than soot during secondary pyrolysis. Essentially all the fuel-N is released as NH_3 during secondary pyrolysis. Note that the abundance of NH_3 with switchgrass, and its higher soot yield and lower CO yield, are the major differences between the two biomass forms.

In contrast, the secondary pyrolysis products from all the coals are dominated by soot which is, by far, the most abundant product. The total hydrocarbon yields are comparable from all coals, but less than a fourth of the hydrocarbon yields from the biomass. Hydrogen yields are also comparable, and double those from biomass. The yields of the oxygenated gases diminish with coals of progressively higher rank, in accord with the trend in the coal-O levels. But even the highest CO yield from JR coal is only about one-quarter the CO yield from the biomass. The only predicted N-species is HCN although, in actuality, a minor amount of NH_3 may have been released from JR coal (but none of the others). The N-species yields are directly proportional to the coal-N levels, as expected.

Table 4-5. Distributions of Secondary Pyrolysis Products and Char Properties.

Component	SD	SG	JR	GL	PR	JW
Volatiles, daf wt. %						
Wt. Loss	86.1	86.0	65.2	56.5	59.8	39.7
Soot	4.3	13.4	30.1	33.7	37.9	26.8
CH_4	7.1	7.4	0.7	0.4	0.5	0.3
C_2H_2	2.2	1.3	1.5	1.0	1.3	2.3
C_2H_4	1.4	1.5	0.0	0.0	0.0	0.0
H_2	2.1	1.7	3.4	3.6	4.0	3.5
CO	48.4	41.5	12.9	7.2	6.1	1.7
CO_2	8.2	8.0	6.4	2.2	1.7	1.0
H_2O	12.1	7.7	7.6	4.9	4.3	1.8
HCN	0.0	0.0	1.26	2.47	2.24	1.52
NH_3	0.24	2.90	0.0	0.0	0.0	0.0
H_2S	0.0	0.44	0.42	1.17	1.91	0.96
Char Comp., daf wt. %						
C	94.7	97.1	98.9	98.4	98.5	98.2
H	3.4	2.5	0.5	0.5	0.4	0.5
O	1.9	0.4	0.0	0.0	0.0	0.0
N	0.0	0.0	0.4	1.1	1.0	1.26
S	0.0	0.0	0.1	0.1	0.1	0.0
Char ash, wt. %	2.5	75.7	15.9	14.2	30.9	21.8
Char size, μm	97.6	103.6	29.9	59.1	54.1	41.7

Char compositions are very similar among all six fuels, except that the most abundant heteroatoms in biomass chars are H and O versus H and N in the coal-derived chars. The char-N levels are negligible in biomass chars – so the assignment of the conversion factor for char-N to NO is inconsequential for biomass (and no factors are reported in Table 4-6, below, in Section 4.5.3.1.1). They are comparable but lower for the coal-derived chars and certainly not negligible. Perhaps the most significant variation in char properties is among the char-ash levels. The values for SG and PR are definitely high enough to inhibit char oxidation during the latest stages of burnout, according to the ash inhibition mechanism in CBK; in fact, the huge ash loading in SG char will prevent predictions of complete burnout for any reasonable thermal history. The mean char sizes are disparate for the biomass and coal chars, but more similar than the whole coal values because biomass shrinks and the coals swell during devolatilization, especially the bituminous coals.

It is worth remembering that both biomass forms generate an abundance of NO_X reductants – hydrocarbons, CO, and H_2 – and release all their nitrogen into the gas phase as NH_3. Their low soot yields compound their NO_X reduction efficacy because soot scavenges radicals from the gas phase that would otherwise drive the N-conversion chemistry toward completion under the reducing conditions in the near-burner flame zone.

4.5.2 Flame Structures

The chemical structures of the various regions of the flowfield will be developed in three stages: (1) volatiles combustion and NO production followed by NO reduction in the flame core; (2) N-species conversion, synthesis gas combustion, and soot oxidation in the mixing layer; and (3) char oxidation in the OFA and burnout regions, with essentially frozen N-conversion chemistry in the gas phase. The first predictions in this section are for the baseline PR-only flame with 15 % OFA and 3.5 % exhaust O_2. The predicted NO_X emission essentially equals the reported value of 328 ppm @ 3% dry O_2 for this case. Succeeding sections review the major differences in the structures of cofired SG and SD flames at the same operating conditions. Whereas the qualitative structures for all other flames are similar, there are significant quantitative differences among the various cases, which will be presented in Sec. 4.5.3, below.

4.5.2.1 Baseline PR-Only Flame Structure

4.5.2.1.1 Flame Core The predicted structure of the flame core for the PR-only baseline flame appears in Figure 4-12. In counterclockwise order from the upper left, the four panels of this figure display the variations in the gas temperature and S. R. values for the gas phase only; the mass fractions of O_2 and CO; the extents of burnout for char and soot; and the mass concentrations of the major N-species. The S. R. values do not include the combustibles in either soot or char, and therefore indicate the oxidation potential for the gas phase chemistry. Each parameter is plotted versus the mean residence time. Recall that discrete sets of operating conditions are imposed across the CSTR-series in the simulations, so the continuous curves in Figure 4-12 may be misleading. For this particular test, devolatilization is completed within 70 ms, and the flow leaves the core at 163 ms.

Neither H_2 nor any of the hydrocarbon fuels are present in cores in significant amounts. The H_2 mass fraction stays under 500 ppmw after the first 10 ms. Hydrocarbons are never present above this threshold. Gaseous hydrocarbons ignite the flow, but are otherwise unimportant. They are certainly not effective NO_X reductants, because NO forms well after they have been eliminated.

The gas temperature increases rapidly during the first 25 ms, then gradually approaches 1450°C at the core outlet. Since the overall S. R. value for the flame core (based on the flows of coal and primary air) is only 0.39, we are inclined to expect N-species conversion under extremely rich conditions in the flame core. Actually, the S. R. value for the gas phase begins at infinity, which is the nominal value for pure primary air. It then falls sharply while volatiles are released into the flow, making it more reducing. But it does not become very low, despite the abundant yield of volatiles from this coal, because a very large portion of volatiles are converted into soot, which does not factor into the S. R. value for the gas phase. Even at the end of devolatilization, the S. R. value is 1.014, which is two-and-one-half times larger than the whole-coal-based value. Clearly, the chemical environment in the core is much more oxidizing than expected. The volatiles ignite at roughly 750°C, based on the decay in the O_2 concentration and the decay in the CO concentration. At this point, two-thirds of the ultimate volatiles yield has been released. All accumulated hydrocarbons are consumed at ignition, and the hydrocarbon concentrations remain very low throughout. The O_2 concentration decays sharply during volatiles combustion, then decays more gradually after the char and soot ignite at 25 ms. The CO concentration decays during the ignition period, then gradually increases during the oxidation of char and soot. Its ultimate value reflects water gas shifting once all O_2 has been consumed.

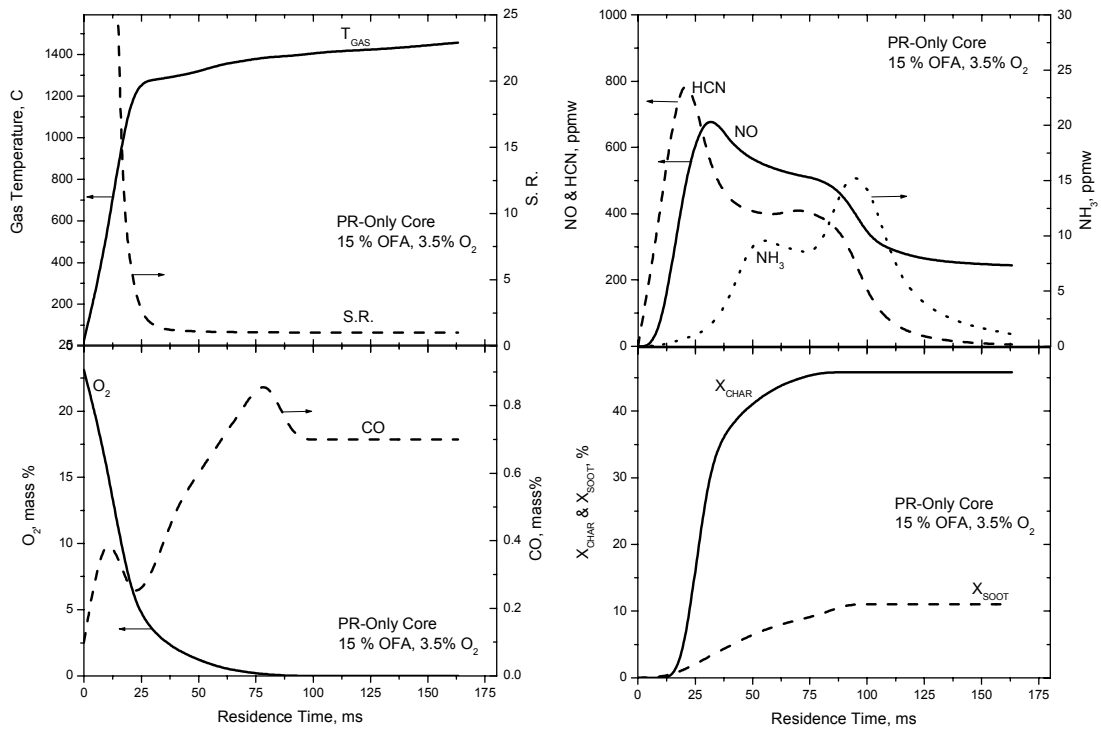

Figure 4-12. Structure of the core of the baseline PR-only flame showing, in counterclockwise order from the upper left, the operating conditions, major species, char and soot burnout, and N-species.

Char competes very effectively with the gaseous fuel compounds for the available O_2 in the core, due to the very rapid burning rates of the smallest char particles in the PSD. The char ignites when the gas temperature is 929°C, and loses almost a third of its mass before the annealing mechanism in CBK comes into play. Subsequent burnout is much slower due to the combined influences of annealing and O_2 depletion. Nevertheless almost half the char burns out in the core. Despite its very small size, soot is much harder to bring to the fully ignited state because of its low intrinsic oxidation reactivity. Consequently, only 11 % of the soot burns out in the core of this flame.

Obviously, the N-conversion chemistry expected for the gross S. R. value does not materialize within the flame core. The NO concentration initially surges to 729 ppmw due to the rapid conversion of HCN, the primary volatile-N species, in the lean section of the core, where the S. R. value falls from 5 to unity. But once the available O_2 falls below 5 %, the NO concentration diminishes in tandem with the decaying HCN concentration. Ammonia appears as soon as NO reduction begins, but its concentration never exceeds 16 ppmw in this core. The NO reduction stage (during which no additional volatiles are released) coincides with the second surge of NH_3 and with the final rapid decay the HCN concentration. At the end of the core, there is 244 ppmw NO, but only 5 ppmw HCN and 1 ppmw NH_3.

4.5.2.1.2 Mixing Layer Profiles through the mixing layer from the PR-only baseline flame appear in Figure 4-13. This region has the highest temperatures in the flame, due to the mixing of all the secondary air with combustibles from the core. The gas temperature history exhibits the peaked profile expected for flames of segregated fuel and air streams. It reaches its maximum value of 1550°C in just under 150 ms, then gradually diminishes over the remaining 400 ms. The S. R. history closely follows the cumulative entrainment fraction, increasing with the addition of secondary air from close to unity to just under 1.4. Eventually, the S. R. values diminish due to the gasification of combustibles in char and soot, which tends to pull the S. R. values toward unity. But the accumulation of O_2 in the layer is impeded by its rapid consumption during soot oxidation. While soot is present, the O_2 concentration rises to 0.4 % by mass. Then, after most of the soot has burned out, the O_2 concentration rises to 1.8 % during the last quarter of char burnout. As the gas phase becomes more oxidizing, the CO concentration diminishes and, ultimately, vanishes after the soot has burned away.

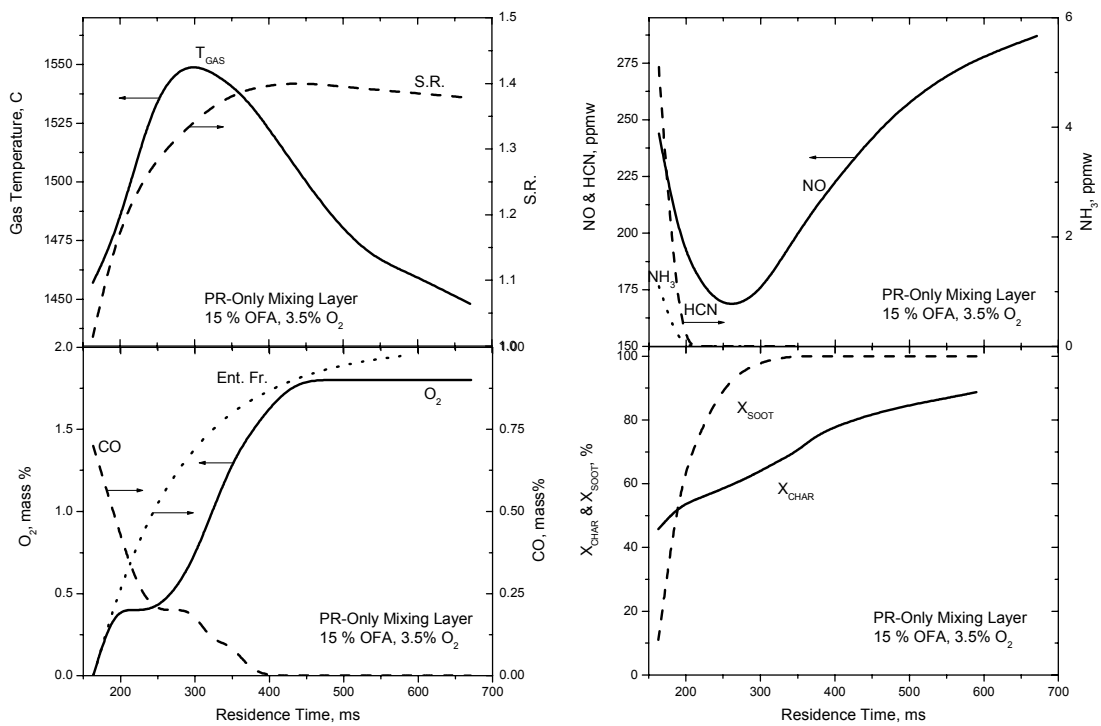

Figure 4-13. Structure of the mixing layer of the baseline PR-only flame showing, in counterclockwise order from the upper left, the operating conditions, major species plus entrainment fraction of secondary air, char and soot burnout, and N-species.

The inlet temperature to the mixing layer exceeds the threshold for rapid ignition of soot, and the soot burning rate accelerates while the gas temperature increases. The soot is completely burned out when the gases reach their maximum temperature. Char burns much slower than soot in the mixing layer, in contrast to the order of their burning rates in the cooler flame core. Both the higher temperatures in the mixing layer and the stronger annealing mechanism in the char oxidation rate are responsible for the reversal.

The N-species chemistry is only interesting at the inlet to the mixing layer. Both HCN and NH_3 are eliminated very quickly, continuing the tendency for NO production established late in the flame core. The NO concentration initially falls due to the addition of secondary air. It then rises across the later two-thirds of the mixing layer, while the conversion of char-N into NO supplements the NO inventory. Since there are no reducing agents in the rest of this region, gas-phase chemistry has been decoupled from char-N conversion. In fact, chemistry in the gas phase remains unimportant throughout the remainder of this furnace.

4.5.2.1.3 OFA and Burnout Regions The only chemistry in the OFA and burnout zone is char oxidation, with simultaneous NO production from the conversion of char-N. As seen in Figure 4-14, the O_2 concentration surges to almost 4.5 % during the addition of OFA, then diminishes to 4 % during the latest stages of burnout. The ultimate O_2 concentration equals 3.7 % by volume, which is close to the value in the corresponding test. The gas temperature is quenched by 150°C during OFA injection, then gradually cools to 1150°C at the furnace exit. The extent of char burnout asymptotically approaches 100 % across the OFA and burnout zones. The burning rate diminishes throughout due to the combined influences of the falling gas and wall temperatures, annealing during the previous thermal treatments, and, perhaps, ash encapsulation. The ultimate extent of burnout is 99.1 %, which corresponds to a LOI value of 2.0 wt. %. This prediction is almost double the measured value of 1.2 %.

The NO concentration across the OFA region falls from 287 to 270 ppmw, then rises to 290 ppmw across the BO region. The corrected exhaust concentration of 335 ppm @ 3% dry O_2 essentially equals the measured value of 328 ppm for this test.

Extents of char burnout are resolved over the char PSD at the ends of the four regions of this flame in Figure 4-15. Only particles smaller than 150 μm have ignited by the end of the core, yet the consumption of O_2 by char oxidation is significant because particles smaller than 60 μm have mostly burned out. The entire PSD has ignited by the end of the mixing layer. But the acute size dependence persists through the end of the OFA region. By the end of the burnout region, particles smaller than 150 μm have completely burned out, so only the largest char particles contribute to UBC. For CRF-type flames, which do not disperse or recirculate particles off the furnace centerline, our analysis predicts that UBC comprises the remnants of only the largest particles in the char PSD.

4.5.2.2 Co-Milled PR/20%SG Flame Structure The predicted structure of the flame core for the PR/20%SG flame appears in Figure 4-16. Even though the SG has much more fuel-N than PR coal (2.4 vs. 1.8 daf wt.%), the cofired flame generates 40% less NO_X. So the structure of this flame should illustrate how biomass affects the flame chemistry to reduce NO_X.

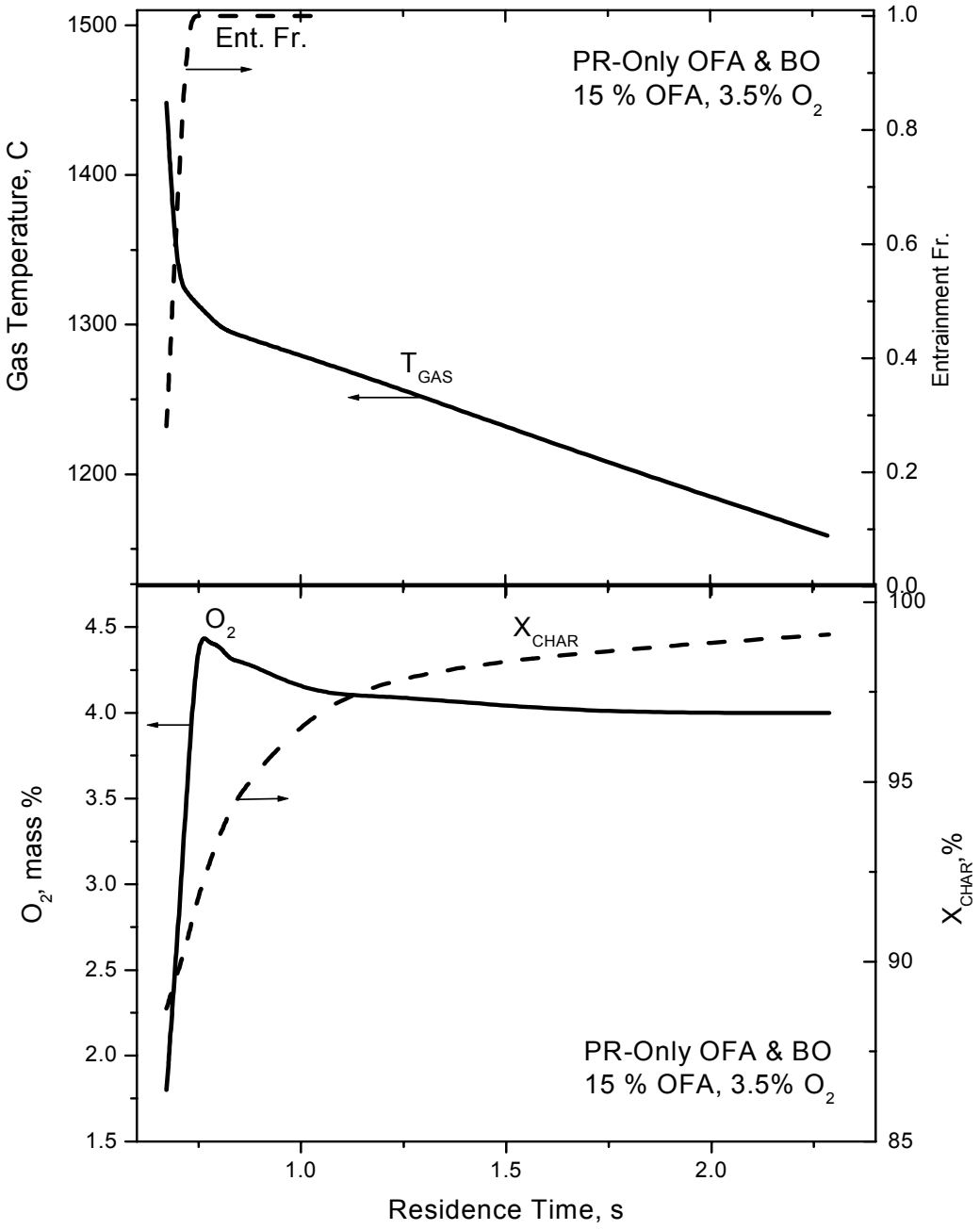

Figure 4-14. Structure of the OFA and BO regions of the baseline PR-only flame showing (top) the operating conditions and (bottom) O_2 concentration and char burnout.

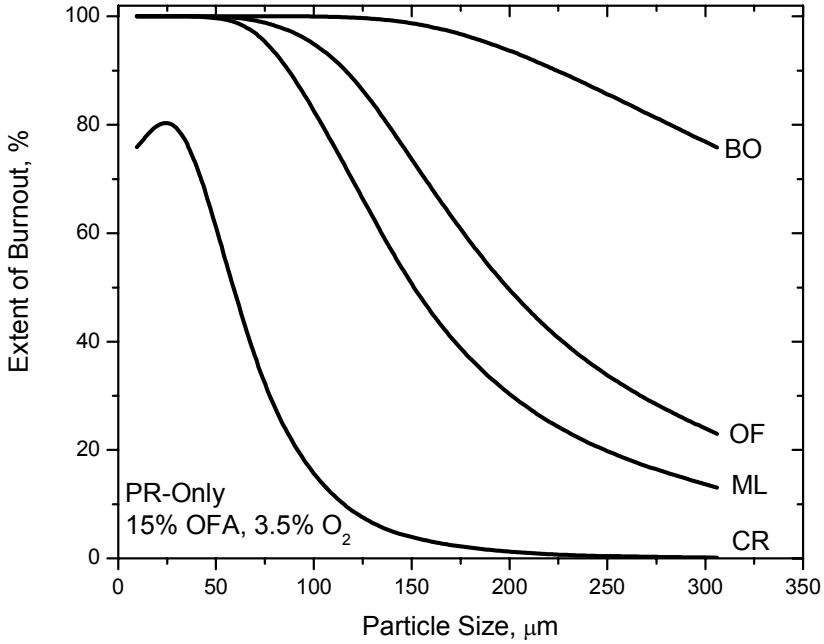

Figure 4-15. Extent of char burnout versus char size at the ends of the core, mixing layer, OFA region, and burnout region.

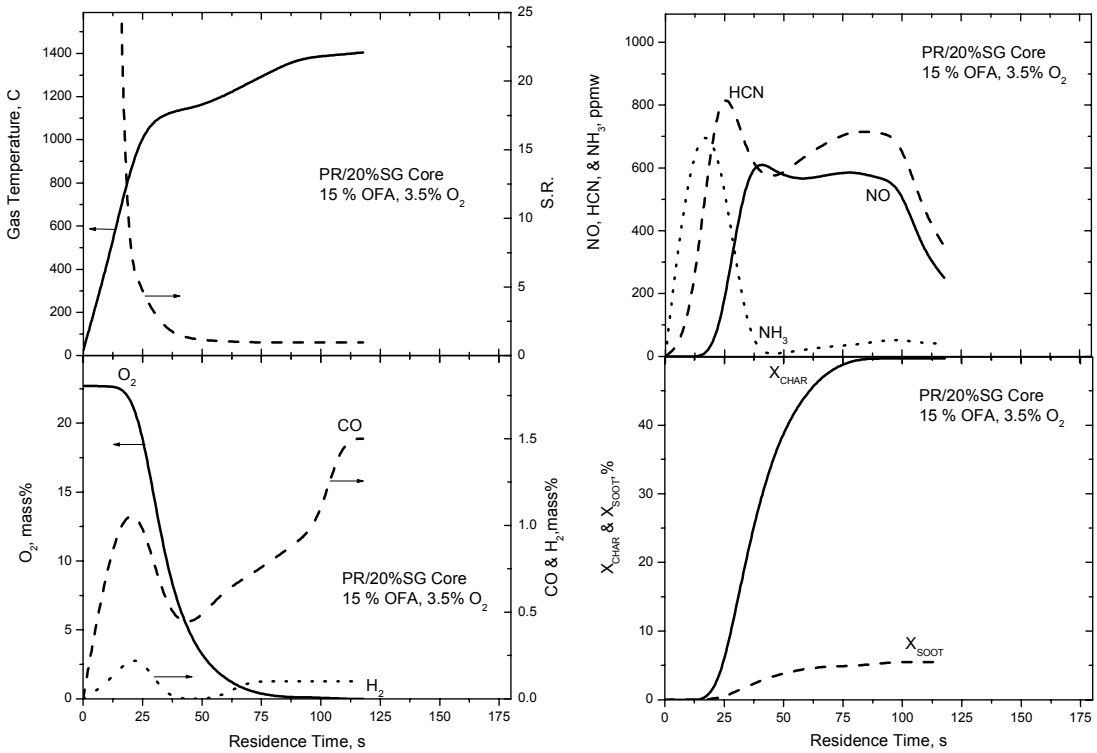

Figure 4-16. Structure of the core of the PR/20%SG flame showing, in counterclockwise order from the upper left, the operating conditions, major species, char and soot burnout, and N-species.

In counterclockwise order from the upper left, the four panels of this figure display the variations in the gas temperature and S. R. values for the gas phase only; the mass fractions of O_2, CO, and H_2; the extents of burnout for char and soot; and the mass concentrations of the major N-species. The same time scale used for the core of the PR-only flame has been retained to show that the cofired flame burns faster in the near-burner region, as expected. The S. R. values do not include the combustibles in either soot or char. For this particular test, devolatilization is completed within 80 ms, and the flow leaves the core at 118 ms.

The gas temperature increases at a slightly slower heating rate than in the PR-only flame, primarily because SG contains eight times more moisture than PR coal. As expected, the S. R. value for the gas phase falls sharply while volatiles are released into the flow, making it more reducing; it then relaxes to an ultimate value 0.951. The gas phase is more reducing than the PR-only flame core because there is much less soot and more volatiles from SG.

The volatiles ignite at roughly 650°C, based on the decay in the O_2 concentration. The O_2 concentration decays sharply during volatiles combustion, then decays more gradually after the char and soot ignite at 25 ms. As for the baseline PR flame, gaseous hydrocarbons ignite the flow, but are otherwise unimportant. But the H_2 mass fraction persists at roughly 1000 ppmw across the entire core, and there is twice as much CO. Initially, the CO concentration surges during the ignition period, then increases more gradually during the oxidation of char and soot. Its ultimate value and the persistence of H_2 reflect water gas shifting once all O_2 has been consumed. Almost half the char but only 5 % of the soot burn out in the core, just like the burnout in the PR-only flame.

Whereas the macroscopic combustion characteristics discussed to this point are very similar in the cofired and baseline flames, there are crucial differences in the N-species conversion chemistry. Most important, all three of the major fixed-N species are present at similar concentrations. Ammonia is expelled by SG to a maximum concentration of 729 ppmw. But it is converted to HCN in only 40 ms, demonstrating that the primary forms of volatile-N are unimportant, because gas phase chemistry governs the nitrogen speciation. The distribution of N-species is determined by the S. R. value in the gas phase which, in this flame, is too lean to sustain much NH_3. The HCN concentration surges above 1000 ppmw, then decays in tandem with NH_3 while the NO concentration grows to 660 ppmw. Thereafter all the fixed-N species concentrations remain fairly constant, before they plummet at the exit of the core. Although the exit NO level from this core is the same as from the PR-only flame core, the HCN level is much higher at 350 ppmw.

When the gases from the core contact secondary air in the mixing layer, the NO concentration relaxes to 170 ppmw by the time that both the other fixed-N species have been eliminated, which is essentially identical to the 179 ppmw NO at this same condition in the PR-only flame. Beyond this point, gas phase chemistry becomes inconsequential. But the remaining inventory of char-N in the biomass cofired flame is much lower, because 68 % of the PR-char had burned out when NO became the only fixed-N species, versus 53 % in the PR-only flame. The fact that the residual SG-char contains no nitrogen compounds this difference. Hence, the reason that the exhaust NO_X emissions are lower for the SG-cofired flame is that the fuel blend releases a much larger portion of the fuel-N into the core, which then becomes subject to NO reduction in the gas

phase chemistry. This enhancement was due to two independent factors: First, PR-char competes more effectively for the available O_2 than SG-char, due to its smaller size, so the extent of burnout for PR-char is higher in the cofired flame than in the PR-only flame. As the extent of burnout increases, the amount of residual char-N diminishes. Second, SG completely releases its fuel-N during devolatilization, and therefore does not convey any char-N into the downstream regions of the flame.

Of course, higher concentrations of HCN and NH_3 in the core promote NO reduction. Moreover, the higher levels of CO and H_2 associated with the lower S. R. value promote NO reduction in the core as well as in the inlet to the mixing layer. Even though more NO can be produced early in the core when more volatile-N species are released, the cores in CRF-flames provide sufficient residence times to reduce it away. However, the shorter residence time in the core of the SG-cofired flame did not enable all the HCN to be eliminated, as it was in the PR-only flame. It is therefore conceivable that the NO emissions could have been reduced further if there was some way to extend the duration of this core.

The competitive burnout of the PR- and SG-chars is apparent in Figure 4-17. The predicted extents of burnout are plotted versus the sizes in the initial PSDs of these chars. PR-particles smaller than 160 μm have ignited by the end of the core. Slightly larger SG-particles have also ignited because the initial char oxidation reactivity of biomass is much faster than any coal's reactivity. But by the end of the mixing layer, PR-char smaller than 120 μm burns faster than this portion of the SG-PSD. The reactivity reversal reflects the huge ash content in SG-chars (76 %), which is 2.5 times greater than PR's. According to CBK, the ash forms a layer around the combustibles that inhibits O_2 penetration, and thereby reduces the burning rate. By the end of the OFA region, the entire PR-PSD burns faster than all the SG-PSD. And at the furnace exit, essentially all the predicted UBC is composed of portions of the largest SG-particles. The predicted LOI emission of 1.9 wt.% compares well with the reported value of 1.6 %.

4.5.2.3 Co-Milled PR/20%SD Flame Structure The predicted structure of the flame core for the PR/20%SD flame appears in Figure 4-18. In contrast to SG, SD has almost no fuel-N. However, this cofired flame still generates 40% less NO_X than the PR-only baseline flame, which is double the reduction expected from the removal of fuel-N alone. So the structure of this flame reflects the reduction in volatile-N species as well as distinctive chemical effects.

The time scale in Figure 4-18 has been extended to depict the core as well as the first quarter of the mixing layer. The gas temperature profile was assigned from a CFD simulation for the PR/20%SD flame (which was also imposed on the PR/20%SG flame analysis). For this particular test, devolatilization is completed within 80 ms, and the flow leaves the core at 118 ms. The total residence time in the mixing layer is 476 ms, but only the first 150 ms are shown in Figure 4-18.

As seen with both the previous flames, the S. R. value for the gas phase falls sharply while volatiles are released into the flow, making it more reducing. It then relaxes to an ultimate value 0.864, which is significantly more reducing than the PR/20%SG flame. Although SD and SG have identical volatiles yields, the gas phase in the SD-core becomes more reducing because more CO and less soot are produced by the primary volatiles from SD.

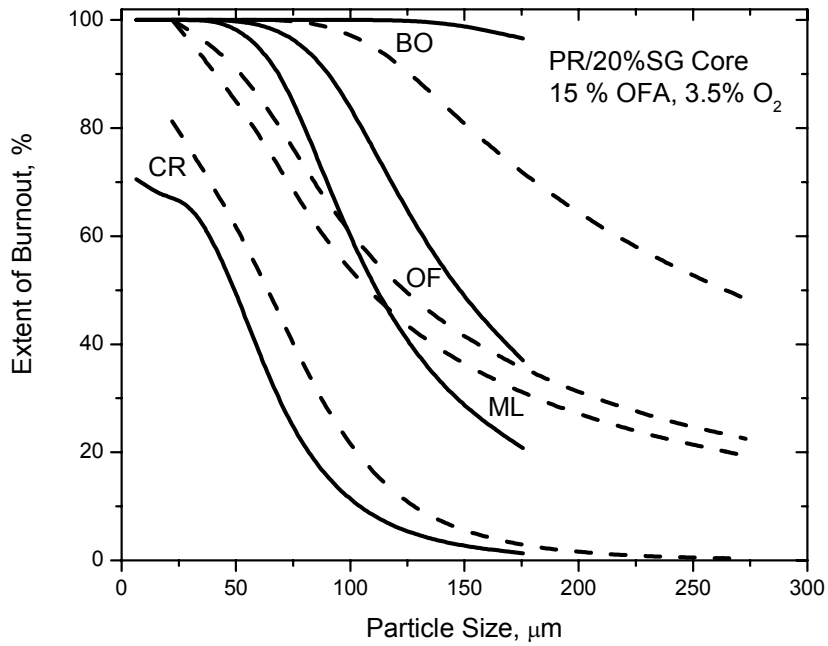

Figure 4-17. Extent of char burnout of PR-char (solid curves) and SG-char (dashed curves) versus initial char size at the ends of the core, mixing layer, OFA region, and burnout region in the PR/20%SG flame.

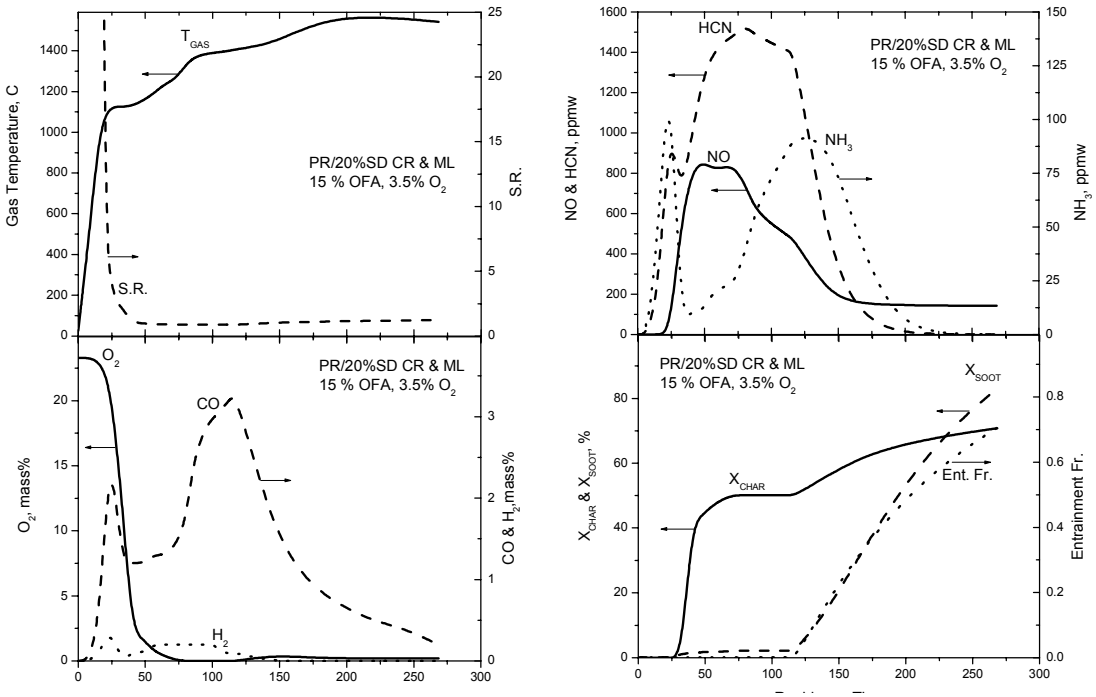

Figure 4-18. Structure of the core of the PR/20%SD flame showing, in counterclockwise order from the upper left, the operating conditions, major species, char and soot burnout, and N-species.

Initially, the CO concentration surges during the ignition period, then increases more gradually during the oxidation of char and soot. Its ultimate value and the persistence of H_2 reflect water gas shifting once all O_2 has been consumed. The maximum CO concentration is double that in the PR/20%SG flame. The H_2 mass fraction persists at roughly 1000-2000 ppmw across the entire core. Moreover, hydrocarbons, especially C_2H_2 (not shown), persist at 1000 ppmw or more across the entire devolatilization zone. This is the first flame core with an appreciable amount of hydrocarbons in the presence of NO, although their concentration is still much lower than those of CO and H_2. As for the other flames, almost half the char burns out in the core, but hardly any soot burns out in this particular core.

The more reducing character of the gas phase in this core imparts several distinctive features to the N-species conversion chemistry. The N-speciation is dominated by HCN and NO, as for the PR-only baseline flame. The NH_3 released by the SD is rapidly converted to HCN and NO within 40 ms. But NO does not accumulate at the expense of HCN, as in both of the other flame cores. Instead, the HCN concentration surges while NO accumulates. Some prompt N-fixation mechanisms involving N_2 in air must be responsible because the total maximum amount of fixed-N species is double the maximum value in the PR/20%SG flame, and the SG-cofired flame has significantly more volatile-N. NO reduction begins at 75 ms but by the exit of the core, there is still 1390 ppmw HCN and 465 ppmw NO, which are both much higher than in either of the other flames.

Very early in the mixing layer, NO reduction accelerates while the HCN concentration plummets. The NH_3 concentration reaches 92 ppm before vanishing with the HCN concentration. The ultimate NO concentration after both other fixed-N species have been eliminated is only 143 ppmw, which is 25 ppm lower than the analogous level in the PR/20%SG flame. Even though there was a higher concentration of fixed-N species in the core, the greater reducing potential yielded a lower NO concentration in the mixing layer after chemistry in the gas phase was exhausted. Since the extents of char burnout at this point are comparable for the PR/20%SG and PR/20%SD flames, the 20 ppmw reduction for the PR/20%SD flame persists in the exhaust emissions as well.

A surge in the extent of soot burnout coincides with the entrainment of secondary air. Due to the high maximum temperatures in the mixing layer, the extent of soot oxidation eventually overtakes the extent of char oxidation at 220 ms. The soot burns out in the mixing layer, whereas char is carried over into the OFA and BO regions.

The extents of burnout of the PR- and SD-chars in Figure 4-19 show that this biomass char wins the competition for O_2, in contrast to the ash-laden SG-char. There is only 2.5 % ash in the SD-char, versus 30.9 % for the PR-char. So the advantage of the biomass's faster initial reactivity persists throughout the entire furnace. Indeed, the UBC from this flame is predicted to consist entirely of fragments of unreacted PR-char, which is the opposite of the character of the LOI emission from the PR/20%SG flame.

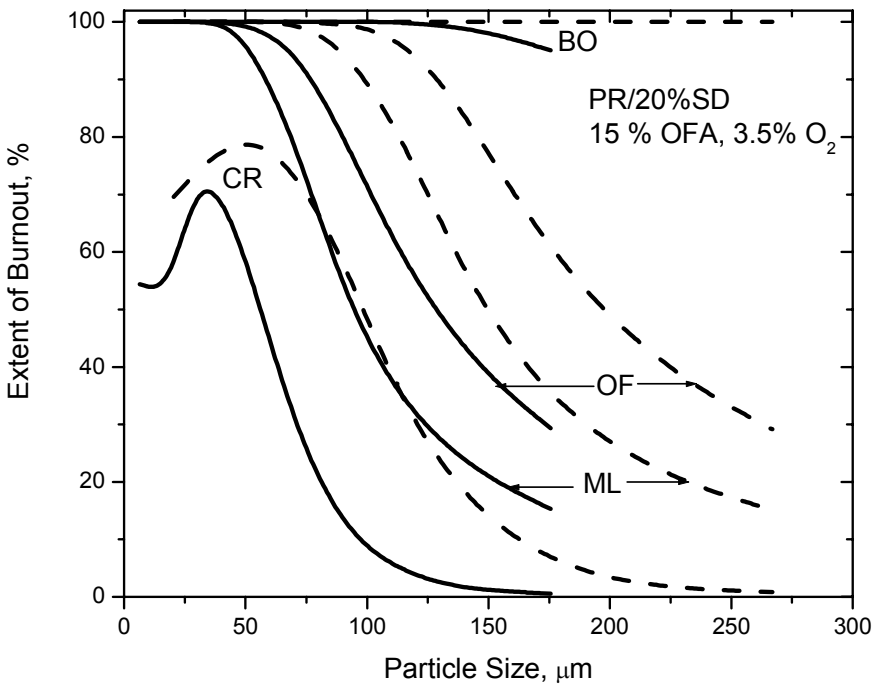

Figure 4-19. Extent of char burnout of PR-char (solid curves) and SD-char (dashed curves) versus initial char size at the ends of the core, mixing layer, OFA region, and burnout region in the PR/20%SD flame.

4.5.3 NO_X Predictions

This section evaluates the predicted NO_X emissions with the measured values across the entire CRF database. In turn, separate evaluations illustrate the utility of the predictions for fuel quality impacts, furnace stoichiometry and staging level, and biomass injection configuration.

4.5.3.1 Fuel Quality Impacts

4.5.3.1.1 Calibration Factors As explained in Section 4.4.1.2, two fuel-specific parameters in the APP analysis were specified by fitting the coal-only baseline flames in each test series: F_{NO}, the fraction of char-N converted to NO and A_C, the initial char oxidation reactivity. The assigned values are collected in Table 4-6, where the fuels are arranged in descending order of increasing rank. No values were assigned to F_{NO} for the biomass fuels simply because their chars contained no nitrogen. The values for the coals vary from 0.22 to 0.48 with a weak tendency to decrease for coals of progressively higher rank. Reported values in the literature tend to cluster around 0.4, although there is wide scatter when different ranks are considered. It is therefore difficult to corroborate the assigned values, except to note that they are not unreasonable.

Values for the initial char oxidation reactivity show the tendency to diminish for chars of progressively higher rank, except for char-GL. The reactivity from CBK's internal correlation had to be reduced for GL, whereas that for PR had to be increased, so their rank dependence was juxtaposed. Since there is no reliable means to estimate sample-specific char oxidation reactivities within useful quantitative tolerances, we accept the values in Table 4-6 at face value.

Table 4-6. Fuel-Specific Calibration Factors.

Fuel	F_{NO}	A_C, s^{-1}
SD	Na	2.00×10^9
SG	Na	2.00×10^9
JR	0.48	1.76×10^9
GL	0.22	3.74×10^8
PR	0.38	1.23×10^9
JW	0.24	8.79×10^8

4.5.3.1.2 Fuel Quality Impacts On NO_X Emissions The most extensive coverage of fuel quality impacts in the testing program comprises the cases with co-milled injection. This focus is sharpened by considering all such data at 3.5 % O_2 in separate groups for 15 and 0 % OFA. Summary evaluations for these two subsets appear in Figures 4-20 and 4-21, respectively. The criterion for evaluating the model predictions is the standard error of estimation (SSE), which is defined as follows:

$$SSE = \sqrt{\frac{\sum_{i=1}^{n_S} (p_i^P - p_i^O)^2}{n_S - n_F - 1}} \tag{4.5.1}$$

where n_S is the number of records under evaluation; $p^P{}_i$ is the prediction for the ith record; $p^O{}_i$ is the measured value; and n_F is the number of independent factors accounted for in the model. The number of independent modeling factors is easiest to specify when the model is a multivariate regression; however, it is ambiguous when mechanistic models are involved in the predictions. For the evaluation of fuel quality impacts in this section, n_F was specified as 4, because fuel quality impacts in the modeling were primarily expressed through the C, H, O, and N contents of the various fuels. Since n_S is much greater than n_F, the specification on n_F is unimportant.

A parity plot for the NO_X emissions for all cases with co-milled injection, 3.5 % O_2, and 15 % OFA appears in Figure 4-20. This data subset contains measurements from test series 1, 5, 6, 7, 10, 11, 12, and 13, and therefore represents the complete range of fuel quality in the testing program. The range of measured values, from 140 to 460 ppm, reflects the range in coal quality, from subbituminous through lv bituminous, compounded by the co-firing with both biomass forms. The predicted values show no systematic discrepancies over the entire range. The SSE is 32.4 ppm, which is roughly double the standard deviation assigned for the measured values. The r^2 correlation coefficient for this data subset is 0.834, and the F-factor is 578. The predictions clearly depict the fuel quality impacts within useful quantitative tolerances over the full range in the testing program, without bias. This performance is especially significant since none of the fuel quality parameters in the modeling were adjusted once their values were specified for the baseline, coal-only cases. Only the proximate and ultimate analyses, grind size fractions, and biomass loadings were changed (as in the testing program) to achieve the agreement in Figure 4-20.

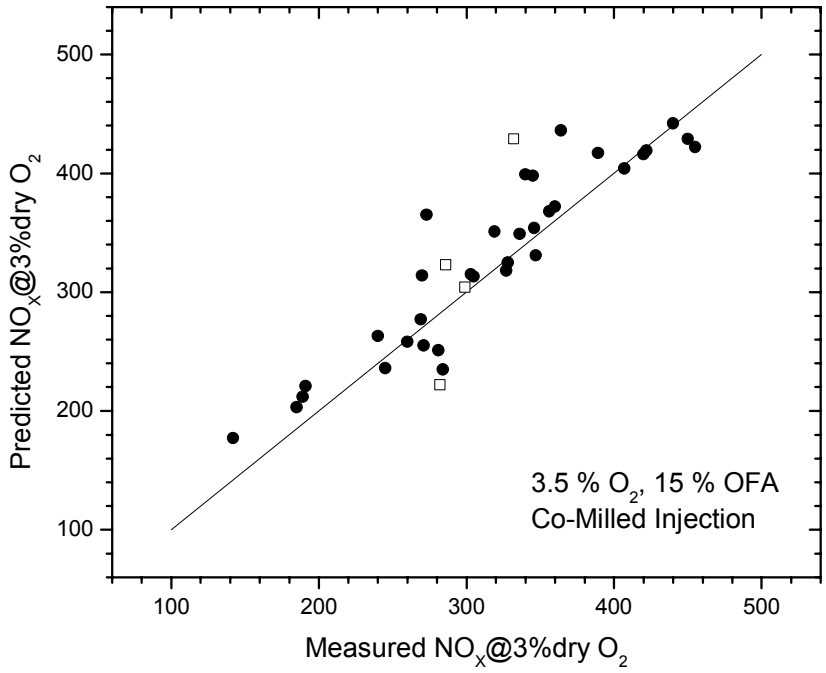

Figure 4-20. Parity plot for the data subset with co-milled injection, 3.5 % O_2, and 15 % OFA where the cases with NH_3 injection (□) are distinguished from all other test results (●).

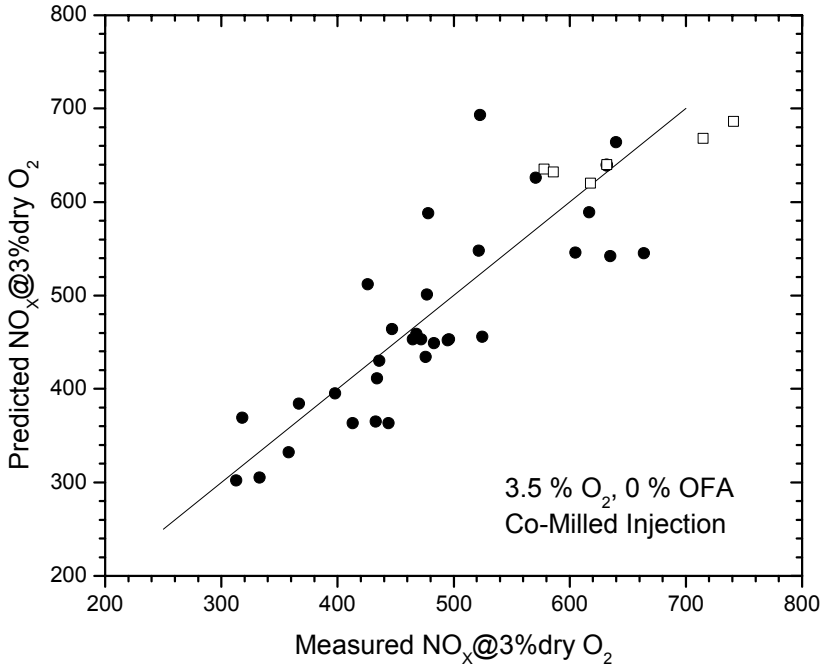

Figure 4-21. Parity plot for the data subset with co-milled injection, 3.5 % O_2, and 0 % OFA where the cases with NH_3 injection (□) are distinguished from all other test results (●).

In addition to the variations in fuel composition, another important aspect of the fuel quality impacts is the dependence on biomass loading. This aspect is apparent in the predictions for individual test series in Table 4-7. In 9 of 10 of the runs with 15 % OFA, the measured NO_X emissions increased for progressively higher biomass loadings. The only exception is for series 5 with SD on GL, for which the emissions exhibit a minimum with biomass loading. The predictions exhibit the correct tendency for lower emissions with higher biomass loadings in 7 of 10 cases. This trend is illustrated in Figure 4-22 for the PR/SD cases from test series 1. The case with PR-only is a calibration point, so the close agreement reflects parameter adjustments. But the predictions for the two cases with SD loadings to 20 % demonstrate the modeling capability to depict the impact of biomass loading essentially within experimental uncertainty.

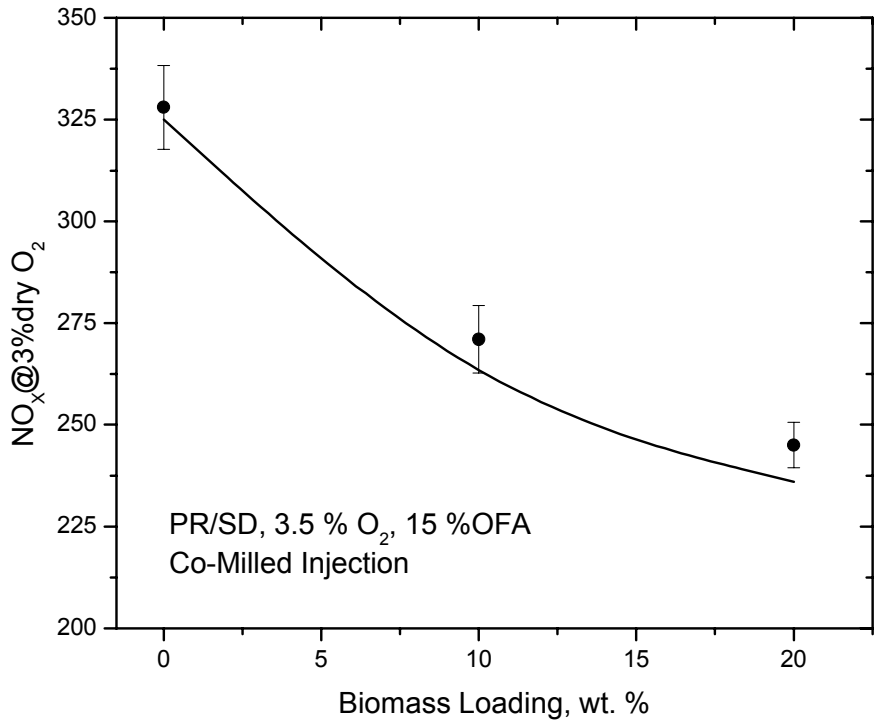

Figure 4-22. Evaluation of the predicted impact of biomass loading on NO_X emissions for PR/SD cases from test series 1.

Among the three series for which the predicted impact of biomass loading is not monotonically decreasing, only two are inaccurate. The predictions for series 13 for JW/SG show essentially no NO_X reduction for SG loadings of 5 and 10 %, in accord with the data, and a reduction to 404 ppm versus a measured value of 407 ppm for a loading of 20 %. Whereas the predictions for GL/SD from series 6 are accurate for 0 and 20 % SD, the one for 10 % SG is 60 ppm too high. Similarly, the predictions for JW/SD from series 12 are accurate at 0 and 5 % SD, but too high by up to 70 ppm for 10 and 20 % SD.

The parity plot for the NO_X emissions for all cases with co-milled injection, 3.5 % O_2, and 0 % OFA appears in Figure 4-21. As with the data subset for 15 % OFA in Figure 4-20, the range of

Table 4-7. Evaluation of Predicted NO_X for Co-Milled, Cofired Flames with 3.5 % O_2.

Series	Fuel	NO_X, ppm @ 3 % dry O_2			
		15% OFA		0% OFA	
		Predicted	Measured	Predicted	Measured
1	PR hv bit	325	328	464	447
	PR/10%SD	255	271	365	433
	PR/20%SD	236	245	363	444
	PR/15%SG	277	269	363	413
	PR/20%SG	258	260	384	367
5	PR hv bit	354	346	453	465
	GL hv bit	372	360	453	472
	GL/10%SD	365	273	459	468
	GL/20%SD	318	327	434	476
6	PR hv bit	351	319	453	496
	PR/20%SD	314	270	411	434
	GL hv bit	368	356	449	483
	GL/10%SG	399	340	501	477
	GL/20%SG	349	336	456	525
7	JR subbit	263	240	395	398
	JR/10%SD	221	191	332	358
	JR/20%SD	212	189	302	313
	JR/10%SG	203	185	305	333
	JR/20%SG	177	142	369	318
10	PR hv bit	315	303	452	495
	PR fine	235	284	430	436
11	GL hv bit	398	345	602	568
			w/6.1 NH_3	640	632
			w/13.1 NH_3	620	618
	GL/5%SD	331	347	693	523
			w/9.6 NH_3	668	715
	GL/10%SD	313	305	626	571
	w/0.8 NH_3	304	299		
	w/10.3 NH_3	323	286		
			w/7.0 NH_3	686	741
	GL/20%SD	251	281	588	478
	w/2.6 NH_3	222	282		
	w/12.0 NH_3	429	332		
			w/7.2 NH_3	635	578
			w/10.8 NH_3	632	586
12	JW lv bit	419	422	639	632
	JW/5%SD	416	420	546	605
	JW/10%SD	417	389	548	522
	JW/20%SD	436	364	542	635
13	JW lv bit	429	450	664	640
	JW/5%SG	422	455	545	664
	JW/10%SG	442	440	589	617
	JW/20%SG	404	407	512	426

measured values reflects the broad range in fuel quality in the testing program, but it has been shifted upward to 300 to 750 ppm by the higher near-burner S. R. in unstaged flames. The predicted values show no systematic discrepancies over the entire range. The SSE is 59.0 ppm, which is roughly double the value for the 15 % OFA subset. The r^2 correlation coefficient for this data subset is 0.718 and the F-factor is 340. The statistics are weaker, in part, because of the greater uncertainties in the tests with unstaged flames. Notwithstanding, the predictions clearly depict the fuel quality impacts within useful quantitative tolerances over the full range in the testing program, without bias. Only the proximate and ultimate analyses, grind size fractions, and biomass loadings were changed (as in the testing program) to achieve the agreement in Figure 4-21.

The effect of biomass loading is also more complex in unstaged flames than in the tests with 15 % OFA. Among the ten fuel combinations in the data subset, only six had measured NO_X emissions that monotonically decreased for progressively higher biomass loadings. Two combinations exhibited no change (PR/SD from series 1 and GL/SD from series 6); one exhibited a minimum (JW/SD from series 12); and one had higher emissions with the highest biomass loading (GL/SG from series 6). The predictions for this subset were also more varied. Four cases had substantial NO_X reductions for 10 % biomass but no further reductions for 20 %. Three (PR/SD from series 6; JR/SD from series 7; and GL/SD from series 11) had monotonic decreases with higher loadings; two showed no change (GL/SD from series 5 and GL/SG from series 6); and one exhibited a minimum in NO_X vs. loading (JR/SG from series 7). Evaluations for three of these dependences appear in Figure 4-23. The evaluation from series 13 illustrates a substantial reduction for low loadings, but minimal additional reduction for 15 % biomass; that from series 5 shows no change; and that from series 7 shows a monotonic decrease. The predictions are essentially within experimental uncertainty over the full range of biomass loadings, except for the highest loading in series 13. The detailed evaluations for all other cases in this data subset are collected in Table 4-7.

The final aspect of fuel quality in the database are the cases with NH_3 injection to simulate the very high fuel-N levels in poultry litter. These tests were run with GL coal and with sawdust as a surrogate for the organics in the litter, to 20 wt. % loading. Ammonia was injected into the primary air stream in the CRF burner at various flowrates to raise the fuel-N levels. These cases are collected under test series 11 in Table 4-7, and labeled with the NH_3 flowrate, in lb/hr; typically, an NH_3 injection flowrate of 10 lb/hr corresponds to about 4.3 % fuel-N with 10 % SD.

Unfortunately, this portion of the evaluations are inconclusive. As seen in Figures 4-20 and 4-21, the discrepancies with half the cases with 15 % OFA and all cases with 0 % OFA are within the expected tolerances for these respective data subsets. But it is still not clear if NH_3 injection increases or decreases NO_X, primarily because the data show no consistent trend. With 15 % OFA, increasing the NH_3 flowrate from 0.8 to 10.3 lb/hr reduced measured NO_X from 299 to 286 ppm for GL/10%SD, compared to the baseline value of 305 ppm. But with GL/20%SD, increasing the NH_3 flowrate from 2.6 to 12.0 lb/hr increased NO_X from 282 to 332 ppm, compared to the baseline value of 281. Only the change for the highest NH_3 flowrate with GL/20%SD is statistically significant. Similarly, the predicted NO_X emissions are essentially the same for all cases with GL/10%SD, and 30 ppm lower for the lowest NH_3 injection rate with GL/20%SD. But the predicted NO_X emission surges to 429 ppm for 12 lb/hr NH_3, which is

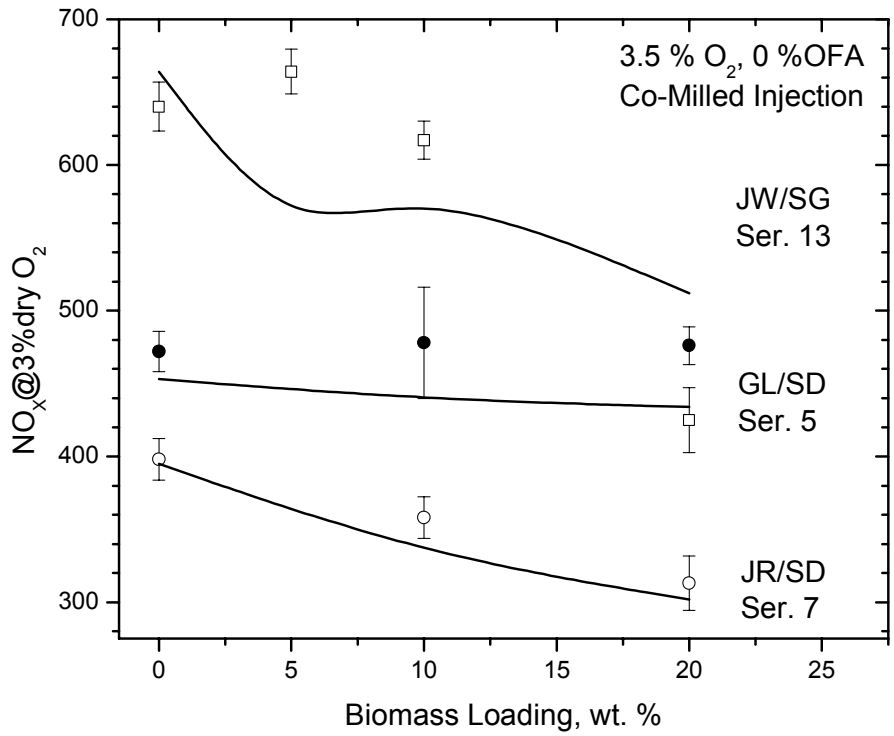

Figure 4-23. Evaluation of the predicted effect of biomass loading on NO_X emissions for test series with co-milled injection, 3.5 % O_2, and 0 % OFA.

qualitatively correct but too high by 100 ppm. With 0 % OFA, the predicted NO_X emissions with both NH_3 injection levels with pure GL coal are within experimental uncertainty. But with GL/5%SD, NH_3 injection raised the measured NO_X by 190 ppm, whereas the prediction fell by 25 ppm. With 10 and 20 % SD, the predicted NO_X increased for all levels of NH_3 injection, but not by as much as the measured values.

Whereas the qualitative tendencies with NH_3 injection are evident in the predictions, the quantitative evaluations are obscured by discrepancies in the reference values for the co-fired cases, without NH_3 injection. More work is necessary to sort through the various factors in this portion of the database, although additional tests with actual poultry litter would surely be more definitive.

4.5.3.2 Impacts of Furnace Stoichiometry and PSD Obviously, staged flames produce less NO_X than unstaged flames, and this behavior is clearly evident in the predictions in Table 4-7. In addition to staging, the testing program characterized variations in furnace stoichiometry and, to a much lesser extent, variations in particle size. Predictions describing these influences are evaluated in this section for the co-milled injection configuration.

Furnace stoichiometry was varied to obtain exhaust O_2 levels from 2.5 to almost 5 %. The predictions over this range in the various test series with 15 % OFA are evaluated in Figure 4-24. The cases for test series 11 were omitted for lack of space. For each series, predictions for a

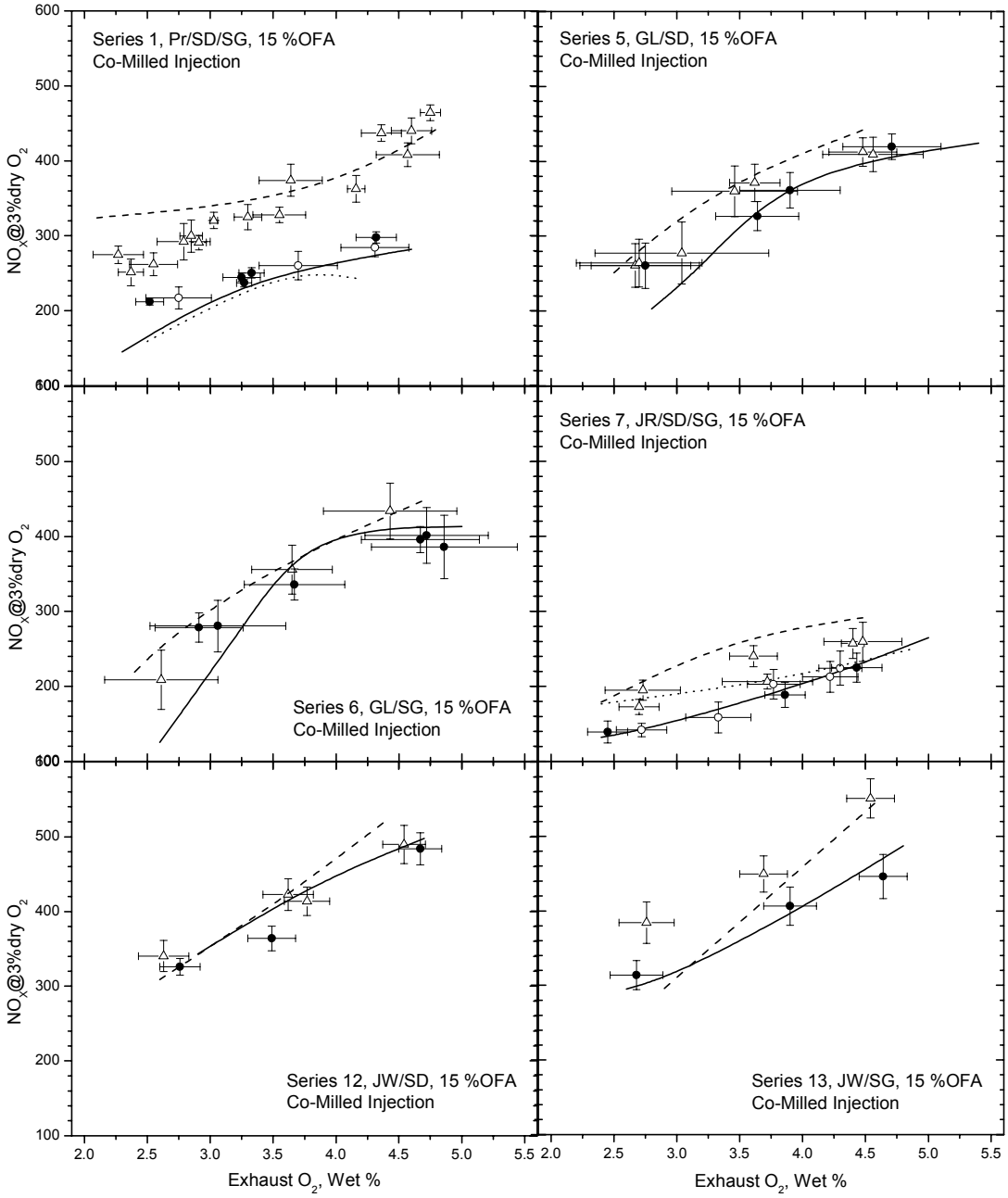

Figure 4-24. Evaluation for the full range of exhaust O_2 with 15 % OFA and co-milled injection. Each case contains a coal-only baseline (Δ, dashed curve) and, if available, cofired cases with 20 % SD (●, solid curve) and 20 % SG (○, dotted curve).

coal-only baseline are evaluated along with those for one or two co-fired cases. In series 1 and 7 the coals were cofired with both biomass forms, whereas the rest were cofired with either SD or SG. All cofiring cases in Figure 4-24 had 20 % biomass. The error bars indicate the standard deviations reported by Southern Research staff for each run.

As explained in Section 4.4.2, the only exhaust O_2 in any of the CFD simulations was 3.5 %. So the predictions for both other levels (2.5 and 4.5 %) represent capabilities in the reaction mechanisms as well as the extrapolation procedures for furnace stoichiometry (cf. Table 4-3 and Section 4.4.2.1). The evaluation in Figure 4-24 highlights the mechanistic capability, because a single calibration procedure was applied uniformly to all test series with 15 % OFA.

The predictions are generally within experimental uncertainty across the full range of exhaust O_2 for all coal types and for all cofiring cases. The only sizeable discrepancies are for the PR-baseline in series 1 for O_2 levels below 2.7 %; for the JR/20%SG case in series 7 for O_2 levels below 3 %; and for the JW-baseline in series 13 for O_2 levels below 3 %. Cofiring (up to 20 wt. %) hardly perturbs the measured dependence on furnace stoichiometry, and this tendency is evident in the predictions for all cases except series 6. But even this distinctive O_2 dependence remains within experimental uncertainty.

The predictions over the full range of exhaust O_2 in the various test series with 0 % OFA are evaluated in Figure 4-25. The cases for test series 7 were omitted for lack of space. For each series, predictions for a coal-only baseline are evaluated along with those for one or two co-fired cases. All cofiring cases in Figure 4-25 had 20 % biomass.

The predictions are generally within experimental uncertainty across the full range of exhaust O_2 for all coal types and for all cofiring cases. The only sizeable discrepancies are for the PR/SD case in series 1 at 3.5 % O_2; for the GL/20%SD cases in series 11 for O_2 levels above 3 %; and for all the JW/20%SD cases in series 13. Cofiring (up to 20 wt. %) hardly perturbed the measured dependence on furnace stoichiometry, and this tendency is evident in the predictions for all cases except series 6 (not shown).

The evaluation in Figure 4-25 is not as straightforward as that for 15 % OFA in Figure 4-24. The reason is apparent in Figure 4-25 in the large differences among the measured NO_X emissions in series 5 and 11 for nominally the same operating conditions. This is because the measured values for the GL-baseline in series 11 are higher by 100 to 160 ppm than those for the same conditions in series 5 and 6. Yet the NO_X emissions for GL/20%SD from both series are the same, within experimental uncertainty. Obviously these series could not be analyzed with the same baseline calibration procedure. Such discrepancies were managed with essentially two calibration procedures for the data subset of unstaged flames, as follows.

The calibration procedure consists of independent factors for temperature enhancements, diverted secondary air, and the secondary air mixing intensity. The same temperature enhancements were applied to all test series. The factor for mixing intensity was the same for all series except series 5 and 6, which had a lower mixing factor. The factors for diverted secondary air were the same in series 1, 5, 6, and 7. More secondary air was diverted in the simulations for series 12 and 13, but only at the lowest furnace stoichiometry. Even more was diverted in series

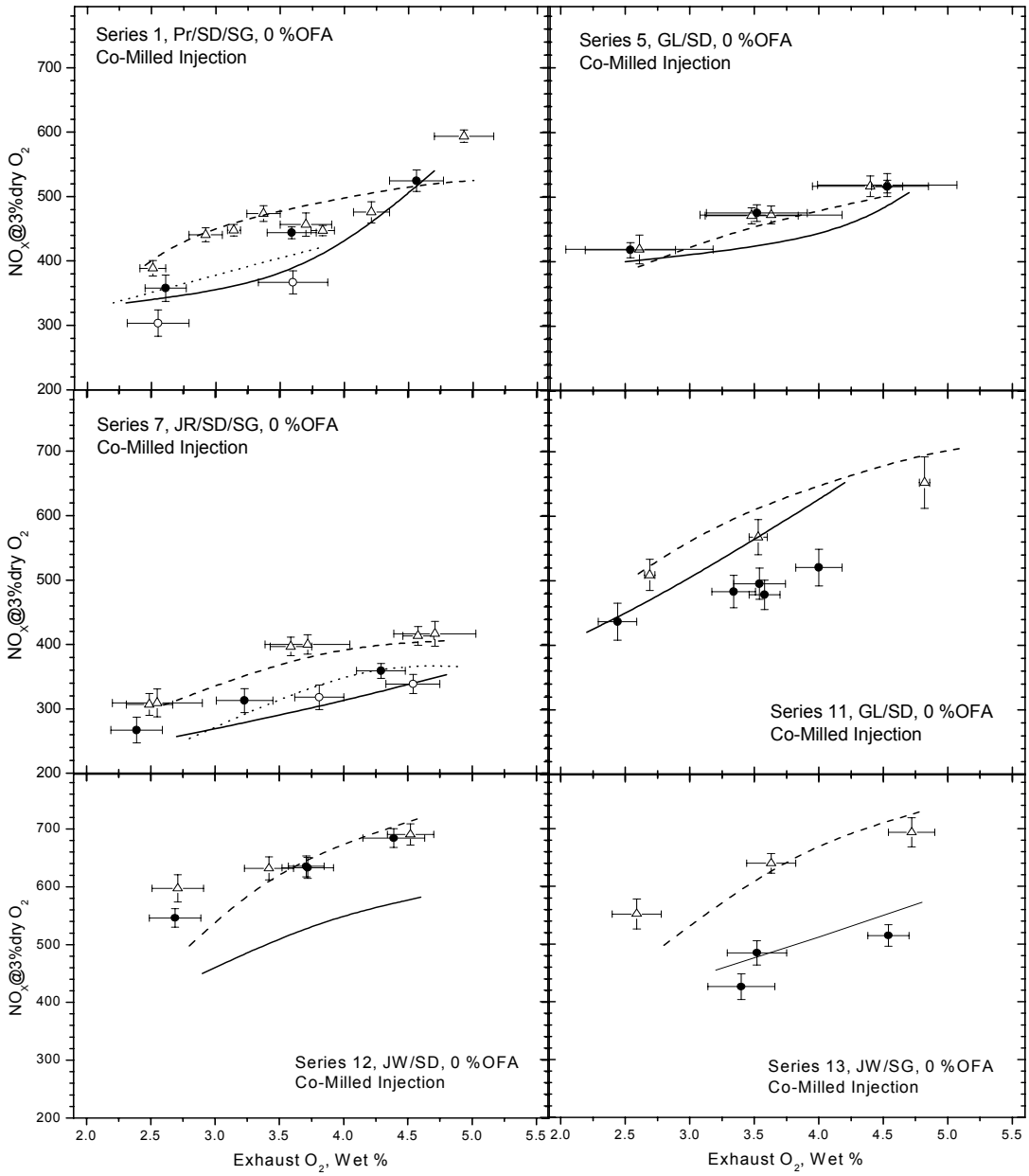

Figure 4-25. Evaluation for the full range of exhaust O_2 with 0 % OFA and co-milled injection. Each case contains a coal-only baseline (Δ, dashed curves) and, if available, cofired cases with 20 % SD (●, solid curves) and 20 % SG (○, dotted curves).

11, and this enhancement was applied uniformly for all furnace stoichiometries. These adjustments suggest that the underlying cause to the greater variability in the operation of unstaged flames in the CRF could be due to instabilities at the burner outlet that promote entrainment of more secondary air into the primary stream upstream of the mixing layer. It would be worth examining whether such instabilities became more prevalent in certain ranges of secondary air flowrates.

Series 10 evaluated the impact of finer grinds on the NO_X emissions from PR-only flames with 0 and 15 % OFA. This study was motivated by characterization work showing that coal PSDs were significantly finer after co-milling with biomass than when milled alone, which raised the possibility that some or all of the NO_X reduction attributed to cofiring was actually due to finer grinds. The predictions for this series were based on the calibration factors and model parameters assigned for series 1, because the operating conditions were nominally the same. The only change was the fineness of the grinds, which was substantial enough to reduce the mean size from 36.2 to 17.9 μm.

As seen in Figure 4-26, the measured impact of the size reduction was negligible for 15 % OFA. For 0 % OFA, NO_X emissions with the finer grind were lower by roughly 40 ppm. The predicted impact is greater than that, but still relatively small. For 15 % OFA, the baseline predictions are within experimental uncertainty throughout, but predicted NO_X emissions for the finer grind are 60 ppm lower for all furnace stoichiometries. For 0% OFA, the predictions for both grinds are essentially the same, but still lower than the measurements by 40 – 60 ppm for the base grind and by 20 ppm for the finer grind. Only the prediction for 3.6 % O_2 appears because the case for 4.3 % O_2 would not converge and no data was taken for 2.5 % O_2.

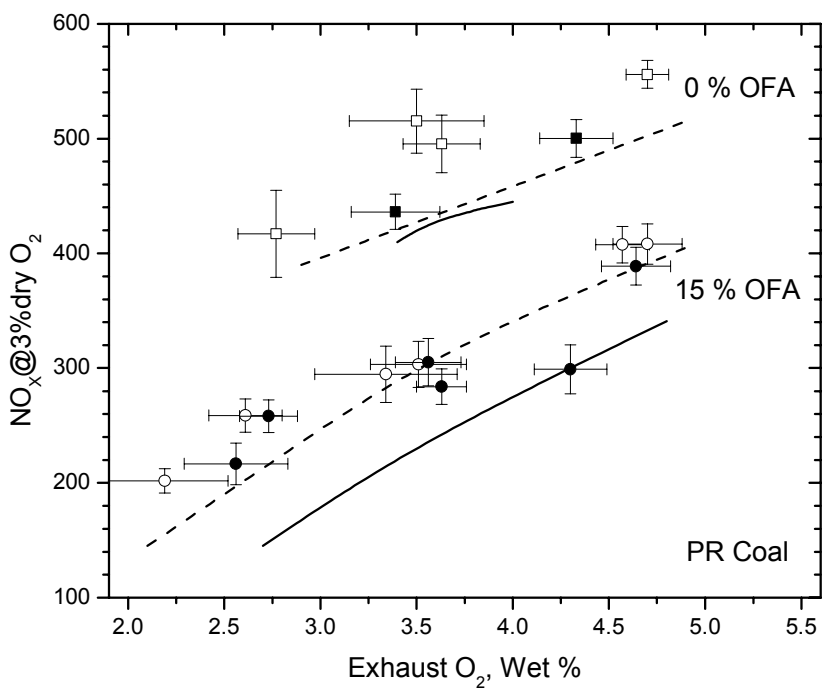

Figure 4-26. Evaluation of predicted NO_X emissions for finer grinds (filled symbols and solid curves) compared to baseline values (open symbols and dashed curves).

4.5.3.3 Effect of Biomass Injection Configuration All cases considered to this point were based on the injection of co-milled biomass as an integral component of the primary fuel stream into the burner. The testing program also characterized three alternate injection configurations, albeit not nearly as thoroughly because none performed as well as co-milling. These alternatives were described in the review of the experimental data in Section 3. Core injection was evaluated with PR and JR in series 3 and 8, respectively, and side injection was evaluated with PR in series 4. In addition, co-milled mixtures were also evaluated in a DRB in series 9. However, only the cases with core injection were simulated because side injection actually increased NO_X in most tests with 15 % OFA and was abandoned early in the project, and because no CFD simulations were developed for the DRB.

The evaluation for a uniform exhaust O_2 level of 3.5 % appears in Table 4-8. These simulations used the char-N conversion factors, initial char oxidation reactivities, and the extrapolation procedures specified for the comparable test series with co-milled injection. Consequently, even the coal-only baselines represent predictions because no parameter adjustments were involved. The measured values show that cofiring with core injection reduced the NO_X emissions in proportion to the biomass loading in series 3 with PR coal, but increased them by 30 to 100 ppm in most cases from series 8 with JR coal. The same tendencies are evident with 0 and 15 % OFA. The predicted values for series 8 with 15 % OFA show essentially no impact of cofiring and are within experimental uncertainty for all cases except JR/10%SD. The predictions for 0 % OFA exhibit increased NO_X emissions for the highest biomass loadings and are also within experimental uncertainty, except for the JR/20% SG case (which underpredicts the NO_X enhancement). But the predictions for series 3 are the worst in the entire database. Whereas the measured NO_X emissions decrease in proportion to biomass loading, the predictions increase for all cofiring cases. The prediction for PR/10%SG failed to converge.

Table 4-8. Evaluation of Predicted NO_X for Core-Injected Co-Fired Flames with 3.5 % O_2.

Series	Fuel	NO_X, ppm @ 3 % dry O_2			
		15% OFA		0% OFA	
		Predicted	Measured	Predicted	Measured
3	PR hv bit	424	425	504	472
	PR/10%SD	514	362	582	411
	PR/20%SD	474	390	556	389
	PR/10%SG	Na	355	659	464
	PR/20%SG	577	344	640	411
8	JR subbit	229	171	304	345
	JR/10%SD	208	260	299	297
	JR/15%SD	235	240	343	372
	JR/10%SG	213	203	314	303
	JR/20%SG	239	247	362	441

Since the predictions for series 8 are generally consistent with the data, there is little reason to believe that the reaction mechanisms are inadequate for core injection. Indeed, the discrepancies for series 3 are probably due to insufficient CFD simulations. The inaccurate predictions for series 3 were based on a single CFD simulation for the PR-only baseline with core injection from REI, whereas those for series 8 were based on CFD simulations prepared by Southern Research for JR-only without core air injection, and for JR/15%SD and JR/20%SG with core injection. The lack of CFD simulations for any of the cofired cases in series 3 introduced major uncertainties into the predictions, because there was no rational basis to assign the mean residence times in the core, which is a crucial parameter in the NO_X reduction stage of the flame chemistry. Also, it may have been too ambitious to apply the extrapolation procedures specified for co-milled injection to core injection cases although, without additional CFD simulations, there was no alternative. In this regard, the good agreement for the JR-only baseline cases in Table 5.4 is misleading, because they omit core air injection. If the core air flow affected the near-burner flow patterns, especially the diversion of secondary air into the primary stream, then different extrapolation procedures would be called for. Additional CFD simulations are needed to clarify this important aspect in future work. Also, future testing with core injection should include core air injection in all baseline tests.

Due to the limitations on the predictions for series 3, the predicted impact of variations in furnace stoichiometry will be evaluated only for series 8. As seen in Figure 4-27, furnace stoichiometry was varied to obtain exhaust O_2 levels from 2.5 to almost 5 %. For each staging level, predictions for the JR-only baseline are evaluated with those for co-firing with both biomass forms, as JR/15%SD and JR/20%SG.

The predictions are generally within experimental uncertainty across the full range of exhaust O_2 for the cofired cases, but not the coal-only baselines. Among the cofired cases, the only significant discrepancy is for the JR/20%SG case with 0 % OFA, where the scatter in the data is also excessive. The somewhat greater propensity for NO_X reduction with SG, even though the loading was lower, is also evident in the predictions. But both of the baseline cases exhibit large discrepancies, especially for intermediate O_2 levels with 15 % OFA and for low O_2 levels with 0 % OFA. This flaw is probably a reflection of inadequate extrapolation procedures, which were noted above.

4.5.4 LOI Predictions

This section evaluates the predicted LOI emissions with the measured values across the entire CRF database. The LOI predictions did not receive nearly the same technical attention as NO_X emissions during the course of the project, due to limitations on schedule and budget. Indeed, various flaws in the evaluations will simply be presented without detailed interpretations. These flaws should not be regarded as intrinsic limitations in the associated reaction mechanisms, particularly CBK, pending a deeper examination of the simulation results.

Also, one potential source of uncertainty on the LOI determinations from the testing program needs to be considered. The flyash loadings and, perhaps, compositions, are usually affected by sedimentation in the horizontal ductwork of the CRF. As much as one-half the flyash may settle out before the collection devices, so this effect may be significant for several reasons. First, UBC and flyash have different aerodynamic characteristics and can therefore settle out at

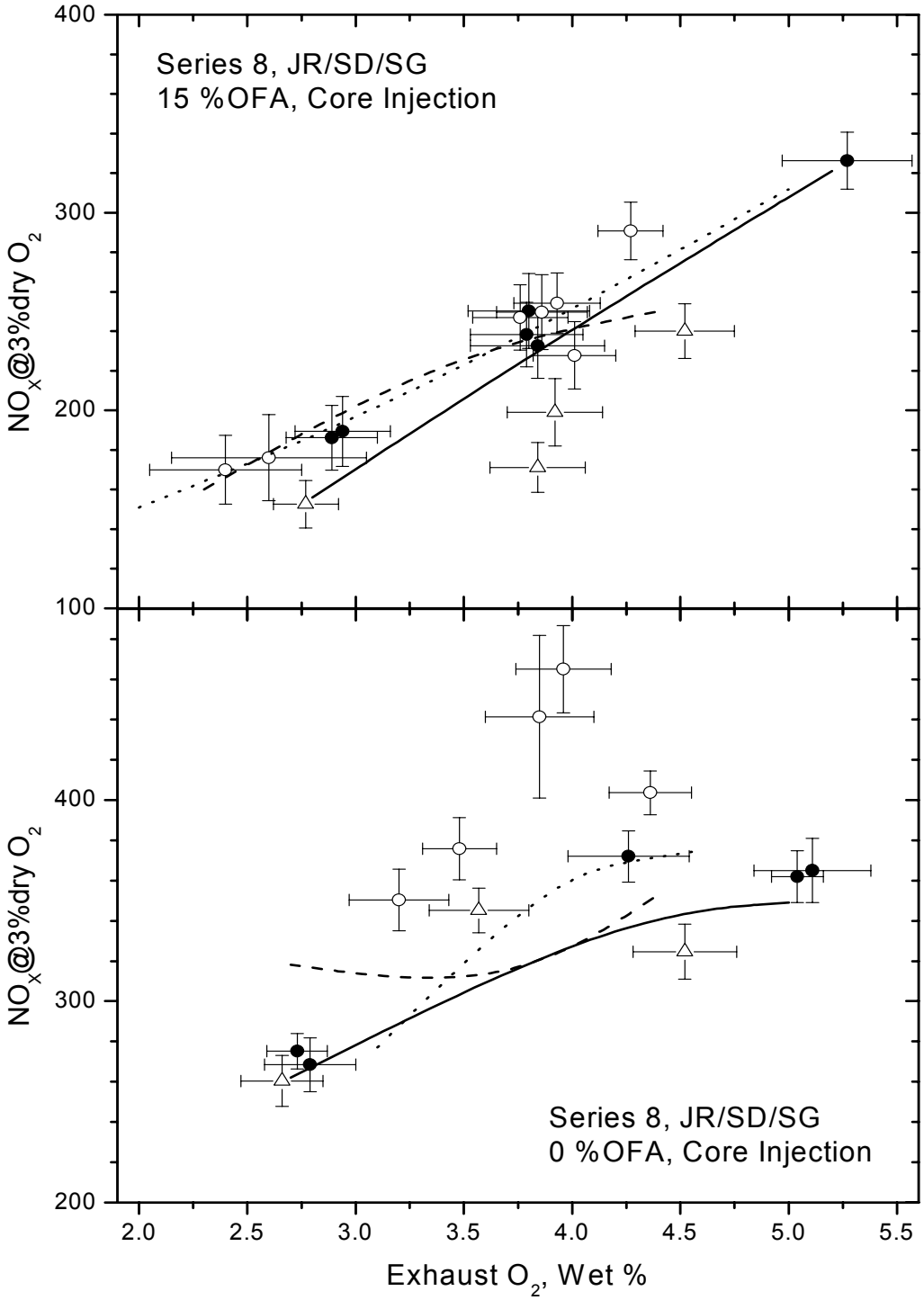

Figure 4-27. Evaluation for the full range of exhaust O_2 for core injection. Each case contains a coal-only baseline (Δ, dashed curves) and cofired cases with 15 % SD (●, solid curves) and 20 % SG (○, dotted curves).

different rates. Second, flyashes from different coals have different aerodynamic characteristics so the fraction that fails to reach the particle collection device can vary among different fuel types. Third, in the modeling, we applied the predicted UBC value to all the ash in the coal to specify LOI. This calculation should be adjusted for the portions of flyash and UBC that settled out, but the necessary information was not available. This omission will bias the LOI predictions in cases with preferential sedimentation of either flyash or UBC.

4.5.4.1 Fuel Quality Effects A parity plot for the LOI predictions for all cases with co-milled injection, 3.5 % O_2, and 15 % OFA appears in Figure 4-28. This data subset contains measurements from test series 1, 5, 6, 7, 10, 11, 12, and 13, and therefore represents the complete range of fuel quality in the testing program. The range of measured values, from 0.1 to 6.0 wt. % reflects the range in coal quality, from subbituminous through lv bituminous, compounded by the co-firing with both biomass forms. The predicted values are systematically high over the entire range. The overprediction is minor for all cases involving PR and GL either with or without SD or SG. But all cases involving JR are overpredicted well beyond the limits of useful quantitative tolerances. The overpredictions for JW-cases are less severe but still 2 to 3 times the measured values.

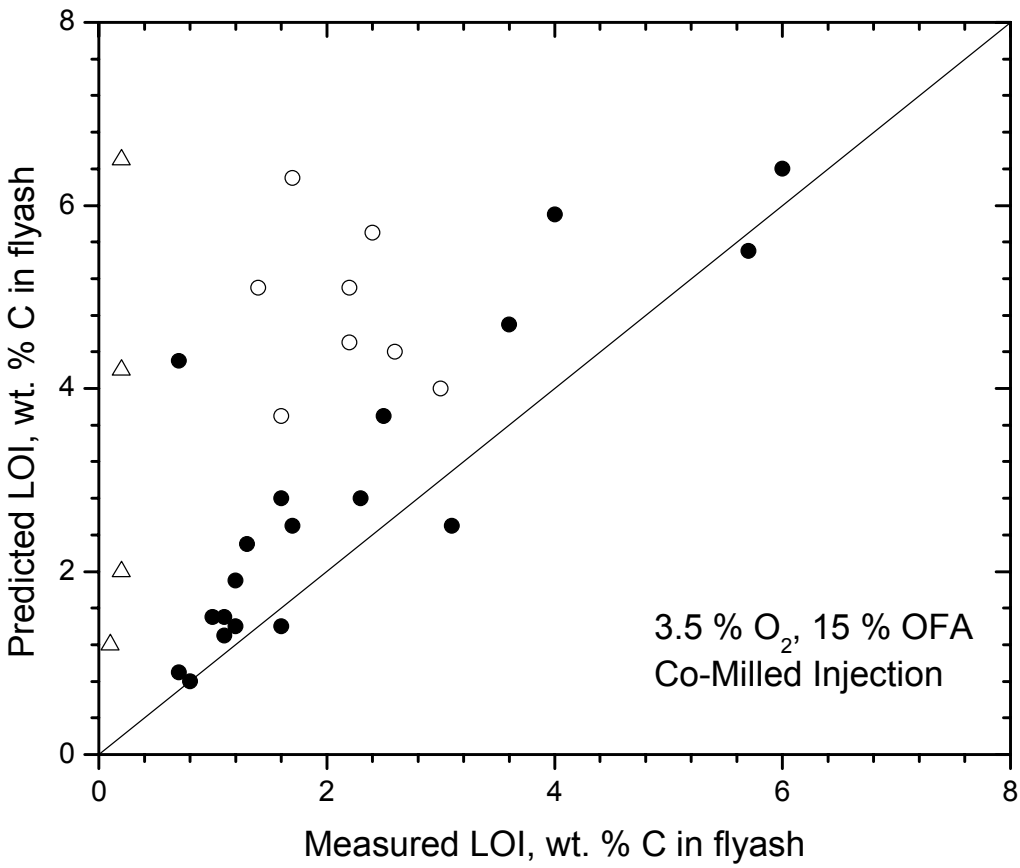

Figure 4-28. Parity plot for the data subset with co-milled injection, 3.5 % O_2, and 15 % OFA where the cases with JR (Δ) and JW (○) are distinguished from all other test results (●).

As seen in the tabulation of this data subset in Table 4-9, biomass cofiring did not necessarily reduce the measured LOI values. Cofiring cases with JW were consistently lower than the baseline values but, with GL, cofiring reduced LOI in series 6 and 11 and increased LOI in series 5 for SD cofiring. The LOI data in series 7 for JR and in series 1 for PR show no impact of cofiring. Even in cases with significant cofiring impacts, the LOI data do not change in proportion to the biomass loading. The predicted impact of cofiring on LOI is correct for PR in series 1, where cofiring has no effect, and for GL in series 5 and 11, where cofiring reduced LOI. Cofiring is incorrectly predicted to have no impact with JW, and to increase LOI with JR, especially SG cofiring.

The parity plot for the LOI predictions for all cases with co-milled injection, 3.5% O_2, and 0 % OFA appears in Figure 4-29. As with the data subset for 15 % OFA in Figure 4-28, the range of measured values reflects the broad range in fuel quality in the testing program, but it has been substantially shifted downward to 0.1 to 1.5 wt. % by the higher near-burner S. R. in the unstaged flames. The predicted values seriously overestimate LOI for all fuel types, and the overpredictions are again much worse for cases with JR and JW. Since all the measured values are so low, there is no apparent effect of cofiring on LOI in this data subset. But the predicted LOI values for series 5 and 11 with GL, and for series 7 with JR and for series 12 with JW are higher with cofiring either biomass form. They are lower for PR in series 1 and for GL in series 5, and essentially unchanged for JW in series 13.

4.5.4.2 Effects of Furnace Stoichiometry and PSD Staged flames produce more LOI than unstaged flames, and this behavior is clearly evident in almost all the predictions in Table 4-9. In addition to staging, the testing program characterized variations in furnace stoichiometry and, to a much lesser extent, variations in particle size. Furnace stoichiometry was varied to obtain exhaust O_2 levels from 2.5 to almost 5 % for both staging levels in all test series. However, the poor accuracy in the LOI predictions for 3.5 % O_2 for all fuels with 0 % OFA and for JR and JW with 15 % OFA provide little incentive for a comprehensive review of this influence. Instead, we focus on the predictions for PR and GL with 15 % OFA.

The predictions for these cases are evaluated in Figure 4-30. The cases for test series 11 were omitted for lack of space. For each series, predictions for a coal-only baseline are evaluated along with those for one or two co-fired cases, except for the PR data from series 6, which did not include LOI for any cofiring tests. The error bars indicate the standard deviations reported by Southern Research staff for each run.

The only predictions within experimental uncertainty across the full range of exhaust O_2 are for the PR-cofiring cases in series 1. For exhaust O_2 levels up to 4 %, the predictions for the other cases exhibit the correct tendency for lower LOI with higher O_2 levels, but the predicted dependence is stronger than the observed one, except for the PR-only baseline in series 6. At the highest O_2 levels the predictions exhibit a curious tendency to become independent of the O_2 level. It is conceivable that this defect reflects the annealing mechanism in CBK. Since the maximum flame temperatures were hotter for the highest overall S. R. values, the annealing mechanism would tend to reduce the oxidation reactivity to a greater extent for these cases. Ultimately, this effect would exert the strongest impact during the very latest stages of burnout and, thereby, enhance LOI levels.

Table 4-9. Evaluation of Predicted LOI for Co-Milled, Co-Fired Flames with 3.5 % O_2.

Series	Fuel	LOI as weight % UBC in ash			
		15% OFA		0% OFA	
		Predicted	Measured	Predicted	Measured
1	PR hv bit	1.4	1.2	2.4	0.9
	PR/10%SD	1.3	1.1	0.8	0.3
	PR/20%SD	1.5	1.1	0.6	1.3
	PR/15%SG	1.9	1.2	1.5	0.5
	PR/20%SG	1.4	1.6	1.6	1.2
5	PR hv bit	0.9	0.7	0.7	0.4
	GL hv bit	4.3	0.7	1.8	0.9
	GL/10%SD	2.8	2.3	4.0	1.3
	GL/20%SD	2.5	1.7	4.5	0.5
6	PR hv bit	2.3	1.3	1.6	0.3
	PR/20%SD	1.4	Na	1.9	0.2
	GL hv bit	6.4	6.0	5.6	0.6
	GL/10%SG	2.8	1.6	2.2	0.9
	GL/20%SG	2.5	3.1	1.6	0.6
7	JR subbit	1.2	0.1	3.0	0.1
	JR/10%SD	2.0	0.2	4.8	0.2
	JR/20%SD	4.2	0.2	2.8	0.2
	JR/10%SG	6.5	0.2	6.0	0.1
	JR/20%SG	12.8	0.2	10.5	0.2
10	PR hv bit	1.5	1.0	1.6	0.4
	PR fine	0.8	0.8	0.8	0.2
11	GL hv bit	5.5	5.7	1.9	1.2
	GL/5%SD	5.9	4.0	2.6	1.5
	GL/10%SD	4.7	3.6	3.0	1.0
	GL/20%SD	3.7	2.5	2.7	0.4
12	JW lv bit	5.7	2.4	3.9	0.9
	JW/5%SD	5.1	2.2	4.7	0.7
	JW/10%SD	5.1	1.4	4.5	0.8
	JW/20%SD	6.3	1.7	5.9	0.7
13	JW lv bit	4.0	3.0	3.4	0.9
	JW/5%SG	3.7	1.6	3.3	0.6
	JW/10%SG	4.5	2.2	2.8	0.8
	JW/20%SG	4.4	2.6	3.9	1.0

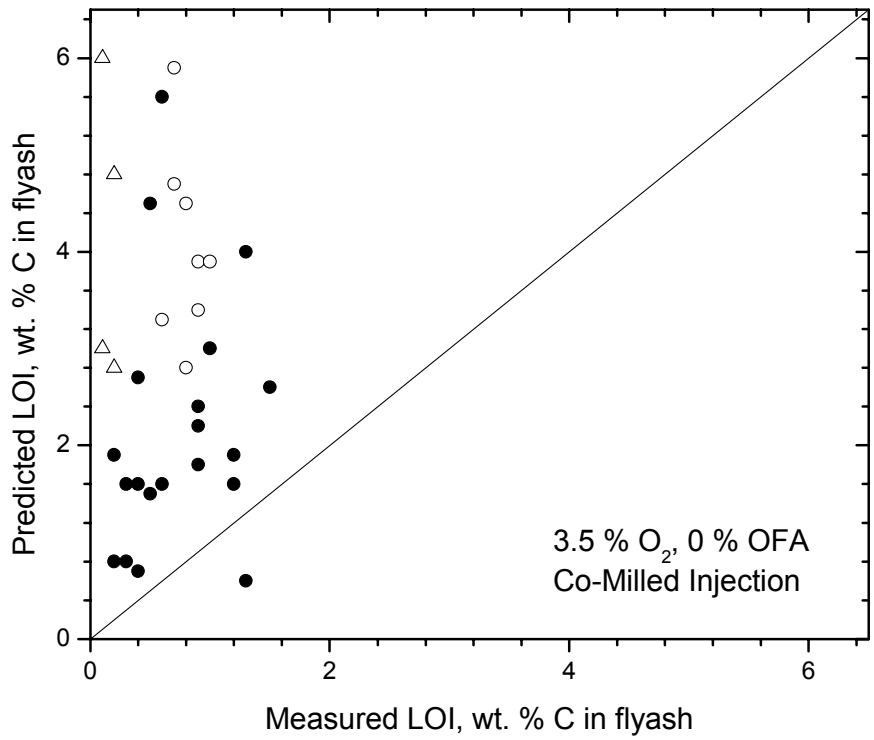

Figure 4-29. Parity plot for the data subset with co-milled injection, 3.5 % O_2, and 0 % OFA where the cases with JR (Δ) and JW (○) are distinguished from all other test results (●).

The other possibility is that the convergence tolerance applied to the oxygen balance for each reactor element in the simulations was not small enough to resolve char conversion during the latest stages of burnout. Early in the project it became apparent that our analysis could not be driven to essentially complete combustion, even with very large increases in the initial char oxidation reactivities. This behavior is not consistent with the performance of CBK for the combustion histories of individual particles subjected to furnace conditions. It probably reflects conversion levels during the latest stages of char burnout under CRF conditions that were below the convergence threshold applied to the oxygen balances. Note that the predicted extents of char burnout were usually greater than 99 % for almost all test conditions, so the neglect of even small burnout fractions would significantly affect the LOI predictions. This effect needs to be examined closely in future applications of APP to CRF test conditions.

An evaluation for the grind size study in series 10 appears in Figure 4-31. The predictions for this series were based on the calibration factors and model parameters assigned for series 1, because the operating conditions were nominally the same. The only change was the fineness of the grinds, which was substantial enough to reduce the mean size from 36.2 to 17.9 μm. The predictions exhibit the correct tendency for lower LOI with finer grinds, but tend to underestimate the impact at lower O_2 levels and conversely at moderate O_2 levels.

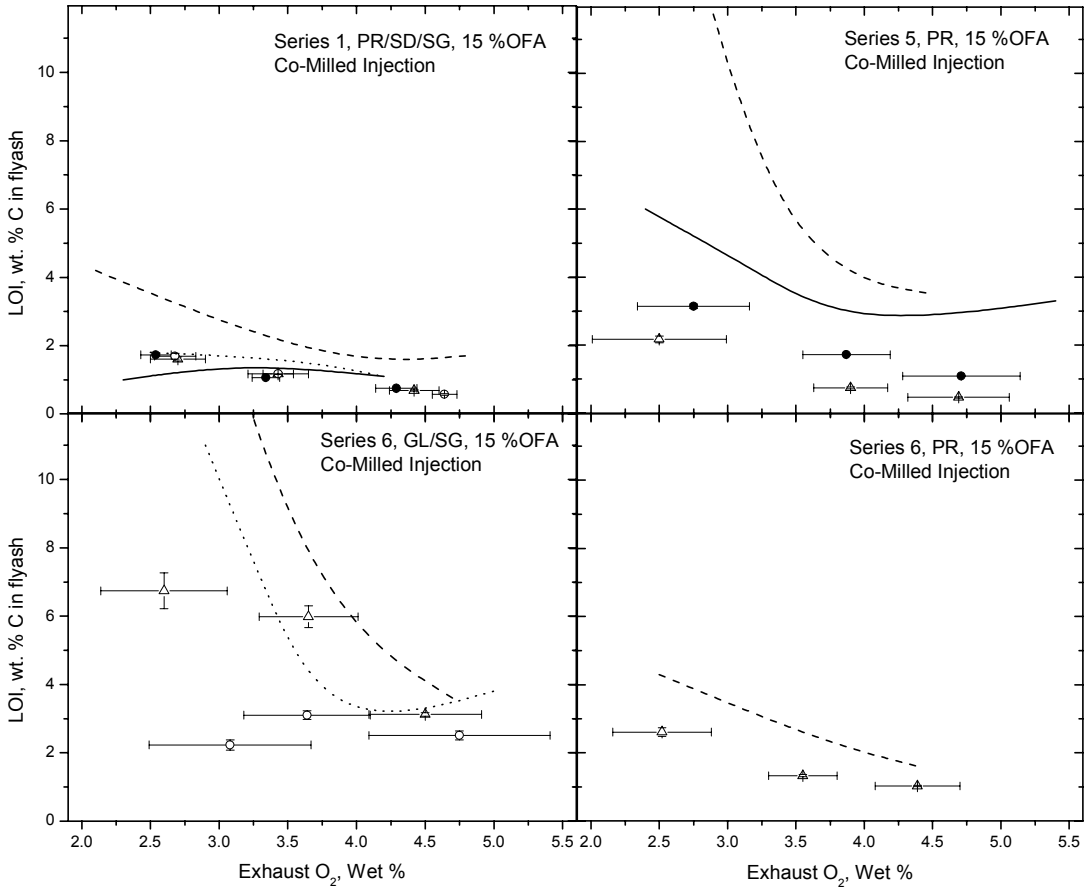

Figure 4-30. Evaluation for the full range of exhaust O_2 with 15 % OFA and co-milled injection. Each case contains a coal-only baseline (Δ, dashed curves) and, if available, cofired cases with 20 % SD (●, solid curves) and 20 % SG (○, dotted curves).

4.5.4.3 Effect of Biomass Injection Configuration The evaluation of the LOI measurements for core injection from series 3 and 8 for a uniform exhaust O_2 level of 3.5 % appears in Table 4-10. The measured values show that cofiring with core injection did not change the LOI levels, as expected. It did not change the predicted values for series 8 either, although the predictions are slightly higher for series 3 with PR. But SG cofiring on JR is predicted to dramatically increase LOI, at odds with the measurements. The prediction for PR/10%SG failed to converge.

4.5.5 Interpretations

The flame structures developed in Section 4.5.2 and the predicted distributions of secondary pyrolysis products in Table 4-5 define the vocabulary needed to interpret the impact of fuel quality and CRF operating conditions. At this point, our interpretations emphasize NO_X emissions, simply because the NO_X predictions were generally within useful quantitative tolerances for the entire database, whereas the LOI predictions were not. Before interpreting the impact of all test variables, we first introduce a parameter set to gauge the various contributions to the exhaust NO_X emissions.

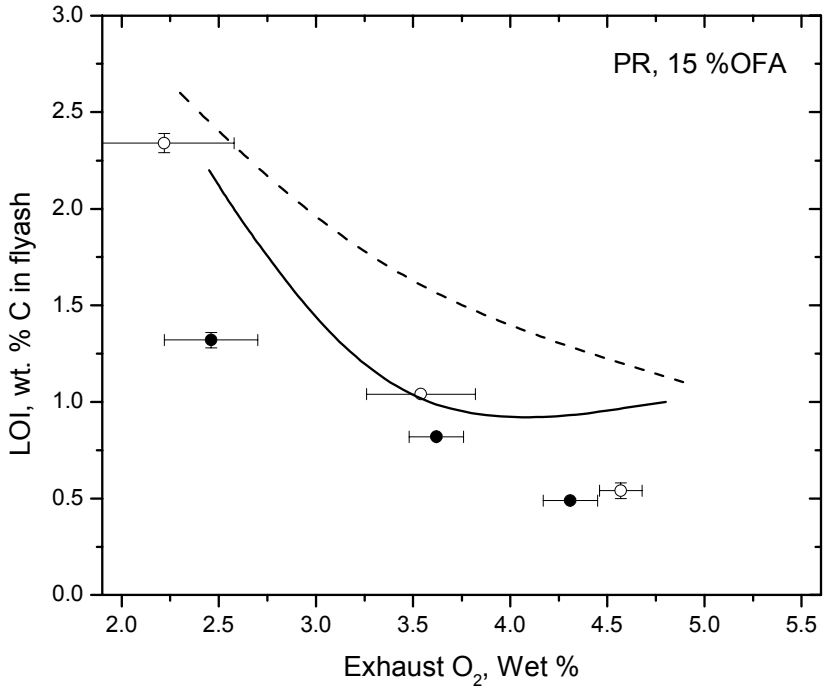

Figure 4-31. Evaluation of predicted LOI for finer grinds (●and solid curve) compared to baseline values with 15 % OFA (○ and dashed curve).

Table 4-10. Evaluation of Predicted LOI for Core-Injected Co-Fired Flames with 3.5 % O_2.

Series	**Fuel**	**LOI, wt. % C in flyash**			
		15% OFA		**0% OFA**	
		Predicted	**Measured**	**Predicted**	**Measured**
3	PR hv bit	2.5	1.8	1.3	1.2
	PR/10%SD	2.3	0.8	2.0	0.5
	PR/20%SD	2.9	0.7	2.6	0.7
	PR/10%SG	Na	1.1	3.1	0.6
	PR/20%SG	3.1	0.9	3.3	0.4
8	JR subbit	2.9	0.1	3.3	0.1
	JR/10%SD	2.2	0.4	2.3	0.2
	JR/15%SD	1.5	0.3	3.3	0.2
	JR/10%SG	7.0	0.2	6.0	0.2
	JR/20%SG	13.5	0.8	11.3	0.5

4.5.5.1 Flame Structure Parameters There are four distinct stages of NO_X production in CRF flames, as follows:

(1) **Near-burner NO production.** Very substantial NO levels are inevitable, mostly due to conversion of volatile-N species under oxidizing conditions in the gas phase (while $(S.R.)_{GAS}$ falls from 5 to 1). The contribution from prompt NO may also be important, due to conversion of hydrocarbons during ignition at moderate temperatures (650-750°C).

(2) **NO reduction in the flame core.** Near-burner NO can be eliminated, provided that (i) $(S.R.)_{GAS}$ is near-unity or lower; (ii) sufficient residence time is available in the core; and (iii) sufficient HCN is available.

(3) **Complete conversion of all volatile-N species in the mixing layer.** Any residual HCN or NH_3 from the core is completely eliminated very early in the mixing layer. The partitioning of these species into additional NO and N_2 is determined by the entrainment rate of secondary air and the temperature, and by the proportions of NO and HCN.

(4) **Burnout of residual char-N**. Once the HCN and NH_3 have been eliminated, the conversion of residual char-N is completely decoupled from chemistry in the gas phase. A fixed fraction of the char-N entering the mixing layer will inevitably form NO. Whereas the fractional char-N conversion factor varies with fuel rank, the amount of char-N entering the mixing layer is determined by a fuel's devolatilization behavior and char oxidation reactivity.

Throughout our interpretations, we will characterize the shifts among these four stages due to variations in fuel quality, staging level, and furnace stoichiometry. Such shifts are clearly related to shifts in the underlying chemical reaction mechanisms, and the APP analysis accommodates quantitative sensitivity analysis to identify which particular reactions are primarily responsible for variations in the NO_X emissions. Unfortunately, due to limitations on schedule and budget, the formal sensitivity analyses had to be relegated to follow-on work. Instead, we introduce a family of parameters that gauges the relative contributions from the four distinct stages, as follows.

The parameter set was identified from the coal-quality impacts on NO_X emissions in the simulations of the baseline, coal-only flames. They are compiled in Table 4-11. The number attached to the coal label denotes the test series. Conditions in the flame core are characterized with several parameters. The maximum near-burner NO concentration, NO_M, always occurred while volatiles were still being released. The ratio of the NO and HCN concentrations, R_{DV}, was evaluated at the end of devolatilization as a measure of the potential for NO reduction. The minimum value of $(S.R.)_G$ also pertains to the NO reduction stage. The core residence time, τ_C, is reported along with the concentrations of NO, HCN, and NH_3 at this time. N-species conversion in the mixing layer is characterized with NO_{VOL}, the NO concentration at the point where all HCN and NH_3 have been eliminated; and $F_{Char\text{-}N}$, the absolute flowrate of char-N into the mixing layer. The maximum gas temperatures were also surveyed but found to be very similar for all coals. For example, the maximum gas temperature in the cores were 1411°C with

Table 4-11. Predicted N-Conversion Parameters for Coal-Only Flames with 15 % OFA and 3.5 % O_2.

Coal	Core							Mixing Layer		Exhaust
	NO_M	R_{DV}	$(S.R.)_G$	τ_C	NO_C	HCN_C	NH_{3C}	NO_{VOL}	F_{CharN}	NO_{EX}
JR-7	533	0.62	0.96	.121	130	344	77	161	0.10	263
GL-5	767	2.23	1.05	.163	325	9	2	256	0.18	360
GL-6	769	2.28	1.05	.163	363	11	2	260	0.17	368
GL-11	757	1.99	1.05	.163	283	14	3	207	0.18	345
PR-1	747	1.35	1.01	.163	256	5	1	209	0.18	325
PR-5	708	0.87	0.99	.163	189	17	5	165	0.20	354
PR-6	694	0.81	0.98	.163	159	30	10	153	0.20	351
PR-10	759	1.23	0.97	.163	256	39	10	206	0.16	315
JW-12	704	2.85	0.98	.150	498	18	1	341	0.15	419
JW-13	743	3.15	0.99	.150	518	15	1	355	0.15	429

JR, 1462°C with PR and GL, and 1436°C with JW. All the cases in this table are for 15 % OFA and an exhaust O_2 level of 3.5 %, so the mixing characteristics are directly comparable.

The maximum NO_X concentrations in the cores are at least 700 ppm, except for the JR-flame. The distinctive value reflects JR's significantly lower N-content (cf. Table 4.3.1). The minimum S. R. values are very similar, which is surprising because the total volatiles yields range from 40 daf wt. % for JW to 65 % for JR. However, most of this difference is compensated for by the variations in the yields of soot, CO_2, and H_2O, which do not affect the S. R. value. For the gaseous fuel compounds, the yields vary from 10.1 daf wt. % for JW to 16 % for GL and PR to 21 % for JR. However, the greater yield of hydrocarbons and lower yield of CO from JW increases the O_2 requirement for volatiles combustion, thereby compensating for its lower combustible gas yield. The relatively short residence time in the core of the JR-flame is partly responsible for the low NO concentration and the very substantial amounts of HCN and NH_3 leaving this core. But, as demonstrated shortly, the very low ratio of NO to HCN is also responsible for the relatively weak conversion of volatile-N in this flame core.

The only flame with a higher NO concentration in the mixing layer than in the core is the JR-flame, due to its high residual amounts of HCN and NH_3. All the other values of NO_{VOL} are determined by dilution with secondary air starting from the NO_C concentration in the core flows. Dilution in the mixing layer alone reduces NO_C by about 20 %. This factor implies that, without supplemental NO in the JR-mixing layer, NO_{VOL} would have been 104 ppmw. The additional 57 ppm in the value of NO_{VOL} corresponds to a conversion of 13 % of the residual HCN and NH_3 into NO.

It is interesting that the rank ordering of the exhaust NO_X emissions for these flames is essentially established by the magnitudes of NO_{VOL}, the NO produced via conversion of volatile-N. The values of F_{CharN} determine the total amount of nitrogen added to the gaseous products during burnout of the remaining char, and show significant variations only for JW and one of the PR-flames. The difference between NO_{VOL} and NO_{EX} is roughly proportional to this parameter,

with attenuation by the variations in the exhaust gas flowrates (of up to 7 %) and the different units applied to NO_{EX}.

Hence, the parameters in Table 4-11 gauge near-burner NO production (NO_M); NO reduction in the flame core (R_{DV} and τ_C); additional NO from HCN/NH_3 conversion in the mixing layer (NO_{VOL} vs. NO_C); and the NO from char-N conversion (F_{CharN}). Parameter R_{DV} has an especially strong mechanistic connection which will be illustrated before the parameter set is used to interpret the impact of all the test variables on NO_X emissions.

A correlation of NO_C versus R_{DV} appears in Figure 4-32. It is remarkably strong, with an r^2-correlation coefficient of 0.948 and a std. dev. of 31.8 ppmw. This implies that the NO emissions from CRF flame cores are governed by the proportions of HCN and NO at the end of devolatilization, provided that the residence time is sufficient to complete the NO reduction. This factor alone is responsible for the significantly higher core-NO with GL than PR, because their core residence times were the same. It is the dominant factor underlying the excessive NO emissions from JW-cores, because these core residence times were not too short to convert all the available HCN and NH_3; rather, JW releases too little volatile-N to provide enough HCN to reduce away its near-burner NO. And the overabundance of HCN in JR-cores is responsible for its very low core-NO level; indeed, had the residence time been longer, the NO emissions would have been even lower.

A mechanistic basis for the relationship between NO_C and R_{DV} appears in Figure 4-33. At the near-unity $(S.R.)_{GAS}$ values in these flame cores, the main radical chain carrier is OH, and the levels of O-atoms would be negligible. The dominant conversion channel for HCN is therefore (1) HCN conversion into CN via OH attack; followed by (2) CN oxidation into NCO. (3) The NCO subsequently reduces NO into N_2. Due to the high core temperatures, the competing NO reduction channel that produces N_2O would not be important. This mechanistic interpretation remains to be validated with sensitivity calculations, but the strength of the correlation in Figure. 4-32 points to a predominant role for NCO, the primary decomposition product of HCN under flame core conditions.

<u>4.5.5.2 Fuel Quality Effects on NO_X Cofiring</u> The flame structure parameters for biomass cofiring with 15 % OFA and 3.5 % O_2 are compiled in Table 4-12. The JW/20%SD case was omitted because the predictions were not within useful quantitative tolerances. The only consistent effect for all fuel combinations is that cofiring significantly reduces the amount of char-N that leaves the flame cores. As explained in connection with Figure 4-16, two factors are responsible for this effect: First, the coal char competes more effectively for the available core-O_2 due to the larger size of the biomass char, so the extent of burnout of the coal is higher in cofired flame cores than in coal-only cores. The residual char-N decreases in proportion to the extent of char burnout. Second, the biomass expels all its fuel-N during devolatilization and does not convey any char-N into the mixing layer.

But the impact of cofiring on volatile-N conversion is surprisingly complex. With JR, cofiring reduces NO_M with SD and raises it with SG, consistent with the N-contents of these biomass samples. Both biomass forms raise R_{DV}, which yields significantly more NO_C. Since the core

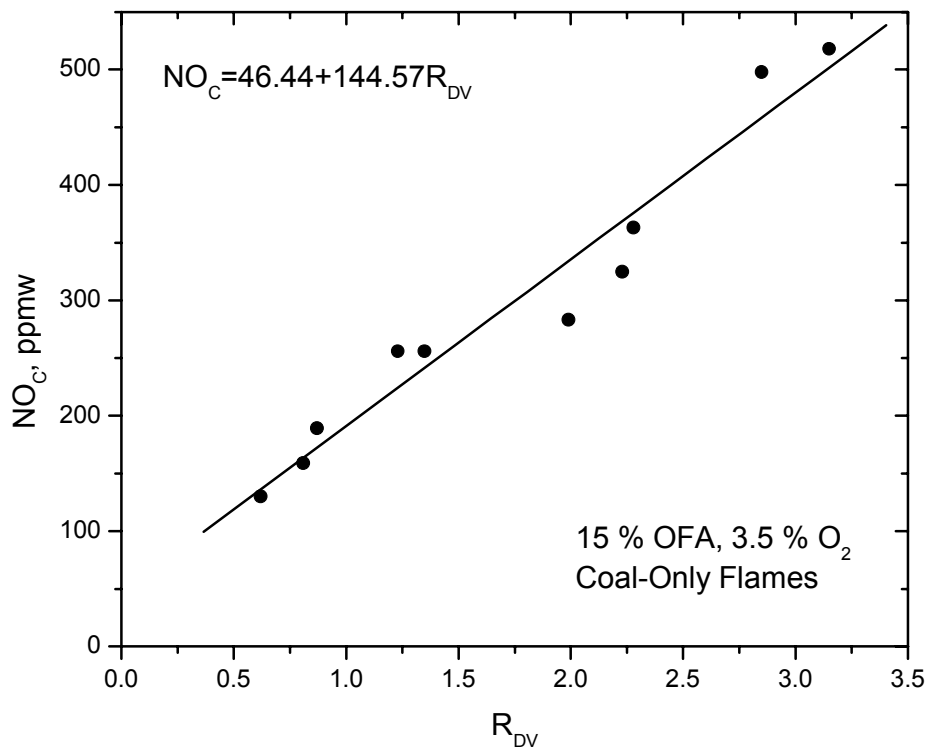

Figure 4-32. Correlation of NO_C versus R_{DV} for coal-only flames.

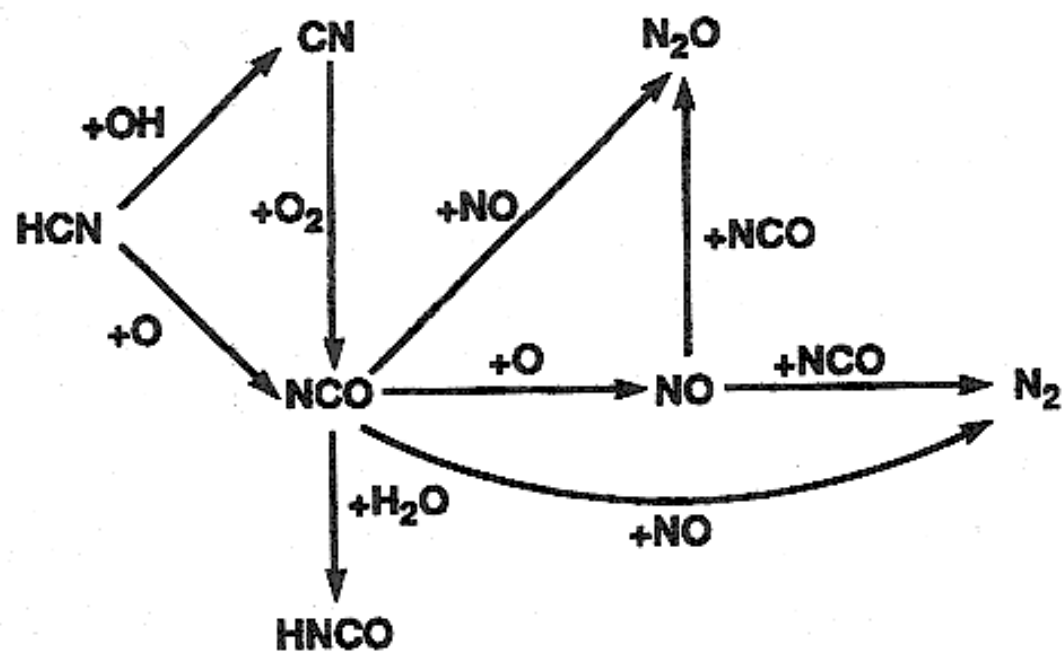

Figure 4-33. Submechanism for HCN oxidation in post-flame regions (Glarborg and Miller 1994).

Table 4-12. Predicted N-Conversion Parameters for Cofired Flames with 15 % OFA and 3.5 % O_2.

Fuel	Core							Mixing Layer		Exhaust
	NO_M	R_{DV}	$(S.R.)_G$	τ_C	NO_C	HCN_C	NH_{3C}	NO_{VOL}	F_{CharN}	NO_{EX}
JR-7	533	0.62	0.96	.121	130	344	77	161	0.10	263
w/20SD	405	0.67	0.95	.158	164	79	19	182	0.07	212
w/20SG	644	0.74	0.95	.158	208	172	32	171	0.07	177
GL-11	757	1.99	1.05	.163	283	14	3	207	0.18	345
w/20SD	595	0.98	1.01	.118	300	50	7	256	0.13	251
GL-6	769	2.28	1.05	.163	363	11	2	260	0.17	368
w/20SG	760	2.86	1.03	.118	524	14	1	354	0.15	349
PR-1	747	1.35	1.01	.163	256	5	1	209	0.18	325
w/20SD	858	0.49	0.86	.118	465	1388	92	143	0.15	236
w/20SG	660	0.71	0.95	.118	250	350	41	163	0.14	258
JW-13	743	3.15	0.99	.150	518	15	1	355	0.15	429
w/20SG	722	3.26	1.01	.165	510	31	2	384	0.13	404

residence times are longer with cofiring, the residual HCN and NH_3 concentrations are correspondingly lower, and the ultimate values of NO_{VOL} are higher for both biomass forms. Despite the higher NO generated from volatile-N conversion, the reduced char-N levels are responsible for the lower exhaust NO_X emissions.

Cofiring SD with GL reduces NO_M, as expected. But NO reduction in the core is hindered by the much shorter residence time, which ultimately yields higher NO_{VOL}. The same situation pertains to SG cofiring, compounded by no reduction in NO_M and less HCN in the core (so R_{DV} is higher). Since the reduction in char-N is small, the exhaust NO_X emissions are nearly the same as for the GL-only baseline. The most surprising aspect of cofiring SD on PR is the much higher NO_M, which we already attributed to prompt NO (in Sec. 4.5.2.3). The short residence time and low S. R. deliver very high concentrations of NO, HCN, and NH_3 out of the core. Nevertheless, the abundance of HCN in the early mixing layer yields a much lower NO_{VOL}. When compounded by the slight reduction in char-N, this benefit yields a substantial reduction in the exhaust NO_X emissions. There is no prompt NO with SG cofiring, but the shorter residence time again enables an abundance of HCN to pass into the early mixing layer. This again lowers NO_{VOL}, but not by as much as the huge excess during SD cofiring.

SG cofiring with JW hardly perturbs volatile-N conversion, so the minor reduction in char-N hardly changes the exhaust NO_X emissions.

Hence, the only universal effect of biomass cofiring on NO_X emissions is the reduction in the amount of char-N released into the char burnout regions. Cofiring can perturb volatile-N conversion by promoting prompt NO formation or, conversely, by reducing NO_M. But the main effect on volatile-N conversion is to lower the core residence time, which conveys more NO, HCN, and NH_3 into the early mixing layer, where it may or may not lower the NO_{VOL}

contribution. The various alternatives are determined by the chemistry among the biomass form and the baseline coal, and cannot be foreseen in the standard coal properties.

4.5.5.3 Effect of Operating Conditions on NO_X

4.5.5.3.1 Effect of Staging The flame structure parameters for coal-only flames with 0 % OFA and 3.5 % O_2 are compiled in Table 4-13. Unstaged CRF flames in the testing program had higher flowrates of secondary air, which diverted 10 to 15 % more secondary air into the primary stream. The maximum gas temperatures were hotter by roughly 70°C, but core residence times were the same. Whereas the NO_M values in Table 4-13 are essentially the same as for staged flames and the $(S.R.)_G$ are only slightly perturbed upward, the R_{DV} values are significantly greater. Even small increases in the O_2-inventory will significantly shift the N-speciation toward more NO and less HCN in the vicinity of the stoichiometric point. Consequently, the extents of NO reduction in the cores of unstaged flames are significantly lower than in staged flames, and all HCN and NH_3 were eliminated in the cores, except for the small residual amounts from the JR-core. Without HCN, there is no supplemental NO reduction in the mixing layer so NO_{VOL} usually equals NO_C. Less char-N is carried into the mixing layer than in staged flames, simply because unstaged flames sustain higher extents of char burnout due to the greater amounts of O_2. Of course, the exhaust NO_X emissions are greater, due to the less effective reduction of near-burner NO in the flame cores.

Table 4-13. Predicted N-Conversion Parameters for Coal-Only Flames with 0 % OFA and 3.5 % O_2.

Coal	Core							Mixing Layer		Exhaust
	NO_M	R_{DV}	$(S.R.)_G$	τ_C	NO_C	HCN_C	NH_{3C}	NO_{VOL}	F_{CharN}	NO_{EX}
JR-7	603	1.01	0.98	.121	294	15	3	248	0.07	395
GL-5	798	3.48	1.07	.163	453	1	0	453	0.16	453
GL-6	798	3.47	1.07	.163	451	1	0	451	0.16	449
GL-11	850	6.84	1.09	.163	600	0	0	600	0.15	640
PR-1	777	2.08	1.02	.163	436	0	0	436	0.16	464
PR-5	766	2.01	1.02	.163	364	0	0	364	0.19	453
PR-6	762	1.67	1.01	.163	381	0	0	381	0.19	453
PR-10	871	2.01	1.00	.163	480	1	0	480	0.13	452
JW-12	718	4.76	1.01	.150	586	0	0	586	0.12	639
JW-13	765	5.59	1.01	.150	630	0	0	630	0.12	664

Most of the same differences are evident among the flame structure parameters for cofired flames with and without staging. The parameters for the unstaged cofired flames are compiled in Table 4-14. The NO_M values are again roughly the same, and the R_{DV} values are significantly higher, indicating a reduced potential for NO reduction in the flame cores. The NO_C values are correspondingly higher, but residual HCN and NH_3 from the cofired flames are carried into the core. The residual concentrations are substantial with JR/20%SD, but low for the other fuel combinations. The char-N levels are lower in all cofired cases, as expected. But exhaust NO_X emission are much higher than in the staged flames due to less effective reduction of near-burner NO in the flame cores.

Table 4-14. Predicted N-Conversion Parameters for Cofired Flames with 0 % OFA and 3.5 % O_2.

Fuel	Core							Mixing Layer		Exhaust
	NO_M	R_{DV}	$(S.R.)_G$	τ_C	NO_C	HCN_C	NH_{3C}	NO_{VOL}	F_{CharN}	NO_{EX}
JR-7	603	1.01	0.98	.121	294	15	3	248	0.07	395
w/20SD	660	1.05	0.91	.158	115	475	130	229	0.04	302
w/20SG	591	1.30	1.00	.131	353	2	0	293	0.06	369
GL-5	798	3.48	1.07	.163	453	1	0	453	0.16	453
w/20SD	748	2.85	1.05	.118	457	8	1	362	0.13	434
GL-6	798	3.47	1.07	.163	451	1	0	451	0.16	449
w/20SG	814	4.05	1.05	.118	527	7	1	404	0.14	456
PR-6	762	1.67	1.01	.163	381	0	0	381	0.19	453
w/20SD	599	0.99	0.96	.118	329	25	4	252	0.17	411
PR-1	777	2.08	1.02	.163	436	0	0	436	0.16	464
w/20SG	669	1.45	0.98	.118	406	13	2	335	0.10	384
JW-13	765	5.59	1.01	.150	630	0	0	630	0.12	664
w/20SG	748	5.50	1.02	.165	595	2	0	460	0.10	512

In Table 4-14 it may seem curious that the NO_{VOL} values are much lower than the NO_C values when so little HCN_C and NH_{3C} are present in the cofired flames. The reason is that NO_{VOL} was evaluated at the point in the mixing layer where the HCN and NH_3 concentrations decreased to less than 1 ppmw. All concentrations at this point within the mixing layer were affected by dilution with secondary air, and the extents of entrainment of secondary air were not necessarily the same in all cases. So dilution, not NO reduction, was mostly responsible for the reduced values of NO_{VOL}.

4.5.5.3.2 Effect of Furnace Stoichiometry At this point the impact of furnace stoichiometry on coal-only and cofired flames is easy to anticipate. The flame structure parameters for JR and JR/20%SD flames at the three nominal exhaust O_2 levels are collected in Table 4-15. Since core residence times are unaffected, the main effect at progressively higher O_2 levels on volatile-N conversion is to decrease the inventory of HCN available for near-burner NO reduction. Consequently, more NO and less HCN and NH_3 leave the flame core at higher O_2 levels, and NO_{VOL} values are correspondingly higher. This detrimental effect is partially compensated for by lower values of F_{CharN}, but the predicted exhaust NO_X emissions are still greater for higher exhaust O_2 levels, as they should be.

4.5.5.3.3 Effect of Cofiring Configuration Since cofiring with core injection increases the air flow into the core, its impact is entirely analogous to firing at higher exhaust O_2 levels with co-milled injection.

<u>4.5.5.4 LOI Predictions</u> The LOI predictions were within useful quantitative tolerances for cases involving GL and PR with 15 % OFA, but not with any of the cases for JR and JW or with any of the fuels with 0 % OFA. Such poor performance probably indicts one of the mechanisms in CBK, but there are also other factors to consider.

Table 4-15. Predicted N-Conversion Parameters for JR and JR/20%SD Flames with 15 % OFA.

Fuel	Core							Mixing Layer		Exhaust
	NO_M	R_{DV}	$(S.R.)_G$	τ_C	NO_C	HCN_C	NH_{3C}	NO_{VOL}	F_{CharN}	NO_{EX}
JR										
2.5%O_2	516	0.44	0.93	.121	182	848	94	98	0.12	179
3.5%O_2	533	0.62	0.96	.121	130	344	77	161	0.10	263
4.5%O_2	549	1.00	0.99	.121	196	24	8	172	0.09	292
JR/20SD										
2.5%O_2	462	0.87	0.87	.158	208	922	70	130	0.08	148
3.5%O_2	405	0.67	0.95	.158	164	79	19	182	0.07	212
4.5%O_2	493	0.97	0.97	.158	286	9	2	245	0.05	265

CBK includes a mechanism for ash inhibition during the latest stages of burnout whereby the accumulating layer of ash becomes progressively thicker as the combustible matter burns away. At some point, the ash layer hinders the penetration of O_2 into the core of combustibles, thereby reducing the overall burning rate. This effect is clearly seen in the predictions for SG cofiring (cf. Figure 4-17), where large unburned SG-particles comprise essentially all the LOI at much higher levels than in the comparable coal-only flames. The same ash inhibition effect comes into play with JR, and also with PR due to its high ash content. This mechanism has already been used to accurately interpret the burnout behavior of several low-rank coals and, by extension, applied uniformly to all biomass samples, albeit without strong confirmation by lab data.

Unfortunately, the LOI data from the CRF do not corroborate an important role for ash inhibition. Based on the poor performance in this project, it now appears that CBK overestimates the impact of ash inhibition on biomass chars, and also on some low-rank coal chars.

The overpredicted LOI in the JW-cases are much harder to rationalize. With 89 % daf wt. % carbon, this coal is clearly a low volatile bituminous. There is an enormous database that established that chars of this rank have substantially lower intrinsic oxidation reactivities than hv bituminous chars, and CBK incorporates this tendency into its default reactivity assignments. To describe the CRF datasets, the assigned initial reactivity for JW was only 30 % lower than for PR (cf. Table 4-6), which is an unusually small adjustment for such a marked difference in coal rank. Our predictions did account for the smaller grind with JW than with the other bituminous coals, and CBK has already been validated for predictions over a broad range of sizes. We do not understand the very low measured LOI values with JW.

We strongly suspect that the problems in the JW cases and with all the 0 % OFA cases are related to an inadequate convergence tolerance in the simulations during the latest stages of burnout (described further in Section 4.5.4.2). Before any attempts are made to modify or replace CBK for applications such as this one, a convergence procedure for APP must be developed that enables predictions of no LOI for arbitrarily high initial char oxidation reactivities for CRF operating conditions. In fact, NEA already developed such a procedure in a more recent

APP project that could fruitfully be applied in more detailed interpretations of the LOI data from this project. It would also help to clarify the impact of preferential sedimentation of UBC in horizontal sections of the ductwork during CRF tests on the measured LOI values.

4.6 Recommendations for Full-Scale Applications

4.6.1 T-Fired Furnace Applications

The flame structures assigned for CRF flames are directly applicable to the near-injector regions in full-scale T-fired utility furnaces. Indeed, CRF emissions have already been qualified against those from full-scale, T-fired boilers and NEA has already used APP to determine the near-injector flame structures in a full-scale, T-fired utility furnace. Moreover, the CRF database compiled for this project spans the complete domain of fuel quality, cofiring level, staging level, and furnace stoichiometry in full-scale applications.

Since the flame structures are comparable, we can confidently expect that the greatest benefits from cofiring on NO_X emissions will be realized with co-milled injection, just like in the CRF. This observation is restricted to cases for biomass injection into the furnace fuel injection elevations, and should not be compared to biomass injection into the upper furnace for p. f .-on-p. f. reburning, which could conceivably be more effective.

Questions as to whether cofiring would be quantitatively as effective in the CRF tests should not be addressed without additional APP simulations. The reason is that we already identified very significant differences among the operating conditions near fuel injectors in a full-scale furnace, compared to the specifications on CRF flames. The major differences include the following:

(1) Full-scale fuel injectors have lags of up to a few hundred ms in the time required to heat fuel suspensions to the onset temperature for devolatilization due to very fast injection velocities, whereas CRF flames do not.

(2) Residence times in the flame cores tend to be much more variable than in CRF flames.

(3) Times to mix auxiliary and close-coupled OFA air streams with the primary streams tend to be much longer than the mixing times for secondary air in the CRF.

(4) Interactions among the flows from adjacent fuel injectors and across different injection elevations are very important. They often govern the amounts of HCN and NH_3 carried from fuel injection zone into the much more oxidizing upper furnace elevations. Such interactions were absent in the CRF tests.

We have already established that the time available to reduce away near-burner NO is a key influence on the conversion of volatile-N into NO. Items 1 and 2, above, directly affect this condition. We have also seen that the conversion of residual HCN and NH_3 from the core at the early times in mixing layers is often a significant contribution to the conversion of volatile-N into NO during biomass cofiring. Items 3 and 4, above, directly affect this chemistry. In principle, all the itemized differences would tend to lengthen the time available for NO

reduction, both in flame cores and in the early mixing layers, and the performance for co-milled biomass injection should be at least as good as in the CRF tests.

However, the interactions among neighboring injection streams in a full-scale T-fired furnace dominate over all the other factors. These interactions can dramatically reduce residence times into the upper furnace, via short circuits, or extend them, via collisions that deflect the streams downward. In NEA's previous APP analysis of a T-fired furnace, the NO_X emissions attributed to individual fuel injectors varied by more than a factor of four, due to the extreme variations among the interactions of neighboring injection streams. Both the lowest emissions and the highest were determined by such interactions. Consequently, we see no way to quantitatively estimate the performance of biomass cofiring in applications in T-fired utility furnaces short of a complete APP analysis. One always hopes that much simpler heuristics will emerge from the detailed analysis, along the lines of our interpretations with the flame structure parameters in this project. But at least one or two complete simulations are needed to identify the basis for the heuristics.

4.6.2 Applications Involving Other Firing Configurations

We seriously doubt that the favorable performance of biomass cofiring with co-milled injection demonstrated in the CRF tests can be anticipated for wall- or cyclone firing conditions. These burners sustain completely different flame structures, and the cofiring performance could very well be better with a different injection configuration. This project established that near-burner NO is inevitable, and that biomass can significantly enhance the reduction of near-burner NO and the favorable conversion of volatile-N into N_2, provided that its volatiles are available within NO reduction zones. Once the locations and residence times of these reduction zones for other firing configurations have been established with APP analyses, it becomes much simpler to optimize the biomass injection configuration.

4.7 Recommendations for Further Development

APP clearly sets the standard on accuracy for predicted NO_X emissions from large-scale p. f. flames of diverse fuel types. It also resolves near-burner phenomena far better than conventional CFD post-processing for NO_X, which is the crucial ingredient needed to advance current burner design practices. Whereas this project demonstrated these capabilities for a 1.7 MW_t single-burner furnace, NEA has already used APP to predict NO_X and CO emissions from a full-scale T-fired furnace rated in excess of 500 MW_e. APP is definitely scalable over the complete domain of commercial interest. We also believe that we are now in a position to automate most, if not all, of the APP methodology.

This unique capability should be implemented in both near- and long-term applications that aim to reduce NO_X emissions from p. f. fired boilers, as follows:

(1) Identify the determining near-burner flame structures in dual-register burners (with internal recirculation) for wall-fired applications. Then identify optimal firing strategies for multi-burner arrays in wall-fired furnaces, and optimize the flame structures in burner design applications.

(2) Identify the determining near-burner flame structures in cyclone burners, and evaluate predictions with test data from full-scale cyclone furnaces.

(3) Develop APP for gas-on-p.f. reburning and for p.f.-on-p.f. reburning systems.

All of these near-term applications can accommodate any type of coal, biomass, or petroleum coke with the chemical reaction mechanisms used in this project. Extensions to other opportunity fuels, such as black liquor, residual crude fractions, municipal solid wastes, and waste plastics, are straightforward, based on NEA's extensive expertise in formulating predictive reaction mechanisms for diverse p. f. types.

In the far-term, APP is especially promising in gasification applications, where chemical kinetics are usually the determining factor (in contrast to furnace flames, where mixing-limited formulations can be applied). NEA has already developed a version of CBK for char gasification by CO_2, H_2, and H_2O with inhibition by CO, and validated the predictions against the available database of lab measurements reported in English. APP is immediately applicable to entrained-flow systems, for which the flow and thermal fields can be characterized with conventional CFD, and for fluidized systems, provided that state-of-the-art Eulerian/Eulerian fields for the gas and particle phases are available. APP can also be applied within the conventional chemical engineering framework for fluidized systems, which combines heuristic correlations for the flow characteristics with various reactor network combinations to represent mixing. This approach is probably the best way to develop expedient engineering calculations for advanced fluidized gasification systems.

Within the context of biomass cofiring, APP should immediately be used in two ways. First, the crucial elements of cofired flame structure identified in this project for fuel injectors should be resolved for dual register burners, to enable optimization of wall-fired cofiring applications. Second, APP should be used to identify the optimal biomass injection configuration for cofiring in full-scale systems. This project clearly established that the injection configuration is crucial for effective NO_X abatement via cofiring. This same issue needs to be addressed in the analysis of full-scale burner arrays, where residence times, mixing intensities, and the thermal fields are, by no means, the same as in the CRF. Based on our analysis, we would expect that careful management of several near-burner operating conditions will be needed to reap the benefits of biomass cofiring in full-scale furnaces. APP provides the most expedient way to identify the most effective injection strategies.

Of course, the accuracy of the LOI predictions must be improved. This project established the poor performance and identified several potential causes. Follow-on work is needed to resolve and rectify the outstanding technical issues, and to evaluate the predictions with data from systems that better represent the typical LOI values in full-scale systems. Whereas the accuracy of the NO_X predictions was firmly established for the CRF database, deeper sensitivity analyses are needed to validate our preliminary interpretations, which were based on the flame structure parameters.

5.0 RESULTS AND DISCUSSION

5.1 Introduction

The purpose of this project was to construct and validate a predictive computer model of biomass cofiring. To reach this goal, two advances were required in the state of the art. First, numerous well-characterized sets of emissions data were needed to define what efficiencies or penalties could be realized from biomass cofiring. Second, a comprehensive NO_X and UBC emissions model should be developed and validated against the sets of experimental test results.

5.2 Testing

All testing was carried out at a single combustion source whose emissions are representative of a full-scale boiler where a rigorous testing campaign was designed to precisely define and assess those parameters most likely to affect NO_X and UBC emissions for biomass cofiring. These parameters include the type of biomass, type of coal, biomass injection configuration, burner geometry and staging, and furnace stoichiometry. Thus, the emissions database compiled for this project spans the complete domain of burner geometry, fuel quality, cofiring level, staging level, and furnace stoichiometry in practical applications of biomass cofiring. The burner type emphasized in the model evaluations sustains the near-burner flame structures found in full-scale T-fired utility furnaces, and emissions from the CRF have already been shown to mimic those from such full-scale systems.

The testing matrix employed for this project included four types of US coal - Powder River Basin (JR), Eastern bituminous high-volatility (PR), Eastern bituminous low-volatility(JW), and Illinois Basin coal (GL) and two biomasses – sawdust (SD) and switchgrass (SG). Poultry litter was simulated by adding anhydrous ammonia to the primary air line (to increase fuel nitrogen) while a comilled mixture of coal and sawdust was combusted. Four discrete levels of biomass addition were tested, always as a percentage of the total mass fired (0%, 5%, 10% or 15%, and 20%). However, not every coal was tested at the four levels of biomass addition.

Fourteen separate test series were required to generate the database of 422 results that was used for the model development and validation portion of this project. Table 5-1 lists these tests by coal, biomass, injection geometry, and burner. Inspection of this table shows that 76% of all test conditions were for pulverized coal (32%) or for coal comilled with biomass (44%). This relatively high proportion is indicative of the relative importance of testing with comilled biomass for validating the model as compared to the other injection geometries. Tests with center-burner injection (16%) and side injection (8%) constitute the balance of the database of results.

Results from this database were used to develop and validate a computer-based model for biomass cofiring. The model development relies on a new Advanced Post Processing (APP) technique to incorporate all of the fundamental chemistry pertinent for NO_X and unburned carbon (UBC) production in flames of pulverized coal and biomass.

Table 5-1. Summary of test conditions in the database.

COAL	TYPE	BIOMASS	BURNER GEOMETRY				TOTAL
			Single Register			Dual-Register	
			Comilled	Center	Side	Comilled	
JR	PRB	None	6	7			**13**
		SD	13	15			**28**
		SG	13	17			**30**
GL	Ill. Basin	None	26			6	**32**
		None-NH_3	2				**2**
		SD	42			12	**54**
		SD-NH_3	14				**14**
		SG	17			14	**31**
PR	hv bit.	None	54	8	8		**70**
		SD	30	11	13		**54**
		SG	16	11	12		**39**
JW	lv bit.	None	13				**13**
		SD	21				**21**
		SG	21				**21**
TOTAL			**288**	**69**	**33**	**32**	**422**

5.3 Model Development

It has not been possible to incorporate detailed chemical reaction mechanisms into conventional CFD simulations of pulverized fuel (p. f.) flames. Therefore, to predict NO_X emissions at a combustion source a common approach is to complete a CFD simulation of that source with a particular fuel and then use the results of that simulation for input to simplified chemical submodels to predict NO_X emissions. This approach, called post-processing, has been applied to pulverized coal flames with varying degrees of success. The modeling protocol developed for this project also relies on post processing of a CFD simulation of the CRF for a particular fuel and biomass. However, in this model development, a new methodology was employed to perform the post processing and is able to incorporate all significant chemical mechanisms that are responsible for NO_X production and UBC emissions.

Since chemistry in the gas phase, especially volatile-N conversion chemistry, was suspected to play a dominant role in NO_X production during biomass cofiring, the modeling partner for this project, Niksa Energy Associates (NEA) developed a new computational approach for this application based on an "Advanced Post-Processing" or APP method. This approach proceeds through three stages: First, conventional computational fluid dynamics (CFD) simulations characterize the bulk flow patterns. Second, the bulk flow patterns are analyzed to specify an equivalent network of idealized reactors for the flow. Third, detailed chemical reaction mechanisms are used to determine the chemical composition across the entire reactor network, including the most important emissions.

Project partner Reaction Engineering International (REI) performed the CFD simulations of the CRF for many of the test cases in the experimental database. Other CFD simulations were performed at Southern Research, using REI's Configurable Fireside Simulator (CFS) for the CRF. The CFS is a stand-alone implementation of REI's proprietary *Glacier*© CFD code that imposes a fixed computational grid on the calculations, and is therefore suitable for parametric case studies with the same firing configurations.

In the APP method, the reactor network is a computational environment that accommodates realistic chemical reaction mechanisms. Under this formalism, mechanisms with a few thousand elementary chemical reactions can now be simulated on an ordinary personal computer, provided that the flow structures are restricted to the limiting cases of plug flow or perfectly stirred tanks. The network is equivalent to the CFD flowfield in so far as it represents the bulk flow patterns in the flow. Such equivalence is actually implemented in terms of the following set of operating conditions: The residence time distributions (RTDs) in the major flow structures are the same in the CFD flowfield and in the section of the reactor network that represents the flow region under consideration. Mean gas temperature histories and the effective ambient temperature for radiant heat transfer are also the same. The entrainment rates of surrounding fluid into a particular flow region are evaluated directly from the CFD simulation. To the extent that the RTD, thermal history, and entrainment rates are similar in the CFD flowfield and reactor network, the chemical kinetics evaluated in the network represent the chemistry in the CFD flowfield.

Model predictions have been validated across the database of test results to within useful quantitative tolerances. *This level of performance was achieved without any adjustments to the model parameters for any of the biomass cofiring cases*. Instead, calibration factors were specified to match the predicted and observed emissions for the coal-only tests for all excess O_2 levels, and extents of air staging.

5.4 Results of the Model Development

The APP analysis of the CRF furnace establishes the following milestones in simulations of large-scale, commercially relevant p.f. flames:

(1) For the first time, the complete range of fuel quality in biomass cofiring applications was simulated without heuristic parameter adjustments. None of the parameters in the mechanisms for devolatilization, soot chemistry, or chemistry in the gas phase, including N-species conversion, were adjusted to fit anything in the simulations program. The conversion factors for char-N and the initial char oxidation reactivities were specified to match the NO_X emissions from coal-only flames with 15 % OFA and 3.5 % exhaust O_2. These values were not changed to simulate any of the other fuel combinations or operating conditions.

(2) Only a handful of CFD simulations were required to enable predictions with the complete reaction mechanisms over the full operating domain. The same extrapolation procedures for staging and furnace stoichiometry were applied to the entire data subset with 15 % OFA. Minor additional adjustments to the fractions of secondary air immediately injected into the primary stream were necessary to cover the data subset on unstaged flames (suggesting that this aspect may be responsible for the unpredictable swings in the measured characteristics

of unstaged CRF flames for nominally identical operating conditions). APP incorporates additional information from CFD simulations but does not entail any additional computational burden. Each CRF flame simulation took 15 to 50 min on a 1.5 GHz P4 microprocessor.

(3) Predicted NO_X emissions for the data subset with comilled injection, 15 % OFA, and 3.5 % O_2 represent the complete range of fuel quality within useful quantitative tolerances. The standard error of estimation (SSE) for this evaluation is 32.4 ppm, which is twice the stated experimental uncertainty but within the scatter in the data for replicate cases. These predictions show no systematic discrepancies over the entire range of fuel quality. The predictions also depicted the dependence on biomass loading within useful quantitative tolerances for all fuel combinations.

(4) Predicted NO_X emissions for the data subset with co-milled injection, 0 % OFA, and 3.5 % O_2 also show no systematic discrepancies over the entire range of fuel quality. The SSE for this evaluation is 59.0 ppm, reflecting the larger experimental uncertainties associated with unstaged CRF flames as well as extrapolations away from the staged flames that were characterized with CFD simulations. The predictions over the range of biomass loadings were generally within experimental uncertainty, except for the highest loadings with SG on JW.

(5) The evaluation of predictions for cases with NH_3 injection into PR/SD flames, which simulated cofiring with poultry litter, was inconclusive because the measured baseline levels differed from replicate cases in other test series, and because the discrepancies were substantial in only about half the test cases.

(6) Predicted NO_X emissions over the full range of furnace stoichiometry were generally within experimental uncertainty for both staged and unstaged flames with 15 % OFA, validating the extrapolation procedure developed for this operating condition.

(7) The predicted impact of finer grinds on NO_X emissions was comparable to the measured impact with unstaged flames, but larger by roughly 30 ppm than the measured impact with staged flames.

(8) Predicted NO_X emissions for core injection of biomass were within experimental uncertainty for cases with JR, but not within useful quantitative tolerances for cases with PR. The latter flaw was attributed to insufficient CFD simulations for this injection configuration, not to deficiencies in the reaction mechanisms.

(9) LOI predictions were within useful quantitative tolerances only for staged flames with PR and GL. Predictions for cases with JR were especially poor, although the LOI values from JW-flames were also substantially overestimated. LOI was also consistently overpredicted for lower exhaust O_2 levels with all fuel types, even in staged flames. The predicted impact of finer grind on LOI was qualitatively correct. The serious flaws in the LOI evaluations could be attributed to an overemphasis in CBK of ash inhibition during the later stages of burnout of biomass and JR chars; an inadequate convergence tolerance for the later stages of burnout in the flame simulations; and preferential sedimentation of UBC in horizontal ductwork in the CRF exhaust system, upstream of the particle collection device.

The outstanding quantitative accuracy of the predicted NO_X emissions can be attributed to the unparalleled resolution of chemistry in near-burner flame structures that APP delivers. Indeed, the predicted exhaust NO_X emissions can be resolved into separate contributions from near-burner NO; NO reduction in flame cores by HCN and NH_3; conversion of residual HCN and NH_3 at the inlet to the mixing layer; and the inevitable conversion of fixed portions of char-N into NO in all char burnout regions. The flame structure parameters assigned directly from the APP simulations gauge these various contributions.

The NO emissions from CRF flame cores are governed by the proportions of HCN and NO at the end of devolatilization, provided that the residence time is sufficient to complete the NO reduction. This factor alone is responsible for the significantly higher core-NO with GL than PR, and it is the dominant factor underlying the excessive NO emissions from JW-cores. An overabundance of HCN in JR-cores is responsible for its very low core-NO level, which could have been even lower given additional residence time in the flame core.

The only universal effect of biomass cofiring on NO_X emissions is the reduction in the amount of char-N released into the char burnout regions. Cofiring can perturb volatile-N conversion by promoting prompt NO formation or, conversely, by reducing NO_M. But the main effect on volatile-N conversion is to lower the core residence time, which conveys more NO, HCN, and NH_3 into the early mixing layer, where it may or may not lower the NO_{VOL} contribution. The various alternatives are determined by the chemistry among the biomass form and the baseline coal, and cannot be foreseen in the standard coal properties.

Whereas unstaged CRF flames had only slightly more O_2 in their flame cores than staged flames, even small increases in the O_2-inventory will significantly shift the N-speciation toward more NO and less HCN in the vicinity of the stoichiometric point. Consequently, the extents of NO reduction in the cores of unstaged flames are significantly lower than in staged flames, and all HCN and NH_3 were eliminated in the flame cores. Less char-N is carried into the mixing layer than in staged flames, simply because unstaged flames sustain higher extents of char burnout due to the greater amounts of O_2. But the exhaust NO_X emissions are greater, due to the less effective reduction of near-burner NO in the flame cores.

Similarly, the main effect on volatile-N conversion at progressively higher O_2 levels is to decrease the inventory of HCN available for near-burner NO reduction. Consequently, more NO and less HCN and NH_3 leave the flame core at higher O_2 levels, and NO_{VOL} values are correspondingly higher. This detrimental effect is partially compensated for by lower values of F_{CharN}, but the predicted exhaust NO_X emissions are still greater for higher exhaust O_2 levels, as they should be. Since cofiring with core injection increases the air flow into the core, its impact is entirely analogous to firing at higher exhaust O_2 levels with co-milled injection.

Detailed interpretations of the LOI predictions were not feasible within the limitations on schedule and budget.

6.0 CONCLUSION

The purpose of this project was to construct and validate a predictive computer model of biomass cofiring that could be used as a tool to predict NO_X and UBC emissions for an arbitrary biomass cofiring configuration. In order for this effort to reach a successful conclusion, two advances were required in the state of the art. First, numerous well-characterized sets of emissions data were needed to define what efficiencies or penalties could be realized from biomass cofiring. These data must be representative of full-scale pulverized coal-fired boilers. Second, a comprehensive NO_X and UBC emissions model had to be developed and validated against the various sets of experimental test results.

These project goals have been reached. A large database of emissions results is now available for inspection and further analysis. Also, a new formalism for predicting NO_X and unburned carbon emissions has been successfully developed, implemented, and tested against the emissions database. The modeling procedure incorporates a novel post-processing formalism (advanced post processing, or APP) that combines all relevant combustion chemistry with conventional CFD calculations to predict NO_X and UBC emissions for any biomass cofiring configuration. Because the APP formalism unbinds the chemical kinetics associated with NO_X generation and UBC production from the CFD calculation, predicting the emissions resulting from biomass cofiring is now a straightforward, though involved, procedure.

The versatile APP formalism now sets the standard of accuracy for predicted NO_X emissions from large-scale pulverized fuel flames from diverse fuels. It also resolves near-burner phenomena far better than conventional CFD post-processing for NO_X, which is the crucial ingredient needed to advance current burner design practice. Whereas this project demonstrated these capabilities for a 1.7 MW_t single-burner furnace, our project partner, NEA, has already used APP to predict NO_X and CO emissions from a full-scale T-fired furnace rated in excess of 500 MW_e.[14] Thus, APP is definitely scalable over the complete domain of commercial interest. NEA has privately continued development of the APP procedure and asserts they are now in a position to automate most, if not all, of the APP methodology.

While this project was meant to develop and prove of a specific tool to enable the prediction of NO_X and UBC emissions from biomass cofiring, a tool of greater utility has emerged and application of the APP formalism has already been generalized beyond the original development effort sponsored by the DOE. Specific recommendations are included in Section 5 of this report for other avenues of development for this tool.

7.0 REFERENCES

1. Bush, P.V.; Boylan, D.M.; Bransby, D.I.; Smith, H.A.; Taylor, C.R., *Evaluation of Switchgrass as a Co-Firing Fuel in the Southeast*, Final Technical Report, DOE Cooperative Agreement DE-FC36-98GO10349, National Renewable Energy Laboratory, Golden, CO, November, 2001.
2. Felix, L.G., *Testing Mixtures of Sericea Lespedeza and Pratt Seam Coal in Southern Research and Southern Company's Combustion Research Facility*, Final Report submitted to the Alabama Department of Economic and Community Affairs, Montgomery, AL, October, 2000.
3. Bush, et al, Figure 18, page 38.
4. Dayton, D., *A Summary of NO_X Emissions Reduction from Biomass Cofiring*, Technical Report, DOE Contract DE-AC36-99-GO10337, Task No.BP02.1030, National Renewable Energy Laboratory, Golden, CO, May, 2002, NREL/TP-510-32260.
5. Tillman, D.A., *EPRI-USDOE Cooperative Agreement: Cofiring Biomass with Coal,* Final Report, DOE Contract DE-FC22-96PC96252, U.S. DOE, National Energy Technology Laboratory, Pittsburgh PA, September 2001.
6. Prinzing, D.E.; Hunt, E.; Battista, J., *Cofiring Biomass with Coal in Shawville,* Bioenergy '96 – The 7th National Bioenergy Conference, Nashville, TN, 1996.
7. Tillman, D.A.; Payette, K.; Plasynski, S., *Cofiring Woody Biomass at the Allegheny Energy: Results from Willow Island and Albright Generating Station,* Proceedings of the 28th International Technical Conference on Coal Utilization & Fuel Systems, Vol. 2, U.S. Department of Energy, Coal Technology Association, and ASME, Fuels & Combustion Technologies Division, Clearwater, FL, March 9-13, 2003, pp 1161-1171.
8. Dayton, Figure 1, page 4.
9. Monroe, L.S.; Clarkson, R.J.; Stallings, J., *Comparison of Pilot-Scale Furnace Experiments to Full-Scale Boiler Performance of Compliance Coals*, EPRI/EPA 1995 Joint Symposium on Stationary Combustion NO_X Control, Kansas City, MO, May 16-19, 1995.
10. Pedersen, L. S., P. Glarborg, et al.. *A chemical engineering model for predicting NO emissions and burnout from pulverized coal flames*, Combust. Sci. and Technol. **132**: 251-314, 1998
11 Benedetto, D., S. Pasini, M. Falcitelli, C. La Marca, and L. Tognotti (2000). *NO_X emission prediction from 3-D complete modeling to reactor network analysis*. Combust. Sci. and Technol. **153**: 279-294, 2000.
12 Falcitelli, M., L. Tognotti, and S. Pasini. *An algorithm for extracting chemical reaction network network models from CFD simulation of industrial combustion systems*. Combust. Sci. and Technol. **174**(11-12): 27-42, 2002
13 Felix, L.G., Bush, P.V., 5th Quarterly Progress Report, DOE Cooperative Agreement DE-FC26-00NT40895, "*Development of a Validated Model for Use in Minimizing NO_X Emissions and Maximizing Carbon Utilization when Cofiring Biomass with Coal.*" January 31, 2002.
14. Niksa, S.; Liu, G., *Advanced CFD Post Processing for P. F. Flame Structure and Emissions,* Proceedings of the 28th International Technical Conference on Coal Utilization & Fuel Systems, Vol. 1, U.S. Department of Energy, Coal Technology Association, and ASME, Fuels & Combustion Technologies Division, Clearwater, FL, March 9-13, 2003, pp 165-176.

APPENDIX A

Emissions Database

Table A-1A. Gas Flow Data from Tests PR-1, PR-1R, PR-2, and PR-10, Part 1.

Test PR-1 – Comilling of SG and SD with PR Coal														
Furnace Flow Data					------ FURNACE AIR FLOWS, SCFM (60°F, 29.92 in. Hg) ----								Fuel Feed	
Test Condition	FEO, Wet %		NO_x, 3% O_2, ppm		Total Air		Pri. Air (150°F)		Sec. Air (600°F)		OFA (600°F)		Rate, lb/hr	
	Avg.	S.D.	Avg.	S.D.	Avg.	S.D.	Avg.	S.D.	Avg.	S.D.	Avg.	S.D.	Avg.	S.D.
100% PR - 0% OFA														
	2.51	0.10	388.6	11.9	650.3	2.9	123.5	0.1	526.8	2.8	0.0	0.0	309.4	8.9
	2.92	0.13	440.7	11.1	680.1	2.3	129.2	0.2	550.9	2.2	0.0	0.0	309.8	8.8
	3.14	0.05	447.7	8.9	680.1	2.0	129.2	0.2	551.0	2.0	0.0	0.0	309.4	8.7
	3.37	0.13	473.3	12.3	680.0	2.8	129.2	0.2	550.5	1.8	0.2	1.8	308.3	8.8
	3.70	0.20	456.5	18.4	667.3	2.9	120.0	0.3	547.3	0.3	0.0	0.0	294.8	9.4
	3.83	0.09	447.2	8.0	699.9	2.1	133.0	0.2	566.9	2.0	0.0	0.0	310.1	8.8
	4.21	0.14	475.7	16.6	684.4	4.2	120.0	0.2	564.4	0.2	0.0	0.0	293.8	8.5
	4.93	0.23	593.6	9.7	750.3	3.2	142.5	0.2	607.8	0.2	0.0	0.0	292.8	8.5
100% PR - 15% OFA														
	2.27	0.20	274.6	11.6	659.8	1.8	125.4	0.1	435.5	1.7	99.0	0.1	309.4	9.2
	2.37	0.10	251.3	17.8	651.4	3.2	123.5	0.2	430.4	3.2	97.4	0.4	310.4	9.0
	2.55	0.19	261.9	15.1	640.1	6.2	120.0	0.2	426.2	0.2	93.9	1.1	293.1	9.4
	2.79	0.21	292.1	24.2	643.1	3.5	120.0	2.9	428.6	2.9	94.5	0.2	293.7	9.9
	2.85	0.09	299.7	21.6	679.6	2.1	129.2	0.2	448.4	2.0	102.0	0.1	309.4	8.6
	2.91	0.06	291.0	9.7	680.3	1.8	129.2	0.2	449.1	1.7	102.0	0.2	310.9	9.1
	3.03	0.03	320.5	11.0	679.7	2.9	129.2	0.2	448.4	2.9	102.0	0.1	309.9	8.8
	3.30	0.11	324.9	16.7	720.0	1.8	136.8	0.2	475.2	1.7	108.0	0.2	308.8	9.0
	3.55	0.21	327.7	10.3	719.8	2.3	136.8	0.2	475.1	2.3	108.0	0.1	309.1	9.0
	3.64	0.25	374.0	21.3	710.8	3.5	134.9	0.2	469.3	0.2	106.5	0.1	293.2	9.1
	4.15	0.07	362.7	17.8	719.3	2.1	136.8	0.2	474.5	2.0	108.0	0.1	309.5	9.5
	4.36	0.16	437.0	11.0	720.5	3.2	122.5	1.9	489.9	1.9	108.0	0.2	294.7	9.2
	4.57	0.25	408.1	15.6	750.3	2.2	142.5	0.2	495.3	0.2	112.5	0.1	293.2	8.7
	4.60	0.16	439.9	17.3	769.3	1.8	146.3	0.2	507.5	1.7	115.5	0.2	309.8	9.1
	4.75	0.08	464.2	10.4	770.2	6.8	146.3	0.3	508.4	6.8	115.5	0.3	310.2	8.7
100% PR - 30% OFA														
	3.49	0.17	192.0	9.7	684.2	4.3	120.0	0.2	360.2	0.2	204.0	0.5	293.2	9.4
	3.66	0.25	213.2	12.2	684.2	3.9	120.0	0.5	360.1	0.5	204.0	0.4	294.3	9.4
90% PR 10% SD 0% OFA														
	2.74	0.19	327.7	15.9	658.7	4.2	133.0	0.2	525.6	0.2	0.0	0.0	305.1	7.7
	4.02	0.14	433.5	13.0	716.8	4.2	133.0	0.2	583.7	0.2	0.0	0.0	304.7	8.5
	4.47	0.24	476.6	12.9	748.0	2.7	133.0	0.2	615.0	0.2	0.0	0.0	304.0	9.2
90% PR 10% SD 15% OFA														
	2.54	0.15	228.9	8.1	675.7	3.3	133.0	0.3	442.3	0.3	100.5	0.2	304.3	8.8
	3.44	0.18	274.2	12.2	716.5	3.8	133.0	0.2	475.5	0.2	108.0	0.2	304.3	8.9
	3.36	0.18	270.7	8.4	715.9	2.8	133.0	0.2	474.9	0.2	108.0	0.2	304.0	8.4
	4.55	0.10	332.0	11.9	772.9	3.0	133.0	0.2	521.3	0.2	118.5	0.2	304.2	8.6
90% PR 10% SD 30% OFA														
	3.47	0.14	177.4	4.8	716.4	4.1	132.9	0.2	367.5	0.2	215.9	0.4	304.5	9.1
	3.56	0.13	184.4	4.7	715.3	3.5	133.0	0.2	366.3	0.2	216.0	0.3	304.7	9.3
	3.54	0.06	178.0	1.6	717.6	3.9	133.1	0.2	368.5	0.2	216.0	0.2	305.8	8.5
	4.24	0.16	198.2	5.6	764.5	3.4	133.0	0.1	397.5	0.1	234.0	0.4	304.5	8.9
80% PR 20% SD 0% OFA														
	2.61	0.16	357.8	20.6	666.0	3.8	133.0	0.1	533.0	0.1	0.0	0.0	317.6	6.0
	3.59	0.19	443.8	9.1	724.2	3.0	133.0	0.2	591.2	0.2	0.0	0.0	318.9	8.1
	4.56	0.21	524.6	16.7	760.3	5.1	133.0	0.2	627.3	0.2	0.0	0.0	316.1	6.3
80% PR 20% SD 15% OFA														
	2.52	0.11	212.1	4.4	685.1	3.9	133.0	0.2	450.1	0.2	102.0	0.1	320.0	8.9
	3.25	0.15	244.7	5.6	715.6	2.4	133.0	0.2	474.6	0.2	108.0	0.2	316.9	6.7
	3.27	0.06	237.2	5.4	716.0	2.1	133.0	0.1	475.0	0.1	108.0	0.1	318.2	7.9
	3.33	0.10	250.3	7.1	715.7	2.8	133.0	0.2	474.7	0.2	108.0	0.3	317.2	7.3
	4.32	0.16	297.9	7.5	765.4	4.7	133.0	0.2	515.3	0.2	117.1	0.3	318.3	8.4

Table A-1B. Gas Flow Data from Tests PR-1, PR-1R, PR-2, and PR-10, Part 2.

Test PR-1 – Comilling of SG and SD with PR Coal														
Gas Sampling Data					------ FURNACE AIR FLOWS, SCFM (60°F, 29.92 in. Hg) ----								Fuel Feed	
Test Condition	FEO, Wet %		NOx, 3% O_2, ppm		Total Air		Pri. Air (150°F)		Sec. Air (600°F)		OFA (600°F)		Rate, lb/hr	
	Avg.	S.D.	Avg.	S.D.	Avg.	S.D.	Avg.	S.D.	Avg.	S.D.	Avg.	S.D.	Avg.	S.D.
80% PR 20% SD 30% OFA														
	2.78	0.18	203.7	5.6	703.8	5.1	133.0	0.2	359.5	0.2	211.3	1.9	316.3	7.0
	3.52	0.23	191.8	4.9	731.8	3.9	133.0	0.2	376.9	0.2	221.9	0.8	317.6	7.7
	4.40	0.14	212.8	9.6	770.3	6.1	133.0	0.2	401.4	0.2	235.9	1.5	316.5	7.6
85% PR 15% SG 0% OFA														
	2.76	0.22	338.1	13.4	676.1	5.9	133.0	0.2	543.1	0.2	0.0	0.0	317.9	7.1
	3.60	0.17	413.5	12.2	716.1	2.9	133.0	0.2	583.1	0.2	0.0	0.0	315.3	8.8
	3.59	0.31	406.4	16.3	720.0	3.5	133.0	0.2	587.0	0.2	0.0	0.0	316.4	7.2
	4.07	0.24	463.5	13.5	740.6	4.1	133.1	0.3	607.6	0.3	0.0	0.0	317.3	7.6
85% PR 15% SG 15% OFA														
	2.63	0.10	211.0	7.4	682.8	2.1	133.0	0.2	447.8	0.2	102.0	0.2	317.1	8.1
	3.52	0.15	269.1	9.7	732.6	2.9	133.0	0.2	488.6	0.2	111.0	0.2	316.8	8.2
	4.27	0.23	303.2	10.3	773.8	4.3	133.0	0.3	523.5	0.3	117.3	8.2	317.0	6.8
	4.61	0.08	308.2	6.1	772.6	2.5	133.0	0.2	521.1	0.2	118.5	0.1	317.3	7.8
85% PR 15% SG 30% OFA														
	3.58	0.18	172.9	4.2	732.6	4.4	133.0	0.2	377.4	0.2	222.2	0.7	317.2	7.8
80% PR 20% SG 0% OFA														
	2.55	0.24	303.6	20.6	622.3	5.2	135.0	0.2	487.3	0.2	0.0	0.0	312.7	6.5
	3.60	0.28	366.8	17.8	677.3	3.2	135.0	0.2	542.3	0.2	0.0	0.0	313.9	6.4
80% PR 20% SG 15% OFA														
	2.75	0.27	217.2	14.6	653.3	2.7	135.0	0.2	422.3	0.2	96.0	0.1	314.9	8.3
	3.70	0.32	260.3	18.9	701.9	2.9	135.0	0.2	461.9	0.2	105.0	0.2	316.1	7.4
	4.31	0.27	284.1	12.1	726.1	2.7	135.0	0.3	481.6	0.3	109.5	0.3	315.2	8.4

Table A-1C. Gas Flow Data for UBC Measurements from Tests PR-1, PR-1R, PR-2, and PR-10.

Test PR-1 - Comilling of SG and SD with PR Coal																
Unburned Carbon Data							----- FURNACE AIR FLOWS, SCFM (60°F, 29.92 in. Hg) ------								Fuel Feed	
Test Condition	FEO, Wet %		NO_x, 3% O_2, ppm		% UBC		Total Air		Pri. Air (150°F)		Sec. Air (600°F)		OFA (600°F)		Rate, lb/hr	
	Avg.	S.D.	Avg.	S.D.	Avg.	S.D.	Avg.	S.D.	Avg.	S.D.	Avg.	S.D.	Avg.	S.D.	Avg.	S.D.
100% PR - 0% OFA																
	3.63	0.18	403.7	20.1	0.94	0.01	696.1	3.4	133.0	0.2	563.1	3.4	0.0	0.0	297.1	8.4
100% PR - 15% OFA																
	2.70	0.20	238.2	9.7	1.61	0.06	708.2	3.3	133.0	0.2	468.7	3.2	106.5	0.1	296.7	8.7
	3.43	0.22	273.4	20.0	1.17	0.04	675.3	2.5	133.0	0.2	441.7	2.4	100.5	0.1	296.8	9.1
	4.42	0.18	323.1	13.7	0.69	0.02	765.2	3.4	133.0	0.2	515.1	3.3	117.0	0.1	297.2	8.5
100% PR - 30% OFA																
	3.35	0.29	181.7	14.6	1.69	0.01	700.0	12.8	133.0	0.3	356.9	8.9	210.1	4.3	293.3	34.6
90% PR 10% SD 0% OFA																
	4.02	0.14	434.5	12.8	0.56	0.04	717.2	4.4	133.0	0.2	584.2	4.4	0.0	0.0	304.8	8.7
90% PR 10% SD 15% OFA																
	2.55	0.14	230.3	7.6	1.57	0.03	675.3	3.0	133.0	0.2	441.8	2.9	100.5	0.2	304.1	8.8
	3.53	0.18	276.5	19.4	1.34	0.03	716.1	3.4	133.0	0.2	475.1	3.3	108.0	0.2	303.9	8.6
	4.55	0.11	333.3	13.7	0.68	0.01	772.9	3.0	133.0	0.2	521.3	2.8	118.5	0.2	303.9	8.7
90% PR 10% SD 30% OFA																
	3.56	0.18	177.7	16.0	1.31	0.03	720.3	6.6	133.0	0.3	370.0	5.2	217.3	1.9	305.3	9.2
80% PR 20% SD 0% OFA																
	3.58	0.17	442.7	9.1	0.34	0.01	723.9	2.6	133.0	0.2	590.9	2.6	0.0	0.0	318.1	8.0
80% PR 20% SD 15% OFA																
	2.54	0.11	212.3	4.5	1.73	0.03	685.0	4.1	133.0	0.2	450.0	4.1	102.0	0.2	319.2	9.0
	3.34	0.10	255.0	8.0	1.06	0.01	716.3	2.8	133.0	0.2	475.3	2.7	108.0	0.1	317.6	8.2
	4.29	0.15	300.1	8.3	0.75	0.02	765.1	4.9	133.0	0.2	515.1	4.6	117.0	0.3	317.4	8.2
80% PR 20% SD 30% OFA																
	3.54	0.23	191.9	5.5	0.61	0.01	732.0	3.4	133.0	0.2	377.0	3.3	222.0	0.3	317.2	7.9
85% PR 15% SG 0% OFA																
	3.60	0.28	405.1	16.2	0.54	0.03	719.6	3.2	133.0	0.2	586.6	3.2	0.0	0.0	316.6	7.6
85% PR 15% SG 15% OFA																
	2.68	0.15	217.2	15.3	1.69	0.08	683.6	2.2	133.0	0.2	448.6	2.2	102.0	0.1	316.9	8.4
	3.43	0.11	266.4	13.3	1.17	0.01	732.0	2.7	133.0	0.2	488.0	2.7	111.0	0.2	316.2	8.2
	4.64	0.09	310.0	8.1	0.57	0.02	772.7	2.8	133.0	0.2	521.2	2.7	118.5	0.1	317.3	8.2
85% PR 15% SG 30% OFA																
	3.55	0.15	173.9	4.5	0.62	0.01	731.2	3.2	133.0	0.2	376.2	3.1	222.1	0.3	316.9	8.4
80% PR 20% SG 0% OFA																
	3.62	0.30	366.3	19.8	1.19	0.04	677.7	3.2	135.0	0.2	542.8	3.1	0.0	0.0	314.1	6.6
80% PR 20% SG 15% OFA																
	2.75	0.29	216.4	14.1	1.84	0.06	653.4	2.0	135.0	0.2	422.4	2.0	96.0	0.1	315.1	8.6
	3.66	0.28	256.8	16.2	1.57	0.07	701.7	3.2	135.0	0.2	461.8	3.1	105.0	0.1	316.6	6.6
	4.29	0.24	285.3	12.4	1.07	0.02	726.2	2.9	135.0	0.3	481.6	2.6	109.5	0.2	316.0	7.5

Table A-1D. Gas Sampling Data from Tests PR-1, PR-1R, PR-2, and PR-10, Part 1.

Test 1 – Comilling of SG and SD with PR Coal														
Gas Sampling Data														
Test Condition	FEO, Wet %		NOx, 3% O_2, ppm		CO, 3% O_2, ppm		CO_2, 3% O_2, %		SO_2, 3% O_2, ppm		SO_2, lb/10^6Btu		NO_x, lb/10^6Btu	
	Avg.	S.D.	Avg.	S.D.	Avg.	S.D.	Avg.	S.D.	Avg.	S.D.	Avg.	S.D.	Avg.	S.D.
100% PR - 0% OFA														
	2.51	0.10	388.6	11.9	84.5	2.4	16.2	0.2	1176.0	11.1	1.58	0.01	0.52	0.02
	2.92	0.13	440.7	11.1	71.1	1.9	16.2	0.2	1190.4	7.1	1.60	0.01	0.59	0.02
	3.14	0.05	447.7	8.9	69.0	2.3	16.3	0.2	1156.9	8.2	1.56	0.01	0.60	0.01
	3.37	0.13	473.3	12.3	68.0	2.2	16.4	0.2	1209.2	8.2	1.63	0.01	0.64	0.02
	3.70	0.20	456.5	18.4	88.1	3.0	16.2	0.3	1078.5	11.5	1.45	0.02	0.61	0.02
	3.83	0.09	447.2	8.0	72.5	2.3	16.1	0.2	1199.7	7.6	1.62	0.01	0.60	0.01
	4.21	0.14	475.7	16.6	80.2	2.4	16.1	0.1	1089.2	16.4	1.46	0.02	0.65	0.02
	4.93	0.23	593.6	9.7	76.8	3.2	16.0	0.3	1106.2	12.0	1.48	0.02	0.80	0.01
100% PR - 15% OFA														
	2.27	0.20	274.6	11.6	71.5	2.0	16.3	0.2	1233.8	10.8	1.66	0.01	0.37	0.02
	2.37	0.10	251.3	17.8	83.7	1.9	16.2	0.1	1179.9	27.8	1.59	0.04	0.34	0.02
	2.55	0.19	261.9	15.1	81.8	2.6	16.3	0.3	1125.7	16.6	1.51	0.02	0.35	0.02
	2.79	0.21	292.1	24.2	89.6	7.3	16.1	0.2	1110.2	10.8	1.49	0.01	0.39	0.03
	2.85	0.09	299.7	21.6	69.9	2.1	16.5	0.2	1233.4	8.2	1.66	0.01	0.40	0.03
	2.91	0.06	291.0	9.7	69.4	1.8	16.4	0.1	1233.2	8.8	1.66	0.01	0.39	0.01
	3.03	0.03	320.5	11.0	70.0	1.9	16.4	0.1	1245.0	5.4	1.68	0.01	0.43	0.01
	3.30	0.11	324.9	16.7	71.9	2.6	16.2	0.2	1167.3	9.0	1.57	0.01	0.44	0.02
	3.55	0.21	327.7	10.3	83.1	1.8	16.2	0.2	1204.1	8.0	1.62	0.01	0.44	0.01
	3.64	0.25	374.0	21.3	85.5	2.5	16.0	0.2	1139.6	32.5	1.53	0.04	0.50	0.03
	4.15	0.07	362.7	17.8	75.1	2.0	16.5	0.2	1104.7	28.3	1.49	0.04	0.49	0.02
	4.36	0.16	437.0	11.0	76.5	2.6	15.9	0.2	1070.2	7.1	1.44	0.01	0.59	0.01
	4.57	0.25	408.1	15.6	87.2	2.5	16.0	0.2	1133.2	8.8	1.52	0.01	0.55	0.02
	4.60	0.16	439.9	17.3	72.2	2.2	16.0	0.2	1189.1	8.1	1.60	0.01	0.59	0.02
	4.75	0.08	464.2	10.4	81.4	3.1	15.9	0.2	1147.0	5.1	1.55	0.01	0.63	0.01
100% PR - 30% OFA														
	3.49	0.17	192.0	9.7	81.2	2.4	16.1	0.2	1119.9	11.6	1.50	0.02	0.26	0.01
	3.66	0.25	213.2	12.2	78.3	2.4	16.0	0.2	1087.6	13.7	1.46	0.02	0.29	0.02
90% PR 10% SD 0% OFA														
	2.74	0.19	327.7	15.9	89.1	2.4	16.2	0.2	1111.8	9.4	1.49	0.01	0.44	0.02
	4.02	0.14	433.5	13.0	83.7	2.6	15.8	0.2	1054.7	7.3	1.42	0.01	0.58	0.02
	4.47	0.24	476.6	12.9	89.1	2.7	15.8	0.3	1092.4	9.6	1.47	0.01	0.64	0.02
90% PR 10% SD 15% OFA														
	2.54	0.15	228.9	8.1	83.8	2.8	16.2	0.2	1093.5	12.7	1.47	0.02	0.31	0.01
	3.44	0.18	274.2	12.2	85.9	2.3	16.1	0.2	1123.1	6.9	1.51	0.01	0.37	0.02
	3.36	0.18	270.7	8.4	87.4	2.4	16.0	0.3	1124.8	9.1	1.51	0.01	0.36	0.01
	4.55	0.10	332.0	11.9	86.6	2.7	15.8	0.2	1063.6	8.4	1.43	0.01	0.45	0.02
90% PR 10% SD 30% OFA														
	3.47	0.14	177.4	4.8	87.4	2.4	16.0	0.2	1101.6	8.5	1.48	0.01	0.24	0.01
	3.56	0.13	184.4	4.7	82.6	8.4	16.0	0.1	1099.6	23.3	1.48	0.03	0.25	0.01
	3.54	0.06	178.0	1.6	89.2	3.2	15.9	0.1	1092.2	7.0	1.47	0.01	0.24	0.00
	4.24	0.16	198.2	5.6	92.6	3.2	15.9	0.2	1085.5	10.2	1.46	0.01	0.27	0.01
80% PR 20% SD 0% OFA														
	2.61	0.16	357.8	20.6	64.0	2.0	16.6	0.2	1129.9	9.4	1.52	0.01	0.48	0.03
	3.59	0.19	443.8	9.1	77.2	2.2	16.3	0.2	1066.7	8.5	1.43	0.01	0.60	0.01
	4.56	0.21	524.6	16.7	59.4	2.5	16.3	0.2	1120.7	18.9	1.50	0.03	0.70	0.02
80% PR 20% SD 15% OFA														
	2.52	0.11	212.1	4.4	82.7	2.5	16.3	0.1	1112.8	6.1	1.49	0.01	0.28	0.01
	3.25	0.15	244.7	5.6	87.1	2.9	16.2	0.2	1104.7	10.8	1.48	0.01	0.33	0.01
	3.27	0.06	237.2	5.4	106.8	3.5	16.0	0.2	1053.4	6.6	1.41	0.01	0.32	0.01
	3.33	0.10	250.3	7.1	89.6	4.2	16.2	0.2	1072.2	4.6	1.44	0.01	0.34	0.01
	4.32	0.16	297.9	7.5	82.7	2.8	16.1	0.2	1069.8	7.6	1.44	0.01	0.40	0.01

Table A-1E. Gas Sampling Data from Tests PR-1, PR-1R, PR-2, and PR-10, Part 2.

Test 1 - Comilling of SG and SD with PR Coal														
Gas Sampling Data														
Test Condition	FEO, Wet %		NOx, 3% O_2, ppm		CO, 3% O_2, ppm		CO_2, 3% O2, %		SO_2, 3% O_2, ppm		SO_2, lb/10^6Btu		NO_x, lb/10^6Btu	
	Avg.	S.D.	Avg.	S.D.	Avg.	S.D.	Avg.	S.D.	Avg.	S.D.	Avg.	S.D.	Avg.	S.D.
80% PR 20% SD - 30% OFA														
	2.78	0.18	203.7	5.6	61.5	1.8	16.6	0.2	1131.0	10.6	1.52	0.01	0.27	0.01
	3.52	0.23	191.8	4.9	66.6	3.6	16.5	0.2	1089.1	10.2	1.46	0.01	0.26	0.01
	4.40	0.14	212.8	9.6	67.8	3.2	16.3	0.2	1091.2	7.4	1.46	0.01	0.29	0.01
85% PR 15% SG - 0% OFA														
	2.76	0.22	338.1	13.4	84.7	2.2	16.1	0.2	1134.1	6.1	1.52	0.01	0.45	0.02
	3.60	0.17	413.5	12.2	79.4	2.2	15.9	0.2	1080.7	10.4	1.45	0.01	0.55	0.02
	3.59	0.31	406.4	16.3	74.9	2.8	16.1	0.2	1085.4	10.2	1.46	0.01	0.55	0.02
	4.07	0.24	463.5	13.5	87.6	10.1	15.9	0.3	1099.2	17.1	1.48	0.02	0.62	0.02
85% PR 15% SG - 15% OFA														
	2.63	0.10	211.0	7.4	83.2	2.3	16.1	0.2	1090.9	10.6	1.46	0.01	0.28	0.01
	3.52	0.15	269.1	9.7	83.9	2.1	16.0	0.2	1092.3	8.2	1.47	0.01	0.36	0.01
	4.27	0.23	303.2	10.3	81.5	3.5	15.8	0.3	1071.1	12.9	1.44	0.02	0.41	0.01
	4.61	0.08	308.2	6.1	83.5	2.1	15.8	0.2	1063.7	8.1	1.43	0.01	0.41	0.01
85% PR 15% SG - 30% OFA														
	3.58	0.18	172.9	4.2	79.6	2.2	16.1	0.2	1094.3	9.5	1.47	0.01	0.23	0.01
80% PR 20% SG - 0% OFA														
	2.55	0.24	303.6	20.6	65.9	4.2	16.4	0.3	1095.9	11.0	1.47	0.01	0.41	0.03
	3.60	0.28	366.8	17.8	68.0	3.7	16.2	0.3	1085.9	11.9	1.46	0.02	0.49	0.02
80% PR 20% SG - 15% OFA														
	2.75	0.27	217.2	14.6	80.7	5.9	16.3	0.3	1114.6	12.8	1.50	0.02	0.29	0.02
	3.70	0.32	260.3	18.9	85.2	2.4	16.1	0.4	1134.2	15.6	1.52	0.02	0.35	0.03
	4.31	0.27	284.1	12.1	73.8	2.5	16.1	0.4	1073.0	16.6	1.44	0.02	0.38	0.02

Table A-1F. Gas Sampling Data for UBC Measurements from Tests PR-1, PR-1R, PR-2, and PR-10.

Test 1 - Comilling of SG and SD with PR Coal																
Unburned Carbon Data																
Test Condition	FEO, Wet %		NOx, 3% O_2, ppm		% UBC		CO, 3% O_2, ppm		CO_2, 3% O_2, %		SO_2, 3% O_2, ppm		SO_2, lb/10^6Btu		NO_X, lb/10^6Btu	
	Avg.	S.D.	Avg.	S.D.	Avg.	S.D.	Avg.	S.D.	Avg.	S.D.	Avg.	S.D.	Avg.	S.D.	Avg.	S.D.
100% PR - 0% OFA																
	3.63	0.18	403.7	20.1	0.9	0.0	79.6	2.3	15.9	0.2	1143.9	10.1	1.54	0.01	0.54	0.03
100% PR - 15% OFA																
	2.70	0.20	238.2	9.7	1.6	0.1	79.7	2.1	16.0	0.2	1131.0	6.8	1.52	0.01	0.32	0.01
	3.43	0.22	273.4	20.0	1.2	0.0	75.4	4.5	14.7	1.1	1035.8	81.2	1.39	0.11	0.37	0.03
	4.42	0.18	323.1	13.7	0.7	0.0	81.9	2.4	15.5	0.3	1087.9	8.1	1.46	0.01	0.43	0.02
100% PR - 30% OFA																
	3.35	0.29	181.7	14.6	1.7	0.0	83.7	5.0	16.0	1.1	1158.7	23.0	1.56	0.03	0.24	0.02
90% PR 10% SD - 0% OFA																
	4.02	0.14	434.5	12.8	0.6	0.0	83.9	2.5	15.9	0.2	1053.6	6.9	1.41	0.01	0.58	0.02
90% PR 10% SD - 15% OFA																
	2.55	0.14	230.3	7.6	1.6	0.0	83.8	2.5	16.2	0.2	1093.5	10.2	1.47	0.01	0.31	0.01
	3.53	0.18	276.5	19.4	1.3	0.0	85.9	2.2	16.0	0.2	1123.5	6.3	1.51	0.01	0.37	0.03
	4.55	0.11	333.3	13.7	0.7	0.0	86.9	2.7	15.7	0.2	1061.5	6.4	1.42	0.01	0.45	0.02
90% PR 10% SD - 30% OFA																
	3.56	0.18	177.7	16.0	1.3	0.0	92.4	8.0	16.0	0.2	1098.7	16.5	1.47	0.02	0.24	0.02
80% PR 20% SD - 0% OFA																
	3.58	0.17	442.7	9.1	0.3	0.0	77.1	2.4	16.3	0.2	1065.9	8.1	1.43	0.01	0.59	0.01
80% PR 20% SD - 15% OFA																
	2.54	0.11	212.3	4.5	1.7	0.0	82.9	2.3	16.3	0.1	1113.7	5.9	1.50	0.01	0.28	0.01
	3.34	0.10	255.0	8.0	1.1	0.0	92.5	5.4	16.0	0.2	1070.6	29.3	1.44	0.04	0.34	0.01
	4.29	0.15	300.1	8.3	0.7	0.0	82.7	3.1	16.2	0.2	1069.9	8.6	1.44	0.01	0.40	0.01
80% PR 20% SD - 30% OFA																
	3.54	0.23	191.9	5.5	0.6	0.0	66.5	3.1	16.4	0.3	1090.2	11.5	1.46	0.02	0.26	0.01
85% PR 15% SG - 0% OFA																
	3.60	0.28	405.1	16.2	0.5	0.0	75.6	2.5	16.1	0.2	1083.7	10.3	1.45	0.01	0.54	0.02
85% PR 15% SG - 15% OFA																
	2.68	0.15	217.2	15.3	1.7	0.1	83.4	2.5	16.1	0.2	1098.3	11.1	1.47	0.01	0.29	0.02
	3.43	0.11	266.4	13.3	1.2	0.0	83.2	2.2	16.1	0.3	1088.7	10.6	1.46	0.01	0.36	0.02
	4.64	0.09	310.0	8.1	0.6	0.0	83.3	2.1	15.8	0.2	1088.7	41.8	1.46	0.06	0.42	0.01
85% PR 15% SG - 30% OFA																
	3.55	0.15	173.9	4.5	0.6	0.0	80.2	2.2	16.0	0.2	1094.4	8.8	1.47	0.01	0.23	0.01
80% PR 20% SG - 0% OFA																
	3.62	0.30	366.3	19.8	1.2	0.0	67.9	4.1	16.2	0.3	1083.4	12.6	1.45	0.02	0.49	0.03
80% PR 20% SG - 15% OFA																
	2.75	0.29	216.4	14.1	1.8	0.1	80.0	6.5	16.3	0.4	1111.7	12.0	1.49	0.02	0.29	0.02
	3.66	0.28	256.8	16.2	1.6	0.1	84.7	3.0	16.0	0.4	1135.7	16.2	1.52	0.02	0.34	0.02
	4.29	0.24	285.3	12.4	1.1	0.0	73.5	2.7	16.1	0.4	1079.7	12.4	1.45	0.02	0.38	0.02

Table A-2A. Gas Flow Data from Test PR-3.

Test 3 – Axial Injection of SG and SD with PR														
Furnace Flow Data					------- FURNACE AIR FLOWS, SCFM (60°F, 29.92 in. Hg) ------								Fuel Feed	
Test Condition	FEO, Wet %		NOx, 3% O_2, ppm		Total Air		Pri. Air (150°F)		Sec. Air (600°F)		OFA (600°F)		Rate, lb/hr	
	Avg.	S.D.	Avg.	S.D.	Avg.	S.D.	Avg.	S.D.	Avg.	S.D.	Avg.	S.D.	Avg.	S.D.
100% PR - 0% OFA														
	3.03	0.24	488.2	14.7	582.3	4.3	120.6	2.5	461.7	4.3	0.0	0.0	283.1	8.8
	3.53	0.20	471.7	22.9	627.2	3.1	120.1	0.2	507.1	3.1	0.0	0.0	283.8	10.5
	3.78	0.28	485.2	12.7	614.7	4.2	120.7	2.1	494.0	3.8	0.0	0.0	283.3	11.4
	4.67	0.19	522.9	15.8	660.6	4.1	125.4	0.4	535.2	4.0	0.0	0.0	282.8	10.1
100% PR - 15% OFA														
	2.83	0.23	375.2	28.7	603.6	3.5	120.1	2.6	395.0	2.8	88.5	0.2	283.6	10.5
	3.02	0.12	293.6	12.6	639.5	1.7	121.6	0.2	421.9	1.7	96.0	0.1	282.1	11.6
	3.66	0.26	425.3	26.2	647.4	5.1	119.3	2.1	431.6	4.5	96.5	0.8	282.9	10.8
	3.83	0.13	399.5	17.3	650.0	3.2	123.5	0.2	428.9	3.1	97.5	0.2	281.1	16.0
	4.68	0.20	459.7	17.7	689.5	2.9	124.2	0.4	463.3	12.1	102.0	12.5	283.5	9.5
90% PR 10% SG - 0% OFA														
	2.58	0.17	427.6	14.8	582.1	3.5	120.0	0.2	462.1	3.5	0.0	0.0	267.1	10.5
	4.80	0.15	476.1	10.9	679.7	3.6	129.2	0.3	550.5	3.5	0.0	0.0	267.1	10.4
90% PR 10% SG - 15% OFA														
	2.56	0.23	330.1	19.4	597.8	10.9	120.1	0.7	389.0	8.8	88.7	1.5	266.6	10.7
	3.04	0.24	354.9	21.6	621.8	9.0	120.0	0.2	408.8	9.2	93.0	0.2	267.2	10.8
	4.35	0.17	463.5	18.4	679.2	3.6	129.2	0.3	448.0	3.6	102.0	0.2	266.5	10.4
80% PR 20% SG - 0% OFA														
	3.27	0.21	411.2	17.5	589.1	2.6	120.0	0.2	469.1	2.5	0.0	0.0	249.6	10.8
	4.95	0.15	474.4	11.2	669.3	3.3	127.3	0.4	542.1	3.3	0.0	0.0	248.7	10.6
80% PR 20% SG - 15% OFA														
	2.51	0.20	310.3	21.9	598.0	3.1	120.0	0.2	389.6	3.1	88.5	0.1	248.9	10.7
	3.37	0.30	344.4	25.6	639.8	2.6	121.6	0.2	422.2	2.5	96.0	0.1	249.2	10.1
	4.37	0.19	454.4	22.4	679.6	2.9	129.2	0.3	448.4	2.8	102.0	0.1	249.3	10.8
90% PR 10% SD - 0% OFA														
	2.51	0.25	370.2	17.7	589.9	3.0	120.0	0.2	469.9	3.0	0.0	0.0	265.7	10.1
	3.47	0.21	411.3	13.5	629.8	1.8	120.0	0.2	509.8	1.9	0.0	0.0	266.0	10.2
	4.21	0.31	386.8	28.6	670.4	3.0	127.3	0.2	543.0	2.9	0.0	0.0	266.7	9.7
90% PR 10% SD - 15% OFA														
	2.20	0.37	282.0	27.6	592.2	12.8	120.2	1.3	384.6	9.4	87.4	2.2	265.6	10.3
	3.64	0.21	362.4	25.1	650.4	3.6	123.5	0.2	429.4	3.5	97.5	0.2	265.7	10.6
	4.33	0.32	460.1	23.9	690.0	3.3	131.1	0.2	455.3	3.3	103.5	0.2	265.6	10.3
80% PR 20% SD - 0% OFA														
	2.42	0.23	380.6	13.9	577.6	3.3	120.0	0.2	457.6	3.2	0.0	0.0	246.6	10.7
	3.47	0.46	388.8	16.5	617.6	2.2	120.0	0.2	497.6	2.2	0.0	0.0	247.5	10.8
	4.46	0.17	446.3	8.1	681.0	4.1	129.2	0.2	551.8	4.1	0.0	0.0	247.9	10.7
80% PR 20% SD - 15% OFA														
	2.83	0.14	337.0	29.1	607.4	11.9	120.1	1.0	397.2	10.0	90.1	1.2	246.0	10.9
	3.72	0.32	390.5	33.7	650.1	2.7	123.5	0.2	429.0	2.6	97.5	0.2	246.3	10.4
	4.51	0.18	466.7	19.3	681.4	4.5	129.6	0.5	449.6	4.0	102.2	0.6	246.6	11.0

Table A-2B. Gas Flow Data for UBC Measurements from Test PR-3.

Test 3 – Axial Injection of SG and SD with PR																
Unburned Carbon Data							----- FURNACE AIR FLOWS, SCFM (60°F, 29.92 in. Hg) ------								Fuel Feed	
Test Condition	FEO, Wet %		NO_x, 3% O_2, ppm		% UBC		Total Air		Pri. Air (150°F)		Sec. Air (600°F)		OFA (600°F)		Rate, lb/hr	
	Avg.	S.D.	Avg.	S.D.	Avg.	S.D.	Avg.	S.D.	Avg.	S.D.	Avg.	S.D.	Avg.	S.D.	Avg.	S.D.
100% PR - 0% OFA	3.74	0.30	488.6	26.6	0.73	0.02	616.4	7.3	120.9	2.0	495.5	7.2	0.0	0.0	283.3	10.6
	3.03	0.26	503.6	55.5	1.18	0.02	582.6	6.1	120.4	2.5	462.2	6.0	0.0	0.0	282.8	9.3
	4.71	0.17	526.8	14.5	0.22	0.01	660.4	3.6	125.3	0.4	535.1	3.5	0.0	0.0	282.9	10.8
100% PR - 15% OFA	2.83	0.23	371.5	24.3	2.74	0.14	603.9	3.3	120.1	2.6	395.3	2.5	88.5	0.2	283.4	10.8
	3.61	0.24	425.1	30.6	1.81	0.03	645.1	3.1	119.9	2.2	429.1	3.1	96.1	0.2	282.5	10.8
	4.68	0.23	466.0	39.6	0.63	0.01	691.1	10.0	124.2	0.4	463.4	10.0	103.5	0.2	283.1	10.3
PR, 10% SG - 0% OFA	2.62	0.16	420.6	21.5	0.61	0.04	582.4	4.0	120.0	0.2	462.4	4.0	0.0	0.0	267.4	10.9
	3.56	0.15	440.1	12.8	0.56	0.03	615.0	4.4	120.0	0.3	494.2	3.5	0.8	3.3	267.7	11.2
	4.78	0.18	471.7	15.9	0.22	0.01	680.1	4.0	129.2	0.3	550.9	3.9	0.0	0.0	267.3	10.7
PR, 10% SG - 15% OFA	2.74	0.48	341.7	69.3	1.45	0.04	600.6	16.0	120.0	0.2	392.1	16.1	88.5	0.6	267.4	11.2
	3.21	0.47	382.6	65.0	1.11	0.04	628.5	23.6	120.0	0.3	415.4	23.5	93.1	0.6	267.2	10.9
	4.44	0.48	496.3	79.3	0.50	0.01	687.0	27.4	129.2	0.5	455.8	27.7	102.0	1.0	267.0	10.6
PR, 20% SG - 0% OFA	3.25	0.24	407.1	22.7	0.52	0.01	589.0	3.0	120.0	0.2	469.0	2.9	0.0	0.0	249.4	11.1
	4.07	0.26	502.4	18.8	0.35	0.02	640.2	3.7	121.6	0.2	518.5	3.7	0.0	0.0	248.8	11.0
	4.96	0.15	467.0	17.2	0.27	0.02	669.6	3.2	127.2	0.4	542.4	3.1	0.0	0.0	249.2	10.8
PR, 20% SG - 15% OFA	2.47	0.20	307.5	22.8	1.39	0.11	598.1	2.9	120.0	0.2	389.5	2.8	88.5	0.1	248.3	10.9
	3.47	0.45	367.0	64.3	0.89	0.03	639.9	3.2	121.6	0.2	422.4	3.2	96.0	0.1	249.0	10.3
	4.35	0.22	452.6	23.7	0.51	0.06	679.6	2.4	129.2	0.3	448.4	2.3	102.0	0.1	249.9	10.7
PR, 10% SD - 0% OFA	2.50	0.25	370.3	18.8	0.75	0.05	589.6	2.4	120.1	0.2	469.5	2.4	0.0	0.0	265.4	9.8
	3.49	0.22	425.5	54.0	0.46	0.01	629.9	2.6	120.0	0.2	509.8	2.6	0.0	0.0	266.1	10.2
	4.22	0.33	385.6	28.8	0.39	0.00	670.5	3.1	127.3	0.2	543.2	3.1	0.0	0.0	266.4	9.5
PR, 10% SD - 15% OFA	2.20	0.43	284.2	35.6	2.02	0.35	589.8	2.5	120.0	0.2	382.8	2.5	86.9	0.2	265.2	11.0
	3.70	0.53	368.4	36.6	0.83	0.02	649.9	4.4	123.5	0.2	428.9	4.2	97.5	0.3	266.4	9.7
	4.30	0.40	460.1	23.7	0.57	0.04	690.0	3.3	131.1	0.2	455.3	3.3	103.5	0.2	265.6	10.3
PR, 20% SD - 0% OFA	2.49	0.37	381.7	21.5	1.02	0.02	577.6	3.1	120.0	0.2	457.6	3.0	0.0	0.0	247.3	10.5
	3.50	0.49	394.8	28.5	0.67	0.01	617.4	1.9	120.0	0.2	497.4	1.9	0.0	0.0	246.8	10.8
	4.53	0.41	451.4	22.6	0.35	0.03	680.8	3.9	129.2	0.2	551.6	3.8	0.0	0.0	247.6	10.5
PR, 20% SD - 15% OFA	3.02	0.31	339.7	39.1	1.02	0.07	607.8	9.9	120.0	0.2	397.8	9.9	90.0	0.3	246.3	10.7
	3.75	0.29	383.7	29.8	0.70	0.02	650.4	3.4	123.5	0.2	429.4	3.3	97.5	0.2	246.5	10.4
	4.56	0.22	461.3	33.0	0.40	0.01	679.8	2.9	129.2	0.3	448.7	2.9	102.0	0.3	247.4	10.7

Table A-2C. Gas Sampling Data from Test PR-3.

Test 3 – Axial Injection of SG and SD with PR Coal																
Unburned Carbon Data																
Test Condition	FEO, Wet %		NO_x, 3% O_2, ppm		% UBC		CO, 3% O_2, ppm		CO_2, 3% O_2, %		SO_2, 3% O_2, ppm		SO_2, lb/10^6Btu		NO_x, lb/10^6Btu	
	Avg.	S.D.	Avg.	S.D.	Avg.	S.D.	Avg.	S.D.	Avg.	S.D.	Avg.	S.D.	Avg.	S.D.	Avg.	S.D.
100% PR Coal - 0% OFA																
	3.74	0.30	488.6	26.6	0.73	0.02	79.3	2.4	15.9	0.2	1133.0	9.2	1.53	0.01	0.66	0.04
	3.03	0.26	503.6	55.5	1.18	0.02	77.1	2.2	16.2	0.2	1142.9	108.8	1.54	0.15	0.68	0.07
	4.71	0.17	526.8	14.5	0.22	0.01	74.5	2.1	16.0	0.2	1130.1	6.5	1.52	0.01	0.71	0.02
100% PR Coal - 15% OFA																
	2.83	0.23	371.5	24.3	2.74	0.14	89.9	2.5	16.1	0.2	1168.5	9.6	1.57	0.01	0.50	0.03
	3.61	0.24	425.1	30.6	1.81	0.03	86.5	2.6	16.1	0.2	1135.4	9.7	1.53	0.01	0.57	0.04
	4.68	0.23	466.0	39.6	0.63	0.01	78.5	3.3	15.9	0.2	1129.6	9.4	1.52	0.01	0.63	0.05
90% PR 10% SG 0% OFA																
	2.62	0.16	420.6	21.5	0.61	0.04	75.6	1.9	16.3	0.2	1155.7	7.9	1.56	0.01	0.57	0.03
	3.56	0.15	440.1	12.8	0.56	0.03	80.4	3.5	16.3	0.2	1140.2	10.3	1.54	0.01	0.59	0.02
	4.78	0.18	471.7	15.9	0.22	0.01	78.2	2.5	15.9	0.3	1112.3	8.4	1.50	0.01	0.64	0.02
90% PR 10% SG 15% OFA																
	2.74	0.48	341.7	69.3	1.45	0.04	86.5	2.7	16.3	0.3	1156.4	11.4	1.56	0.02	0.46	0.09
	3.21	0.47	382.6	65.0	1.11	0.04	85.0	2.5	16.3	0.4	1146.9	15.4	1.55	0.02	0.52	0.09
	4.44	0.48	496.3	79.3	0.50	0.01	80.0	3.0	16.0	0.3	1124.7	18.4	1.52	0.02	0.67	0.11
80% PR 20% SG 0% OFA																
	3.25	0.24	407.1	22.7	0.52	0.01	75.2	2.2	16.4	0.4	1105.4	12.5	1.49	0.02	0.55	0.03
	4.07	0.26	502.4	18.8	0.35	0.02	75.6	2.3	16.5	0.3	1053.8	13.1	1.42	0.02	0.68	0.03
	4.96	0.15	467.0	17.2	0.27	0.02	76.5	2.5	16.2	0.3	1070.0	12.4	1.44	0.02	0.63	0.02
80% PR 20% SG 15% OFA																
	2.47	0.20	307.5	22.8	1.39	0.11	77.7	2.0	16.8	0.2	1071.6	12.0	1.44	0.02	0.41	0.03
	3.47	0.45	367.0	64.3	0.89	0.03	77.8	7.8	16.6	0.6	994.8	211.0	1.34	0.28	0.49	0.09
	4.35	0.22	452.6	23.7	0.51	0.06	78.1	2.2	16.5	0.4	1051.2	9.9	1.42	0.01	0.61	0.03
90% PR 10% SD 0% OFA																
	2.50	0.25	370.3	18.8	0.75	0.05	72.2	2.0	16.5	0.2	-----	-----	-----	-----	0.50	0.03
	3.49	0.22	425.5	54.0	0.46	0.01	72.9	6.6	16.3	0.4	-----	-----	-----	-----	0.57	0.07
	4.22	0.33	385.6	28.8	0.39	0.00	74.1	2.4	16.2	0.3	-----	-----	-----	-----	0.52	0.04
90% PR 10% SD 15% OFA																
	2.20	0.43	284.2	35.6	2.02	0.35	80.8	2.9	16.5	0.3	1129.9	17.5	1.52	0.02	0.38	0.05
	3.70	0.53	368.4	36.6	0.83	0.02	78.2	2.6	16.4	0.3	1102.0	19.2	1.48	0.03	0.50	0.05
	4.30	0.40	460.1	23.7	0.57	0.04	77.1	2.3	16.2	0.2	1093.8	10.8	1.47	0.01	0.62	0.03
80% PR 20% SD 0% OFA																
	2.49	0.37	381.7	21.5	1.02	0.02	81.4	2.2	16.4	0.4	1046.0	17.1	1.41	0.02	0.51	0.03
	3.50	0.49	394.8	28.5	0.67	0.01	82.1	2.5	16.3	0.5	1050.9	24.9	1.42	0.03	0.53	0.04
	4.53	0.41	451.4	22.6	0.35	0.03	84.6	2.7	16.1	0.5	996.0	23.9	1.34	0.03	0.61	0.03
80% PR 20% SD 15% OFA																
	3.02	0.31	339.7	39.1	1.02	0.07	77.7	3.2	16.4	0.3	1056.9	11.1	1.42	0.01	0.46	0.05
	3.75	0.29	383.7	29.8	0.70	0.02	77.5	2.4	16.4	0.4	1027.8	18.9	1.38	0.03	0.52	0.04
	4.56	0.22	461.3	33.0	0.40	0.01	79.3	2.2	16	0	1029.8	21.7	1.39	0.03	0.62	0.04

Table A-2D. Gas Sampling Data for UBC Measurements from Test PR-3.

Test 3 – Axial Injection of SG and SD with PR Coal																
Unburned Carbon Data																
Test Condition	FEO, Wet %		NO_x, 3% O_2, ppm		% UBC		CO, 3% O_2, ppm		CO_2, 3% O_2, %		SO_2, 3% O_2, ppm		SO_2, lb/10^6Btu		NO_x, lb/10^6Btu	
	Avg.	S.D.	Avg.	S.D.	Avg.	S.D.	Avg.	S.D.	Avg.	S.D.	Avg.	S.D.	Avg.	S.D.	Avg.	S.D.
100% PR Coal - 0% OFA																
	3.74	0.30	488.6	26.6	0.73	0.02	79.3	2.4	15.9	0.2	1133.0	9.2	1.53	0.01	0.66	0.04
	3.03	0.26	503.6	55.5	1.18	0.02	77.1	2.2	16.2	0.2	1142.9	108.8	1.54	0.15	0.68	0.07
	4.71	0.17	526.8	14.5	0.22	0.01	74.5	2.1	16.0	0.2	1130.1	6.5	1.52	0.01	0.71	0.02
100% PR Coal - 15% OFA																
	2.83	0.23	371.5	24.3	2.74	0.14	89.9	2.5	16.1	0.2	1168.5	9.6	1.57	0.01	0.50	0.03
	3.61	0.24	425.1	30.6	1.81	0.03	86.5	2.6	16.1	0.2	1135.4	9.7	1.53	0.01	0.57	0.04
	4.68	0.23	466.0	39.6	0.63	0.01	78.5	3.3	15.9	0.2	1129.6	9.4	1.52	0.01	0.63	0.05
90% PR 10% SG 0% OFA																
	2.62	0.16	420.6	21.5	0.61	0.04	75.6	1.9	16.3	0.2	1155.7	7.9	1.56	0.01	0.57	0.03
	3.56	0.15	440.1	12.8	0.56	0.03	80.4	3.5	16.3	0.2	1140.2	10.3	1.54	0.01	0.59	0.02
	4.78	0.18	471.7	15.9	0.22	0.01	78.2	2.5	15.9	0.3	1112.3	8.4	1.50	0.01	0.64	0.02
90% PR 10% SG 15% OFA																
	2.74	0.48	341.7	69.3	1.45	0.04	86.5	2.7	16.3	0.3	1156.4	11.4	1.56	0.02	0.46	0.09
	3.21	0.47	382.6	65.0	1.11	0.04	85.0	2.5	16.3	0.4	1146.9	15.4	1.55	0.02	0.52	0.09
	4.44	0.48	496.3	79.3	0.50	0.01	80.0	3.0	16.0	0.3	1124.7	18.4	1.52	0.02	0.67	0.11
80% PR 20% SG 0% OFA																
	3.25	0.24	407.1	22.7	0.52	0.01	75.2	2.2	16.4	0.4	1105.4	12.5	1.49	0.02	0.55	0.03
	4.07	0.26	502.4	18.8	0.35	0.02	75.6	2.3	16.5	0.3	1053.8	13.1	1.42	0.02	0.68	0.03
	4.96	0.15	467.0	17.2	0.27	0.02	76.5	2.5	16.2	0.3	1070.0	12.4	1.44	0.02	0.63	0.02
80% PR 20% SG 15% OFA																
	2.47	0.20	307.5	22.8	1.39	0.11	77.7	2.0	16.8	0.2	1071.6	12.0	1.44	0.02	0.41	0.03
	3.47	0.45	367.0	64.3	0.89	0.03	77.8	7.8	16.6	0.6	994.8	211.0	1.34	0.28	0.49	0.09
	4.35	0.22	452.6	23.7	0.51	0.06	78.1	2.2	16.5	0.4	1051.2	9.9	1.42	0.01	0.61	0.03
90% PR 10% SD 0% OFA																
	2.50	0.25	370.3	18.8	0.75	0.05	72.2	2.0	16.5	0.2	-----	-----	-----	-----	0.50	0.03
	3.49	0.22	425.5	54.0	0.46	0.01	72.9	6.6	16.3	0.4	-----	-----	-----	-----	0.57	0.07
	4.22	0.33	385.6	28.8	0.39	0.00	74.1	2.4	16.2	0.3	-----	-----	-----	-----	0.52	0.04
90% PR 10% SD 15% OFA																
	2.20	0.43	284.2	35.6	2.02	0.35	80.8	2.9	16.5	0.3	1129.9	17.5	1.52	0.02	0.38	0.05
	3.70	0.53	368.4	36.6	0.83	0.02	78.2	2.6	16.4	0.3	1102.0	19.2	1.48	0.03	0.50	0.05
	4.30	0.40	460.1	23.7	0.57	0.04	77.1	2.3	16.2	0.2	1093.8	10.8	1.47	0.01	0.62	0.03
80% PR 20% SD 0% OFA																
	2.49	0.37	381.7	21.5	1.02	0.02	81.4	2.2	16.4	0.4	1046.0	17.1	1.41	0.02	0.51	0.03
	3.50	0.49	394.8	28.5	0.67	0.01	82.1	2.5	16.3	0.5	1050.9	24.9	1.42	0.03	0.53	0.04
	4.53	0.41	451.4	22.6	0.35	0.03	84.6	2.7	16.1	0.5	996.0	23.9	1.34	0.03	0.61	0.03
80% PR 20% SD 15% OFA																
	3.02	0.31	339.7	39.1	1.02	0.07	77.7	3.2	16.4	0.3	1056.9	11.1	1.42	0.01	0.46	0.05
	3.75	0.29	383.7	29.8	0.70	0.02	77.5	2.4	16.4	0.4	1027.8	18.9	1.38	0.03	0.52	0.04
	4.56	0.22	461.3	33.0	0.40	0.01	79.3	2.2	16	0	1029.8	21.7	1.39	0.03	0.62	0.04

Table A-3A. Gas Flow Data from Test PR-4.

Test 4 – Co-Injection of PR Coal with SD and Switchgrass into Burner														
Furnace Flow Data					------- FURNACE AIR FLOWS, SCFM (60°F, 29.92 in. Hg) ------								Fuel Feed	
Test Condition	FEO, Wet %		NOx, 3% O_2, ppm		Total Air		Pri. Air (150°F)		Sec. Air (600°F)		OFA (600°F)		Rate, lb/hr	
	Avg.	S.D.	Avg.	S.D.	Avg.	S.D.	Avg.	S.D.	Avg.	S.D.	Avg.	S.D.	Avg.	S.D.
SIDE-100% PR-0% OFA														
	2.67	0.15	407.7	16.0	640.1	3.0	121.6	0.2	518.4	2.9	0.0	0.0	307.1	8.8
	2.76	0.32	413.7	22.3	640.0	3.0	121.6	0.2	518.4	3.0	0.0	0.0	307.1	8.8
	3.52	0.13	430.2	14.3	679.5	5.1	129.1	1.0	550.5	4.3	0.0	0.0	306.6	10.3
	3.65	0.37	431.2	18.7	680.1	2.5	129.2	0.2	550.9	2.4	0.0	0.0	306.1	10.0
	4.39	0.17	488.4	16.3	720.0	2.6	136.8	0.2	583.2	2.6	0.0	0.0	306.7	10.0
SIDE-100% PR-15% OFA														
	2.83	0.13	256.4	13.2	660.0	2.1	125.4	0.2	435.6	2.0	99.0	0.2	306.9	10.1
	3.63	0.13	306.4	11.8	699.8	2.0	133.0	0.3	461.8	1.8	105.0	0.2	306.8	9.5
	3.73	0.25	307.5	21.3	700.0	2.2	133.0	0.2	461.9	1.9	105.0	0.2	307.1	9.2
	4.55	0.12	334.7	15.4	739.5	2.0	140.6	0.3	487.9	1.8	111.0	0.2	307.6	10.6
	4.63	0.23	336.2	20.0	739.8	1.5	140.6	0.3	488.2	1.3	111.0	0.2	307.4	11.0
SIDE-90% PR-10%SG-0%OFA														
	2.57	0.22	370.7	10.6	640.0	1.6	121.6	0.2	518.4	1.6	0.0	0.0	287.1	9.9
	3.46	0.26	484.9	14.0	679.7	2.1	129.2	0.2	550.5	2.1	0.0	0.0	287.4	10.3
	3.44	0.19	488.8	17.6	680.2	2.4	129.2	0.2	551.0	2.3	0.0	0.0	286.8	10.3
	4.22	0.19	453.8	18.7	720.0	2.5	136.8	0.3	583.2	2.4	0.0	0.0	286.1	10.6
SIDE-90% PR-10%SG-15%OFA														
	2.73	0.18	329.9	19.6	659.7	2.0	125.4	0.2	435.3	1.8	99.0	0.2	286.9	10.4
	3.67	0.37	370.9	32.4	700.4	2.7	133.0	0.3	462.4	2.5	105.0	0.2	286.8	11.4
	3.63	0.20	361.6	22.6	700.3	2.5	133.0	0.2	462.2	2.3	105.0	0.2	286.7	11.3
	4.59	0.24	475.9	21.8	740.0	2.3	140.6	0.3	488.4	2.0	111.0	0.3	286.8	9.5
SIDE-80% PR-20%SG-0%OFA														
	2.95	0.23	346.1	15.7	622.0	3.0	120.0	0.2	502.0	2.9	0.0	0.0	264.6	10.3
	3.96	0.34	380.5	29.2	659.9	2.4	125.4	0.2	534.5	2.3	0.0	0.0	264.2	10.0
	3.87	0.16	396.9	13.5	659.7	2.5	125.4	0.2	534.3	2.5	0.0	0.0	264.3	9.9
	4.64	0.15	460.1	10.4	700.2	2.5	133.0	0.3	567.2	2.4	0.0	0.0	265.5	8.7
SIDE-80% PR-20%SG-15%OFA														
	2.91	0.25	267.3	24.3	639.8	1.6	121.6	0.2	422.2	1.4	96.0	0.1	263.5	10.3
	3.10	0.42	274.8	32.0	640.0	1.5	121.6	0.2	422.4	1.3	96.0	0.1	263.4	10.4
	3.53	0.22	357.8	27.5	679.8	2.0	129.2	0.3	448.6	1.8	102.0	0.2	264.4	9.7
	4.63	0.16	351.2	17.4	710.4	2.3	134.9	0.2	468.9	2.1	106.5	0.2	264.0	10.1
SIDE-90% PR-10% SD-0%OFA														
	2.67	0.20	337.8	13.2	630.6	2.2	120.0	0.2	510.6	2.1	0.0	0.0	287.2	9.8
	3.46	0.19	373.2	14.0	670.3	1.7	127.3	0.2	543.0	1.6	0.0	0.0	287.4	9.7
	4.33	0.16	480.2	15.8	719.8	3.2	136.8	0.3	583.0	3.1	0.0	0.0	286.7	10.5
	4.38	0.14	435.0	13.2	719.8	1.8	136.8	0.4	583.0	1.6	0.0	0.0	287.0	9.7
	4.52	0.37	445.4	20.9	719.8	1.6	136.9	0.3	583.0	1.4	0.0	0.0	286.9	9.6
SIDE-90% PR-10% SD-15%OFA														
	2.38	0.25	214.0	7.9	639.9	1.9	121.6	0.2	422.4	1.8	96.0	0.1	287.3	10.3
	3.48	0.18	299.4	16.7	690.3	2.1	131.1	0.2	455.7	1.9	103.5	0.3	287.5	10.0
	3.57	0.32	287.2	16.6	690.0	2.5	131.1	0.3	455.4	2.3	103.5	0.2	287.1	10.4
	4.72	0.10	297.3	11.9	740.2	2.3	140.6	0.3	488.6	2.0	111.0	0.2	287.6	10.7
	4.81	0.20	298.6	19.8	740.0	2.0	140.6	0.3	488.4	1.8	111.0	0.2	287.2	10.9
SIDE-80% PR-20% SD-0%OFA														
	3.11	0.36	404.4	18.3	634.7	2.1	120.7	0.3	514.0	2.0	0.0	0.0	262.1	31.4
	3.99	0.29	447.1	14.7	679.9	2.1	129.2	0.2	550.7	2.0	0.0	0.0	265.4	10.3
	4.19	0.51	454.0	15.0	680.1	2.0	129.2	0.2	550.9	1.9	0.0	0.0	265.9	9.8
SIDE-80% PR-20% SD-15%OFA														
	2.75	0.24	211.7	12.3	630.2	2.3	120.0	0.2	415.7	2.2	94.5	0.2	266.1	9.8
	3.80	0.19	301.8	14.6	700.0	2.4	133.0	0.3	462.0	2.2	105.0	0.2	266.2	10.1
	4.23	0.45	292.7	40.8	700.4	2.2	133.0	0.3	462.4	2.1	105.0	0.2	266.6	9.2
	4.19	0.33	251.6	14.4	699.9	2.4	133.0	0.3	461.9	2.1	105.0	0.2	265.6	11.5
	4.75	0.25	351.2	46.7	730.1	2.4	138.7	0.3	481.9	2.3	109.5	0.2	265.9	9.5
	4.78	0.21	390.6	24.2	730.2	2.7	138.7	0.3	482.0	2.4	109.5	0.2	265.6	9.9

Table A-3B. Gas Flow Data for UBC Measurements from Test PR-4.

Test 4 – Co-Injection of PR Coal with SD and Switchgrass into Burner																
Unburned Carbon Data							----- FURNACE AIR FLOWS, SCFM (60°F, 29.92 in. Hg) ------								Fuel Feed	
Test Condition	FEO, Wet %		NOx, 3% O_2, ppm		% UBC		Total Air		Pri. Air (150°F)		Sec. Air (600°F)		OFA (600°F)		Rate, lb/hr	
	Avg.	S.D.	Avg.	S.D.	Avg.	S.D.	Avg.	S.D.	Avg.	S.D.	Avg.	S.D.	Avg.	S.D.	Avg.	S.D.
SIDE-100% PR-0% OFA	2.76	0.32	413.7	22.3	1.41	0.02	640.0	3.0	121.6	0.2	518.4	3.0	0.0	0.0	307.1	8.8
	3.65	0.37	431.2	18.7	0.80	0.01	680.1	2.5	129.2	0.2	550.9	2.4	0.0	0.0	306.1	10.0
	4.55	0.42	492.1	22.9	0.27	0.01	720.0	2.3	136.8	0.2	583.2	2.3	0.0	0.0	306.3	10.3
SIDE-100% PR-15% OFA	2.92	0.23	260.2	21.2	1.23	0.03	660.5	2.5	125.4	0.2	436.0	2.4	99.0	0.2	306.6	10.5
	3.73	0.25	307.5	21.3	0.85	0.04	700.0	2.2	133.0	0.2	461.9	1.9	105.0	0.2	307.1	9.2
	4.63	0.23	336.2	20.0	0.55	0.01	739.8	1.5	140.6	0.3	488.2	1.3	111.0	0.2	307.4	11.0
SIDE-90% PR-10%SG-0%OFA	2.65	0.31	380.5	25.5	1.17	0.05	639.5	1.7	121.6	0.1	517.9	1.7	0.0	0.0	287.0	10.2
	3.46	0.26	484.9	14.0	0.41	0.01	679.7	2.1	129.2	0.2	550.5	2.1	0.0	0.0	287.4	10.3
	4.36	0.43	455.3	24.1	0.33	0.02	719.8	2.6	136.8	0.3	583.1	2.5	0.0	0.0	285.9	10.7
SIDE-90% PR-10%SG-15%OFA	2.75	0.25	330.7	24.5	1.26	0.01	659.7	2.1	125.4	0.2	435.3	1.9	99.0	0.3	287.1	10.5
	3.67	0.37	370.9	32.4	0.78	0.04	700.4	2.7	133.0	0.3	462.4	2.5	105.0	0.2	286.8	11.4
	4.67	0.28	477.9	25.8	0.45	0.02	739.9	2.2	140.6	0.3	488.3	1.9	111.0	0.3	286.7	9.7
SIDE-80% PR-20%SG-0%OFA	3.01	0.31	351.3	16.3	0.80	0.02	621.8	1.9	120.0	0.2	501.9	1.9	0.0	0.0	264.9	10.4
	3.96	0.34	380.5	29.2	0.43	0.01	659.9	2.4	125.4	0.2	534.5	2.3	0.0	0.0	264.2	10.0
	4.71	0.31	461.5	12.7	0.30	0.00	700.1	2.5	133.0	0.3	567.2	2.4	0.0	0.0	265.6	8.7
SIDE-80% PR-20%SG-15%OFA	3.10	0.42	274.8	32.0	0.88	0.01	640.0	1.5	121.6	0.2	422.4	1.3	96.0	0.1	263.4	10.4
	3.72	0.58	365.3	36.6	0.78	0.01	679.7	1.9	129.2	0.2	448.6	1.7	102.0	0.2	264.2	10.3
	4.75	0.37	356.6	26.8	0.45	0.01	710.4	2.3	134.9	0.2	469.0	2.2	106.5	0.2	263.9	10.2
SIDE-90% PR-10% SD-0%OFA	2.75	0.29	341.4	15.9	1.04	0.04	630.5	2.5	120.0	0.2	510.5	2.4	0.0	0.0	287.5	9.6
	3.57	0.38	376.6	16.4	0.68	0.02	670.2	1.7	127.3	0.3	542.9	1.6	0.0	0.0	286.9	9.9
	4.52	0.37	445.4	20.9	0.26	0.01	719.8	1.6	136.9	0.3	583.0	1.4	0.0	0.0	286.9	9.6
SIDE-90% PR-10% SD-15%OFA	2.42	0.29	215.3	8.5	2.10	0.05	640.3	2.0	121.6	0.2	422.7	1.9	96.0	0.1	287.0	10.7
	3.72	0.40	293.5	25.2	1.06	0.03	690.1	2.3	131.1	0.3	455.4	2.0	103.5	0.3	287.0	10.0
	4.81	0.20	298.6	19.8	0.69	0.01	740.0	2.0	140.6	0.3	488.4	1.8	111.0	0.2	287.2	10.9
SIDE-80% PR-20% SD-0%OFA	4.19	0.51	454.0	15.0	0.20	0.01	680.1	2.0	129.2	0.2	550.9	1.9	0.0	0.0	265.9	9.8
SIDE-80% PR-20% SD-15%OFA	2.83	0.23	212.3	7.4	1.39	0.06	630.0	1.7	120.0	0.2	415.5	1.7	94.5	0.2	266.0	10.0
	4.23	0.45	292.7	40.8	0.64	0.01	700.4	2.2	133.0	0.3	462.4	2.1	105.0	0.2	266.6	9.2
	4.75	0.25	351.2	46.7	0.45	0.02	730.1	2.4	138.7	0.3	481.9	2.3	109.5	0.2	265.9	9.5

Table A-3C. Gas Sampling Data from Test PR-4.

Test 4 – Co-Injection of PR Coal with SD and SG into Burner														
Gas Sampling Data														
Test Condition	FEO, Wet %		NO_x, 3% O_2, ppm		CO, 3% O_2, ppm		CO_2, 3% O_2, %		SO_2, 3% O_2, ppm		SO_2, lb/10^6Btu		NO_x, lb/10^6Btu	
	Avg.	S.D.	Avg.	S.D.	Avg.	S.D.	Avg.	S.D.	Avg.	S.D.	Avg.	S.D.	Avg.	S.D.
SIDE-100% PR-0% OFA														
	2.67	0.15	407.7	16.0	88.2	2.1	16.1	0.2	1187.9	18.5	1.61	0.03	0.56	0.03
	2.76	0.32	413.7	22.3	88.2	2.2	16.1	0.3	1188.2	18.9	1.61	0.03	0.56	0.03
	3.52	0.13	430.2	14.3	89.6	2.3	15.9	0.3	1178.0	16.4	1.59	0.02	0.59	0.02
	3.65	0.37	431.2	18.7	89.3	2.2	15.9	0.3	1177.8	17.0	1.59	0.02	0.58	0.03
	4.39	0.17	488.4	16.3	91.1	2.5	15.8	0.4	1111.4	23.7	1.50	0.03	0.67	0.03
SIDE-100% PR-15% OFA														
	2.83	0.13	256.4	13.2	105.4	2.0	16.1	0.3	1203.1	12.9	1.63	0.02	0.35	0.02
	3.63	0.13	306.4	11.8	108.2	2.6	16.0	0.3	1164.9	19.2	1.57	0.03	0.42	0.03
	3.73	0.25	307.5	21.3	108.2	2.3	16.1	0.3	1166.2	16.2	1.58	0.02	0.42	0.03
	4.55	0.12	334.7	15.4	109.8	2.1	15.8	0.3	1175.4	16.9	1.59	0.02	0.46	0.03
	4.63	0.23	336.2	20.0	109.8	2.1	15.8	0.3	1175.2	15.6	1.59	0.02	0.45	0.03
SIDE-90% PR-10%SG-0%OFA														
	2.57	0.22	370.7	10.6	99.1	2.6	16.2	0.2	1109.3	10.6	1.50	0.01	0.51	0.02
	3.46	0.26	484.9	14.0	98.1	2.4	16.1	0.3	1102.7	11.9	1.49	0.02	0.66	0.02
	3.44	0.19	488.8	17.6	98.0	2.3	16.1	0.3	1103.2	13.1	1.49	0.02	0.66	0.03
	4.22	0.19	453.8	18.7	103.7	2.6	15.9	0.3	1065.3	14.4	1.44	0.02	0.62	0.03
SIDE-90% PR-10%SG-15%OFA														
	2.73	0.18	329.9	19.6	94.8	2.4	16.3	0.2	1133.7	12.4	1.53	0.02	0.45	0.03
	3.67	0.37	370.9	32.4	95.7	2.8	16.1	0.3	1136.6	12.2	1.54	0.02	0.50	0.04
	3.63	0.20	361.6	22.6	95.1	2.7	16.1	0.3	1133.5	13.1	1.53	0.02	0.49	0.04
	4.59	0.24	475.9	21.8	98.9	3.1	15.9	0.3	1108.7	15.1	1.50	0.02	0.65	0.04
SIDE-80% PR-20%SG-0%OFA														
	2.95	0.23	346.1	15.7	106.0	2.9	16.1	0.3	1030.0	13.1	1.39	0.02	0.47	0.02
	3.96	0.34	380.5	29.2	102.9	3.5	16.0	0.3	1022.0	14.5	1.38	0.02	0.51	0.04
	3.87	0.16	396.9	13.5	100.4	3.3	16.0	0.4	1036.0	23.7	1.40	0.03	0.54	0.02
	4.64	0.15	460.1	10.4	101.7	2.8	15.9	0.2	1010.6	15.6	1.37	0.02	0.62	0.02
SIDE-80% PR-20%SG-15%OFA														
	2.91	0.25	267.3	24.3	96.4	3.4	16.3	0.3	1066.3	15.9	1.44	0.02	0.37	0.04
	3.10	0.42	274.8	32.0	96.4	4.1	16.3	0.4	1064.0	17.9	1.44	0.02	0.37	0.04
	3.53	0.22	357.8	27.5	98.7	4.5	16.3	0.4	1049.7	29.5	1.42	0.04	0.49	0.05
	4.63	0.16	351.2	17.4	97.8	2.4	16.1	0.3	1044.3	14.8	1.41	0.02	0.48	0.03
SIDE-90% PR-10% SD-0%OFA														
	2.67	0.20	337.8	13.2	93.9	2.4	16.1	0.2	1124.7	13.3	1.52	0.02	0.46	0.02
	3.46	0.19	373.2	14.0	93.6	2.0	16.0	0.3	1109.4	12.7	1.50	0.02	0.51	0.02
	4.33	0.16	480.2	15.8	95.5	3.2	15.8	0.4	1098.2	16.5	1.48	0.02	0.65	0.02
	4.38	0.14	435.0	13.2	94.3	2.6	15.8	0.4	1100.8	14.5	1.49	0.02	0.59	0.02
	4.52	0.37	445.4	20.9	94.7	2.6	15.9	0.3	1098.9	15.6	1.49	0.02	0.60	0.03
SIDE-90% PR-10% SD-15%OFA														
	2.38	0.25	214.0	7.9	104.6	2.3	16.2	0.2	1121.1	14.1	1.52	0.02	0.29	0.01
	3.48	0.18	299.4	16.7	102.0	3.0	16.1	0.3	1098.5	13.3	1.48	0.02	0.41	0.03
	3.57	0.32	287.2	16.6	107.1	2.7	16.0	0.3	1103.3	15.0	1.49	0.02	0.39	0.03
	4.72	0.10	297.3	11.9	110.1	2.4	15.8	0.3	1085.1	11.5	1.47	0.02	0.41	0.03
	4.81	0.20	298.6	19.8	110.3	2.4	15.8	0.3	1083.6	13.5	1.46	0.02	0.40	0.03
SIDE-80% PR-20% SD-0%OFA														
	3.11	0.36	404.4	18.3	99.0	6.4	16.3	0.5	1001.8	72.2	1.35	0.10	0.55	0.04
	3.99	0.29	447.1	14.7	120.3	5.4	16.0	0.4	1005.6	18.1	1.36	0.02	0.61	0.02
	4.19	0.51	454.0	15.0	123.3	3.3	16.1	0.4	1013.6	17.2	1.37	0.02	0.61	0.02
SIDE-80% PR-20% SD-15%OFA														
	2.75	0.24	211.7	12.3	100.5	2.4	16.5	0.4	1027.5	25.9	1.39	0.03	0.29	0.02
	3.80	0.19	301.8	14.6	107.7	3.2	16.1	0.4	998.6	17.0	1.35	0.02	0.41	0.03
	4.23	0.45	292.7	40.8	105.3	3.1	16.1	0.5	1007.5	27.4	1.36	0.04	0.40	0.06
	4.19	0.33	251.6	14.4	103.8	2.6	16.0	0.5	1010.6	24.9	1.37	0.03	0.35	0.03
	4.75	0.25	351.2	46.7	103.1	2.9	16.1	0.5	976.6	17.7	1.32	0.02	0.47	0.06
	4.78	0.21	390.6	24.2	103.3	2.3	16.1	0.4	975.0	15.3	1.32	0.02	0.53	0.03

Table A-3D. Gas Sampling Data for UBC Measurements from Test PR-4.

Test 4 - Co-Injection of PR Coal with SD and SG into Burner																
Unburned Carbon Data																
Test Condition	FEO, Wet %		NOx, 3% O_2, ppm		% UBC		CO, 3% O_2, ppm		CO_2, 3% O_2, %		SO_2, 3% O_2, ppm		SO_2, lb/10^6Btu		NO_x, lb/10^6Btu	
	Avg.	S.D.	Avg.	S.D.	Avg.	S.D.	Avg.	S.D.	Avg.	S.D.	Avg.	S.D.	Avg.	S.D.	Avg.	S.D.
SIDE-100% PR-0% OFA																
	2.76	0.32	413.7	22.3	1.41	0.02	88.2	2.2	16.1	0.3	1188.2	18.9	1.61	0.03	0.56	0.03
	3.65	0.37	431.2	18.7	0.80	0.01	89.3	2.2	15.9	0.3	1177.8	17.0	1.59	0.02	0.58	0.03
	4.55	0.42	492.1	22.9	0.27	0.01	91.6	2.7	15.8	0.4	1107.0	19.2	1.50	0.03	0.67	0.03
SIDE-100% PR-15% OFA																
	2.92	0.23	260.2	21.2	1.23	0.03	104.7	2.1	16.1	0.3	1205.2	13.2	1.63	0.02	0.35	0.03
	3.73	0.25	307.5	21.3	0.85	0.04	108.2	2.3	16.1	0.3	1166.2	16.2	1.58	0.02	0.42	0.03
	4.63	0.23	336.2	20.0	0.55	0.01	109.8	2.1	15.8	0.3	1175.2	15.6	1.59	0.02	0.45	0.03
SIDE-90% PR-10%SG-0%OFA																
	2.65	0.31	380.5	25.5	1.17	0.05	99.0	2.6	16.2	0.2	1109.8	11.3	1.50	0.02	0.51	0.03
	3.46	0.26	484.9	14.0	0.41	0.01	98.1	2.4	16.1	0.3	1102.7	11.9	1.49	0.02	0.66	0.02
	4.36	0.43	455.3	24.1	0.33	0.02	104.2	2.5	15.9	0.4	1063.0	15.1	1.44	0.02	0.62	0.03
SIDE-90% PR-10%SG-15%OFA																
	2.75	0.25	330.7	24.5	1.26	0.01	94.8	2.3	16.3	0.2	1133.6	13.3	1.53	0.02	0.45	0.03
	3.67	0.37	370.9	32.4	0.78	0.04	95.7	2.8	16.1	0.3	1136.6	12.2	1.54	0.02	0.50	0.04
	4.67	0.28	477.9	25.8	0.45	0.02	99.9	2.8	15.9	0.3	1109.4	16.9	1.50	0.02	0.65	0.03
SIDE-80% PR-20%SG-0%OFA																
	3.01	0.31	351.3	16.3	0.80	0.02	107.4	2.4	16.0	0.2	1025.1	12.3	1.39	0.02	0.47	0.02
	3.96	0.34	380.5	29.2	0.43	0.01	102.9	3.5	16.0	0.3	1022.0	14.5	1.38	0.02	0.51	0.04
	4.71	0.31	461.5	12.7	0.30	0.00	101.8	2.8	15.9	0.2	1010.7	15.9	1.37	0.02	0.62	0.02
SIDE-80% PR-20%SG-15%OFA																
	3.10	0.42	274.8	32.0	0.88	0.01	96.4	4.1	16.3	0.4	1064.0	17.9	1.44	0.02	0.37	0.04
	3.72	0.58	365.3	36.6	0.78	0.01	98.1	2.8	16.3	0.4	1045.1	27.2	1.41	0.04	0.49	0.05
	4.75	0.37	356.6	26.8	0.45	0.01	97.7	2.3	16.1	0.3	1044.1	15.2	1.41	0.02	0.48	0.04
SIDE-90% PR-10% SD-0%OFA																
	2.75	0.29	341.4	15.9	1.04	0.04	93.9	2.4	16.1	0.2	1127.5	11.9	1.52	0.02	0.46	0.02
	3.57	0.38	376.6	16.4	0.68	0.02	92.7	3.9	16.0	0.3	1108.9	13.3	1.50	0.02	0.51	0.02
	4.52	0.37	445.4	20.9	0.26	0.01	94.7	2.6	15.9	0.3	1098.9	15.6	1.49	0.02	0.60	0.03
SIDE-90% PR-10% SD-15%OFA																
	2.42	0.29	215.3	8.5	2.10	0.05	104.9	2.4	16.1	0.3	1118.3	13.7	1.51	0.02	0.29	0.01
	3.72	0.40	293.5	25.2	1.06	0.03	108.1	2.1	16.0	0.3	1103.6	15.2	1.49	0.02	0.40	0.03
	4.81	0.20	298.6	19.8	0.69	0.01	110.3	2.4	15.8	0.3	1083.6	13.5	1.46	0.02	0.40	0.03
SIDE-80% PR-20% SD-0%OFA																
	4.19	0.51	454.0	15.0	0.20	0.01	123.3	3.3	16.1	0.4	1013.6	17.2	1.37	0.02	0.61	0.02
SIDE-80% PR-20% SD-15%OFA																
	2.83	0.23	212.3	7.4	1.39	0.06	100.4	2.3	16.5	0.4	1035.7	19.0	1.40	0.03	0.29	0.01
	4.23	0.45	292.7	40.8	0.64	0.01	105.3	3.1	16.1	0.5	1007.5	27.4	1.36	0.04	0.40	0.06
	4.75	0.25	351.2	46.7	0.45	0.02	103.1	2.9	16.1	0.5	976.6	17.7	1.32	0.02	0.47	0.06

Table A-4A. Gas Flow Data from Test GL-5 and PR-5.

Test 5 – Comilling of SD with GL and 100% PR														
Furnace Flow Data					------- FURNACE AIR FLOWS, SCFM (60°F, 29.92 in. Hg) ------								Fuel Feed	
Test Condition	FEO, Wet %		NO_x, 3% O_2, ppm		Total Air		Pri. Air (150°F)		Sec. Air (600°F)		OFA (600°F)		Rate, lb/hr	
	Avg.	S.D.	Avg.	S.D.	Avg.	S.D.	Avg.	S.D.	Avg.	S.D.	Avg.	S.D.	Avg.	S.D.
100%PR-0% OFA														
	2.90	0.35	390.8	21.8	669.7	2.7	127.3	0.3	542.4	2.7	0.0	0.0	300.9	9.8
	2.99	0.32	403.5	21.2	670.0	3.0	127.3	0.3	542.7	3.0	0.0	0.0	301.1	9.8
	2.99	0.31	398.2	21.6	669.4	1.3	127.2	0.3	542.1	1.2	0.0	0.0	300.1	9.7
	3.37	0.28	386.0	14.9	670.9	2.5	127.4	0.4	543.6	2.4	0.0	0.0	301.2	7.5
	3.44	0.23	386.5	20.7	670.1	1.9	127.3	0.3	542.8	1.9	0.0	0.0	301.0	11.1
	3.84	0.43	433.9	27.2	730.0	2.3	138.7	0.2	591.3	2.3	0.0	0.0	300.1	10.7
	3.79	0.40	460.3	20.3	730.1	2.6	138.7	0.3	591.4	2.5	0.0	0.0	302.1	9.8
	4.08	0.47	443.5	26.7	729.9	1.8	138.8	0.2	591.1	1.7	0.0	0.0	301.6	9.8
	4.29	0.24	491.9	15.1	730.3	2.4	138.7	0.3	591.5	2.4	0.0	0.0	301.5	10.4
	4.64	0.27	435.0	21.5	729.9	1.9	138.7	0.3	591.2	1.8	0.0	0.0	301.1	10.5
	4.66	0.30	442.9	12.9	730.3	2.5	138.7	0.2	591.5	2.6	0.0	0.0	298.9	11.6
	4.78	0.24	441.6	20.4	729.7	1.4	138.6	0.3	591.0	1.3	0.0	0.0	301.3	9.5
	4.81	0.48	479.5	16.1	780.2	2.5	148.2	0.3	632.0	2.4	0.0	0.0	300.4	9.7
	4.98	0.30	502.8	20.3	780.5	2.8	148.2	0.3	632.3	2.7	0.0	0.0	303.3	10.2
100%PR-15% OFA														
	2.62	0.28	231.0	20.2	659.9	1.9	125.3	0.4	435.6	1.7	99.0	0.2	300.9	10.1
	3.93	0.30	344.5	20.3	729.5	2.1	138.7	0.3	481.4	1.9	109.5	0.3	301.4	10.6
	4.69	0.18	403.7	12.5	779.6	2.1	148.2	0.3	514.4	1.9	117.0	0.2	302.1	8.5
100%GL-0%OFA														
	2.61	0.57	419.0	22.2	660.4	4.2	125.5	0.7	534.9	3.9	0.0	0.0	288.3	9.9
	3.48	0.36	471.2	12.4	704.3	4.6	133.9	0.3	570.4	4.6	0.0	0.0	292.3	8.2
	3.63	0.55	472.4	13.8	704.8	4.3	133.9	0.3	570.9	4.3	0.0	0.0	289.7	9.7
	4.40	0.45	516.8	15.8	749.1	3.7	142.5	0.4	606.6	3.5	0.0	0.0	287.3	10.6
	4.53	0.54	518.8	17.7	749.3	5.0	142.4	0.8	606.9	4.4	0.0	0.0	286.4	11.9
100%G-15%OFA														
	2.67	0.44	260.9	29.1	664.7	2.3	126.4	0.4	438.6	2.2	99.8	0.2	291.0	10.0
	2.70	0.50	264.2	31.9	665.0	2.5	126.4	0.4	438.9	2.3	99.8	0.2	290.2	11.4
	3.04	0.69	277.4	41.5	670.3	2.2	127.4	0.3	442.4	2.2	100.5	0.2	285.2	13.4
	3.46	0.50	360.0	34.0	704.9	2.0	133.9	0.3	465.3	1.9	105.7	0.2	289.7	10.0
	3.62	0.20	371.3	24.9	750.6	2.5	142.5	0.3	495.6	2.5	112.5	0.2	305.6	7.3
	4.48	0.27	412.4	19.2	750.0	2.1	142.6	0.3	495.0	1.9	112.5	0.2	290.3	7.1
	4.56	0.40	409.1	22.9	750.1	1.9	142.6	0.3	495.0	1.8	112.5	0.2	287.6	8.5
90%GL+10%SD-0%OFA														
	2.44	0.30	338.0	19.9	680.6	6.9	129.4	0.6	551.2	6.5	0.0	0.0	299.9	8.1
	3.38	0.42	468.2	38.2	719.8	4.9	136.8	0.4	583.0	4.8	0.0	0.0	299.3	7.8
	4.20	0.37	487.1	27.4	760.2	3.0	144.3	0.6	615.9	2.9	-0.1	1.1	298.8	7.2
90%GL+10%SD-15%OFA														
	2.75	0.41	247.7	24.6	679.7	2.0	129.3	0.3	448.4	1.9	102.0	0.2	295.6	7.4
	3.49	0.25	272.6	25.1	740.1	2.6	140.6	0.4	488.4	2.4	111.0	0.2	316.0	9.7
	3.72	0.26	276.1	13.4	730.1	1.6	138.7	0.4	481.9	1.6	109.5	0.1	297.8	8.6
	4.18	0.37	344.0	21.2	759.3	7.7	144.3	1.0	503.4	10.5	111.6	16.5	301.1	7.8
80%GL+20%SD-0%OFA														
	2.53	0.35	418.0	11.8	650.1	2.2	123.5	0.6	526.6	2.1	0.0	0.0	310.2	8.1
	3.52	0.39	475.6	12.9	704.7	4.0	133.8	1.0	570.9	3.5	0.0	0.0	310.6	9.1
	4.30	0.12	516.6	9.8	750.2	2.3	142.6	0.4	607.6	2.1	0.0	0.0	307.5	7.6
80%GL+20%SD-15%OFA														
	2.75	0.42	260.7	30.3	660.8	9.5	125.6	1.4	436.1	7.1	99.1	1.1	307.9	10.9
	3.64	0.33	326.7	19.4	710.1	1.9	134.9	0.3	468.7	1.8	106.5	0.2	310.3	8.7
	3.90	0.40	361.3	23.8	715.0	2.5	135.9	0.4	471.9	2.2	107.3	0.2	308.8	9.6
	4.71	0.39	419.5	17.0	759.8	2.0	144.4	0.5	501.4	1.8	114.0	0.2	309.2	9.7

Table A-4B. Gas Flow Data for UBC Measurements from Test GL-5 and PR-5.

Test 5 – Comilling of SD with GL and 100% PR																
Unburned Carbon Data							----- FURNACE AIR FLOWS, SCFM (60°F, 29.92 in. Hg) ------								Fuel Feed	
Test Condition	FEO, Wet %		NO_x, 3% O_2, ppm		% UBC		Total Air		Pri. Air (150°F)		Sec. Air (600°F)		OFA (600°F)		Rate, lb/hr	
	Avg.	S.D.	Avg.	S.D.	Avg.	S.D.	Avg.	S.D.	Avg.	S.D.	Avg.	S.D.	Avg.	S.D.	Avg.	S.D.
100% PR - 0% OFA	3.86	0.39	461.2	16.2	0.37	0.01	729.6	2.0	138.7	0.3	590.9	1.9	0.0	0.0	304.8	7.5
	2.99	0.31	408.6	18.9	0.87	0.04	669.9	2.8	127.3	0.3	542.6	2.7	0.0	0.0	300.3	10.5
	5.61	0.30	483.8	17.1	0.17	0.00	779.7	2.6	148.2	0.3	631.5	2.5	0.0	0.0	300.1	10.0
100% PR - 15% OFA	3.90	0.27	348.7	16.2	0.74	0.03	729.5	1.7	138.7	0.3	481.3	1.6	109.5	0.2	303.7	8.0
	2.50	0.49	224.0	25.9	2.17	0.10	659.7	1.8	125.3	0.4	435.4	1.6	99.0	0.2	301.2	8.9
	4.69	0.37	400.4	13.3	0.46	0.02	779.9	2.3	148.3	0.3	514.7	2.1	117.0	0.2	304.3	7.1
100% GL - 0% OFA	3.48	0.36	471.2	12.4	0.86	0.02	704.3	4.6	133.9	0.3	570.4	4.6	0.0	0.0	292.3	8.2
	2.59	0.55	416.0	18.3	2.41	0.02	659.8	3.1	125.3	0.6	534.5	3.0	0.0	0.0	288.5	10.2
	4.40	0.45	516.8	15.8	0.35	0.04	749.1	3.7	142.5	0.4	606.6	3.5	0.0	0.0	287.3	10.6
100% GL - 15% OFA	2.67	0.44	260.9	29.1	6.93	0.68	664.7	2.3	126.4	0.4	438.6	2.2	99.8	0.2	291.0	10.0
	3.62	0.20	371.3	24.9	4.38	0.41	750.6	2.5	142.5	0.3	495.6	2.5	112.5	0.2	305.6	7.3
	4.48	0.27	412.4	19.2	2.44	0.06	750.0	2.1	142.6	0.3	495.0	1.9	112.5	0.2	290.3	7.1
90%GL+10%SD-0%OFA	3.30	0.36	628.4	11.3	1.33	0.01	720.1	2.6	136.8	0.4	583.4	2.6	0.0	0.0	300.1	7.7
	2.39	0.40	339.9	21.2	4.24	0.12	682.4	12.6	129.6	1.2	552.8	11.5	0.0	0.0	300.2	7.6
	4.17	0.35	484.5	22.3	0.51	0.04	760.5	2.8	144.3	0.4	616.1	2.6	0.0	0.5	300.0	7.3
90%GL+10%SD-15%OFA	3.52	0.25	263.5	21.9	2.33	0.03	740.0	1.7	140.7	0.4	488.3	1.5	111.0	0.2	315.6	9.7
	2.76	0.40	248.4	25.0	3.03	0.09	679.7	1.9	129.3	0.3	448.3	1.8	102.0	0.2	295.6	6.1
	4.14	0.36	342.1	19.1	1.85	0.01	760.5	2.5	144.4	0.4	502.1	2.2	114.0	0.2	301.1	7.7
80%GL+20%SD-0%OFA	3.55	0.40	477.2	13.2	0.48	0.05	704.8	3.0	133.9	0.4	570.9	3.0	0.0	0.0	311.5	9.4
	2.59	0.35	419.1	11.0	1.16	0.02	650.1	2.3	123.6	0.6	526.6	2.1	0.0	0.0	310.3	8.1
	4.53	0.12	515.2	9.1	0.17	0.00	750.1	2.3	142.6	0.4	607.5	2.1	0.0	0.0	307.2	7.6
80%GL+20%SD-15%OFA	3.87	0.32	361.5	21.8	1.72	0.02	714.8	1.2	135.9	0.3	471.6	1.1	107.3	0.1	310.8	7.2
	2.75	0.41	262.2	32.5	3.14	0.07	659.9	1.7	125.4	0.4	435.5	1.7	99.0	0.1	308.1	11.5
	4.71	0.43	420.8	17.9	1.09	0.01	759.8	2.4	144.4	0.5	501.3	2.1	114.0	0.2	308.7	10.3

Table A-4C. Gas Sampling Data from Test GL-5 and PR-5.

Test 5 – Comilling of Sawdust with Galatia and 100% Pratt Seam														
Gas Sampling Data														
Test Condition	FEO, Wet %		NO_x, 3% O_2, ppm		CO, 3% O_2, ppm		CO_2, 3% O_2, %		SO_2, 3% O_2, ppm		SO_2, lb/10^6Btu		NO_x, lb/10^6Btu	
	Avg.	S.D.	Avg.	S.D.	Avg.	S.D.	Avg.	S.D.	Avg.	S.D.	Avg.	S.D.	Avg.	S.D.
100%PR-0% OFA														
	2.90	0.35	390.8	21.8	84.1	24.5	16.1	0.3	1034.4	33.0	1.44	0.05	0.54	0.03
	2.99	0.32	403.5	21.2	105.9	3.0	16.0	0.4	1169.6	16.6	1.63	0.02	0.56	0.03
	2.99	0.31	398.2	21.6	98.3	3.1	16.0	0.2	1172.8	13.3	1.63	0.02	0.56	0.03
	3.37	0.28	386.0	14.9	95.3	2.3	16.1	0.3	1091.9	20.3	1.52	0.03	0.53	0.02
	3.44	0.23	386.5	20.7	98.2	2.6	16.1	0.2	1163.7	20.4	1.62	0.03	0.54	0.03
	3.84	0.43	433.9	27.2	82.5	3.2	16.0	0.5	979.3	28.7	1.36	0.04	0.61	0.03
	3.79	0.40	460.3	20.3	111.0	2.7	15.7	0.5	1125.8	26.0	1.57	0.04	0.65	0.02
	4.08	0.47	443.5	26.7	99.7	2.5	15.8	0.5	1159.9	22.7	1.61	0.03	0.62	0.04
	4.29	0.24	491.9	15.1	81.7	2.1	15.9	0.3	917.5	21.3	1.28	0.03	0.68	0.02
	4.64	0.27	435.0	21.5	98.9	3.1	15.8	0.4	1162.8	26.1	1.62	0.04	0.60	0.03
	4.66	0.30	442.9	12.9	98.3	2.6	15.9	0.4	1010.9	22.3	1.41	0.03	0.62	0.02
	4.78	0.24	441.6	20.4	105.1	3.1	15.9	0.3	1103.4	15.1	1.53	0.02	0.61	0.03
	4.81	0.48	479.5	16.1	101.8	2.4	15.8	0.4	1010.8	19.8	1.41	0.03	0.67	0.02
	4.98	0.30	502.8	20.3	93.6	3.0	15.7	0.3	1132.6	11.7	1.57	0.02	0.70	0.03
100%PR-15% OFA														
	2.62	0.28	231.0	20.2	92.6	5.2	16.1	0.3	1192.0	24.5	1.66	0.03	0.32	0.03
	3.93	0.30	344.5	20.3	95.5	3.7	15.8	0.4	1140.7	21.4	1.59	0.03	0.48	0.03
	4.69	0.18	403.7	12.5	93.5	2.5	15.6	0.4	1095.7	30.5	1.52	0.04	0.56	0.03
100%GL-0%OFA														
	2.61	0.57	419.0	22.2	92.0	16.5	16.3	0.3	662.4	19.0	0.92	0.03	0.58	0.03
	3.48	0.36	471.2	12.4	87.8	2.4	16.2	0.2	630.4	18.1	0.88	0.03	0.66	0.02
	3.63	0.55	472.4	13.8	88.0	2.5	16.2	0.3	631.7	18.1	0.88	0.03	0.66	0.02
	4.40	0.45	516.8	15.8	89.0	3.0	16.1	0.3	596.1	19.2	0.83	0.03	0.72	0.02
	4.53	0.54	518.8	17.7	89.9	3.4	16.0	0.4	599.7	18.4	0.83	0.03	0.72	0.02
100%G-15%OFA														
	2.67	0.44	260.9	29.1	117.8	2.6	16.1	0.4	742.9	19.0	1.03	0.03	0.36	0.04
	2.70	0.50	264.2	31.9	118.7	2.8	16.1	0.4	740.2	17.5	1.03	0.02	0.37	0.04
	3.04	0.69	277.4	41.5	92.1	2.5	16.3	0.3	700.7	20.1	0.97	0.03	0.39	0.06
	3.46	0.50	360.0	34.0	118.1	4.4	16.3	0.5	715.8	15.7	1.00	0.02	0.50	0.05
	3.62	0.20	371.3	24.9	119.6	2.9	16.3	0.3	745.9	11.7	1.04	0.02	0.52	0.03
	4.48	0.27	412.4	19.2	113.2	2.6	15.9	0.3	709.9	17.6	0.99	0.02	0.57	0.03
	4.56	0.40	409.1	22.9	113.6	2.6	15.9	0.3	714.3	18.8	0.99	0.03	0.57	0.03
90%GL+10%SD-0%OFA														
	2.44	0.30	338.0	19.9	107.8	7.2	16.2	0.3	619.8	15.7	0.86	0.02	0.47	0.03
	3.38	0.42	468.2	38.2	91.2	12.3	15.7	2.3	630.6	28.7	0.88	0.04	0.65	0.05
	4.20	0.37	487.1	27.4	101.0	2.8	16.0	0.3	518.2	15.9	0.72	0.02	0.68	0.04
90%GL+10%SD-15%OFA														
	2.75	0.41	247.7	24.6	98.7	8.8	16.2	0.4	686.9	12.4	0.96	0.02	0.34	0.03
	3.49	0.25	272.6	25.1	99.1	3.6	16.1	0.3	690.4	11.8	0.96	0.02	0.38	0.03
	3.72	0.26	276.1	13.4	99.7	2.5	16.1	0.3	610.8	15.1	0.85	0.02	0.38	0.03
	4.18	0.37	344.0	21.2	101.6	3.5	15.8	0.3	658.1	10.9	0.92	0.02	0.48	0.03
80%GL+20%SD-0%OFA														
	2.53	0.35	418.0	11.8	95.4	2.0	16.4	0.3	581.7	9.1	0.81	0.01	0.58	0.02
	3.52	0.39	475.6	12.9	96.3	2.1	16.2	0.3	568.2	10.4	0.79	0.01	0.66	0.02
	4.30	0.12	516.6	9.8	89.7	2.3	16.1	0.3	548.2	9.6	0.76	0.01	0.72	0.01
80%GL+20%SD-15%OFA														
	2.75	0.42	260.7	30.3	97.9	2.2	16.3	0.4	528.4	17.0	0.73	0.02	0.36	0.04
	3.64	0.33	326.7	19.4	90.8	2.3	16.4	0.2	590.5	11.4	0.82	0.02	0.45	0.03
	3.90	0.40	361.3	23.8	95.7	2.6	16.1	0.4	564.4	16.4	0.78	0.02	0.50	0.03
	4.71	0.39	419.5	17.0	95.7	2.4	16.0	0.4	541.3	11.8	0.75	0.02	0.58	0.02

Table A-4D. Gas Sampling Data for UBC Measurements from Test GL-5 and PR-5.

Test 5 - Comilling of Sawdust with Galatia and 100% Pratt Seam																
Unburned Carbon Data																
	FEO, Wet %		NOx, 3% O_2, ppm		% UBC		CO, 3% O_2, ppm		CO_2, 3% O_2, %		SO_2, 3% O_2, ppm		SO_2, lb/10^6Btu		NO_X, lb/10^6Btu	
Test Condition	Avg.	S.D.	Avg.	S.D.	Avg.	S.D.	Avg.	S.D.	Avg.	S.D.	Avg.	S.D.	Avg.	S.D.	Avg.	S.D.
100% PR - 0% OFA	3.86	0.39	461.2	16.2	0.37	0.01	111.3	3.0	15.7	0.3	1118.0	19.0	1.55	0.03	0.64	0.02
	2.99	0.31	408.6	18.9	0.87	0.04	106.0	3.1	15.9	0.4	1170.2	16.9	1.63	0.02	0.57	0.03
	5.61	0.30	483.8	17.1	0.17	0.00	102.0	2.9	15.8	0.4	980.2	24.0	1.36	0.03	0.67	0.02
100% PR - 15% OFA	3.90	0.27	348.7	16.2	0.74	0.03	96.3	3.3	15.8	0.4	1135.3	17.7	1.58	0.02	0.48	0.02
	2.50	0.49	224.0	25.9	2.17	0.10	94.9	14.6	16.1	0.3	1198.0	26.6	1.67	0.04	0.31	0.04
	4.69	0.37	400.4	13.3	0.46	0.02	93.2	2.5	15.7	0.3	1082.1	37.4	1.50	0.05	0.56	0.02
100% GL - 0% OFA	3.48	0.36	471.2	12.4	0.86	0.02	87.8	2.4	16.2	0.2	630.4	18.1	0.88	0.03	0.66	0.02
	2.59	0.55	416.0	18.3	2.41	0.02	90.8	3.7	16.3	0.3	662.3	18.0	0.92	0.02	0.58	0.03
	4.40	0.45	516.8	15.8	0.35	0.04	89.0	3.0	16.1	0.3	596.1	19.2	0.83	0.03	0.72	0.02
100% GL - 15% OFA	2.67	0.44	260.9	29.1	6.93	0.68	117.8	2.6	16.1	0.4	742.9	19.0	1.03	0.03	0.36	0.04
	3.62	0.20	371.3	24.9	4.38	0.41	119.6	2.9	16.3	0.3	745.9	11.7	1.04	0.02	0.52	0.03
	4.48	0.27	412.4	19.2	2.44	0.06	113.2	2.6	15.9	0.3	709.9	17.6	0.99	0.02	0.57	0.03
90%GL+10%SD-0%OFA	3.30	0.36	628.4	11.3	1.33	0.01	98.4	2.8	16.1	0.3	566.9	14.5	0.79	0.02	0.87	0.02
	2.39	0.40	339.9	21.2	4.24	0.12	106.6	3.2	16.3	0.3	619.1	15.4	0.86	0.02	0.47	0.03
	4.17	0.35	484.5	22.3	0.51	0.04	101.6	2.5	16.0	0.3	516.5	13.1	0.72	0.02	0.67	0.03
90%GL+10%SD-15%OFA	3.52	0.25	263.5	21.9	2.33	0.03	98.4	3.4	16.1	0.2	686.0	11.9	0.95	0.02	0.37	0.03
	2.76	0.40	248.4	25.0	3.03	0.09	99.0	10.0	16.2	0.4	686.0	12.1	0.95	0.02	0.35	0.03
	4.14	0.36	342.1	19.1	1.85	0.01	100.5	3.3	15.7	0.3	656.9	10.7	0.91	0.01	0.48	0.03
80%GL+20%SD-0%OFA	3.55	0.40	477.2	13.2	0.48	0.05	95.7	2.6	16.1	0.3	570.5	11.3	0.79	0.02	0.66	0.02
	2.59	0.35	419.1	11.0	1.16	0.02	95.2	1.7	16.4	0.2	581.0	8.5	0.81	0.01	0.58	0.02
	4.53	0.12	515.2	9.1	0.17	0.00	92.0	45.0	13.3	6.2	504.6	217.6	0.70	0.30	0.71	0.33
80%GL+20%SD-15%OFA	3.87	0.32	361.5	21.8	1.72	0.02	95.7	2.7	16.0	0.3	560.6	9.9	0.78	0.01	0.50	0.03
	2.75	0.41	262.2	32.5	3.14	0.07	97.8	2.1	16.4	0.4	532.3	14.9	0.74	0.02	0.36	0.05
	4.71	0.43	420.8	17.9	1.09	0.01	96.2	2.2	16.0	0.4	542.7	12.7	0.75	0.02	0.59	0.02

Table A-5A. Gas Flow Data from Test GL-6.

Test 6 – Comilling of SD with GL and 100% PR														
Furnace Flow Data					------- FURNACE AIR FLOWS, SCFM (60°F, 29.92 in. Hg) ------								Fuel Feed	
Test Condition	FEO, Wet %		NOx, 3% O_2, ppm		Total Air		Pri. Air (150°F)		Sec. Air (600°F)		OFA (600°F)		Rate, lb/hr	
	Avg.	S.D.	Avg.	S.D.	Avg.	S.D.	Avg.	S.D.	Avg.	S.D.	Avg.	S.D.	Avg.	S.D.
100%PR-0% OFA														
	2.66	0.19	506.4	14.6	660.2	2.1	125.4	0.2	534.8	2.0	0.0	0.0	288.5	4.0
	2.71	0.22	503.8	15.8	660.4	2.3	125.4	0.2	534.9	2.2	0.0	0.0	288.4	4.2
	3.73	0.18	495.5	20.0	709.9	2.8	135.0	0.2	574.9	2.7	0.0	0.0	289.7	3.1
	4.70	0.32	561.3	14.7	749.8	2.1	142.5	0.3	607.3	2.0	0.0	0.0	289.7	2.9
100%PR-15% OFA														
	2.52	0.36	251.0	20.2	660.3	1.9	125.4	0.2	435.9	1.8	99.0	0.2	288.5	6.0
	2.47	0.18	242.4	13.5	659.7	2.4	125.4	0.2	435.3	2.3	99.0	0.2	288.0	5.0
	3.51	0.19	319.2	12.1	709.9	1.7	134.9	0.2	468.5	1.5	106.5	0.2	289.1	3.8
	4.36	0.28	369.6	12.9	749.9	2.5	142.5	0.2	494.9	2.4	112.5	0.2	289.1	3.7
100%GL-0%OFA														
	3.90	0.41	483.1	14.1	689.5	1.8	131.1	0.2	558.3	1.7	0.0	0.0	271.9	4.2
100%GL-15%OFA														
	2.61	0.45	208.6	39.7	666.7	25.1	126.7	3.9	442.3	28.0	97.7	13.8	272.0	5.2
	3.65	0.32	355.6	32.6	710.1	2.1	134.9	0.3	468.7	1.9	106.5	0.2	271.6	3.4
	4.43	0.53	433.7	37.2	760.3	2.2	144.4	0.3	501.8	1.9	114.0	0.3	271.5	3.7
90%GL+10%SG-0%OFA														
	2.75	0.23	410.0	12.8	660.2	2.2	125.4	0.3	534.8	2.2	0.0	0.0	282.3	4.6
	3.75	0.29	476.8	16.0	700.1	2.6	133.0	0.3	567.0	2.5	0.0	0.0	281.0	4.2
	3.82	0.25	498.3	11.9	700.0	2.3	133.0	0.3	567.0	2.2	0.0	0.0	281.6	4.5
	4.57	0.21	519.1	21.3	750.2	3.1	142.5	0.4	607.7	2.9	0.0	0.0	283.3	4.4
	4.60	0.25	517.0	18.1	750.2	2.9	142.5	0.4	607.7	2.7	0.0	0.0	283.3	4.8
90%GL+10%SG-15%OFA														
	2.87	0.33	277.4	21.6	660.1	1.7	125.4	0.3	435.7	1.6	99.0	0.2	281.8	4.9
	3.72	0.26	340.0	19.6	699.9	2.9	133.0	0.3	461.8	2.7	105.0	0.2	281.9	4.4
	3.81	0.29	331.7	23.3	699.7	2.0	132.9	0.3	461.8	1.8	105.0	0.2	281.6	4.3
	4.49	0.28	393.6	16.2	739.8	1.6	140.6	0.3	488.2	1.4	111.0	0.2	281.7	4.6
80%GL+20%SG-0%OFA														
	2.59	0.36	446.2	11.6	650.1	2.4	123.5	0.3	526.5	2.4	0.0	0.0	292.1	5.3
	3.51	0.20	526.0	11.2	689.7	2.0	131.0	0.4	558.6	1.9	0.0	0.0	292.1	5.4
	4.49	0.71	510.7	23.6	750.0	3.1	142.5	0.7	607.5	2.7	0.0	0.0	292.1	3.7
	4.61	0.24	527.5	10.9	748.3	4.2	142.2	0.8	606.1	3.6	0.0	0.0	291.9	5.2
80%GL+20%SG-15%OFA														
	2.91	0.35	278.5	19.7	660.8	2.6	125.4	0.3	436.3	2.5	99.1	0.1	292.1	6.2
	2.95	0.23	278.9	23.8	660.5	2.3	125.5	0.3	436.0	2.2	99.0	0.1	291.5	7.7
	3.61	0.21	335.5	15.9	699.8	2.4	133.0	0.3	461.9	2.1	105.0	0.3	292.1	4.7
	4.64	0.26	395.6	18.4	739.5	3.1	140.7	0.5	487.7	2.8	111.1	0.2	292.3	6.3
	4.78	0.38	407.7	23.5	740.0	1.9	140.5	0.4	488.5	1.7	111.0	0.2	292.3	7.9
	4.96	0.37	394.7	18.0	740.3	2.0	140.7	0.7	488.6	1.5	111.0	0.2	293.3	5.0
80%PR+20%SD-0%OFA														
	2.49	0.24	396.3	21.3	658.9	1.9	125.4	0.2	533.5	1.8	0.0	0.0	309.4	3.2
	2.59	0.30	395.1	17.4	659.8	2.0	125.4	0.2	534.4	1.9	0.0	0.0	309.0	5.5
	2.65	0.28	397.5	16.5	659.9	2.0	125.4	0.2	534.5	1.9	0.0	0.0	308.9	5.7
	3.64	0.28	433.5	15.5	700.1	2.6	133.0	0.3	567.1	2.4	0.0	0.0	304.0	43.9
	3.77	0.22	413.8	14.3	699.9	1.8	133.0	0.2	566.9	1.8	0.0	0.0	310.9	4.0
	3.89	0.20	421.8	13.3	699.8	2.5	133.0	0.3	566.9	2.4	0.0	0.0	310.1	4.0
	3.89	0.17	442.6	14.4	699.5	2.8	133.1	0.3	566.5	2.8	0.0	0.0	310.3	3.4
	3.94	0.16	430.0	16.3	700.1	2.1	133.0	0.3	567.1	2.0	0.0	0.0	309.8	3.3
	4.46	0.27	447.2	11.6	740.0	3.0	140.6	0.4	599.4	2.8	0.0	0.0	310.4	3.8
80%PR+20%SD-15%OFA														
	3.45	0.24	269.7	12.6	699.7	4.7	133.0	0.3	462.9	3.7	103.9	7.6	310.7	3.9

Table A-5B. Gas Flow Data for UBC Measurements from Test GL-6.

Test 6 – Comilling of SD with GL and 100% PR																
Unburned Carbon Data							----- FURNACE AIR FLOWS, SCFM (60°F, 29.92 in. Hg) ------								Fuel Feed	
Test Condition	FEO, Wet %		NOx, 3% O_2, ppm		% UBC		Total Air		Pri. Air (150°F)		Sec. Air (600°F)		OFA (600°F)		Rate, lb/hr	
	Avg.	S.D.	Avg.	S.D.	Avg.	S.D.	Avg.	S.D.	Avg.	S.D.	Avg.	S.D.	Avg.	S.D.	Avg.	S.D.
100%PR-0% OFA	3.74	0.19	495.6	21.3	0.27	0.00	710.0	2.3	135.0	0.2	575.0	2.2	0.0	0.0	289.4	2.9
	2.71	0.22	503.8	15.8	0.39	0.02	660.4	2.3	125.4	0.2	534.9	2.2	0.0	0.0	288.4	4.2
	4.72	0.35	562.5	14.6	0.14	0.00	749.5	1.8	142.5	0.3	607.0	1.7	0.0	0.0	289.4	3.1
100%PR-15% OFA	3.55	0.25	320.1	12.9	1.33	0.03	710.0	1.7	134.9	0.2	468.5	1.5	106.5	0.2	288.6	3.8
	2.52	0.36	251.0	20.2	2.61	0.13	660.3	1.9	125.4	0.2	435.9	1.8	99.0	0.2	288.5	6.0
	4.39	0.31	369.3	11.9	1.03	0.02	750.3	3.1	142.5	0.2	495.3	2.9	112.5	0.2	289.3	3.8
100%GL-0%OFA	3.90	0.41	483.1	14.1	0.55	0.03	689.5	1.8	131.1	0.2	558.3	1.7	0.0	0.0	271.9	4.2
100%GL-15%OFA	4.50	0.41	437.7	37.0	3.12	0.05	760.3	1.9	144.4	0.3	501.9	1.7	114.0	0.2	272.6	2.9
	3.65	0.36	356.0	34.1	5.98	0.32	710.0	2.1	134.9	0.3	468.6	2.0	106.5	0.2	271.0	3.8
	2.60	0.46	202.9	31.3	6.74	0.52	665.3	24.0	126.5	3.7	439.1	17.2	99.8	3.2	271.7	5.5
90%GL+10%SG-0%OFA	3.84	0.27	499.4	12.2	0.89	0.06	700.1	2.3	133.0	0.3	567.1	2.2	0.0	0.0	281.6	4.4
	2.74	0.24	409.8	13.5	0.37	0.06	660.2	2.0	125.4	0.3	534.7	1.9	0.0	0.0	282.6	4.6
	4.57	0.21	519.1	21.3	1.27	0.08	750.2	3.1	142.5	0.4	607.7	2.9	0.0	0.0	283.3	4.4
90%GL+10%SG-15%OFA	3.81	0.29	331.7	23.3	1.57	0.19	699.7	2.0	132.9	0.3	461.8	1.8	105.0	0.2	281.6	4.3
	2.85	0.37	273.9	21.7	1.35	0.15	660.1	1.9	125.4	0.3	435.7	1.8	99.0	0.2	281.9	5.1
	4.49	0.25	394.4	17.5	0.27	0.01	740.0	1.6	140.6	0.3	488.3	1.4	111.0	0.2	281.9	4.8
80%GL+20%SG-0%OFA	3.56	0.40	523.4	14.0	0.43	0.03	689.5	1.9	131.1	0.3	558.5	1.7	0.0	0.0	292.2	5.2
	2.60	0.39	446.3	11.6	0.59	0.01	649.6	1.6	123.5	0.3	526.1	1.6	0.0	0.0	291.9	5.6
	4.49	0.71	510.7	23.6	0.34	0.04	750.0	3.1	142.5	0.7	607.5	2.7	0.0	0.0	292.1	3.7
80%GL+20%SG-15%OFA	3.64	0.46	337.9	17.4	3.10	0.13	699.7	2.1	133.1	0.3	461.7	1.9	105.0	0.2	291.3	4.4
	3.08	0.59	281.2	36.8	2.23	0.15	660.4	2.3	125.4	0.4	435.9	2.1	99.0	0.1	291.6	8.6
	4.75	0.66	397.9	34.8	2.51	0.13	740.1	1.9	140.6	0.5	488.5	1.6	111.0	0.2	292.0	8.5
80%PR+20%SD-15%OFA	3.94	0.16	430.0	16.3	0.19	0.01	700.1	2.1	133.0	0.3	567.1	2.0	0.0	0.0	309.8	3.3
	2.65	0.28	397.5	16.5	0.38	0.01	659.9	2.0	125.4	0.2	534.5	1.9	0.0	0.0	308.9	5.7
	4.43	0.25	446.2	10.8	0.12	0.00	740.2	2.4	140.6	0.3	599.6	2.2	0.0	0.0	310.4	3.8

Table A-5C. Gas Sampling Data from Test GL-6.

Test 6 – Comilling of SD with GL and 100% PR														
Gas Sampling Data														
Test Condition	FEO, Wet %		NO_x, 3% O_2, ppm		CO, 3% O_2, ppm		CO_2, 3% O_2, %		SO_2, 3% O_2, ppm		SO_2, lb/10^6Btu		NO_x, lb/10^6Btu	
	Avg.	S.D.	Avg.	S.D.	Avg.	S.D.	Avg.	S.D.	Avg.	S.D.	Avg.	S.D.	Avg.	S.D.
100%PR-0% OFA														
	2.66	0.19	506.4	14.6	132.1	2.8	15.9	0.2	1065.2	10.6	1.48	0.01	0.70	0.02
	2.71	0.22	503.8	15.8	131.6	2.6	16.0	0.2	1067.3	11.1	1.48	0.02	0.70	0.02
	3.73	0.18	495.5	20.0	131.8	4.3	15.8	0.2	N/A	N/A	N/A	N/A	0.69	0.03
	4.70	0.32	561.3	14.7	101.3	3.2	15.6	0.1	1022.8	9.0	1.42	0.01	0.78	0.02
100%PR-15% OFA														
	2.52	0.36	251.0	20.2	130.2	3.2	16.3	0.3	1035.6	267.8	1.44	0.37	0.35	0.03
	2.47	0.18	242.4	13.5	130.6	3.3	16.2	0.2	1005.4	363.9	1.40	0.51	0.34	0.02
	3.51	0.19	319.2	12.1	133.9	3.2	16.0	0.3	1182.1	425.0	1.64	0.59	0.44	0.02
	4.36	0.28	369.6	12.9	132.8	2.8	16.0	0.2	1062.9	40.6	1.48	0.06	0.51	0.02
100%GL-0%OFA														
	3.90	0.41	483.1	14.1	88.8	3.3	16.1	0.3	NA	NA	NA	NA	0.67	0.02
100%GL-15%OFA														
	2.61	0.45	208.6	39.7	127.1	4.5	16.0	0.4	489.0	133.7	0.68	0.19	0.29	0.06
	3.65	0.32	355.6	32.6	145.4	63.2	15.9	0.5	251.9	257.3	0.35	0.36	0.49	0.05
	4.43	0.53	433.7	37.2	125.2	15.0	15.6	0.5	702.6	145.3	0.98	0.20	0.60	0.05
90%GL+10%SG-0%OFA														
	2.75	0.23	410.0	12.8	101.1	4.7	16.0	0.3	628.3	9.7	0.87	0.01	0.57	0.02
	3.75	0.29	476.8	16.0	96.7	2.3	15.9	0.3	605.4	14.0	0.84	0.02	0.66	0.02
	3.82	0.25	498.3	11.9	87.4	3.0	16.0	0.3	635.6	10.6	0.88	0.01	0.69	0.02
	4.57	0.21	519.1	21.3	108.6	5.8	15.5	0.3	565.0	10.0	0.79	0.01	0.72	0.03
	4.60	0.25	517.0	18.1	109.9	5.4	15.5	0.3	568.2	10.9	0.79	0.02	0.72	0.03
90%GL+10%SG-15%OFA														
	2.87	0.33	277.4	21.6	113.9	2.8	16.3	0.3	687.4	12.2	0.96	0.02	0.39	0.03
	3.72	0.26	340.0	19.6	113.2	2.7	16.1	0.3	676.9	9.3	0.94	0.01	0.47	0.03
	3.81	0.29	331.7	23.3	115.0	2.7	16.1	0.3	677.9	12.4	0.94	0.02	0.46	0.03
	4.49	0.28	393.6	16.2	112.7	3.1	16.0	0.3	660.4	8.8	0.92	0.01	0.55	0.02
80%GL+20%SG-0%OFA														
	2.59	0.36	446.2	11.6	89.4	3.7	16.2	0.3	604.9	8.9	0.84	0.01	0.62	0.02
	3.51	0.20	526.0	11.2	103.7	2.8	16.1	0.3	601.1	10.9	0.84	0.02	0.73	0.02
	4.49	0.71	510.7	23.6	101.4	3.1	16.0	0.5	571.1	15.0	0.79	0.02	0.71	0.03
	4.61	0.24	527.5	10.9	100.0	3.4	15.9	0.3	570.0	10.9	0.79	0.02	0.73	0.02
80%GL+20%SG-15%OFA														
	2.91	0.35	278.5	19.7	97.1	2.0	16.4	0.3	626.2	8.7	0.87	0.01	0.39	0.03
	2.95	0.23	278.9	23.8	111.7	1.9	16.3	0.4	624.2	12.8	0.87	0.02	0.39	0.05
	3.61	0.21	335.5	15.9	94.9	2.7	16.2	0.4	617.8	14.1	0.86	0.02	0.47	0.03
	4.64	0.26	395.6	18.4	115.3	6.1	16.2	0.5	595.3	48.2	0.83	0.07	0.55	0.02
	4.78	0.38	407.7	23.5	119.2	4.1	16.0	0.5	600.3	16.6	0.83	0.02	0.56	0.05
	4.96	0.37	394.7	18.0	117.5	4.6	16.1	0.7	603.2	17.1	0.84	0.02	0.54	0.06
80%PR+20%SD-0%OFA														
	2.49	0.24	396.3	21.3	92.6	4.7	16.3	0.4	1011.2	12.1	1.41	0.02	0.55	0.03
	2.59	0.30	395.1	17.4	89.1	2.3	16.2	0.2	1015.1	10.3	1.41	0.01	0.55	0.02
	2.65	0.28	397.5	16.5	88.9	2.3	16.2	0.3	1016.2	9.5	1.41	0.01	0.55	0.02
	3.64	0.28	433.5	15.5	82.7	3.4	16.1	0.2	1009.6	9.8	1.40	0.01	0.60	0.02
	3.77	0.22	413.8	14.3	101.6	2.9	16.1	0.3	1010.8	14.9	1.41	0.02	0.58	0.02
	3.89	0.20	421.8	13.3	91.6	3.1	16.0	0.2	983.8	9.5	1.37	0.01	0.59	0.02
	3.89	0.17	442.6	14.4	94.3	2.5	16.0	0.2	983.9	13.4	1.37	0.02	0.62	0.02
	3.94	0.16	430.0	16.3	93.5	2.3	16.0	0.2	985.6	9.8	1.37	0.01	0.60	0.02
	4.46	0.27	447.2	11.6	90.9	2.4	15.9	0.2	991.7	9.4	1.38	0.01	0.62	0.02
80%PR+20%SD-15%OFA														
	3.45	0.24	269.7	12.6	107.9	3.0	16.0	0.2	1036.0	10.1	1.44	0.01	0.38	0.02

Table A-5D. Gas Sampling Data for UBC Measurements from Test GL-6.

Test 6 - Comilling of SD with GL and 100% PR																
Unburned Carbon Data																
	FEO, Wet %		NOx, 3% O_2, ppm		% UBC		CO, 3% O_2, ppm		CO_2, 3% O_2, %		SO_2, 3% O_2, ppm		SO_2, lb/10^6Btu		NO_x, lb/10^6Btu	
Test Condition	Avg.	S.D.	Avg.	S.D.	Avg.	S.D.	Avg.	S.D.	Avg.	S.D.	Avg.	S.D.	Avg.	S.D.	Avg.	S.D.
100%PR-0% OFA																
	3.74	0.19	495.6	21.3	0.27	0.00	133.4	2.9	15.8	0.2	NA	NA	NA	NA	0.69	0.03
	2.71	0.22	503.8	15.8	0.39	0.02	131.6	2.6	16.0	0.2	1067.3	11.1	1.48	0.02	0.70	0.02
	4.72	0.35	562.5	14.6	0.14	0.00	101.8	2.6	15.6	0.2	1022.5	8.2	1.42	0.01	0.78	0.02
100%PR-15% OFA																
	3.55	0.25	320.1	12.9	1.3	0.0	134.5	2.9	16	0	1100.6	449.3	1.53	0.62	0.45	0.02
	2.52	0.36	251.0	20.2	2.61	0.13	130.2	3.2	16.3	0.3	1035.6	267.8	1.44	0.37	0.35	0.03
	4.39	0.31	369.3	11.9	1.03	0.02	132.3	2.5	16.0	0.2	1033.4	34.0	1.44	0.05	0.51	0.02
100%GL-0%OFA																
	3.90	0.41	483.1	14.1	0.55	0.03	88.8	3.3	16.1	0.3	NA	NA	NA	NA	0.67	0.02
100%GL-15%OFA																
	4.50	0.41	437.7	37.0	3.12	0.05	124.5	9.7	15.6	0.4	708.2	75.0	0.98	0.10	0.61	0.05
	3.65	0.36	356.0	34.1	5.98	0.32	145.6	84.9	15.8	0.5	337.5	116.9	0.47	0.16	0.50	0.05
	2.60	0.46	202.9	31.3	6.74	0.52	127.0	4.7	16.0	0.4	479.3	117.1	0.67	0.16	0.28	0.04
90%GL+10%SG-0%OFA																
	3.84	0.27	499.4	12.2	0.89	0.06	88.1	2.8	16.0	0.3	634.3	11.2	0.88	0.02	0.69	0.02
	2.74	0.24	409.8	13.5	0.37	0.06	103.8	2.7	15.9	0.3	629.3	10.2	0.87	0.01	0.57	0.02
	4.57	0.21	519.1	21.3	1.27	0.08	108.6	5.8	15.5	0.3	565.0	10.0	0.79	0.01	0.72	0.03
90%GL+10%SG-15%OFA																
	3.81	0.29	331.7	23.3	1.57	0.19	115.0	2.7	16.1	0.3	677.9	12.4	0.94	0.02	0.46	0.03
	2.85	0.37	273.9	21.7	1.35	0.15	113.9	2.9	16.3	0.3	687.0	9.5	0.96	0.01	0.38	0.03
	4.49	0.25	394.4	17.5	0.27	0.01	112.1	3.1	16.0	0.3	660.2	8.8	0.92	0.01	0.55	0.02
80%GL+20%SG-0%OFA																
	3.56	0.40	523.4	14.0	0.43	0.03	103.6	2.7	16.1	0.3	600.1	10.8	0.83	0.02	0.73	0.02
	2.60	0.39	446.3	11.6	0.59	0.01	89.0	3.2	16.2	0.3	604.9	9.2	0.84	0.01	0.62	0.02
	4.49	0.71	510.7	23.6	0.34	0.04	101.4	3.1	16.0	0.5	571.1	15.0	0.79	0.02	0.71	0.03
80%GL+20%SG-15%OFA																
	3.64	0.46	337.9	17.4	3.10	0.13	94.2	2.3	16.1	0.4	627.6	12.8	0.87	0.02	0.47	0.02
	3.08	0.59	281.2	36.8	2.23	0.15	112.2	2.2	16.3	0.5	625.0	16.4	0.87	0.02	0.39	0.05
	4.75	0.66	397.9	34.8	2.51	0.13	121.8	5.0	15.9	0.5	602.5	17.5	0.84	0.02	0.55	0.05
80%PR+20%SD-0%OFA																
	3.94	0.16	430.0	16.3	0.19	0.01	93.5	2.3	16.0	0.2	985.6	9.8	1.37	0.01	0.60	0.02
	2.65	0.28	397.5	16.5	0.38	0.01	88.9	2.3	16.2	0.3	1016.2	9.5	1.41	0.01	0.55	0.02
	4.43	0.25	446.2	10.8	0.12	0.00	90.8	2.5	15.9	0.2	993.3	9.4	1.38	0.01	0.62	0.01

Table A-6A. Gas Flow Data from Test JR-7.

Test 7 – Co-milling of JR with SG and SD														
Furnace Flow Data					------- FURNACE AIR FLOWS, SCFM (60°F, 29.92 in. Hg) ------								Fuel Feed	
Test Condition	FEO, Wet %		NOx, 3% O_2, ppm		Total Air		Pri. Air (150°F)		Sec. Air (600°F)		OFA (600°F)		Rate, lb/hr	
	Avg.	S.D.	Avg.	S.D.	Avg.	S.D.	Avg.	S.D.	Avg.	S.D.	Avg.	S.D.	Avg.	S.D.
100%JR-0% OFA														
	2.49	0.18	306.9	17.0	630.7	6.3	120.1	1.1	510.6	5.2	0.0	0.0	352.1	3.1
	2.55	0.35	309.3	21.7	630.1	2.7	120.0	0.3	510.2	2.6	0.0	0.0	352.5	2.6
	3.59	0.16	396.9	14.3	680.2	3.1	129.2	0.4	551.0	2.9	0.0	0.0	351.9	3.5
	3.72	0.33	400.1	15.1	680.6	2.5	129.2	0.3	551.4	2.3	0.0	0.0	352.1	3.3
	4.58	0.12	413.4	14.7	730.3	2.8	138.8	0.4	591.5	2.7	0.0	0.0	352.3	3.5
	4.71	0.32	416.7	19.3	730.0	3.0	138.8	0.3	591.2	2.8	0.0	0.0	352.2	3.6
100%JR-15% OFA														
	2.70	0.16	172.6	10.2	630.5	2.2	120.0	0.2	416.1	2.0	94.5	0.2	352.5	3.8
	2.73	0.30	195.0	13.4	630.3	1.9	119.9	0.2	415.9	1.8	94.5	0.2	352.4	3.9
	3.61	0.19	240.3	14.0	740.3	2.7	140.6	0.3	488.7	2.4	111.0	0.3	381.5	3.8
	3.72	0.36	206.4	10.0	740.3	2.4	140.6	0.3	488.7	2.1	111.0	0.2	381.7	4.0
	4.39	0.09	257.3	20.1	720.2	2.2	136.8	0.3	475.4	1.9	108.0	0.2	351.5	3.7
	4.48	0.31	259.6	26.1	719.9	3.9	136.8	0.4	475.1	3.3	108.0	0.5	351.5	3.9
90%JR+10% SG-0%OFA														
	2.58	0.18	273.7	16.2	631.2	1.4	120.0	0.3	511.2	1.3	0.0	0.0	358.2	4.4
	2.77	0.14	282.5	14.5	630.4	2.6	120.0	0.3	510.4	2.6	0.0	0.0	357.9	5.5
	3.65	0.18	333.2	15.4	680.4	3.4	129.2	0.4	551.2	3.2	0.0	0.0	357.3	4.8
	3.81	0.26	332.1	18.4	679.9	3.3	129.2	0.4	550.7	3.0	0.0	0.0	357.8	5.1
	4.51	0.21	356.5	12.0	720.7	3.1	136.9	0.4	583.9	2.9	0.0	0.0	357.8	3.9
90%JR+10% SG-15%OFA														
	2.71	0.12	136.4	8.3	630.4	2.0	120.0	0.3	415.9	1.8	94.5	0.2	357.2	6.3
	3.76	0.13	184.6	14.7	680.1	2.3	129.2	0.4	448.9	1.9	102.0	0.3	357.7	4.4
	4.66	0.15	236.5	16.5	720.1	3.1	136.8	0.4	475.2	2.7	108.0	0.3	357.7	4.8
80%JR+20% SG-0%OFA														
	3.81	0.19	318.1	19.0	700.3	3.1	133.0	0.5	567.3	2.9	0.0	0.0	365.8	12.4
	4.54	0.21	338.8	14.7	740.2	3.5	140.6	0.6	599.6	3.1	0.0	0.0	366.2	10.4
80%JR+20% SG-15%OFA														
	2.72	0.20	141.8	8.9	631.9	1.8	120.2	0.3	417.0	1.5	94.7	0.2	371.7	4.1
	3.33	0.26	158.7	20.4	669.8	2.2	127.3	0.5	442.0	1.8	100.5	0.3	365.2	10.1
	3.77	0.21	202.9	19.6	717.7	5.3	136.5	1.0	473.5	4.0	107.7	0.7	382.5	8.7
	4.22	0.22	212.7	20.3	709.0	2.6	134.9	0.6	467.7	1.9	106.5	0.3	367.7	6.2
	4.30	0.17	224.4	22.6	710.0	2.5	134.9	0.6	468.5	1.7	106.5	0.4	365.3	8.5
80%JR+20% SD-0%OFA														
	2.39	0.20	267.2	20.0	630.5	2.0	120.0	0.3	510.5	1.9	0.0	0.0	367.5	7.7
	3.22	0.22	313.0	18.6	670.7	6.2	127.4	0.8	543.3	5.6	0.0	0.0	367.1	7.7
	4.29	0.19	359.1	11.6	719.6	3.1	136.8	0.5	582.8	2.9	0.0	0.0	367.8	7.9
80%JR+20% SD-15%OFA														
	2.45	0.16	139.2	14.6	630.0	1.7	120.0	0.3	415.5	1.6	94.5	0.2	365.7	10.1
	3.86	0.16	188.7	16.6	679.8	2.2	129.2	0.4	448.6	1.9	102.0	0.2	366.2	9.5
	4.43	0.20	225.0	19.3	720.0	2.1	136.8	0.4	475.2	1.8	108.0	0.3	367.3	9.1
80%JR+10% SD-0%OFA														
	3.31	0.17	306.8	37.7	629.8	2.6	120.0	0.4	509.9	2.3	0.0	0.0	356.9	8.8
	3.35	0.18	343.7	9.4	630.3	2.5	120.0	0.3	510.3	2.3	0.0	0.0	357.4	10.0
	3.37	0.23	317.8	40.9	630.1	2.5	120.0	0.3	510.1	2.3	0.0	0.0	357.2	10.3
	3.94	0.21	357.7	14.3	669.8	2.1	127.3	0.4	542.5	1.9	0.0	0.0	356.3	11.1
	5.28	0.20	428.9	15.5	720.0	2.7	136.8	0.5	583.1	2.3	0.0	0.0	356.5	8.8
80%JR+10% SD-15%OFA														
	2.82	0.20	148.2	10.7	630.0	2.0	120.0	0.4	415.5	1.8	94.5	0.2	355.9	9.8
	3.61	0.19	190.9	16.3	668.8	6.1	127.1	1.0	441.4	4.4	100.3	1.0	356.8	9.8
	4.68	0.21	260.5	16.9	720.2	3.4	136.8	0.5	475.4	3.0	108.0	0.3	357.2	8.8
	4.78	0.19	265.8	18.9	720.3	3.5	136.8	0.6	475.5	2.9	108.0	0.3	356.8	10.3

Table A-6B. Gas Flow Data for UBC Measurements from Test JR-7.

Test 7 – Co-milling of JR with SG and SD																
Unburned Carbon Data							----- FURNACE AIR FLOWS, SCFM (60°F, 29.92 in. Hg) ------								Fuel Feed	
Test Condition	FEO, Wet %		NOx, 3% O_2, ppm		% UBC		Total Air		Pri. Air (150°F)		Sec. Air (600°F)		OFA (600°F)		Rate, lb/hr	
	Avg.	S.D.	Avg.	S.D.	Avg.	S.D.	Avg.	S.D.	Avg.	S.D.	Avg.	S.D.	Avg.	S.D.	Avg.	S.D.
100%JR-0% OFA	2.55	0.35	309.3	21.7	0.11	0.01	630.1	2.7	120.0	0.3	510.2	2.6	0.0	0.0	352.5	2.6
	3.72	0.33	400.1	15.1	0.12	0.01	680.6	2.5	129.2	0.3	551.4	2.3	0.0	0.0	352.1	3.3
	4.71	0.32	416.7	19.3	0.24	0.10	730.0	3.0	138.8	0.3	591.2	2.8	0.0	0.0	352.2	3.6
100%JR-15% OFA	2.73	0.30	195.0	13.4	0.18	0.02	630.3	1.9	119.9	0.2	415.9	1.8	94.5	0.2	352.4	3.9
	3.72	0.36	206.4	10.0	0.14	0.01	740.3	2.4	140.6	0.3	488.7	2.1	111.0	0.2	381.7	4.0
	4.48	0.31	259.6	26.1	0.12	0.00	719.9	3.9	136.8	0.4	475.1	3.3	108.0	0.5	351.5	3.9
90%JR+10% SG-0%OFA	2.74	0.26	281.1	19.4	0.20	0.02	630.4	2.9	120.0	0.3	510.4	2.8	0.0	0.0	357.6	4.9
	3.81	0.26	332.1	18.4	0.14	0.01	679.9	3.3	129.2	0.4	550.7	3.0	0.0	0.0	357.8	5.1
	4.50	0.44	313.2	38.2	0.14	0.00	718.8	3.1	136.8	0.5	582.0	2.8	0.0	0.0	357.1	5.1
90%JR+10% SG-15%OFA	2.74	0.20	138.4	15.8	0.18	0.00	630.3	1.9	120.0	0.3	415.9	1.8	94.5	0.2	357.3	5.9
	3.77	0.34	187.4	24.9	0.15	0.01	680.3	2.1	129.3	0.4	449.1	1.6	102.0	0.3	356.8	5.2
	4.70	0.31	238.1	22.7	0.14	0.00	720.2	3.6	136.8	0.5	475.3	3.1	108.0	0.4	357.1	4.9
80%JR+20% SG-0%OFA	3.87	0.33	319.3	22.6	0.23	0.00	700.3	3.3	133.0	0.5	567.3	3.1	0.0	0.0	366.1	12.2
	4.54	0.22	343.5	15.3	0.24	0.02	739.9	3.0	140.5	0.6	599.4	2.7	0.0	0.0	365.7	11.7
80%JR+20% SG-15%OFA	2.72	0.20	141.8	8.9	0.62	0.02	631.9	1.8	120.2	0.3	417.0	1.5	94.7	0.2	371.7	4.1
	3.32	0.33	154.9	16.3	0.24	0.01	669.9	2.3	127.3	0.5	442.1	1.8	100.5	0.3	366.4	9.7
	4.22	0.22	212.7	20.3	0.23	0.01	709.0	2.6	134.9	0.6	467.7	1.9	106.5	0.3	367.7	6.2
80%JR+20% SD-0%OFA	2.37	0.18	265.3	11.7	0.18	0.03	630.4	1.9	120.0	0.3	510.5	1.8	0.0	0.0	367.0	7.9
	3.19	0.23	316.3	15.4	0.18	0.03	670.5	4.2	127.3	0.4	543.2	4.0	0.0	0.0	366.8	7.4
	4.34	0.27	357.4	18.4	0.18	0.02	719.6	3.1	136.8	0.5	582.8	2.9	0.0	0.0	367.9	8.0
80%JR+20% SD-15%OFA	2.41	0.17	138.7	12.2	0.37	0.00	630.0	1.9	119.9	0.3	415.6	1.7	94.5	0.2	365.1	10.6
	3.87	0.24	183.7	11.3	0.19	0.03	679.6	2.3	129.2	0.4	448.5	1.9	102.0	0.2	366.6	8.9
	4.42	0.21	222.0	20.4	0.14	0.01	719.7	2.2	136.8	0.5	474.9	1.7	108.0	0.3	366.7	8.7
80%JR+10% SD-0%OFA	3.37	0.23	317.8	40.9	0.19	0.07	630.1	2.5	120.0	0.3	510.1	2.3	0.0	0.0	357.2	10.3
	3.96	0.24	351.2	25.5	0.16	0.04	669.9	2.4	127.3	0.4	542.6	2.1	0.0	0.0	356.0	10.8
	5.31	0.42	425.8	16.2	0.11	0.00	720.0	3.0	136.8	0.5	583.2	2.6	0.0	0.0	356.9	8.9
80%JR+10% SD-15%OFA	2.87	0.22	150.0	10.7	0.17	0.01	630.1	1.8	120.0	0.4	415.6	1.5	94.5	0.2	356.4	10.3
	3.58	0.15	193.1	16.2	0.18	0.02	669.7	1.8	127.3	0.4	441.9	1.5	100.5	0.3	357.1	10.1
	4.78	0.19	265.8	18.9	0.14	0.01	720.3	3.5	136.8	0.6	475.5	2.9	108.0	0.3	356.8	10.3

Table A-6C. Gas Sampling Data from Test JR-7.

Test 7 – Co-milling of JR with SG and SD														
Gas Sampling Data														
Test Condition	FEO, Wet %		NO_x, 3% O_2, ppm		CO, 3% O_2, ppm		CO_2, 3% O_2, %		SO_2, 3% O_2, ppm		SO_2, lb/10^6Btu		NO_x, lb/10^6Btu	
	Avg.	S.D.	Avg.	S.D.	Avg.	S.D.	Avg.	S.D.	Avg.	S.D.	Avg.	S.D.	Avg.	S.D.
100%JR-0% OFA														
	2.49	0.18	306.9	17.0	104.6	3.9	18.6	0.3	301.9	4.8	0.41	0.01	0.42	0.02
	2.55	0.35	309.3	21.7	104.4	3.3	18.5	0.3	302.4	5.8	0.41	0.01	0.42	0.03
	3.59	0.16	396.9	14.3	112.4	3.4	18.7	0.3	295.0	5.6	0.40	0.01	0.54	0.02
	3.72	0.33	400.1	15.1	113.3	3.4	18.7	0.3	296.0	6.0	0.40	0.01	0.54	0.02
	4.58	0.12	413.4	14.7	99.3	3.3	17.9	0.3	257.8	9.6	0.35	0.01	0.56	0.02
	4.71	0.32	416.7	19.3	99.0	3.8	17.8	0.4	253.5	6.3	0.34	0.01	0.57	0.03
100%JR-15% OFA														
	2.70	0.16	172.6	10.2	120.2	4.4	18.9	0.6	286.6	9.0	0.39	0.01	0.23	0.01
	2.73	0.30	195.0	13.4	135.9	6.0	21.3	0.8	322.8	13.6	0.44	0.02	0.27	0.02
	3.61	0.19	240.3	14.0	123.9	4.5	18.5	0.7	261.4	9.2	0.36	0.01	0.33	0.02
	3.72	0.36	206.4	10.0	113.3	3.4	18.7	0.3	296.0	6.0	0.40	0.01	0.54	0.02
	4.39	0.09	257.3	20.1	116.2	3.1	18.7	0.3	280.9	7.3	0.38	0.01	0.35	0.03
	4.48	0.31	259.6	26.1	117.0	3.9	18.6	0.4	275.7	13.3	0.38	0.02	0.35	0.04
90%JR+10% SG-0%OFA														
	2.58	0.18	273.7	16.2	86.6	3.7	17.7	0.2	218.9	8.1	0.30	0.01	0.37	0.02
	2.77	0.14	282.5	14.5	86.4	2.7	17.7	0.3	224.8	8.8	0.31	0.01	0.38	0.02
	3.65	0.18	333.2	15.4	94.0	3.5	17.7	0.5	211.0	9.3	0.29	0.01	0.45	0.02
	3.81	0.26	332.1	18.4	95.7	12.4	17.6	0.6	211.5	11.0	0.29	0.01	0.45	0.03
	4.51	0.21	356.5	12.0	91.9	3.0	17.6	0.4	230.2	9.9	0.31	0.01	0.49	0.02
90%JR+10% SG-15%OFA														
	2.71	0.12	136.4	8.3	84.9	2.5	17.7	0.3	263.7	9.5	0.36	0.01	0.19	0.01
	3.76	0.13	184.6	14.7	88.1	3.2	17.6	0.4	251.3	9.2	0.34	0.01	0.25	0.02
	4.66	0.15	236.5	16.5	91.6	2.8	17.6	0.4	242.3	11.8	0.33	0.02	0.32	0.02
80%JR+20% SG-0%OFA														
	3.81	0.19	318.1	19.0	88.5	3.1	17.1	0.4	167.8	13.6	0.23	0.02	0.43	0.03
	4.54	0.21	338.8	14.7	90.6	3.3	17.0	0.4	161.7	11.1	0.22	0.02	0.46	0.02
80%JR+20% SG-15%OFA														
	2.72	0.20	141.8	8.9	86.5	3.2	17.3	0.3	189.6	10.2	0.26	0.01	0.19	0.01
	3.33	0.26	158.7	20.4	87.9	2.1	17.1	0.4	197.4	13.9	0.27	0.02	0.22	0.03
	3.77	0.21	202.9	19.6	87.9	2.6	17.5	0.4	188.5	11.1	0.26	0.02	0.28	0.03
	4.22	0.22	212.7	20.3	93.6	40.9	17.4	0.5	170.5	11.0	0.23	0.01	0.29	0.04
	4.30	0.17	224.4	22.6	89.0	3.2	17.3	0.4	173.8	10.6	0.24	0.01	0.31	0.03
80%JR+20% SD-0%OFA														
	2.39	0.20	267.2	20.0	86.0	2.9	17.3	0.4	191.8	9.5	0.26	0.01	0.36	0.03
	3.22	0.22	313.0	18.6	91.9	34.0	17.3	0.4	184.3	10.6	0.25	0.01	0.43	0.03
	4.29	0.19	359.1	11.6	90.9	2.6	17.1	0.3	172.5	9.1	0.23	0.01	0.49	0.02
80%JR+20% SD-15%OFA														
	2.45	0.16	139.2	14.6	88.8	2.7	17.3	0.4	264.0	30.1	0.36	0.04	0.19	0.02
	3.86	0.16	188.7	16.6	83.6	2.7	17.3	0.4	189.3	9.1	0.26	0.01	0.26	0.02
	4.43	0.20	225.0	19.3	85.6	3.7	17.2	0.6	179.3	11.5	0.24	0.02	0.31	0.03
80%JR+10% SD-0%OFA														
	3.31	0.17	306.8	37.7	87.3	3.7	17.1	0.3	212.7	11.5	0.29	0.02	0.42	0.05
	3.35	0.18	343.7	9.4	87.3	2.5	17.1	0.3	210.0	9.2	0.29	0.01	0.47	0.01
	3.37	0.23	317.8	40.9	87.7	3.1	17.1	0.4	213.8	11.1	0.29	0.02	0.44	0.06
	3.94	0.21	357.7	14.3	87.0	3.0	17.0	0.5	201.3	9.2	0.27	0.01	0.49	0.02
	5.28	0.20	428.9	15.5	93.6	3.2	16.8	0.5	200.0	10.8	0.27	0.01	0.58	0.02
80%JR+10% SD-15%OFA														
	2.82	0.20	148.2	10.7	79.7	2.3	17.2	0.3	213.7	10.0	0.29	0.01	0.20	0.01
	3.61	0.19	190.9	16.3	82.8	2.5	17.1	0.4	204.7	10.7	0.28	0.01	0.26	0.02
	4.68	0.21	260.5	16.9	85.8	2.3	16.9	0.4	201.8	9.0	0.27	0.01	0.35	0.02
	4.78	0.19	265.8	18.9	86.5	3.6	16.8	0.8	204.2	15.4	0.28	0.02	0.38	0.06

Table A-6D. Gas Sampling Data for UBC Measurements from Test JR-7.

Test 7 - Co-milling of JR with SG and SD																
Unburned Carbon Data																
Test Condition	FEO, Wet %		NOx, 3% O_2, ppm		% UBC		CO, 3% O_2, ppm		CO_2, 3% O_2, %		SO_2, 3% O_2, ppm		SO_2, lb/10^6Btu		NO_x, lb/10^6Btu	
	Avg.	S.D.	Avg.	S.D.	Avg.	S.D.	Avg.	S.D.	Avg.	S.D.	Avg.	S.D.	Avg.	S.D.	Avg.	S.D.
100%JR-0% OFA																
	2.55	0.35	309.3	21.7	0.11	0.01	104.4	3.3	18.5	0.3	302.4	5.8	0.41	0.01	0.42	0.03
	3.72	0.33	400.1	15.1	0.12	0.01	113.3	3.4	18.7	0.3	296.0	6.0	0.40	0.01	0.54	0.02
	4.71	0.32	416.7	19.3	0.24	0.10	99.0	3.8	17.8	0.4	253.5	6.3	0.34	0.01	0.57	0.03
100%JR-15% OFA																
	2.73	0.30	195.0	13.4	0.18	0.02	135.9	6.0	21.3	0.8	322.8	13.6	0.44	0.02	0.27	0.02
	3.72	0.36	206.4	10.0	0.14	0.01	108.2	3.8	15.7	0.4	221.8	6.5	0.30	0.01	0.28	0.01
	4.48	0.31	259.6	26.1	0.12	0.00	117.0	3.9	18.6	0.4	275.7	13.3	0.38	0.02	0.35	0.04
90%JR+10% SG-0%OFA																
	2.74	0.26	281.1	19.4	0.20	0.02	86.7	2.7	17.7	0.4	220.5	9.9	0.30	0.01	0.39	0.03
	3.81	0.26	332.1	18.4	0.14	0.01	95.7	12.4	17.6	0.6	211.5	11.0	0.29	0.01	0.45	0.03
	4.50	0.44	313.2	38.2	0.14	0.00	94.5	2.5	17.7	0.5	205.1	11.7	0.28	0.02	0.43	0.05
90%JR+10% SG-15%OFA																
	2.74	0.20	138.4	15.8	0.18	0.00	84.7	2.6	17.6	0.3	266.2	11.3	0.36	0.02	0.19	0.03
	3.77	0.34	187.4	24.9	0.15	0.01	87.0	2.9	17.6	0.4	248.9	9.7	0.34	0.01	0.26	0.03
	4.70	0.31	238.1	22.7	0.14	0.00	91.9	2.4	17.6	0.5	238.7	12.7	0.32	0.02	0.32	0.03
80%JR+20% SG-0%OFA																
	3.87	0.33	319.3	22.6	0.23	0.00	98.1	58.1	17.1	0.7	166.4	15.5	0.23	0.02	0.45	0.05
	4.54	0.22	343.5	15.3	0.24	0.02	92.6	4.9	17.0	0.7	159.8	11.3	0.22	0.02	0.48	0.05
80%JR+20% SG-15%OFA																
	2.72	0.20	141.8	8.9	0.62	0.02	86.5	3.2	17.3	0.3	189.6	10.2	0.26	0.01	0.19	0.01
	3.32	0.33	154.9	16.3	0.24	0.01	88.6	3.6	17.1	0.6	200.9	13.6	0.27	0.02	0.23	0.06
	4.22	0.22	212.7	20.3	0.23	0.01	93.6	40.9	17.4	0.5	170.5	11.0	0.23	0.01	0.29	0.04
80%JR+20% SD-0%OFA																
	2.37	0.18	265.3	11.7	0.18	0.03	86.4	3.3	17.2	0.8	192.2	13.3	0.26	0.02	0.37	0.04
	3.19	0.23	316.3	15.4	0.18	0.03	90.8	29.5	17.1	0.7	186.0	11.5	0.25	0.02	0.44	0.03
	4.34	0.27	357.4	18.4	0.18	0.02	91.1	3.7	17.1	0.5	173.7	9.6	0.24	0.01	0.49	0.03
80%JR+20% SD-15%OFA																
	2.41	0.17	138.7	12.2	0.37	0.00	89.5	3.9	17.1	0.7	278.3	31.0	0.38	0.04	0.21	0.07
	3.87	0.24	183.7	11.3	0.19	0.03	84.5	3.8	17.2	0.7	190.4	10.9	0.26	0.01	0.26	0.05
	4.42	0.21	222.0	20.4	0.14	0.01	86.0	4.2	17.1	0.7	182.1	13.0	0.25	0.02	0.31	0.05
80%JR+10% SD-0%OFA																
	3.37	0.23	317.8	40.9	0.19	0.07	87.7	3.1	17.1	0.4	213.8	11.1	0.29	0.02	0.44	0.06
	3.96	0.24	351.2	25.5	0.16	0.04	87.8	2.8	17.0	0.5	204.0	9.6	0.28	0.01	0.49	0.05
	5.31	0.42	425.8	16.2	0.11	0.00	93.7	3.3	16.7	0.6	200.4	11.0	0.27	0.01	0.58	0.03
80%JR+10% SD-15%OFA																
	2.87	0.22	150.0	10.7	0.17	0.01	80.3	3.0	17.1	0.6	215.8	15.5	0.29	0.02	0.22	0.06
	3.58	0.15	193.1	16.2	0.18	0.02	83.6	3.9	17.0	0.7	206.7	14.9	0.28	0.02	0.28	0.06
	4.78	0.19	265.8	18.9	0.14	0.01	86.5	3.6	16.8	0.8	204.2	15.4	0.28	0.02	0.38	0.06

Table A-7A1. Gas Flow Data from Test JR-8, Part 1.

Test 8 - JR Coal with Core Injection of SG and SD														
Furnace Flow Data					------- FURNACE AIR FLOWS, SCFM (60°F, 29.92 in. Hg) ------								Fuel Feed	
Test Condition	FEO, Wet %		NOx, 3% O_2, ppm		Total Air		Pri. Air (150°F)		Sec. Air (600°F)		OFA (600°F)		Rate, lb/hr	
	Avg.	S.D.	Avg.	S.D.	Avg.	S.D.	Avg.	S.D.	Avg.	S.D.	Avg.	S.D.	Avg.	S.D.
100%JR-0% OFA - NO flow through burner core biomass injector														
	2.66	0.19	260.4	12.6	630.5	1.8	120.0	0.3	510.5	1.7	0.0	0.0	362.9	5.2
	3.57	0.23	345.2	11.1	669.9	2.2	127.3	0.4	542.6	2.0	0.0	0.0	363.0	5.7
	4.52	0.23	240.1	13.9	710.1	2.3	134.9	0.4	575.2	2.1	0.0	0.0	362.3	5.4
100%JR-15% OFA - NO flow through burner core biomass injector														
	2.77	0.15	152.6	12.0	630.0	2.1	120.0	0.3	415.6	1.9	94.5	0.2	363.2	6.0
	3.84	0.22	171.2	12.6	670.1	1.8	127.3	0.4	442.3	1.4	100.5	0.2	363.1	6.1
	3.92	0.22	199.1	17.0	669.9	3.4	127.3	0.4	442.1	3.0	100.5	0.4	361.9	7.3
	4.52	0.24	324.6	13.6	709.9	2.8	134.9	0.4	468.5	2.5	106.5	0.2	362.5	5.7
90%JR+10% SG-0%OFA														
	2.56	0.28	230.7	12.8	606.2	2.4	120.0	0.3	486.2	2.4	0.0	0.0	333.2	5.9
	2.61	0.31	236.4	14.0	606.4	2.5	120.0	0.3	486.4	2.4	0.0	0.0	332.8	6.4
	3.42	0.21	302.7	12.4	639.8	3.1	121.6	0.4	518.2	3.0	0.0	0.0	333.7	6.0
	4.55	0.16	359.1	12.4	700.0	2.4	133.0	0.3	567.0	2.3	0.0	0.0	334.0	6.1
	4.62	0.17	350.4	15.2	700.1	2.6	133.0	0.3	567.1	2.6	0.0	0.0	334.6	5.2
90%JR+10% SG-15%OFA														
	2.77	0.18	175.2	16.2	605.9	2.4	120.0	0.3	395.8	2.3	90.0	0.2	334.1	5.8
	2.81	0.24	170.1	16.4	606.4	3.1	120.1	0.3	396.3	2.9	90.1	0.2	334.3	5.7
	3.66	0.16	203.1	14.4	639.9	3.1	121.6	0.3	422.3	2.9	96.0	0.3	333.9	5.9
	4.42	0.14	283.7	13.1	680.6	4.1	129.2	0.4	449.4	3.7	102.0	0.4	332.8	6.0
80%JR+20% SG-0%OFA														
	3.20	0.23	350.4	15.3	597.8	3.1	120.0	0.3	477.8	3.0	0.0	0.0	305.1	6.2
	3.48	0.17	375.8	15.5	640.0	1.7	121.6	0.3	518.4	1.5	0.0	0.0	304.6	6.0
	3.85	0.25	441.4	40.4	640.4	3.2	121.6	0.3	518.8	3.1	0.0	0.0	304.0	5.9
	3.96	0.21	465.1	21.7	640.4	3.5	121.6	0.3	518.7	3.3	0.0	0.0	304.2	5.7
	4.36	0.19	403.6	10.8	660.3	2.7	125.4	0.3	534.8	2.6	0.0	0.0	305.2	5.4

Table A-7A2. Gas Flow Data from Test JR-8, Part 2.

Test 8 - JR Coal with Core Injection of SG and SD														
Furnace Flow Data					------- FURNACE AIR FLOWS, SCFM (60°F, 29.92 in. Hg) ------								Fuel Feed	
Test Condition	FEO, Wet %		NOx, 3% O_2, ppm		Total Air		Pri. Air (150°F)		Sec. Air (600°F)		OFA (600°F)		Rate, lb/hr	
	Avg.	S.D.	Avg.	S.D.	Avg.	S.D.	Avg.	S.D.	Avg.	S.D.	Avg.	S.D.	Avg.	S.D.
80%JR+20% SG-15%OFA														
	2.40	0.35	170.0	17.4	581.7	2.7	120.0	0.3	376.2	2.5	85.5	0.3	304.8	6.1
	2.60	0.45	176.2	21.7	581.4	2.3	120.0	0.3	375.9	2.2	85.5	0.2	304.6	5.6
	3.76	0.22	247.0	16.5	630.0	2.1	120.0	0.3	415.5	1.9	94.5	0.2	304.8	5.8
	3.86	0.21	249.7	18.9	630.3	2.7	120.0	0.4	415.9	2.4	94.5	0.3	304.9	5.8
	3.93	0.20	254.3	15.2	630.5	2.5	120.0	0.4	416.1	2.3	94.5	0.2	305.5	6.2
	4.01	0.19	227.8	17.0	649.6	2.0	123.5	0.3	428.6	1.8	97.5	0.2	305.0	5.1
	4.27	0.15	290.7	14.5	679.9	1.7	129.2	0.3	448.7	1.5	102.0	0.2	304.2	6.2
90%JR+10% SD-0%OFA														
	2.48	0.25	241.6	14.3	572.3	9.0	120.0	0.5	452.3	8.7	0.0	0.0	334.7	4.3
	2.53	0.35	245.0	15.3	573.5	4.8	120.0	0.3	453.5	4.7	0.0	0.0	334.7	4.4
	3.59	0.31	296.7	9.8	601.4	3.0	120.0	0.4	481.4	2.9	0.0	0.0	334.9	4.0
	4.42	0.28	396.2	13.1	679.4	5.5	129.0	0.9	550.4	4.8	0.0	0.0	336.0	4.9
	4.50	0.25	400.6	13.8	680.6	3.3	129.2	0.3	551.4	3.2	0.0	0.0	336.0	4.5
90%JR+10% SD-15%OFA														
	3.19	0.21	241.8	15.4	598.6	2.4	120.0	0.3	390.0	2.3	88.5	0.2	333.3	5.6
	3.24	0.35	244.0	17.5	598.4	2.5	120.0	0.3	389.8	2.4	88.5	0.2	333.4	5.5
	3.70	0.24	233.7	14.6	629.7	2.0	120.0	0.3	415.2	1.9	94.5	0.2	335.3	5.6
	3.72	0.16	282.5	17.1	630.1	2.1	120.0	0.3	415.6	2.0	94.5	0.2	334.3	6.5
	3.79	0.24	261.9	14.5	630.2	2.1	120.0	0.3	415.7	2.0	94.5	0.2	333.9	5.8
	5.03	0.16	339.9	13.9	679.8	2.2	129.2	0.4	448.6	1.9	102.0	0.2	334.9	5.1
85%JR+15% SD-0%OFA														
	2.73	0.14	275.1	8.8	581.6	2.8	120.0	0.3	461.6	2.7	0.0	0.0	313.8	5.7
	2.79	0.21	268.4	13.4	582.3	2.7	120.0	0.2	462.3	2.7	0.0	0.0	314.4	5.6
	4.26	0.28	372.0	12.7	630.2	2.4	119.9	0.3	510.2	2.2	0.0	0.0	315.1	6.5
	5.04	0.12	361.9	12.9	680.6	2.4	129.2	0.3	551.4	2.3	0.0	0.0	314.0	4.4
	5.11	0.27	364.9	16.0	680.5	2.5	129.2	0.3	551.3	2.3	0.0	0.0	314.0	4.5
85%JR+15% SD-15%OFA														
	2.89	0.21	186.2	16.4	581.5	2.4	120.0	0.3	376.1	2.2	85.5	0.2	314.5	5.5
	2.94	0.22	189.4	17.7	581.2	1.8	120.0	0.3	375.7	1.6	85.5	0.2	314.1	5.3
	3.79	0.26	238.3	16.2	632.4	5.6	120.3	0.7	417.2	4.3	94.8	0.7	335.7	5.3
	3.80	0.28	250.3	18.9	621.9	2.3	120.0	0.4	408.9	1.9	93.0	0.3	314.1	5.1
	3.84	0.31	232.8	16.6	622.2	2.3	120.0	0.3	409.2	2.1	93.0	0.2	314.0	4.2
	5.27	0.30	326.3	14.4	680.0	2.6	129.2	0.3	448.8	2.4	102.0	0.2	313.5	5.8

Table A-7B. Gas Flow Data for UBC Measurements from Test JR-8.

Test 8 - JR Coal with Core Injection of SG and SD																
Unburned Carbon Data							----- FURNACE AIR FLOWS, SCFM (60°F, 29.92 in. Hg) ------								Fuel Feed	
Test Condition	FEO, Wet %		NOx, 3% O_2, ppm		% UBC		Total Air		Pri. Air (150°F)		Sec. Air (600°F)		OFA (600°F)		Rate, lb/hr	
	Avg.	S.D.	Avg.	S.D.	Avg.	S.D.	Avg.	S.D.	Avg.	S.D.	Avg.	S.D.	Avg.	S.D.	Avg.	S.D.
100%JR-0% OFA - NO flow through burner core biomass injector																
	2.64	0.20	263.8	13.5	0.09	0.01	630.6	1.8	120.0	0.3	510.6	1.7	0.0	0.0	362.7	5.1
	3.60	0.32	342.5	13.0	0.10	0.01	669.7	2.2	127.2	0.4	542.5	1.9	0.0	0.0	362.5	6.0
	4.57	0.24	321.2	12.1	0.08	0.02	709.9	2.0	134.9	0.4	575.0	1.9	0.0	0.0	362.3	6.2
100%JR-15% OFA - NO flow through burner core biomass injector																
	2.73	0.19	153.1	13.4	0.10	0.01	630.2	2.4	120.0	0.3	415.7	2.1	94.5	0.2	363.7	6.1
	3.90	0.21	194.8	14.9	0.12	0.02	669.6	2.3	127.3	0.4	441.8	1.9	100.5	0.3	362.1	7.1
	4.50	0.20	243.8	11.9	0.08	0.00	710.0	2.2	134.9	0.3	468.6	1.9	106.5	0.2	362.2	5.7
90%JR+10% SG-0%OFA																
	2.61	0.31	236.4	14.0	0.13	0.01	606.4	2.5	120.0	0.3	486.4	2.4	0.0	0.0	332.8	6.4
	3.45	0.22	305.2	12.2	0.16	0.01	639.8	3.1	121.6	0.4	518.2	3.0	0.0	0.0	334.0	6.2
	4.62	0.17	350.4	15.2	0.18	0.04	700.1	2.6	133.0	0.3	567.1	2.6	0.0	0.0	334.6	5.2
90%JR+10% SG-15%OFA																
	2.81	0.24	170.1	16.4	0.18	0.02	606.4	3.1	120.1	0.3	396.3	2.9	90.1	0.2	334.3	5.7
	3.67	0.15	204.6	14.2	0.17	0.01	640.3	2.9	121.6	0.3	422.8	2.6	96.0	0.3	333.9	6.2
	4.42	0.14	286.4	15.3	0.11	0.03	680.3	2.4	129.2	0.4	449.1	2.2	102.0	0.2	333.1	6.1
80%JR+20% SG-0%OFA																
	3.18	0.22	350.0	14.8	0.31	0.02	598.1	2.1	120.0	0.3	478.1	2.0	0.0	0.0	305.2	6.4
	3.85	0.25	441.4	40.4	0.45	0.04	640.4	3.2	121.6	0.3	518.8	3.1	0.0	0.0	304.0	5.9
	4.35	0.20	403.3	10.9	0.20	0.01	660.3	2.7	125.4	0.3	534.9	2.6	0.0	0.0	305.1	5.3
80%JR+20% SG-15%OFA																
	2.60	0.45	176.2	21.7	0.85	0.05	581.4	2.3	120.0	0.3	375.9	2.2	85.5	0.2	304.6	5.6
	3.86	0.21	249.7	18.9	0.81	0.28	630.3	2.7	120.0	0.4	415.9	2.4	94.5	0.3	305.0	5.9
	4.27	0.17	293.9	19.3	0.75	0.11	679.9	2.3	129.2	0.4	448.7	1.9	102.0	0.2	304.5	6.3
90%JR+10% SD-0%OFA																
	2.53	0.35	245.0	15.3	0.23	0.04	573.5	4.8	120.0	0.3	453.5	4.7	0.0	0.0	334.7	4.4
	3.56	0.21	298.3	12.3	0.15	0.01	601.1	2.6	120.0	0.3	481.1	2.5	0.0	0.0	334.5	4.8
	4.42	0.28	396.2	13.1	0.23	0.06	679.4	5.5	129.0	0.9	550.4	4.8	0.0	0.0	336.0	4.9
90%JR+10% SD-15%OFA																
	3.19	0.21	241.8	15.4	0.40	0.04	598.6	2.4	120.0	0.3	390.0	2.3	88.5	0.2	333.2	5.5
	3.80	0.26	261.7	14.4	0.39	0.05	629.9	2.3	120.0	0.3	415.5	2.2	94.5	0.2	334.1	5.5
	5.09	0.16	338.2	14.4	0.20	0.06	680.1	2.4	129.2	0.4	448.9	2.1	102.0	0.3	335.1	5.0
85%JR+15% SD-0%OFA																
	2.79	0.21	268.4	13.4	0.27	0.02	582.3	2.7	120.0	0.2	462.3	2.7	0.0	0.0	314.4	5.6
	4.30	0.25	378.5	16.2	0.21	0.01	630.0	2.3	119.9	0.3	510.1	2.2	0.0	0.0	314.6	6.7
	5.11	0.27	364.9	16.0	0.12	0.00	680.5	2.5	129.2	0.3	551.3	2.3	0.0	0.0	314.0	4.5
85%JR+15% SD-15%OFA																
	2.94	0.22	189.4	17.7	0.32	0.04	581.2	1.8	120.0	0.3	375.7	1.6	85.5	0.2	314.1	5.3
	3.79	0.26	238.3	16.2	0.21	0.03	632.4	5.6	120.3	0.7	417.2	4.3	94.8	0.7	335.7	5.3
	3.80	0.28	250.3	18.9	0.33	0.03	621.9	2.3	120.0	0.4	408.9	1.9	93.0	0.3	314.1	5.1
	5.28	0.32	326.2	15.3	0.17	0.01	680.0	2.3	129.2	0.4	448.8	2.0	102.0	0.2	313.4	5.9

Table A-7C1. Gas Sampling Data from Test JR-8, Part 1.

Test 8 - JR Coal with Core Injection of SG and SD														
Gas Sampling Data														
Test Condition	FEO, Wet %		NO_x, 3% O_2, ppm		CO, 3% O_2, ppm		CO_2, 3% O_2, %		SO_2, 3% O_2, ppm		SO_2, lb/10^6Btu		NO_x, lb/10^6Btu	
	Avg.	S.D.	Avg.	S.D.	Avg.	S.D.	Avg.	S.D.	Avg.	S.D.	Avg.	S.D.	Avg.	S.D.
100%JR-0% OFA - NO flow through burner core biomass injector														
	2.66	0.19	260.4	12.6	84.2	1.9	17.2	0.2	243.5	16.6	0.33	0.02	0.35	0.02
	3.57	0.23	345.2	11.1	85.6	2.6	17.1	0.3	238.2	15.4	0.32	0.02	0.47	0.02
	4.52	0.23	240.1	13.9	88.0	2.3	17.0	0.3	233.9	18.2	0.32	0.02	0.33	0.02
100%JR-15% OFA - NO flow through burner core biomass injector														
	2.77	0.15	152.6	12.0	83.7	2.1	17.2	0.2	240.2	16.6	0.33	0.02	0.21	0.02
	3.84	0.22	171.2	12.6	85.4	2.3	17.1	0.2	242.7	15.2	0.33	0.02	0.23	0.02
	3.92	0.22	199.1	17.0	92.3	3.0	17.3	0.3	245.4	18.0	0.33	0.02	0.27	0.02
	4.52	0.24	324.6	13.6	89.0	2.7	17.0	0.3	235.3	18.2	0.32	0.02	0.44	0.02
90%JR+10% SG-0%OFA														
	2.56	0.28	230.7	12.8	85.6	2.3	17.1	0.2	222.5	15.6	0.30	0.02	0.31	0.02
	2.61	0.31	236.4	14.0	84.9	1.8	17.0	0.2	222.9	15.8	0.30	0.02	0.32	0.02
	3.42	0.21	302.7	12.4	86.7	2.5	16.9	0.2	207.8	15.8	0.28	0.02	0.41	0.02
	4.55	0.16	359.1	12.4	98.5	2.7	16.6	0.2	189.3	18.6	0.26	0.03	0.49	0.02
	4.62	0.17	350.4	15.2	98.7	2.6	16.6	0.3	183.5	19.4	0.25	0.03	0.48	0.02
90%JR+10% SG-15%OFA														
	2.77	0.18	175.2	16.2	82.9	2.0	17.1	0.2	217.6	16.2	0.30	0.02	0.24	0.02
	2.81	0.24	170.1	16.4	82.7	2.2	17.1	0.2	221.9	20.2	0.30	0.03	0.23	0.02
	3.66	0.16	203.1	14.4	84.0	2.6	17.1	0.2	217.9	17.6	0.30	0.02	0.28	0.02
	4.42	0.14	283.7	13.1	89.2	2.3	16.9	0.3	199.4	19.0	0.27	0.03	0.39	0.02
80%JR+20% SG-0%OFA														
	3.20	0.23	350.4	15.3	99.6	2.4	17.1	0.2	172.0	15.5	0.23	0.02	0.48	0.02
	3.48	0.17	375.8	15.5	101.7	2.3	17.1	0.2	147.5	15.7	0.20	0.02	0.51	0.02
	3.85	0.25	441.4	40.4	104.4	2.9	17.1	0.2	148.9	16.7	0.20	0.02	0.60	0.05
	3.96	0.21	465.1	21.7	105.3	2.4	17.0	0.2	150.2	17.7	0.20	0.02	0.63	0.03
	4.36	0.19	403.6	10.8	106.7	2.3	17.0	0.2	153.2	16.5	0.21	0.02	0.55	0.01
80%JR+20% SG-15%OFA														
	2.40	0.35	170.0	17.4	95.2	2.7	17.3	0.2	173.1	14.0	0.24	0.02	0.23	0.02
	2.60	0.45	176.2	21.7	95.8	2.6	17.3	0.2	172.4	14.2	0.23	0.02	0.24	0.03
	3.76	0.22	247.0	16.5	102.1	2.7	17.1	0.2	175.1	16.7	0.24	0.02	0.34	0.02
	3.86	0.21	249.7	18.9	103.0	2.8	17.1	0.3	169.0	15.5	0.23	0.02	0.34	0.03
	3.93	0.20	254.3	15.2	103.5	3.0	17.1	0.3	169.2	16.4	0.23	0.02	0.35	0.02
	4.01	0.19	227.8	17.0	98.3	2.9	16.9	0.2	170.0	16.1	0.23	0.02	0.31	0.02
	4.27	0.15	290.7	14.5	106.4	2.4	17.0	0.2	144.9	15.0	0.20	0.02	0.40	0.02

Table A-7C2. Gas Sampling Data from Test JR-8, Part 2.

Test 8 - JR Coal with Core Injection of SG and SD														
Gas Sampling Data														
Test Condition	FEO, Wet %		NOx, 3% O_2, ppm		CO, 3% O_2, ppm		CO_2, 3% O_2, %		SO_2, 3% O_2, ppm		SO_2, lb/10^6Btu		NO_x, lb/10^6Btu	
	Avg.	S.D.	Avg.	S.D.	Avg.	S.D.	Avg.	S.D.	Avg.	S.D.	Avg.	S.D.	Avg.	S.D.
90%JR+10% SD-0%OFA														
	2.48	0.25	241.6	14.3	90.0	4.0	17.4	0.2	197.2	19.7	0.27	0.03	0.33	0.02
	2.53	0.35	245.0	15.3	92.2	2.4	17.3	0.2	202.9	22.1	0.28	0.03	0.33	0.02
	3.59	0.31	296.7	9.8	89.7	2.2	17.3	0.2	186.1	16.7	0.25	0.02	0.40	0.01
	4.42	0.28	396.2	13.1	104.3	2.5	16.9	0.2	153.5	14.7	0.21	0.02	0.54	0.02
	4.50	0.25	400.6	13.8	105.0	2.9	16.9	0.2	156.8	16.1	0.21	0.02	0.54	0.02
90%JR+10% SD-15%OFA														
	3.19	0.21	241.8	15.4	88.0	2.8	17.4	0.2	224.4	17.5	0.31	0.02	0.33	0.02
	3.24	0.35	244.0	17.5	87.9	2.8	17.4	0.2	224.1	18.6	0.30	0.03	0.33	0.02
	3.70	0.24	233.7	14.6	99.5	2.4	17.1	0.2	170.5	14.9	0.23	0.02	0.32	0.02
	3.72	0.16	282.5	17.1	90.7	2.7	17.3	0.2	190.7	17.4	0.26	0.02	0.38	0.02
	3.79	0.24	261.9	14.5	89.1	2.3	17.4	0.2	209.8	19.6	0.29	0.03	0.36	0.02
	5.03	0.16	339.9	13.9	99.0	3.3	17.2	0.2	170.6	20.7	0.23	0.03	0.46	0.02
85%JR+15% SD-0%OFA														
	2.73	0.14	275.1	8.8	84.4	2.6	17.2	0.2	156.0	16.4	0.21	0.02	0.37	0.01
	2.79	0.21	268.4	13.4	84.8	2.8	17.2	0.2	159.0	17.2	0.22	0.02	0.37	0.02
	4.26	0.28	372.0	12.7	87.1	2.6	17.0	0.3	136.5	17.6	0.19	0.02	0.51	0.02
	5.04	0.12	361.9	12.9	93.8	3.3	16.8	0.2	134.4	20.6	0.18	0.03	0.49	0.02
	5.11	0.27	364.9	16.0	93.9	3.4	16.9	0.2	130.3	21.2	0.18	0.03	0.50	0.02
85%JR+15% SD-15%OFA														
	2.89	0.21	186.2	16.4	84.7	2.3	17.3	0.3	170.0	18.8	0.23	0.03	0.25	0.02
	2.94	0.22	189.4	17.7	84.2	2.6	17.3	0.2	169.3	19.0	0.23	0.03	0.26	0.02
	3.79	0.26	238.3	16.2	99.9	3.0	17.1	0.2	169.1	15.6	0.23	0.02	0.32	0.02
	3.80	0.28	250.3	18.9	93.7	3.5	17.0	0.2	153.2	18.5	0.21	0.03	0.34	0.03
	3.84	0.31	232.8	16.6	95.8	3.3	17.0	0.3	160.7	18.3	0.22	0.02	0.32	0.02
	5.27	0.30	326.3	14.4	91.8	2.9	16.9	0.2	134.2	20.8	0.18	0.03	0.44	0.02

Table A-7D. Gas Sampling Data for UBC Measurements from Test JR-8.

Test 8 - JR Coal with Core Injection of SG and SD																
Unburned Carbon Data																
Test Condition	FEO, Wet %		NOx, 3% O_2, ppm		% UBC		CO, 3% O_2, ppm		CO_2, 3% O_2, %		SO_2, 3% O_2, ppm		SO_2, lb/10^6Btu		NO_x, lb/10^6Btu	
	Avg.	S.D.	Avg.	S.D.	Avg.	S.D.	Avg.	S.D.	Avg.	S.D.	Avg.	S.D.	Avg.	S.D.	Avg.	S.D.
100%JR-0% OFA - NO flow through burner core biomass injector																
	2.64	0.20	263.8	13.5	0.09	0.01	84.3	1.9	17.1	0.2	242.1	16.1	0.33	0.02	0.36	0.02
	3.60	0.32	342.5	13.0	0.10	0.01	85.5	2.5	17.1	0.3	240.8	16.6	0.33	0.02	0.47	0.02
	4.57	0.24	321.2	12.1	0.08	0.02	89.3	2.8	17.0	0.2	235.9	17.9	0.32	0.02	0.44	0.02
100%JR-15% OFA - NO flow through burner core biomass injector																
	2.73	0.19	153.1	13.4	0.10	0.01	83.6	2.3	17.2	0.2	239.3	16.1	0.33	0.02	0.21	0.02
	3.90	0.21	194.8	14.9	0.12	0.02	91.4	2.7	17.3	0.4	246.3	17.8	0.34	0.02	0.26	0.02
	4.50	0.20	243.8	11.9	0.08	0.00	88.1	2.6	17.0	0.2	234.2	18.9	0.32	0.03	0.33	0.02
90%JR+10% SG-0%OFA																
	2.61	0.31	236.4	14.0	0.13	0.01	84.8	1.8	17.0	0.3	222.7	15.6	0.30	0.02	0.32	0.02
	3.45	0.22	305.2	12.2	0.16	0.01	86.7	2.5	16.9	0.2	208.5	15.7	0.28	0.02	0.42	0.02
	4.62	0.17	350.4	15.2	0.18	0.04	98.7	2.6	16.6	0.3	183.5	19.4	0.25	0.03	0.48	0.02
90%JR+10% SG-15%OFA																
	2.81	0.24	170.1	16.4	0.18	0.02	82.7	2.2	17.1	0.2	221.9	20.2	0.30	0.03	0.23	0.02
	3.67	0.15	204.6	14.2	0.17	0.01	84.4	2.7	17.1	0.2	212.4	15.7	0.29	0.02	0.28	0.02
	4.42	0.14	286.4	15.3	0.11	0.03	89.2	2.2	16.9	0.2	198.5	19.3	0.27	0.03	0.39	0.02
80%JR+20% SG-0%OFA																
	3.18	0.22	350.0	14.8	0.31	0.02	99.5	2.4	17.1	0.2	172.7	15.1	0.23	0.02	0.48	0.02
	3.85	0.25	441.4	40.4	0.45	0.04	104.4	2.9	17.1	0.2	148.9	16.7	0.20	0.02	0.60	0.05
	4.35	0.20	403.3	10.9	0.20	0.01	106.8	2.3	17.0	0.2	153.4	16.5	0.21	0.02	0.55	0.01
80%JR+20% SG-15%OFA																
	2.60	0.45	176.2	21.7	0.85	0.05	95.8	2.6	17.3	0.2	172.4	14.2	0.23	0.02	0.24	0.03
	3.86	0.21	249.7	18.9	0.81	0.28	103.1	2.8	17.1	0.2	169.1	15.6	0.23	0.02	0.34	0.03
	4.27	0.17	293.9	19.3	0.75	0.11	108.1	2.8	17.0	0.2	148.9	16.9	0.20	0.02	0.40	0.03
90%JR+10% SD-0%OFA																
	2.53	0.35	245.0	15.3	0.23	0.04	92.2	2.4	17.3	0.2	202.9	22.1	0.28	0.03	0.33	0.02
	3.56	0.21	298.3	12.3	0.15	0.01	90.1	2.7	17.3	0.2	181.8	17.0	0.25	0.02	0.41	0.02
	4.42	0.28	396.2	13.1	0.23	0.06	104.3	2.5	16.9	0.2	153.5	14.7	0.21	0.02	0.54	0.02
90%JR+10% SD-15%OFA																
	3.19	0.21	241.8	15.4	0.40	0.04	88.0	2.8	17.4	0.2	224.3	17.5	0.31	0.02	0.33	0.02
	3.80	0.26	261.7	14.4	0.39	0.05	89.0	2.2	17.4	0.2	209.9	19.1	0.29	0.03	0.36	0.02
	5.09	0.16	338.2	14.4	0.20	0.06	99.3	3.2	17.1	0.3	172.4	21.0	0.23	0.03	0.46	0.02
85%JR+15% SD-0%OFA																
	2.79	0.21	268.4	13.4	0.27	0.02	84.8	2.8	17.2	0.2	159.0	17.2	0.22	0.02	0.37	0.02
	4.30	0.25	378.5	16.2	0.21	0.01	87.6	2.4	17.1	0.3	133.5	18.6	0.18	0.03	0.51	0.02
	5.11	0.27	364.9	16.0	0.1	0.0	93.9	3.4	16.9	0.2	130.3	21.2	0.18	0.03	0.50	0.02
85%JR+15% SD-15%OFA																
	2.94	0.22	189.4	17.7	0.3	0.0	84.2	2.6	17.3	0.2	169.3	19.0	0.23	0.03	0.26	0.02
	3.79	0.26	238.3	16.2	0.2	0.0	99.9	3.0	17.1	0.2	169.1	15.6	0.23	0.02	0.32	0.02
	3.80	0.28	250.3	18.9	0.3	0.0	93.7	3.5	17.0	0.2	153.2	18.5	0.21	0.03	0.34	0.03
	5.28	0.32	326.2	15.3	0.2	0.0	91.4	2.7	16.9	0.3	131.1	20.8	0.18	0.03	0.44	0.02

Table A-8A. Gas Flow Data from Test GL-9.

Test 9 – Dual Register Burner – GL Coal with Comilled Switchgrass and SD														
Furnace Flow Data					------- FURNACE AIR FLOWS, SCFM (60°F, 29.92 in. Hg) ------								Fuel Feed	
Test Condition	FEO, Wet %		NOx, 3% O_2, ppm		Total Air		Pri. Air (150°F)		Sec. Air (600°F)		TA (600°F)		Rate, lb/hr	
	Avg.	S.D.	Avg.	S.D.	Avg.	S.D.	Avg.	S.D.	Avg.	S.D.	Avg.	S.D.	Avg.	S.D.
100%GL-16% TA														
	2.49	0.13	313.4	21.2	699.5	2.2	126.0	0.1	461.6	2.2	112.0	0.2	266.6	2.9
	3.82	0.29	365.2	21.3	760.1	2.0	136.8	0.2	501.7	1.8	121.6	0.2	267.9	1.7
	4.33	0.09	378.2	10.8	799.9	1.8	144.0	0.2	527.9	1.6	128.0	0.2	268.0	1.7
100%GL-30% TA														
	2.61	0.19	334.8	17.9	715.3	4.3	122.7	1.4	388.3	2.4	204.4	2.3	268.0	2.0
	3.61	0.11	438.9	19.6	739.0	3.8	133.0	1.0	384.4	2.1	221.6	1.6	267.5	2.1
	4.56	0.15	446.4	22.9	800.1	3.3	144.0	0.2	416.1	3.2	240.0	0.2	268.2	1.8
90%GL+10% Switchgrass-16% TA														
	2.60	0.15	251.8	16.2	700.1	1.7	126.0	0.2	462.0	1.6	112.0	0.2	278.2	1.8
	3.48	0.16	331.1	14.0	749.8	1.9	135.0	0.3	494.8	1.7	120.0	0.2	278.5	2.1
	4.54	0.15	371.1	12.5	799.9	2.1	144.0	0.3	527.9	2.0	128.0	0.2	279.1	1.9
90%GL+10% Switchgrass-30% TA														
	2.69	0.21	327.7	22.4	694.4	1.8	120.0	0.2	379.4	1.7	195.0	0.3	278.9	2.0
	3.20	0.20	394.7	23.3	715.0	2.0	126.0	0.2	378.9	2.0	210.1	0.4	279.6	2.0
	3.31	0.20	282.8	17.2	714.9	2.8	125.9	0.6	379.2	2.8	209.8	1.6	276.6	2.9
	4.09	0.19	426.3	15.7	819.6	2.1	147.6	0.2	426.0	2.0	246.0	0.3	278.6	1.9
	4.54	0.09	473.0	15.5	800.3	2.5	144.0	0.3	416.3	2.4	240.0	0.3	278.4	1.8
80%GL+20% Switchgrass-16% TA														
	2.34	0.26	238.5	20.0	679.7	1.7	122.4	0.3	448.5	1.6	108.8	0.1	288.5	5.3
	3.44	0.23	353.1	17.9	760.4	1.8	136.8	0.3	501.9	1.5	121.6	0.2	289.4	3.8
	3.61	0.21	368.1	21.2	750.2	2.0	135.0	0.4	495.2	1.8	120.0	0.2	288.1	6.9
	3.72	0.28	408.2	19.7	789.6	1.7	142.2	0.2	521.0	1.6	126.4	0.2	289.8	3.5
	4.44	0.27	336.3	12.9	799.7	2.3	144.0	0.5	527.8	2.1	128.0	0.2	288.2	6.3
80%GL+20% Switchgrass-30% TA														
	2.68	0.17	431.4	24.1	702.0	2.5	122.4	0.3	375.6	2.4	204.0	0.4	288.6	7.9
	3.15	0.24	449.2	35.6	723.9	2.6	129.6	0.4	378.3	2.3	216.0	0.5	285.4	10.8
	4.48	0.21	573.0	15.9	769.9	2.5	138.6	0.4	400.4	2.4	230.9	0.4	289.6	4.9
90%GL+10% SD-16% TA														
	2.75	0.09	244.0	7.7	720.0	1.9	129.6	0.2	475.3	1.8	115.2	0.2	279.5	3.0
	3.87	0.13	269.9	7.8	779.7	1.7	140.4	0.2	514.5	1.5	124.8	0.2	279.3	3.2
	4.55	0.17	304.5	10.1	799.8	1.6	143.9	0.2	527.8	1.5	128.0	0.1	277.3	5.0
90%GL+10% SD-30% TA														
	2.60	0.18	605.6	12.2	702.5	2.0	122.4	0.2	376.1	1.9	204.0	0.2	277.3	5.4
	3.49	0.11	628.5	12.5	729.3	2.2	131.4	0.2	378.8	2.1	219.0	0.3	279.4	3.0
	4.62	0.22	698.0	14.1	799.7	3.3	143.9	0.3	415.9	3.3	239.9	0.3	280.1	3.1
85%GL+20% SD-16% TA														
	2.31	0.20	215.3	9.1	720.5	2.4	129.6	0.2	475.7	2.2	115.2	0.3	289.9	3.0
	3.48	0.19	292.7	12.5	770.1	2.6	138.6	0.3	508.4	2.5	123.2	0.3	289.8	3.4
	4.60	0.18	335.3	10.4	850.1	1.7	153.0	0.3	561.0	1.5	136.0	0.2	290.6	3.4
85%GL+20% SD-30% TA														
	3.00	0.25	326.2	20.6	712.3	2.9	128.0	0.7	371.1	2.5	213.3	1.0	288.6	6.5
	3.69	0.16	379.8	12.0	779.8	2.3	140.4	0.3	405.4	2.2	234.0	0.7	291.7	3.4
	4.63	0.26	402.7	14.4	800.2	3.3	144.0	0.5	416.2	3.2	240.0	0.5	288.3	7.9

Table A-8B. Gas Flow Data for UBC Measurements from Test GL-9.

Test 9 – Dual Register Burner – GL Coal with Comilled Switchgrass and SD																
Unburned Carbon Data							----- FURNACE AIR FLOWS, SCFM (60°F, 29.92 in. Hg) ------								Fuel Feed	
Test Condition	FEO, Wet %		NOx, 3% O_2, ppm		% UBC		Total Air		Pri. Air (150°F)		Sec. Air (600°F)		TA (600°F)		Rate, lb/hr	
	Avg.	S.D.	Avg.	S.D.	Avg.	S.D.	Avg.	S.D.	Avg.	S.D.	Avg.	S.D.	Avg.	S.D.	Avg.	S.D.
100%GL-16% TA	2.63	0.27	324.3	24.7	3.2	0.1	699.6	1.9	126.0	0.2	461.6	1.9	112.0	0.1	266.5	3.3
	3.85	0.27	361.8	15.9	0.8	0.0	760.4	2.0	136.9	0.2	501.9	1.8	121.7	0.2	267.6	2.1
	4.36	0.15	380.5	9.8	0.8	0.0	800.2	2.4	144.0	0.3	528.1	2.1	128.0	0.2	267.8	1.8
100%GL-30% TA																
	2.51	0.37	334.2	25.9	2.1	0.1	710.5	8.4	122.1	0.8	385.4	5.6	203.0	2.6	267.7865586	
	3.62	0.12	442.0	19.5	0.7	0.0	739.8	2.0	133.2	0.2	384.6	1.7	222.0	0.4	267.56	2.26
	5.50	0.56	453.4	21.0	0.2	0.0	800.4	2.7	144.0	0.3	416.4	2.4	240.0	0.3	267.43	2.05
90%GL+10% Switchgrass-16% TA																
	2.61	0.17	251.3	16.1	2.3	0.0	700.2	1.7	126.0	0.2	462.1	1.7	112.0	0.1	278.1	1.9
	3.49	0.15	334.1	12.5	0.8	0.0	750.1	2.0	135.0	0.3	495.1	1.8	120.0	0.2	278.8	1.8
	4.54	0.17	369.1	12.5	0.45	0.06	800.0	1.8	144.0	0.2	527.9	1.7	128.0	0.2	278.8	2.1
90%GL+10% Switchgrass-30% TA																
	2.79	0.22	332.0	22.1	0.79	0.04	700.4	12.1	121.6	4.2	379.1	1.9	199.6	8.5	278.9	1.7
	3.21	0.20	391.8	24.5	0.59	0.03	715.1	2.1	126.0	0.2	379.0	2.1	210.0	0.4	279.5	2.1
	4.57	0.09	471.2	14.6	0.17	0.01	800.1	2.4	144.0	0.3	416.1	2.2	240.0	0.3	278.2	2.0
80%GL+20% Switchgrass-16% TA																
	2.28	0.24	236.7	22.7	4.87	0.33	679.5	1.5	122.4	0.3	448.2	1.5	108.8	0.1	288.1	5.8
	3.55	0.24	354.3	26.4	2.28	0.02	750.3	3.0	135.0	0.3	495.3	2.7	120.0	0.3	284.9	9.8
	4.60	0.42	337.2	20.1	2.02	0.06	800.1	2.2	144.0	0.4	528.1	2.0	128.0	0.2	287.9	6.8
80%GL+20% Switchgrass-30% TA																
	2.71	0.17	429.2	24.7	1.53	0.19	701.9	2.7	122.4	0.3	375.6	2.5	204.0	0.3	288.4	7.4
	3.27	0.54	451.3	28.1	1.73	0.25	724.0	2.5	129.6	0.4	378.3	2.2	216.0	0.5	284.2	11.3
	4.50	0.22	575.3	16.4	0.50	0.04	769.8	2.6	138.6	0.4	400.3	2.5	230.9	0.4	289.2	5.7
90%GL+10% SD-16% TA																
	2.77	0.10	246.2	8.1	3.04	0.24	720.1	2.1	129.6	0.2	475.4	2.0	115.2	0.2	279.4	3.1
	3.88	0.14	270.4	6.5	1.88	0.05	779.9	1.5	140.4	0.3	514.7	1.4	124.8	0.2	278.5	3.3
	4.56	0.16	301.5	10.9	1.09	0.08	799.9	1.6	144.0	0.2	527.9	1.5	128.0	0.1	276.9	5.0
90%GL+10% SD-30% TA																
	2.61	0.20	606.1	11.2	2.90	0.31	702.5	2.2	122.4	0.2	376.1	2.1	204.0	0.2	276.4	5.7
	3.52	0.10	629.0	13.6	1.88	0.16	729.8	2.0	131.4	0.2	379.3	1.8	219.1	0.3	279.1	3.1
	4.58	0.21	695.2	16.4	0.70	0.01	799.5	3.2	143.9	0.4	415.6	3.0	239.9	0.5	280.4	2.8
85%GL+20% SD-16% TA																
	2.30	0.18	220.3	12.5	5.71	0.35	718.8	4.8	129.4	0.6	474.4	3.9	115.0	0.6	289.5	2.8
	3.57	0.22	296.4	15.6	1.55	0.08	770.0	3.2	138.6	0.3	508.2	3.1	123.2	0.2	289.3	3.8
	4.65	0.17	334.9	11.2	0.67	0.03	850.0	1.8	153.0	0.4	561.0	1.6	136.0	0.2	290.9	3.3
85%GL+20% SD-30% TA																
	3.03	0.25	323.9	19.8	2.49	0.27	712.0	2.4	127.8	0.4	371.2	2.1	213.0	0.4	287.7	7.0
	3.70	0.16	379.6	12.0	0.50	0.03	779.8	2.4	140.4	0.3	405.4	2.2	234.0	0.7	291.7	3.4
	4.65	0.26	403.0	14.3	0.45	0.05	800.3	3.5	144.0	0.5	416.3	3.2	240.0	0.6	287.9	7.4

Table A-8C. Gas Sampling Data from Test GL-9.

Test 9 – Dual Register Burner – GL Coal with Comilled Switchgrass and SD														
Gas Sampling Data														
Test Condition	FEO, Wet %		NO_x, 3% O_2, ppm		CO, 3% O_2, ppm		CO_2, 3% O_2, %		SO_2, 3% O_2, ppm		SO_2, lb/10^6Btu		NO_x, lb/10^6Btu	
	Avg.	S.D.	Avg.	S.D.	Avg.	S.D.	Avg.	S.D.	Avg.	S.D.	Avg.	S.D.	Avg.	S.D.
100%GL-16% TA														
	2.49	0.13	313.4	21.2	97.6	3.0	16.7	0.2	743.9	8.9	0.99	0.01	0.42	0.03
	3.82	0.29	365.2	21.3	90.6	3.0	16.5	0.2	741.6	11.1	0.99	0.01	0.49	0.03
	4.33	0.09	378.2	10.8	92.7	3.0	16.5	0.2	744.3	12.3	0.99	0.02	0.51	0.01
100%GL-30% TA														
	2.61	0.19	334.8	17.9	88.3	3.0	16.8	0.2	736.4	16.6	0.98	0.02	0.45	0.02
	3.61	0.11	438.9	19.6	88.6	3.0	16.6	0.3	729.3	12.0	0.97	0.02	0.59	0.03
	4.56	0.15	446.4	22.9	88.4	2.4	16.7	0.2	637.6	42.1	0.85	0.06	0.60	0.03
90%GL+10% Switchgrass-16% TA														
	2.60	0.15	251.8	16.2	90.4	2.7	16.8	0.2	693.3	9.5	0.93	0.01	0.34	0.02
	3.48	0.16	331.1	14.0	83.8	3.0	16.8	0.3	676.7	10.2	0.90	0.01	0.44	0.02
	4.54	0.15	371.1	12.5	86.2	3.2	16.6	0.3	679.1	7.7	0.91	0.01	0.50	0.02
90%GL+10% Switchgrass-30% TA														
	2.69	0.21	327.7	22.4	92.1	4.2	16.6	0.3	717.8	15.5	0.96	0.02	0.44	0.03
	3.20	0.20	394.7	23.3	88.6	3.1	16.6	0.3	688.9	7.9	0.92	0.01	0.53	0.03
	3.31	0.20	282.8	17.2	136.8	4.9	16.7	0.2	742.3	10.2	0.99	0.01	0.38	0.02
	4.09	0.19	426.3	15.7	129.0	4.3	16.8	0.3	710.7	18.1	0.95	0.02	0.57	0.02
	4.54	0.09	473.0	15.5	98.7	4.3	16.5	0.4	722.5	10.0	0.97	0.01	0.63	0.02
80%GL+20% Switchgrass-16% TA														
	2.34	0.26	238.5	20.0	128.6	10.3	17.3	0.2	690.4	18.4	0.92	0.02	0.32	0.03
	3.44	0.23	353.1	17.9	136.1	5.1	16.9	0.5	700.6	14.4	0.94	0.02	0.47	0.02
	3.61	0.21	368.1	21.2	122.3	4.2	17.1	0.2	687.0	17.6	0.92	0.02	0.49	0.03
	3.72	0.28	408.2	19.7	134.0	3.8	16.8	0.3	732.3	14.9	0.98	0.02	0.55	0.03
	4.44	0.27	336.3	12.9	98.4	4.2	17.2	0.3	699.1	14.2	0.93	0.02	0.45	0.02
80%GL+20% Switchgrass-30% TA														
	2.68	0.17	431.4	24.1	91.5	4.2	16.7	0.2	668.8	16.4	0.89	0.02	0.58	0.03
	3.15	0.24	449.2	35.6	100.7	3.2	16.9	0.2	692.1	14.9	0.92	0.02	0.60	0.05
	4.48	0.21	573.0	15.9	97.6	4.0	16.6	0.2	620.2	12.4	0.83	0.02	0.77	0.02
90%GL+10% SD-16% TA														
	2.75	0.09	244.0	7.7	90.5	2.4	16.7	0.1	867.4	8.8	1.16	0.01	0.33	0.01
	3.87	0.13	269.9	7.8	93.8	2.4	16.6	0.1	862.1	7.4	1.15	0.01	0.36	0.01
	4.55	0.17	304.5	10.1	87.6	2.8	16.4	0.2	866.3	11.8	1.16	0.02	0.41	0.01
90%GL+10% SD-30% TA														
	2.60	0.18	605.6	12.2	115.1	2.9	14.9	0.2	606.4	7.2	0.81	0.01	0.81	0.02
	3.49	0.11	628.5	12.5	125.0	3.2	15.5	0.2	628.7	7.4	0.84	0.01	0.84	0.02
	4.62	0.22	698.0	14.1	127.1	3.2	17.1	0.2	694.9	8.8	0.93	0.01	0.93	0.02
85%GL+20% SD-16% TA														
	2.31	0.20	215.3	9.1	117.4	4.1	16.6	0.1	856.5	11.4	1.14	0.02	0.29	0.01
	3.48	0.19	292.7	12.5	102.9	3.3	16.5	0.2	827.8	12.3	1.11	0.02	0.39	0.02
	4.60	0.18	335.3	10.4	102.4	3.0	16.5	0.1	837.7	9.6	1.12	0.01	0.45	0.01
85%GL+20% SD-30% TA														
	3.00	0.25	326.2	20.6	98.0	3.2	16.8	0.2	756.8	19.8	1.01	0.03	0.44	0.03
	3.69	0.16	379.8	12.0	97.7	3.3	16.5	0.1	848.5	7.4	1.13	0.01	0.51	0.02
	4.63	0.26	402.7	14.4	98.9	3.2	16.7	0.2	712.9	15.0	0.95	0.02	0.54	0.02

Table A-8D. Gas Sampling Data for UBC Measurements from Test GL-9.

Test 9 - Dual Register Burner - GL Coal with Comilled Switchgrass and SD																
Unburned Carbon Data																
Test Condition	FEO, Wet %		NOx, 3% O_2, ppm		% UBC		CO, 3% O_2, ppm		CO_2, 3% O_2, %		SO_2, 3% O_2, ppm		SO_2, lb/10^6Btu		NO_x, lb/10^6Btu	
	Avg.	S.D.	Avg.	S.D.	Avg.	S.D.	Avg.	S.D.	Avg.	S.D.	Avg.	S.D.	Avg.	S.D.	Avg.	S.D.
100%GL-16% TA	2.63	0.27	324.3	24.7	3.2	0.1	96.9	2.7	17	0	745.5	10.8	1.04	0.01	0.45	0.03
	3.85	0.27	361.8	15.9	0.8	0.0	89.9	2.9	17	0	739.1	10.6	1.03	0.01	0.50	0.02
	4.36	0.15	380.5	9.8	0.8	0.0	92.4	3.3	17	0	747.8	11.0	1.04	0.02	0.53	0.01
100%GL-30% TA																
	2.51	0.37	334.2	25.9	2.1	0.1	89.8	3.6	17	0	744.8	12.6	1.04	0.02	0.46	0.04
	3.62	0.12	442.0	19.5	0.7	0.0	88.9	3.1	17	0	729.9	12.9	1.01	0.02	0.61	0.03
	5.50	0.56	453.4	21.0	0.2	0.0	89.1	3.0	17	0	499.8	53.1	0.69	0.07	0.63	0.03
90%GL+10% Switchgrass-16% TA																
	2.61	0.17	251.3	16.1	2.3	0.0	90.6	2.6	17	0	692.3	8.2	0.96	0.01	0.35	0.02
	3.49	0.15	334.1	12.5	0.8	0.0	82.4	3.0	17	0	673.5	8.1	0.94	0.01	0.46	0.02
	4.54	0.17	369.1	12.5	0.4	0.1	85.7	3.1	17	0	677.9	8.5	0.94	0.01	0.51	0.02
90%GL+10% Switchgrass-30% TA																
	2.79	0.22	332.0	22.1	0.8	0.0	94.5	4.5	17	0	725.4	13.8	1.01	0.02	0.46	0.03
	3.21	0.20	391.8	24.5	0.6	0.0	88.5	3.3	17	0	687.3	7.1	0.96	0.01	0.54	0.03
	4.57	0.09	471.2	14.6	0.2	0.0	98.8	4.4	16	0	720.1	8.8	1.00	0.01	0.66	0.02
80%GL+20% Switchgrass-16% TA																
	2.28	0.24	236.7	22.7	4.9	0.3	128.6	11.4	17	0	693.9	15.3	0.96	0.02	0.33	0.03
	3.55	0.24	354.3	26.4	2.3	0.0	127.6	7.8	17	0	685.9	19.0	0.95	0.03	0.49	0.04
	4.60	0.42	337.2	20.1	2.0	0.1	96.2	3.1	17	0	699.4	17.0	0.97	0.02	0.47	0.03
80%GL+20% Switchgrass-30% TA																
	2.71	0.17	429.2	24.7	1.5	0.2	93.0	3.8	17	0	667.6	17.7	0.93	0.02	0.60	0.04
	3.27	0.54	451.3	28.1	1.7	0.2	100.7	3.1	17	0	692.4	14.7	0.96	0.02	0.63	0.04
	4.50	0.22	575.3	16.4	0.5	0.0	98.0	4.2	17	0	622.2	13.4	0.87	0.02	0.80	0.02
90%GL+10% SD-16% TA																
	2.77	0.10	246.2	8.1	3.0	0.2	89.9	2.2	17	0	871.8	5.8	1.21	0.01	0.34	0.01
	3.88	0.14	270.4	6.5	1.9	0.1	93.6	2.1	17	0	862.3	7.8	1.20	0.01	0.38	0.01
	4.56	0.16	301.5	10.9	1.1	0.1	87.7	2.8	16	0	861.7	9.7	1.20	0.01	0.42	0.02
90%GL+10% SD-30% TA																
	2.61	0.20	606.1	11.2	2.9	0.3	114.8	2.7	15	0	607.0	7.5	0.84	0.01	0.84	0.02
	3.52	0.10	629.0	13.6	1.9	0.2	124.8	3.3	15	0	628.4	7.8	0.87	0.01	0.87	0.02
	4.58	0.21	695.2	16.4	0.7	0.0	126.0	3.5	17	0	692.5	11.3	0.96	0.02	0.97	0.02
85%GL+20% SD-16% TA																
	2.30	0.18	220.3	12.5	5.7	0.4	118.5	4.1	17	0	847.6	14.2	1.18	0.02	0.31	0.02
	3.57	0.22	296.4	15.6	1.6	0.1	102.3	2.9	17	0	821.6	9.2	1.14	0.01	0.41	0.02
	4.65	0.17	334.9	11.2	0.7	0.0	102.5	3.0	16	0	835.7	9.7	1.16	0.01	0.47	0.02
85%GL+20% SD-30% TA																
	3.03	0.25	323.9	19.8	2.5	0.3	97.8	3.1	17	0	755.9	16.1	1.05	0.02	0.45	0.03
	3.70	0.16	379.6	12.0	0.5	0.0	97.6	3.3	17	0	848.5	7.5	1.18	0.01	0.53	0.02
	4.65	0.26	403.0	14.3	0.4	0.0	98.6	3.1	17	0	713.4	14.9	0.99	0.02	0.56	0.02

Table A-9A. Gas Flow Data from Test PR-10.

Test 10 - Fine and Normal Grinds of PR Coal														
Furnace Flow Data					------- FURNACE AIR FLOWS, SCFM (60°F, 29.92 in. Hg) ------								Fuel Feed	
Test Condition	FEO, Wet %		NOx, 3% O_2, ppm		Total Air		Pri. Air (150°F)		Sec. Air (600°F)		OFA (600°F)		Rate, lb/hr	
	Avg.	S.D.	Avg.	S.D.	Avg.	S.D.	Avg.	S.D.	Avg.	S.D.	Avg.	S.D.	Avg.	S.D.
PR - Regular Grind - 0% OFA														
	2.77	0.20	417.0	37.8	669.9	2.0	127.3	0.2	542.5	2.0	0.0	0.0	296.8	1.6
	3.50	0.35	515.2	27.8	710.4	2.2	134.9	0.3	575.5	2.0	0.0	0.0	296.9	1.6
	3.63	0.19	495.3	25.1	710.5	2.6	134.9	0.2	575.7	2.5	0.0	0.0	297.0	1.7
	4.70	0.11	556.0	12.1	760.0	2.0	144.4	0.2	615.6	1.9	0.0	0.0	296.8	1.7
PR - Regular Grind - 15% OFA														
	2.19	0.33	201.7	10.5	659.6	1.7	125.4	0.2	435.2	1.7	99.0	0.2	296.3	2.5
	2.61	0.19	258.7	14.4	670.1	2.3	127.3	0.2	442.3	2.1	100.5	0.1	296.5	1.4
	3.34	0.37	294.7	24.4	699.7	1.2	133.0	0.2	461.7	1.1	105.0	0.1	296.8	1.7
	3.51	0.25	303.2	20.0	700.3	2.5	133.0	0.2	462.3	2.4	105.0	0.2	295.7	2.0
	4.57	0.14	407.5	16.0	760.6	2.2	144.4	0.2	502.2	2.1	114.0	0.2	297.0	1.8
	4.70	0.18	408.1	17.5	760.3	2.1	144.4	0.2	501.9	2.0	114.0	0.1	296.3	1.9
PR - Fine Grind - 0% OFA														
	3.39	0.23	436.2	15.3	710.1	2.2	134.9	0.2	575.3	2.1	0.0	0.0	297.4	1.5
	4.33	0.19	500.1	16.5	750.4	3.0	142.5	0.4	607.8	2.9	0.0	0.0	297.4	1.8
PR - Fine Grind - 15% OFA														
	2.56	0.27	216.5	18.1	669.8	2.2	127.3	0.2	442.0	2.0	100.5	0.2	296.8	1.6
	2.73	0.15	258.1	14.1	669.9	2.4	127.3	0.3	442.2	2.2	100.4	0.3	297.1	1.6
	3.56	0.17	305.1	20.8	710.2	1.5	134.9	0.2	468.8	1.4	106.5	0.2	297.4	1.8
	3.63	0.13	283.9	15.3	709.8	1.6	134.9	0.2	468.4	1.5	106.5	0.2	296.5	1.4
	4.30	0.19	299.0	21.4	750.3	2.4	142.5	0.3	496.4	12.0	111.3	11.8	297.2	1.7
	4.64	0.18	388.9	16.3	760.6	1.9	144.4	0.2	502.2	1.9	114.0	0.1	296.8	1.4

Table A-9B. Gas Flow Data for UBC Measurements from Test PR-10.

Test 10 - Fine and Normal Grinds of PR Coal																
Unburned Carbon Data							----- FURNACE AIR FLOWS, SCFM (60°F, 29.92 in. Hg) ------								Fuel Feed	
Test Condition	FEO, Wet %		NOx, 3% O_2, ppm		% UBC		Total Air		Pri. Air (150°F)		Sec. Air (600°F)		OFA (600°F)		Rate, lb/hr	
	Avg.	S.D.	Avg.	S.D.	Avg.	S.D.	Avg.	S.D.	Avg.	S.D.	Avg.	S.D.	Avg.	S.D.	Avg.	S.D.
PR - Regular Grind - 0% OFA																
	2.77	0.22	422.0	39.9	1.0	0.1	669.9	2.1	127.3	0.2	542.6	2.0	0.0	0.0	296.7	1.7
	3.64	0.20	492.9	24.6	0.4	0.0	710.6	2.7	134.9	0.2	575.7	2.6	0.0	0.0	297.0	1.6
	4.68	0.13	554.9	11.5	0.1	0.0	759.9	1.7	144.4	0.2	615.5	1.6	0.0	0.0	296.7	1.8
PR - Regular Grind - 15% OFA																
	2.22	0.36	201.6	10.4	2.3	0.0	659.8	1.7	125.4	0.2	435.4	1.6	99.0	0.2	296.4	2.4
	3.54	0.28	304.5	20.1	1.0	0.0	700.3	2.7	133.0	0.2	462.3	2.5	105.0	0.2	295.5	2.1
	4.57	0.11	403.9	13.4	0.5	0.0	760.5	1.9	144.4	0.2	502.1	1.8	114.0	0.2	296.8	2.0
PR - Fine Grind - 0% OFA																
	2.51	0.21	366.6	27.7	0.9	0.1	670.2	2.0	127.3	0.3	542.9	2.0	0.0	0.0	297.3	1.5
	3.40	0.23	436.4	15.5	0.2	0.0	710.2	2.2	134.9	0.2	575.3	2.2	0.0	0.0	297.4	1.5
	4.35	0.18	497.7	15.6	0.1	0.0	750.1	2.7	142.5	0.4	607.6	2.6	0.0	0.0	297.4	1.9
PR - Fine Grind - 15% OFA																
	2.46	0.24	216.3	14.6	1.3	0.0	670.3	2.1	127.3	0.2	442.5	2.0	100.5	0.2	296.9	1.6
	3.62	0.14	284.7	17.3	0.8	0.0	709.4	1.5	134.9	0.2	468.0	1.4	106.5	0.1	296.3	1.4
	4.31	0.14	299.6	11.9	0.5	0.0	750.7	2.6	142.6	0.3	495.6	2.3	112.5	0.2	297.3	1.8

Table A-9C. Gas Sampling Data from Test PR-10.

Test 10 - Fine and Normal Grinds of PR Coal														
Gas Sampling Data														
Test Condition	FEO, Wet %		NOx, 3% O_2, ppm		CO, 3% O_2, ppm		CO_2, 3% O_2, %		SO_2, 3% O_2, ppm		SO_2, lb/10^6Btu		NO_X, lb/10^6Btu	
	Avg.	S.D.	Avg.	S.D.	Avg.	S.D.	Avg.	S.D.	Avg.	S.D.	Avg.	S.D.	Avg.	S.D.
PR - Regular Grind - 0% OFA														
	2.77	0.20	417.0	37.8	97.8	94.1	16.3	0.3	1299.3	33.7	1.77	0.05	0.57	0.05
	3.50	0.35	515.2	27.8	83.4	3.0	16.6	0.3	1259.4	28.4	1.71	0.04	0.70	0.04
	3.63	0.19	495.3	25.1	86.9	2.7	16.1	0.2	1210.3	20.4	1.65	0.03	0.67	0.03
	4.70	0.11	556.0	12.1	84.3	2.5	16.2	0.2	1260.4	16.6	1.71	0.02	0.76	0.02
PR - Regular Grind - 15% OFA														
	2.19	0.33	201.7	10.5	90.8	14.6	16.5	0.3	1306.1	29.0	1.78	0.04	0.27	0.01
	2.61	0.19	258.7	14.4	85.6	2.4	16.6	0.2	1316.9	17.9	1.79	0.02	0.35	0.02
	3.34	0.37	294.7	24.4	87.9	2.7	16.5	0.2	1302.5	31.2	1.77	0.04	0.40	0.03
	3.51	0.25	303.2	20.0	80.1	2.6	16.5	0.3	1247.9	23.1	1.70	0.03	0.41	0.03
	4.57	0.14	407.5	16.0	92.9	2.9	16.2	0.2	1221.7	17.5	1.66	0.02	0.55	0.02
	4.70	0.18	408.1	17.5	88.0	2.6	16.5	0.2	1321.7	16.6	1.80	0.02	0.56	0.02
PR - Fine Grind - 0% OFA														
	3.39	0.23	436.2	15.3	88.2	2.7	16.4	0.2	1229.0	15.4	1.67	0.02	0.59	0.02
	4.33	0.19	500.1	16.5	91.3	2.6	16.4	0.2	1169.3	33.7	1.59	0.05	0.68	0.02
PR - Fine Grind - 15% OFA														
	2.56	0.27	216.5	18.1	94.3	17.1	16.6	0.2	1277.3	18.0	1.74	0.02	0.29	0.02
	2.73	0.15	258.1	14.1	92.3	15.4	17.3	0.2	1256.6	19.9	1.71	0.03	0.35	0.02
	3.56	0.17	305.1	20.8	91.2	3.5	17.1	0.2	1208.2	24.3	1.64	0.03	0.42	0.03
	3.63	0.13	283.9	15.3	89.2	2.9	16.7	0.2	1280.5	18.1	1.74	0.02	0.39	0.02
	4.30	0.19	299.0	21.4	94.5	2.5	16.4	0.2	1235.9	15.2	1.68	0.02	0.41	0.03
	4.64	0.18	388.9	16.3	91.3	2.9	17.2	0.2	1258.8	15.1	1.71	0.02	0.53	0.02

Table A-9D. Gas Sampling Data for UBC Measurements from Test PR-10.

Test 10 - Fine and Normal Grinds of PR Coal																
Unburned Carbon Data																
Test Condition	FEO, Wet %		NOx, 3% O_2, ppm		% UBC		CO, 3% O_2, ppm		CO_2, 3% O_2, %		SO_2, 3% O_2, ppm		SO_2, lb/10^6Btu		NO_X, lb/10^6Btu	
	Avg.	S.D.	Avg.	S.D.	Avg.	S.D.	Avg.	S.D.	Avg.	S.D.	Avg.	S.D.	Avg.	S.D.	Avg.	S.D.
PR - Regular Grind - 0% OFA																
	2.77	0.22	422.0	39.9	0.97	0.05	102.2	110.3	16.3	0.3	1301.3	34.5	1.77	0.05	0.57	0.05
	3.64	0.20	492.9	24.6	0.39	0.04	86.9	2.8	16.1	0.2	1212.4	19.9	1.65	0.03	0.67	0.03
	4.68	0.13	554.9	11.5	0.13	0.01	84.4	2.5	16.2	0.2	1261.2	16.9	1.72	0.02	0.75	0.02
PR - Regular Grind - 15% OFA																
	2.22	0.36	201.6	10.4	2.34	0.05	91.7	15.3	16.4	0.3	1305.4	30.0	1.78	0.04	0.27	0.01
	3.54	0.28	304.5	20.1	1.04	0.00	79.4	2.4	16.6	0.3	1246.8	22.3	1.70	0.03	0.41	0.03
	4.57	0.11	403.9	13.4	0.54	0.04	92.7	3.0	16.2	0.2	1218.1	15.2	1.66	0.02	0.55	0.02
PR - Fine Grind - 0% OFA																
	2.51	0.21	366.6	27.7	0.91	0.05	126.1	199.6	16.5	0.2	1237.4	18.1	1.68	0.02	0.50	0.04
	3.40	0.23	436.4	15.5	0.21	0.00	88.3	2.7	16.4	0.2	1229.0	15.5	1.67	0.02	0.59	0.02
	4.35	0.18	497.7	15.6	0.14	0.02	91.7	2.7	16.4	0.2	1171.1	36.3	1.59	0.05	0.68	0.02
PR - Fine Grind - 15% OFA																
	2.46	0.24	216.3	14.6	1.32	0.04	95.6	22.2	16.6	0.2	1279.7	16.5	1.74	0.02	0.29	0.02
	3.62	0.14	284.7	17.3	0.82	0.01	88.2	2.6	16.7	0.2	1281.1	17.9	1.74	0.02	0.39	0.02
	4.31	0.14	299.6	11.9	0.5	0.0	94.4	2.5	16.3	0.2	1235.0	13.6	1.68	0.02	0.41	0.02

Table A-10A. Gas Flow Data from Test GL-11.

Test 11 – GL Coal Comilled with SD, Ammonia Added to Increase Fuel N (as with Chicken Litter)																
Furnace Flow Data					------- FURNACE AIR FLOWS, SCFM (60°F, 29.92 in. Hg) ------								Fuel Feed		NH_3	
Test Condition	FEO, Wet %		NO_x, 3% O_2, ppm		Total Air		Pri. Air (150°F)		Sec. Air (600°F)		OFA (600°F)		Rate, lb/hr		Feed	Fuel N
	Avg.	S.D.	Avg.	S.D.	Avg.	S.D.	Avg.	S.D.	Avg.	S.D.	Avg.	S.D.	Avg.	S.D.	lb/hr	% Total
100%GL-0% OFA																
	2.69	0.04	509.1	24.2	649.7	2.7	123.5	0.2	526.1	2.7	0.0	0.0	268.4	1.8	0.00	1.70
	2.88	0.14	617.8	79.7	690.3	1.9	131.1	0.2	559.2	1.8	0.0	0.0	268.2	2.7	13.11	5.46
	3.08	0.14	632.2	58.7	690.0	2.3	131.1	0.2	558.9	2.3	0.0	0.0	267.7	2.8	6.09	3.49
	3.52	0.07	567.6	27.1	690.0	2.1	131.1	0.3	558.8	1.9	0.0	0.0	268.6	2.2	0.00	1.70
	4.82	0.04	651.9	40.0	750.5	3.3	142.6	0.3	607.9	3.1	0.0	0.0	268.8	1.7	0.00	1.70
100%GL-15% OFA																
	2.61	0.07	248.3	21.3	649.8	2.1	123.5	0.2	428.8	2.0	97.6	1.3	269.4	2.1	0.00	1.70
	3.65	0.12	344.6	17.2	690.3	2.2	131.1	0.2	455.6	2.0	103.5	0.2	268.8	1.6	0.00	1.70
	4.63	0.06	426.8	20.7	739.8	1.9	140.6	0.2	488.1	1.7	111.0	0.2	268.3	2.2	0.00	1.70
95%GL+5% SD-0%OFA																
	2.57	0.09	520.3	26.8	649.6	1.6	123.5	0.2	526.2	1.6	0.0	0.0	273.5	2.0	0.00	1.62
	3.27	0.13	715.4	67.4	699.3	2.2	132.9	0.2	566.3	2.1	0.0	0.0	274.1	2.1	9.58	4.35
	3.44	0.16	502.2	24.4	700.1	2.4	133.0	0.2	567.1	2.3	0.0	0.0	275.0	2.4	0.00	1.62
	3.46	0.17	526.8	25.2	689.9	2.1	131.1	0.2	558.8	2.0	0.0	0.0	274.3	1.9	0.00	1.62
	3.66	0.19	623.1	36.3	700.0	1.9	133.0	0.2	567.0	1.8	0.0	0.0	274.7	2.5	0.00	1.62
	4.52	0.19	581.3	22.9	750.3	2.1	142.5	0.3	607.8	1.9	0.0	0.0	274.0	2.3	0.00	1.62
95%GL+5% SD-15%OFA																
	2.65	0.16	257.4	16.6	649.9	1.5	123.5	0.2	428.9	1.5	97.5	0.1	273.4	2.6	0.00	1.62
	3.82	0.15	347.4	18.1	700.0	2.1	133.0	0.2	462.0	2.0	104.7	1.3	273.8	2.1	0.00	1.62
	4.59	0.18	375.0	19.1	740.1	2.0	140.6	0.2	488.5	1.8	105.4	24.3	273.5	2.6	0.00	1.62
90%GL+10% SD-0%OFA																
	2.32	0.16	473.7	15.5	640.4	2.4	121.6	0.2	518.8	2.4	0.0	0.0	279.6	2.8	0.00	1.53
	3.02	0.09	549.5	45.0	677.9	5.2	129.2	0.2	548.7	5.3	0.0	0.0	279.9	2.3	10.21	4.37
	3.11	0.17	728.2	69.6	710.5	2.3	134.9	0.2	575.6	2.2	0.0	0.0	280.3	2.8	13.35	5.20
	3.18	0.14	547.1	23.4	679.8	1.9	129.2	0.2	550.6	1.8	0.0	0.0	279.7	2.5	0.00	1.53
	3.33	0.15	741.4	59.0	710.0	2.0	134.9	0.2	575.2	2.0	0.0	0.0	279.7	2.8	7.01	3.51
	3.41	0.17	652.8	79.5	700.3	2.2	133.0	0.2	567.3	2.1	0.0	0.0	279.5	2.4	0.00	1.53
	3.43	0.20	573.1	21.4	679.6	2.8	129.2	0.3	550.5	2.6	0.0	0.0	278.9	2.7	0.00	1.53
	4.37	0.15	631.6	25.2	729.9	2.0	138.7	0.2	591.3	2.0	0.0	0.0	279.6	2.5	0.00	1.53
90%GL+10% SD-15%OFA																
	2.60	0.16	233.5	14.3	639.8	1.8	121.6	0.2	422.2	1.8	96.0	0.2	280.2	3.4	0.00	1.53
	3.05	0.22	286.2	22.8	700.0	1.9	133.1	0.2	461.9	1.7	105.1	0.1	278.5	3.2	10.33	4.42
	3.44	0.13	299.3	16.6	699.7	1.8	133.0	0.2	461.7	1.6	105.0	0.1	279.7	2.2	0.82	1.77
	3.62	0.15	306.0	13.6	699.3	1.5	133.0	0.2	461.3	1.3	105.0	0.2	278.9	2.8	0.00	1.53
	3.91	0.18	313.3	17.3	690.1	1.8	131.1	0.2	455.5	1.7	103.5	0.2	279.3	2.5	0.00	1.53
	4.35	0.17	368.7	20.1	719.4	1.8	136.8	0.2	474.6	1.7	103.9	20.9	279.4	2.8	0.00	1.53
80%GL+20% SD-0%OFA																
	2.44	0.15	429.8	16.6	660.2	1.5	125.4	0.2	534.8	1.5	0.0	0.0	290.9	2.8	0.00	1.43
	2.89	0.15	586.0	40.9	700.4	1.7	133.0	0.2	567.4	1.6	0.0	0.0	291.8	2.5	10.76	4.31
	3.13	0.14	577.6	47.0	700.1	1.3	133.0	0.2	567.1	1.2	0.0	0.0	291.3	2.0	7.20	3.38
	3.34	0.17	481.4	22.9	700.1	2.4	133.0	0.2	567.1	2.3	0.0	0.0	292.1	2.9	0.00	1.43
	3.54	0.20	496.8	22.9	709.6	2.6	134.9	0.3	574.7	2.4	0.0	0.0	292.2	2.6	0.00	1.43
	3.58	0.12	476.5	20.9	690.2	2.4	131.2	0.2	559.1	2.3	0.0	0.0	292.2	2.7	0.00	1.43
	4.00	0.18	521.2	29.2	730.0	2.0	138.7	0.2	591.4	1.9	0.0	0.0	290.6	3.4	0.00	1.43
80%GL+20% SD-15%OFA																
	2.65	0.23	246.4	15.5	699.5	1.5	133.0	0.2	461.5	1.4	105.0	0.1	291.8	2.4	0.00	1.43
	2.73	0.12	214.6	15.4	660.2	1.2	125.4	0.2	435.7	1.2	99.0	0.1	291.2	3.2	0.00	1.43
	3.29	0.13	282.3	19.1	700.0	2.2	133.0	0.2	462.0	2.1	104.6	3.4	291.7	2.4	2.55	2.13
	3.40	0.16	279.8	19.4	700.2	2.6	133.0	0.2	462.1	2.4	105.0	0.2	291.5	3.0	0.00	1.43
	3.40	0.14	283.7	15.8	700.5	2.3	132.9	0.2	462.6	2.2	105.0	0.1	291.7	2.6	0.00	1.43
	3.50	0.18	332.1	21.5	759.6	1.9	144.4	0.3	501.2	1.7	114.0	0.1	291.6	1.7	12.02	4.63
	4.14	0.17	355.1	11.9	760.6	2.9	144.4	0.2	502.2	2.8	114.0	0.2	291.3	1.8	0.89	1.68
	4.24	0.17	355.6	16.0	760.4	2.4	144.4	0.2	502.0	2.3	113.1	2.7	292.1	2.8	0.00	1.43
	4.43	0.09	317.6	17.8	730.0	1.6	138.7	0.3	481.7	1.5	109.5	0.2	291.9	3.0	0.00	1.43

Table A-10B. Gas Sampling Data from GL-11.

Test 11 – GL Coal Comilled with SD, Ammonia Added to Increase Fuel N (as with Chicken Litter)																
Gas Sampling Data																
Test Condition	FEO, Wet %		NOx, 3% O_2, ppm		CO, 3% O_2, ppm		CO_2, 3% O_2, %		SO_2, 3% O_2, ppm		SO_2, lb/10^6Btu		NO_x, lb/10^6Btu		NH_3	Fuel N
	Avg.	S.D.	Avg.	S.D.	Avg.	S.D.	Avg.	S.D.	Avg.	S.D.	Avg.	S.D.	Avg.	S.D.	lb/hr	% Total
100%GL-0% OFA																
	2.69	0.04	509.1	24.2	86.7	2.0	16.7	0.2	931.1	11.0	1.24	0.01	0.67	0.03	0.0	1.70
	2.88	0.14	617.8	79.7	87.2	2.3	16.2	0.2	930.1	12.2	1.24	0.02	0.82	0.11	13.1	5.46
	3.08	0.14	632.2	58.7	86.9	2.2	16.5	0.2	912.1	17.8	1.21	0.02	0.84	0.08	6.1	3.49
	3.52	0.07	567.6	27.1	90.0	2.7	16.6	0.2	946.6	14.6	1.26	0.02	0.75	0.04	0.0	1.70
	4.82	0.04	651.9	40.0	90.3	2.5	16.5	0.3	906.7	12.4	1.21	0.02	0.87	0.05	0.0	1.70
100%GL-15% OFA																
	2.61	0.07	248.3	21.3	106.6	2.9	16.9	0.2	920.4	17.2	1.22	0.02	0.33	0.03	0.0	1.70
	3.65	0.12	344.6	17.2	105.3	3.3	16.6	0.2	918.4	47.0	1.22	0.06	0.46	0.02	0.0	1.70
	4.63	0.06	426.8	20.7	100.1	2.9	16.8	0.2	946.6	13.6	1.26	0.02	0.56	0.03	0.0	1.70
95%GL+5% SD-0%OFA																
	2.57	0.09	520.3	26.8	86.2	2.6	16.7	0.2	930.7	13.2	1.24	0.02	0.69	0.04	0.0	1.62
	3.27	0.13	715.4	67.4	82.4	2.4	16.4	0.3	914.1	15.8	1.22	0.02	0.98	0.09	9.6	4.35
	3.44	0.16	502.2	24.4	87.5	2.8	16.7	0.2	919.9	16.9	1.22	0.02	0.67	0.03	0.0	1.62
	3.46	0.17	526.8	25.2	89.9	2.7	16.6	0.2	937.5	15.9	1.25	0.02	0.70	0.03	0.0	1.62
	3.66	0.19	623.1	36.3	84.2	3.1	16.8	0.3	951.7	10.3	1.27	0.01	0.83	0.05	0.0	1.62
	4.52	0.19	581.3	22.9	96.0	3.0	16.4	0.2	863.2	11.5	1.15	0.02	0.77	0.03	0.0	1.62
95%GL+5% SD-15%OFA																
	2.65	0.16	257.4	16.6	104.4	2.2	16.7	0.2	913.8	11.5	1.21	0.02	0.34	0.02	0.0	1.62
	3.82	0.15	347.4	18.1	103.7	2.8	16.6	0.3	904.7	12.9	1.20	0.02	0.46	0.02	0.0	1.62
	4.59	0.18	375.0	19.1	103.1	3.3	16.5	0.3	910.2	53.3	1.21	0.07	0.50	0.03	0.0	1.62
90%GL+10% SD-0%OFA																
	2.32	0.16	473.7	15.5	91.6	2.3	16.9	0.2	866.2	8.0	1.15	0.01	0.63	0.02	0.0	1.53
	3.02	0.09	549.5	45.0	86.5	3.0	16.6	0.2	907.5	10.5	1.21	0.01	0.74	0.04	10.2	4.37
	3.11	0.17	728.2	69.6	92.0	2.5	16.2	0.2	831.2	12.6	1.10	0.02	0.97	0.09	13.3	5.20
	3.18	0.14	547.1	23.4	86.9	2.7	16.7	0.2	919.7	11.8	1.22	0.02	0.73	0.03	0.0	1.53
	3.33	0.15	741.4	59.0	91.1	2.7	16.4	0.2	838.3	20.2	1.11	0.03	0.98	0.07	7.0	3.51
	3.41	0.17	652.8	79.5	92.2	4.1	16.6	0.2	914.9	12.8	1.22	0.02	0.88	0.04	0.0	1.53
	3.43	0.20	573.1	21.4	86.5	2.7	16.6	0.2	907.8	8.9	1.21	0.01	0.76	0.03	0.0	1.53
	4.37	0.15	631.6	25.2	88.4	2.6	16.6	0.2	920.3	10.1	1.22	0.01	0.84	0.03	0.0	1.53
90%GL+10% SD-15%OFA																
	2.60	0.16	233.5	14.3	105.0	2.8	16.8	0.2	891.2	12.9	1.18	0.02	0.31	0.02	0.0	1.53
	3.05	0.22	286.2	22.8	100.4	2.4	16.3	0.2	849.3	11.9	1.13	0.02	0.38	0.03	10.3	4.42
	3.44	0.13	299.3	16.6	103.4	3.0	16.8	0.2	865.8	11.0	1.15	0.01	0.40	0.02	0.8	1.77
	3.62	0.15	306.0	13.6	100.8	2.6	16.7	0.2	860.0	8.8	1.14	0.01	0.41	0.02	0.0	1.53
	3.91	0.18	313.3	17.3	105.6	2.7	16.7	0.2	870.6	11.8	1.16	0.02	0.42	0.02	0.0	1.53
	4.35	0.17	368.7	20.1	99.1	2.9	16.6	0.2	897.7	13.4	1.19	0.02	0.49	0.03	0.0	1.53
80%GL+20% SD-0%OFA																
	2.44	0.15	429.8	16.6	89.3	2.3	16.9	0.2	851.3	9.3	1.13	0.01	0.57	0.02	0.0	1.43
	2.89	0.15	586.0	40.9	102.4	3.0	16.5	0.2	811.7	9.9	1.08	0.01	0.78	0.06	10.8	4.31
	3.13	0.14	577.6	47.0	102.8	3.3	16.7	0.2	817.3	12.5	1.09	0.02	0.76	0.06	7.2	3.38
	3.34	0.17	481.4	22.9	91.5	3.0	16.7	0.3	856.0	14.3	1.14	0.02	0.64	0.03	0.0	1.43
	3.54	0.20	496.8	22.9	92.7	2.9	16.8	0.2	860.4	7.8	1.14	0.01	0.66	0.03	0.0	1.43
	3.58	0.12	476.5	20.9	92.1	2.7	16.8	0.2	854.4	14.0	1.14	0.02	0.63	0.03	0.0	1.43
	4.00	0.18	521.2	29.2	93.1	2.4	16.7	0.2	861.4	7.6	1.15	0.01	0.69	0.04	0.0	1.43
80%GL+20% SD-15%OFA																
	2.65	0.23	246.4	15.5	113.7	3.1	17.0	0.2	839.2	9.5	1.12	0.01	0.33	0.02	0.0	1.43
	2.73	0.12	214.6	15.4	101.4	2.5	16.8	0.2	842.6	10.6	1.12	0.01	0.29	0.02	0.0	1.43
	3.29	0.13	282.3	19.1	110.9	3.1	16.9	0.3	832.2	11.2	1.11	0.01	0.37	0.03	2.5	2.13
	3.40	0.16	279.8	19.4	104.4	2.7	16.8	0.2	824.0	12.8	1.10	0.02	0.37	0.03	0.0	1.43
	3.40	0.14	283.7	15.8	110.1	3.8	16.9	0.2	834.7	14.1	1.11	0.02	0.38	0.02	0.0	1.43
	3.50	0.18	332.1	21.5	110.5	3.2	16.5	0.2	823.3	7.4	1.09	0.01	0.45	0.03	12.0	4.63
	4.14	0.17	355.1	11.9	114.0	3.4	16.9	0.2	840.5	23.5	1.12	0.03	0.47	0.02	0.9	1.68
	4.24	0.17	355.6	16.0	114.1	4.5	16.9	0.3	856.3	16.1	1.14	0.02	0.47	0.02	0.0	1.43
	4.43	0.09	317.6	17.8	101.7	2.8	16.7	0.3	831.0	12.6	1.10	0.02	0.42	0.02	0.0	1.43

Table A-10C. Gas Flow Data for UBC Measurements from GL-11.

Test 11 - GL Coal Comilled with SD, Ammonia Added to Increase Fuel N - UBC DATA - NO AMMONIA																
Unburned Carbon Data							----- FURNACE AIR FLOWS, SCFM (60°F, 29.92 in. Hg) ------								Fuel Feed	
Test Condition	FEO, Wet %		NOx, 3% O_2, ppm		% UBC		Total Air		Pri. Air (150°F)		Sec. Air (600°F)		OFA (600°F)		Rate, lb/hr	
	Avg.	S.D.	Avg.	S.D.	Avg.	S.D.	Avg.	S.D.	Avg.	S.D.	Avg.	S.D.	Avg.	S.D.	Avg.	S.D.
100%GL-0% OFA	3.56	0.05	569.5	29.9	1.21	0.09	690.0	2.2	131.1	0.3	558.9	2.0	0.0	0.0	268.5	2.2
100%GL-15% OFA	3.70	0.31	339.9	73.7	5.67	0.40	689.9	2.1	131.1	0.2	455.3	1.7	103.5	0.3	269.5	1.4
95%GL+5% SD-0%OFA	2.58	0.09	515.9	25.0	1.00	0.04	649.7	1.6	123.5	0.2	526.2	1.6	0.0	0.0	273.3	2.3
	3.46	0.18	526.1	22.4	1.46	0.03	689.7	1.8	131.1	0.2	558.6	1.8	0.0	0.0	274.4	1.9
	4.46	0.29	578.8	24.5	0.60	0.02	746.3	12.7	141.8	2.3	604.5	10.5	0.0	0.0	274.3	2.4
95%GL+5% SD-15%OFA	2.65	0.19	256.8	17.1	6.15	0.38	650.1	1.3	123.5	0.2	429.1	1.3	97.5	0.1	273.2	2.5
	3.82	0.15	346.1	18.2	4.03	0.18	700.1	2.4	133.0	0.2	462.1	2.2	105.0	0.2	273.7	2.0
	4.59	0.15	374.4	20.4	3.34	0.21	739.9	1.9	140.6	0.2	488.3	1.8	111.0	0.2	273.5	2.5
90%GL+10% SD-0%OFA	3.43	0.21	569.7	21.2	0.95	0.07	679.5	3.0	129.2	0.3	550.4	2.8	0.0	0.0	279.0	2.7
90%GL+10% SD-15%OFA	3.96	0.20	317.5	18.3	3.59	0.06	690.1	1.9	131.1	0.2	455.5	1.7	103.5	0.2	279.5	2.4
80%GL+20% SD-0%OFA	3.69	0.31	476.8	23.5	0.39	0.01	689.1	5.2	130.9	1.1	558.2	4.3	0.0	0.0	292.1	2.8
80%GL+20% SD-15%OFA	3.55	0.20	288.5	23.5	2.50	0.01	700.2	2.1	133.0	0.2	462.1	2.0	105.0	0.1	292.3	2.4

Table A-10D. Gas Sampling Data for UBC Measurements from GL-11.

Test 11 - GL Coal Comilled with SD, Ammonia Added to Increase Fuel N - UBC DATA - NO AMMONIA																
Unburned Carbon Data																
Test Condition	FEO, Wet %		NOx, 3% O_2, ppm		% UBC		CO, 3% O_2, ppm		CO_2, 3% O_2, %		SO_2, 3% O_2, ppm		SO_2, lb/10^6Btu		NO_x, lb/10^6Btu	
	Avg.	S.D.	Avg.	S.D.	Avg.	S.D.	Avg.	S.D.	Avg.	S.D.	Avg.	S.D.	Avg.	S.D.	Avg.	S.D.
100%GL-0% OFA	3.56	0.05	569.5	29.9	1.21	0.09	90.2	2.8	16.6	0.2	946.1	15.4	1.32	0.02	0.8	0.04
100%GL-15% OFA	3.70	0.31	339.9	73.7	5.67	0.40	112.0	21.1	16.0	3.0	864.4	206.1	1.20	0.29	0.5	0.10
95%GL+5% SD-0%OFA	2.58	0.09	515.9	25.0	1.00	0.04	86.4	2.6	16.7	0.2	928.4	12.5	1.29	0.02	0.7	0.03
	3.46	0.18	526.1	22.4	1.46	0.03	89.7	2.7	16.6	0.2	938.7	17.0	1.31	0.02	0.7	0.03
	4.46	0.29	578.8	24.5	0.60	0.02	95.9	3.1	16.4	0.2	863.6	11.9	1.20	0.02	0.8	0.03
95%GL+5% SD-15%OFA	2.65	0.19	256.8	17.1	6.15	0.38	104.5	2.0	16.7	0.2	920.6	9.0	1.28	0.01	0.4	0.02
	3.82	0.15	346.1	18.2	4.03	0.18	103.8	2.7	16.6	0.3	902.9	11.7	1.26	0.02	0.5	0.03
	4.59	0.15	374.4	20.4	3.34	0.21	103.7	2.6	16.5	0.2	915.2	16.3	1.27	0.02	0.5	0.03
90%GL+10% SD-0%OFA	3.43	0.21	569.7	21.2	0.95	0.07	86.6	2.8	16.7	0.2	909.7	11.7	1.26	0.02	0.8	0.03
90%GL+10% SD-15%OFA	3.96	0.20	317.5	18.3	3.59	0.06	105.3	2.9	16.7	0.3	866.3	13.8	1.20	0.02	0.4	0.03
80%GL+20% SD-0%OFA	3.69	0.31	476.8	23.5	0.39	0.01	91.9	2.7	16.8	0.3	851.7	12.5	1.18	0.02	0.7	0.03
80%GL+20% SD-15%OFA	3.55	0.20	288.5	23.5	2.50	0.01	103.4	3.3	16.8	0.2	821.4	17.3	1.14	0.02	0.4	0.03

Table A-11A. Gas Flow Data from Test JW-12.

Test 12 - Jim Walters #7 Mine Low-Vol Coal Comilled with SD														
Furnace Flow Data					------- FURNACE AIR FLOWS, SCFM (60°F, 29.92 in. Hg) ------								Fuel Feed	
Test Condition	FEO, Wet %		NOx, 3% O_2, ppm		Total Air		Pri. Air (150°F)		Sec. Air (600°F)		OFA (600°F)		Rate, lb/hr	
	Avg.	S.D.	Avg.	S.D.	Avg.	S.D.	Avg.	S.D.	Avg.	S.D.	Avg.	S.D.	Avg.	S.D.
100%JW#7-0% OFA														
	2.71	0.20	597.1	23.6	670.1	2.3	127.3	0.3	542.8	2.2	0.0	0.0	264.4	2.4
	3.42	0.19	631.8	19.7	699.7	2.3	133.0	0.3	566.7	2.2	0.0	0.0	264.3	2.4
	4.52	0.18	690.5	18.4	750.2	2.5	142.5	0.3	607.7	2.4	0.0	0.0	264.1	2.4
100%JW#7-15% OFA														
	2.63	0.20	340.4	20.9	659.8	2.3	125.4	0.2	435.4	2.2	99.0	0.3	264.8	2.8
	3.62	0.20	422.6	21.2	699.1	1.9	133.0	0.2	461.1	1.7	105.0	0.2	264.9	3.2
	3.77	0.17	413.6	19.1	700.2	2.3	133.0	0.2	462.2	2.2	105.0	0.1	264.9	2.1
	4.54	0.17	489.7	25.7	739.5	2.3	140.6	0.3	488.0	1.9	111.0	0.3	264.5	2.8
95%JW#7+5% SD-0%OFA														
	2.56	0.19	576.5	17.8	660.8	8.5	125.6	1.5	535.2	7.1	0.0	0.0	270.9	2.2
	3.51	0.17	605.0	19.7	700.1	2.2	133.0	0.2	567.1	2.1	0.0	0.0	270.7	2.2
	3.53	0.19	601.4	19.9	699.8	3.6	133.0	0.3	566.8	3.4	0.0	0.0	270.7	2.3
	4.54	0.15	678.9	16.1	749.9	2.3	142.5	0.3	607.4	2.2	0.0	0.0	270.8	2.3
95%JW#7+5% SD-15%OFA														
	2.65	0.18	370.0	29.9	660.0	2.0	125.4	0.2	435.5	1.9	99.0	0.1	271.2	2.1
	3.59	0.22	420.4	20.9	700.0	2.5	133.0	0.2	462.0	2.3	105.0	0.8	269.8	2.5
	3.77	0.18	437.9	16.5	698.2	8.4	132.4	1.9	461.2	5.4	104.6	1.5	270.4	2.3
	4.33	0.19	489.8	20.8	740.2	2.1	140.6	0.3	488.6	2.0	111.0	0.1	271.3	2.2
90%JW#7+10% SD-0%OFA														
	2.64	0.17	460.8	17.8	650.1	3.2	123.5	0.2	526.6	3.2	0.0	0.0	275.8	2.6
	3.48	0.14	522.2	17.5	679.6	3.7	129.1	0.7	550.5	3.4	0.0	0.0	275.9	2.2
	4.66	0.18	626.6	15.5	740.2	2.0	140.6	0.2	599.6	1.9	0.0	0.0	275.7	2.3
90%JW#7+10% SD-15%OFA														
	2.83	0.18	318.9	18.5	661.0	3.6	125.4	0.2	436.6	3.5	99.1	0.2	276.2	2.2
	3.74	0.15	388.6	16.9	700.0	2.1	133.0	0.2	462.1	2.0	105.0	0.2	275.8	2.4
	4.69	0.17	420.4	15.3	740.0	2.6	140.7	0.3	489.7	11.5	109.7	12.0	275.5	2.4
80%JW#7+20% SD-0%OFA														
	2.69	0.20	546.1	15.9	660.3	2.6	125.5	0.2	534.8	2.6	0.0	0.0	286.9	2.3
	3.71	0.14	635.2	18.0	699.6	2.2	133.0	0.2	566.6	2.1	0.0	0.0	287.3	2.3
	3.72	0.20	632.7	18.0	700.4	2.7	133.0	0.2	567.4	2.7	0.0	0.0	287.2	2.3
	4.39	0.24	684.0	16.2	740.5	3.1	140.6	0.3	599.9	3.1	0.0	0.0	287.2	2.7
80%JW#7+20% SD-15%OFA														
	2.76	0.16	326.0	11.2	661.4	10.0	125.6	1.6	436.6	7.2	99.2	1.3	286.9	2.6
	3.49	0.19	364.0	16.6	699.4	4.6	132.9	0.9	461.7	3.2	104.9	0.8	286.9	2.2
	4.67	0.17	483.9	21.4	740.0	2.8	140.6	0.3	488.4	2.7	111.0	0.2	287.0	2.4

Table A-11B. Gas Flow Data for UBC Measurements from JW-12.

Test 12 - Jim Walters #7 Mine Low-Vol Coal Comilled with SD																
Unburned Carbon Data							----- FURNACE AIR FLOWS, SCFM (60°F, 29.92 in. Hg) ------								Fuel Feed	
Test Condition	FEO, Wet %		NOx, 3% O_2, ppm		% UBC		Total Air		Pri. Air (150°F)		Sec. Air (600°F)		OFA (600°F)		Rate, lb/hr	
	Avg.	S.D.	Avg.	S.D.	Avg.	S.D.	Avg.	S.D.	Avg.	S.D.	Avg.	S.D.	Avg.	S.D.	Avg.	S.D.
100%JW#7-0% OFA	2.66	0.27	598.0	21.5	1.2	0.1	669.9	2.8	127.3	0.2	542.6	2.7	0.0	0.0	264.6	2.4
	3.51	0.29	630.3	18.3	0.9	0.0	699.8	2.0	133.0	0.3	566.8	1.9	0.0	0.0	264.4	2.5
	4.44	0.16	692.2	20.4	0.5	0.0	750.4	2.5	142.4	0.3	607.9	2.3	0.0	0.0	264.3	2.3
100%JW#7-15% OFA	2.57	0.19	345.0	19.3	4.1	0.5	660.0	2.4	125.4	0.2	435.6	2.3	99.1	0.4	264.5	2.5
	3.66	0.19	428.6	18.8	2.4	0.1	699.5	2.0	132.9	0.2	461.6	1.9	105.0	0.2	265.0	3.1
	4.48	0.20	492.2	21.3	1.8	0.1	740.4	2.3	140.6	0.2	488.8	2.2	111.0	0.2	264.6	2.5
95%JW#7+5% SD-0%OFA	2.61	0.57	581.7	23.2	1.2	0.0	660.0	3.0	125.4	0.2	534.6	2.9	0.0	0.0	270.9	2.2
	3.42	0.22	620.9	25.8	0.7	0.0	699.9	3.1	133.0	0.4	566.9	2.9	0.0	0.0	271.1	2.3
	4.51	0.21	680.0	15.0	0.4	0.0	749.5	2.1	142.5	0.3	606.9	1.9	0.0	0.0	270.7	2.3
95%JW#7+5% SD-15%OFA	2.69	0.22	368.3	28.5	2.9	0.1	660.1	2.0	125.4	0.2	435.7	1.9	99.0	0.1	271.1	2.2
	3.57	0.24	416.8	21.4	2.2	0.1	699.6	2.1	133.0	0.2	461.7	2.0	104.9	0.8	269.5	2.6
	4.35	0.17	488.2	21.2	1.3	0.0	740.3	2.2	140.6	0.3	488.8	2.0	111.0	0.1	271.1	2.2
90%JW#7+10% SD-0%OFA	2.62	0.15	459.9	18.5	1.6	0.1	650.4	2.6	123.5	0.2	526.9	2.6	0.0	0.0	275.9	2.7
	3.56	0.31	530.1	19.2	0.8	0.0	680.4	2.8	129.2	0.3	551.2	2.7	0.0	0.0	275.3	2.5
	4.64	0.19	625.3	15.5	0.4	0.0	740.0	1.8	140.6	0.2	599.4	1.8	0.0	0.0	275.8	2.3
90%JW#7+10% SD-15%OFA	2.96	0.26	326.9	34.8	2.5	0.1	660.6	3.5	125.4	0.2	436.2	3.4	99.0	0.1	276.1	2.3
	3.78	0.17	402.4	12.4	1.4	0.0	700.3	2.4	132.9	0.3	462.4	2.2	105.0	0.2	275.6	2.5
	4.69	0.17	423.6	13.8	1.1	0.1	739.6	2.2	140.6	0.2	488.0	2.1	111.0	0.2	275.4	2.5
80%JW#7+20% SD-0%OFA	2.73	0.27	548.3	17.2	0.8	0.0	660.5	2.6	125.5	0.2	535.0	2.6	0.0	0.0	287.0	2.4
	3.76	0.24	633.9	14.9	0.5	0.0	699.9	2.4	133.0	0.2	566.8	2.3	0.0	0.0	287.1	2.2
	4.39	0.24	684.0	16.2	0.5	0.0	740.5	3.1	140.6	0.3	599.9	3.1	0.0	0.0	287.2	2.7
80%JW#7+20% SD-15%OFA	2.81	0.22	325.5	12.7	2.1	0.1	660.3	2.1	125.4	0.2	435.9	2.0	99.0	0.2	286.6	2.7
	3.34	0.19	382.0	12.1	1.7	0.0	700.0	1.8	133.0	0.2	462.0	1.7	105.0	0.2	286.9	2.4
	4.62	0.29	479.3	25.1	0.8	0.0	740.1	3.1	140.6	0.2	488.5	3.0	111.0	0.3	286.8	2.3

Table A-11C. Gas Sampling Data from JW-12.

Test 12 - Jim Walters #7 Mine Low-Vol Coal Comilled with SD														
Gas Sampling Data														
Test Condition	FEO, Wet %		NOx, 3% O_2, ppm		CO, 3% O_2, ppm		CO_2, 3% O_2, %		SO_2, 3% O_2, ppm		SO_2, lb/10^6Btu		NO_X, lb/10^6Btu	
	Avg.	S.D.	Avg.	S.D.	Avg.	S.D.	Avg.	S.D.	Avg.	S.D.	Avg.	S.D.	Avg.	S.D.
100%JW#7-0% OFA														
	2.71	0.20	597.1	23.6	85.0	2.2	16.7	0.2	540.0	6.6	0.73	0.01	0.81	0.03
	3.42	0.19	631.8	19.7	86.9	2.6	16.6	0.2	532.0	7.5	0.72	0.01	0.86	0.03
	4.52	0.18	690.5	18.4	86.0	3.0	16.6	0.2	485.6	7.2	0.66	0.01	0.94	0.02
100%JW#7-15% OFA														
	2.63	0.20	340.4	20.9	99.1	2.4	16.7	0.2	535.5	8.5	0.73	0.01	0.46	0.03
	3.62	0.20	422.6	21.2	99.6	2.1	16.9	0.2	523.2	6.0	0.71	0.01	0.57	0.03
	3.77	0.17	413.6	19.1	94.4	2.5	16.8	0.2	486.0	6.5	0.66	0.01	0.56	0.03
	4.54	0.17	489.7	25.7	95.7	2.4	16.5	0.2	508.8	5.9	0.69	0.01	0.66	0.03
95%JW#7+5% SD-0%OFA														
	2.56	0.19	576.5	17.8	92.1	2.6	16.8	0.1	486.4	5.3	0.66	0.01	0.78	0.02
	3.51	0.17	605.0	19.7	90.9	2.8	16.7	0.2	498.4	21.4	0.68	0.03	0.82	0.03
	3.53	0.19	601.4	19.9	93.2	2.7	16.7	0.2	479.7	5.8	0.65	0.01	0.81	0.03
	4.54	0.15	678.9	16.1	95.2	2.8	16.6	0.2	450.7	13.1	0.61	0.02	0.92	0.02
95%JW#7+5% SD-15%OFA														
	2.65	0.18	370.0	29.9	98.2	7.2	16.8	0.2	482.2	8.7	0.65	0.01	0.50	0.04
	3.59	0.22	420.4	20.9	95.3	2.7	16.8	0.2	473.1	9.3	0.64	0.01	0.57	0.03
	3.77	0.18	437.9	16.5	98.1	2.6	16.7	0.2	472.2	5.2	0.64	0.01	0.59	0.02
	4.33	0.19	489.8	20.8	99.9	3.0	16.5	0.2	475.8	9.3	0.64	0.01	0.66	0.03
90%JW#7+10% SD-0%OFA														
	2.64	0.17	460.8	17.8	94.1	2.9	17.0	0.2	483.7	24.1	0.66	0.03	0.62	0.02
	3.48	0.14	522.2	17.5	94.8	2.6	16.9	0.2	456.9	6.0	0.62	0.01	0.71	0.02
	4.66	0.18	626.6	15.5	96.2	2.9	16.7	0.2	447.8	12.3	0.61	0.02	0.85	0.02
90%JW#7+10% SD-15%OFA														
	2.83	0.18	318.9	18.5	95.3	2.6	16.8	0.2	474.7	7.6	0.64	0.01	0.43	0.03
	3.74	0.15	388.6	16.9	96.1	2.7	16.7	0.2	457.3	12.4	0.62	0.02	0.53	0.02
	4.69	0.17	420.4	15.3	98.1	2.5	16.6	0.2	475.5	5.7	0.64	0.01	0.57	0.02
80%JW#7+20% SD-0%OFA														
	2.69	0.20	546.1	15.9	85.7	3.0	16.8	0.1	433.6	6.1	0.59	0.01	0.74	0.02
	3.71	0.14	635.2	18.0	88.9	2.9	16.8	0.2	425.9	13.4	0.58	0.02	0.86	0.02
	3.72	0.20	632.7	18.0	88.3	2.4	16.7	0.2	417.0	7.1	0.56	0.01	0.86	0.02
	4.39	0.24	684.0	16.2	89.6	2.2	16.6	0.3	415.3	17.0	0.56	0.02	0.93	0.02
80%JW#7+20% SD-15%OFA														
	2.76	0.16	326.0	11.2	89.4	2.4	16.9	0.1	439.4	11.5	0.60	0.02	0.44	0.02
	3.49	0.19	364.0	16.6	95.0	2.7	16.8	0.2	432.2	8.9	0.59	0.01	0.49	0.02
	4.67	0.17	483.9	21.4	93.7	2.9	16.7	0.2	407.0	7.7	0.55	0.01	0.66	0.03

Table A-11D. Gas Sampling Data for UBC Measurements from JW-12.

Test 12 - Jim Walters #7 Mine Low-Vol Coal Comilled with SD																
Unburned Carbon Data																
Test Condition	FEO, Wet %		NOx, 3% O_2, ppm		% UBC		CO, 3% O_2, ppm		CO_2, 3% O_2, %		SO_2, 3% O_2, ppm		SO_2, lb/10^6Btu		NO_x, lb/10^6Btu	
	Avg.	S.D.	Avg.	S.D.	Avg.	S.D.	Avg.	S.D.	Avg.	S.D.	Avg.	S.D.	Avg.	S.D.	Avg.	S.D.
100%JW#7-0% OFA	2.66	0.27	598.0	21.5	1.18	0.06	85.5	2.3	16.7	0.2	540.5	6.4	0.73	0.01	0.81	0.03
	3.51	0.29	630.3	18.3	0.88	0.01	87.5	2.7	16.7	0.2	524.6	10.9	0.71	0.01	0.85	0.02
	4.44	0.16	692.2	20.4	0.48	0.04	86.5	3.0	16.6	0.1	489.6	6.4	0.66	0.01	0.94	0.03
100%JW#7-15% OFA	2.57	0.19	345.0	19.3	4.09	0.53	98.5	2.3	16.7	0.1	537.4	6.9	0.73	0.01	0.47	0.03
	3.66	0.19	428.6	18.8	2.39	0.06	99.4	2.1	16.8	0.1	522.4	5.1	0.71	0.01	0.58	0.03
	4.48	0.20	492.2	21.3	1.78	0.07	96.3	2.3	16.5	0.2	512.6	6.1	0.69	0.01	0.67	0.03
95%JW#7+5% SD-0%OFA	2.61	0.57	581.7	23.2	1.17	0.05	92.2	2.5	16.8	0.2	486.6	5.4	0.66	0.01	0.79	0.03
	3.42	0.22	620.9	25.8	0.74	0.01	92.5	2.5	16.7	0.2	488.8	12.1	0.66	0.02	0.84	0.03
	4.51	0.21	680.0	15.0	0.41	0.02	95.7	2.6	16.6	0.2	440.7	12.6	0.60	0.02	0.92	0.02
95%JW#7+5% SD-15%OFA	2.69	0.22	368.3	28.5	2.92	0.09	98.1	7.3	16.8	0.2	483.2	7.7	0.65	0.01	0.50	0.04
	3.57	0.24	416.8	21.4	2.20	0.13	95.1	2.9	16.8	0.2	471.7	10.0	0.64	0.01	0.56	0.03
	4.35	0.17	488.2	21.2	1.25	0.05	99.9	3.1	16.5	0.2	473.4	8.5	0.64	0.01	0.66	0.03
90%JW#7+10% SD-0%OFA	2.62	0.15	459.9	18.5	1.64	0.09	94.9	2.7	17.0	0.2	479.7	25.9	0.65	0.04	0.62	0.03
	3.56	0.31	530.1	19.2	0.77	0.05	94.5	2.5	16.9	0.2	469.2	13.8	0.64	0.02	0.72	0.03
	4.64	0.19	625.3	15.5	0.36	0.01	96.0	2.8	16.7	0.2	448.7	13.4	0.61	0.02	0.85	0.02
90%JW#7+10% SD-15%OFA	2.96	0.26	326.9	34.8	2.54	0.12	96.0	2.5	16.8	0.2	475.5	7.0	0.64	0.01	0.44	0.05
	3.78	0.17	402.4	12.4	1.41	0.04	96.3	2.7	16.7	0.2	468.3	10.9	0.63	0.01	0.55	0.02
	4.69	0.17	423.6	13.8	1.14	0.06	98.1	2.6	16.6	0.2	476.3	5.8	0.65	0.01	0.57	0.02
80%JW#7+20% SD-0%OFA	2.73	0.27	548.3	17.2	0.78	0.02	85.8	2.8	16.8	0.2	433.1	6.0	0.59	0.01	0.74	0.02
	3.76	0.24	633.9	14.9	0.48	0.02	88.5	2.8	16.8	0.2	428.0	14.4	0.58	0.02	0.86	0.02
	4.39	0.24	684.0	16.2	0.53	0.02	89.6	2.2	16.6	0.3	415.3	17.0	0.56	0.02	0.93	0.02
80%JW#7+20% SD-15%OFA	2.81	0.22	325.5	12.7	2.06	0.05	89.6	2.5	16.9	0.2	441.9	10.4	0.60	0.01	0.44	0.02
	3.34	0.19	382.0	12.1	1.68	0.03	94.2	2.7	16.8	0.1	440.5	16.6	0.60	0.02	0.52	0.02
	4.62	0.29	479.3	25.1	0.79	0.05	93.7	2.8	16.6	0.3	406.6	8.6	0.55	0.01	0.65	0.03

Table A-12A. Gas Flow Data from Test JW-13.

Test 13 - Jim Walters #7 Mine Low-Vol Coal Comilled with SG														
Furnace Flow Data					------- FURNACE AIR FLOWS, SCFM (60°F, 29.92 in. Hg) ------								Fuel Feed	
Test Condition	FEO, Wet %		NOx, 3% O_2, ppm		Total Air		Pri. Air (150°F)		Sec. Air (600°F)		OFA (600°F)		Rate, lb/hr	
	Avg.	S.D.	Avg.	S.D.	Avg.	S.D.	Avg.	S.D.	Avg.	S.D.	Avg.	S.D.	Avg.	S.D.
100%JW#7-0% OFA														
	2.59	0.19	552.2	25.9	669.9	2.1	127.3	0.2	542.5	2.1	0.0	0.0	265.2	2.5
	3.63	0.19	639.9	16.9	710.4	3.0	134.9	0.3	575.5	3.0	0.0	0.0	265.1	2.3
	4.72	0.18	693.6	25.3	760.0	3.0	144.4	0.3	615.6	2.8	0.0	0.0	265.4	2.2
100%JW#7-15% OFA														
	2.76	0.22	384.3	27.9	669.9	3.8	127.3	0.3	442.1	3.5	100.5	0.4	265.2	2.6
	3.67	0.17	449.1	20.0	710.3	2.2	134.9	0.3	468.9	2.1	106.5	0.2	265.5	2.5
	4.54	0.19	550.8	26.0	749.7	3.3	142.5	0.3	494.7	3.1	112.5	0.3	265.6	2.2
95%JW#7+5% SG-0%OFA														
	2.68	0.18	576.1	25.7	670.2	5.1	127.3	0.6	542.9	4.7	0.0	0.0	271.1	3.4
	3.69	0.17	664.2	15.4	720.1	2.2	136.8	0.2	583.3	2.2	0.0	0.0	270.4	2.0
	4.59	0.17	751.8	15.5	759.9	2.5	144.4	0.3	615.5	2.4	0.0	0.0	270.6	2.1
95%JW#7+5% SG-15%OFA														
	2.88	0.20	420.4	17.4	679.8	1.6	129.2	0.3	448.5	1.4	102.0	0.2	270.4	2.5
	3.69	0.20	454.5	18.3	720.0	1.8	136.8	0.3	475.2	1.6	108.0	0.2	270.5	2.6
	4.65	0.20	550.7	20.0	760.4	2.2	144.4	0.3	502.0	2.0	114.0	0.2	270.1	2.4
90%JW#7+10% SG-0%OFA														
	2.53	0.19	482.3	19.5	670.1	2.7	127.3	0.2	542.8	2.6	0.0	0.0	276.7	2.3
	2.54	0.19	516.3	19.1	670.3	2.3	127.4	0.2	542.9	2.2	0.0	0.0	276.5	2.6
	3.72	0.16	617.0	12.9	720.0	3.0	136.8	0.4	583.2	2.8	0.0	0.0	277.0	2.0
	4.47	0.13	784.0	16.8	759.9	2.3	144.4	0.3	615.5	2.3	0.0	0.0	277.6	2.6
90%JW#7+10% SG-15%OFA														
	2.65	0.19	312.2	22.9	669.9	1.3	127.2	0.2	442.2	1.3	100.5	0.2	275.9	2.5
	2.72	0.20	374.9	24.1	670.3	2.6	127.3	0.3	442.5	2.1	100.5	0.3	276.2	2.7
	3.56	0.19	413.7	19.7	720.0	1.8	136.8	0.3	475.1	1.5	108.0	0.3	276.6	2.9
	3.67	0.17	439.7	20.0	719.8	1.9	136.8	0.3	475.0	1.7	108.0	0.2	276.8	2.5
	4.55	0.14	626.6	19.2	759.9	2.2	144.4	0.3	501.5	2.0	114.0	0.2	276.4	2.5
80%JW#7+20% SG-0%OFA														
	3.40	0.26	426.2	22.3	691.0	2.1	131.1	0.2	559.8	2.2	0.0	0.0	288.8	5.1
	3.52	0.23	484.8	21.3	699.4	2.2	133.0	0.2	566.4	2.1	0.0	0.0	288.6	7.2
	4.54	0.16	514.8	18.5	749.5	2.7	142.4	0.3	607.1	2.6	0.0	0.0	289.3	2.5
80%JW#7+20% SG-15%OFA														
	2.68	0.21	313.8	19.3	649.8	1.9	123.5	0.2	428.8	1.8	97.5	0.2	288.9	3.5
	3.90	0.21	406.5	25.6	710.0	2.0	134.9	0.2	468.6	1.9	106.5	0.2	288.6	2.7
	4.64	0.19	446.0	29.6	740.0	5.2	140.6	0.3	489.5	6.7	109.9	11.3	289.2	5.1

Table A-12B. Gas Sampling Data from JW-13.

Test 13 - Jim Walters #7 Mine Low-Vol Coal Comilled with SG																
Unburned Carbon Data							----- FURNACE AIR FLOWS, SCFM (60°F, 29.92 in. Hg) ------								Fuel Feed	
Test Condition	FEO, Wet %		NOx, 3% O_2, ppm		% UBC		Total Air		Pri. Air (150°F)		Sec. Air (600°F)		OFA (600°F)		Rate, lb/hr	
	Avg.	S.D.	Avg.	S.D.	Avg.	S.D.	Avg.	S.D.	Avg.	S.D.	Avg.	S.D.	Avg.	S.D.	Avg.	S.D.
100%JW#7-0% OFA																
	2.61	0.21	550.4	28.7	2.0	0.1	670.0	2.2	127.3	0.2	542.7	2.1	0.0	0.0	265.5	2.5
	3.58	0.21	632.1	20.6	0.9	0.0	710.6	2.9	134.9	0.2	575.6	2.9	0.0	0.0	265.7	2.3
	4.73	0.18	691.8	22.2	0.8	0.0	759.8	3.0	144.4	0.3	615.4	3.0	0.0	0.0	265.3	2.3
100%JW#7-15% OFA																
	2.74	0.24	380.9	34.7	3.0	0.2	670.6	3.2	127.3	0.3	442.7	3.0	100.5	0.3	265.5	2.6
	3.62	0.11	437.3	18.3	3.0	0.2	710.0	1.4	134.9	0.2	468.6	1.3	106.5	0.1	265.4	2.7
	4.52	0.19	542.6	20.9	2.1	0.0	749.9	2.1	142.5	0.2	494.9	2.0	112.5	0.2	265.5	2.2
95%JW#7+5% SG-0%OFA																
	2.74	0.23	572.4	27.9	0.8	0.0	669.7	3.3	127.3	0.2	542.4	3.2	0.0	0.0	271.2	3.6
	3.69	0.17	661.3	15.6	0.6	0.0	719.9	2.2	136.8	0.2	583.1	2.3	0.0	0.0	270.3	2.0
	4.57	0.27	737.4	19.2	0.5	0.0	760.3	3.0	144.4	0.3	616.0	2.9	0.0	0.0	270.7	2.2
95%JW#7+5% SG-15%OFA																
	2.85	0.21	418.5	19.6	2.2	0.0	679.8	1.3	129.2	0.2	448.6	1.2	102.0	0.1	270.2	2.5
	3.67	0.20	453.4	17.2	1.6	0.1	719.8	1.5	136.7	0.3	475.1	1.3	108.0	0.2	270.7	3.0
	4.67	0.19	553.6	19.9	1.0	0.0	760.4	2.2	144.4	0.2	502.0	2.1	114.0	0.2	270.2	2.5
90%JW#7+10% SG-0%OFA																
	2.50	0.24	483.0	20.0	1.3	0.1	671.1	8.6	127.5	1.6	543.6	7.1	0.0	0.0	276.5	2.3
	3.72	0.16	617.9	12.9	0.8	0.0	719.7	2.3	136.8	0.3	582.9	2.2	0.0	0.0	277.1	2.2
	4.48	0.13	783.1	17.1	0.5	0.0	760.0	2.3	144.4	0.3	615.6	2.2	0.0	0.0	277.5	2.6
90%JW#7+10% SG-15%OFA																
	2.68	0.23	338.0	42.1	2.8	0.2	670.0	1.4	127.2	0.2	442.3	1.4	100.5	0.1	275.9	2.4
	3.58	0.26	405.8	20.2	2.2	0.2	719.9	1.9	136.8	0.4	475.1	1.6	108.0	0.2	276.3	2.6
	4.55	0.14	627.8	19.8	1.5	0.0	759.9	2.3	144.4	0.3	501.5	2.1	114.0	0.2	276.4	2.5
80%JW#7+20% SG-0%OFA																
	3.39	0.26	427.6	20.9	1.4	0.0	690.2	2.7	131.1	0.3	559.1	2.7	0.0	0.0	288.9	5.6
	3.52	0.23	484.8	21.3	1.0	0.1	699.9	2.6	133.0	0.3	567.0	2.5	0.0	0.0	288.7	4.6
	4.53	0.16	514.6	18.8	0.8	0.0	749.7	2.2	142.5	0.3	607.3	2.1	0.0	0.0	289.2	2.6
80%JW#7+20% SG-15%OFA																
	2.67	0.30	316.4	23.1	3.6	0.2	649.6	1.8	123.5	0.2	428.6	1.7	97.5	0.2	289.3	3.7
	3.88	0.20	404.4	22.7	2.6	0.1	710.0	2.2	134.9	0.2	468.6	2.0	106.5	0.2	288.6	2.6
	4.64	0.19	443.8	27.8	2.2	0.1	740.7	1.8	140.6	0.3	489.0	1.6	111.0	0.2	290.0	5.4

Table A-12C. Gas Flow Data for UBC Measurements from JW-13.

Test 13 - Jim Walters #7 Mine Low-Vol Coal Comilled with SG														
Furnace Flow Data														
Test Condition	FEO, Wet %		NOx, 3% O_2, ppm		CO, 3% O_2, ppm		CO_2, 3% O_2, %		SO_2, 3% O_2, ppm		SO_2, lb/10^6Btu		NO_X, lb/10^6Btu	
	Avg.	S.D.	Avg.	S.D.	Avg.	S.D.	Avg.	S.D.	Avg.	S.D.	Avg.	S.D.	Avg.	S.D.
100%JW#7-0% OFA														
	2.59	0.19	552.2	25.9	87.2	2.3	16.8	0.2	476.1	8.6	0.65	0.01	0.75	0.04
	3.63	0.19	639.9	16.9	87.9	2.4	16.8	0.2	459.2	8.8	0.62	0.01	0.87	0.02
	4.72	0.18	693.6	25.3	87.7	2.5	16.6	0.2	438.8	7.9	0.60	0.01	0.94	0.03
100%JW#7-15% OFA														
	2.76	0.22	384.3	27.9	94.2	2.5	16.9	0.2	515.0	9.1	0.70	0.01	0.52	0.04
	3.67	0.17	449.1	20.0	99.1	2.9	16.7	0.1	482.7	7.5	0.66	0.01	0.61	0.03
	4.54	0.19	550.8	26.0	99.6	2.7	16.7	0.2	492.2	10.3	0.67	0.01	0.75	0.04
95%JW#7+5% SG-0%OFA														
	2.68	0.18	576.1	25.7	86.4	1.9	16.9	0.2	489.7	8.8	0.67	0.01	0.78	0.03
	3.69	0.17	664.2	15.4	86.7	2.1	16.8	0.2	477.4	5.7	0.65	0.01	0.90	0.02
	4.59	0.17	751.8	15.5	100.7	2.7	16.5	0.2	454.4	5.9	0.62	0.01	1.02	0.02
95%JW#7+5% SG-15%OFA														
	2.88	0.20	420.4	17.4	91.6	2.2	16.9	0.2	499.4	5.8	0.68	0.01	0.57	0.02
	3.69	0.20	454.5	18.3	91.9	2.5	16.8	0.2	463.1	13.2	0.63	0.02	0.62	0.02
	4.65	0.20	550.7	20.0	92.4	2.6	16.6	0.2	478.3	5.7	0.65	0.01	0.75	0.03
90%JW#7+10% SG-0%OFA														
	2.53	0.19	482.3	19.5	102.3	2.9	16.7	0.1	507.4	6.1	0.69	0.01	0.66	0.03
	2.54	0.19	516.3	19.1	102.0	3.1	16.7	0.1	498.5	6.5	0.68	0.01	0.70	0.03
	3.72	0.16	617.0	12.9	103.4	2.4	16.6	0.2	478.2	5.8	0.65	0.01	0.84	0.02
	4.47	0.13	784.0	16.8	107.2	2.7	16.4	0.2	462.6	5.7	0.63	0.01	1.07	0.02
90%JW#7+10% SG-15%OFA														
	2.65	0.19	312.2	22.9	106.3	3.2	16.8	0.1	483.2	9.2	0.66	0.01	0.42	0.03
	2.72	0.20	374.9	24.1	108.2	2.2	16.8	0.1	488.4	7.1	0.66	0.01	0.51	0.03
	3.56	0.19	413.7	19.7	109.7	3.0	16.6	0.2	467.3	5.5	0.63	0.01	0.56	0.03
	3.67	0.17	439.7	20.0	108.0	2.4	16.6	0.2	468.7	5.9	0.64	0.01	0.60	0.03
	4.55	0.14	626.6	19.2	112.6	2.5	16.5	0.1	464.5	7.4	0.63	0.01	0.85	0.03
80%JW#7+20% SG-0%OFA														
	3.40	0.26	426.2	22.3	94.0	2.7	16.6	0.2	426.4	9.9	0.58	0.01	0.58	0.03
	3.52	0.23	484.8	21.3	91.7	2.6	16.7	0.3	420.0	9.0	0.57	0.01	0.66	0.03
	4.54	0.16	514.8	18.5	92.1	2.7	16.5	0.2	410.4	9.1	0.56	0.01	0.70	0.03
80%JW#7+20% SG-15%OFA														
	2.68	0.21	313.8	19.3	119.0	2.6	16.7	0.2	441.0	6.9	0.60	0.01	0.43	0.03
	3.90	0.21	406.5	25.6	118.3	2.6	16.7	0.2	456.1	7.7	0.62	0.01	0.55	0.03
	4.64	0.19	446.0	29.6	120.8	3.2	16.4	0.3	417.6	13.1	0.57	0.02	0.61	0.04

Table A-12D. Gas Sampling Data for UBC Measurements from JW-13.

Test 13 - Jim Walters #7 Mine Low-Vol Coal Comilled with SG																
Unburned Carbon Data																
Test Condition	FEO, Wet %		NOx, 3% O_2, ppm		% UBC		CO, 3% O_2, ppm		CO_2, 3% O_2, %		SO_2, 3% O_2, ppm		SO_2, lb/10^6Btu		NO_x, lb/10^6Btu	
	Avg.	S.D.	Avg.	S.D.	Avg.	S.D.	Avg.	S.D.	Avg.	S.D.	Avg.	S.D.	Avg.	S.D.	Avg.	S.D.
100%JW#7-0% OFA																
	2.61	0.21	550.4	28.7	2.0	0.1	87.6	2.4	16.8	0.2	478.7	7.5	0.65	0.01	0.75	0.04
	3.58	0.21	632.1	20.6	0.9	0.0	86.4	3.3	16.8	0.2	461.4	7.7	0.62	0.01	0.86	0.03
	4.73	0.18	691.8	22.2	0.8	0.0	87.6	2.4	16.6	0.2	438.9	8.5	0.59	0.01	0.94	0.03
100%JW#7-15% OFA																
	2.74	0.24	380.9	34.7	3.0	0.2	94.2	2.5	16.8	0.2	515.5	8.7	0.70	0.01	0.52	0.05
	3.62	0.11	437.3	18.3	3.0	0.2	100.2	2.4	16.8	0.1	480.9	7.4	0.65	0.01	0.59	0.02
	4.52	0.19	542.6	20.9	2.1	0.0	100.1	2.7	16.7	0.2	489.9	9.4	0.66	0.01	0.74	0.03
95%JW#7+5% SG-0%OFA																
	2.74	0.23	572.4	27.9	0.8	0.0	86.7	2.0	16.8	0.2	492.0	6.1	0.67	0.01	0.77	0.04
	3.69	0.17	661.3	15.6	0.6	0.0	86.2	2.1	16.8	0.2	477.3	5.5	0.65	0.01	0.90	0.02
	4.57	0.27	737.4	19.2	0.5	0.0	91.1	2.2	16.7	0.2	455.4	7.4	0.62	0.01	1.00	0.03
95%JW#7+5% SG-15%OFA																
	2.85	0.21	418.5	19.6	2.2	0.0	91.5	2.1	16.9	0.2	498.9	5.5	0.68	0.01	0.57	0.03
	3.67	0.20	453.4	17.2	1.6	0.1	91.9	2.6	16.8	0.2	456.7	6.8	0.62	0.01	0.61	0.02
	4.67	0.19	553.6	19.9	1.0	0.0	92.7	2.6	16.6	0.2	477.5	5.5	0.65	0.01	0.75	0.03
90%JW#7+10% SG-0%OFA																
	2.50	0.24	483.0	20.0	1.3	0.1	102.1	3.0	16.7	0.1	508.5	5.4	0.69	0.01	0.65	0.03
	3.72	0.16	617.9	12.9	0.8	0.0	103.3	2.1	16.6	0.2	477.9	6.0	0.65	0.01	0.84	0.02
	4.48	0.13	783.1	17.1	0.5	0.0	107.2	2.7	16.4	0.2	462.4	5.6	0.63	0.01	1.06	0.02
90%JW#7+10% SG-15%OFA																
	2.68	0.23	338.0	42.1	2.8	0.2	107.2	2.9	16.8	0.1	486.1	7.5	0.66	0.01	0.46	0.06
	3.58	0.26	405.8	20.2	2.2	0.2	108.9	2.9	16.7	0.2	466.5	6.9	0.63	0.01	0.55	0.03
	4.55	0.14	627.8	19.8	1.5	0.0	112.6	2.6	16.5	0.2	465.2	7.1	0.63	0.01	0.85	0.03
80%JW#7+20% SG-0%OFA																
	3.39	0.26	427.6	20.9	1.4	0.0	94.5	2.7	16.6	0.3	425.9	11.3	0.58	0.02	0.58	0.03
	3.52	0.23	484.8	21.3	1.0	0.1	103.0	62.3	16.5	0.3	418.5	13.6	0.57	0.02	0.75	0.05
	4.53	0.16	514.6	18.8	0.8	0.0	92.2	2.7	16.5	0.2	411.1	9.2	0.56	0.01	0.70	0.03
80%JW#7+20% SG-15%OFA																
	2.67	0.30	316.4	23.1	3.6	0.2	118.6	2.5	16.7	0.2	436.8	8.9	0.59	0.01	0.43	0.03
	3.88	0.20	404.4	22.7	2.6	0.1	119.0	2.4	16.7	0.2	457.3	6.5	0.62	0.01	0.55	0.03
	4.64	0.19	443.8	27.8	2.2	0.1	120.9	3.1	16.4	0.3	415.7	10.9	0.56	0.01	0.60	0.04

APPENDIX B

Curvefits to Emissions Data

Table B-1A. Curvefits to NO_X emissions data for Tests PR-1, P-3, and PR-4.

Test	Fuel	% OFA	Curvefit, NO_X (ppm) = F(%FEO)
PR-1 Comill	100% Coal	0	NOx (ppm) = [exp(0.1359056098 • %FEO)] • 288.6239871
	100% Coal	15	NOx (ppm) = [exp(0.2256171884 • %FEO)] • 144.6827651
	100% Coal	30	NOx (ppm) = [exp(0.1987586042 • %FEO)] • 99.25790084
	+10% SD	0	NOx (ppm) = [exp(0.1359056098 • %FEO)] • 288.6239871
	+10% SD	15	NOx (ppm) = [exp(0.2256171884 • %FEO)] • 144.6827651
	+10% SD	30	NOx (ppm) = [exp(0.1987586042 • %FEO)] • 99.25790084
	+20% SD	0	NOx (ppm) = [exp(0.1885670355 • %FEO)] • 222.2200728
	+20% SD	15	NOx (ppm) = [exp(0.183924822 • %FEO)] • 134.2759303
	+20% SD	30	NOx (ppm) = [exp(0.1127068764 • %FEO)] • 129.0934419
	+15% SG	0	NOx (ppm) = [exp(0.1935383727 • %FEO)] • 203.8764363
	+15% SG	15	NOx (ppm) = [exp(0.1839956081 • %FEO)] • 136.7218973
	+15% SG	30	NOx (ppm) = [exp(0.05665514947 • %FEO)] • 141.0623055
	+20% SG	0	NOx (ppm) = [exp(0.1801735782 • %FEO)] • 191.3432886
	+20% SG	15	NOx (ppm) = [exp(0.16284737 • %FEO)] • 141.2456366
PR-3 Center	100% Coal	0	NOx (ppm) = [exp(0.04556175326 • %FEO)] • 417.420755
	100% Coal	15	NOx (ppm) = [exp(0.1079065902 • %FEO)] • 276.7088555
	+10% SD	0	NOx (ppm) = [exp(0.1022889916 • %FEO)] • 286.9518312
	+10% SD	15	NOx (ppm) = [exp(0.2099132791 • %FEO)] • 175.6148737
	+20% SD	0	NOx (ppm) = [exp(0.07257867972 • %FEO)] • 314.2842947
	+20% SD	15	NOx (ppm) = [exp(0.1926348708 • %FEO)] • 192.7603226
	+10% SG	0	NOx (ppm) = [exp(0.04912649073 • %FEO)] • 374.5455392
	+10% SG	15	NOx (ppm) = [exp(0.1895837052 • %FEO)] • 201.4744111
	+20% SG	0	NOx (ppm) = [exp(0.2083288129 • %FEO)] • 212.9027371
	+20% SG	15	NOx (ppm) = [exp(0.2025577886 • %FEO)] • 183.6443639
PR-4 Side	100% Coal	0	NOx (ppm) = [exp(0.104230848 • %FEO)] • 304.4560448
	100% Coal	15	NOx (ppm) = [exp(0.1618850999 • %FEO)] • 161.3413989
	+10% SD	0	NOx (ppm) = [exp(0.1716657863 • %FEO)] • 212.326962
	+10% SD	15	NOx (ppm) = [exp(0.1401229653 • %FEO)] • 162.3858172
	+20% SD	0	NOx (ppm) = [exp(0.09224916122 • %FEO)] • 306.529237
	+20% SD	15	NOx (ppm) = [exp(0.2925772738 • %FEO)] • 96.28709813
	+10% SG	0	NOx (ppm) = [exp(0.104230848 • %FEO)] • 304.4560448
	+10% SG	15	NOx (ppm) = [exp(0.1618850999 • %FEO)] • 161.3413989
	+20% SG	0	NOx (ppm) = [exp(0.1580186029 • %FEO)] • 217.2154242
	+20% SG	15	NOx (ppm) = [exp(0.1498066874 • %FEO)] • 186.1904124

Table B-1B. Curvefits to NO_X emissions data for Tests GL-5&6, PR-6, JR-7, and JR-8.

Test	Fuel	% OFA	Curvefit, NO_X (ppm) = F(%FEO)
GL-5&6 Comill	100% Coal	0	NOx (ppm) = [exp(0.1099729341 • %FEO)] • 319.8045512
	100% Coal	15	NOx (ppm) = 96.09342342 • (%FEO^1.005718829)
	+10% SD	0	NOx (ppm) = [exp(0.1674797639 • %FEO)] • 241.622634
	+10% SD	15	NOx (ppm) = [exp(0.1869732766 • %FEO)] • 144.5209938
	+20% SD	0	NOx (ppm) = [exp(0.1083144018 • %FEO)] • 321.3434144
	+20% SD	15	NOx (ppm) = 69.12237433 • %FEO + 82.52943888
	+10% SG	0	NOx (ppm) = [exp(0.1121870115 • %FEO)] • 311.7778125
	+10% SG	15	NOx (ppm) = [exp(0.1954040243 • %FEO)] • 161.5653439
	+20% SG	0	NOx (ppm) = [exp(0.0823574732 • %FEO)] • 372.2337779
	+20% SG	15	NOx (ppm) = - 51.8406882•(ln(%FEO)^2) + 369.7425333•ln(%FEO) - 53.01669606,
PR-6 Comill	100% Coal	0	NOx (ppm) = [exp(0.1281674508 • %FEO)] • 306.8779354
	100% Coal	15	NOx (ppm) = [exp(0.2362163406 • %FEO)] • 133.5812879
	+10% SD	0	NOx (ppm) = [exp(0.05802965439 • %FEO)] • 341.5412488
	+10% SD	15	N/A
JR-7 Comill	100% Coal	0	NOx (ppm) = [exp(0.1455589995 • %FEO)] • 219.9179535
	100% Coal	15	NOx (ppm) = [exp(0.2385240056 • %FEO)] • 96.55271511
	+10% SD	0	NOx (ppm) = [exp(0.138339097 • %FEO)] • 205.4999295
	+10% SD	15	NOx (ppm) = [exp(0.278737013 • %FEO)] • 69.0377288
	+20% SD	0	NOx (ppm) = [exp(0.1471869909 • %FEO)] • 191.2601883
	+20% SD	15	NOx (ppm) = [exp(0.2326142899 • %FEO)] • 78.09786552
	+10% SG	0	NOx (ppm) = [exp(0.1406739644 • %FEO)] • 193.0895701
	+10% SG	15	NOx (ppm) = [exp(0.275395431 • %FEO)] • 65.06295601
	+20% SG	0	NOx (ppm) = [exp(0.06499317769 • %FEO)] • 250.5933261
	+20% SG	15	NOx (ppm) = [exp(0.286790813 • %FEO)] • 64.32408276
JR-8 Center	100% Coal	0	NOx (ppm) = [exp(0.1115158002 • %FEO)] • 203.7807106
	100% Coal	15	NOx (ppm) = [exp(0.2321159819 • %FEO)] • 79.31752494
	+10% SD	0	NOx (ppm) = exp(0.01688472271 • %FEO^2) • exp(0.1144523767 • %FEO) • 164.593389
	+10% SD	15	NOx (ppm) = [exp(0.1731513847 • %FEO)] • 138.503919
	+15% SD	0	NOx (ppm) = [exp(0.1380919219 • %FEO)] • 190.7123615
	+15% SD	15	NOx (ppm) = [exp(0.2222286574 • %FEO)] • 99.2225662
	+10% SG	0	NOx (ppm) = 209.4652453 • ln(%FEO) + 41.01501296
	+10% SG	15	NOx (ppm) = 1.628911997 • (%FEO^3)+ 124.0537952
	+20% SG	0	NOx (ppm) = [exp(0.1410166512 • %FEO)] • 231.8222417
	+20% SG	15	NOx (ppm) = 1.598500424 • (%FEO^3) + 152.851728

Table B-1C. Curvefits to NO_X emissions data for Tests GL-9, GL-11&12, and JW-12&13.

Test	Fuel	% OFA	Curvefit, NO_X (ppm) = F(%FEO)

GL-9	100% Coal	16	NOx (ppm) = [exp(0.1013309319 • %FEO)] • 245.5940689
Comill	100% Coal	30	NOx (ppm) = 213.4010436 • ln(%FEO) + 148.3641859
DRB	+10% SD	16	NOx (ppm) = [exp(0.1126259271 • %FEO)] • 177.3720864
	+10% SD	30	NOx (ppm) = [exp(0.06755321616 • %FEO)] • 504.3496336
	+20% SD	16	NOx (ppm) = 168.6112791 • ln(%FEO) + 79.06919633
	+20% SD	30	NOx (ppm) = 168.0136418 • ln(%FEO) + 148.5575102
	+10% SG	16	NOx (ppm) = 208.7307239 • ln(%FEO) + 60.87922996
	+10% SG	30	NOx (ppm) = 241.255893 • ln(%FEO) + 100.9536784
	+20% SG	16	NOx (ppm) = 291.4041716 • ln(%FEO) - 0.1574573267
	+20% SG	30	NOx (ppm) = 275.1196676 • ln(%FEO) + 152.0831588
GL-11&12	100% Coal	0	NOx (ppm) = [exp(0.1115671985 • %FEO)] • 369.1555986
Comill	100% Coal	15	NOx (ppm) = [exp(0.227053187 • %FEO)] • 137.2629569
	+5% SD	0	NOx (ppm) = 0.8263611951•(%FEO^3)+ 491.645388
	+5% SD	15	NOx (ppm) = [exp(0.1910308638 • %FEO)] • 158.845717
	+10% SD	0	NOx (ppm) = [exp(0.1357692364 • %FEO)] • 351.8173708
	+10% SD	15	NOx (ppm) = [exp(0.2407465003 • %FEO)] • 125.3042676
	+20% SD	0	NOx (ppm) = [exp(0.1103455946 • %FEO)] • 330.005491
	+20% SD	15	NOx (ppm) = [exp(0.2104652519 • %FEO)] • 133.4406949
JW-12&13	100% Coal	0	NOx (ppm) = 203.9545613 • ln(%FEO) + 376.3901411
Comill	100% Coal	15	NOx (ppm) = [exp(0.1906927951 • %FEO)] • 216.1582735
	+5% SD	0	NOx (ppm) = 1.350766572•(%FEO^3)+ 549.083231
	+5% SD	15	NOx (ppm) = 10.16397327•(%FEO^2) + 295.1253347
	+10% SD	0	NOx (ppm) = [exp(0.149947911 • %FEO)] • 310.5324638
	+10% SD	15	NOx (ppm) = 54.42365737 • %FEO + 171.5748084
	+20% SD	0	NOx (ppm) = 77.107713 • %FEO + 345.0982038
	+20% SD	15	NOx (ppm) = [exp(0.2052946322 • %FEO)] • 180.9089072
	+5% SG	0	NOx (ppm) = [exp(0.1366611284 • %FEO)] • 400.7129067
	+5% SG	15	NOx (ppm) = 1.672459383•(%FEO^3) + 374.9301534
	+10% SG	0	NOx (ppm) = 3.746454707•(%FEO^3) + 434.0944984
	+10% SG	15	NOx (ppm) = 3.746454707•(%FEO^3) + 261.2634448
	+20% SG	0	NOx (ppm) = 55.24568363 • %FEO + 263.0839291
	+20% SG	15	NOx (ppm) = 67.0186863 • %FEO + 138.4821004

Table B-2. Fuel stoichiometric ratio and volatile to fixed carbon ratio as a function of weight % biomass.

Quantity/Biomass	Coal	Curvefit Coefficients		
		A	B	C
Stoichiometric Ratio*				
SD or SG	JR	1.0070	0.04746	0.004551
	GL	1.0076	0.04484	0.004451
	PR	1.0077	0.04451	0.004439
	JW	1.0079	0.04372	0.004408
Volatile/FC Ratio**				
SD	JR	1.0946	0.01101	5.012E-05
	GL	0.6174	0.01052	9.122E-05
	PR	0.6571	0.01437	1.332E-04
	JW	0.3180	0.00906	6.953E-05
SG	JR	1.0946	0.01043	5.620E-05
	GL	0.6174	0.00876	7.142E-05
	PR	0.6581	0.01126	9.515E-05
	JW	0.3180	0.00853	6.988E-05

*SR = A + B•FEO+C•$(FEO)^2$
**V/FC = A + B•W% + C•$(Wt\%)^2$

Table B-3. Fuel Nitrogen as a function of weight % biomass.

Biomass	Coal	Curvefit Coefficients	
		Slope	B
SD	JR	-0.0080	0.8510
	GL	-0.0142	1.7074
	PR	-0.0088	1.5693
	JW	-0.0120	1.4485
SG	JR	0.0047	0.8521
	GL	-0.0054	1.7074
	PR	-0.0089	1.5731
	JW	-0.0027	1.4482

% Fuel N = Slope•Wt% + B

Table B-4A. Size distributions for coal and comilled biomass with component coal and biomass, Rosin-Rammler distribution fit parameters.

Test	Biomass	% Biomass	Fraction	%< 75μm	RR-Size	RR -Dist

GL-5	SD	10	Coal+SD	69.73	68.0	1.15
			Coal	78.63	53.0	1.50
			SD	0.00	250.0	2.50
	SD	20	Coal+SD	68.40	66.0	0.90
			Coal	83.36	50.0	1.45
			SD	0.00	240.0	3.00
GL-6	SG	10	Coal+SG	69.27	68.0	1.10
			Coal	84.72	52.0	1.70
			SG	0.00	200.0	1.80
	SG	20	Coal+SG	70.50	61.0	0.90
			Coal	91.36	40.0	1.55
			SG	9.68	180.0	1.80
PR-6	SD	20	Coal+SD	69.37	64.0	0.90
			Coal	89.79	40.0	1.45
			SD	11.73	180.0	2.00
JR-7	SG	10	Coal+SG	82.48	40.0	0.65
			Coal	89.54	36.0	1.00
			SG	0.00	290.0	2.30
	SG	20	Coal+SG	69.69	65.0	0.60
			Coal	83.32	45.0	0.90
			SG	0.00	300.0	2.90
	SD	10	Coal+SD	77.08	50.0	0.70
			Coal	87.58	38.0	1.00
			SD	0.00	280.0	2.50
	SD	20	Coal+SD	75.15	45.0	0.50
			Coal	89.39	35.0	1.00
			SD	0.00	300.0	2.80
GL-9	SD	10	Coal+SD	77.02	48.0	0.75
			Coal	85.61	42.0	1.15
			SD	28.00	240.0	0.90
	SD	20	Coal+SD	78.40	40.0	0.58
			Coal	91.15	33.0	1.05
			SD	23.81	220.0	1.20
	SG	10	Coal+SG	79.63	45.0	0.80
			Coal	85.94	41.0	1.10
			SG	39.86	170.0	1.00
	SG	20	Coal+SG	70.93	62.0	0.76
			Coal	82.32	46.0	1.10
			SG	22.58	275.0	1.00

Table B-4B. Size distributions for coal and comilled biomass with component coal and biomass, Rosin-Rammler distribution fit parameters.

Test	Biomass	% Biomass	Fraction	%< 75mm	RR-Size	RR -Dist
GL-11	SD	5	Coal+SD	80.20	41.0	0.81
			Coal	83.00	37.0	0.89
			SD	10.37	800.0	0.90
	SD	10	Coal+SD	76.17	45.0	0.72
			Coal	81.58	41.0	0.95
			SD	23.90	350.0	0.90
	SD	20	Coal+SD	78.35	35.0	0.50
			Coal	91.05	26.0	0.80
			SD	1.45	240.0	3.00
JW-12	SD	5	Coal+SD	78.18	48.0	0.86
			Coal	81.08	42.0	0.92
			SD	24.16	250.0	1.70
	SD	10	Coal+SD	77.23	44.0	0.68
			Coal	85.51	35.5	0.85
			SD	11.55	240.0	1.70
	SD	20	Coal+SD	73.30	52.0	0.62
			Coal	85.85	31.0	0.74
			SD	13.30	225.0	2.00
JW-13	SG	5	Coal+SG	79.96	45.0	0.85
			Coal	82.90	40.0	0.92
			SD	65.82	68.0	0.55
	SG	10	Coal+SG	77.57	45.0	0.74
			Coal	84.53	35.0	0.85
			SD	12.56	270.0	1.40
	SG	20	Coal+SG	74.93	45.0	0.60
			Coal	87.18	28.0	0.75
			SD	19.09	195.0	1.75